

# Biochemical and physiological characterization of PIN auxin efflux carriers from *Arabidopsis thaliana*

Martina Kolb

Vollständiger Abdruck der von der TUM School of Life Sciences der Technischen Universität München zur Erlangung einer  
Doktorin der Naturwissenschaften (Dr. rer. nat.)  
genehmigten Dissertation.

Vorsitz: Prof. Dr. Corinna Dawid

Prüfer der Dissertation:

1. Priv.-Doz. Dr. Ulrich Z. Hammes
2. Prof. Dr. Kay H. Schneitz

Die Dissertation wurde am 25.09.2023 bei der Technischen Universität München eingereicht und durch die TUM School of Life Sciences am 19.01.2024 angenommen.



Für mich.

# Contents

<b>1. ABSTRACT .....</b>	<b>1</b>
<b>2. ZUSAMMENFASSUNG .....</b>	<b>3</b>
<b>3. INTRODUCTION .....</b>	<b>5</b>
<b>3.1 The phytohormone auxin .....</b>	<b>5</b>
<b>3.2 Auxin transport.....</b>	<b>6</b>
<b>3.3 The family of PIN-FORMED proteins.....</b>	<b>8</b>
3.3.1 Protein structure and classification .....	8
3.3.2 Cellular localization.....	10
3.3.3 PIN-mediated directional auxin flow regulates root gravitropism .....	12
3.3.4 Regulation of PINs by means of the loop.....	13
<b>3.4 AGCVIII kinases regulate PIN polarity and activity.....</b>	<b>14</b>
<b>3.5 Aims of this thesis .....</b>	<b>17</b>
3.5.1 Examination of potential modifiers and inhibitors of PIN-mediated IAA transport, in particular, NPA .....	17
3.5.2 Characterization of semi-canonical PIN6 and non-canonical PIN8.....	17
3.5.3 Investigation of the role of the PIN loop in regulating IAA transport activity and localization of PINs.....	18
3.5.4 Examination of the potential of other AGCVIII kinases to activate PINs and identification of additional players in PAT.....	18
<b>4. RESULTS .....</b>	<b>19</b>
<b>4.1 PIN-mediated IAA transport in <i>X. laevis</i> oocytes can be modified by co-injected substances.....</b>	<b>21</b>
<b>4.2 Naphthylphthalamic acid inhibits PIN auxin transporters .....</b>	<b>25</b>
4.2.1 NPA inhibits PIN-mediated IAA transport in the oocyte system.....	25
4.2.2 NPA does not impair PIN phosphorylation.....	28
4.2.3 NPA is not a general transport inhibitor .....	29
<b>4.3 PIN8 is a constitutively active IAA transporter and sensitive to NPA .....</b>	<b>30</b>
<b>4.4 Non-canonical PIN8 adopts properties of a canonical PIN when provided with a canonical loop .....</b>	<b>31</b>
4.4.1 Chimaeras display IAA transport characteristics of their loop donor and TMD donor .....	32
4.4.2 Physiological relevance of the PIN8-2-8 and PIN8-3-8 chimaeras .....	34
4.4.3 PIN8-2-8-GFP localizes at the PM .....	38
<b>4.5 Characterization of semi-canonical PIN6 .....</b>	<b>39</b>
4.5.1 PIN6 is a constitutively active IAA transporter and its transport capacity is enhanced by PID.....	40
4.5.2 $P_{PIN2}:PIN6$ expressed in <i>pin2</i> background enhances the mutant phenotype .....	42
4.5.3 PIN6 expressed in the <i>PIN2</i> domain localizes at the ER and the PM.....	44

<b>4.6</b>	<b>Characterization of new regulators of PIN-mediated IAA transport</b> .....	<b>44</b>
4.6.1	Identification of new players in regulation of PIN-mediated IAA efflux.....	45
4.6.2	Characterization of the interaction between PAX, PIN and BRX .....	46
<b>5.</b>	<b>DISCUSSION</b> .....	<b>51</b>
<b>5.1</b>	<b>Characterization of PIN8 and the transport mechanism of the PINs</b> .....	<b>51</b>
<b>5.2</b>	<b>The canonical loop regulates PIN activity by an inhibitory interaction with the TMD and contributes to IAA transport</b> .....	<b>53</b>
<b>5.3</b>	<b>PIN substrate specificity and modulation of PIN-mediated IAA transport</b> .....	<b>56</b>
5.3.1	NPA directly inhibiting PINs causes the physiological effects of NPA .....	56
5.3.2	Investigation of further potential modulators of PIN IAA transport .....	58
<b>5.4</b>	<b>PIN6 is an exceptional member of the PIN family</b> .....	<b>63</b>
<b>5.5</b>	<b>Identification of new regulators of PIN-mediated IAA transport</b> .....	<b>65</b>
5.5.1	PIN, PAX and BRX constitute a molecular rheostat modulating auxin flux underlying protophloem sieve element differentiation.....	66
5.5.2	Functional divergence of BRX family proteins .....	68
<b>6.</b>	<b>MATERIALS AND METHODS</b> .....	<b>70</b>
<b>6.1</b>	<b>Materials</b> .....	<b>70</b>
6.1.1	Biological material.....	70
6.1.1.1.	Plant lines .....	70
6.1.1.2.	<i>Xenopus laevis</i> oocytes .....	70
6.1.1.3.	Bacterial strains .....	71
6.1.2	Plasmids .....	71
6.1.3	Primers.....	73
<b>6.2</b>	<b>Methods</b> .....	<b>74</b>
6.2.1	Molecular cloning.....	74
6.2.2	Genotyping of plant genomic DNA.....	75
6.2.3	Biochemical methods .....	76
6.2.3.1.	Protein purification of recombinant GST-tagged proteins .....	76
6.2.3.2.	<i>In vitro</i> phosphorylation of purified PIN loop.....	76
6.2.4	Plant growth conditions .....	76
6.2.5	Stable transformation and selection of plant lines .....	77
6.2.6	Crossing of plant lines .....	77
6.2.7	Plant physiology experiments.....	77
6.2.8	Histochemical GUS Staining .....	77
6.2.9	Microscopy and signal quantification .....	78
6.2.10	<i>Xenopus laevis</i> oocyte transport assay.....	78
6.2.11	<i>In silico</i> protein alignment .....	79
<b>7.</b>	<b>LIST OF FIGURES</b> .....	<b>80</b>
<b>8.</b>	<b>LIST OF TABLES</b> .....	<b>82</b>
<b>9.</b>	<b>ABBREVIATIONS</b> .....	<b>83</b>

<b>10.</b>	<b>BIBLIOGRAPHY .....</b>	<b>85</b>
<b>11.</b>	<b>ACKNOWLEDGEMENTS.....</b>	<b>98</b>
<b>12.</b>	<b>APPENDIX .....</b>	<b>101</b>

Ung *et al.*, 2022  
Koh *et al.*, 2021  
Abas *et al.*, 2021  
Marhava *et al.*, 2020  
Marhava *et al.*, 2018  
Abbas *et al.*, 2018

# 1. Abstract

Auxins, a group of phytohormones and particularly their main representative IAA, regulate a plethora of developmental and growth processes in plants, which is largely based on its controlled and directed flux through the plant's body. This so-called polar auxin transport (PAT) critically depends on the PIN-FORMED (PIN) proteins, a family of integral membrane auxin efflux carriers localizing to the plasma membrane (PM) or endoplasmic reticulum (ER) to facilitate PAT and to maintain auxin homeostasis. *Arabidopsis* has eight PINs (PIN1 – PIN8). They consist of two transmembrane domains (TMD) separated by a hydrophilic loop based on whose size they are non-phylogenetically categorized into canonical, non-canonical, and semi-canonical. Canonical PINs (PIN1, PIN2, PIN3, PIN4, and PIN7) are polarly distributed in the PM of many cells, thus conferring directionality to the auxin flux. Their loop is by default auto-inhibitory and PINs need to be activated by phosphorylation. This is carried out by AGCVIII protein kinases like D6 PROTEIN KINASE (D6PK) and PINOID (PID). Non-canonical PINs (PIN5 and PIN8) mainly localize to the ER and are proposed to function in the regulation of auxin homeostasis within cells. The semi-canonical PIN6 localizes both at the PM and at the ER. In this study, I used the *Xenopus laevis* oocyte expression system to investigate the regulation and activation of PINs by means of their loop and kinases, to characterize the lesser-studied family members PIN6 and PIN8, and to investigate modification of PIN-mediated IAA transport by substances like other natural and synthetic auxins as well as inhibitors of auxin transport.

First, I identified the four AGCVIII kinases PROTEIN KINASE ASSOCIATED WITH BRX (PAX), PAXL, AGC1-9, and KCBP-INTERACTING PROTEIN KINASE (KIPK) as yet unknown activators of PINs. Further, I found that AGC1-7, which phosphorylates PINs *in vitro* does not activate PIN-mediated IAA transport. This suggests that phosphorylation is not sufficient to explain activation. In summary, my findings substantially increase the current knowledge about activation of PIN-mediated IAA transport. Second, I found that PIN-mediated IAA transport can be modified by other substances and my results suggest that shape complementary plays a large role in recognition of the PIN substrate. In particular, the widely used PAT inhibitor, N-1-naphthylphthalamic acid (NPA) was found to directly inhibit PINs, which is a parsimonious, mechanistic explanation for NPA's physiological effects on plants that has long been sought after. Third, my characterization of PIN6 and PIN8 in the oocyte system showed for the first time clearly that both transport IAA: I found that PIN8 is a constitutively active IAA transporter operating independently of kinase control. Further, I found that PIN6 is a constitutively active IAA transporter and that its transport capacity is enhanced by PID, but intriguingly, not by D6PK, which is a yet unknown feature within the PIN family. Lastly, I created and studied a chimaera of PIN8 provided with the PIN2 loop and PIN3 loop,

respectively. Alongside IAA transport assays in the oocyte system, I conducted rescue experiments in the agravitropic *pin2* mutant, GUS histochemical staining as well as a subcellular localization analysis using confocal laser scanning microscopy. I found that providing a non-canonical PIN with a canonical loop can turn the non-canonical PIN to some extent into a canonical PIN and that the canonical loop is more than an “on/off” switch of the PINs but determines IAA transport characteristics and contributes to IAA transport activity. Moreover, the results indicate that the inhibitory effect of the canonical loop is mediated through a specific interaction between loop and TMD.



## 2. Zusammenfassung

Auxine, eine Gruppe von Phytohormonen und insbesondere ihr wichtigster Vertreter IAA, regulieren eine Vielzahl von Entwicklungs- und Wachstumsprozessen in Pflanzen, die erheblich auf ihrem kontrollierten und gerichteten Fluss durch den Pflanzenkörper beruhen. Dieser sogenannte polare Auxin-Transport (PAT) hängt maßgeblich von den PIN FORMED (PIN)-Proteinen ab, einer Familie integraler Membranproteine, die Auxin-Efflux-Carrier sind und die in der Plasmamembran (PM) oder dem endoplasmatischen Retikulum (ER) lokalisiert sind, um PAT zu bewerkstelligen und die Auxin-Homöostase aufrechtzuerhalten. *Arabidopsis* besitzt acht PINs (PIN1 - PIN8). Sie bestehen aus zwei Transmembrandomänen (TMD), die durch einen hydrophilen Loop getrennt sind, und werden aufgrund ihrer Größe nicht-phylogenetisch in kanonisch, nicht-kanonisch und semi-kanonisch eingeteilt. Kanonische PINs (PIN1, PIN2, PIN3, PIN4 und PIN7) sind polar in der PM vieler Zellen verteilt und verleihen so dem Auxinfluss seine Richtung. Ihr Loop ist grundsätzlich autoinhibitorisch und die PINs müssen durch Phosphorylierung aktiviert werden. Dies geschieht durch AGCVIII-Proteinkinasen wie D6 PROTEIN KINASE (D6PK) und PINOID (PID). Nicht-kanonische PINs (PIN5 und PIN8) sind hauptsächlich im ER lokalisiert und scheinen bei der Regulierung der Auxin-Homöostase innerhalb der Zellen eine Rolle zu spielen. Der semi-kanonische PIN6 ist sowohl an der PM als auch am ER lokalisiert. In der vorliegenden Studie habe ich das Expressionssystem der *Xenopus laevis* Oozyten verwendet, um die Regulierung und Aktivierung der PINs durch ihren Loop und durch Kinasen zu untersuchen, um die weniger gut erforschten Familienmitglieder PIN6 und PIN8 zu charakterisieren und um die Modifizierung des PIN-vermittelten IAA-Transports durch Substanzen wie andere natürliche und synthetische Auxine sowie durch Inhibitoren des Auxin-Transports zu untersuchen. Erstens identifizierte ich die vier AGCVIII-Kinasen PROTEIN KINASE ASSOCIATED WITH BRX (PAX), PAXL, AGC1-9 und KCBP-INTERACTING PROTEIN KINASE (KIPK) als bisher unbekannte Aktivatoren von PINs. Außerdem habe ich herausgefunden, dass AGC1-7, welche PINs in vitro phosphoryliert, den PIN-vermittelten IAA-Transport nicht aktiviert. Dies deutet darauf hin, dass die Phosphorylierung nicht ausreicht, um Aktivierung zu erklären. Insgesamt erweitern meine Ergebnisse das derzeitige Wissen über die Aktivierung des PIN IAA-Transports erheblich. Zweitens habe ich festgestellt, dass der PIN-vermittelte IAA-Transport durch andere Substanzen modifiziert werden kann, und meine Ergebnisse deuten darauf hin, dass bei der Erkennung des PIN-Substrats die geometrisch komplementäre Struktur eine große Rolle spielt. Insbesondere wurde festgestellt, dass 1-Naphthylphthalamidsäure (NPA), ein weit verbreiteter PAT-Inhibitor, PINs direkt hemmt, was eine schlüssige Erklärung des Mechanismus der physiologischen Wirkungen von NPA auf Pflanzen darstellt, nach der lange gesucht wurde. Drittens zeigte meine

Charakterisierung von PIN6 und PIN8 im Oozyten System zum ersten Mal eindeutig, dass beide IAA transportieren: Ich fand heraus, dass PIN8 ein konstitutiv aktiver IAA-Transporter ist, der unabhängig von der Kontrolle durch Kinasen arbeitet. Außerdem habe ich herausgefunden, dass PIN6 ein konstitutiv aktiver IAA-Transporter ist und dass seine Transportkapazität durch PID erhöht wird, aber interessanterweise nicht durch D6PK, was eine bisher unbekannte Eigenschaft innerhalb der PIN-Familie ist. Schließlich erstellte und untersuchte ich eine Chimäre von PIN8 versehen mit dem PIN2-Loop beziehungsweise dem PIN3-Loop. Neben IAA-Transportversuchen im Oozyten System führte ich Rettungsexperimente in der agravitropen *pin2*-Mutante, histochemische GUS-Färbungen sowie eine Analyse der subzellulären Lokalisierung mittels konfokaler Laser-Scanning-Mikroskopie durch. Ich fand heraus, dass ein nicht-kanonischer PIN durch einen kanonischen Loop zu einem gewissen Grad zu einem kanonischen PIN gemacht werden kann und dass der kanonische Loop mehr als ein „An/Aus“-Schalter der PINs ist, sondern die IAA-Transporteigenschaften bestimmt sowie zur IAA-Transportaktivität beiträgt. Darüber hinaus deuten die Ergebnisse darauf hin, dass die inhibierende Wirkung des kanonischen Loops durch eine spezifische Interaktion zwischen Loop und TMD zustande kommt.

### 3. Introduction

#### 3.1 The phytohormone auxin

The phytohormone auxin controls essentially all aspects of a plant's life (Benjamins and Scheres, 2008). Not only is it of tremendous importance for plant growth and basically all developmental processes, but it is also crucial for a plant's response to the environment, resulting in a seemingly ever-expanding list of processes in which auxin is involved (Finet and Jaillais, 2012; Weijers and Wagner, 2016; Vieten *et al.*, 2007). These aspects make it vitally important to understand how auxin exerts its diverse functions and although the history of auxin research reaches back more than a hundred years (Darwin and Darwin, 1880), we are still far from a comprehensive understanding.

Auxins are defined as low molecular weight organic acids containing an aromatic ring and a carboxyl group (George *et al.*, 1963). Notably, the term auxin describes several chemical compounds - naturally occurring and synthetic ones - that exhibit auxin activity. Thereof, indole-3-acetic acid (IAA) is the most abundant and most studied representative but also other endogenous auxins are typically found in lower concentrations in several plant species (Sauer *et al.*, 2013; Ludwig-Müller, 2022). Inside the cell, IAA initiates countless different transcriptional programs with a wide range of output. The perception of IAA occurs through the auxin receptor TIR1 (TRANSPORT INHIBITOR RESPONSE1) and its close homologs AFB1, 2, and 3 (AUXIN SIGNALING F-BOX1, 2 and 3) (Dharmasiri *et al.*, 2005). TIR1/ AFB receptors are F-box subunits of E3 ubiquitin ligases that promote the degradation of their Aux/IAA (AUXIN/INDOLE-3-ACETIC ACID) co-receptors when IAA is bound. At high IAA concentrations, these receptors initiate a transcriptional response by binding Aux/IAA proteins, leading to their ubiquitinylation and consequently their degradation. Subsequently, the auxin response factors (ARF) are derepressed and gene expression is activated (reviewed in Weijers and Wagner 2016). Apart from this pathway, upstream of gene regulation, IAA forms gradients, as well as maxima and minima, and very often a concentration gradient within a tissue governs the developmental output (Friml, 2003). Therefore, IAA is frequently referred to as a morphogen rather than a phytohormone. An example of this mode of action is the process of protophloem differentiation. Protophloem is the early, initial phloem and it is the first tissue, which differentiates in the root meristem (Rodriguez-Villalon *et al.*, 2014). The process is regulated by the auxin flux running through: The auxin level decreases as the cells divide, and subsequently increases as the cells differentiate (Brunoud *et al.*, 2012; Santuari *et al.*, 2011). Interestingly, the timing of differentiation is not uniform across cell files, so for instance, developing protophloem sieve elements (PPSE) differentiate as their neighboring cells still divide.

IAA is produced primarily in young leaves and the apexes of the root and shoot via tryptophan biosynthesis dependent and independent pathways (Ljung *et al.*, 2001, 2005; Normanly, 2010; Petersson *et al.*, 2009; Zhao, 2010). Additionally, it can be released from IAA conjugates by hydrolytic cleavage of IAA-amino acids, IAA-sugar, and IAA-methyl ester (Bartel, 1997; Li *et al.*, 2008; Woodward and Bartel, 2005; Yang *et al.*, 2008). Passively transported within the phloem, IAA is delivered fast from its site of synthesis to the recipient sink tissue (Cambridge and Morris, 1996). Interconnected with this rather rough way of distribution, the plant body additionally possesses a precise cell-to-cell polar auxin transport (PAT) system, i.e. auxin is moved between cells in a directional manner. By controlling local auxin concentrations, PAT regulates a variety of developmental responses, including gravitropic and phototropic organ growth (Benková *et al.*, 2003; Han *et al.*, 2021; Li *et al.*, 2022). PAT is enabled by an extended network of specialized, plasma membrane (PM)-localized, influx and efflux carriers actively transporting IAA across cells, and the existence of such a transporter network, ensuring the correct time- and space-wise distribution of IAA, makes a unique feature of the phytohormone. Additionally to PAT transport, IAA is intracellularly transported across organelle membranes like the ER and the vacuole for storage and modification, which plays a crucial role in regulating the distribution, activity, and availability of auxin within plant cells (Zhang and Peer, 2017; Ruiz Rosquete *et al.*, 2012). Notably, our current knowledge about transport systems for other auxins than IAA is very limited and the transport of conjugated forms of auxin is barely investigated.

### **3.2 Auxin transport**

PAT is enabled by various PM-localized IAA influx and efflux carriers, whose differential and often polar subcellular localization defines the direction of auxin flow (Armengot *et al.*, 2016; Tanaka *et al.*, 2006; Vieten *et al.*, 2007). Our current knowledge about these transporters and how auxin moves within the plant body is largely built on experiments in which this process is inhibited. In this context, chemicals that are inhibitors of PAT play a big role (Teale and Palme, 2018). Especially the synthetic PAT inhibitor *N*-1-naphthylphthalamic acid (NPA), a herbicide, has been used extensively in research and contributed highly to our current knowledge of the molecular mechanisms of PAT. Interestingly, however, despite its popularity among plant physiologists and its importance as a research tool, NPA's exact mode of action is unclear. It is believed to bind to one or more protein components of the auxin efflux carrier network which mediate PAT, but NPA's exact target has been a matter of debate for centuries (Teale and Palme, 2018).

The chemistry underlying the IAA carrier network is the widely accepted chemiosmotic theory (Rubery and Shelldrake 1973, 1974; Goldsmith and Goldsmith, 1981; Goldsmith *et al.*, 1981):

IAA is a weak organic acid and depending on the compartment pH, it is present either as anion IAA<sup>-</sup> or in its protonated state, HIAA. In the apoplast, at pH 5,5, the majority of IAA is protonated. In this state, it can diffuse freely into the cell. This uptake is further assisted by membrane-resident auxin influx carriers namely AUX1 (AUXIN RESISTANT1) and its homologs LAX1, 2, 3 (LIKE AUX1, 2, 3) (Yang *et al.*, 2006; Swarup *et al.*, 2008). In addition, the nitrate sensor/transporter NRT1.1/NPF6.3/CHL1 (NITRATE TRANSPORTER1.1/NITRATE TRANSPORTER1/PEPTIDE TRANSPORTER FAMILY 6.3/CHLORINA1) facilitates auxin uptake at low NO<sub>3</sub><sup>-</sup> concentration (Krouk *et al.*, 2010).

Once inside the cell, the more alkaline pH of the cytosol causes deprotonation of IAA, thus the molecule cannot pass through the plasma membrane anymore but must be transported actively by efflux carriers. Two protein families are primarily responsible for the export of IAA: The first is the ATP BINDING CASSETTE (ABC) auxin transporters of a MULTIDRUG RESISTANCE (MDR) subfamily (Geisler and Murphy, 2006; Geisler *et al.*, 2005). The second is the family of PIN-FORMED (PIN) auxin efflux carriers. The ABC and the PIN families have been shown to transport auxin independently in heterologous systems and *in planta* (Geisler *et al.*, 2005; Petrášek *et al.*, 2006; Yang and Murphy, 2009; Zourelidou *et al.*, 2014). Furthermore, it is suggested that the families interact in one-way or the other, thus independently and interdependently controlling PAT (Bandyopadhyay *et al.*, 2007; Blakeslee *et al.*, 2007; Titapiwatanakun *et al.*, 2009; Mravec *et al.*, 2008). In particular, some studies suggest that PINs and ABCBs form protein complexes to facilitate IAA efflux *in planta* (Blakeslee *et al.*, 2007; Titapiwatanakun *et al.*, 2009). A major difference between ABCs and PINs is their localization within the cell: Only members of the PIN family show clear polar localization at the PM and thus have the potential to give essential directionality to the auxin flow within the plant (Habets and Offringa, 2014; Adamowski and Friml, 2015). Furthermore, PIN localization correlates with the expected auxin accumulation and depletion sites in the cells, observable by usage of synthetic output (transcriptional) reporters, as well as auxin input reporters (Ulmasov *et al.*, 1997; Sabatini *et al.*, 1999; Benková *et al.*, 2003; Vernoux *et al.*, 2011; Brunoud *et al.*, 2012; Larrieu and Vernoux, 2015; Liao *et al.*, 2015). Therefore, the polar localization of PIN proteins is widely used to predict the auxin flow in plants and the direction of it, as to date there is no possibility of direct visualization. The PINs rightly are often referred to as the key players in PAT and consequently, understanding their function and their regulation is crucial for the understanding of plant growth and development.

Additionally to intercellular transport, IAA is intracellularly transported across organelle membranes like the endoplasmic reticulum (ER) and the vacuole. At the ER, besides members of the PIN family, members of the ER-resident family of PIN-LIKE TRANSPORTERS (PILS) have been suggested to export IAA out of the cytoplasm into the ER and by that to contribute

to the regulation of intracellular auxin distribution (Feraru *et al.*, 2012; Barbez *et al.*, 2012). Further, WALLS ARE THIN1 (WAT1/UmamiT5), which localizes to the tonoplast, was demonstrated to transport IAA out of the vacuole into the cytosol (Ranocha *et al.*, 2013). An overview of all IAA transporters identified to date is given in **Fig. 3-1**.

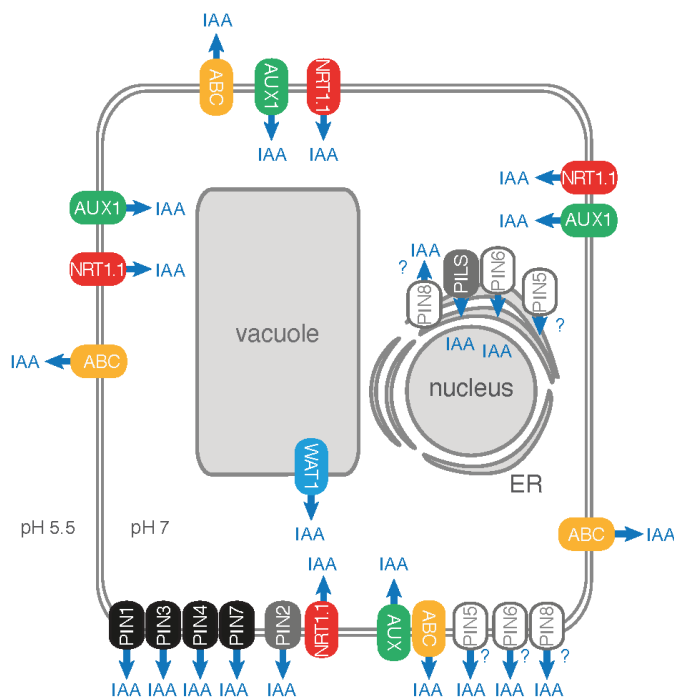


**Fig. 3-1 Overview of the influx and efflux carrier network enabling (polar) IAA transport in *Arabidopsis thaliana*.** Schematic representation of all IAA transporters identified to date, their distribution in the plasma membrane or endomembranes, as well as the direction of auxin transport (arrows). Depending on the pH, IAA is present either as IAA<sup>-</sup> or as HIAA. HIAA can freely diffuse into the cell and its uptake into the cell is further assisted by auxin influx carriers (AUX/LAX and NRT1.1). IAA<sup>-</sup> cannot pass through the PM to exit the cell and needs to be actively transported by the efflux carriers of the PIN and ABC family. Only PINs show a polarity at the PM, regulating the direction of auxin flux. Additionally to intercellular transport, IAA is intracellularly transported across organelle membranes. This is carried out by ER-resident members of the PINs and PILS family and by WAT1, transporting IAA out of the vacuole. Figure modified from Hammes *et al.*, 2022.

### 3.3 The family of PIN-FORMED proteins

#### 3.3.1 Protein structure and classification

The PIN proteins are a plant-specific family of integral membrane transporter proteins (Křeček *et al.* 2009) and their evolutionary origin reaches back to streptophyte algae (Skokan *et al.*, 2019). In *Arabidopsis thaliana*, the family consists of eight members (Křeček *et al.*, 2009). The name of the family refers to PIN1, the first member identified, as the loss-of-function mutant *pin1*, generates pin-formed inflorescences, largely devoid of leaves or flowers (Gälweiler *et al.*, 1998). *Pin2* mutants are agravitropic (Luschnig *et al.*, 1998; Müller *et al.*, 1998) and *pin347* mutants are non-phototropic (Willige *et al.*, 2013). Importantly, the observed phenotypes of *pin* mutants can often be mimicked by the application of auxin transport inhibitors (Müller *et al.*, 1998; Benková *et al.*, 2003; Bliilou *et al.*, 2005), and notably, the application of NPA leads to a *pin1* like phenotype (Okada *et al.*, 1991). The most economical explanation therefor is that NPA directly inhibits PIN1, however, evidence for such a mode of action is conspicuous by its absence and a direct molecular association of NPA with PINs has never been reported so far (Teale and Palme, 2018).

PINs consist of two transmembrane domains (TMD) of five alpha helices each, with the TMDs being separated by a disordered, hydrophilic loop (HL) that reaches into the cytosol (Mravec *et al.*, 2009; Zwiewka *et al.*, 2019; Nodzyński *et al.*, 2016) (**Fig. 3-2 A**). For years, the eight *Arabidopsis* PINs had been classified based on the length of their loop (Mravec *et al.*, 2009; Viaene *et al.*, 2013). This classification was refined by Bennett and colleagues a couple of years ago (Bennett *et al.*, 2014). Their structural analysis showed that most PIN proteins possess a conserved, modular domain within their loop. Consequently, in terms of sequence similarity of this shared “canonical” structure and the length of the loop, the PINs can be grouped into at least two transporter classes: “long” canonical and “short” or “intermediate” non-canonical PINs (Bennett *et al.*, 2014; Adamowski and Friml, 2015) (**Fig. 3-2 B**). The canonical PINs (PIN1, PIN2, PIN3, PIN4, and PIN7) possess long HLs (>350 residues), the two non-canonical PINs (PIN5 and PIN8) possess short HLs (<50 residues), and semi-canonical PIN6 has a HL of intermediate length (>250 residues), that has homology to the canonical structure but lacks most conserved motifs. Bennett and colleagues found that the canonical structure dates back to the last common ancestor of all land plants and although it has previously been proposed that the short-looped PINs are the ancestral form of PINs in land plants (Mravec *et al.*, 2009; Viaene *et al.*, 2013) their results demonstrate that canonical PINs were one ancestral form and that non-canonical PINs with divergent structures have arisen from canonical precursors multiple times in the angiosperms (Bennett *et al.*, 2014). The importance of PIN proteins to PAT is evident: All eight family members have been shown to be involved in the regulation of auxin fluxes *in planta* and their potential to transport auxin has been investigated in several expression systems (Mravec *et al.*, 2008, 2009; Blakeslee *et al.*, 2007; Zourelidou *et al.*, 2014; Band *et al.*, 2014). However, despite their importance and the effort made in the field, their IAA transport activity has only been shown clearly for canonical PINs and the IAA transport mechanism of the PINs is unknown. Moreover, our current knowledge about their biochemical properties is still limited and only little is known about their substrate specificity.

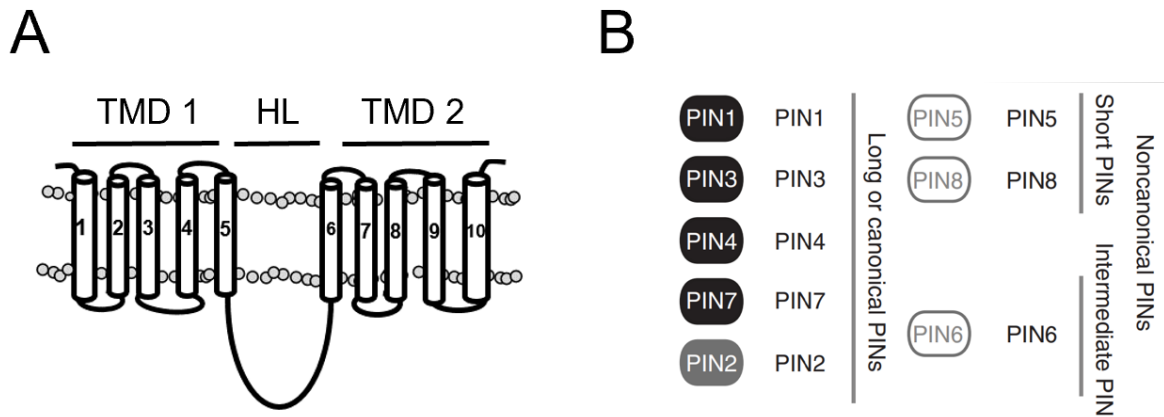


**Fig. 3-2 Structure and classification of PIN proteins from *Arabidopsis*** (A) Schematic structure of a PIN. PINs consist of two transmembrane domains (TMD) of five alpha helices each. The TMDs are separated by a disordered, hydrophilic loop (HL) that reaches into the cytosol and differs in length depending on the PIN. (B) Classification based on sequence similarity and length of the central HL. Figure from Hammes *et al.*, 2022.

### 3.3.2 Cellular localization

The individual PINs show differences in their cellular localization. The canonical PINs localize solely to the PM and they are polarly distributed in many cell types (**Fig. 3-3** left panel). For instance, PIN1 is localized basally (rootward) in root stele cells (Gälweiler *et al.*, 1998) and PIN2 is localized basally in root cortex cells, but apically (shootward) in root epidermal cells (Müller *et al.*, 1998) (**Fig. 3-3** small panel). In the root, polar localization of canonical PINs at the PM combined with their cell type-specific expression pattern is reflected in and sufficient to explain the so-called reverse fountain model of how the IAA flux flows within the root and creates an auxin maximum in the root: IAA is transported upward through the epidermis and partially flows back through the cortex, endodermis, and pericycle to the vasculature, where it returns to the root tip (Kramer and Bennett, 2006; Grieneisen *et al.*, 2007; Mironova *et al.*, 2012; Geisler *et al.*, 2014) (**Fig. 3-3** right panel). In many tissues, different canonical PINs are expressed in the same cell, thus an interaction between different PINs is thinkable. Notably, their localization at the PM is highly dynamic, either during the plant's development or in response to tropic stimuli and PINs continuously cycle between their polar domain at the PM and endosomal compartments (Adamowski and Friml 2015) and depending on the destination of the specific PIN, different pathways are used (Feraru and Friml, 2008). For the investigation of these processes, application of the fungal toxin BFA (Brefeldin A) is often used as a tool. BFA is an inhibitor of subcellular vesicle trafficking. It inhibits GNOM, which belongs to the ARF-GEFs and is responsible for the coordinated delivery of cargo vesicles from the trans-Golgi network to the PM (Steinmann *et al.*, 1999; Geldner *et al.*, 2003). In the presence of BFA, PM-localized PINs aggregate in so-called BFA-compartments inside the cell (Steinmann *et al.*, 1999; Geldner *et al.*, 2001; Ganguly *et al.*, 2010).



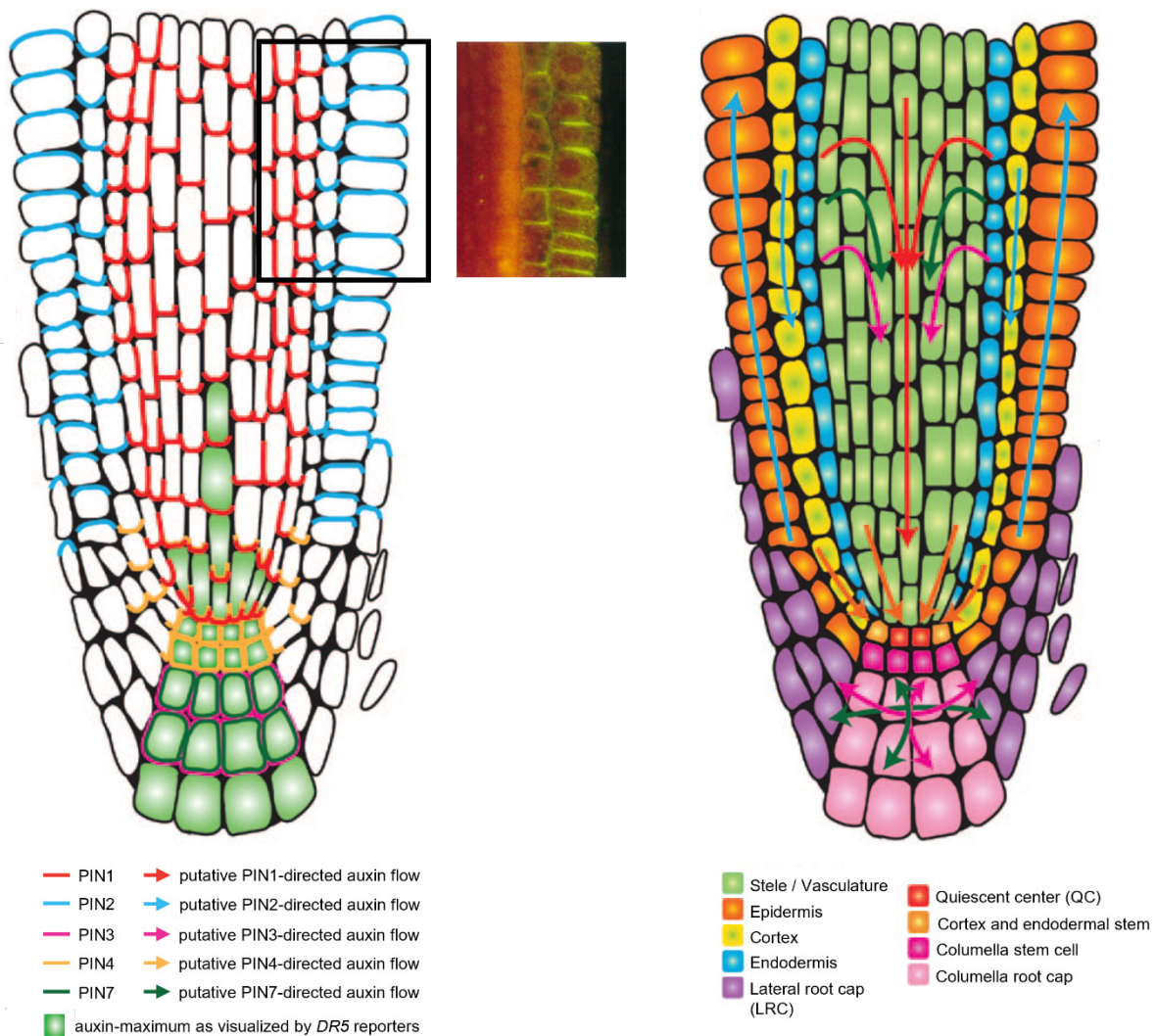


**Fig. 3-3 Localization of canonical PINs in the primary root tip and the auxin flux according to the reverse fountain model.** Schematic representation of a longitudinal root section that shows the localization of the different PINs (left) and the putative auxin fluxes through the root tissues (right). Localization of PIN3 and PIN7 in the stele is redundant with that of PIN1. The small panel shows the dual localization of PIN2, that is basal in cortex cells and apical in epidermis cells. Figure modified from Armengot *et al.*, 2016 and Müller *et al.*, 1998 (small panel).

In contrast to the canonical PINs, the non-canonical, short PINs are unique in that they localize at internal membranes. Both PIN5 (Ganguly *et al.*, 2014; Mravec *et al.*, 2009) and PIN8 (Bosco *et al.*, 2012; Ding *et al.*, 2012) predominantly localize internally to the ER, albeit instances of PM localization have been reported for both of them when expressed ectopically (Ganguly *et al.*, 2014, 2010). Due to their internal localization, PIN5 and PIN8 have been proposed to function in auxin homeostasis within cells rather than IAA transport between cells. At the ER, they are assumed to be responsible for the regulation of the intracellular IAA level in the cell, by facilitating IAA transport into and out of the ER lumen. Inside the ER lumen, auxin is likely unavailable for PAT and nuclear signaling and is potentially inactivated by ER-localized auxin-conjugating enzymes (Mravec *et al.*, 2009). Regarding the role of PIN5 and PIN8, in

particular, a model was presented some years ago, in which PIN5 and PIN8 act antagonistically, with PIN5 transporting IAA into the ER lumen and PIN8 transporting IAA out of the ER into the cytosol (Ding *et al.*, 2012).

Lastly, the cellular localization of semi-canonical PIN6. PIN6 shows a noteworthy dual localization as it is found at the PM as well as at the ER (Simon *et al.*, 2016; Ditengou *et al.*, 2018). Where in the cell PIN6 localizes appears to depend on cell type, expression level, and phosphorylation status of PIN6 (Simon *et al.*, 2016; Ditengou *et al.*, 2018). The PM-residing portion of PIN6 seems to exhibit a certain polarity, which is however not yet clearly determined (Simon *et al.*, 2016; Ditengou *et al.*, 2018). Nevertheless, PIN6 is suggested to be involved in both intercellular PAT and regulation of IAA homeostasis inside the cell by mediating IAA transport into internal compartments (Ditengou *et al.*, 2018; Simon *et al.*, 2016; Cazzonelli *et al.*, 2013). It has been debated whether non-canonical PINs have divergent functions from canonical PINs and one hypothesis in this context is that non-canonical PINs are broader spectrum carriers for auxin-like molecules and auxin conjugates (Bennett *et al.*, 2014).

### **3.3.3 PIN-mediated directional auxin flow regulates root gravitropism**

A mechanism of particular relevance for this thesis is the regulation of root gravitropism by PIN-mediated directional auxin flow. Gravity is perceived primarily in the columella cells, where amyloplasts sediment to the bottom side of the cells (Morita and Tasaka, 2004) and orientation of the root growth according to the gravity vector is provoked by dynamic changes of auxin distribution and asymmetric auxin distribution between the opposite sides of a (gravistimulated) root (Armengot *et al.*, 2016; Sato *et al.*, 2015; Su *et al.*, 2017), which is achieved by differential subcellular PIN distribution (Luschnig *et al.*, 1998; Baster *et al.*, 2012; Zhang *et al.*, 2019a; Tan *et al.*, 2020). Our understanding of the downward movement of the root is based on the Cholodny-Went theory and various interpretations of it ever since (Went, 1928; Cholodny, 1927). According to the theory, accumulation of auxin in the root tip on the side closest to the direction of the gravity vector triggers a decrease in cell elongation within the basal zone of the root cap, which causes the root to bend in the direction of the gravity vector (Geisler *et al.*, 2014; Krieger *et al.*, 2016). This auxin maximum guiding root growth depends on PAT and the IAA flow in the direction of the reverse fountain. PIN2 is the main player mediating shootward auxin transport in root gravitropism. It localizes apically (shootward) in root epidermal cells and together with AUX1, it transports auxin from the root tip to the elongation zone, where root growth is regulated (**Fig. 3-4 A**) (Luschnig *et al.*, 1998; Baster *et al.*, 2012; Zhang *et al.*, 2019a; Tan *et al.*, 2020; Swarup *et al.*, 2001). As mentioned above, *pin2* is agravitropic and it shows a defective auxin distribution (Müller *et al.*, 1998; Lee *et al.*, 2020b). Root reorientation upon gravistimulation (**Fig. 3-4 B**) further requires the activity

of PIN3 and PIN7. Both are expressed in the columella cells, where they localize at the PM in an apolar manner. After the root perceived gravistimulation, for instance, by experimentally turning it by 90°, they polarize to the now downward-facing side of the cells, thus driving the auxin flow towards the lower side of the root tip (Friml *et al.*, 2002; Kleine-Vehn *et al.*, 2010a). Subsequently, the abundance and PM localization of PIN2 is strongly enhanced at the downward-facing side of the root, reinforcing auxin accumulation in this area (Paciorek *et al.*, 2005; Baster *et al.*, 2012; Abas *et al.*, 2006). Ultimately, this cascade leads to the gravitropic response of the root, i.e. growth inhibition at the lower side of the elongation zone, causing downward root bending (Abas *et al.* 2006). Importantly, auxin itself promotes its efflux in the process of gravitropic response, as it was shown that it regulates PIN2 abundance at the PM and PIN2 turnover (Abas *et al.*, 2006; Paciorek *et al.*, 2005).

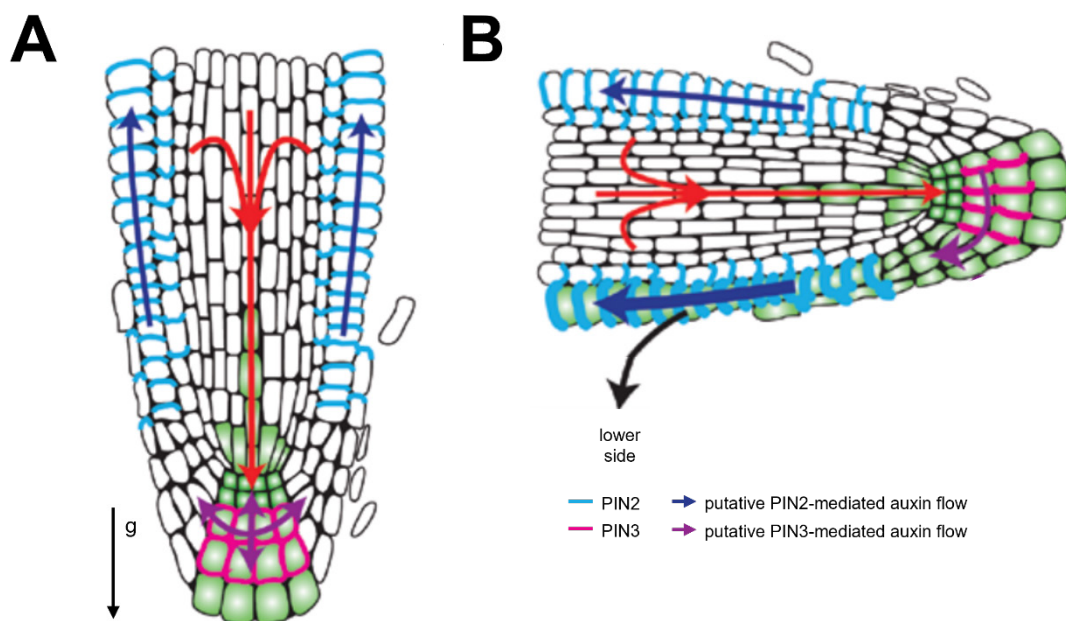


**Fig. 3-4 Auxin flux and PIN localization in root gravitropism.** (A) As per Cholodny-Went theory (Went, 1928; Cholodny, 1927) accumulation of auxin in the root tip on the side closest to the direction of the gravity vector causes the root to bend downward, in the direction of the gravity vector (g). This auxin maximum guiding root growth depends on PAT and the IAA flow in the direction of a reverse fountain, whereat apically localized PIN2 transports IAA shootward through the epidermal cells. (B) Auxin fluxes and localization of PIN2, PIN3, and PIN7 (localization is redundant with that of PIN3) in the primary root tip after gravistimulation. High auxin concentration in the downward-facing side of the root inhibits PIN2 endocytosis which promotes its localization at the PM and reinforces asymmetric auxin localization. The resulting accumulation of auxin locally inhibits cell elongation, thus the root bends. Figure modified from Armengot *et al.*, 2016.

### 3.3.4 Regulation of PINs by means of the loop

The loop of the PINs is suggested to contain the molecular cues for PIN trafficking, stability and, subcellular polarity (Michniewicz *et al.*, 2007; Dhonukshe *et al.*, 2010; Huang *et al.*, 2010; Zhang *et al.*, 2010; Kleine-Vehn *et al.*, 2011; Barbosa and Schwechheimer, 2014; Barbosa *et al.*, 2018) At their loop, PINs undergo constant phosphorylation and dephosphorylation and

their phosphorylation status controls IAA transport activity as well as cellular localization, both time- and space-wise (Michniewicz *et al.*, 2007; Dai *et al.*, 2012; Zourelidou *et al.*, 2014; Weller *et al.*, 2017; Deruere *et al.*, 1999; Rashotte *et al.*, 2005; Shin *et al.*, 2005; Barbosa *et al.*, 2018). Phosphorylation of PINs is carried out by following kinases: (i)  $\text{Ca}^{2+}$ /calmodulin-dependent protein kinase-related kinases (CRKs) (Rigó *et al.*, 2013), (ii) MITOGEN- ACTIVATED PROTEIN (MAP) KINASES (MPKs) (Jia *et al.*, 2016), (iii) CAMEL (CANALIZATION-RELATED AUXIN-REGULATED MALECTIN-TYPE RLK) (Hajný *et al.*, 2020) and (iv) members of the plant-specific subfamily AGCVIII of the AGC kinase family (serine/threonine kinases with homology to mammalian protein kinase A, cGMP-dependent kinase, and protein kinase C) (Galván-Ampudia and Offringa, 2007). The role of the AGCVIII kinases in PIN regulation will be described in more detail in the next chapter. Additionally to the listed kinases, not yet identified kinases also phosphorylate the PIN loop (Barbosa *et al.*, 2018). Phosphorylation is antagonized by dephosphorylation by phosphatases and one player here is the protein phosphatase 2A (PP2A) (Michniewicz *et al.*, 2007; Dai *et al.*, 2012).

In 2014, Ganguly and colleagues performed an interesting experiment to examine the role of the loop (Ganguly *et al.*, 2014). As both non-canonical, short-looped PINs, PIN5 and PIN8, show predominant ER-localization, it was suggested, that they lack the molecular cues for PM trafficking. Thus, to test whether the loop of a PM-resident PIN can provide its original molecular cues to an ER-resident PIN, Ganguly and colleagues inserted the loop of PIN2 into PIN5 and examined the behavior of the resulting PIN5-2-5 chimaera. PIN5 fails to show any detectable phosphorylation *in planta*, the PIN5-2-5 chimaera, however, was found phosphorylated. Furthermore, the incorporation of the PIN2 loop caused the chimaera to be predominantly PM localized in cells where PIN5 showed an internal localization. Thus, it was reasoned that the canonical loop is partially modular for the trafficking behavior of PINs. PIN2's characteristic localization, which is basally in the cortex and apically in the epidermis, was not observed for the chimaera. It was concluded that the introduction of the loop enabled the phosphorylation of the chimaera, but that this phosphorylation is not sufficient for polar localization of the protein. The functionality and the IAA transport activity of the chimaera remained unclear.

### **3.4 AGCVIII kinases regulate PIN polarity and activity**

Members of the AGCVIII kinase family are crucial for the described regulation of PIN IAA transport activity and PIN localization. *Arabidopsis* possesses 23 AGCVIII kinases in total and based on an alignment of their catalytic kinase domains they can be subdivided into four major clades, AGC1 - AGC4 (Galván-Ampudia and Offringa, 2007) (**Fig. 3-5**). The loops of canonical PINs is auto-inhibitory; phosphorylation of the loop overcomes this inhibition and activates PIN

IAA transport activity (Zourelidou *et al.*, 2014). This is carried out by PINOID (PID) and its presumed functional paralogs WAG1 and WAG2 from subclade AGC3 as well as D6 PROTEIN KINASE (D6PK) and the three candidate paralogs D6PK-LIKE (D6PKL) 1–3 from subclade AGC1 (Willige *et al.*, 2013; Weller *et al.*, 2017; Zourelidou *et al.*, 2014). Notably, experiments in the heterologous expression system of *X. laevis* show, that PID activates PIN-mediated IAA transport more efficiently, despite equal levels of both proteins and phosphorylation (Zourelidou *et al.* 2014, Dorina P. Janacek, personal communication). Further, PID and D6PK cannot functionally replace each other (Zourelidou *et al.* 2014). If the canonical loop, the activating kinase, or a combination of both contribute to IAA transport is yet unanswered. Representatives from AGC2 (UCN) and AGC4 (PHOT1) neither phosphorylate PINs nor activate PIN-mediated IAA efflux (Zourelidou *et al.* 2014), thus it is suggested that activation of PINs is restricted to clade AGC1 and AGC3. Not yet identified kinases are likely to also activate PINs, and consequently members of the AGC1 and AGC3 clade make interesting candidates to be tested. Further, it remains to be shown if PIN phosphorylation leads to PIN IAA transport i.e. if phosphorylation is sufficient to explain activation.

AGC2	At1g51170	UNC
	At3g20830	UNC-L
	At3g25250	OXI1
	At4g13000	AGC2.2
AGC4	At3g45780	PHOT1
	At5g58140	PHOT2
AGC3	At2g34650	PINOID
	At2g26700	AGC3.4
	At3g14370	WAG2
	At1g53700	WAG1
AGC1	At3g44610	AGC1.12
	At5g03640	AGC1.8
	At2g36350	AGC1.9
	At3g52890	KIPK
	At3g12690	AGC1.5
	At1g16440	AGC1.6
	At1g79250	AGC1.7
	At3g27580	D6PKL3
	At5g47750	D6PKL2
	At4g26610	D6PKL1
	At5g55910	D6PK
	At5g40030	AGC1.4 (PAXL)
	At2g44830	AGC1.3 (PAX)

**Fig. 3-5 The Arabidopsis AGCVIII protein kinase family, a plant-specific subfamily of the AGC kinase family.** Based on an alignment of their catalytic kinase domains, the 23 members in *Arabidopsis* can be divided into four distinct groups, AGC1 – AGC4. PINOID (PID, orange arrow) and its presumed functional paralogs WAG1 and WAG2 from subclade AGC3 (PID/WAG), as well as D6 PROTEIN KINASE (D6PK, orange arrow) and the three candidate paralogs D6PK-LIKE (D6PKL) 1–3 from subclade AGC1, directly phosphorylate PINs. Figure modified from Galván-Ampudia and Offringa, 2007.

The localization of PINs is regulated by phosphorylation carried out by PID/WAGs. For years it was assumed that this phosphorylation directly initiates PIN localization at the apical PM (Friml *et al.*, 2004; Michniewicz *et al.*, 2007; Huang *et al.*, 2010). Although it is clear now that the correlation is not as simple and other players must be involved (Weller *et al.*, 2017), correct (re)localization of PM-resident PINs critically depends on PID/WAG activity.

At least five serine residues within the canonical loop (S1 – S5) are critical target for PIN phosphorylation and activation by D6PK and PID (Zourelidou *et al.*, 2014) (**Fig. 3-6**). S1-S3 are embedded in a highly conserved TPRXS(N/S) motif and are present in all canonical PINs. S4 and S5, on the contrary, vary both in context and presence (Zourelidou *et al.*, 2014; Barbosa *et al.*, 2018). Even though D6PK and PID phosphorylate the same phosphosites, mutations of specific serines have different effects on the ability of each kinase to activate PINs *in vitro* and in oocyte-based auxin transport assays, which suggests a different mode of PIN binding (Haga *et al.*, 2018; Zourelidou *et al.*, 2014).

D6PKs are broadly expressed and interestingly, D6PK predominantly localizes at the basal PM where it overlaps with basally localized PINs (Barbosa and Schwechheimer, 2014; Zourelidou *et al.*, 2009). PID on the contrary is apolarly distributed at the plasma membrane (Kleine-Vehn *et al.*, 2010b; Dhonukshe *et al.*, 2010; Weller, 2017). This localization pattern indicates that PIN phosphorylation at the basal PM is maintained by D6PK, whereas PID or other non-polar kinases maintain phosphorylation at other PM regions (Barbosa *et al.*, 2018). Similar to the PINs, D6PK is sensitive to BFA and constantly recycles to and from the PM, albeit in comparison to PINs, D6PK recycling is faster (Barbosa *et al.*, 2014; Kleine-Vehn *et al.*, 2010b). On the contrary, PID is BFA-insensitive (Kleine-Vehn *et al.*, 2010b).

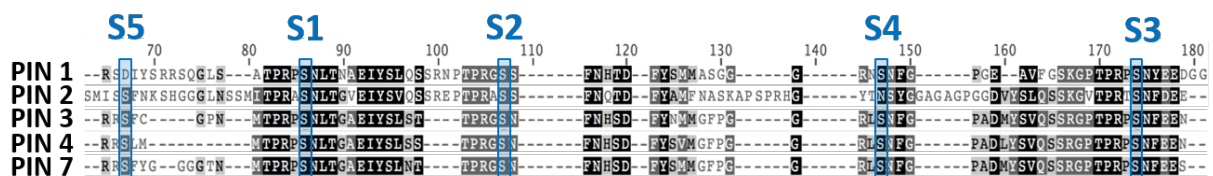


**Fig. 3-6 Alignment of parts of the hydrophilic loop of the canonical PINs.** Serines S1 – S5 are critical phosphorylation targets of D6PK and PID/WAG in the activation and polarity control of canonical PINs. Figure modified from Zourelidou *et al.*, 2014.

## **3.5 Aims of this thesis**

### **3.5.1 Examination of potential modifiers and inhibitors of PIN-mediated IAA transport, in particular, NPA**

One aim of the present thesis was to test selected substances for their potential to modulate PIN-mediated IAA transport and to investigate the sensitivity of PINs to inhibitors of PAT. To do so, I used the heterologous expression system of *X. laevis* oocytes, a well-established system to investigate transport activity by membrane proteins, which is suitable for investigating IAA transport by PIN proteins (Fastner *et al.*, 2017). In oocytes expressing PINs, I examined if the substances affected PIN IAA transport activity and IAA transport rates of PINs. I tested eleven different substances by co-injecting them together with IAA: Two synthetic auxins [2,4-dichlorophenoxyacetic acid (2,4-D) (Peterson, 1967), and 1-Naphthaleneacetic acid (NAA)], Indole-3-butyric acid (IBA), which is another naturally occurring auxin (Ludwig-Müller and Epstein, 1991), the IAA conjugate methylated IAA (Me-IAA), the main IAA precursor tryptophan (Woodward and Bartel, 2005), three inhibitors of (polar) auxin transport [N-1-naphthylphthalamic acid (NPA) (Hoffmann and Smith, 1949), 2,3,5-triiodobenzoic acid (TIBA) (Galston, 1947; Thomson *et al.*, 1973) and quercetin (Jacobs and Rubery, 1988)], trans-Zeatin, which is the most abundant cytokinin, fluorescing IAA (NBD-IAA, Hayashi *et al.*, 2014) and serotonin, which's structure resembles IAA and has been proposed to inhibit auxin activity and transport (Erland *et al.*, 2015; Pelagio-Flores *et al.*, 2011). NPA's inhibitory effect on PAT was investigated in more detail. In the oocyte system, I tested if PINs can transport NPA and if NPA has an inhibitory effect on other PM-localized transporters, namely IAA importer *AtAUX1* (Yang *et al.*, 2006) and Leucine transporter *AtCAT6* (Hammes *et al.*, 2006). In *in vitro* phosphorylation assays, I tested NPA's potential to impair PIN phosphorylation.

### **3.5.2 Characterization of semi-canonical PIN6 and non-canonical PIN8**

Another aim was to investigate the IAA-efflux capability and characteristics of semi-canonical PIN6 and non-canonical PIN8 because to date, their IAA transport ability has only been deduced from experiments based on passive pre-loading, partly not bare of other plant factors (Ding *et al.*, 2012; Petrášek *et al.*, 2006; Simon *et al.*, 2016; Ganguly *et al.*, 2010). Further, regarding PIN8, I could build up on preliminary data of my Master's Thesis, indicating IAA transport by PIN8 (Kolb, 2015). I tested both PIN6 and PIN8 in *X. laevis* oocytes to characterize their IAA transport activity.

Additionally, I aimed to investigate if PIN6 can contribute to gravitropic response, as it has been shown to be involved in root development and formation of correct root morphology (Cazzonelli *et al.* 2013; Simon *et al.* 2016). To this end, I tested the potential of PIN6 to

complement the agravitropic *pin2* mutant when expressed under the control of the *PIN2* promotor.

### **3.5.3 Investigation of the role of the PIN loop in regulating IAA transport activity and localization of PINs**

As a continuation of initial insights from my Master's thesis (Kolb, 2015), I performed structure-function analyses. I asked the question if a non-canonical PIN can be turned into a canonical PIN and by providing non-canonical PIN8 with the loop of PIN2 (PIN8-2-8) and PIN3 (PIN8-3-8), respectively, I aimed to gain insights into how the loop of canonical PINs contributes to regulation of IAA transport activity, to IAA transport *per se* and to localization of the PINs.

In the oocyte system, I examined the IAA transport properties of the two chimaeras and of GFP-fused versions of them. Additionally, I examined the chimaeras *in planta*: First, I tested the potential of both chimaeras to complement the agravitropic *pin2* mutant when expressed under the control of the *PIN2* promotor. Second, I investigated the IAA response of these lines, by crossing them with the IAA reporter construct *P<sub>DR5</sub>:GUS* (Ulmasov *et al.*, 1997). Third, I performed CLSM analyses to investigate the localization of PIN8-2-8-GFP in *pin2*.

### **3.5.4 Examination of the potential of other AGCVIII kinases to activate PINs and identification of additional players in PAT**

From the AGC1 subclade of the AGCVIII kinase family, only D6PK and its three homologs are known to activate PIN auxin transport (Zourelidou *et al.*, 2014), however, additional kinases have been suggested to be involved in regulation and activation of PINs by phosphorylation (Barbosa *et al.*, 2018). To expand the knowledge of kinase-mediated activation of the PIN family, I tested the potential of further kinases from the AGC1 subfamily to do so. Therefore, I tested AGC1-3, AGC1-4, AGC1-7, AGC1-8, AGC1-9, and KIPK in the oocyte system for their potential to activate PIN-mediated IAA transport.

Lastly, in light of the finding that BREVIS RADIX (BRX), a plasma-membrane-associated protein specifically expressed in developing PPSE interacts with AGC1-3 (Christian Hardtke, pers. comm.), I investigated the influence of BRX and its homolog BRXL2 on AGC1 kinase-mediated activation of PINs in the oocyte system.



## 4. Results

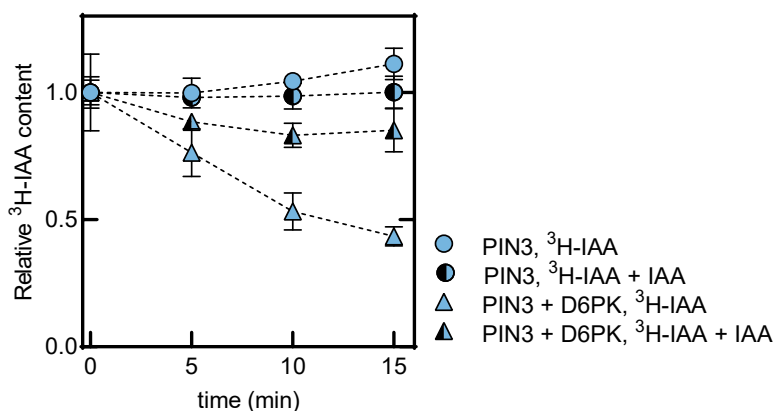
Most of the data I present in this thesis was published. These publications - one shared first authorship and five co-authorships - are listed in **Table 4-1** (see also **12. Appendix**). The data and results that have been published, along with my contributions to these respective publications, will be described and discussed in the following chapters of this thesis.

**Table 4-1 List of the publications presenting data generated within the frame of the present thesis and personal contribution**

<b>Publication</b>	<b>Contribution</b>
Ung, K.L., Winkler, M., Schulz, L., <b>Kolb, M.</b> , Janacek, D.P., Dedic, E., Stokes, D.L., Hammes, U.Z., and Pedersen, B.P. (2022). Structures and mechanism of the plant PIN-FORMED auxin transporter. <b>Nature</b> 609: 605–610.	<b>Co-authorship</b> , Fig. 1a, Extended Data Fig. 2B
Koh, S.W.H., Marhava, P., Rana, S., Graf, A., Moret, B., Bassukas, A.E.L., Zourelidou, M., <b>Kolb, M.</b> , Hammes, U.Z., Schwechheimer, C., and Hardtke, C.S. (2021). Mapping and engineering of auxin-induced plasma membrane dissociation in BRX family proteins. <b>Plant Cell</b> 33: 1945–1960.	<b>Co-authorship</b> , Supplemental Fig S8B
Abas, L., <b>Kolb, M.</b> , Stadlmann, J., Janacek, D.P., Lukic, K., Schwechheimer, C., Sazanov, L.A., Mach, L., Friml, J., and Hammes, U.Z. (2021). Naphthylphthalamic acid associates with and inhibits PIN auxin transporters. <b>Proc. Natl. Acad. Sci.</b> 118: 1–8.	<b>Shared first authorship</b> , Fig. 1A-D, SI Fig. S1A-E
Marhava, P., Aliaga Fandino, A.C., Koh, S.W.H., Jelínková, A., <b>Kolb, M.</b> , Janacek, D.P., Breda, A.S., Cattaneo, P., Hammes, U.Z., Petrášek, J., and Hardtke, C.S. (2020). Plasma Membrane Domain Patterning and Self-Reinforcing Polarity in Arabidopsis. <b>Dev. Cell</b> 52: 223-235.e5.	<b>Co-authorship</b> , Fig. 6I
Marhava, P., Bassukas, A.E.L., Zourelidou, M., <b>Kolb, M.</b> , Moret, B., Fastner, A., Schulze, W.X., Cattaneo, P., Hammes, U.Z., Schwechheimer, C., and Hardtke, C.S. (2018). A molecular rheostat adjusts auxin flux to promote root protophloem differentiation. <b>Nature</b> 558: 1.	<b>Co-authorship</b> , Fig. 2d, 4a-d, and h. Extended Data Fig. 4h, 5j, and 6f
Abbas, M., Hernández-García, J., Pollmann, S., Samodelov, S.L., <b>Kolb, M.</b> , Friml, J., Hammes, U.Z., Zurbriggen, M.D., Blázquez, M.A., and Alabadí, D. (2018). Auxin methylation is required for differential growth in Arabidopsis. <b>Proc. Natl. Acad. Sci.</b> 115: 6864–6869.	<b>Co-authorship</b> , SI Fig. S8

I generated large parts of my data with the use of the heterologous expression system of *X. laevis* oocytes. For this reason, I want to give a detailed introduction to the system.

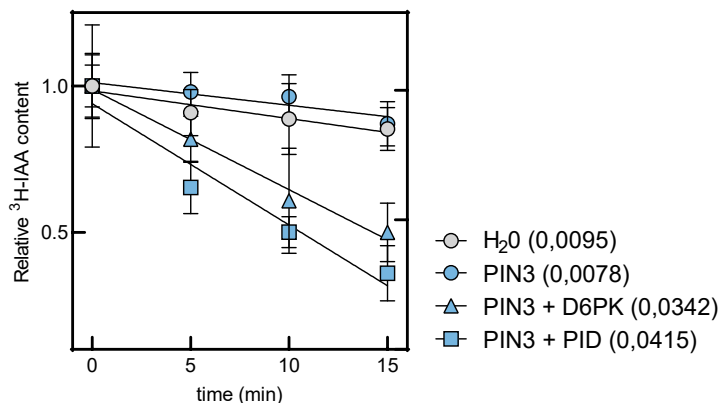
*X. laevis* oocytes are a well-established expression system to investigate transport activity by membrane proteins and suitable for investigating IAA transport by PIN proteins (Fastner *et al.*, 2017; Zourelidou *et al.*, 2014). In the first step, cRNA encoding for PINs (+ activating kinases), is injected into oocytes, leading to protein expression in the oocytes. In the next step,  $^3\text{H}$ -labeled IAA is injected into the oocytes ( $1\mu\text{M}$  internal concentration), and the depletion of the substrate is measured over time by liquid scintillation counting. For this purpose, six to ten oocytes are sampled at different time points post injection and their remaining  $^3\text{H}$ -IAA content is measured by scintillation count. Oocytes expressing canonical PINs alone show very little IAA depletion over time. This does, however, not differ significantly from water-injected control oocytes. If on the contrary, a canonical PIN is co-expressed together with an activating kinase, in most instances in this thesis D6PK or PID, the PIN becomes phosphorylated, the auto-inhibitory effect of the loop is overcome i.e. the PIN is activated by the kinase and finally, it transports IAA out of the oocyte (Zourelidou *et al.* 2014). Transport rates of individual PINs can be determined from the negative value of the slope of the obtained time courses (Absmanner, 2013). A representative experiment for PIN3 and PIN3 co-expressed with D6PK or PID including the corresponding linear regression and the calculated transport rates is shown in **Fig. 4-1**. Both kinases activate PIN-mediated IAA efflux, whereat the trend that PID stimulates the efflux considerably, has been observed before (Absmanner, 2013; Zourelidou *et al.*, 2014). Transport rates from individual biological replicates provided the basis for investigating PIN-mediated IAA transport in this thesis.



**Fig. 4-1** Data of typical experiment of PIN-mediated IAA transport in *X. laevis* oocytes and determination of relative IAA transport rates (Fastner *et al.*, 2017). Reduction of  $^3\text{H}$ -IAA content in oocytes over time after direct injection of the substrate. Counts per minute at time point 0 min were set to 1. Data points show measurements of one biological replicate for oocytes expressing PIN3 ( $r^2=0,8366$ ), PIN3 + D6PK ( $r^2=0,985$ ), and PIN3 + PID ( $r^2=0,9459$ ), respectively, and water-injected control oocytes ( $r^2=0,9023$ ). PIN3 co-expressed with D6PK or PID gets activated by the kinase and transports IAA out of the oocytes. The linear regression graphs serve as a basis for the calculation of transport rates and hence relative IAA efflux (in brackets). Error bars show SEM of technical replicates ( $n=8-10$ ).

#### 4.1 PIN-mediated IAA transport in *X. laevis* oocytes can be modified by co-injected substances

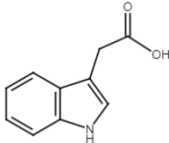
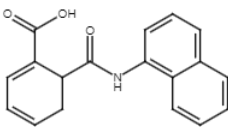
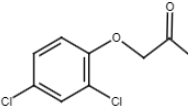
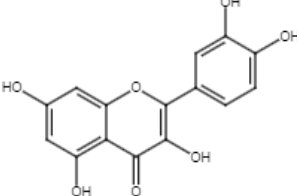
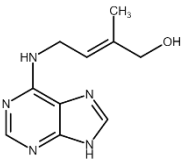
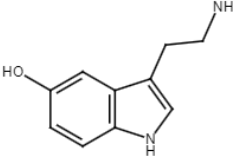
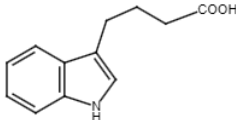
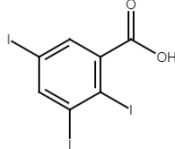
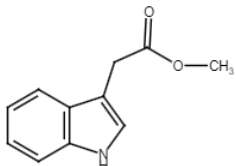
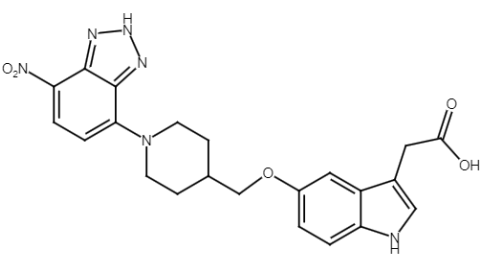
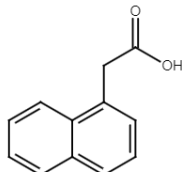
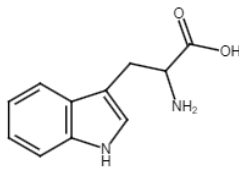
One aim of the present thesis was to investigate the effect of selected substances on PIN-mediated IAA transport and the sensitivity of PINs to inhibitors of PAT. To this end, I co-injected the substances of interest together with  $^3\text{H}$ -IAA into oocytes expressing PINs, with the substance of interest present in 100-fold excess compared to  $^3\text{H}$ -IAA (100  $\mu\text{M}$  and 1  $\mu\text{M}$ , respectively). I then monitored if the PIN-mediated  $^3\text{H}$ -IAA transport was affected by the other substance present. I expected to measure altered  $^3\text{H}$ -IAA transport rates, in case a substance interfered with PIN-mediated transport in the oocytes. Oocytes co-injected with unlabeled IAA together with  $^3\text{H}$ -IAA were used as control. Here, labeled and unlabeled IAA compete for transport. Thus, transport of the measurable fraction of IAA decreases, exemplified shown for PIN3 activated by D6PK in **Fig. 4-2**.



**Fig. 4-2 Effect of unlabeled IAA on the transport of  $^3\text{H}$ -labeled IAA.** Data of a typical experiment performed as control for results in **Fig. 4-3**. Reduction of  $^3\text{H}$ -IAA content over time in oocytes expressing PIN3 (+ D6PK) as specified. Counts per minute at time point 0 min were set to 1. PIN3 transports IAA only when co-expressed with D6PK. Co-injected unlabeled IAA competes with labeled IAA for transport and consequently,  $^3\text{H}$ -IAA content over time only slightly decreases. Data points represent arithmetic mean and standard error from n=6-10 oocytes. The dotted lines support the better visualization of the course of labeled IAA content and do not represent linear regression graphs.

I tested the following eleven selected substances: IBA, which is another naturally occurring auxin (Ludwig-Müller and Epstein, 1991), 2,4-D and NAA, which are synthetic auxins (Peterson, 1967), IAA conjugate Me-IAA, NBD-IAA, which is a synthetic, fluorescing IAA (Hayashi *et al.*, 2014), trans-Zeatin, which is the major cytokinin in *Arabidopsis* (Sakakibara, 2006) and has been shown to be involved in the regulation of PIN expression and PM localization (Osugi and Sakakibara, 2015), serotonin, which's chemical structure resembles IAA, tryptophan, which is the main precursor of IAA (Woodward and Bartel, 2005) and three inhibitors of (polar) auxin transport, namely TIBA (Galston, 1947), NPA (Hoffmann and Smith, 1949), and quercetin (Jacobs and Rubery, 1988). An overview of the substances and their chemical structure is displayed in **Table 4-2**.

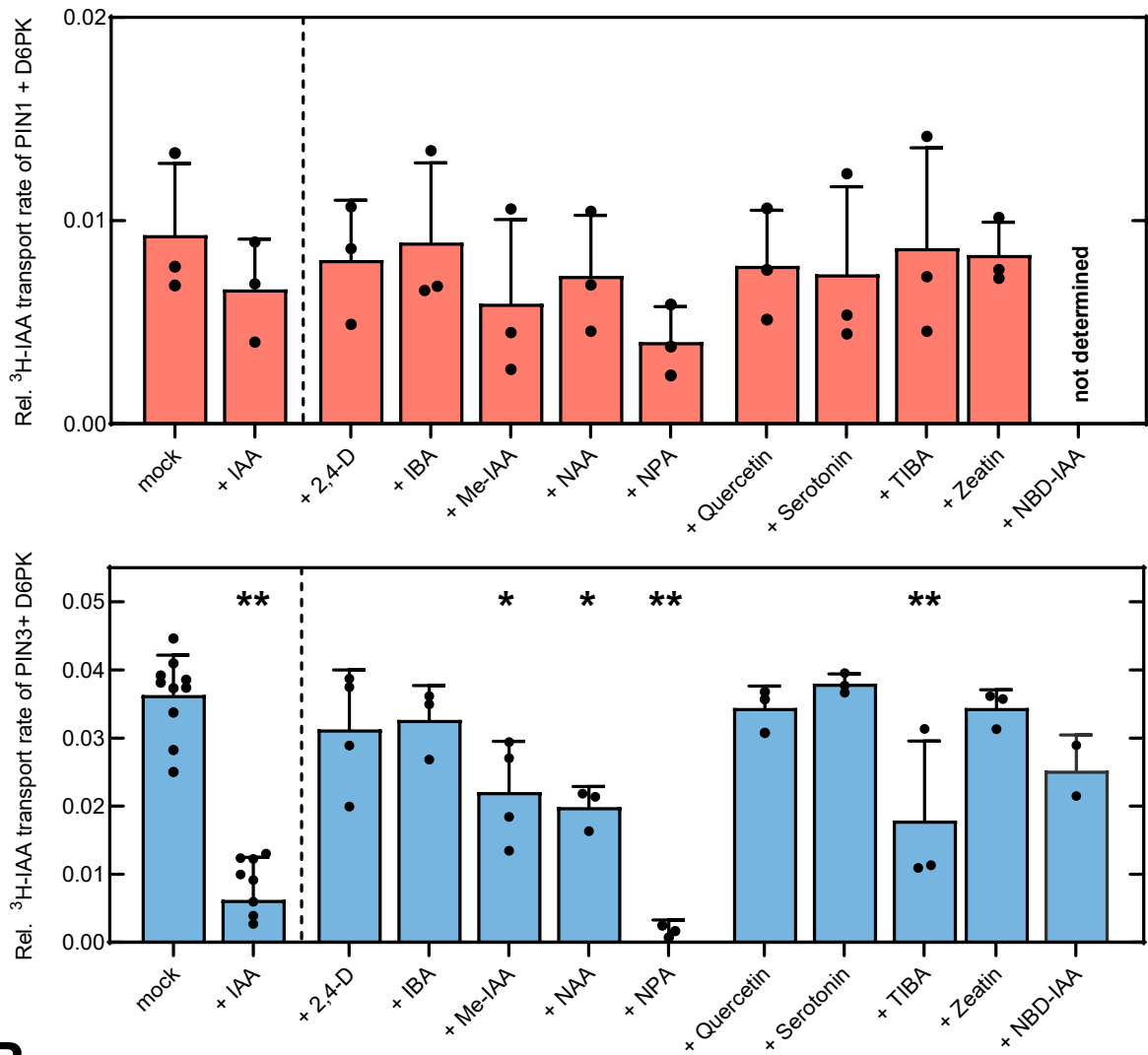
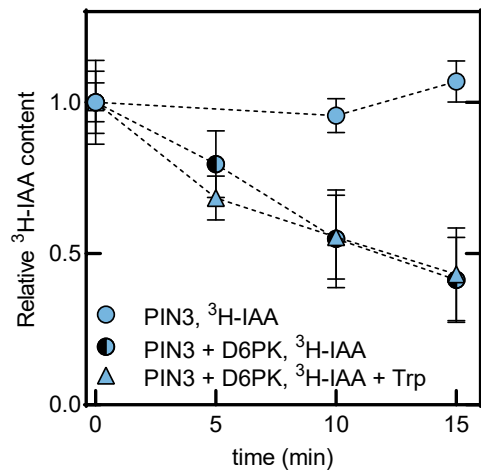
**Table 4-2 Name and chemical structure of the substances tested for their effect on PIN-mediated IAA transport in *X. laevis* oocytes**

Name	Chemical structure	Name	Chemical structure
<b>IAA</b>		<b>NPA</b>	
<b>2,4-D</b>		<b>Quercetin</b>	
<b>Trans-Zeatin</b>		<b>Serotonin</b>	
<b>IBA</b>		<b>TIBA</b>	
<b>Me-IAA</b>		<b>NBD-IAA</b> (Hayashi <i>et al.</i> , 2014)	
<b>NAA</b>		<b>Tryptophan</b>	

I quantified the depletion of  $^3\text{H}$ -IAA over time, calculated the transport rates of the expressed PINs from individual biological replicates, and compared, how the transport rates changed in presence of the additional substance. To obtain more representative data and a better insight, I performed the experiments with PIN1 and PIN3, which differ remarkably in their transport characteristics in the oocyte system: PIN1 shows weak transport activity, PIN3, on the contrary, is a stronger IAA transporter (Zourelidou *et al.*, 2014).

I found that the presence of **trans-Zeatin**, **IBA**, **quercetin**, **serotonin**, and **NBD-IAA** did not significantly change transport rates of neither PIN1 (**Fig. 4-3 A**, upper panel) nor PIN3 (**Fig.**

**4-3 A**, lower panel) (NBD-IAA was only tested with PIN3), suggesting that – in the given scenario - the substances have no effect on PIN1- and PIN3-mediated transport and do not compete with IAA, thus are no PIN substrate or transport modulator. Importantly, the measured counts per minute (cpm) of oocytes injected with  $^3\text{H}$ -IAA + quercetin were many times lower than the cpm of the control oocytes or those measured for any of the other experiments (data not shown). In the case of **2,4-D**, the PIN transport rates did not change significantly, I did however, note a high variability in the transport rates of the individual experiments and the trend that the presence of 2,4-D decreased the transport rates. Co-injection of **Me-IAA** decreased PIN-mediated IAA transport strongly, in the case of PIN3 significantly ( $p < 0.05$ ), suggesting that this was due to a competition of Me-IAA with  $^3\text{H}$ -IAA. These findings are my contribution to a paper dealing with the importance of auxin conjugation (Abbas *et al.* 2018). Co-injection of **NPA** greatly decreased PIN1-mediated IAA efflux, in the case of PIN3 highly significant ( $p < 0.001$ ), close to no transport at all. These findings were considered highly interesting and were investigated in more detail (**4.2**). The findings for **NAA** differed between PIN1 and PIN3 in that in the case of PIN1, NAA had no visible effect, while in the case of PIN3,  $^3\text{H}$ -IAA transport was significantly decreased. The same is true for the IAA transport inhibitor **TIBA**: PIN1-mediated IAA transport was not affected by the presence of TIBA, on the contrary, the  $^3\text{H}$ -IAA transport by PIN3 decreased highly significant ( $p < 0.001$ ). Here, it is noteworthy, that the results of PIN1 and PIN3 cannot necessarily be compared directly. This is because they show differential transport activity in the oocyte system and consequently, the signal-to-noise ratio (“transport to background”) differs. Lastly, I tested if co-injected **tryptophan** affects PIN-mediated IAA transport. In a preliminary experiment, I saw that the presence of tryptophan had no influence on PIN3-mediated IAA transport (**Fig. 4-3 B**) suggesting that in the given scenario tryptophan does not compete with IAA.

**A****B**

**Fig. 4-3 The effect of various substances on PIN-mediated IAA transport in *X. laevis* oocytes.** The substances (100  $\mu$ M) were co-injected together with <sup>3</sup>H-IAA (1  $\mu$ M) as specified, for mock control only <sup>3</sup>H-IAA was injected. **(A)** Bars represent blotted relative <sup>3</sup>H-IAA transport rates of PIN1 (upper panel) and PIN3 (lower panel) activated by D6PK. Black dots represent transport rates from individual experiments, error bars show SEM. Modification of <sup>3</sup>H-IAA transport was observed for Me-IAA, NPA, NAA (PIN3-mediated transport only), and TIBA (PIN3-mediated transport only). Statistical analysis was performed by means of a one-way ANOVA vs. mock control followed by Holm-Sidak post hoc test, asterisks indicate statistical significance (\*=  $p < 0.05$ , \*\*=  $p < 0.001$ ). **(B)** Reduction of <sup>3</sup>H-IAA content over time with or without co-injected tryptophan (Trp) in oocytes expressing PIN3 and D6PK as specified. Counts per minute at time point 0 min were set to 1. PIN3-mediated <sup>3</sup>H-IAA transport is not affected by Trp. Data points represent mean and standard error from  $n = 6-10$  oocytes. The dotted lines support the better visualization of the course of <sup>3</sup>H-IAA content and do not represent linear regression graphs.

## 4.2 Naphthylphthalamic acid inhibits PIN auxin transporters

Our current understanding of how auxin moves and is transported within the plant is largely built on experiments in which this process is inhibited. In this context, the synthetic PAT inhibitor NPA has been used extensively in research and contributed highly to our current knowledge of the molecular mechanisms of PAT. Hitherto, however, NPA's exact mode of action and its target, has been a matter of debate for years (Teale and Palme, 2018). Thus, the finding that NPA inhibits <sup>3</sup>H-IAA transport rates of PIN1 and abolishes <sup>3</sup>H-IAA transport rates of PIN3 when co-injected into oocytes expressing the respective PIN was very interesting and I decided to investigate this in more detail.

I published all results described in this chapter as a co-first author in Abas *et al.*, 2020 and NPA was used as a tool to inhibit PIN transport activity in further experiments investigating PIN6 (4.5) and PIN8 (4.3) as will be described in detail in the respective chapters.

### 4.2.1 NPA inhibits PIN-mediated IAA transport in the oocyte system

To investigate NPA's effect on PIN-mediated IAA transport in more detail, I performed further IAA efflux assays in the oocyte system as described in the former chapter. Due to the higher signal-to-noise ratio and therefore, the clearest readout, the experiments were performed with PIN3.

The transport rates of activated PIN3 treated with 100  $\mu$ M internal NPA are found in the same group as the negative control, non-activated PIN3 (without co-expressed kinase) (**Fig. 4-4 A**). In any case, the internal concentration of 100  $\mu$ M NPA in the oocyte abolished PIN3 transport activity. This effect was independent of the identity of the activating kinase - D6PK or PID - suggesting that the kinase is no target of NPA. Further, I tested a lower internal concentration of NPA (10  $\mu$ M) (**Fig. 4-4 B**). I found that 10  $\mu$ M NPA significantly decreased PIN3-mediated transport. This inhibition of transport, however, was significantly less compared to 100  $\mu$ M NPA internal. Taken together the data indicate that NPA in the oocyte system inhibits PIN-mediated IAA efflux and that the activating kinase is not a crucial factor in the interplay underlying the inhibition.

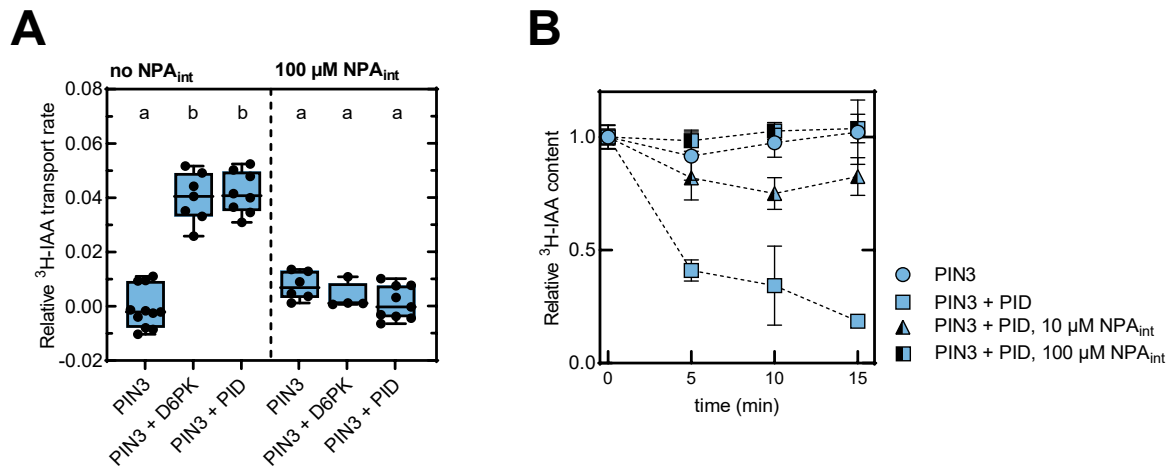


**Fig. 4-4 Concentration effect of NPA on PIN3-mediated IAA transport in the oocyte system.** IAA efflux assay was performed with oocytes expressing PIN3 alone or PIN3 together with either D6PK or PID as activating kinase as specified. Oocytes were injected with only <sup>3</sup>H-IAA or <sup>3</sup>H-IAA + NPA as specified. **(A)** Transport rates of PIN3 from individual biological replicates were calculated and blotted, with one black dot representing the transport rate of one biological replicate, error bars show SEM. Internal application of 100 μM NPA reduces the level of both PIN3 + D6PK and PIN3 + PID <sup>3</sup>H-IAA transport to the level of PIN3 alone (negative control). Different letters indicate significant differences. Statistical analysis was performed by means of a one-way ANOVA followed by Holm-Sidak post hoc test ( $p < 0.050$ ). **(B)** Reduction of <sup>3</sup>H-IAA content over time in oocytes expressing PIN3 or PIN3 + PID. The reduction of the relative <sup>3</sup>H-IAA content over time is significantly weaker in oocytes co-injected with 10 μM NPA ( $p < 0.001$ , student's t-test at time point five, ten, and 15 minutes). Data points represent mean and standard error from  $n = 6-10$  oocytes. The dotted lines support the better visualization of the course of labeled IAA content and do not represent linear regression graphs.

Next, I wanted to investigate if the reduction of PIN-mediated IAA transport rates upon internal NPA application could be explained by competition of NPA with <sup>3</sup>H-IAA for PIN-mediated transport. Thus, I tested if NPA is transported by PINs. To do so, I injected <sup>3</sup>H-NPA (1 μM internal concentration) into oocytes expressing PIN1 (+ D6PK), PIN3 (+ D6PK) or PIN3 (+ PID), respectively, and measured if they released <sup>3</sup>H-NPA over time. The content of <sup>3</sup>H-NPA in the oocytes at the end of the experiment was not lower than at the beginning of the experiment (**Fig. 4-5 A, B, and C**). Also, co-injection of IAA did not lead to a decrease of <sup>3</sup>H-NPA content over time (**Fig. 4-5 A and B**). In summary, as neither oocytes expressing PIN1 + D6PK, nor oocytes expressing PIN3 + D6PK or PIN3 + PID showed a depletion of injected <sup>3</sup>H-NPA over time, I concluded that NPA is not transported by PIN1 or PIN3.



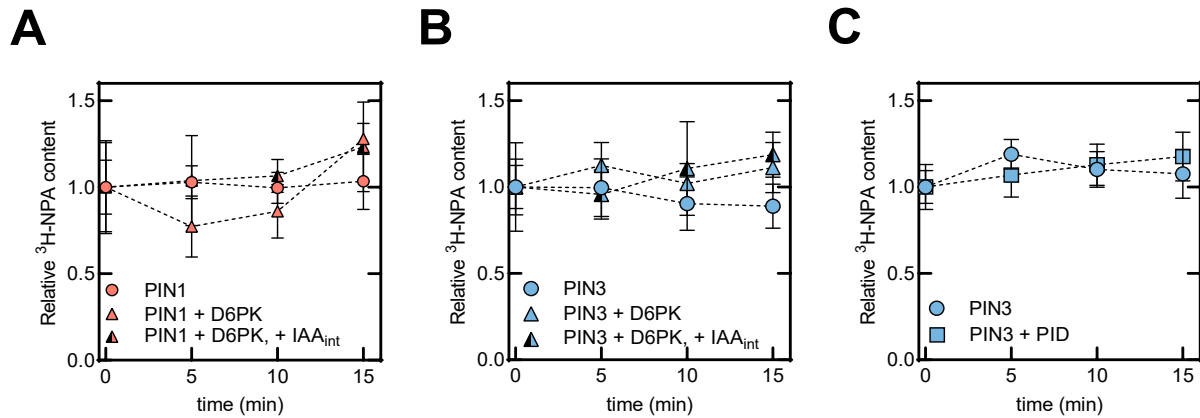


**Fig. 4-5 NPA is not transported by PINs.** Reduction of  $^3\text{H}$ -NPA content over time in oocytes expressing PIN and activating kinase as specified. Oocytes were injected with  $^3\text{H}$ -NPA or  $^3\text{H}$ -NPA and IAA as specified. Counts per minute at time point 0 min were set to 1.  $^3\text{H}$ -NPA is not exported from oocytes expressing (A) PIN1 (+ D6PK), (B) PIN3 (+ D6PK) or (C) PIN3 (+ PID). Data points represent mean and standard error from n=6-10 oocytes. The dotted lines support the better visualization of the course of labeled NPA content and do not represent linear regression graphs.

Upon the observation that NPA inside the oocyte inhibits PIN-mediated IAA transport, I wanted to investigate NPA applied externally. Therefore, I incubated oocytes expressing PIN3 (+ D6PK) in buffer containing  $10\mu\text{M}$  NPA prior to the IAA efflux assay. I tested this at the usual of pH 7.5 (Fastner *et al.*, 2017) and at pH 5.5 which is closer to the physiological situation, and incubated the oocytes either ten minutes or 150 minutes prior to the IAA efflux assay. Oocytes in buffer without NPA were used as controls.

At pH7.5, an incubation time of 10 minutes in the buffer containing NPA did not inhibit PIN3-mediated  $^3\text{H}$ -IAA export (Fig. 4-6 left panel). After a 150 minutes incubation time, however, the  $^3\text{H}$ -IAA transport was significantly reduced, thus a partial inhibition was observed. At pH 5.5, NPA applied for ten minutes decreased PIN3-mediated  $^3\text{H}$ -IAA transport significantly (Fig. 4-6 right panel) and in comparison to the higher pH, this inhibition of  $^3\text{H}$ -IAA transport was remarkably more pronounced. The prolongation of the incubation time to 150 minutes did not lead to a more efficient inhibition. In comparison, co-injection of  $10\mu\text{M}$  NPA caused full inhibition of  $^3\text{H}$ -IAA transport at both pH values (Fig. 4-6 left and right panel). In summary, the results suggest that NPA is able to diffuse into the oocytes in a pH- and time-dependent fashion where it intracellularly inhibits PIN-mediated transport. Furthermore, the pH dependence of the inhibition suggests that NPA, a weak organic acid, diffuses in its protonated, uncharged form.

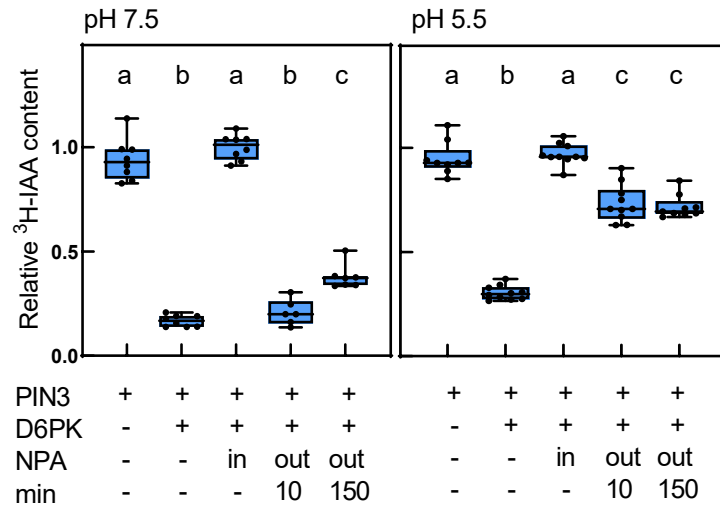


**Fig. 4-6 NPA applied from outside only partly inhibits IAA transport.** Oocytes expressing PIN3 (+ D6PK) as specified were injected with <sup>3</sup>H-IAA. Oocytes were incubated in BARTH's with or without 10 μM NPA (for ten or 150 minutes, as specified) and the <sup>3</sup>H-IAA content of the oocytes at the end of the experiment was measured. <sup>3</sup>H-IAA content at the beginning of the experiment was set to 1. The pH of the incubation buffer was adjusted to 7.5 (**left panel**) or 5.5 (**right panel**). At pH 7.5, PIN3 still transports IAA when oocytes are incubated for ten minutes but is partially inhibited after 150 minutes of incubation time. At pH 5.5 the partial inhibition of PIN3 is more pronounced and equally strong after ten or 150 minutes of incubation. At both pH values, co-injection of NPA causes full inhibition of <sup>3</sup>H-IAA transport. Data points represent mean and standard error from n = 6 - 10 oocytes. (ANOVA; p < 0.0001 for all subsets).

#### 4.2.2 NPA does not impair PIN phosphorylation

PIN1 and PIN3 transport activity critically depends on phosphorylation of their loop (Zourelidou *et al.*, 2014). Thus, I wanted to examine if the observed inhibition of PIN-mediated IAA transport was due to NPA affecting kinase activity. In *in vitro* phosphorylation assays using <sup>32</sup>P-ATP, it has been shown that GST-D6PK autophosphorylates itself and transphosphorylates the GST-tagged loop of PIN1 and PIN3 (Zourelidou *et al.*, 2014, 2009). To examine if NPA affects D6PK-mediated phosphorylation, I performed this assay in the presence and absence of NPA.

I found that at a concentration of 100 μM NPA in the reaction buffer, GST-D6PK autophosphorylates itself and transphosphorylates GST-tagged PIN1 loop (**Fig. 4-7 A**) as well as GST-tagged PIN3 loop (**Fig. 4-7 B**). Thus, I concluded that NPA does not cause any changes in the D6PK phosphorylation pattern and that NPA does not inhibit phosphorylation of PINs.

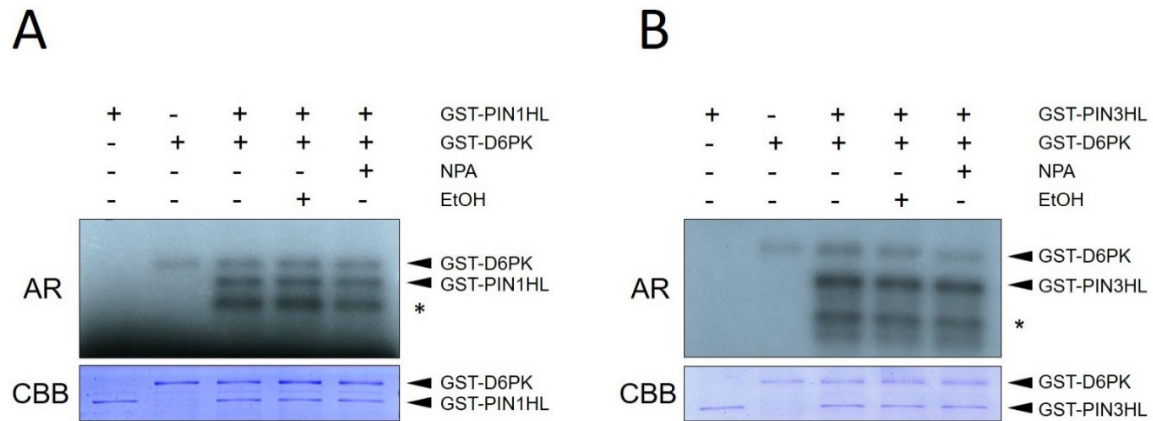


**Fig. 4-7 NPA does not inhibit *in vitro* D6PK autophosphorylation or trans-phosphorylation of PIN1 or PIN3 hydrophilic loop (HL).** *In vitro* phosphorylation assay performed with recombinant purified GST-D6PK and GST-PIN1HL (**A**) or GST-PIN3HL (**B**) in the presence of radiolabeled  $^{32}\text{P}$ -ATP. NPA was applied in a concentration of 100  $\mu\text{M}$  (in Ethanol (EtOH)). The phosphorylation pattern of GST-D6PK auto-phosphorylation and trans-phosphorylation of PIN1HL (**A**) and PIN3HL (**B**) did not change in the presence of NPA. EtOH only was used as solvent control. Asterisks mark PIN degradation products as described before (Zourelidou *et al.*, 2014). AR, autoradiogram; CBB, Coomassie Brilliant Blue.

### 4.2.3 NPA is not a general transport inhibitor

To investigate the effect of NPA on other PM-localized transporters and to see, if NPA generally compromises (IAA) transport activity, I tested if NPA influences the transport activity of *AtAUX1*, an IAA importer (Yang *et al.*, 2006) and *AtCAT6*, a Leucin transporter (Hammes *et al.*, 2006). Oocytes expressing *AUX1* or *CAT6*, respectively, were injected with NPA (100  $\mu\text{M}$  internal concentration) and thereafter incubated in their respective radiolabeled substrates. Water-injected oocytes served as a control. I measured the amount of substrate the oocytes had taken up after 30 minutes.

As expected, oocytes expressing *AUX1* accumulated significantly more  $^3\text{H}$ -IAA than water-injected oocytes. The increase was similar in the presence and absence of internal NPA (**Fig. 4-8 A**). Similarly, oocytes expressing *CAT6* accumulated significantly more  $^{14}\text{C}$ -Leucin independent of internal NPA (**Fig. 4-8 B**). I concluded that the inhibition of PIN activity was not due to deleterious effects on general oocyte viability and that NPA does not compromise transport activity in general.

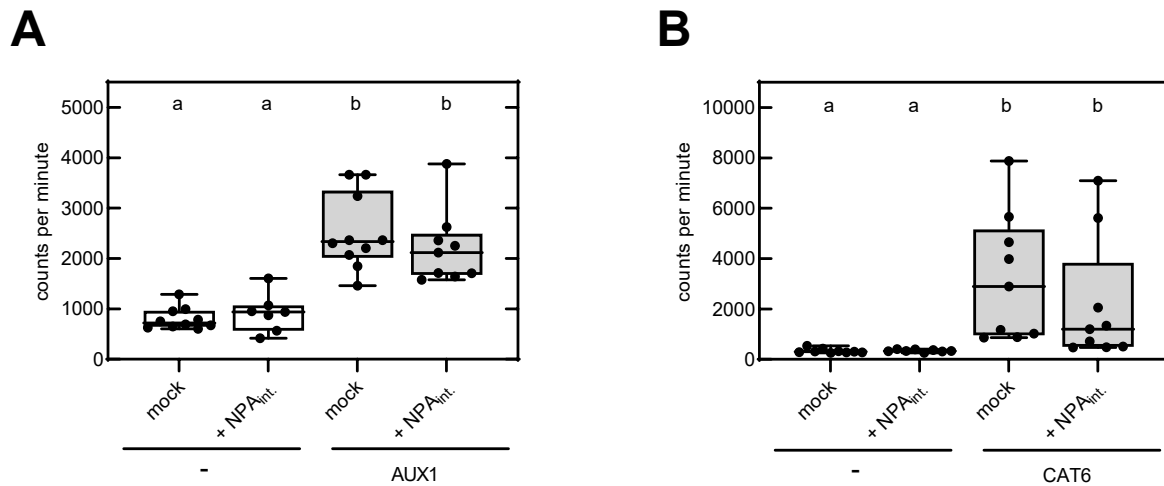


**Fig. 4-8 NPA does not affect transport the activity of *AtAUX1* or *AtCAT6*.** Import assay with oocytes expressing (A) AUX1 or (B) CAT6 were injected with NPA (100  $\mu$ M internal concentration) or buffer for mock control and incubated in their respective substrates  $^3$ H-IAA or  $^{14}$ C-Leucin. cpm were measured after 30 minutes. (A) Oocytes expressing AUX1 took up significantly more  $^3$ H-IAA than water-injected oocytes and this was not affected by injected NPA (ANOVA,  $n=7-10$ ; ab,  $p < 0.032$ ). (B) Oocytes expressing CAT6 took up significantly more  $^{14}$ C-Leucin than water-injected oocytes and this was not affected by injected NPA (ANOVA,  $n = 9-10$ ; ab,  $p < 0.045$ ).

### 4.3 PIN8 is a constitutively active IAA transporter and sensitive to NPA

The non-canonical, short-looped PIN8 has been reported to localize at internal membranes where it is postulated to mediate IAA export from internal compartments into the cell lumen to maintain the intracellular IAA homeostasis (Ding *et al.*, 2012). This, however, is still a matter of debate and when I started my doctorate, PIN8's IAA transport activity had only been deduced from experiments based on passive pre-loading and not shown clearly. However, preliminary data from my Master's thesis indicated IAA transport by PIN8 (Kolb, 2015). To examine the potential of PIN8 to mediate IAA efflux, I heterologously expressed PIN8 in the oocyte system and performed IAA transport assays. I calculated its transport rates and compared the results to canonical PIN3, the strongest transporter in the oocyte system.

I found that IAA transport rates of PIN8 without kinase were significantly higher than transport rates of inactive PIN3 (Fig. 4-9 A), indicating that PIN8 is able to transport IAA without the necessity of a co-expressed, activating kinase. Furthermore, co-expression of neither D6PK nor PID affected this PIN8-mediated IAA transport, as there was no significant difference between transport rates of PIN8 alone in comparison to PIN8 co-expressed with D6PK or PID. These results were published within the frame of a collaboration (Ung *et al.*, 2022) and they suggest that PIN8 is a constitutively active IAA transporter. To further support this suggestion, I tested whether PIN8-mediated IAA transport was sensitive to NPA, as I had observed that NPA inhibits PIN-mediated IAA transport (4.2). I co-injected NPA together with  $^3$ H-IAA into oocytes expressing PIN8 and expected to observe a decrease of IAA transport. Indeed, I saw

the trend of NPA decreasing PIN8-mediated  $^3\text{H}$ -IAA transport (**Fig. 4-9 B**). In summary, my findings demonstrate that non-canonical PIN8 is a constitutively active IAA transporter which is not controlled by a kinase and that the inhibition of PIN-mediated IAA efflux by NPA is not restricted to canonical PINs, but that NPA also inhibits non-canonical PINs.

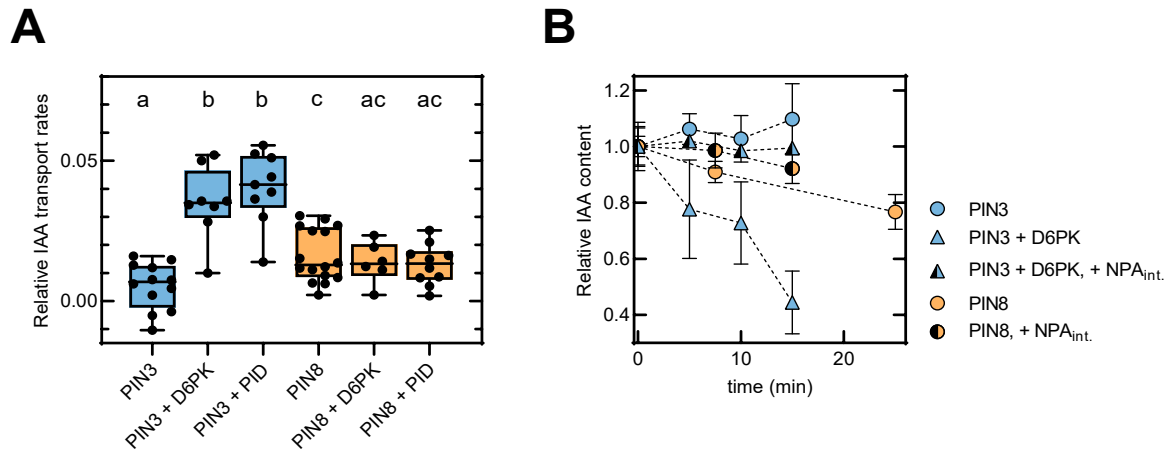


**Fig. 4-9 PIN8 is a constitutive active IAA transporter sensitive to NPA.** IAA efflux assay was performed with oocytes expressing PINs and kinases as specified. **(A)** Transport rates of PIN3 and PIN8 from individual biological replicates were calculated and blotted, with one black dot representing the transport rate of one biological replicate, error bars show SEM. Transport rates of PIN8 alone are significantly higher than transport rates of PIN3 alone (negative control) and this constitutive active transport does not significantly vary upon co-expression with D6PK or PID. Different letters indicate significant differences. Statistical analysis was performed by means of a one-way ANOVA followed by Holm-Sidak post hoc test ( $p < 0.050$ ). **(B)** Reduction of  $^3\text{H}$ -IAA content over time, oocytes were injected with  $^3\text{H}$  IAA only or  $^3\text{H}$  IAA + 100  $\mu\text{M}$  NPA as specified. PIN8-mediated  $^3\text{H}$ -IAA transport is reduced by internal NPA. Data points represent mean and standard error from  $n = 6 - 10$  oocytes. The dotted lines support the better visualization of the course of labeled IAA content and do not represent linear regression graphs.

#### 4.4 Non-canonical PIN8 adopts properties of a canonical PIN when provided with a canonical loop

I was interested in the question to which extent the cellular localization and the IAA transport characteristics of PINs are based on or controlled by the nature of the loop and if the loop contributes to IAA transport. To answer these questions, I provided non-canonical PIN8 with the canonical loop of PIN2 (PIN8-2-8) or PIN3 (PIN8-3-8), respectively, by inserting the loop between the PIN8 TMDs (Ganguly *et al.*, 2014, Kolb, 2015) (**Fig. 4-10**) and examined, which characteristics the resulting chimaeras showed in terms of IAA transport and cellular localization.

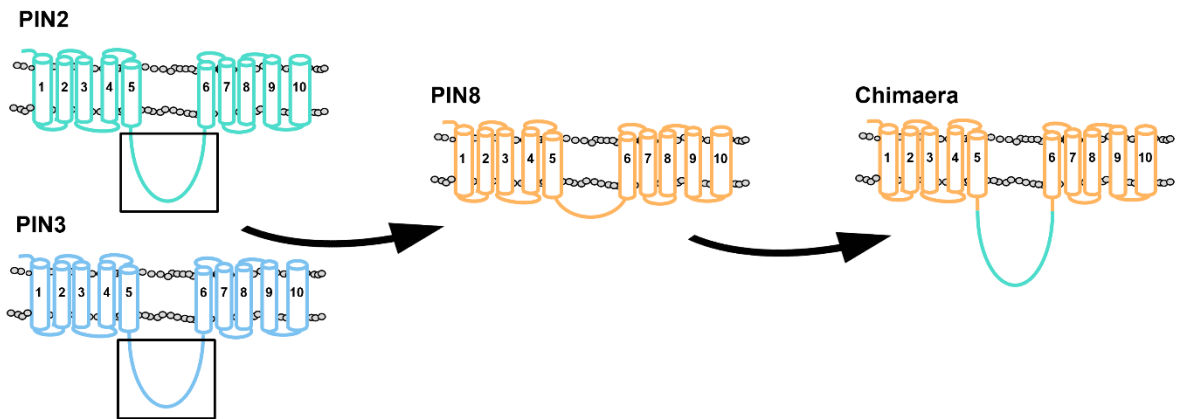


**Fig. 4-10 Schematic presentation of the generation of the PIN8 chimaeras.** The chimaeras were cloned by inserting the canonical loop of PIN2 or PIN3, respectively between the two TMDs of PIN8 (Ganguly *et al.* 2014), mimicking the structure of a canonical PIN.

#### 4.4.1 Chimaeras display IAA transport characteristics of their loop donor and TMD donor

IAA transport characteristics of the PIN8-2-8 and the PIN8-3-8 chimaeras were examined in IAA transport assays in the oocyte system. I performed several individual experiments and calculated the transport rates. Then, the transport rates of the chimaeras were compared to the transport rates of loop donor PIN3 and TMD donor PIN8 (**Fig. 4-11 A**). Data of loop donor PIN2 could not be included in the comparison, as to the time I was performing the experiments, measurement of PIN2-mediated IAA transport in the oocyte system was not possible due to technical problems.

I found that the relative transport rates of PIN8-2-8 alone were significantly higher than the negative control PIN3 and that they were in the same range as constitutively active PIN8 (**4.3**). This indicates that the PIN8-2-8 chimaera, like its transmembrane donor PIN8, is constitutively active and suggests that the auto-inhibitory effect of the PIN2 loop is not present in the PIN8 TM context. Additionally, PIN8-2-8 showed characteristics of canonical PINs: Upon co-expressing D6PK or PID, the transport rates increased, in the case of PID significantly. Moreover, the trend that PID activates IAA efflux more efficiently than D6PK (Zourelidou *et al.*, 2014), was visible. The PIN8-3-8 chimaera behaved differently in that in the absence of a kinase, transport rates of PIN8-3-8 did not differ from the negative control PIN3. This suggests that PIN8-3-8 alone is not transporting IAA and I concluded that the auto-inhibitory effect of the PIN3 loop is present in the PIN8 TMD context. Co-expression of the activating kinases D6PK or PID increased PIN8-3-8 IAA transport rates significantly and activation by PID was more pronounced than activation by D6PK.

Lastly, I performed IAA transport assays with GFP-tagged versions of the chimaeras, PIN8-2-8-GFP and PIN8-3-8-GFP, respectively (**Fig. 4-11 B and C**). In these chimaeras, GFP was inserted into the loop at a position described before (Wiśniewska *et al.*, 2006). I found

that PIN8-2-8-GFP, like PIN8-2-8, exhibited constitutively active IAA transport which was enhanced by co-expression of either D6PK or PID (Fig. 4-11 B) and that PIN8-3-8-GFP, like PIN8-3-8, was inactive when expressed alone, whereat co-expression of either D6PK or PID, activated its IAA transport (Fig. 4-11 C). I concluded that both GFP-tagged chimaeras are functional transporters in the oocyte system, displaying transport characteristics resembling their untagged, “native” versions.

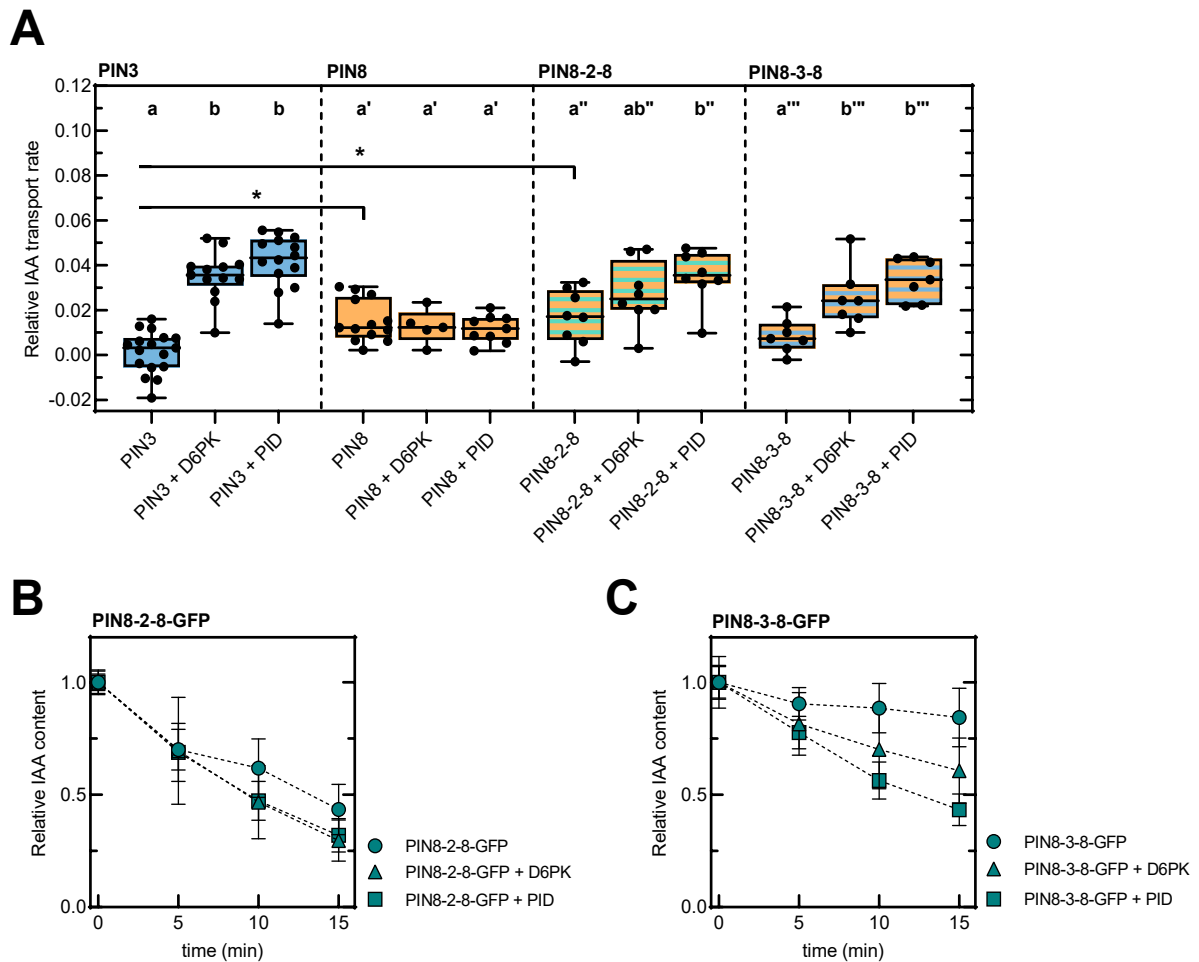


**Fig. 4-11 The chimaeras PIN8-2-8, PIN8-3-8, and their GFP-tagged versions are functional IAA transporter in the oocyte system and display characteristics from both their parents.** IAA efflux assays were performed with oocytes expressing PINs, PIN-chimaeras, and kinases as specified. **(A)** Transport rates of PINs and PIN-chimaeras from individual biological replicates were calculated and blotted, with one black dot representing the transport rate of one biological replicate, error bars show SEM. The auto-inhibitory effect of the PIN2 loop is not present in PIN8-2-8, which transports  $^3\text{H}$ -IAA without a kinase co-expressed. Upon co-expression with D6PK or PID, the transport rates increase, in the case of PID significantly. PIN8-3-8 transports  $^3\text{H}$ -IAA only when co-expressed with an activating kinase. Also here, activation by PID is more pronounced. Different letters indicate significant differences. Statistical analysis was performed by means of a one-way ANOVA (All Pairwise Multiple Comparison Procedures) followed by Holm-Sidak post hoc test ( $p < 0.050$ ). Oocytes expressing **(B)** PIN8-2-8-GFP and **(C)** PIN8-3-8-GFP as indicated, reduction of  $^3\text{H}$ -IAA content was measured over time. Both GFP-tagged chimaeras transport  $^3\text{H}$ -IAA in the oocyte system, with transport characteristics similar to their untagged, “native” versions. Data points represent mean and standard error from  $n = 6 - 10$  oocytes. The dotted lines support the better visualization of the course of labeled IAA content and do not represent linear regression graphs.

#### 4.4.2 Physiological relevance of the PIN8-2-8 and PIN8-3-8 chimaeras

From the oocyte system I had learned that both PIN8 chimaeras, PIN8-2-8 and PIN8-3-8 are functional IAA transporters and that by providing PIN8 with a canonical loop, it can to some extent be turned into a canonical PIN. I was curious if these findings have physiological relevance. Therefore, I performed experiments to test if the chimeras can complement the agravitropic growth phenotype of the *pin2* mutant (Müller *et al.*, 1998) when expressed in the *PIN2* domain. I introduced PIN8-2-8 and PIN8-3-8 under the control of the *PIN2* promoter into the *pin2* mutant background, all lines were genotyped for the *pin2* background and the T-DNA construct. I then scored the gravitropic growth of these transgenic plant lines ( $P_{PIN2}:PIN8-2-8$  and  $P_{PIN2}:PIN8-3-8$ , respectively) in comparison to the wild type (ecotype Col-0) and the *pin2* mutant. Besides PIN8-2-8 and PIN8-3-8, I included PIN8-2-8-GFP, TMD donor PIN8, loop donor PIN3 and loop donor PIN2 in the assay ( $P_{PIN2}:PIN8-2-8-GFP$ ,  $P_{PIN2}:PIN8$ ,  $P_{PIN2}:PIN3$  and  $P_{PIN2}:PIN2$ , respectively). To evaluate the phenotypic rescue, I used two-well established parameters (Fig. 4-12). Firstly, I measured the root angle, which is small for a *Wt*-like, gravitropic root and big for a *pin2*-like, agravitropic root. Furthermore, for *pin2* seedlings, the root angle shows a higher variability in its size compared to *Wt* roots and thus has a scattered distribution pattern when more individuals of one line are measured. Secondly, I calculated the vertical growth index (VGI, Grabov *et al.*, 2005), which is defined as the ratio between the root tip ordinate and the root length. If a root grows perfectly downward, its root angle equals 0 and its VGI equals 1, whereas an agravitropic root has a VGI smaller than 1.

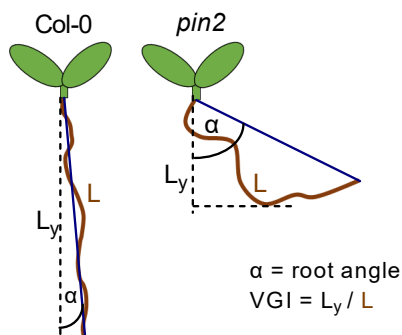


**Fig. 4-12 Quantification of root geometry of *Arabidopsis* with use of the root angle and the vertical growth index (VGI)**  $L$  is the length of the root,  $L_y$  is the ordinate of the root tip,  $\alpha$  is an angular coordinate of the root tip. The VGI is defined as the ratio between the root tip ordinate and the root length. Gravitropic Col-0 seedlings will generate a relatively small  $\alpha$  and relatively big VGI, whereas the agravitropic *pin2* seedlings generate a bigger  $\alpha$  and thus smaller VGI in comparison to *Wt* seedlings. VGI as published in Grabov *et al.*, 2005.

I worked with 5-day-old seedlings of the segregating T2 generation, thus it must be considered that 25% of the transgenic individuals are *pin2* mutants. I evaluated a minimum of seven individual transgenic lines per construct. To this end, I plated 120 individual seedlings per line and calculated the mean of their root angles and the mean of their VGIs.

The root angle distribution pattern of the individual evaluated seedlings of both  $P_{PIN2}:PIN8-2-8$  and  $P_{PIN2}:PIN8-2-8-GFP$  shifted from the *pin2* distribution pattern closer to the *Wt* (Col-0) distribution pattern (Fig. 4-13 A, B, and G, upper panel). When I plotted the means of all



evaluated lines, I found that also here, both the mean of the root angles and the mean of the VGIs were shifted from *pin2* closer to the *Wt* phenotype (**Fig. 4-13 G** middle panel and lower panel). Hence, both PIN8-2-8 and PIN8-2-8-GFP decreased the intensity of the *pin2* growth phenotype. In contrast, in  $P_{PIN2}:PIN8$  the distribution pattern of the root angles was highly scattered (**Fig. 4-13 C**). The mean of the VGI did not differ from *pin2* and the mean of the root angles was even higher than in the *pin2* seedlings (**Fig. 4-13 G** upper, middle and lower panel), suggesting that PIN8 was not able to complement the *pin2* mutant phenotype, which is in line with Ganguly *et al* (2014). The distribution pattern of the root angles of  $P_{PIN2}:PIN8-3-8$  was highly scattered (**Fig. 4-13 E**) and neither the mean of root angles nor the mean of VGIs of the lines differed from *pin2* (**Fig. 4-13 G** upper, middle, and lower panel). This suggests that  $P_{PIN2}:PIN8-3-8$  behaved like *pin2* and that PIN8-3-8 was not able to complement the *pin2* mutant phenotype. For  $P_{PIN2}:PIN3$ , I observed that the root angle distribution pattern resembled the *Wt* roots and both the mean of the root angles and the mean of the VGIs fell in between the *Wt* and *pin2* control plants (**Fig. 4-13 F, G** upper, middle, and lower panel), suggesting that the construct partially complemented the *pin2* root phenotype. The  $P_{PIN2}:PIN2$  control behaved as expected and grew gravitropic roots (**Fig. 4-13 D and G** upper, middle, and lower panel).

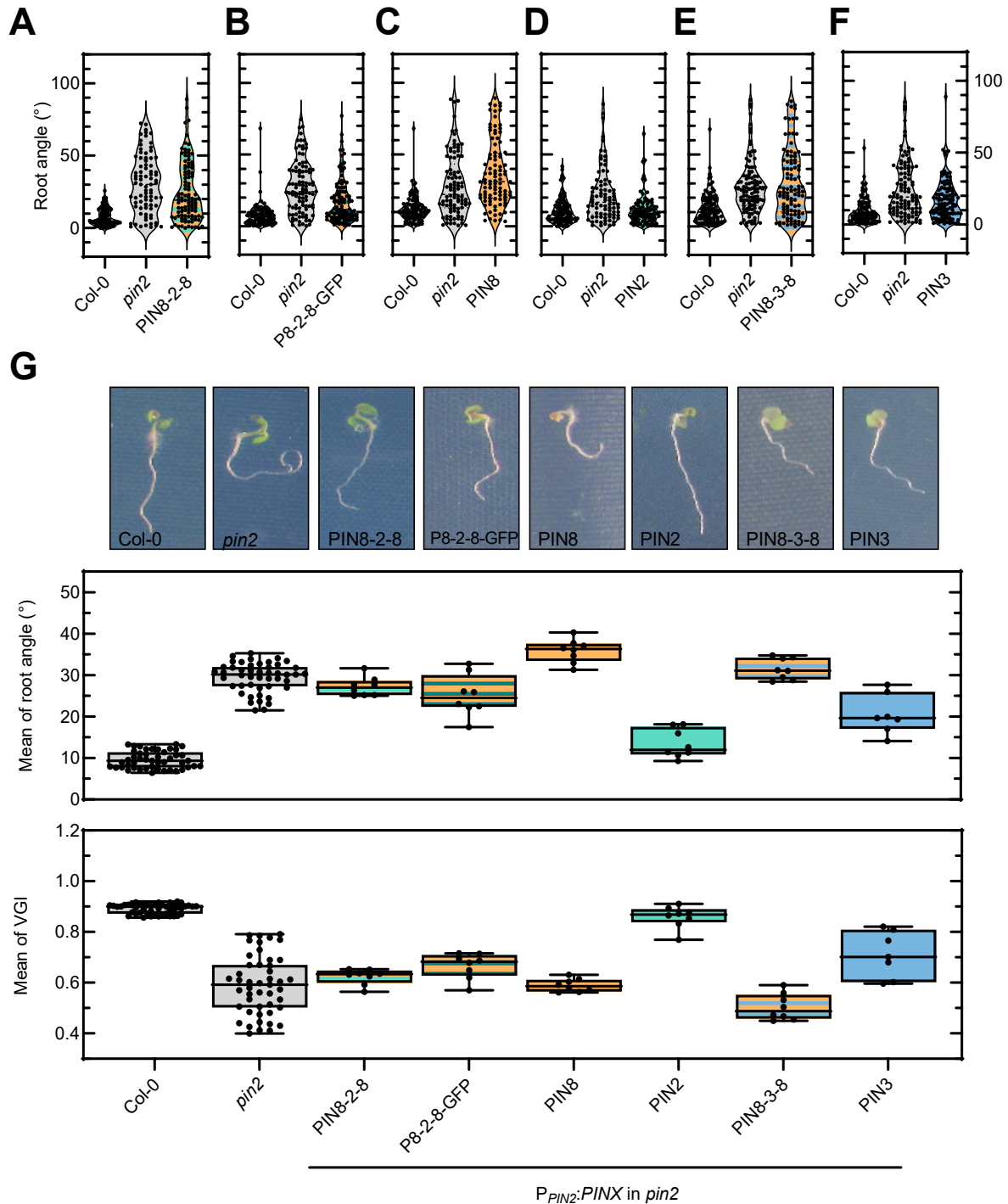


**Fig. 4-13 Quantification of *pin2* rescue with use of the root angle and VGI (Grabov et al., 2005).** All transgenic lines have a *pin2* background and were analyzed in T2 generation.  $P_{PIN2}:PINX$  genotypes with the Wt and *pin2* controls as indicated. **(A-F)** Pattern of root angle distribution of representative lines.  $P_{PIN2}:PIN8-2-8$ ,  $P_{PIN2}:PIN8-2-8-GFP$  and  $P_{PIN2}:PIN3$  show a distribution pattern shifted from the *pin2*-like distribution pattern closer to the Wt-like distribution pattern. On the contrary,  $P_{PIN2}:PIN8$ , and  $P_{PIN2}:PIN8-3-8$  show a distribution pattern like *pin2*. **(G)** Phenotype of 5-day-old seedlings, genotypes as indicated (upper panel), with mean of root angles (middle panel) and mean of VGI (lower panel), respectively, of all lines as indicated.  $P_{PIN2}:PIN8-2-8$  and  $P_{PIN2}:PIN8-2-8-GFP$  minor the *pin2* mutant phenotype and  $P_{PIN2}:PIN3$  partially complements.  $P_{PIN2}:PIN8$  and  $P_{PIN2}:PIN8-3-8$  were not able to complement the *pin2* mutant phenotype.

For root gravitropism, polar IAA transport is pivotal (Armengot *et al.*, 2016; Sato *et al.*, 2015; Su *et al.*, 2017). Thus, I was also interested in the IAA response of the transgenic lines. To this end, I utilized the IAA reporter construct  $P_{DR5}:GUS$  (Ulmasov *et al.*, 1997). DR5 includes an auxin-responsive element and a 35S promoter element. In the presence of IAA, *GUS* is expressed and this IAA response can be made visible by histochemical staining for GUS activity. I crossed the  $P_{DR5}:GUS$  reporter into all  $P_{PIN2}:PINX$  (*pin2*) lines described in the previous chapter and in the *Wt* and *pin2* background as controls. All lines were genotyped for the *pin2* background and the T-DNA construct. I quantified the GUS histochemical staining (Béziat, Kleine-Vehn, *et al.*, 2017) by converting the blue color intensity into gray values and measuring the signal intensity of a linear, horizontal region of interest (ROI) along the root through the quiescent center (QC) (**Fig. 4-14 A**). I then compared the resulting profiles of the different genotypes. the DR5 response in Col-0 was restricted to the QC, columella stem cells, and the columella root cap as has been described before (Sabatini *et al.*, 1999) and caused one peak in the gray values at the region around the QC and second, slightly higher peak in the lower part of the columella region (**Fig. 4-14 B**). By contrast, the GUS signal in *pin2* was widespread and distributed undefinedly over the whole root tip in all cell types (**Fig. 4-14 C**). In the intensity profile, this was reflected in a high and stretched peak above the QC area and comparatively low peak in the columella root cap.  $P_{PIN2}:PIN8-2-8$ ,  $P_{PIN2}:PIN8-2-8-GFP$  and  $P_{PIN2}:PIN3$  (**Fig. 4-14 D, E, and I**) showed an DR5 response resembling the *Wt* scenario, whereas the staining in  $P_{PIN2}:PIN8$  and  $P_{PIN2}:PIN8-3-8$  (**Fig. 4-14 F and H**) was widespread and distributed undefinedly, resembling the scenario in *pin2* roots. The DR5 response of the positive control  $P_{PIN2}:PIN2$  equated to Col-0 roots. In a parsimonious interpretation, the data obtained in the experiment emphasizes the observations made in the gravitropism rescue experiment, and I concluded that both PIN8-2-8 and PIN8-2-8-GFP mitigate and that PIN3 partially rescues the *pin2* mutant phenotype when expressed under the control of the *PIN2* promotor, whereas PIN8 and PIN-3-8 cannot rescue the *pin2* mutant.

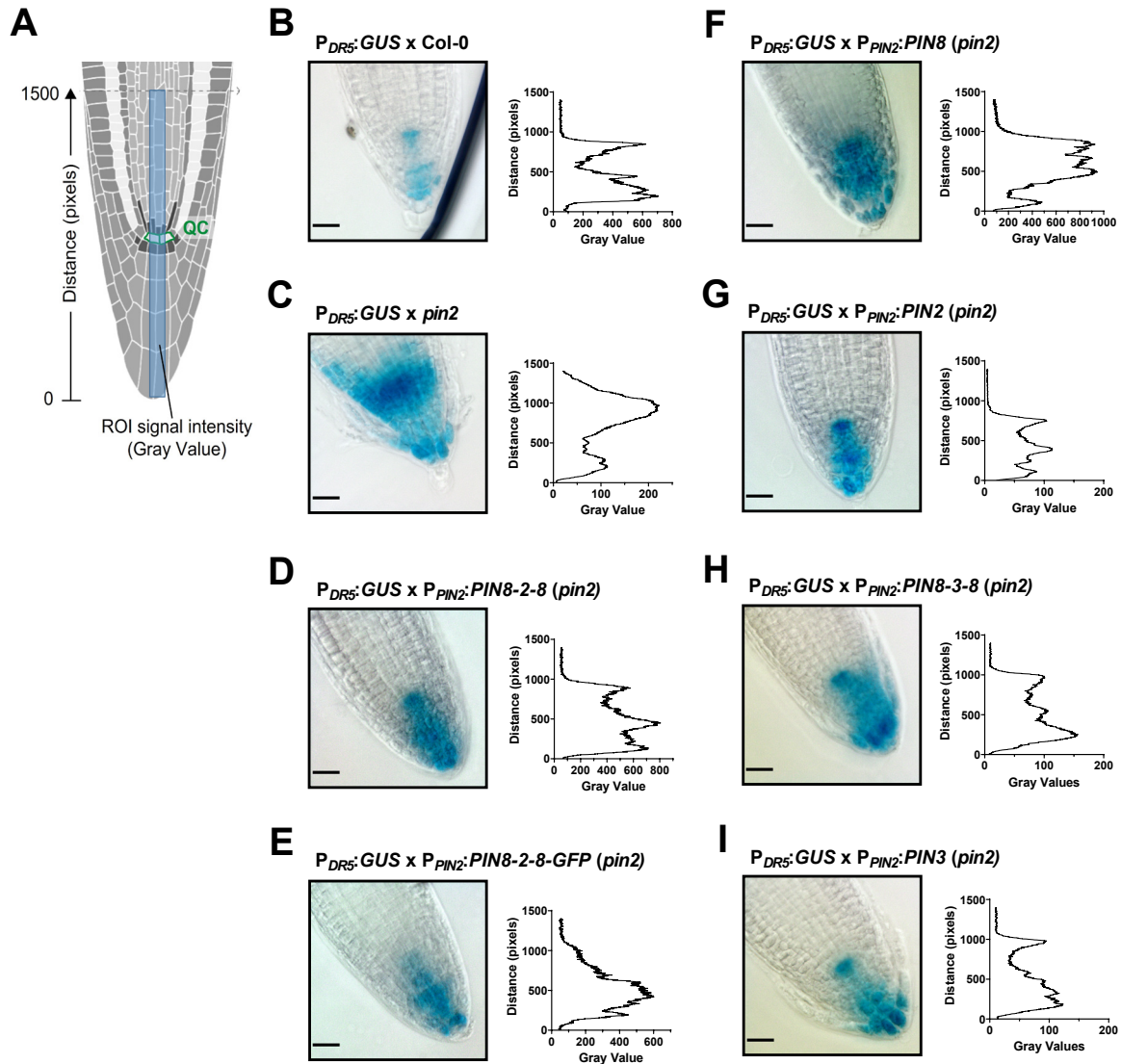


**Fig. 4-14 Auxin response of Col-0, *pin2*, and *PIN2:PINX (pin2)* lines, visualized by GUS-staining (Ulmasov *et al.*, 1997) and its quantification. (A) Schematic presentation of the root and the linear region of interest (ROI) selection, where the signal intensity of gray values was measured, reflecting the GUS intensity (Béziat *et al.*, 2017). Figure modified from (Rahni and Birnbaum, 2019). (B – I) Scale bars represent 100  $\mu$ m. Genotypes as indicated. (B) DR5 response of Col-0 roots is restricted to the QC and columella cells, whereas the DR5 response in (C) *pin2* seedlings is widespread and undefined distributed over the whole root. (D) *PIN2:PIN8-2-8*, (E) *PIN2:PIN8-2-8-GFP*, and (I) *PIN2:PIN3* show a DR5 response similar to the Col-0, whereas the GUS staining in (F) *PIN2:PIN8* and (H) *PIN2:PIN8-3-8* resembles the *pin2* scenario. (G) The DR5 response of the positive control *PIN2:PIN2* equates to Col-0 roots.**

#### 4.4.3 PIN8-2-8-GFP localizes at the PM

Canonical PINs are predominantly located in the PM, whereas non-canonical PINs are found at internal membranes (Ding *et al.*, 2012; Ditengou *et al.*, 2018; Mravec *et al.*, 2009). In root tissue, PINs show distinctive localization: *PIN2* is expressed in the epidermis and cortex of the lateral root, where it displays a dual polarity, namely basal PM localization in the cortex, and apical PM localization in the epidermis (Müller *et al.*, 1998). Defects in this polarity or *PIN2*

expression cause agravitropic root phenotypes (Müller *et al.*, 1998; Abas *et al.*, 2006; Rahman *et al.*, 2010). PIN8 localizes internally in the root meristem (Lee *et al.*, 2020a), but it displays predominantly a PM localization pattern when ectopically expressed in the *PIN2* domain, even though it fails to show polar localization (Ganguly *et al.*, 2014).

To assess the subcellular localization of the chimeric PIN8-2-8 and PIN 8-2-8-GFP proteins, and to determine if these PIN8 chimeric proteins exhibit similarities to the PIN2 subcellular localization, I took confocal images of roots of 5-day-old seedlings. I found that the PIN8-2-8-GFP fusion protein was expressed in cortex cells and lateral epidermis cells, where it localized to the PM (Fig. 4-15). Whether the chimaera showed a distinct polar localization pattern and thus, if providing PIN8 with the PIN2-loop is sufficient to evoke the PIN2-unique localization pattern could not be estimated at this point.

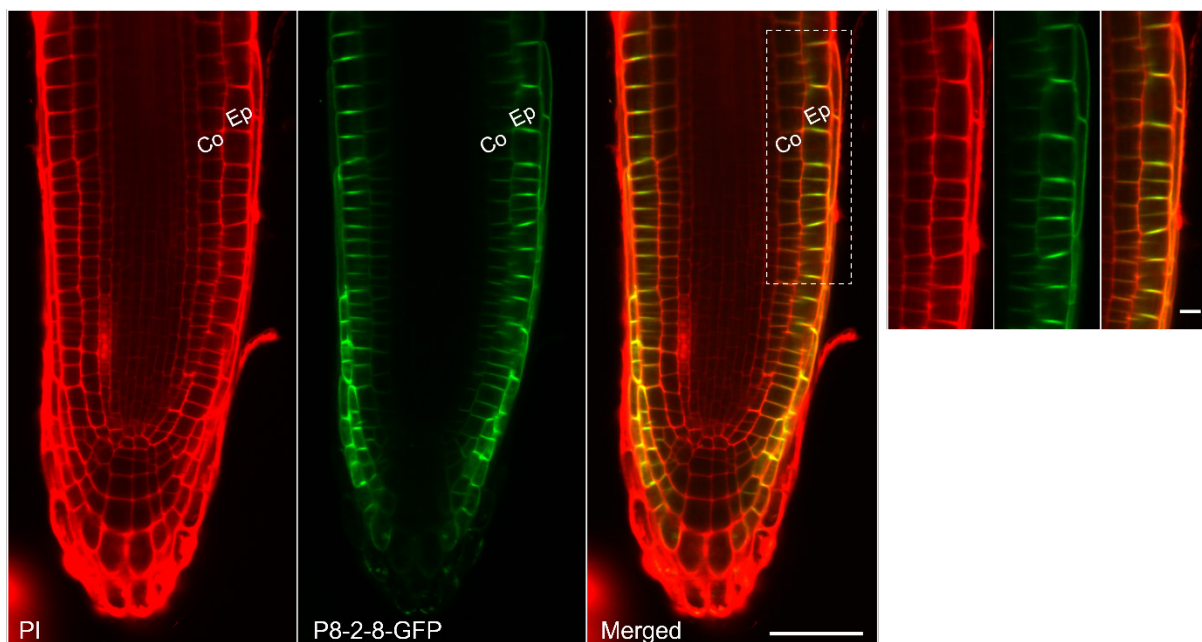


**Fig. 4-15 PIN8-2-8 localizes at the PM in epidermis and cortex in 5-day-old *P<sub>PIN2</sub>:PIN8-2-8-GFP* (*pin2*) roots.** Representative confocal images of root cells after Propidium iodide (PI) staining of transgenic seedlings. PI signal, PIN8-2-8-GFP signal, and merged signals as indicated with magnification of epidermis and cortex (right panel). PIN8-2-8-GFP localizes to the PM in the *PIN2* expression domain. Co = Cortex, Ep = Epidermis. Scale bar: 50  $\mu$ m (Merge), 10  $\mu$ m (Magnification).

## 4.5 Characterization of semi-canonical PIN6

In terms of sequence similarity and the length of its loop, semi-canonical PIN6 is a unique member of the PIN family, it is however closer related to the canonical PINs and in particular to PIN2 (Bennett *et al.* 2014). In terms of its cellular localization, in the root, PIN6 localizes both in endomembrane domains and at the PM (Simon *et al.*, 2016; Ditengou *et al.*, 2018). PIN6 has been shown to be involved in root development and formation of correct root morphology: It is suggested to contribute to intracellular auxin homeostasis during root growth

and to play a critical role in both lateral and adventitious root development (Simon *et al.*, 2016) and overexpression of *PIN6* leads to a pronounced root-waving phenotype, a significant reduction in root length and an absence of root hair outgrowth (Cazzonelli *et al.*, 2013; Simon *et al.*, 2016; Ditengou *et al.*, 2018). As to date, *PIN6* and its biological role are only little characterized and its IAA transport activity has not been shown clearly, I performed IAA efflux assays and included *PIN6* in the root gravitropism assay.

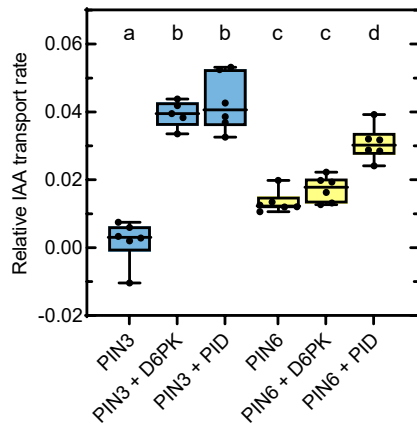
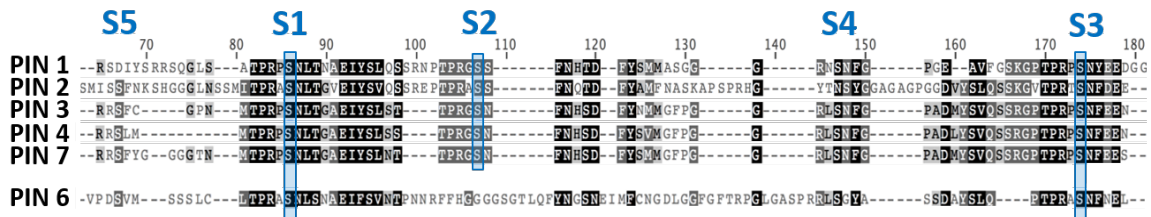
Parts of the data displayed in this chapter have been published as described in more detail below (Abas *et al.*, 2021).

#### **4.5.1 PIN6 is a constitutively active IAA transporter and its transport capacity is enhanced by PID**

The IAA transport activity of *PIN6* has so far only been suggested from experiments in tobacco BY-2 cells using synthetic auxins, or in yeast cells (Simon *et al.*, 2016). To directly examine its IAA transport, I expressed *PIN6* either alone or together with D6PK or PID in the oocyte system, performed IAA transport assays, and calculated the IAA transport rates of *PIN6*. *PIN3* (+ D6PK or + PID) was used as control.

I found that the transport rates of *PIN6* alone were significantly higher than the negative control *PIN3* alone (**Fig. 4-16 A**). This implies that *PIN6* constitutively transports IAA, without a co-expressed kinase. Furthermore, I saw that this transport activity of *PIN6* was significantly enhanced by one of the kinases only, PID. Co-expression of D6PK, in contrast, increased the transport rates of *PIN6* only marginal. In terms of its IAA transport, *PIN6* therefore resembles the *PIN8-2-8* chimera and even more so the closely related *PIN2* (Dorina P. Janacek, pers. comm.).

PID is known to phosphorylate three serines (S1 – S3) embedded in a highly conserved TPRXS(N/S) motif in the canonical PIN loop (Zourelidou *et al.*, 2014). Upon the finding that PID enhances *PIN6* transport activity, I performed a sequence alignment of the loop regions of all canonical PINs and semi-canonical *PIN6* to identify potential PID phosphorylation targets in the semi-canonical *PIN6* loop. (**Fig. 4-16 B**). I found that two of the three known PID sites, S1 and S3, are conserved within the *PIN6* loop. Taken together, this suggests that kinase regulation in *PIN6* is different from other PINs and that PID not only is involved in regulation of *PIN6* polarity as previously suggested (Ditengou *et al.*, 2018) but also plays a role in control of *PIN6* IAA transport by phosphorylation at S1 and S3.

**A****B**

**Fig. 4-16 PIN6 is a constitutively active IAA transporter and its transport capacity is enhanced by PID.** (A) IAA efflux assay was performed with oocytes expressing PINs and kinases as specified. Transport rates of PINs (+ kinase) from individual biological replicates were calculated and blotted, with one black dot representing the transport rate of one biological replicate, error bars show SEM. PIN6 alone transports IAA independently of a co-expressed activating kinase, as its transport rates are significantly higher than PIN3 alone (negative control). PID significantly increases the transport rates of PIN6, whereas D6PK has only a marginal effect. Different letters indicate significant differences, statistical analysis was performed by means of a one-way ANOVA (All Pairwise Multiple Comparison Procedures) followed by Holm-Sidak post hoc test ( $p < 0.050$ ). (B) Sequence alignment of the loop of all canonical PINs and semi-canonical PIN6. PID phosphorylates S1-S3 embedded in a highly conserved TPRXS(N/S) motif (Zourelidou *et al.*, 2014). Only S1 and S3 are conserved in the PIN6 loop.

Internal NPA inhibits PIN-mediated IAA transport independently from the co-expressed kinase (4.2) and a sensitivity of PIN6-mediated auxin transport towards NPA has been observed previously (Simon *et al.*, 2016). Thus, I reasoned that IAA transport by both PIN6 alone and PIN6 + PID must decrease equipollent in the presence of internal NPA. Indeed, I could observe that transport rates of both PIN6 alone and PIN6 + PID showed the trend to decrease in the presence of NPA inside the oocyte (Fig. 4-17). The finding that NPA reduces the transport rates of a constitutively active PIN further supports the suggestion that inhibition by NPA is independent of the activating kinase and the data were published within the frame of my collaboration investigating the effect of NPA on PIN-mediated IAA transport (Abas *et al.* 2020).

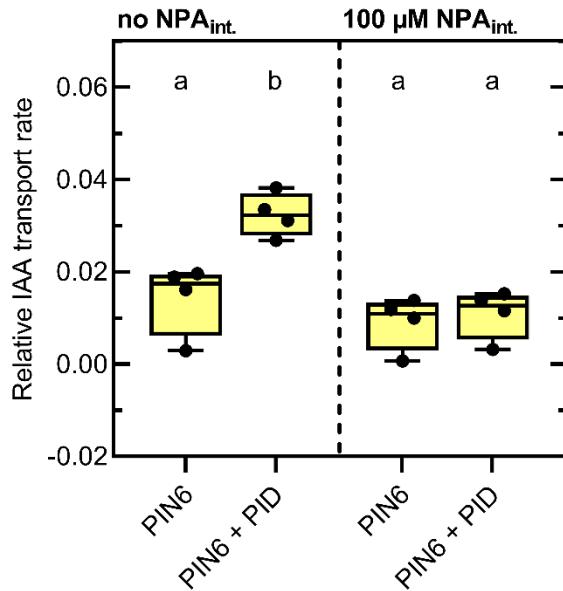


**Fig. 4-17 PIN6-mediated IAA transport in the oocyte system is sensitive to NPA.** IAA efflux assay was performed with oocytes expressing PINs and kinases as specified. Transport rates of PINs (+ kinase) from individual biological replicates were calculated and blotted, with one black dot representing the transport rate of one biological replicate, error bars show SEM. Oocytes were injected with only 3H-IAA or 3H-IAA + NPA as specified. The 3H-IAA transport rates of both PIN6 alone and PIN6 + PID show the trend to decrease in the presence of NPA inside the oocyte. Different letters indicate significant differences, statistical analysis was performed by means of a one way ANOVA (All Pairwise Multiple Comparison Procedures) followed by Holm-Sidak post hoc test ( $p < 0.050$ ).

#### 4.5.2 $P_{PIN2}:PIN6$ expressed in $pin2$ background enhances the mutant phenotype

Compared with PM-localized canonical PIN2, PIN6 has been detected both at the PM and at the ER membrane (Simon *et al.*, 2016). Given the close relationship to PIN2 and the similarities in IAA transport characteristics, I was curious about how PIN6 performs in the gravitropism assay (4.4.2). I introduced *PIN6* under the control of the *PIN2* promoter into the agravitropic *pin2* mutant plant line and evaluated the root gravitropism of eight transgenic  $P_{PIN2}:PIN6$  T2 lines in comparison to the *Wt* and *pin2*. All lines were genotyped for the *pin2* background and the T-DNA construct.

I found that the means of the root angles of the  $P_{PIN2}:PIN6$  lines did not differ from *pin2* seedlings (Fig. 4-18 A) and concluded that PIN6 is not able to complement the agravitropic *pin2* phenotype. Interestingly however, I observed the opposite, as all lines showed an enhancement of the root phenotype and grew roots, which were strikingly impaired in their growth (Fig. 4-18 B - E): depending on the individual line, the roots were either highly wavy (Fig. 4-18 D), i.e. resembling the phenotype described for *PIN6* overexpressing lines (Ditengou *et al.*, 2018; Cazzonelli *et al.*, 2013), or highly cloddy (Fig. 4-18 E). Therefore, especially in the latter case, measurement of the root length was not possible. This parameter is a prerequisite for the VGI, which consequently, I could not calculate. To describe the heavily disturbed root system architecture, included new parameters in the assay: I measured the area the roots occupied (root area,  $R_a$ ) and calculated the relation to the rectangular the root “spanned” (root rectangular,  $R_r$ ) (Fig. 4-18 F). With these parameters and the quotient  $R_a/R_r$  (occupancy index), I qualitatively evaluated the observed enhancement of the root phenotype



of the  $P_{PIN2}:PIN6$  lines. I found that  $P_{PIN2}:PIN6$  roots occupied a significantly smaller area than both *Wt* roots and *pin2* roots (Fig. 4-18 G) and that the area of the root rectangular was significantly smaller (Fig. 4-18 H). Also, the resulting occupancy index of the  $P_{PIN2}:PIN6$  lines was significantly higher, reflecting the observed enhancement of the *pin2* root phenotype (Fig. 4-18 I). I concluded that *PIN6* driven from *PIN2* promoter further impairs correct formation of the root system architecture, phenocopying *PIN6* overexpressing lines.

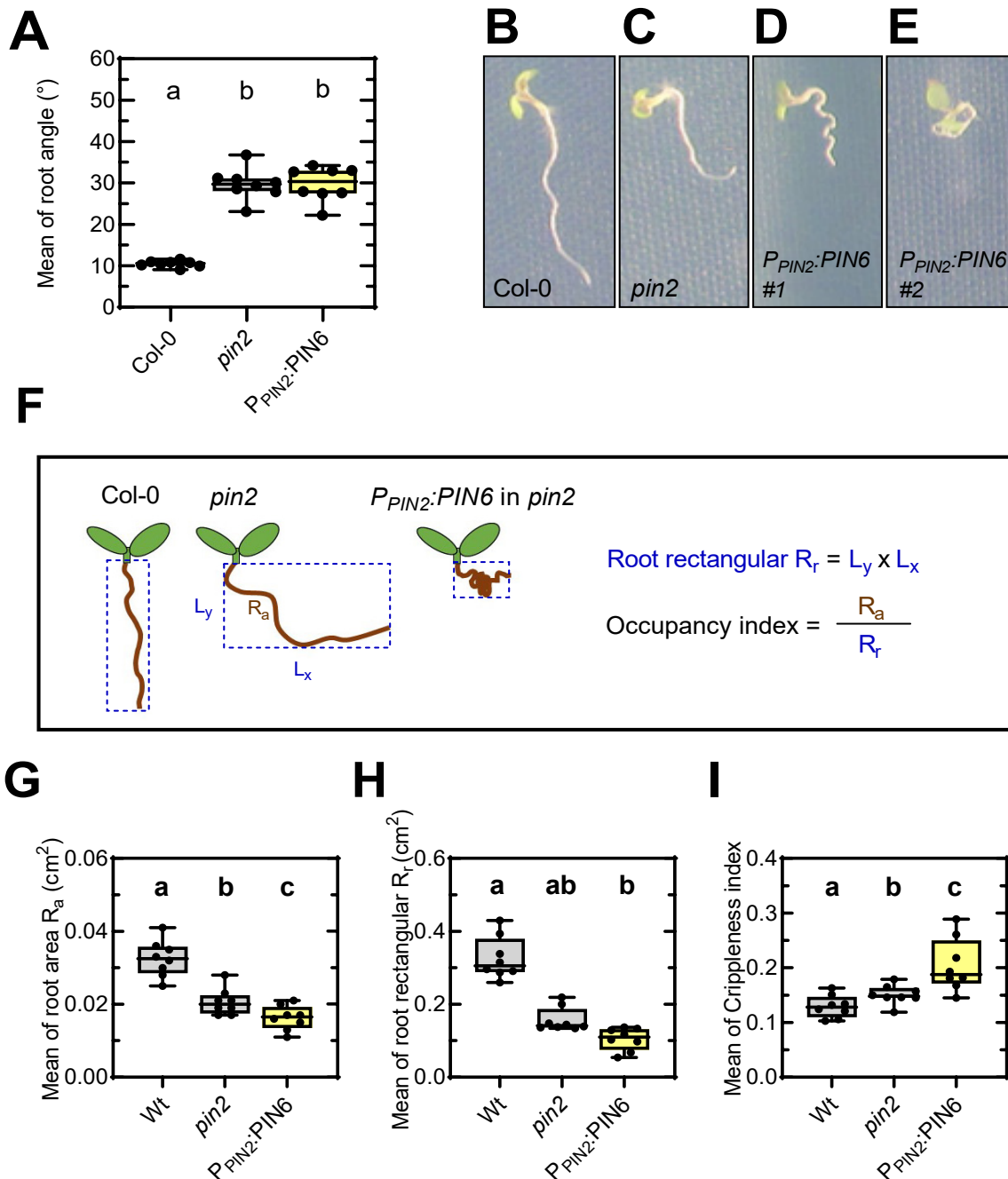


**Fig. 4-18**  $P_{PIN2}:PIN6$  in *pin2* enhances the agravitropic *pin2* phenotype (A) Means of root angle of eight  $P_{PIN2}:PIN6$  T2 lines in *pin2* background in comparison to Col-0 and *pin2* controls.  $P_{PIN2}:PIN6$  does not differ from *pin2*. (B - E) Phenotype of 5-days-old seedlings, genotypes as indicated.  $P_{PIN2}:PIN6$  grows cripple, partly highly wavy (D), partly cloddy (E) roots. (F) Quantification of root geometry of *Arabidopsis*.  $R_r$  is defined as the area of

the rectangular surrounding the whole root from its origin to the root tip (blue).  $R_a$  is defined as the area the root actually occupies (brown). The occupancy index was calculated from the ratio between  $R_a$  and  $R_r$ . (**G - I**) Mean of root area  $R_a$ , root rectangular ( $R_r$ ) and occupancy index of eight  $P_{PIN2}:PIN6$  T2 lines in comparison to Col-0 and  $pin2$  controls.  $P_{PIN2}:PIN6$  showed an intensification of all three parameters, i.e. an enhancement of the  $pin2$  phenotype. Different letters indicate significant differences, statistical analysis was performed by means of a one-way ANOVA (All Pairwise Multiple Comparison Procedures) followed by Holm-Sidak post hoc test ( $p < 0.050$ ).

#### 4.5.3 PIN6 expressed in the *PIN2* domain localizes at the ER and the PM

Upon the observation that the transgenic  $P_{PIN2}:PIN6$  ( $pin2$ ) lines showed an intensified malformation of the agravitropic  $pin2$  phenotype, I wanted to investigate the cellular localization of the construct within the root. I cloned a GFP-fused version of PIN6 (Sawchuk *et al.*, 2013) and investigated its localization in the root tip when driven from the *PIN2* promoter in  $pin2$  background ( $P_{PIN2}:PIN6-GFP$ ) by CLSM analysis of the T2 lines. Interestingly, I saw that also in the *PIN2* domain, PIN6 localized both at the ER and at the PM of epidermis and cortex cells (**Fig. 4-19**).

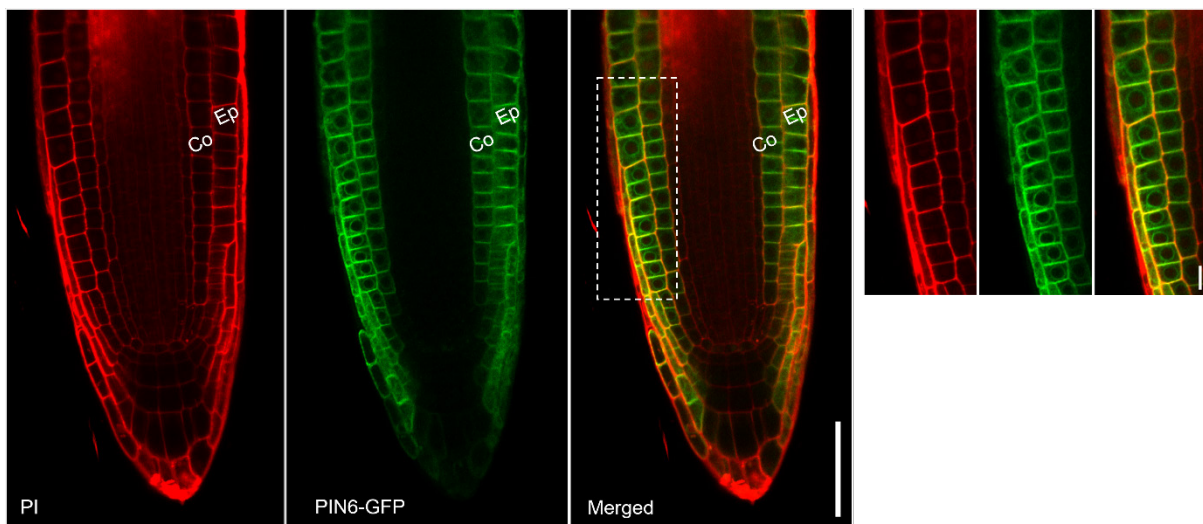


**Fig. 4-19 PIN6 localizes at the ER and the PM in 5-day-old  $P_{PIN2}:PIN6-GFP$  roots.** Representative confocal images of root cells after Propidium iodide (PI) staining of transgenic seedlings. PI signal, PIN6-GFP signal, and merged signals as indicated with magnification of epidermis and cortex (right panel). PIN6-GFP localizes at the ER and the PM as indicated by overlapping signal with PI staining. Co = Cortex, Ep = Epidermis. Scale bar: 50  $\mu$ m (Merge), 10  $\mu$ m (Magnification).

#### 4.6 Characterization of new regulators of PIN-mediated IAA transport

Members of the AGCVIII kinase family are crucial for the activation and regulation of PIN-mediated IAA transport (Zourelidou *et al.*, 2014; Galván-Ampudia and Offringa, 2007) but our knowledge in this context is still limited, as for instance, other candidates must be involved in regulation of PIN-mediated IAA transport that still await characterization and not all members of the AGCVIII family have been examined for their potential to activate PINs. Thus,

one goal of my thesis was to broaden our knowledge in the context of regulators of PINs and PIN IAA transport activity.

Parts of the data presented in this chapter are my contribution to three publications (Koh *et al.*, 2021; Marhava *et al.*, 2018, 2020) as will be described in detail below.

#### **4.6.1 Identification of new players in regulation of PIN-mediated IAA efflux**

The AGCVIII kinase family consists of the four subfamilies AGC1 – AGC4 (Galván-Ampudia and Offringa, 2007). Before the start of my thesis, it was known that D6PK from the AGC1 clade and PID and WAG1 from the AGC3 clade directly activate PINs, whereas UCN from the AGC2 clade and PHOT1 from the AGC4 clade do not (Zourelidou *et al.*, 2014). Consequently, PIN activation seems to be restricted to clade AGC1 and AGC3, however, not all clade members have yet been examined for their potential to activate PINs. Thus, I tested six members of the AGC1 subclade for their potential to activate PIN-mediated IAA transport in the oocyte system: AGC1-3, AGC1-4, AGC1-7, AGC1-8, AGC1-9 and KCBP-INTERACTING PROTEIN KINASE (KIPK). Notably, AGC1-3 was named PROTEIN KINASE ASSOCIATED WITH BRX (PAX) and PAX1-4 was named PAX-LIKE (PAXL) during my doctorate research (Marhava *et al.*, 2018). I co-expressed the kinases of interest together with PINs and measured the depletion of <sup>3</sup>H-IAA over time.

**AGC1-7** was tested for its potential to activate PIN1, PIN3, and PIN6 in individual experiments (**Fig. 4-20 A - C**). None of all three tested PINs co-expressed with AGC1-7 showed an increase of IAA depletion over time in comparison to the respective PIN expressed alone. I concluded that AGC1-7 does not activate PIN1, PIN3 or PIN6 and likely no other PINs.

**PAX, AGC1-8, AGC1-9, and KIPK** were tested exclusively with PIN3. Here, I performed several individual experiments (biological replicates) and calculated and plotted the relative transport rates (**Fig. 4-20 D**). In comparison to PIN3 alone, transport rates increased significantly upon co-expression with AGC1-9 and PAX and highly significantly upon co-expression with KIPK. Importantly, I noted, however, that transport rates were not as high as upon co-expressing with D6PK or PID. I extended the experiments in that I tested PAX additionally with PIN1 and further included **PAXL**, the closest homolog of PAX (Galván-Ampudia and Offringa, 2007). I could confirm the findings insofar as also PIN1 showed the trend to be activated by PAX, whereat the trend was even more pronounced upon co-expression with PAXL (**Fig. 4-20 E**).

In summary, I concluded that AGC1-7 and AGC1-8 do not, whereas PAX, PAXL, AGC1-9, and KIPK do activate PIN-mediated IAA efflux in *X. laevis* oocytes. The finding that PAX and PAXL activate PIN-mediated transport was published in Marhava *et al.*, 2018.

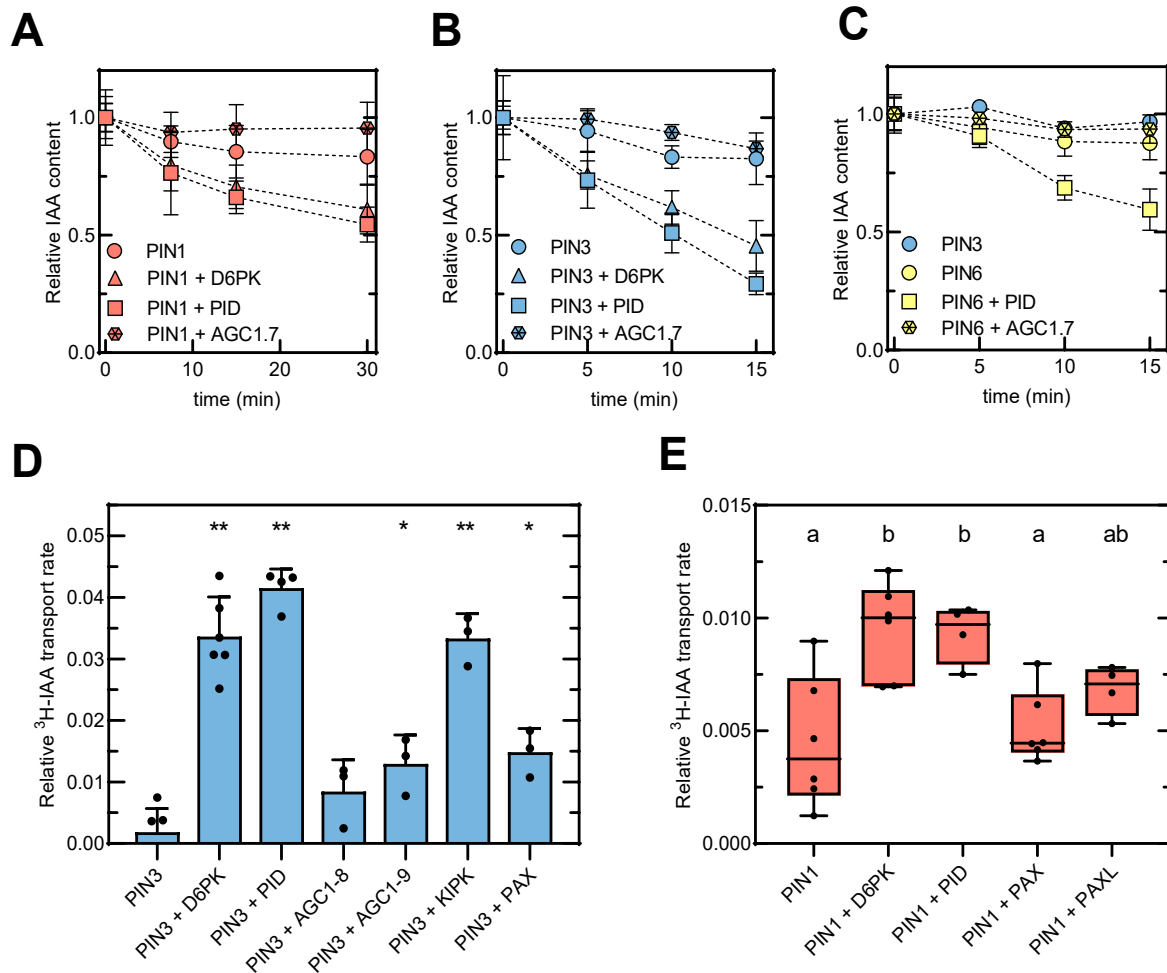


**Fig. 4-20 Potential of selected AGC1 clade kinases to activate PIN-mediated IAA transport.** IAA efflux assay was performed with oocytes expressing PINs and kinases as specified. Reduction of <sup>3</sup>H-IAA content over time, data points represent mean and standard error from n=6-10 oocytes. Co-expression of AGC1.7 did not activate IAA transport by (A) PIN1, (B) PIN3, and (C) PIN6. The dotted lines support the better visualization of the course of labeled IAA content and do not represent linear regression graphs. (D) Calculated transport rates from individual biological replicates. PIN3-mediated IAA transport was activated by AGC1-9, KIPK, and PAX. Statistical analysis was performed by means of a one-way ANOVA (no kinase) followed by Holm-Sidak post hoc test, asterisks indicate statistical significance (\* = P<0.05, \*\* = P<0.001). (E) Calculated transport rates from individual biological replicates. PIN1 showed the trend to be activated by PAX and PAXL. Different letters indicate significant differences. Statistical analysis was performed by means of a one-way ANOVA (All Pairwise Multiple Comparison Procedures) followed by Holm-Sidak post hoc test (p<0.050).

#### 4.6.2 Characterization of the interaction between PAX, PIN and BRX

PAX was found to phosphorylate the PIN loop *in vitro* (Lanassa Bassukas, pers. comm.). Phosphoproteomics indicated auxin-induced phosphorylation of phosphoserine S596 in the PAX activation loop and interestingly, a phosphomimicking variant of PAX (PAX-S596D) is more efficient than wild type PAX or a phospho-mutant variant of PAX (PAX-S596A) (Lanassa Bassukas, pers. comm.). Thus, I wondered if PAX, PAX-S596D, and PAX-S596A activate PIN-mediated IAA transport with different efficiency and if a more efficient phosphorylation *in vitro* was reflected in a more efficient stimulation of the PIN IAA transport. In the oocyte system,

I co-expressed the three PAX variants together with PIN3 (**Fig. 4-21**). Matching the biochemical observation, PAX-S596D stimulated auxin efflux considerably more than wild type PAX, to a level approximately equal to D6PK. Activation by PAX-S596A was as efficient as activation by wild type PAX. I concluded that a more efficient phosphorylation by PAX leads to a more efficient activation of PINs, suggesting that a fine-tuning of PAX activity is a feature to correctly fulfill its role in PIN phosphorylation and activation. I published the data in Marhava *et al.*, 2018.

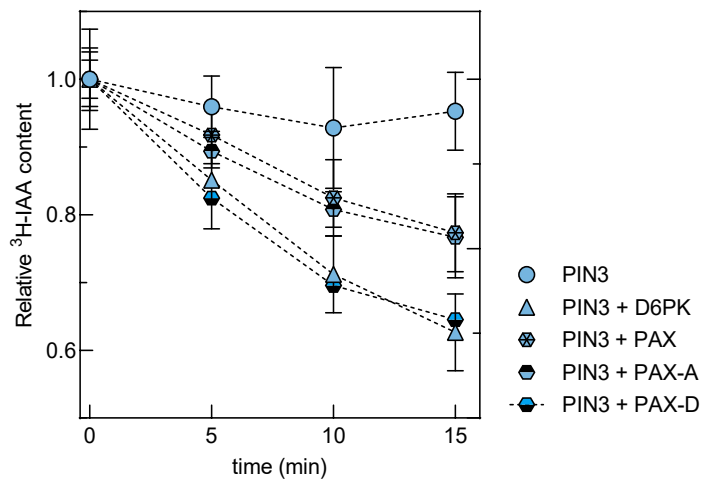


**Fig. 4-21 Potential of wild type PAX, a phosphomimicking variant (PAX-S596D, PAX-D) and a phospho-mutant variant (PAX-S596A, PAX-A) to activate PIN3-mediated IAA transport.** Oocytes expressing PIN3 (+ D6PK or + PAX or + PAX variant) as specified were injected with  $^3\text{H}$ -IAA. Data points represent mean and standard error from n=8-10 oocytes. Activation by PAX-D is more efficient in stimulation of PIN-mediated IAA transport than wild type PAX and PAX-A, to a level approximately equal to activation by D6PK. Activation by PAX-A was as efficient as activation by wild type PAX. The dotted lines support the better visualization of the course of labeled IAA content and do not represent linear regression graphs.

Following the finding that PAX activates PIN-mediated IAA efflux, I extended the experiment with another player: BREVIS RADIX (BRX), a regulator of cell proliferation and elongation in the root (Mouchel *et al.*, 2004). BRX is a PM-associated protein, localizing at the basal PM in the PIN1 domain (Scacchi *et al.*, 2009) and it was identified as PAX interactor by immunoprecipitation (Christian Hardtke, pers. comm.). I tested the influence of BRX influence on PIN-mediated IAA transport in the oocyte system.

I found that oocytes expressing PIN1 + BRX and oocytes expressing PIN3 + BRX did not show an increase in IAA depletion over time in comparison to the respective PIN expressed alone (**Fig. 4-22**). I concluded that BRX does not activate PIN IAA transport and the data described was published in Marhava *et al.*, 2018.

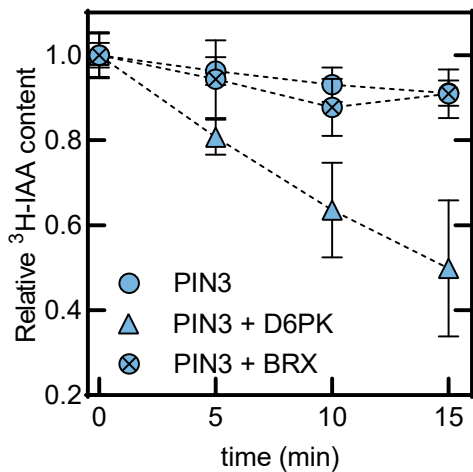


**Fig. 4-22 BRX does not activate PIN3-mediated IAA transport in the oocyte system.** IAA efflux assay was performed with oocytes expressing PIN3 (and D6PK or BRX) as specified. Reduction of  $^3\text{H}$ -IAA content over time, data points represent mean and standard error from  $n=6-10$  oocytes. Oocytes expressing PIN3 + BRX does not show an increase of  $^3\text{H}$ -IAA depletion over time in comparison to PIN3 expressed alone. The dotted lines support the better visualization of the course of labeled IAA content and do not represent linear regression graphs.

Interestingly, however, in oocytes expressing PIN3 + PAX + BRX, I found that the PIN3-mediated IAA transport was strongly reduced in the presence of BRX (**Fig. 4-23 A**), suggesting that BRX substantially inhibited the PAX-mediated stimulation of PIN3. I was curious if this hold true also for other activating kinases of the AGCVIII kinase family. First, I tested the influence of BRX on PIN3 activation by D6PK, which is like PAX, a member of the AGC1 subclade. In oocytes expressing PIN3 + D6PK + BRX, I saw that the IAA transport by PIN3 was lower in comparison to oocytes expressing only PIN3 + D6PK (**Fig. 4-23 B**). This inhibitory effect of BRX had been observed also for PIN1 + D6PK (Fastner, unpublished), thus I concluded that BRX inhibits activation by D6PK. Next, I tested BRX's influence on PID, which belongs to the AGC3 subclade. Interestingly, I saw that PIN3-mediated IAA transport in oocytes expressing PIN3 + PID + BRX was just as strong as in oocytes expressing only PIN3 + PID (**Fig. 4-23 C**). I reasoned that BRX does not inhibit the more distantly related PID, but only members of the AGC1 subclade and this was published as contribution to Marhava *et al.*, 2018.

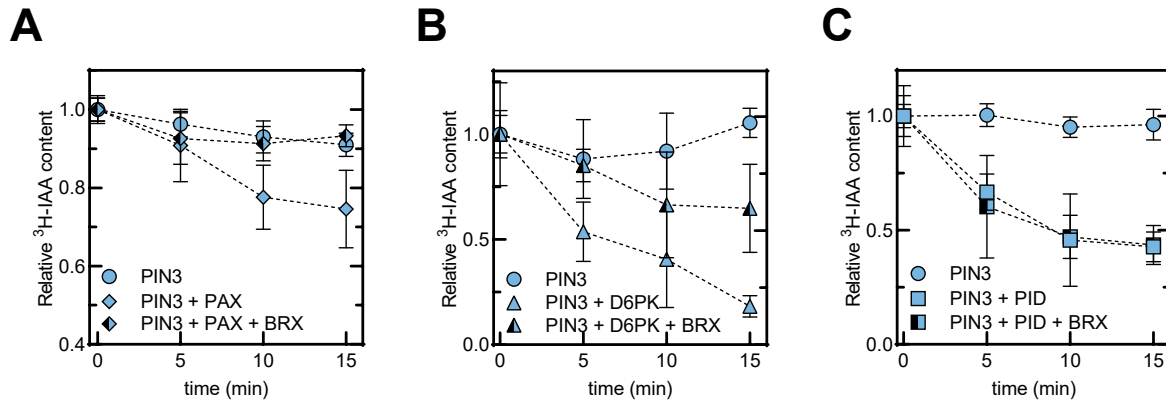


**Fig. 4-23 Effect of BRX on PIN-mediated IAA efflux activated by AGC1 or AGC3 kinases.** IAA efflux assay was performed with oocytes expressing PINs and kinases as specified. Reduction of  $^3\text{H}$ -IAA content over time, data points represent mean and standard error from  $n=6-10$  oocytes. The dotted lines support the better visualization of the course of labeled IAA content and do not represent linear regression graphs. Co-expression of BRX inhibits activation of PIN3 by (A) PAX and (B) D6PK from the AGC1 subclade, but not activation by (C) PID from AGC3 the subclade.

The *Arabidopsis* genome encodes five BRX family proteins, BRX and BRX-LIKE (BRXL) 1 to 4 and my results prompted me to further examine BRX function as well as the role of the other BRX family proteins. The respective proteins exhibit high sequence similarity and contain four highly conserved domains (Briggs *et al.*, 2006): the N-terminus which confers PM association (Scacchi *et al.*, 2009), an adjacent domain with a conserved “KDMA” motif and two so-called “BRX domains” in tandem (Christian Hardtke, pers. comm.). Further, BRX is suggested to constitute potential target sites for AGC kinases such as D6PK or PAX (Christian Hardtke, pers. comm.). I was interested if BRXL2 inhibits PAX activation of PINs as efficiently as BRX.

In the IAA efflux assays I performed, the reduction of  $^3\text{H}$ -IAA content over time of oocytes expressing either PIN1 + PAX + BRX and PIN1 + PAX + BRXL2, respectively differed marginal (**Fig. 4-24 A** left panel) and therefore, an interpretation of the result in this way was not possible. Thus, I decided to plot the exported IAA (fmol) after the end of the experiment as compared to the baseline set by the average of the PIN1 sample (**Fig. 4-24** right panel). I found that BRXL2 could not reduce auxin efflux of PIN1 + PAX to the same extent as BRX, suggesting that in comparison to BRX, BRXL2 is only a weak antagonist of PAX. This result was published as a contribution to Marhava *et al.* 2020.

Moreover, I included a BRX variant in my experiments, in which the three serines in the potential D6PK/PAX R(D/E)S target sites were substituted by alanines (BRX-KO). BRX-KO was tested for its inhibitory effect on PIN3 + D6PK in individual experiments and I calculated the respective transport rates (**Fig. 4-24 B**). I found that BRX-KO was as efficient as wildtype BRX in inhibiting D6PK-stimulated auxin efflux. This suggests that PAX- and D6PK-targeted

phosphosites contribute to the fine-tuning of BRX function. This result was published as a contribution to Koh *et al.*, 2021.

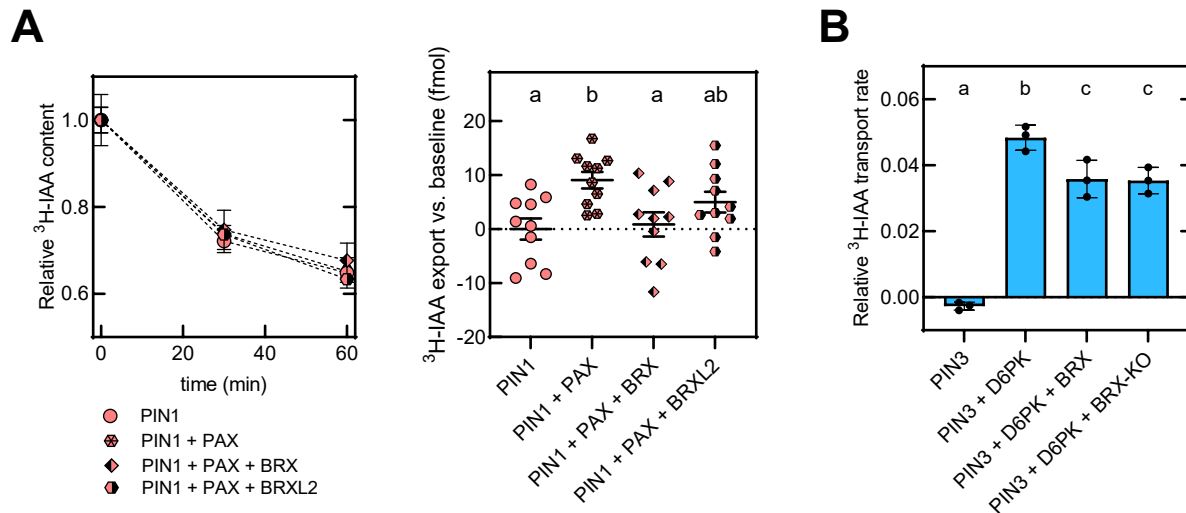


**Fig. 4-24 Effect of BRXL2 and BRX-KO (serines in the potential D6PK/PAX target sites are substituted by alanines) on PIN-mediated IAA efflux in comparison to wild type BRX in *X. laevis* transport assays.** IAA efflux assay was performed with oocytes expressing proteins as specified. **(A)** Left panel: Reduction of  $^3\text{H}$ -IAA content over time, data points represent mean and standard error from  $n=9-10$  oocytes. The dotted lines support the better visualization of the course of labeled IAA content and do not represent linear regression graphs. The individual constructs differ marginally. Right panel: Data points indicate fmol of  $^3\text{H}$ -IAA exported after 60 minutes as compared to the baseline set by the average of the PIN1 sample ( $n = 10$  oocytes per time point). Statistically significant different groups (a and b, one-way ANOVA) are indicated. BRXL2 does not reduce auxin efflux of PIN1 + PAX to the same extent as BRX. **(B)** Calculated transport rates from three individual biological replicates. BRX-KO is as efficient as wild type BRX in inhibiting D6PK-stimulated auxin efflux. Different letters indicate significant differences. Statistical analysis was performed by means of a one-way ANOVA (All Pairwise Multiple Comparison Procedures) followed by Tukey post hoc test.



## 5. Discussion

### 5.1 Characterization of PIN8 and the transport mechanism of the PINs

Non-canonical PIN8 predominantly localizes at internal membranes, and it is postulated to mediate IAA export from internal compartments into the cell lumen to maintain intracellular IAA homeostasis (Bosco *et al.*, 2012; Ding *et al.*, 2012; Lee *et al.*, 2020a). Specifically, a model has been described in which ER-resident PIN5 and PIN8 act antagonistically, with PIN5 transporting IAA into the ER lumen and PIN8 transporting IAA out of the ER into the cytosol (Ding *et al.*, 2012). However, if PIN8 transports IAA remained to be shown, even though preliminary data from my Master's thesis (Kolb, 2015) pointed in that direction. PIN5 on the contrary does not show IAA transport in the oocyte system (Kolb, 2015).

When expressed in the oocyte system, transport rates (**Fig. 4-1**) of PIN8 were significantly higher than non-activated PIN3 (**Fig. 4-9 A**), similar to activated PIN1 (Ung *et al.*, 2022). This transport activity was independent of the identity of co-expressed kinases, D6PK or PID (**Fig. 4-9 A**) and sensitive to the inhibitor NPA (**Fig. 4-9 B**). Collectively, this demonstrates for the first time clearly that PIN8 is a functional IAA efflux carrier in the absence of a kinase and draws a more profound picture of its suggested role in regulating intracellular IAA homeostasis required for pollen and lateral root development (Bosco *et al.*, 2012; Ding *et al.*, 2012; Lee *et al.*, 2020a).

Building up on my data, biophysical analyses of PIN8 were performed within the frame of a collaboration (Ung *et al.*, 2022). In this collaboration, we used solid supported membrane (SSM) electrophysiology (Schulz *et al.*, 2008) to measure PIN8 IAA transport activity and to describe its kinetics. The Michaelis constant  $K_m$ , defined as the concentration of substrate that is transported at half the maximal velocity of transport, is a measure of the affinity of the transporter for its substrate. We showed that PIN8 has a relatively low apparent affinity for IAA with  $K_m = 356 \pm 136 \mu\text{M}$ , which is 5-500-fold lower than the physiological concentrations of auxin in plant tissues of 0.1-10  $\mu\text{M}$  (Petersson *et al.*, 2009). Further, the dissociation constant ( $K_d$ ) of IAA binding was measured to be 39.9  $\mu\text{M}$ . These findings indicate that at physiological IAA concentrations, PIN8 transport rates are linear i.e. significantly below  $K_m$ . This is true for canonical PINs, as has recently been shown (Janacek *et al.*, submitted), and implies that the distinct functions of AtPINs in the plant body in regulating PAT are not enabled by direct modulation of their substrate affinity but rather by other factors like their expression level, differing abundance in the PM, localization and auto-inhibition properties (Hammes *et al.*, 2022).

We used single-particle cryo-EM and solved three structures of PIN8: two outward-facing conformations with and without auxin, and one inward-facing conformation bound to NPA (Ung *et al.*, 2022). The latter confirms Abas *et al.* (2020) and more on this mechanism will be discussed below (5.3.1). In the structures, PIN8 is seen as a dimer. Each monomer is composed of ten transmembrane helices and divided into a scaffold domain (Helices 1, 2, 6, and 7) and a transporter domain (Helices 3 – 5 and 8 - 10), whereat the scaffold domain creates the dimer interface. The transporter domain harbors an X-shaped crossover by helices 4 and 9, constituting a clearly defined auxin binding site (**Fig. 5-1 A**). All residues defining the binding pocket show high sequence conservation across different plant species and are fully conserved in all *AtPIN* proteins except for PIN5 (**Fig. 5-1 B**). The high conservation of the binding pocket indicates that the observations regarding PIN-mediated IAA transport can be generalized (Bennett *et al.*, 2014) and that PIN8 is more closely related to the canonical PINs than it is to non-canonical PIN5 and semi-canonical PIN6, suggesting that PIN8 lost the loop during evolution. This draws a new picture of the clustering of the PIN family members in comparison to previous alignments (Mravec *et al.*, 2009; Bennett *et al.*, 2014; Viaene *et al.*, 2013). Further, it ascribes a certain peculiarity to PIN5 and questions if PIN5 is an IAA transporter, which would be in line with the fact that PIN5 is the only *AtPIN* that does not show IAA transport in the oocyte system. With the structural data obtained, PIN8 is the only non-canonical PIN for which convincing evidence exists that it is an IAA transporter. Next to the binding site, we found what was called “support site”, with several key residues that seem essential for the transport mechanism and the structure revealed that the ligand recognition of the PINs is based on shape complementarity.

Collectively, our data suggest that PINs are secondary active uniporters, independent of proton and ion gradients, probably driven by the negative charge of auxin, and that they work by a cross-over elevator mechanism. We propose the following model for PIN-mediated IAA transport (**Fig. 5-1 A**): At the cytosolic side, deprotonated IAA<sup>-</sup> enters the binding site between the transport and scaffold domains of the PIN (inward-facing conformation). The molecule is stabilized and held in place via its negatively charged carboxylate group, while the two crossover motifs of the scaffold domain recognize the carbon backbone and indole ring. This is followed by a transition to the outward-facing conformation by a rotation of the crossover and the auxin binding site in the scaffold domain is translated away from the cytosol. At the non-cytosolic side, IAA is released, probably facilitated by a pH shift that protonates and neutralizes the carboxylate. After the release of IAAH, the PIN reverts to the inward-open state.

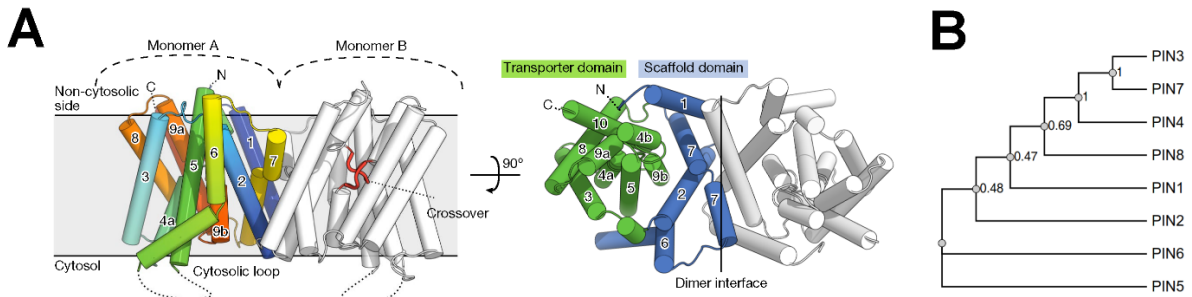


**Fig. 5-1 The structure of PIN8 and a dendrogram of the relationship between AtPIN1 – PIN8. (A)** Left: Side view of dimer PIN8 composed of monomers A and B with TMD 1–10 of each monomer labeled. The central crossover of helices within TMD4 and TMD9 is highlighted in red. Right: Top view from the non-cytosolic side displays the dimer interface and the transporter domain (green) and the scaffold domain (blue) in each monomer. **(B)** The dendrogram is based on sequence-alignments of the IAA binding site and the numbers denote bootstrap values of 500 trials. PIN8 is in a clade with the canonical PINs, unlike semi-canonical PIN6 and non-canonical PIN5. Figure modified from Ung *et al.*, 2022.

The discovery of the structure of the PINs and their IAA transport mechanism we published in Ung *et al.*, is groundbreaking as it has been sought after since the cloning of the first PIN family member (Gälweiler *et al.*, 1998). Our clustering of the PIN family members shifted the perspective towards the PIN family members and their relationship to each other. Lastly, our results call into question if PIN5 is an IAA transporter and with PIN8 transporting IAA out of the cytosol, we disprove the topology and antagonistic function of PIN5 and PIN8 stated by Ding *et al.* (2012): If at all ER-localized PIN5 transports IAA antagonistically to PIN8, I postulate based on my results that PIN5 transports IAA out of the ER-lumen into the cytosol and not the other way round.

## 5.2 The canonical loop regulates PIN activity by an inhibitory interaction with the TMD and contributes to IAA transport

The function and role of the PIN loop and TMDs have been a matter of debate since the prediction of the tripartite domain structure. The canonical loop includes diverse motifs for phosphorylation, crucial for polarity control (Kleine-Vehn *et al.* 2009, 2011; Dhonukshe *et al.* 2010; Huang *et al.* 2010; Ding *et al.* 2011; Ganguly *et al.* 2012, 2014; Weller *et al.* 2017) and regulation of IAA transport (Zourelidou *et al.*, 2014). Regarding the latter, the auto-inhibitory effect of the loop is overcome by phosphorylation carried out by AGCVIII protein kinases like D6PK and PID (Zourelidou *et al.*, 2014). The details of this process have been unresolved to date, however, a similar mechanism similar has been described quite recently for SbtA, a sodium-dependent bicarbonate symporter found in the carbon uptake mechanism of cyanobacteria (Fang *et al.*, 2021; Liu *et al.*, 2021). SbtA forms a complex with its partner protein SbtB, which allosterically regulates the transport activity of SbtA. It was found that in

the presence of AMP, the loop of SbtB binds to SbtA, locks it in an inward-facing state and inhibits its transport activity.

Transport assays of loop donor PIN2 could not be performed when I was working in the lab due to technical reasons. However, my colleague Dorina Janacek is now able to measure PIN2-mediated IAA transport. She found that PIN2 and PIN3 differ in their transport properties in that PIN2 is not as efficient in transporting IAA as PIN3 (Dorina P. Janacek, pers. comm.). When I measured IAA transport activity of PIN8-2-8 and PIN8-3-8 (**Fig. 4-11 A**), I found that the chimaeras vary in the characteristics they adopt from their “parents” in that PIN8-2-8 is constitutively active like TMD-donor PIN8, whereat PIN8-3-8 needs to be activated by co-expressed D6PK or PID for IAA transport, i.e. in the same TMD context, only the PIN3 loop is inhibitory. This means that i) the inhibitory effect of the canonical loop is mediated not solely by the canonical loop but by a specific interaction between loop and TMD or certain motives within it and that ii) given the predicted co-evolution of PIN loop and PIN TMD (Zhang *et al.*, 2020a) this interaction can only take place between the more closely related PIN3 and PIN8 (**Fig. 5-1**), but not between the more distant related PIN8 and PIN2. In both cases, co-expression of the kinases enhances transport activity and here, like seen in canonical PINs (Zourelidou *et al.*, 2014), PID is more efficient in activating than D6PK. This implies that providing a non-canonical PIN with a canonical loop can turn the non-canonical PIN to some extent into a canonical PIN and that the loop carries features determining IAA transport properties of canonical PINs. Moreover, the fact that the transport rates of both chimaeras were upon activation higher than the transport rates of PIN8, implies that the loop is more than an “on/off” switch of the PINs but that the loop contributes to IAA transport carried out by PINs - either “alone” or together with the TMD (context) and the kinase.

Regarding the inhibitory effect of the loop, it is possible that the interaction between loop and TMD results in that the loop “covers” the IAA binding side so IAA binding is prevented and that phosphorylation of the loop resolves the interaction, so that the binding site is accessible and transport can occur. However, in the light of the close relationship of PINs to HCO<sub>3</sub><sup>-</sup>/Na<sup>+</sup> symporter (Ung *et al.*, 2022), it seems more likely that the canonical loop operates by a similar mechanism like observed for the allosteric inhibition of SbtA by SbtB, i.e. the loop locks the PIN in its inward-facing conformation, which is resolved by phosphorylation, allowing the PIN to switch in its outward-facing state. The additive effect of the kinase seems to have structural reasons and suggests that IAA transport by the loop and inhibition by the loop must be considered two different mechanisms. As an interesting next step, chimaeras could be created with truncated versions of the canonical loop to unravel elements of the loop which account for regulation of transport and inhibition. The fact that PIN monomers work independently, but nevertheless form homo- and possibly hetero-dimers (Ung *et al.*, 2022),

and might be in complex with the activating kinase as well as phosphatases, adds additional complexity to the regulation of PIN transport activity *in planta*, which will be interesting to unravel.

Regarding PIN subcellular localization, even though the cell type seems to contribute, it is suggested that the mutual matching of TMDs between the N- and C-termini is crucial for the correct localization and moreover, that not only the canonical loop is decisive for correct PM localization as has long been thought, but that the PINs underwent an intramolecular domain-domain coevolution between loop and TMD to jointly determine the subcellular membrane localization (Zhang *et al.*, 2020a). PIN2 shows a polar localization in epidermal (apical) and cortical (basal) cells of the root (Luschnig *et al.*, 1998; Müller *et al.*, 1998) and defects in PIN2 polarity or expression cause the agravitropic *pin2* root phenotype (Müller *et al.*, 1998; Abas *et al.*, 2006; Rahman *et al.*, 2010). Apically localized PIN2 exclusively transports auxin from the root tip to the elongation zone to mediate root gravitropic growth (Müller *et al.*, 1998; Baster *et al.*, 2012; Zhang *et al.*, 2019b) and apical localization to mediate shootward auxin flux is crucial to replace PIN2 (Zhang *et al.*, 2019b). Of the canonical PINs only PIN2 is able to fully complement the defective root gravitropism phenotype of *pin2*, the other canonical PINs rescue partially (Zhang *et al.*, 2019b). PIN8-2-8-2 slightly mitigated the *pin2* phenotype in gravitropism (**Fig. 4-13**) and GUS-staining pattern (**Fig. 4-14**), and PIN8-2-8-GFP localized to the PM (**Fig. 4-15**). PIN8-3-8 had no moderating effect on the root phenotype (**Fig. 4-13** and **Fig. 4-14**). Still, considering that TMD-donor PIN8 is not expressed in root tissue, pointing to structural limitations of the fully synthetic chimaeras *in planta*, the results may serve as a proof of concept for the conclusions drawn from the transport assays that a non-canonical PIN is turned into a canonical PIN when provided with a canonical loop. Performing rescue experiments with the chimaeras in other canonical PIN mutants might be an interesting alternative: The non-phototropic *pin347* mutant (Willige *et al.*, 2013) can be rescued by complementation with single PIN3, PIN4 or PIN7 (Wang *et al.*, 2021; Zourelidou *et al.*, 2014) and consequently, rescue experiments in the *pin347* mutant make an interesting alternative to put the hypothesis to the test. Further, it would be of interest to see if other properties of the canonical PINs, NPA-sensitivity and BFA-sensitivity (Zhang *et al.*, 2020b), are displayed by the chimaeras and their functional GFP-tagged versions (**Fig. 4-11**). Lastly, if providing PIN8 with the PIN2-loop is sufficient to evoke PIN2-like polarity (Müller *et al.*, 1998) remains to be estimated.

### 5.3 PIN substrate specificity and modulation of PIN-mediated IAA transport

One goal of my thesis was to investigate if PIN-mediated IAA transport can be modulated by other substances present. The oocyte system allows for the direct injection of substances, enabling precise internal application in controlled doses. I co-injected different substances of interest together with  $^3\text{H}$ -IAA into oocytes and expected to observe altered PIN  $^3\text{H}$ -IAA transport rates in case a substance interfered with PIN-mediated transport. The presence of unlabeled IAA, competing with the radiolabeled  $^3\text{H}$ -IAA, led to a decrease of  $^3\text{H}$ -IAA transport rates (**Fig. 4-2** and **Fig. 4-3 A** upper and lower panel). This was highly significant in the case of PIN3, which is a strong IAA transporter in the oocyte system, and visible, although not significant in the case of PIN1, which is a weak IAA transporter in the oocyte system. This can be explained by the fact that for a transporter, which shows only weak transport activity, the signal-to-noise ratio is low, and an alteration of the transport rates is only marginal. Still, the data gained for PIN1 is in decent agreement with the results of PIN3 and collectively, the oocyte system and the chosen set-up were found to be generally suitable to investigate the effect of potential modifiers of PIN-mediated IAA transport (**Table 4-2** and **Fig. 4-3 A** upper and lower panel), most of which were later tested if they elicit a current response in PIN8 using SSM electrophysiology within the frame of a collaboration (Ung *et al.* 2022, **Fig. 5-2**).

#### 5.3.1 NPA directly inhibiting PINs causes the physiological effects of NPA

The PAT inhibitor **NPA** is a popular tool among plant physiologists investigating IAA transport. Despite its frequent use, its exact mode of action and where exactly it binds has been sought after for decades and many potential NPA binding targets have been debated. For instance, ABCBs showed high-affinity NPA binding and NPA-sensitive auxin export (Petrášek *et al.*, 2006; Geisler *et al.*, 2017; Noh, 2001; Bailly *et al.*, 2008) as well as their chaperone TWD1 binds NPA though only under certain conditions (Bailly *et al.*, 2008). On the contrary, a substantial body of literature clearly points to the PIN family as the target of NPA, not least the fact that NPA treatment phenocopies the pin-shaped *pin1* (Okada *et al.*, 1991; Reinhardt *et al.*, 2000; Xu *et al.*, 2005), the agravitropic *pin2* (Brown *et al.*, 2001; Rashotte *et al.*, 2000) and the non-phototropic *pin3* (Matsuda *et al.*, 2011) mutant, respectively. Nevertheless, a direct molecular association of NPA with PINs has never been reported (Kim *et al.*, 2010; Teale and Palme, 2018). In addition, NPA acting through the regulation of protein phosphorylation has been proposed and in particular, PID has been debated as NPA target: For instance, Benjamins *et al.* describe PID to be NPA sensitive based on the observation that root defects of *35S::PID* alleles can be rescued by NPA treatment (Benjamins *et al.*, 2001) while on the

contrary, studies by Henrichs *et al.* show that PID phosphorylation activity is NPA-insensitive (Henrichs *et al.*, 2012).

My observation that NPA abolished both PIN1- and PIN3-mediated <sup>3</sup>H-IAA export in the oocyte system suggested the PINs to be direct target of NPA. However, at first glance, it allowed for several explanations. To start with, the possibility of NPA negatively affecting the activating kinases D6PK and PID could be ruled out by several lines of evidence: First, inhibition of both PIN1 and PIN3 transport activity was independent of the identity of the activating kinase (**Fig. 4-3** and **Fig. 4-4**). Second, PIN6 and PIN8, which transport IAA independent of activating kinases (**Fig. 4-9 A** and **Fig. 4-16**), could be inhibited by NPA (**Fig. 4-9 B** and **Fig. 4-17**). Third, D6PK auto- and trans-phosphorylation activity was not impaired in presence of NPA (**Fig. 4-7**). Thus, my results disprove suggestions that NPA acts through the regulation of protein phosphorylation and support Henrichs *et al.* (2012), who state that NPA does not target PID. Next up, the possibility of NPA competing for IAA transport could be rejected as I showed that <sup>3</sup>H-NPA is not transported by PINs (**Fig. 4-5**), which is in line with previously published data, demonstrating that NPA is not polarly transported in maize (Thomson *et al.*, 1973). Lastly, the possibility of NPA being a general (IAA) transport inhibitor was ruled out by the fact that the transport activity of neither IAA importer *AtAUX1* (Yang *et al.*, 2006) nor Leucin transporter *AtCAT6* (Hammes *et al.*, 2006) was affected by co-injected NPA (**Fig. 4-8 A** and **B**). By applying NPA outside, I found that adding NPA to the external medium of pH 7.5 at the start of the assay was ineffective in inhibiting PIN-mediated <sup>3</sup>H-IAA export, as has been observed before (Absmanner, 2013) and only a prolonged incubation time or changing to a plant-type medium of pH 5.5 led again to an inhibition of PIN-mediated <sup>3</sup>H-IAA transport (**Fig. 4-6 A** and **B**). This is in line with previous reports, suggesting passive and pH-dependent IAA uptake into maize coleoptiles (Sussman and Goldsmith, 1981), and shows that NPA must be inside the oocyte in order to inhibit <sup>3</sup>H-IAA efflux. Collectively, my data highly suggest an intracellular interaction of NPA with PINs.

Together with the work of colleagues within the frame of a collaboration (Abas *et al.* 2020), my suggestions were confirmed by several lines of evidence including classical *in situ* membrane binding assays in heterologously PIN-enriched oocyte, yeast, and *N. benthamiana* membranes and quantitative multiplexed mass spectrometry (QMS), leaving the PINs as the most plausible binding target. Collectively, in Abas *et al.* 2020 we showed for the first time clearly that NPA directly targets and inhibits PINs, independently of any plant-derived components and other potential NPA-binding proteins. Shortly after, our findings were confirmed by another group (Teale *et al.*, 2021). Importantly to note is that in our paper, we suggested that NPA inhibits PINs allosterically. This was based on the finding that in the binding assay in *N. benthamiana* microsomal membranes heterologously enriched for PINs,

an addition of excess IAA (10 $\mu$ M) did not wash out <sup>3</sup>H-NPA. Within the frame of my more recent collaboration (Ung *et al.*, 2022) this assumption was overruled and we were able to investigate the NPA-PIN interaction in more detail. By using SSM electrophysiology (**Fig. 5-2**) and by measuring the current response of NPA-bound PIN8 towards IAA titration, we found that NPA inhibits PINs competitively with an inhibition constant ( $K_i$ ) of 1.9  $\mu$ M. This suggests an affinity of PINs towards NPA one order of magnitude higher than the affinity of PINs towards IAA. Consequently, the concentration of IAA used in the binding assay in Abas *et al.* was too low to wash out the bound NPA. Further, using single-particle cryo-EM, we solved the structure of the inward-facing conformation of NPA-bound PIN8. In the NPA-bound form of the PIN8 dimer, the scaffold domains and the dimeric interface were unchanged relative to the apo-PIN8, but the two transporter domains were rotated, resulting in a translocation of the binding site. Due to a different and particularly stronger interaction of the NPA molecule with the residues in the IAA binding pocket and several new interactions with the scaffold domain, the PIN gets stalled in the inward-open state. This means that we can explain PIN inhibition by NPA i) by a stronger binding of NPA due to engagement of additional residues from the scaffold domain and ii) by NPA preventing the transition of the PIN to the outward, IAA releasing state due to NPA's larger size (**Table 4-2**).

By now, with PIN1 (Yang *et al.*, 2022) and PIN3 (Su *et al.* 2022), three structures of PINs are published in total and all of them see NPA bound to the protein. This means that it is now established beyond doubt that PINs are the NPA target and that this interaction is the reason for the known physiological effects of NPA on plant growth by PAT-inhibition. This parsimonious, mechanistic explanation has long been sought after and disproves numerous publications stating that NPA does not bind to PINs. The findings inform our understanding of the substrate recognition and transport mechanisms of PINs and set up a framework for future research on polar auxin transport, which is one of the most crucial processes underlying plant development. The NPA-bound structure could provide the basis for structure-based development of novel herbicides and in the light of the data, reinterpretation of past publications to reconsider possible overlooked effects or contributions due to NPA binding by PINs should be considered.

### **5.3.2 Investigation of further potential modulators of PIN IAA transport**

**2,4-D** is the canonical synthetic auxin and the first to be commercially developed (Peterson *et al.*, 2016). At low concentrations it efficiently stimulates plant growth, whereat its application at high dosages is toxic for dicot development. It mimics IAA at the molecular level, whereas in comparison to IAA, 2,4-D is more stable (Grossmann, 2010, 2000; Song, 2014). 2,4-D not only is a widely used herbicide but also is used extensively to study auxin-related activities.



However, its intercellular transport is not fully understood: Whereat the import of 2,4-D into the cell likely is mediated by AUX1 (Marchant *et al.*, 2002), its export out of the cell is in question. It has been suggested that 2,4-D is not transported by auxin efflux carriers (Delbarre *et al.*, 1996), but by PDR9/ABCG37 (Ito and Gray, 2006; Strader *et al.*, 2008). Other studies on the contrary, suggested that PIN6 has the potential to transport 2,4-D (Simon *et al.*, 2016) and cultured tobacco BY-2 cells expressing PIN proteins display IAA and 2,4-D efflux (Petrášek *et al.*, 2006). Further, a sensitivity of 2,4-D transport towards NPA has been observed (Hošek *et al.*, 2012; Goggin *et al.*, 2016) and with PINs being inhibitable by NPA as shown in this thesis, this indicates that PINs transport 2,4-D. In my experiments, even though co-injection into the oocytes displayed a high variability in affecting PIN-mediated IAA transport, it showed a clear trend to decrease the transport rates. Further, 2,4-D elicited a current response in PIN8 as strong as IAA (Ung *et al.*, 2022). Collectively, the results suggest that in addition to other transporters, PINs transport 2,4-D, mediating its export out of the plant cell.

**NAA**, another synthetic auxin analog, is used broadly to exogenous manipulate auxin distribution and signaling. Here, NAA is often favored over the endogenous IAA, even though there are indications that IAA and NAA have differential activities in the cell (Paciorek *et al.*, 2005). NAA competes with IAA for transport (Depta *et al.*, 1983) and cultured tobacco BY-2 cells expressing PIN proteins display <sup>3</sup>H-NAA efflux (Petrášek *et al.*, 2006). In my experiments co-injected NAA significantly reduced PIN-mediated IAA transport and further, NAA elicited a current response in PIN8 similar to IAA (Ung *et al.*, 2022). Taken together, this strongly suggests that PINs transport NAA and that in this context it is feasible to thoughtfully draw conclusions from experiments using exogenous NAA to study (PIN-mediated) auxin transport.

**TIBA** is known to inhibit the polar transport of auxin in plants (Thomson *et al.*, 1973). As it is a weak aromatic acid, protonated TIBA is thought to diffuse into cells in a way similar to IAA (Depta *et al.*, 1983) and it has been suggested to be polarly transported in a manner similar to IAA (Thomson *et al.*, 1973; Depta *et al.*, 1983). It has been shown that TIBA inhibits the binding of IAA to membranes *in vitro* (Thomson *et al.*, 1973) and that it competes with IAA in *in vitro* binding assays in plant tissue (Jablanović and Noodén, 1974). With regards to the PINs, TIBA has been shown to interfere with PIN PM cycling (Geldner *et al.*, 2001) and it is debated whether PINs transport TIBA, but there is no compelling evidence for this consideration. In my oocyte experiments, TIBA decreased PIN-mediated IAA transport and further, TIBA elicited a current response in PIN8 similar to IAA (Ung *et al.*, 2022). The way I interpret the results is that TIBA is a straightforward competitor for the PIN IAA binding site. If this however also leads to PINs transporting TIBA or if TIBA binds to PINs but is not transported (de Boer *et al.*, 2020) remains to be shown.

Regulated input from the auxin precursor **IBA** towards the pool of active IAA is a cellular mechanism to regulate auxin levels and response in addition to the biosynthesis of IAA and conversion of IBA to active IAA modulates developmental processes like lateral root formation (Strader and Bartel, 2011; Zolman *et al.*, 2008; Michniewicz *et al.*, 2019). Similar to IAA, IBA is thought to move long distances through the plant and several IBA transporters have been described (reviewed in Strader and Bartel 2011). For instance, IBA efflux is promoted by ABCG36/PDR8/PEN3 (Strader and Bartel, 2009) and ABCG37/PDR9/PIS1 (Růžička *et al.*, 2010; Strader *et al.*, 2008) and more recently, TOB1 has been identified as a vacuolar IBA transporter (Michniewicz *et al.*, 2019). Further, IBA seems to use carriers distinct from those that efflux IAA: Examined transporters of IAA, including PINs, are considered to not facilitate the transport of IBA (reviewed in Michniewicz *et al.* 2014). For instance, PIN inhibitor NPA does not alter IBA movement, suggesting that IBA transport is mediated by other proteins than PINs (Rashotte *et al.*, 2003). However, Ding *et al.* state that in competitive uptake assays with ER-enriched vesicle fraction from *PIN8OX* IBA competes with <sup>3</sup>H-IAA for uptake by PIN8 and they suggested that IBA is a substrate for PIN8 (Ding *et al.*, 2012). In my experiments, co-injection of IBA had no significant effect on PIN IAA transport rates and the current response IBA elicited in PIN8 was significantly lower than IAA (Ung *et al.*, 2022). Collectively, this suggests that PINs do not transport IBA, which is in line with the general opinion and contradicts Ding *et al.*, whose conclusions might be based on an artifact due to a missing positive control in their assay.

**Me-IAA** is generated by methylation of IAA by an IAA CARBOXYL METHYLTRANSFERASE (IAMT) (Qin *et al.*, 2005) and Me-IAA is an IAA conjugate, which contribute to the maintenance of auxin homeostasis in various processes (Woodward and Bartel, 2005). At the time I started my doctorate research, Miguel A. Blázquez. and colleagues were investigating the role of Me-IAA in maintaining the auxin homeostasis, particularly in the regulation of asymmetric auxin distribution across the hypocotyl as a prerequisite for differential growth in gravitropic response. They supposed that Me-IAA was an inactive form of IAA and that the conversion of IAA into Me-IAA was a fine-tuning mechanism that generates or maintains the correct local auxin concentrations in the hypocotyl of seedlings responding to gravistimulation. However, the possibility remained that a reduction in auxin methylation can indirectly affect auxin conjugation, or that Me-IAA itself has a direct role as a modulator of auxin signaling or transport. Upon the finding that co-injected Me-IAA reduced both PIN1- and PIN3-mediated IAA efflux to the same extent as IAA, we suggested that Me-IAA is transported by PINs and competes with IAA and that is rather unlikely that it acts as an allosteric inhibitor (Abbas *et al.*, 2018). This suggestion, however, is in conflict with the SSM electrophysiology findings of my more recent collaboration (Ung *et al.*, 2022). Here, it was found that the current response

elicited by Me-IAA was significantly lower than the response elicited by IAA. This indicates that Me-IAA is not transported by PIN8 and likely not by any other PIN, even though we cannot rule out the possibility that the observed current response was influenced by the different electrostatic potentials of uncharged Me-IAA and IAA. Consequently, the reduction of IAA transport by Me-IAA in the oocytes was not due to Me-IAA transport by PINs but due to other reasons.

**Tryptophan**, an essential aromatic amino acid, made an interesting candidate to be tested for its effect on IAA transport, as tryptophan is the main IAA precursor in the *de novo* IAA synthesis through the tryptophan-dependent pathway. This pathway involves various parallel routes with many intermediates, with many molecular components still largely unknown (Ljung *et al.*, 2001, 2005; Normanly, 2010; Petersson *et al.*, 2009; Zhao, 2010). Tryptophan resembles IAA as both contain an indole ring, the 3-position of which is connected to an amino acid moiety in tryptophan and a carboxyl group in IAA (**Table 4-2**). Cultured tobacco BY-2 cells expressing PIN proteins display efflux of IAA, NAA, and 2,4-D, but not of tryptophan (Petrášek *et al.*, 2006), and in line with this, in my experiments, co-injection of tryptophan did not reduce IAA transport rates. This implies that tryptophan does not modulate PIN-mediated IAA transport, suggesting, that tryptophan is no substrate for PIN transport.

The indolamine **serotonin** is a well-studied neurotransmitter with structural similarities to IAA (**Table 4-2**). There are several reports highlighting the roles of serotonin in plant development (Mukherjee *et al.*, 2014; Erland *et al.*, 2019a); it has been proposed to inhibit auxin activity and transport (Erland *et al.*, 2015; Pelagio-Flores *et al.*, 2011) and has been published to be transported in a polar manner through the vasculature towards the root tip in a manner reminiscent of auxin (Erland *et al.*, 2019b). In the oocyte system, I did not observe an impact of serotonin on PIN-mediated IAA transport. This is in line with results of the SSM electrophysiology assays, where serotonin did not evoke a current response in PIN8 (Ung *et al.* 2022). Collectively, the data suggest that the auxin effect of serotonin is mediated by auxin recognition and that serotonin transport through the vasculature is not carried out by PINs but by other membrane transporters.

**Trans-Zeatin** is the main cytokine, a group of plant hormones, which in crosstalk with auxin control various aspects of plant development at multiple levels (Moubayidin *et al.*, 2009). Three types of membrane transporters have been recognized and implicated in cytokinin transmembrane transport and intercellular translocation. These proteins include the subsets of purine permeases (PUPs), equilibrative nucleoside transporters (ENTs), and the ATP-binding cassette transporter G subfamily member (Liu *et al.*, 2019). Co-injected trans-Zeatin did not affect PIN-mediated IAA transport in the oocyte system and the current response the substance elicited was significantly lower than IAA (Ung *et al.*, 2022). We cannot

rule out the possibility that the observed current response was influenced by the different electrostatic potentials of uncharged trans-Zeatin and IAA, however the data collectively highly suggests that trans-Zeatin and likely cytokines in general are no substrate for PIN transport and that other membrane proteins mediate intercellular cytokine transport as has been suggested before.

**Quercetin** belongs to flavonoids, a class of secondary plant metabolites, which have been suspected to modulate auxin transport and tropic responses, but the identity of specific flavonoid compounds involved, and their molecular function and targets *in vivo* are not yet fully understood. Quercetin is a broadly used inhibitor of PAT (Jacobs and Rubery, 1988), seemingly by inhibiting PID (Henrichs *et al.*, 2012) and application of quercetin partially restores *pin2* root gravitropism (Santelia *et al.*, 2008), making quercetin an interesting candidate to be investigated in the context of PIN-mediated IAA transport. At first glance, co-injected quercetin did not influence IAA transport, however, the calculated  $^3\text{H}$ -IAA transport rates are an artifact: The measured cpm of oocytes injected with  $^3\text{H}$ -IAA + quercetin were many times lower than cpm of the control oocytes or the cpm measured for any of the other experiments (data not shown), and consequently, the calculated transport rates are falsified. The reason for the low cpm could be that quercetin acts as a chemical quencher in liquid scintillation counting and thus falsified the measured amount of radioactivity in the oocytes. Another possible explanation is that it affects the oolemma, making it porous for  $^3\text{H}$ -IAA. Collectively, I found the oocyte system to be unsuitable to investigate quercetin's effect on PIN-mediated IAA transport and another experimental setup should be chosen for future experiments to answer the question if quercetin specifically alters PIN-mediated IAA transport. A similar point can be made for **NBD-IAA**, a fluorescing IAA compound, which has been introduced as a promising tool to visualize IAA transport and transport sites (Hayashi *et al.*, 2014). Co-injection of NBD-IAA resulted in seemingly reduced IAA transport rates, however, it has to be taken into account that other than the other substrates tested, NBD-IAA was dissolved in the solvent DMSO. DMSO enhances the permeability of lipid membranes (Notman *et al.*, 2006), which likely affected the oolemma and consequently falsified the results. Thus, the experimental setup was unsuitable to investigate if NBD-IAA is a modulator of PIN-mediated IAA transport and no conclusion can be drawn from the results at this point.

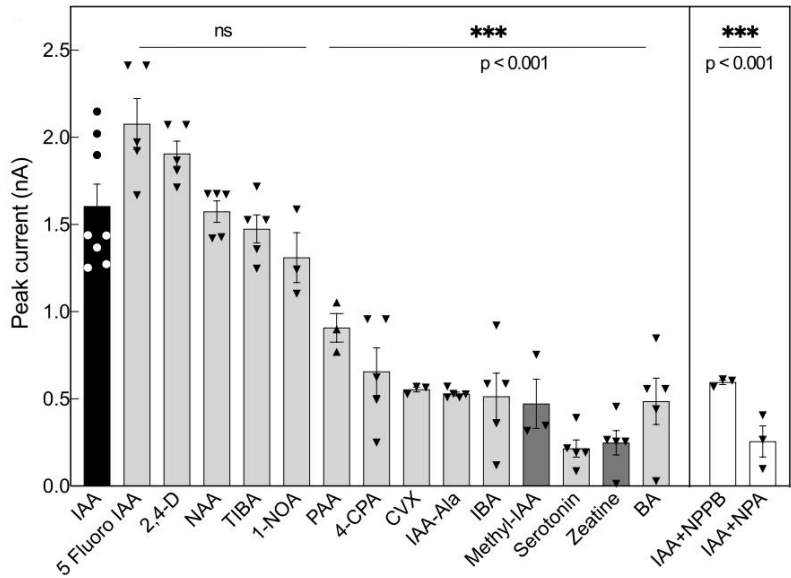


**Fig. 5-2 Results of SSM electrophysiology investigating substrate specificity of PIN8.** Peak currents elicited by IAA (●) or a range of putative substrates tested at 100 μM (▼). Experiments were performed at pH 7.4. 5-Fluoro IAA (NBD IAA)  $p = 0.011$ ; 2,4-D  $p = 0.272$ ; NAA  $p = 0.999$ ; TIBA  $p = 0.989$ ; 1-NOA  $p = 0.539$ ; PAA  $p = 0.0007$ ; 4-CPA  $p < 0.0001$ ; CVX  $p < 0.0001$ ; IAA-Ala  $p < 0.0001$ ; IBA  $p < 0.0001$ ; Methyl-IAA  $p < 0.0001$ ; Serotonin  $p < 0.0001$ ; Zeatin (trans-Zeatin)  $p < 0.0001$ ; BA  $p < 0.0001$ ; IAA+NPPB  $p < 0.0001$ ; IAA+NPA  $p < 0.0001$ . Substrates shown in dark grey are uncharged. Figure from Ung *et al.*, 2022.

In summary, the comparison of all substrates tested suggests that in PIN-mediated transport, shape complementary plays a large role in recognition of the substrate: While all synthetic auxins tested are likely a PIN substrate, the larger size of IBA, trans-Zeatin, and serotonin might be the reason that they are not transported by PINs and thus clearly questions transport of the relatively big NBD-IAA and the possibility to use it as a tool to visualize IAA transport (Hayashi *et al.* 2014). Given the high sequence conservation of the IAA binding pocket in all PINs (Ung *et al.*, 2022) it is rather unlikely that non-canonical and canonical PINs differ in their substrate spectrum as has been hypothesized (Bennett *et al.* 2014).

## 5.4 PIN6 is an exceptional member of the PIN family

Semi-canonical PIN6 has often been referred to as the intermediate PIN, due to the intermediate length of its loop as well as due to its dual subcellular localization that is PIN6 localizes both in endomembrane domains and at the PM (Simon *et al.*, 2016). In regulation of this localization, *PIN6* expression level and post-transcriptional modifications play a role. The PM-residing fraction of PIN6 exhibits a polarity and in polarity regulation, PID has been suggested to be involved (Simon *et al.*, 2016; Ditengou *et al.*, 2018). In terms of evolutions, recent results suggest that PIN6 is an invention of angiosperms and that it shares much closer common descent with canonical PINs such as PIN2, rather than with the non-canonical PINs and consequently that PIN6 is closer related to the canonical PINs than to the non-canonical PINs (Zhang *et al.*, 2020a; Bennett *et al.*, 2014; Ung *et al.*, 2022). In addition to its role in nectary function and regulation of nectary production (Bender *et al.*, 2013) PIN6 plays a role during auxin-mediated lateral and adventitious root organogenesis (Simon *et al.*, 2016), and

35S promoter overexpressing lines grow wavy roots, which are devoid of root hairs (Ditengou *et al.*, 2018; Cazzonelli *et al.*, 2013). Root hair growth is proportional to internal auxin levels in the root hair cell (Ganguly *et al.*, 2010), which suggests that overexpression of *PIN6* interferes with auxin availability in these cells and it has been hypothesized that auxin efflux inhibits, and auxin influx enhances, the outgrowth of the root hair cell (Cho *et al.*, 2008; Weijers and Wagner, 2016).

I showed for the first time clearly that *PIN6* transports IAA (**Fig. 4-16 A** and **Fig. 4-17**, Abas *et al.* 2020b). Moreover, the fact that the constitutive transport of IAA can be enhanced only by *PID* but not by *D6PK* has not been described before for any other *PIN* and therefore is a unique feature of *PIN6* within the *PIN* family. The identification of two TPRXS(N/S) *PID* target motifs within the *PIN6* loop (**Fig. 4-16 B**) is in line with previous publications (Ditengou *et al.*, 2018; Huang *et al.*, 2010) and the additive effect of *PID* on *PIN6* transport rates possibly involves *PID* phosphorylating the *PIN6* loop at these two sites, which remains to be shown. Considering the dual localization of *PIN6* at PM and ER, one intriguing interpretation of my results is that *PIN6* may have distinct functions based on its cellular location: When ER-localized, it constitutively transports IAA and contributes to regulation of intracellular auxin homeostasis by sequestering auxin from the cytosol into the lumen of the ER. When localized at the PM, it contributes to the intercellular IAA transport, and here, where it coincides with PM-localized *PID* (Barbosa *et al.*, 2014; Kleine-Vehn *et al.*, 2010b) its transport activity is enhanced by phosphorylation by *PID*, ascribing *PID*-mediated phosphorylation a role in regulation of *PIN6* polarity as well as *PIN6* IAA transport activity.

When expressed in the *PIN2* domain in *pin2* background, in my CLSM analysis *PIN6* localized both in endomembrane domains and at the PM (**Fig. 4-19**) and in the gravitropism assay, the agravitropic *pin2* phenotype could not be complemented (**Fig. 4-18 A**), which is in line with a recent publication (Zhang, Hartinger, *et al.* 2020). Further, I observed that the lines showed an impairment of the *pin2* phenotype with cloddy and wavy roots (**Fig. 4-18 B - I**), phenocopying *PIN6* overexpressing lines. Given the close relationship between *PIN2* and *PIN6*, this suggests that the expression of *PIN6* under the *PIN2* promoter is even higher than under the 35S promoter and that an increase in *PIN6* activity in the *PIN2* domain leads to an increase of malformation of root architecture *i.e.* a dose effect. In this sense, it would be interesting to investigate if the absence of root hair outgrowths described for the *PIN6* overexpressing lines is also found in my  $P_{PIN2}:PIN6$  lines as this would further underline the role of *PIN6*-mediated IAA transport in root hair development.

## 5.5 Identification of new regulators of PIN-mediated IAA transport

One member of the AGC1 clade (D6PK) as well as members of the AGC3 clade (PID/WAG) directly activate canonical PINs by phosphorylating the loop, while representatives from AGC2 (UCN) and AGC4 (PHOT) do not activate PIN-mediated IAA efflux (Zourelidou *et al.* 2014). Consequently, activation of PINs seems to be restricted to members of clades AGC1 and AGC3. As it has been suggested before that other, yet unknown kinases must be involved in activation of PINs (Weller *et al.*, 2017; Barbosa *et al.*, 2018), I tested further members of the AGC1 clade - AGC1-3 (PAX), AGC1-4 (PAXL), AGC1-7, AGC1-8, AGC1-9, and KIPK - for their potential to activate PINs in the oocyte system, of which PAX (Marhava *et al.*, 2018), AGC1.7 (Hiromasa Shikata, pers. comm.) and KIPK (Weller, 2017) have been shown to phosphorylate PINs *in vitro*. I found that co-expression of PAX, PAXL, AGC1-9, and KIPK does activate PIN-mediated IAA efflux and that co-expression of AGC1-7 and AGC1-8 does not activate PIN-mediated IAA efflux (**Fig. 4-20**). With that, I identified PAX, PAXL, AGC1-9 and KIPK as new, yet unknown direct activators of PINs, and my data suggests that AGC1-7 and AGC1-8 are not directly implicated in the activation of PIN-mediated IAA transport. Moreover, the finding that AGC1-7, which phosphorylates the PIN loop *in vitro* but does not activate IAA transport, suggests that phosphorylation is not sufficient to explain PIN activation. My findings significantly expand our current understanding of kinase-mediated activation of PINs (**Fig. 5-3**), which is indispensable for a better understanding of the regulation of PAT.

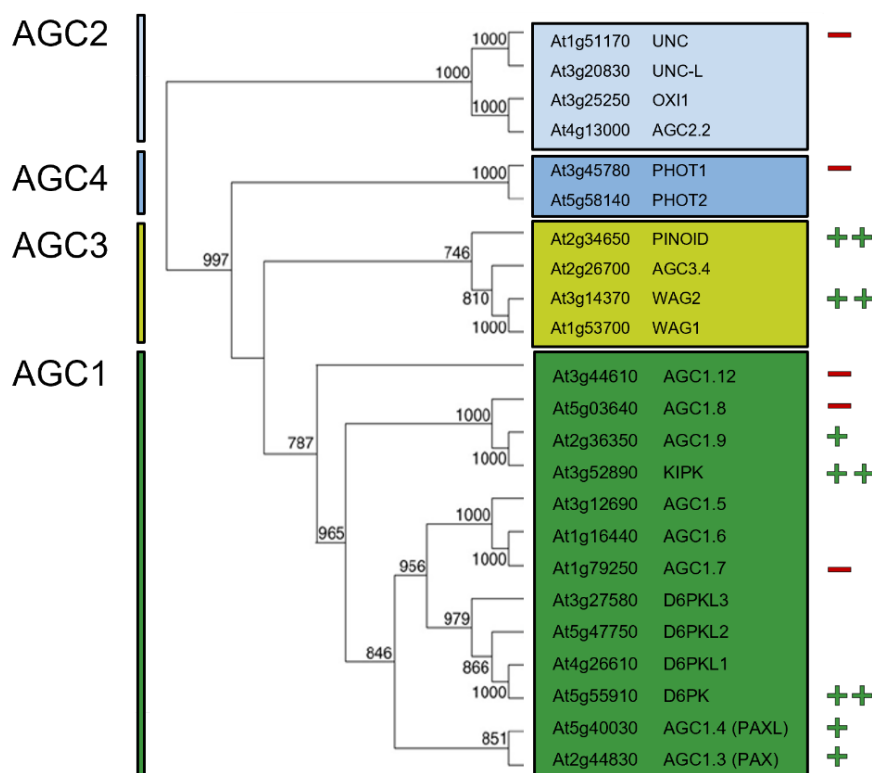


**Fig. 5-3 Members of the AGCVIII kinase family and their potential to activate PIN-mediated IAA transport.** Summary of previous data (Absmanner, 2013, Zourelidou *et al.*, 2014) and the results of this thesis as an overview of the current understanding of the activation of PIN-mediated IAA transport by AGCVIII kinases. Respective members of the family have been tested in the oocyte system and do not (-), do (+), or do strongly (++) activate PINs. Figure modified from Galván-Ampudia *et al.*, 2008 according to previous data (Absmanner, 2013, Zourelidou *et al.*, 2014) and data described in this thesis.

If PIN transport rates correlate with their phosphorylation status and if the kinases phosphorylate PINs with varying intensity is still not fully understood. Proteomics data of my colleague Dorina Janacek showed that the different PINs as well as the activating kinases D6PK and PID show similar abundance in the oocytes (Janacek, unpublished). In light of the observed kinase effect on the PIN kinetics, i.e. the finding that transport rates of activated canonical PINs vary depending on the co-expressed kinase, this suggests that PINs and different activating kinases form a heterodimer mediating IAA transport. A variation in phosphorylation intensity, willingness to phosphorylate and a different phosphosite preference hint at a differential mode of PIN binding or PIN activation by the kinases (Zourelidou *et al.*, 2014; Haga *et al.*, 2018) even though results from *in situ* analyses suggest that differential phosphosite preference does not necessarily have to be biologically relevant (Zourelidou *et al.*, 2014; Weller *et al.*, 2017; Barbosa and Schwechheimer, 2014).

Considering the close relationship and sequence similarity among the AGC1 kinases, particularly AGC1-7 and D6PK (Galván-Ampudia and Offringa, 2007; Humphrey *et al.*, 2015), an unanswered question pertains to why certain AGC1 kinases activate PIN-mediated IAA transport while others do not, and what underlies this functional divergence. Finding these answers will be exciting future research.

### **5.5.1 PIN, PAX and BRX constitute a molecular rheostat modulating auxin flux underlying protophloem sieve element differentiation**

In protophloem sieve element (PPSE) differentiation, the timing of differentiation is not uniform across cell files, and developing PPSEs differentiate as their neighboring cells still divide (Santuari *et al.*, 2011; Brunoud *et al.*, 2012). In this process, BREVIS RADIX (BRX) promotes the commitment of precursor cells to the differentiation program (Scacchi *et al.*, 2009; Beuchat *et al.*, 2010; Rodriguez-Villalon *et al.*, 2014) and within the frame of three of my collaborations, the role of BRX in PPSE differentiation was investigated.

BRX is specifically expressed in the developing protophloem cells, where it localizes basally at the PM (Scacchi *et al.*, 2009; Marhava *et al.*, 2018) and this PM association is negatively regulated by auxin threshold levels (Scacchi *et al.*, 2009). The *brx* mutant is characterized by a signature “gap phenotype” in the developing sieve element strand continuity (Anne and Hardtke, 2018; Rodriguez-Villalon *et al.*, 2014, 2015; Scacchi *et al.*, 2009), which manifests in a systemically reduced auxin response throughout the meristem (Gujas *et al.*, 2012; Rodriguez-Villalon *et al.*, 2014). Strikingly, the *pax* mutant represents a (hypomorphic) phenocopy of *brx* mutants and when my colleagues performed an expression analysis of PAX, they found it to co-localize with BRX (Marhava *et al.*, 2018). Moreover, in *pax* PPSEs BRX abundance was severely reduced (Marhava *et al.*, 2018), suggesting that PAX is required for



efficient BRX PM recruitment. Notably, PIN abundance was not affected in *pax* PPSEs (Marhava *et al.*, 2018). I found that BRX does not activate PIN-mediated IAA transport ( **Fig. 4-22**), but that it substantially inhibits IAA transport stimulated by PAX and also by D6PK (**Fig. 4-23 A and B**) whereat activation by the more distantly related PID was not affected by co-expression of BRX (**Fig. 4-23 C**). This suggests that BRX affects a subset of related AGC kinases and that its inhibitory effect is determined by the identity of the kinase.

The PM association of PAX is not sensitive to auxin, but auxin stimulates its kinase activity: phosphoproteomics indicated an auxin-induced phosphorylation of the PAX activation loop at phosphoserine S596, which correlated with simultaneously increased PIN1 phosphorylation (Marhava *et al.*, 2018). Phosphorylation of PAX may be conferred by recently identified, functionally redundant upstream regulators of D6PK and PAX, the 3-PHOSPHOINOSITIDE-DEPENDENT PROTEIN KINASES (PDK1) and PDK2 (Zegzouti *et al.*, 2006; Tan *et al.*, 2020; Xiao and Offringa, 2020). Matching our phosphoproteomics data, the PAX-S596D phosphomimic variant displayed an increased phosphorylation activity towards PIN1 in comparison to wild type PAX (Marhava *et al.*, 2018) and also in my oocyte experiments, the recombinant PAX-S596D stimulated auxin efflux considerably more than PAX or PAX-S596A, to a level approximately equal to D6PK (**Fig. 4-21**). However, unlike the wild type PAX, PAX-S596D not only is unable to rescue the *pax* mutant but also generated maldeveloped roots (Marhava *et al.*, 2018), collectively suggesting a highly fine-tuned auxin-dependent PAX activity in PPSE development.

BRX possesses three potential D6PK/PAX R(D/E)S target sites embedding the serines S217, S123, and S228 (Koh *et al.*, 2021). These serines seem to contribute to the fine-tuning of BRX function and modulate its auxin-responsiveness, as a BRX variant in which the serines were substituted by alanines shows normal expression and localization *in planta*, largely rescues the *brx* mutant phenotype (Koh *et al.*, 2021) and is still about as efficient as wild type BRX in inhibiting D6PK-stimulated auxin efflux in my oocyte assays (**Fig. 4-24 B**), but its PM-association does no longer display a significant auxin response (Koh *et al.*, 2021).

In summary, we postulate in Marhava *et al.* 2018 that PIN, PAX, and BRX constitute a “molecular rheostat” that fine-tunes the auxin flux through the developing sieve element cell file. In our model, BRX interacts with PAX at the PM, where inhibition of PAX by BRX suppresses PIN efflux activity at lower auxin levels. This in turn leads to increases in cytosolic auxin levels due to reduced PIN-mediated auxin efflux. Eventually, BRX dissociates, accompanied by PAX activation. PAX increasingly stimulates PIN-mediated IAA efflux by phosphorylation. Ultimately, reinforced through decreasing cellular auxin levels and auxin-induced BRX transcription (Scacchi *et al.*, 2009; Santuari *et al.*, 2011), BRX returns to the plasma membrane, where again, it inhibits PAX and PIN-mediated auxin efflux.

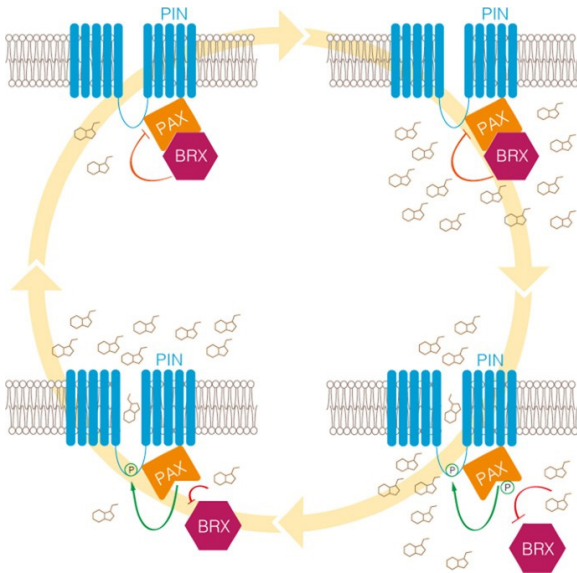


**Fig. 5-4 PAX and BRX constitute a “molecular rheostat” that regulates and fine-tunes PIN-mediated auxin efflux.** BRX interacts with PAX at the PM, where it inhibits PAX and consequently suppresses PIN efflux activity at low auxin levels. With increasing auxin level, eventually, BRX dissociates, and PAX becomes activated and stimulates PIN-mediated IAA transport by phosphorylation. Ultimately, reinforced through decreasing cellular auxin levels and auxin-induced BRX transcription, BRX returns to the PM, where again, it inhibits PAX and auxin efflux. This interplay modulates auxin flux through developing PPSEs, thereby timing PPSE differentiation. Figure from Marhava *et al.*, 2018.

### 5.5.2 Functional divergence of BRX family proteins

*BRX* has four homologs in *A. thaliana*, *BRXL1-4*. All five BRX family proteins display four conserved domains: the N-terminus, which confers PM association in the case of BRX (Scacchi *et al.*, 2009; Rowe *et al.*, 2019) a domain with a conserved “KDMA” motif and two signature “BRX domains” in tandem (Koh *et al.*, 2021). The domains are separated by variable spacer regions (Koh *et al.*, 2021). Previous data suggested limited yet tangible redundancy between BRX and other family members in the root (Koh *et al.*, 2021). The closest homolog of BRX, *BRXL1*, is mainly expressed in the mature vasculature (Scacchi *et al.*, 2009; Cattaneo *et al.*, 2019) and shows only a weak expression in the protophloem (Koh *et al.*, 2021). However, *BRXL1* can rescue the *brx* mutant phenotype when ectopically expressed (Beuchat *et al.*, 2010; Briggs *et al.*, 2006; Koh *et al.*, 2021) while by contrast, the more distantly related *BRXL2-4* can at best partial rescue the *brx* mutant phenotype, even though other characteristics are shared (Marhava *et al.*, 2020; Koh *et al.*, 2021). Notably, in contrast to BRX, PM association of *BRXL2* is not auxin responsive (Marhava *et al.*, 2020). I found that *BRXL2* is only a weak antagonist of PAX, which does not reduce auxin efflux to the same extent as BRX (**Fig. 4-24 A**), collectively suggesting that BRX and *BRXL2* differ in their activities and function and that these differential features might be responsible for the incapacity of *BRXL2* to fully substitute for BRX function. In the context of this differential activity of BRX and *BRXL2*, results of domain swapping experiments suggest that the linker between the tandem BRX domains has a crucial function. In the case of BRX, this linker contains the three putative R(D/E)S phosphosites, which are targeted by PAX or D6PK. *BRXL2* lacks these phosphosites (Koh *et al.*, 2021). A BRX variant in which all three sites were substituted by alanines (*BRX-KO*) shows normal expression and localization, but is not anymore able to fully rescue

the *brx* mutant phenotype (Koh *et al.*, 2021) indicating an impairment of its function. Further, PM association of BRX-KO does not display a significant auxin response anymore (Koh *et al.*, 2021), while interestingly, the variant was still about as efficient as wild type BRX in inhibiting D6PK-stimulated auxin efflux in my oocyte experiments (**Fig. 4-24 B**). Conversely, providing BRXL2 with S123, S217, and S228 imparts an BRX-like auxin responsiveness on BRXL2 and increases its functionality in the context of PPSE development (Koh *et al.*, 2021), where the native BRXL2 can only partially replace BRX (Briggs *et al.*, 2006; Beuchat *et al.*, 2010; Marhava *et al.*, 2020). Taken together, this suggests that the functional divergence within the BRX protein family resides mainly in the linker between the tandem BRX domains and that the PAX-and D6PK-targeted phosphosites S123, S217 and S228, contribute to the fine-tuning of BRX function and modulate its auxin-responsiveness. Further, the lack of auxin responsiveness seems to be one main difference between BRX and BRXL2 and auxin-responsive PM dissociation quantitatively determine BRX activity in the protophloem context.

## 6. Materials and Methods

### 6.1 Materials

#### 6.1.1 Biological material

##### 6.1.1.1. Plant lines

All *Arabidopsis thaliana* plants used in this study are based on ecotype Columbia Col-0, which is referred to as wild type in all experiments. The homozygous *pin2* mutant line (Müller *et al.*, 1998) was ordered from the Salk Institute for Biological Studies. All (transgenic) *Arabidopsis* lines used in this study are listed in **Table 6-1**.

Table 6-1 (Transgenic) *Arabidopsis* lines used in this study

Background	T-DNA construct	Provided by/Reference
Col-0	P <sub>DR5</sub> :GUS	Ulrich Z. Hammes / Ulmasov <i>et al</i> 1997a
<i>pin2</i>	P <sub>PIN2</sub> :PIN2 CDS	Dorina P. Janacek
<i>pin2</i>	P <sub>PIN2</sub> :PIN3 CDS	Dorina P. Janacek
<i>pin2</i>	P <sub>PIN2</sub> :PIN6	This thesis (Floral dip)
<i>pin2</i>	P <sub>PIN2</sub> :PIN6-GFP	This thesis (Floral dip)
<i>pin2</i>	P <sub>PIN2</sub> :PIN8	This thesis (Floral dip)
<i>pin2</i>	P <sub>PIN2</sub> :PIN8-2-8	This thesis (Floral dip)
<i>pin2</i>	P <sub>PIN2</sub> :PIN8-2-8-GFP	This thesis (Floral dip)
<i>pin2</i>	P <sub>PIN2</sub> :PIN8-3-8	This thesis (Floral dip)
<i>pin2</i>	P <sub>PIN2</sub> :PIN2, P <sub>DR5</sub> :GUS	This thesis (Crossing with transgenic line)
<i>pin2</i>	P <sub>PIN2</sub> :PIN3, P <sub>DR5</sub> :GUS	This thesis (Crossing with transgenic line)
<i>pin2</i>	P <sub>PIN2</sub> :PIN6, P <sub>DR5</sub> :GUS	This thesis (Crossing with transgenic line)
<i>pin2</i>	P <sub>PIN2</sub> :PIN8, P <sub>DR5</sub> :GUS	This thesis (Crossing with transgenic line)
<i>pin2</i>	P <sub>PIN2</sub> :PIN8-2-8, P <sub>DR5</sub> :GUS	This thesis (Crossing with transgenic line)
<i>pin2</i>	P <sub>PIN2</sub> :PIN8-2-8-GFP, P <sub>DR5</sub> :GUS	This thesis (Crossing with transgenic line)
<i>pin2</i>	P <sub>PIN2</sub> :PIN8-3-8, P <sub>DR5</sub> :GUS	This thesis (Crossing with transgenic line)
<i>pin2</i>	P <sub>DR5</sub> :GUS	This thesis (Crossing with transgenic line)

##### 6.1.1.2. *Xenopus laevis* oocytes

Stage V and VI *Xenopus laevis* oocytes were used for the transport assays. Frogs that provided the oocytes were kept in strict accordance with the recommendations and guidelines based on the Tierschutzgesetz (TierSchG) of the Federal Republic of Germany at the Research Department of Food and Nutrition at the Center of Life and Food Sciences Weihenstephan. I explicitly want to thank Angela Alkofer, Franziska Anzenberger,

Ulrich Hammes, Dorina Janacek, Katrin Petzold, and Helene Prunkl for taking care of the frogs and performing the surgeries. Occasionally, oocytes of stages V and VI were ordered and used for experiments.

### 6.1.1.3. Bacterial strains

*Escherichia coli* (*E. coli*) DH5 $\alpha$  was used for GreenGate cloning, *E. coli* One Shot Mach1 was used for blunt-end cloning, *E. coli* BL21 was used for expression of recombinant GST:D6PK, GST:PIN1HL (PIN1 loop), and GST:PIN3HL (PIN3 loop). *Agrobacterium tumefaciens* (*A. tumefaciens*, GV3101/pMP90 pSOUP) was used for floral dip of *Arabidopsis thaliana*.

### 6.1.2 Plasmids

Table 6-2 Plasmids used in this thesis

Name	Module/Construct/Usage	Provided by/ Reference
pBLAB001	Template for eGFP CDS PCR amplification	Andrea Bleckmann
pDest15-D6PK	Protein purification of D6PK via GST-tag	Alkistis E. Lanassa Bassukas, Zourelidou <i>et al.</i> , 2014
pDest15-PIN1HL	Protein purification of the PIN1 loop via GST-tag	Alkistis E. Lanassa Bassukas, Zourelidou <i>et al.</i> , 2014
pDest15-PIN3HL	Protein purification of the PIN3 loop via GST-tag	Alkistis E. Lanassa Bassukas, Zourelidou <i>et al.</i> , 2014
pGGF009	BASTA resistance cassette	Lampropoulos <i>et al.</i> , 2013
pGGZ003	Destination vector, floral dip	Lampropoulos <i>et al.</i> , 2013
pKOM018	pOO2, <i>in vitro</i> cRNA synthesis of <i>PIN8</i> cRNA for oocyte injection	Kolb, 2015
pKOM019	pOO2, <i>in vitro</i> cRNA synthesis of <i>PIN8-2-8</i> cRNA for oocyte injection	Kolb, 2015
pKOM020	pOO2, <i>in vitro</i> cRNA synthesis of <i>PIN8-3-8</i> cRNA for oocyte injection	Kolb, 2015
pKOM110	pGGZ003, <i>P<sub>PIN2</sub>:PIN8-2-8 CDS</i> / BASTA cassette, Generation of transgenic lines via floral dip	This thesis
pKOM111	pGGZ003, <i>P<sub>PIN2</sub>:PIN8-2-8-GFP CDS</i> / BASTA cassette, Generation of transgenic lines via floral dip	This thesis
pKOM117	pOO2, <i>in vitro</i> cRNA synthesis of <i>PIN8-2-8-GFP</i> cRNA for oocyte injection	This thesis
pKOM118	pOO2, <i>in vitro</i> cRNA synthesis of <i>PIN8-3-8-GFP</i> cRNA for oocyte injection	This thesis
pKOM127	pGGZ003, <i>P<sub>PIN2</sub>:PIN8 CDS</i> / BASTA cassette, Generation of transgenic lines via floral dip	This thesis

pKOM129	pGGZ003, P <sub>PIN2</sub> :PIN6 CDS / BASTA cassette, Generation of transgenic lines via floral dip	This thesis
pKOM130	pGGZ003, P <sub>PIN2</sub> :PIN6-GFP CDS / BASTA cassette, Generation of transgenic lines via floral dip	This thesis
pKOM135	pGGZ003, P <sub>PIN2</sub> :PIN8-3-8 CDS / BASTA cassette, Generation of transgenic lines via floral dip	This thesis
pOO2-AGC1-3 CDS	pOO2, <i>in vitro</i> cRNA synthesis of AGC1-3 cRNA for oocyte injection	Julia Karmann
pOO2-AGC1-3-S596A CDS	pOO2, <i>in vitro</i> cRNA synthesis of AGC1-3-S596A cRNA for oocyte injection	Alkistis E. Lanassa Bassukas
pOO2-AGC1-3-S596D CDS	pOO2, <i>in vitro</i> cRNA synthesis of AGC1-3-S596D cRNA for oocyte injection	Alkistis E. Lanassa Bassukas
pOO2-AGC1-4 CDS	pOO2, <i>in vitro</i> cRNA synthesis of AGC1-4 cRNA for oocyte injection	Julia Karmann
pOO2-AGC1-7 CDS	pOO2, <i>in vitro</i> cRNA synthesis of AGC1-7 cRNA for oocyte injection	Hiromasa Shikata
pOO2-AGC1-8 CDS	pOO2, <i>in vitro</i> cRNA synthesis of AGC1-8 cRNA for oocyte injection	Julia Karmann
pOO2-AGC1-9 CDS	pOO2, <i>in vitro</i> cRNA synthesis of AGC1-9 cRNA for oocyte injection	Julia Karmann
pOO2-AUX1 CDS	pOO2, <i>in vitro</i> cRNA synthesis of AUX1 cRNA for oocyte injection	Ulrich Z. Hammes, Yang <i>et al.</i> 2006
pOO2-BRX CDS	pOO2, <i>in vitro</i> cRNA synthesis of BRX cRNA for oocyte injection	Ulrich Z. Hammes
pOO2-BRXL CDS	pOO2, <i>in vitro</i> cRNA synthesis of BRXL cRNA for oocyte injection	Ulrich Z. Hammes
pOO2-CAT6 CDS	pOO2, <i>in vitro</i> cRNA synthesis of CAT6 cRNA for oocyte injection	Ulrich Z. Hammes, Hammes <i>et al.</i> 2006
pOO2-KIPK CDS	pOO2, <i>in vitro</i> cRNA synthesis of KIPK cRNA for oocyte injection	Julia Karmann
pOO2-PIN1	pOO2, <i>in vitro</i> cRNA synthesis of PIN1 cRNA for oocyte injection	Absmanner, 2013
pOO2-PIN3	pOO2, <i>in vitro</i> cRNA synthesis of PIN3 cRNA for oocyte injection	Absmanner, 2013
pOO2-PIN5	pOO2, <i>in vitro</i> cRNA synthesis of PIN5 cRNA for oocyte injection	Kolb, 2015
pOO2-PIN6	pOO2, <i>in vitro</i> cRNA synthesis of PIN6 cRNA for oocyte injection, PIN6 CDS cured of Bsal sites and framed with BamHI sites	Ulrich Z. Hammes
pOO2-PIN8	pOO2, <i>in vitro</i> cRNA synthesis of PIN8 cRNA for oocyte injection	Kolb, 2015
pOO2-PIN8-2-8	pOO2, <i>in vitro</i> cRNA synthesis of PIN8-2-8 cRNA for oocyte injection	Kolb, 2015
pOO2-PIN8-3-8	pOO2, <i>in vitro</i> cRNA synthesis of PIN8-3-8 cRNA for oocyte injection	Kolb, 2015
pOO2-PINOID	pOO2, <i>in vitro</i> cRNA synthesis of PINOID cRNA for oocyte injection	Absmanner, 2013
pOO2-YFP-D6PK	pOO2, <i>in vitro</i> cRNA synthesis of YFP-D6PK for oocyte injection	Absmanner, 2013

### 6.1.3 Primers

All transgenic lines generated within the frame of this work were genotyped for *pin2* background and the T-DNA insertion by PCR with the primers listed in **Table 6-3**. Primers were ordered at Merck KGaA (Darmstadt).

**Table 6-3 Primers used for genotyping in this study**

Name	T-DNA insertion	Sequence (5' - 3')
pGGZ003_LB_REV	LB in pGGZ003, REV	GATCTTGGCAGGATATATTGTGGTGTAAACGTT
pGGZ003_RB_FWD	RB in pGGZ003, FWD	CRACTTAGTTTTACCCGCCAATATATCCTGTCAAGG
OlexTATA FWD	OlexTATA-35s Box, FWD	TGCATGCCAGCTTGGGCTGCAGGTCGAGGC
KOM138	PIN8 CDS, FWD	ATGATCTCCTGGCTCGATATCTACCATGTTGTTTTCA GC
KOM139	PIN8 CDS, REV	TCATAGGTCCAATAGAAAATAATATGCCAAAGTTGT TGG
KOM142	PIN2 loop, FWD	GCTAAGCTTCTCATCTCCGAGCAGTTCCCGG
KOM143	PIN2 loop, REV	ACTCGCCGGCGGCATCTGCTGTTTCCTAGG
KOM144	PIN3 loop, FWD	GCCAAGATGCTCATCATGGAGCAGTTCCCTG
KOM145	PIN3 loop, REV	ACTCGCCGGAGGCATATTTTTTTCGTTGACTTGC
KOM146	PIN8 CDS TMD1, REV	CCTTGCGGCGTTAAGCTCGAACAAAAAGAGC
KOM147	PIN2 loop, REV	CCGGGAAGTCTCGGAGATGAGAAGCTTAGC
KOM149	PIN8 CDS, FWD	ACAACCTTTGGCATATTATTTTCTATTGGACCTATG
KOM150	PIN8 CDS, FWD	ACTTTGGCATATTATTTTCTATTGGACCTATG
KOM151	eGFP, FWD	GGGATCACTCTCGGCATGGACGAGCTGTACAAG
KOM153	PIN3 loop, REV	CAGGGAACTGCTCCATGATGAGCATCTTGGC
KOM154	eGFP, FWD	ATGGTGAGCAAGGGCGAGGAGCTGTTACCG
KOM155	eGFP, REV	CTTGACAGCTCGTCCATGCCGAGAGTGATCC
KOM157	PIN2 Promoter, FWD	AACACAAACAACATTAATTAATATCGTCTCAAGGA AC
KOM160	PIN2 loop, FWD	GTCCCGGTCTTAGGAAACAGCAGATGCCGCGGCG GAG
KOM161	PIN3 loop, FWD	GCAAGTCAACGAAAAAATATGCCTCCGGCGAG
KOM162	PIN6 CDS, FWD	ATGATAACGGGAAACGAATTCTACAC
KOM163	PIN6 CDS, FWD	CTATTTTGTACTACGTCCTCTTGGGC
KOM164	PIN6 CDS, REV	TCATAGGCCCAAGAGGACGTAGTAC
KOM165	PIN6 loop, FWD	GCAGCGAGGTTGCTTATCCGAGC
KOM166	PIN6 loop, FWD	GGCCGCAAGCTTTCTCGAAACCCTAAC
KOM167	PIN6 loop, REV	GTTAGGGTTTTCGAGAAAGCTTGCGGCC
KOM168	eGFP, REV	GCTCCTCGCCCTTGCTCACCAT
KOM169	PIN2 Promoter, REV	ACACTTTCTGAGCGATCTGC
KOM170	PIN8 CDS, FWD	AGCTCTTCTCACCCGAACAATGCGC
KOM171	PIN2 loop, REV	CCGACACCGGAGAAGCACTCGAACT
KOM172	PIN6 CDS, REV	GTAGAATTCTGTTTCCCGTTATCAT
KOM173	PIN6 loop, REV	GCTCGGATAAGCAACCTCGCTGC
KOM 175	PIN2 loop, FWD	AGACGGTAATAACGGGGGAAAG

KOM 176	PIN2 Terminator (UTR), REV	GCAAATACGTTTTGATAATAAC
GUS_START_FWD	$\beta$ -Glucuronidase CDS, FWD	ATGGTCCGTCCTGTAGAAACCC
GUS_STOP_REV	$\beta$ -Glucuronidase CDS, REV	TCATTGTTTGCCTCCCTGCTGCGG
GUS_MITTE_FWD	$\beta$ -Glucuronidase CDS, FWD	TTTGGTCGTCATGAAGATGCGG
GUS_MITTE_REV	$\beta$ -Glucuronidase CDS, REV	GCCAGTAAAGTAGAACGGTTTGTGG
KOM178	PIN2 loop, FWD	TAAAGTTTCTATTCTCCTCACGAC
KOM179	PIN2 loop, FWD	CCTTTTTTGCCCATGTAAGGTGA
KOM180	eGFP, FWD	GGAGCTGTTACCGGGGTGGTGCCC
KOM181	eGFP, REV	GGGCACCACCCCGGTGAACAGCTCC
KOM182	eGFP, FWD	GGAGTTCGTGACCGCCGCGGG
KOM183	eGFP, REV	CCCGGCGGCGGTCACGA ACTCC
KOM184	PIN8 TMD CDS/PIN2 Loop, FWD	GTTCGAGCTTAACGCCGCAAGGGCTAAGCTTC
KOM185	PIN2 loop/PIN8 TMD CDS, REV	GAAGCTCCAGAAGATGGTAACGCACTCGCCGG
LP01	<i>pin2</i> SALK T-DNA insertion	AACCCTGCTACTGATTTTCCG
LBb1.3	<i>pin2</i> SALK T-DNA insertion	ATTTTGCCGATTTTCGGAAC
RP01	<i>pin2</i> SALK T-DNA insertion	TATGGTCAGTTCCGTCGTACC

## 6.2 Methods

Standard methods of molecular biology were performed according to Sambrook *et al.* 1989 using molecular-grade reagents.

### 6.2.1 Molecular cloning

The plasmids and vectors used and cloned within the frame of this work are listed in **Table 6-2**. All plasmids were cloned with the coding sequences (CDS) of the respective genes/constructs. The *PIN2* promoter (1132 bp) and the *PIN2* terminator (500 bp) were PCR amplified from *Arabidopsis* genomic DNA. Constructs cloned into pGGZ003 (Lampropoulos *et al.*, 2013) were assembled using fragments, which were PCR amplified with *Bsa*I sites overhangs, a BASTA resistance cassette conferred BASTA (phosphinothricin) resistance to select for transformants. Primers were designed using the online NEBridge™ Golde Gate Assembly Tool. eGFP CDS was amplified from pBla001 (Andrea Bleckmann, pGGB000, Lampropoulos *et al.* 2013). cDNAs were cloned blunt into pOO2 (Ludewig *et al.*, 2002) as described before (Absmanner 2013; Zourelidou *et al.* 2014).



The compositions of the CDS of the PIN8-2-8 and PIN8-3-8 chimaeras (Ganguly *et al.*, 2014), their GFP-fused version, and the PIN6-GFP fusion (Sawchuk *et al.*, 2013) are illustrated in Fig. 6-1.

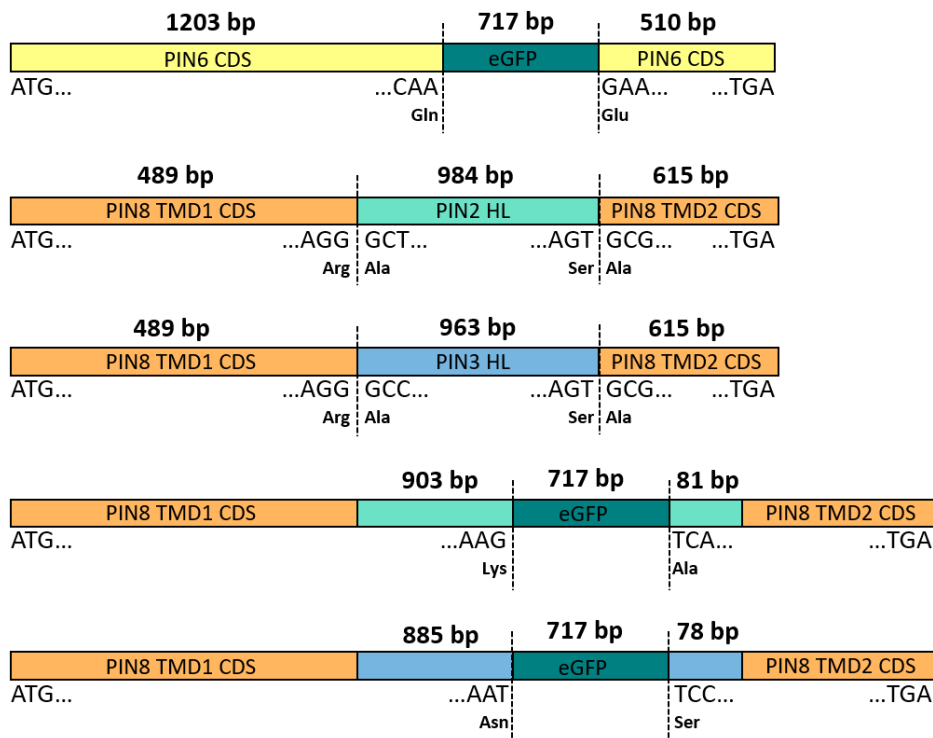


Fig. 6-1 Illustration of the cloning strategy of the cDNAs of the two chimaeras, their GFP-fused version, and *PIN6-GFP*

## 6.2.2 Genotyping of plant genomic DNA

Genomic DNA was extracted from ca. 50 mg leave/plant material. The plant material was put in 2 ml reaction tubes filled with glass beads, frozen in liquid nitrogen, and ground with a QIAGEN® TissueLyser at 30 Hz for 2 minutes. 750 µl extraction buffer [50 mM Tris-HCl (pH 8.0), 10 mM EDTA (pH 8.0), 100 mM NaCl, 10 mM 2-Mercaptoethanol, 1% (w/v) SDS, 2-Mercaptoethanol and SDS were added just before usage of the buffer] were added and the mixture was left to incubate at 65°C in a water bath for 15 min. 200 µl 5 M KAc were added followed by incubation on ice for 20 min. After centrifugation (10 min, 13000 rpm), 700 µl of the supernatant was transferred to a new tube and 700 µl isopropanol was added. After another centrifugation, the supernatant was removed, 600 µl 70% (w/v) Ethanol was added to the pellet and incubated for five minutes at room temperature. After another centrifugation, the supernatant was removed, and the pellet was air-dried and dissolved in 100 µl ddH<sub>2</sub>O overnight at 8°C. The *Arabidopsis* lines were genotyped for *pin2* background and the T-DNA insertion by PCR using Taq DNA polymerase and the primers listed in **Table 6-3** according to standard operating protocol.

## **6.2.3 Biochemical methods**

### **6.2.3.1. Protein purification of recombinant GST-tagged proteins**

For protein purification of recombinant GST-tagged proteins, *E. coli* BL21 were transformed with pDest15 encoding for GST:D6PK, GST:PIN1-loop or GST:PIN3-loop respectively freshly the day before purification. A pre-culture was inoculated and shaken at 37°C overnight. The pre-culture was used the next day to inoculate a 200 ml culture which was shaken at 37°C until OD600 = 0,6 – 0,7 was reached. Subsequently, protein synthesis was induced by adding IPTG (0,5 mM end concentration) and the culture was shaken at 18°C for roughly 21 more hours. Cells were harvested in 50 ml tubes by centrifugation (4000g, 10 min, 4°C) and frozen at -80°C to help cell disruption and for storage.

For purification, the cell pellet was firstly thawed on ice and resuspended in 8 ml extraction buffer [1x PBS, 10% Glycerol, 1% Triton X, 50 mg / 50 ml Lysozyme, protease inhibitor cocktail PIC (Sigma-Aldrich, St. Louis, MO)]. Thereafter, the cells were disrupted by ultrasonication while cooling them constantly with ice. After a centrifugation step (10,000 g, 10 min, 4°C), the supernatant was transferred into a new 50 ml reaction tube and PBS + PIC buffer was added to a final volume of 35 ml. 100 µl of GSH beads were added and the reaction was rotated for 30 min at 4°C. After another centrifugation step, 30 ml of the supernatant was discarded carefully, and the beads were washed two times with 20 ml PBS + PIC buffer with each one centrifugation step in between. After washing, the beads were transferred in a new 1,5 ml reaction tube, centrifuged and the supernatant was removed completely. For elution with glutathione, 50 µl of a 50 mM stock was added to the beads, which were then rotated for 30 min at 4°C. A last centrifugation step was performed to separate the elution from the beads. The protein elution was checked on a SDS gel with a subsequent CBB staining.

### **6.2.3.2. *In vitro* phosphorylation of purified PIN loop**

*In vitro* phosphorylation experiments were carried out as described (Zourelidou *et al.*, 2014). For NPA treatment, NPA was solved in EtOH and added to the reaction buffer to a final concentration of 100 µM. The equivalent volume of EtOH only was used as solvent control.

## **6.2.4 Plant growth conditions**

For growth of plants on plates under sterile conditions, *Arabidopsis* seeds were sterilized with chlorine gas (50 ml NaOCl + 3 ml 37% HCl) for one hour. Sterile seeds were placed under a sterile hood on solid growth medium (Murashige & Skoog medium (MS) medium with 1% sucrose) and stratification was performed on plates for 48 – 72 hours at 4°C in the dark. Seedlings were grown under long-day conditions (120 µmol m<sup>-2</sup> s<sup>-1</sup>, 16 hours light / 8 hours

darkness), vertically in a Sanyo chamber. For growth on soil, seeds were put on soil and transferred to plant growth chambers under long-day conditions.

### **6.2.5 Stable transformation and selection of plant lines**

The individual constructs were introduced into *pin2* background using the “Floral dipping method” (Clough and Bent, 1998). The *Agrobacterium* suspension was prepared by the addition of 5% (w/v) sucrose and 0.05 Silwet® L-77. Positive seedlings were preselected by applying BASTA® solution [0.1% (v/v) BASTA® solution (Bayer), 0.1% (v/v) Tween® 20] three times every third day and genotyped for *pin2* background and T-DNA insertion (see 6.2.2).

### **6.2.6 Crossing of plant lines**

For crossing (transgenic) *pin2* mutant lines with *P<sub>DR5</sub>:GUS* plants, flowers of the *pin2* lines were emasculated and pollinated with *P<sub>DR5</sub>:GUS* pollen. Mature siliques were harvested and seeds were sown out on soil. Plants that contained the *P<sub>DR5</sub>:GUS* reporter and the respective *PIN2* promoter-driven construct were preselected by applying BASTA® solution [0.1% (v/v) BASTA® solution (Bayer), 0.1% (v/v) Tween® 20] three times every third day and genotyped for *pin2* background and T-DNA insertion (see 6.2.2).

### **6.2.7 Plant physiology experiments**

*Arabidopsis* seedlings were grown as described in 6.2.4 for five days, then pictures were taken for evaluation. Evaluation of the roots was performed using the Fiji (ImageJ) “Simple Neurite Tracer” plugin, the rectangle tool, and the “Angle root script” to give the value of the root angle simultaneously, which was kindly provided by José Antonio Villacéjica Aguilar. Root length, root angle, and VGI were defined according to Grabov *et al.*, 2005. Statistical analysis was performed using SigmaPlot 14.0 software (Systat Software Inc), blotting of data was performed using GraphPad Prism 8 Software (GraphPad Software) with default settings.

### **6.2.8 Histochemical GUS Staining**

For histochemical GUS staining, *Arabidopsis* seedlings were grown as described in 6.2.4 for five days. Afterwards, roots of the seedlings were cut off and each root was transferred into one well of a 24-well-plate containing 250 µl freshly prepared GUS staining solution [100 mM NaPO<sub>4</sub> (pH 7.0), 10 mM EDTA (pH 7.0), 1 mM K<sub>3</sub>Fe(CN)<sub>6</sub>, 1 mM K<sub>4</sub>Fe(CN)<sub>6</sub>, 10% Triton X-100 (v/v), 1.25 mM X-Gluc]. For a stock GUS staining solution, X-Gluc was dissolved in DMSO and kept in the dark at 8 °C. The seedlings were left on the plates and grown for three more days to allow for gDNA extraction for genotyping. The well plate with the roots was incubated at 37°C in the dark for one hour. Afterwards samples were washed three times in 0.05 NaPO<sub>4</sub>

(pH 7.2) and subsequently analyzed by DIC (differential interference contrast) microscopy at an Olympus BX61 microscope (see 6.2.9).

### **6.2.9 Microscopy and signal quantification**

Confocal microscopy images were acquired with an Olympus BX61 microscope equipped with a FV1000 confocal laser scanning unit (Olympus, Hamburg). Propidium iodide staining was performed as described (Müller *et al.* 2015). Images were processed only for brightness and contrast adjustments using Fiji (ImageJ).

GUS-stained samples were analyzed by DIC microscopy at an Olympus BX61 microscope. The GUS stained samples were mounted in chloral hydrate solution [50% (w/v) chloral hydrate, 10% (v/v) glycerol]. ImageJ-based quantification of the staining was carried out as described (Béziat *et al.* 2017).

### **6.2.10 *Xenopus laevis* oocyte transport assay**

General procedure was performed according to Absmanner, 2013 and Fastner *et al.*, 2017 with changes as stated below.

#### *In vitro* transcription of cRNA

For *in vitro* transcription of cRNA (see step 2 in Fastner *et al.*, 2017), 10 µg of vector containing the gene of interest was linearized, preferentially with *MluI* in an overnight reaction. To achieve a high yield of cRNA (see step 12), the maximum of template DNA was used and the reaction was incubated for two hours at 37°C. After mRNA synthesis, template DNA was removed by adding 1 µl of TURBO DNase.

For oocyte injection with cRNA (see step 4), cRNA working solutions were prepared as described in (Absmanner, 2013; Zourelidou *et al.*, 2014).

#### Efflux experiments with <sup>3</sup>H-IAA or <sup>3</sup>H-NPA

For efflux experiments with radioactive labeled substances (<sup>3</sup>H-IAA or <sup>3</sup>H-NPA), oocytes were injected at room temperature (see step 4), kept in the “recovery” plate for two minutes (see steps 8 and 15), and washed in two Petri dishes containing Barth’s solution which was exchanged at times (see step 13).

For experiments with NPA applied from outside, NPA (prepared in 180 mM stock solution, solved in EtOH) was added to Barth’s solution (pH 7.6 and pH 5.5) to obtain a concentration of 10 µM. Oocytes were incubated for ten or 150 min before at room temperature. Thereafter, the efflux experiment with <sup>3</sup>H-IAA was performed.

### Co-injection of potential modifiers of <sup>3</sup>H-IAA efflux

The concentrations of the solutions were calculated in a way to obtain an internal concentration of 100 μM (or 10 μM) of the different chemicals/substances and 1 μM of <sup>3</sup>H-IAA upon injecting the solution together with <sup>3</sup>H-IAA into the oocytes. Stock solutions (180 mM and 18 mM in the case of Quercetin) of the different substances were prepared by solving the substance either in H<sub>2</sub>O (Serotonin, trans-Zeatin, tryptophan) or EtOH (IAA, Me-IAA, IBA, 2,4-D, NAA, quercetin, NPA, TIBA) according to The Merck Index (Merck & Co., Inc.). To perform the assays, working solutions (1,8 mM) were prepared freshly by diluting the stock solutions with Barth's solution. NBD-IAA (in DMSO, stock concentration undetermined) was mixed 1:5 with Barth's solution to serve as a working solution. <sup>3</sup>H-IAA was diluted 1:2.5 in Barth's + Gent and the <sup>3</sup>H-IAA solution was mixed with the respective working solution of the substance to be co-injected (or Barth's solution only for mock control) in a ratio of 1:1.

### Uptake experiments with <sup>3</sup>H-IAA and <sup>14</sup>C-leucine

For the uptake experiments, Barth's solution with pH 5.5 was used for all incubation steps. Prior to the uptake experiment, oocytes were injected with Barth's solution with NPA (100 μM internal concentration, see "Co-injection of potential modifiers of <sup>3</sup>H-IAA efflux") or without NPA. Subsequently, they were incubated on ice for two minutes, thereafter uptake experiments with <sup>3</sup>H-IAA (Yang *et al.*, 2006) or <sup>14</sup>C-leucine (Hammes *et al.*, 2006) were performed as described. Here, 1.5 reaction tubes provided with 50 μl of the respective substrate-solution were used. Oocytes were incubated for five or 30 minutes at room temperature, and afterwards washed three times with Barth's solution with cold substrate in 12 well plates. Thus, the oocytes were separated and cpm in oocytes were determined.

### Determination of transport rates

The relative transport rates were calculated from the obtained time courses as described before (Absmanner, 2013). Only those parts of the curve in which the auxin content decreased in a linear fashion were considered. For assays with PIN1 this was 0 – 30 minutes, for assays with PIN3, PIN6, PIN8, PIN8-2-8, PIN8-3-8, and the respective GFP-fused versions this was 0 – 15 minutes.

## **6.2.11 *In silico* protein alignment**

Protein alignment of the PIN hydrophilic loops was performed as described (Zourelidou *et al.* 2014).

## 7. List of figures

Fig. 3-1 Overview of the influx and efflux carrier network enabling (polar) IAA transport in <i>Arabidopsis thaliana</i> .....	8
Fig. 3-2 Structure and classification of PIN proteins from <i>Arabidopsis</i> . ....	10
Fig. 3-3 Localization of canonical PINs in the primary root tip and the auxin flux according to the reverse fountain model .....	11
Fig. 3-4 Auxin flux and PIN localization in root gravitropism.....	13
Fig. 3-5 The <i>Arabidopsis</i> AGCVIII protein kinase family, a plant-specific subfamily of the AGC kinase family .....	15
Fig. 3-6 Alignment of parts of the hydrophilic loop of the canonical PINs. ....	16
Fig. 4-1 Data of typical experiment of PIN-mediated IAA transport in <i>X. laevis</i> oocytes and determination of relative IAA transport rates.....	20
Fig. 4-2 Effect of unlabeled IAA on the transport of <sup>3</sup> H-labeled IAA.....	21
Fig. 4-3 The effect of various substances on PIN-mediated IAA transport in <i>X. laevis</i> oocytes .....	21
Fig. 4-4 Concentration effect of NPA on PIN3-mediated IAA transport in the oocyte system. ....	26
Fig. 4-5 NPA is not transported by PINs .....	27
Fig. 4-6 NPA applied from outside only partly inhibits IAA transport.....	28
Fig. 4-7 NPA does not inhibit <i>in vitro</i> D6PK autophosphorylation or trans-phosphorylation of PIN1 or PIN3 hydrophilic loop (HL). ....	29
Fig. 4-8 NPA does not affect transport the activity of <i>AtAUX1</i> or <i>AtCAT6</i> . ....	30
Fig. 4-9 PIN8 is a constitutive active IAA transporter sensitive to NPA.....	31
Fig. 4-10 Schematic presentation of the generation of the PIN8 chimaeras.....	32
Fig. 4-11 The chimaeras PIN8-2-8, PIN8-3-8, and their GFP-tagged versions are functional IAA transporter in the oocyte system and display characteristics from both their parents. ....	33
Fig. 4-12 Quantification of root geometry of <i>Arabidopsis</i> with use of the root angle and the vertical growth index (VGI ) .....	34
Fig. 4-13 Quantification of <i>pin2</i> rescue with use of the root angle and VGI (Grabov <i>et al.</i> , 2005.) .....	36
Fig. 4-14 Auxin response of Col-0, <i>pin2</i> , and <i>P<sub>PIN2</sub>:PINX (pin2)</i> lines, visualized by GUS-staining (Ulmasov <i>et al.</i> , 1997) and its quantification.....	38

Fig. 4-15 PIN8-2-8 localizes at the PM in epidermis and cortex in 5-day-old <i>P<sub>PIN2</sub>:PIN8-2-8-GFP (pin2)</i> roots.....	39
Fig. 4-16 PIN6 is a constitutively active IAA transporter and its transport capacity is enhanced by PID.....	41
Fig. 4-17 PIN6-mediated IAA transport in the oocyte system is sensitive to NPA. ....	42
Fig. 4-18 <i>P<sub>PIN2</sub>:PIN6</i> in <i>pin2</i> enhances the agravitropic <i>pin2</i> phenotype .....	43
Fig. 4-19 PIN6 localizes at the ER and the PM in 5-day-old <i>P<sub>PIN2</sub>:PIN6-GFP</i> roots.....	44
Fig. 4-20 Potential of selected AGC1 clade kinases to activate PIN-mediated IAA transport. ....	46
Fig. 4-21 Potential of wild type PAX, a phosphomimicking variant (PAX-S596D, PAX-D) and a phospho-mutant variant (PAX-S596A, PAX-A) to activate PIN3-mediated IAA transport .....	47
Fig. 4-22 BRX does not activate PIN3-mediated IAA transport in the oocyte system .....	48
Fig. 4-23 Effect of BRX on PIN-mediated IAA efflux activated by AGC1 or AGC3 kinases ..	49
Fig. 4-24 Effect of BRXL2 and BRX-KO (serines in the potential D6PK/PAX target sites are substituted by alanines) on PIN-mediated IAA efflux in comparison to wild type BRX in <i>X. laevis</i> transport assays .....	50
Fig. 5-1 The structure of PIN8 and a dendrogram of the relationship between AtPIN1 – PIN8. ....	53
Fig. 5-2 Results of SSM electrophysiology investigating substrate specificity of PIN8.....	63
Fig. 5-3 Members of the AGCVIII kinase family and their potential to activate PIN-mediated IAA transport .....	65
Fig. 5-4 PAX and BRX constitute a “molecular rheostat” that regulates and fine-tunes PIN-mediated auxin efflux.....	68
Fig. 6-1 Illustration of the cloning strategy of the cDNAs of the two chimaeras, their GFP-fused version, and <i>PIN6-GFP</i> .....	75

## 8. List of tables

Table 4-1 List of the publications presenting data generated within the frame of the present thesis and personal contribution.....	19
Table 4-2 Name and chemical structure of the substances tested for their effect on PIN mediated IAA transport in <i>X. laevis</i> oocytes.....	22
Table 8-1 (Transgenic) <i>Arabidopsis</i> lines used in this study .....	70
Table 8-2 Plasmids used in this thesis .....	71
Table 8-2 Primers used for genotyping in this study.....	73



## 9. Abbreviations

2,4-D	2,4-dichlorophenoxyacetic acid
AA	Amino acid
ANOVA	Analysis of Variance
ARF	Auxin response factors
ATP	Adenosine triphosphate
AUX	AUXIN RESISTANT
AUX/IAA	AUXIN/INDOLE-3-ACETIC ACID
BRX	BREVIS RADIX
BRXL	BREVIS RADIX-LIKE
CAT	Cationic amino acid transporters
CDS	Coding sequence
Col-0	Columbia 0
cpm	Counts per minute
D6PK	D6 PROTEIN KINASE
D6PKL	D6 PROTEIN KINASE-LIKE
DR5	DIRECT REPEAT 5
ER	Endoplasmic reticulum
GEF	Guanine-nucleotide exchange factor
GFP	GREEN FLOURESCENT PROTEIN
GN	GNOM
GUS	β-GLUCURONIDASE
HL	Hydrophilic loop
IAA	Indole-3-acetic acid
IBA	Indole-3-butyric acid
KIPK	KCBP-INTERACTING PROTEIN KINASE
LAX	LIKE AUX
MAP	MITOGEN-ACTIVATED PROTEIN
MAPK	MITOGEN-ACTIVATED PROTEIN KINASE
MDR/PGP	MULTIDRUG RESISTANCE/P-GLYCOPROTEIN
Me-IAA	Methylated IAA
NAA	1-Naphthaleneacetic acid
NBD-IAA	7-nitro-2,1,3- benzoxadiazole-conjugated IAA (Hayashi <i>et al.</i> , 2014)
NPA	N-1-naphthylphthalamic acid
PAT	Polar auxin transport
PAX	PROTEIN KINASE ASSOCIATED WITH BRX
PAXL	PROTEIN KINASE ASSOCIATED WITH BRX LIKE
PPSE	Protophloem sieve element
phot	Phototropin
PI	Propidium Iodide
PID	PINOID
PILS	PIN-LIKES
PIN	PIN-FORMED
PM	Plasma membrane
PP2A	PROTEIN PHOSPHATASE 2A
QC	Quiescent center

ROI	Region of interest
SDS/PAGE	Sodium dodecyl sulfate/polyacrylamide gel electrophoresis
SEM	Standard error of the mean
TIBA	2,3,5-triiodobenzoic acid
TIR	TRANSPORT INHIBITOR RESPONSE
TMD	Transmembrane domaine
TOB	TRANSPORTER OF IBA
Trp	Tryptophan
UNC	UNICORN
VGI	Vertical growth index (Grabov <i>et al.</i> , 2005)
WAG	WAVY GROWTH
WAT	WALLS ARE THIN

## 10. Bibliography

- Abas, L., Benjamins, R., Malenica, N., Paciorek, T., Wiśniewska, J., Moulinier–Anzola, J.C., Sieberer, T., Friml, J., and Luschnig, C.** (2006). Intracellular trafficking and proteolysis of the Arabidopsis auxin-efflux facilitator PIN2 are involved in root gravitropism. *Nat. Cell Biol.* **8**: 249–256.
- Abas, L., Kolb, M., Stadlmann, J., Janacek, D.P., Lukic, K., Schwechheimer, C., Sazanov, L.A., Mach, L., Friml, J., and Hammes, U.Z.** (2021). Naphthylphthalamic acid associates with and inhibits PIN auxin transporters. *Proc. Natl. Acad. Sci.* **118**: 1–8.
- Abbas, M., Hernández-García, J., Pollmann, S., Samodelov, S.L., Kolb, M., Friml, J., Hammes, U.Z., Zurbriggen, M.D., Blázquez, M.A., and Alabadí, D.** (2018). Auxin methylation is required for differential growth in Arabidopsis. *Proc. Natl. Acad. Sci. U. S. A.* **115**: 6864–6869.
- Absmanner, B.** (2013). Regulation of PIN-FORMED-mediated auxin transport and the role of auxin and cytokinin responses in plant - nematode interactions. Dissertation Universität. Regensburg.
- Adamowski, M. and Friml, J.** (2015). PIN-Dependent Auxin Transport: Action, Regulation, and Evolution. *Plant Cell* **27**: 20–32.
- Anne, P. and Hardtke, C.S.** (2018). Phloem function and development — biophysics meets genetics. *Curr. Opin. Plant Biol.* **43**: 22–28.
- Armengot, L., Marquès-Bueno, M.M., and Jaillais, Y.** (2016). Regulation of polar auxin transport by protein and lipid kinases. *J. Exp. Bot.* **67**: 4015–4037.
- Bailly, A., Sovero, V., Vincenzetti, V., Santelia, D., Bartnik, D., Koenig, B. W., Mancuso, S., Martinoia, E., and Geisler, M.** (2008). Modulation of P-glycoproteins by auxin transport inhibitors is mediated by interaction with immunophilins. *J. Biol. Chem.* **283**: 21817–21826.
- Band, L.R. Band, L.R., Wells, D.M., Fozard, J.A., Ghetiu, T., French, A.P., Pound, M.P., Wilson, M.H., Yu, L., Li, W., Hijazi, H.I., Oh, J., Pearce, S.P., Perez-Amador, M.A., Yun, J., Kramer, E., Alonso, J.M., Godin, C., Vernoux, T., Hodgman, T.C., Pridmore, T.P., Swarup, R., King, J.R., and Bennett, M.J.** (2014). Systems Analysis of Auxin Transport in the Arabidopsis Root Apex. *Plant Cell* **26**: 862–875.
- Bandyopadhyay, A., Blakeslee, J.J., Lee, O.R., Mravec, J., Sauer, M., Titapiwatanakun, B., Makam, S.N., Bouchard, R., Geisler, M., Martinoia, E., Friml, J., Peer, W.A., and Murphy, A.S.** (2007). Interactions of PIN and PGP auxin transport mechanisms. *Biochem. Soc. Trans.* **35**: 137–141.
- Barbez, E., Kubeš, M., Rolčík, J., Béziat, C., Pěňčík, A., Wang, B., Rosquete, M. R., Zhu, J., Dobrev, P. I., Lee, Y., Zažímalová, E., Petrášek, J., Geisler, M., Friml, J., and Kleine-Vehn, J.** (2012). A novel putative auxin carrier family regulates intracellular auxin homeostasis in plants. *Nature* **485**: 119–122.
- Barbosa, I.C.R. and Schwechheimer, C.** (2014). Dynamic control of auxin transport-dependent growth by AGCVIII protein kinases. *Curr. Opin. Plant Biol.* **22**: 108.
- Barbosa, I.C.R., Hammes, U.Z., and Schwechheimer, C.** (2018). Activation and Polarity Control of PIN-FORMED Auxin Transporters by Phosphorylation. *Trends Plant Sci.* **23**: 523–538.
- Barbosa, I.C.R., Zourelidou, M., Willige, B.C., Weller, B., and Schwechheimer, C.** (2014). D6 PROTEIN KINASE Activates Auxin Transport-Dependent Growth and PIN-FORMED Phosphorylation at the Plasma Membrane. *Dev. Cell* **29**: 674–685.
- Bartel, B.** (1997). Auxin biosynthesis. *Annu. Rev. Plant Biol.* **48**: 51–66.
- Baster, P., Robert, S., Kleine-Vehn, J., Vanneste, S., Kania, U., Grunewald, W., De Rybel, B., Beeckman, T., and Friml, J.** (2012). SCFTIR1/AFB-auxin signalling regulates PIN vacuolar trafficking and auxin fluxes during root gravitropism. *EMBO J.* **32**: 260–274.
- Bender, R.L., Fekete, M.L., Klinkenberg, P.M., Hampton, M., Bauer, B., Malecha, M., Lindgren, K., Maki, J.A., Perera, M.A.D.N., Nikolau, B.J., and Carter, C.J.** (2013).

- PIN6 is required for nectary auxin response and short stamen development.: 893–904.
- Benjamins, R., Quint, A., Weijers, D., Hooykaas, P., and Offringa, R.** (2001). The PINOID protein kinase regulates organ development in Arabidopsis by enhancing polar auxin transport. *Development* **128**: 4057–4067.
- Benjamins, R. and Scheres, B.** (2008). Auxin: The Looping Star in Plant Development. *Annu. Rev. Plant Biol.* **59**: 443–465.
- Benková, E., Michniewicz, M., Sauer, M., Teichmann, T., Seifertová, D., Jürgens, G., and Friml, J.** (2003). Local, Efflux-Dependent Auxin Gradients as a Common Module for Plant Organ Formation. *Cell* **115**: 591–602.
- Bennett, T., Brockington, S.F., Rothfels, C., Graham, S.W., Stevenson, D., Kutchan, T., Rolf, M., Thomas, P., Wong, G.K.-S., Leyser, O., Glover, B.J., and Harrison, C.J.** (2014). Paralogous Radiations of PIN Proteins with Multiple Origins of Noncanonical PIN Structure. *Mol. Biol. Evol.* **31**: 2042–2060.
- Beuchat, J., Scacchi, E., Tarkowska, D., Ragni, L., Strnad, M., and Hardtke, C.S.** (2010). BRX promotes Arabidopsis shoot growth. *New Phytol.* **188**: 23–29.
- Béziat, C., Kleine-Vehn, J., and Feraru, E.** (2017). *Plant Hormones*. J. Kleine-Vehn and M. Sauer, eds (Springer New York: New York, NY).
- Blakeslee, J.J., Bandyopadhyay, A., Lee, O. R., Mravec, J., Titapiwatanakun, B., Sauer, M., Makam, S. N., Cheng, Y., Bouchard, R., Adamec, J., Geisler, M., Nagashima, A., Sakai, T., Martinoia, E., Friml, J., Peer, W. A., and Murphy, A. S.** (2007). Interactions among PIN-FORMED and P-Glycoprotein Auxin Transporters in Arabidopsis. *Plant Cell* **19**: 131–147.
- Blilou, I., Xu, J., Wildwater, M., Willemsen, V., Paponov, I., Friml, J., Heidstra, R., Aida, M., Palme, K., and Scheres, B.** (2005). The PIN auxin efflux facilitator network controls growth and patterning in Arabidopsis roots. *Nature* **433**: 39–44.
- de Boer, M., Cordes, T., and Poolman, B.** (2020). Kinetic Modelling of Transport Inhibition by Substrates in ABC Importers. *J. Mol. Biol.* **432**: 5565–5576.
- Bosco, C.D., Dovzhenko, A., Liu, X., Woerner, N., Rensch, T., Eismann, M., Eimer, S., Hegermann, J., Paponov, I. A., Ruperti, B., Heberle-Bors, E., Touraev, A., Cohen, J. D., and Palme, K.** (2012). The endoplasmic reticulum localized PIN8 is a pollen-specific auxin carrier involved in intracellular auxin homeostasis. *Plant J.* **71**: 860–870.
- Briggs, G.C., Mouchel, C.F., and Hardtke, C.S.** (2006). Characterization of the Plant-Specific BREVIS RADIX Gene Family Reveals Limited Genetic Redundancy Despite High Sequence Conservation. *Plant Physiol.* **140**: 1306–1316.
- Brown, D.E., Rashotte, A.M., Murphy, A.S., Normanly, J., Tague, B.W., Peer, W. a, Taiz, L., and Muday, G.K.** (2001). Flavonoids Act as Negative Regulators of Auxin Transport in Vivo in Arabidopsis. *Plant Physiol.* **126**: 524–535.
- Brunoud, G., Wells, D.M., Oliva, M., Larrieu, A., Mirabet, V., Burrow, A.H., Beeckman, T., Kepinski, S., Traas, J., Bennett, M.J., and Vernoux, T.** (2012). A novel sensor to map auxin response and distribution at high spatio-temporal resolution. *Nature* **482**: 103–106.
- Cambridge, A. and Morris, D.** (1996). Transfer of exogenous auxin from the phloem to the polar auxin transport pathway in pea (*Pisum sativum* L.). *Planta* **199**: 583–588.
- Cattaneo, P., Graeff, M., Marhava, P., and Hardtke, C.S.** (2019). Conditional effects of the epigenetic regulator JUMONJI 14 in Arabidopsis root growth. *Dev.* **146**.
- Cazonelli, C.I., Vanstraelen, M., Simon, S., Yin, K., Carron-Arthur, A., Nisar, N., Tarle, G., Cuttriss, A. J., Searle, I. R., Benkova, E., Mathesius, U., Masle, J., Friml, J., and Pogson, B. J.** (2013). Role of the Arabidopsis PIN6 Auxin Transporter in Auxin Homeostasis and Auxin-Mediated Development. *PLoS One* **8**: e70069.
- Cho, M., Lee, S.H., and Cho, H.-T.** (2008). P-Glycoprotein4 Displays Auxin Efflux Transporter-Like Action in Arabidopsis Root Hair Cells and Tobacco Cells. *Plant Cell* **19**: 3930–3943.
- Cholodny, N.** (1927). Wuchshormone und Tropismen bei den Pflanzen. *Biol. Zent. Bl.* **47**: 604–626.
- Clough, S.J. and Bent, A.F.** (1998). Floral dip: a simplified method for Agrobacterium-

- mediated transformation of *Arabidopsis thaliana*. *Plant J.* **16**: 735–743.
- Dai, M., Zhang, C., Kania, U., Chen, F., Xue, Q., Mccray, T., Li, G., Qin, G., Wakeley, M., Terzaghi, W., Wan, J., Zhao, Y., Xu, J., Friml, J., Deng, X. W., and Wang, H.** (2012). A PP6-Type Phosphatase Holoenzyme Directly Regulates PIN Phosphorylation and Auxin Efflux in *Arabidopsis*. *Plant Cell* **24**: 2497–2514.
- Darwin, C. and Darwin, F.** (1880). *The power of movement in plants* (London, John Murray).
- Depta, H., Eisele, K.-H., and Hertel, R.** (1983). Specific inhibitors of auxin transport: Action on tissue segments and in vitro binding to membranes from maize coleoptiles. *Plant Sci. Lett.* **31**: 181–192.
- Deruere, J., Jackson, K., Garbers, C., Soll, D., and DeLong, A.** (1999). The RCN1-encoded A subunit of protein phosphatase 2A increases phosphatase activity in vivo. *Plant J.* **20**: 389–399.
- Dharmasiri, N., Dharmasiri, S., and Estelle, M.** (2005). The F-box protein TIR1 is an auxin receptor. *Nature* **435**: 441–445.
- Dhonukshe, P., Aniento, F., Hwang, I., Robinson, D.G., Mravec, J., Stierhof, Y.-D., and Friml, J.** (2007). Clathrin-Mediated Constitutive Endocytosis of PIN Auxin Efflux Carriers in *Arabidopsis*. *Curr. Biol.* **17**: 520–527.
- Dhonukshe, P., Huang, F., Galvan-Ampudia, C.S., Mähönen, A.P., Kleine-Vehn, J., Xu, J., Quint, A., Prasad, K., Friml, J., Scheres, B., and Offringa, R.** (2010). Plasma membrane-bound AGC3 kinases phosphorylate PIN auxin carriers at TPRXS(N/S) motifs to direct apical PIN recycling. *Development* **137**: 3245–3255.
- Ding, Z., Wang, B., Moreno, I., Dupláková, N., Simon, S., Carraro, N., Reemmer, J., Pěňčík, A., Chen, X., Tejos, R., Skůpa, P., Pollmann, S., Mravec, J., Petrášek, J., Zažímalová, E., Honys, D., Rolčík, J., Murphy, A., Orellana, A., Geisler, M., and Friml, J.** (2012). ER-localized auxin transporter PIN8 regulates auxin homeostasis and male gametophyte development in *Arabidopsis*. *Nat. Commun.* **3**: 941.
- Ding, Z., Galván-Ampudia, C.S., Demarsy, E., Łangowski, Ł., Kleine-Vehn, J., Fan, Y., Morita, M.T., Tasaka, M., Fankhauser, C., Offringa, R., and Friml, J.** (2011). Light-mediated polarization of the PIN3 auxin transporter for the phototropic response in *Arabidopsis*. *Nat. Cell Biol.* **13**: 447–452.
- Ditengou, F.A., Gomes, D., Nziengui, H., Kochersperger, P., Lasok, H., Medeiros, V., Paponov, I. A., Nagy, S. K., Náday, T. V., Mészáros, T., Barnabás, B., Ditengou, B. I., Rapp, K., Qi, L., Li, X., Becker, C., Li, C., Dóczi, R., and Palme, K.** (2018). Characterization of auxin transporter PIN6 plasma membrane targeting reveals a function for PIN6 in plant bolting. *New Phytol.* **217**: 1610–1624.
- Eerland, L.A.E., Murch, S.J., Reiter, R.J., and Saxena, P.K.** (2015). A new balancing act: The many roles of melatonin and serotonin in plant growth and development. *Plant Signal. Behav.* **10**: e1096469.
- Eerland, L.A.E., Turi, C.E., and Saxena, P.K.** (2019a). Serotonin in Plants. In *Serotonin* (Elsevier), pp. 23–46.
- Eerland, L.A.E., Yasunaga, A., Li, I.T.S., Murch, S.J., and Saxena, P.K.** (2019b). Direct visualization of location and uptake of applied melatonin and serotonin in living tissues and their redistribution in plants in response to thermal stress. *J. Pineal Res.* **66**: e12527.
- Fang, S., Huang, X., Zhang, X., Zhang, M., Hao, Y., Guo, H., Liu, L.-N., Yu, F., and Zhang, P.** (2021). Molecular mechanism underlying transport and allosteric inhibition of bicarbonate transporter SbtA. *Proc. Natl. Acad. Sci.* **118**: 1–8.
- Fastner, A., Absmanner, B., and Hammes, U.Z.** (2017). *Plant Hormones J.* Kleine-Vehn and M. Sauer, eds (Springer New York: New York, NY).
- Feraru, E. and Friml, J.** (2008). PIN polar targeting. *Plant Physiol.* **147**: 1553–1559.
- Feraru, E., Vosolsobě, S., Feraru, M.I., Petrášek, J., and Kleine-Vehn, J.** (2012). Evolution and structural diversification of PILS putative auxin carriers in plants. *Front. Plant Sci.* **3**.
- Finet, C. and Jaillais, Y.** (2012). AUXOLOGY: When auxin meets plant evo-devo. *Dev. Biol.* **369**: 19–31.
- Friml, J., Yang, X., Michniewicz, M., Weijers, D., Quint, A., Tietz, O., Benjamins, R.,**

- Ouwerkerk, P. B. F., Ljung, K., Sandberg, G., Hooykaas, P. J. J., Palme, K., and Offringa, R.** (2004). A PINOID-Dependent Binary Switch in Apical-Basal PIN Polar Targeting Directs Auxin Efflux. *Science* (80-. ). **306**: 862–865.
- Friml, J.** (2003). Auxin transport — shaping the plant. *Curr. Opin. Plant Biol.* **6**: 7–12.
- Friml, J., Wiśniewska, J., Benková, E., Mendgen, K., and Palme, K.** (2002). Lateral relocation of auxin efflux regulator PIN3 mediates tropism in Arabidopsis. *Nature* **415**: 806–809.
- Galston, A.W.** (1947). The Effect of 2,3,5-Triiodobenzoic Acid on the Growth and Flowering of Soybeans. *Am. J. Bot.* **34**: 356.
- Galván-Ampudia, C.S. and Offringa, R.** (2007). Plant evolution: AGC kinases tell the auxin tale. *Trends Plant Sci.* **12**: 541–547.
- Gälweiler, L., Guan, C., Müller, A., Wisman, E., Mendgen, K., Yephremov, A., and Palme, K.** (1998). Regulation of Polar Auxin Transport by AtPIN1 in Arabidopsis Vascular Tissue. *Science* (80-. ). **282**: 2226–2230.
- Ganguly, A., Lee, S.H., and Cho, H.T.** (2012). Functional identification of the phosphorylation sites of Arabidopsis PIN-FORMED3 for its subcellular localization and biological role. *Plant J.* **71**: 810–823.
- Ganguly, A., Lee, S.H., Cho, M., Lee, O.R., Yoo, H., and Cho, H.-T.** (2010). Differential Auxin-Transporting Activities of PIN-FORMED Proteins in Arabidopsis Root Hair Cells. *Plant Physiol.* **153**: 1046–1061.
- Ganguly, A., Park, M., Kesawat, M.S., and Cho, H.-T.** (2014). Functional Analysis of the Hydrophilic Loop in Intracellular Trafficking of Arabidopsis PIN-FORMED Proteins. *Plant Cell* **26**: 1570–1585.
- Geisler, M. Blakeslee, J. J., Bouchard, R., Lee, O. R., Vincenzetti, V., Bandyopadhyay, A., Titapiwatanakun, B., Peer, W. A., Bailly, A., Richards, E. L., Ejendal, K. F. K., Smith, A. P., Baroux, C., Grossniklaus, U., Müller, A., Hrycyna, C. A., Dudler, R., Murphy, A. S., and Martinoia, E.** (2005). Cellular efflux of auxin catalyzed by the Arabidopsis MDR/PGP transporter AtPGP1. *Plant J.* **44**: 179–194.
- Geisler, M., Aryal, B., di Donato, M., and Hao, P.** (2017). A Critical View on ABC Transporters and Their Interacting Partners in Auxin Transport. *Plant Cell Physiol.* **58**: 1601–1614.
- Geisler, M. and Murphy, A.S.** (2006). The ABC of auxin transport: The role of p-glycoproteins in plant development. *FEBS Lett.* **580**: 1094–1102.
- Geisler, M., Wang, B., and Zhu, J.** (2014). Auxin transport during root gravitropism: transporters and techniques. *Plant Biol.* **16**: 50–57.
- Geldner, N., Anders, N., Wolters, H., Keicher, J., Kornberger, W., Muller, P., Delbarre, A., Ueda, T., Nakano, A., and Jürgens, G.** (2003). The Arabidopsis GNOM ARF-GEF Mediates Endosomal Recycling, Auxin Transport, and Auxin-Dependent Plant Growth. *Cell* **112**: 219–230.
- Geldner, N., Friml, J., Stierhof, Y.-D., Jürgens, G., and Palme, K.** (2001). Auxin transport inhibitors block PIN1 cycling and vesicle trafficking. *Nature* **413**: 425–428.
- George, E.** (2007). *Plant Propagation by Tissue Culture Volume 1. The Background.* E.F. George, M.A. Hall, and G.-J. De Klerk, eds (Springer Netherlands: Dordrecht).
- Goggin, D.E., Cawthray, G.R., and Powles, S.B.** (2016). 2,4-D resistance in wild radish: reduced herbicide translocation via inhibition of cellular transport. *J. Exp. Bot.* **67**: 3223–3235.
- Goldsmith, M.H.M. and Goldsmith, T.H.** (1981). Quantitative predictions for the chemiosmotic uptake of auxin. *Planta* **153**: 25–33.
- Goldsmith, M.H.M., Goldsmith, T.H., and Martin, M.H.** (1981). Mathematical analysis of the chemiosmotic polar diffusion of auxin through plant tissues. *Proc. Natl. Acad. Sci.* **78**: 976–980.
- Grabov, A., Ashley, M.K., Rigas, S., Hatzopoulos, P., Dolan, L., and Vicente-Agullo, F.** (2005). Morphometric analysis of root shape. *New Phytol.* **165**: 641–652.
- Grieneisen, V.A., Xu, J., Marée, A.F.M., Hogeweg, P., and Scheres, B.** (2007). Auxin

- transport is sufficient to generate a maximum and gradient guiding root growth. *Nature* **449**: 1008–1013.
- Grossmann, K.** (2010). Auxin herbicides: Current status of mechanism and mode of action. *Pest Manag. Sci.* **66**: 113–120.
- Grossmann, K.** (2000). Mode of action of auxin herbicides: a new ending to a long, drawn out story. *Trends Plant Sci.* **5**: 506–508.
- Gujas, B., Alonso-Blanco, C., and Hardtke, C.S.** (2012). Natural Arabidopsis brx Loss-of-Function Alleles Confer Root Adaptation to Acidic Soil. *Curr. Biol.* **22**: 1962–1968.
- Habets, M.E.J. and Offringa, R.** (2014). PIN-driven polar auxin transport in plant developmental plasticity: a key target for environmental and endogenous signals. *New Phytol.* **203**: 362–377.
- Haga, K., Frank, L., Kimura, T., Schwechheimer, C., and Sakai, T.** (2018). Roles of AGCVIII Kinases in the Hypocotyl Phototropism of Arabidopsis Seedlings. *Plant Cell Physiol.* **59**: 1060–1071.
- Hajný, J., Prát, T., Rydza, N., Rodriguez, L., Tan, S., Verstraeten, I., Domjan, D., Mazur, E., Smakowska-Luzan, E., Smet, W., Mor, E., Nolf, J., Yang, B., Grunewald, W., Molnár, G., Belkhadir, Y., De Rybel, B., and Friml, J.** (2020). Receptor kinase module targets PIN-dependent auxin transport during canalization. *Science (80-. )*. **370**: 550–557.
- Hammes, U.Z., Murphy, A.S., and Schwechheimer, C.** (2022). Auxin Transporters—A Biochemical View. *Cold Spring Harb. Perspect. Biol.* **14**: a039875.
- Hammes, U.Z., Nielsen, E., Honaas, L.A., Taylor, C.G., and Schachtman, D.P.** (2006). AtCAT6, a sink-tissue-localized transporter for essential amino acids in Arabidopsis. *Plant J.* **48**: 414–426.
- Han, H., Adamowski, M., Qi, L., Alotaibi, S.S., and Friml, J.** (2021). PIN-mediated polar auxin transport regulations in plant tropic responses. *New Phytol.* **232**: 510–522.
- Hayashi, K., Nakamura, S., Fukunaga, S., Nishimura, T., Jenness, M.K., Murphy, A.S., Motose, H., Nozaki, H., Furutani, M., and Aoyama, T.** (2014). Auxin transport sites are visualized in planta using fluorescent auxin analogs. *Proc. Natl. Acad. Sci.* **111**: 11557–11562.
- Henrichs, S., Wang, B., Fukao, Y., Zhu, J., Charrier, L., Bailly, A., Oehring, S. C., Linnert, M., Weiwad, M., Endler, A., Nanni, P., Pollmann, S., Mancuso, S., Schulz, A., and Geisler, M.** (2012). Regulation of ABCB1/PGP1-catalysed auxin transport by linker phosphorylation. *EMBO J.* **31**: 2965–2980.
- Hoffmann, O.L. and Smith, A.E.** (1949). A New Group of Plant Growth Regulators. *Science (80-. )*. **109**: 588–588.
- Hošek, P., Kubeš, M., Laňková, M., Dobrev, P.I., Klíma, P., Kohoutová, M., Petrášek, J., Hoyerová, K., Jiřina, M., and Zažímalová, E.** (2012). Auxin transport at cellular level: new insights supported by mathematical modelling. *J. Exp. Bot.* **63**: 3815–3827.
- Huang, F., Kemel Zago, M., Abas, L., van Marion, A., Galván-Ampudia, C.S., and Offringa, R.** (2010). Phosphorylation of Conserved PIN Motifs Directs Arabidopsis PIN1 Polarity and Auxin Transport. *Plant Cell* **22**: 1129–1142.
- Humphrey, T. V., Haasen, K.E., Aldea-Brydges, M.G., Sun, H., Zayed, Y., Indriolo, E., and Goring, D.R.** (2015). PERK–KIPK–KCBP signalling negatively regulates root growth in Arabidopsis thaliana. *J. Exp. Bot.* **66**: 71–83.
- Ito, H. and Gray, W.M.** (2006). A Gain-of-Function Mutation in the Arabidopsis Pleiotropic Drug Resistance Transporter PDR9 Confers Resistance to Auxinic Herbicides. *Plant Physiol.* **142**: 63–74.
- Jablanović, M. and Noodén, L.D.** (1974). Changes in competitive IAA binding in relation to bud development in pea seedlings<sup>1</sup>. *Plant Cell Physiol.* **15**: 687–692.
- Jacobs, M. and Rubery, P.H.** (1988). Naturally occurring auxin transport regulators. *Science* **241**: 346–349.
- Jia, W., Li, B., Li, S., Liang, Y., Wu, X., Ma, M., Wang, J., Gao, J., Cai, Y., Zhang, Y., Wang, Y., Li, J., and Wang, Y.** (2016). Mitogen-Activated Protein Kinase Cascade MKK7-MPK6

- Plays Important Roles in Plant Development and Regulates Shoot Branching by Phosphorylating PIN1 in Arabidopsis. *PLOS Biol.* **14**: e1002550.
- Kim, J.-Y., Henrichs, S., Bailly, A., Vincenzetti, V., Sovero, V., Mancuso, S., Pollmann, S., Kim, D., Geisler, M., and Nam, H.-G.** (2010). Identification of an ABCB/P-glycoprotein-specific Inhibitor of Auxin Transport by Chemical Genomics. *J. Biol. Chem.* **285**: 23309–23317.
- Kleine-Vehn, J., Ding, Z., Jones, A.R., Tasaka, M., Morita, M.T., and Friml, J.** (2010a). Gravity-induced PIN transcytosis for polarization of auxin fluxes in gravity-sensing root cells. *Proc. Natl. Acad. Sci.* **107**: 22344–22349.
- Kleine-Vehn, J., Huang, F., Naramoto, S., Zhang, J., Michniewicz, M., Offringa, R., and Friml, J.** (2010b). PIN Auxin Efflux Carrier Polarity Is Regulated by PINOID Kinase-Mediated Recruitment into GNOM-Independent Trafficking in Arabidopsis. *Plant Cell* **21**: 3839–3849.
- Kleine-Vehn, J., Wabnik, K., Martinière, A., Łangowski, Ł., Willig, K., Naramoto, S., Leitner, J., Tanaka, H., Jakobs, S., Robert, S., Luschnig, C., Govaerts, W., W Hell, S., Runions, J., and Friml, J.** (2011). Recycling, clustering, and endocytosis jointly maintain PIN auxin carrier polarity at the plasma membrane. *Mol. Syst. Biol.* **7**: 540.
- Koh, S.W.H., Marhava, P., Rana, S., Graf, A., Moret, B., Bassukas, A.E.L., Zourelidou, M., Kolb, M., Hammes, U.Z., Schwechheimer, C., and Hardtke, C.S.** (2021). Mapping and engineering of auxin-induced plasma membrane dissociation in BRX family proteins. *Plant Cell* **33**: 1945–1960.
- Kolb, M.** (2015). Characterization of the putative auxin efflux transporters PIN5, PIN6 and PIN8 - A domain-swapping approach. Master's Thesis, Universität Regensburg.
- Kramer, E.M. and Bennett, M.J.** (2006). Auxin transport: a field in flux. *Trends Plant Sci.* **11**: 382–386.
- Křeček, P., Skůpa, P., Libus, J., Naramoto, S., Tejos, R., Friml, J., and Zažímalová, E.** (2009). The PIN-FORMED (PIN) protein family of auxin transporters. *Genome Biol.* **10**: 249.
- Krieger, G., Shkolnik, D., Miller, G., and Fromm, H.** (2016). Reactive oxygen species tune root tropic responses. *Plant Physiol.* **Oct;172(2)**: 1209-1220
- Krouk, G., Lacombe, B., Bielach, A., Perrine-Walker, F., Malinska, K., Mounier, E., Hoyerova, K., Tillard, P., Leon, S., Ljung, K., Zazimalova, E., Benkova, E., Nacry, P., and Gojon, A.** (2010). Nitrate-Regulated Auxin Transport by NRT1.1 Defines a Mechanism for Nutrient Sensing in Plants. *Dev. Cell* **18**: 927–937.
- Lampropoulos, A., Sutikovic, Z., Wenzl, C., Maegele, I., Lohmann, J.U., and Forner, J.** (2013). GreenGate - A Novel, Versatile, and Efficient Cloning System for Plant Transgenesis. *PLoS One* **8**: e83043.
- Larrieu, A. and Vernoux, T.** (2015). Comparison of plant hormone signalling systems. *Essays Biochem.* **58**: 165–181.
- Lee, H., Ganguly, A., Lee, R.D., Park, M., and Cho, H.-T.** (2020a). Intracellularly Localized PIN-FORMED8 Promotes Lateral Root Emergence in Arabidopsis. *Front. Plant Sci.* **10**: 1–11.
- Lee, H., Kim, H., Park, J.M., Cho, H.S., and Jeon, J.H.** (2020b). PIN-mediated polar auxin transport facilitates root-obstacle avoidance. *New Phytol.* **225**: 1285–1296.
- Li, L., Gallei, M., and Friml, J.** (2022). Bending to auxin: fast acid growth for tropisms. *Trends Plant Sci.* **27**: 440–449.
- Li, L., Hou, X., Tsuge, T., Ding, M., Aoyama, T., Oka, A., Gu, H., Zhao, Y., and Qu, L.-J.** (2008). The possible action mechanisms of indole-3-acetic acid methyl ester in Arabidopsis. *Plant Cell Rep.* **27**: 575–584.
- Liao, C.-Y., Smet, W., Brunoud, G., Yoshida, S., Vernoux, T., and Weijers, D.** (2015). Reporters for sensitive and quantitative measurement of auxin response. *Nat. Methods* **12**: 207–210.
- Liu, C.-J., Zhao, Y., and Zhang, K.** (2019). Cytokinin Transporters: Multisite Players in Cytokinin Homeostasis and Signal Distribution. *Front. Plant Sci.* **10**: 1–9.



- Liu, X.-Y., Hou, W.-T., Wang, L., Li, B., Chen, Y., Chen, Y., Jiang, Y.-L., and Zhou, C.-Z.** (2021). Structures of cyanobacterial bicarbonate transporter SbtA and its complex with PII-like SbtB. *Cell Discov.* **7**: 63.
- Ljung, K., Bhalerao, R.P., and Sandberg, G.** (2001). Sites and homeostatic control of auxin biosynthesis in *Arabidopsis* during vegetative growth. *Plant J.* **28**: 465–474.
- Ljung, K., Hull, A.K., Celenza, J., Yamada, M., Estelle, M., Normanly, J., and Sandberg, G.** (2005). Sites and regulation of auxin biosynthesis in *Arabidopsis* roots. *Plant Cell* **17**: 1090–1104.
- Ludwig-Müller, J.** (2022). Auxins in the right space and time regulate pea fruit development. *J. Exp. Bot.* **73**: 3831–3835.
- Ludwig-Müller, J. and Epstein, E.** (1991). Occurrence and in Vivo Biosynthesis of Indole-3-Butyric Acid in Corn (*Zea mays* L.). *Plant Physiol.* **97**: 765–770.
- Luschnig, C., Gaxiola, R.A., Grisafi, P., and Fink, G.R.** (1998). EIR1, a root-specific protein involved in auxin transport, is required for gravitropism in *Arabidopsis thaliana*. *Genes Dev.* **12**: 2175–2187.
- Marchant, A., Bhalerao, R., Casimiro, I., Eklöf, J., Casero, P.J., Bennett, M., and Sandberg, G.** (2002). AUX1 Promotes Lateral Root Formation by Facilitating Indole-3-Acetic Acid Distribution between Sink and Source Tissues in the *Arabidopsis* Seedling. *Plant Cell* **14**: 589–597.
- Marhava, P., Aliaga Fandino, A.C., Koh, S.W.H., Jelínková, A., Kolb, M., Janacek, D.P., Breda, A.S., Cattaneo, P., Hammes, U.Z., Petrášek, J., and Hardtke, C.S.** (2020). Plasma Membrane Domain Patterning and Self-Reinforcing Polarity in *Arabidopsis*. *Dev. Cell* **52**: 223-235.e5.
- Marhava, P., Bassukas, A.E.L., Zourelidou, M., Kolb, M., Moret, B., Fastner, A., Schulze, W.X., Cattaneo, P., Hammes, U.Z., Schwechheimer, C., and Hardtke, C.S.** (2018). A molecular rheostat adjusts auxin flux to promote root protophloem differentiation. *Nature* **558**: 1.
- Matsuda, S., Kajizuka, T., Kadota, A., Nishimura, T., and Koshiba, T.** (2011). NPH3- and PGP-like genes are exclusively expressed in the apical tip region essential for blue-light perception and lateral auxin transport in maize coleoptiles. *J. Exp. Bot.* **62**: 3459–3466.
- Michniewicz, M., Zago, M. K., Abas, L., Weijers, D., Schweighofer, A., Meskiene, I., Heisler, M. G., Ohno, C., Zhang, J., Huang, F., Schwab, R., Weigel, D., Meyerowitz, E. M., Luschnig, C., Offringa, R., and Friml, J.** (2007). Antagonistic Regulation of PIN Phosphorylation by PP2A and PINOID Directs Auxin Flux. *Cell* **130**: 1044–1056.
- Michniewicz, M., Ho, C., Enders, T.A., Floro, E., Damodaran, S., Gunther, L.K., Powers, S.K., Frick, E.M., Topp, C.N., Frommer, W.B., and Strader, L.C.** (2019). TRANSPORTER OF IBA1 Links Auxin and Cytokinin to Influence Root Architecture. *Dev. Cell* **50**: 599-609.e4.
- Michniewicz, M., Powers, S.K., and Strader, L.C.** (2014). IBA Transport by PDR Proteins. In *Plant ABC Transporters*, pp. 313–331.
- Mironova, V. V., Omelyanchuk, N.A., Novoselova, E.S., Doroshkov, A. V., Kazantsev, F. V., Kochetov, A. V., Kolchanov, N.A., Mjolsness, E., and Likhoshvai, V.A.** (2012). Combined in silico/in vivo analysis of mechanisms providing for root apical meristem self-organization and maintenance. *Ann. Bot.* **110**: 349–360.
- Morita, M.T. and Tasaka, M.** (2004). Gravity sensing and signaling. *Curr. Opin. Plant Biol.* **7**: 712–718.
- Moubayidin, L., Di Mambro, R., and Sabatini, S.** (2009). Cytokinin–auxin crosstalk. *Trends Plant Sci.* **14**: 557–562.
- Mouchel, C.F., Briggs, G.C., and Hardtke, C.S.** (2004). Natural genetic variation in *Arabidopsis* identifies BREVIS RADIX, a novel regulator of cell proliferation and elongation in the root. *Genes Dev.* **18**: 700–714.
- Mravec, J., Skůpa, P., Bailly, A., Hoyerová, K., Křeček, P., Bielach, A., Petrášek, J., Zhang, J., Gaykova, V., Stierhof, Y-D., Dobrev, P. I., Schwarzerová, K., Rolčík, J., Seifertová, D., Luschnig, C., Benková, E., Zažímalová, E., Geisler, M., and Friml, J.**

- (2009). Subcellular homeostasis of phytohormone auxin is mediated by the ER-localized PIN5 transporter. *Nature* **459**: 1136–1140.
- Mravec, J., Kubeš, M., Bielach, A., Gaykova, V., Petrášek, J., Skupa, P., Chand, S., Benková, E., Zažímalová, E., and Friml, J.** (2008). Interaction of PIN and PGP transport mechanisms in auxin distribution-dependent development. *Development* **135**: 3345–3354.
- Mukherjee, S., David, A., Yadav, S., Baluška, F., and Bhatla, S.C.** (2014). Salt stress-induced seedling growth inhibition coincides with differential distribution of serotonin and melatonin in sunflower seedling roots and cotyledons. *Physiol. Plant.* **152**: 714–728.
- Müller, A., Guan, C., Gälweiler, L., Tänzler, P., Huijser, P., Marchant, A., Parry, G., Bennett, M., Wisman, E., and Palme, K.** (1998). AtPIN2 defines a locus of Arabidopsis for root gravitropism control. *EMBO J.* **17**: 6903–6911.
- Müller, B., Fastner, A., Karmann, J., Mansch, V., Hoffmann, T., Schwab, W., Suter-Grotemeyer, M., Rentsch, D., Truernit, E., Ladwig, F., Bleckmann, A., Dresselhaus, T., and Hammes, U. Z.** (2015). Amino Acid Export in Developing Arabidopsis Seeds Depends on UmamiT Facilitators. *Curr. Biol.* **25**: 3126–3131.
- Nodzyński, T., Vanneste, S., Zwiewka, M., Pernisová, M., Hejátko, J., and Friml, J.** (2016). Enquiry into the Topology of Plasma Membrane-Localized PIN Auxin Transport Components. *Mol. Plant* **9**: 1504–1519.
- Noh, B., Murphy, A. S., and Spalding, E. P.** (2001). Multidrug Resistance-like Genes of Arabidopsis Required for Auxin Transport and Auxin-Mediated Development. *Plant Cell* **13**: 2441–2454.
- Normanly, J.** (2010). Approaching Cellular and Molecular Resolution of Auxin Biosynthesis and Metabolism. *Cold Spring Harb. Perspect. Biol.* **2**: a001594–a001594.
- Notman, R., Noro, M., O'Malley, B., and Anwar, J.** (2006). Molecular Basis for Dimethylsulfoxide (DMSO) Action on Lipid Membranes. *J. Am. Chem. Soc.* **128**: 13982–13983.
- Okada, K., Ueda, J., Komaki, M.K., Bell, C.J., Shimura, Y., Okadalat, K., Uedalb, J., Komaki, M.K., and Bell, C.J.** (1991). Requirement of the Auxin Polar Transport System in Early Stages of Arabidopsis Floral Bud Formation. *Plant Cell* **3**: 677–684.
- Osugi, A. and Sakakibara, H.** (2015). Q and A: How do plants respond to cytokinins and what is their importance? *BMC Biol.* **13**: 102.
- Paciorek, T., Zažímalová, E., Ruthardt, N., Petrášek, J., Stierhof, Y.-D., Kleine-Vehn, J., Morris, D.A., Emans, N., Jürgens, G., Geldner, N., and Friml, J.** (2005). Auxin inhibits endocytosis and promotes its own efflux from cells. *Nature* **435**: 1251–1256.
- Pelagio-Flores, R., Ortíz-Castro, R., Méndez-Bravo, A., Macías-Rodríguez, L., and López-Bucio, J.** (2011). Serotonin, a Tryptophan-Derived Signal Conserved in Plants and Animals, Regulates Root System Architecture Probably Acting as a Natural Auxin Inhibitor in Arabidopsis thaliana. *Plant Cell Physiol.* **52**: 490–508.
- Peterson, G.E.** (1967). The Discovery and Development of 2,4-D. *Agric. Hist.* **41**: 243–254.
- Peterson, M.A., McMaster, S.A., Riechers, D.E., Skelton, J., and Stahlman, P.W.** (2016). 2,4-D Past, Present, and Future: A Review. *Weed Technol.* **30**: 303–345.
- Petersson, S. V., Johansson, A.I., Kowalczyk, M., Makoveychuk, A., Wang, J.Y., Moritz, T., Grebe, M., Benfey, P.N., Sandberg, G., and Ljung, K.** (2009). An Auxin Gradient and Maximum in the Arabidopsis Root Apex Shown by High-Resolution Cell-Specific Analysis of IAA Distribution and Synthesis. *Plant Cell* **21**: 1659–1668.
- Petrášek, J., Mravec, J., Bouchard, R., Blakeslee, J. J., Abas, M., Seifertová, D., Wiśniewska, J., Tadele, Z., Kubeš, M., Čovanová, M., Dhonukshe, P., Skůpa, P., Benková, E., Perry, L., Křeček, P., Lee, O. R., Fink, G. R., Geisler, M., Murphy, A. S., Luschnig, C., Zažímalová, E., and Friml, J.** (2006). PIN Proteins Perform a Rate-Limiting Function in Cellular Auxin Efflux. *Science* (80-. ). **312**: 914–918.
- Qin, G., Gu, H., Zhao, Y., Ma, Z., Shi, G., Yang, Y., Pichersky, E., Chen, H., Liu, M., Chen, Z., and Qu, L.-J.** (2005). An Indole-3-Acetic Acid Carboxyl Methyltransferase Regulates Arabidopsis Leaf Development. *Plant Cell* **17**: 2693–2704.

- Rahman, A., Takahashi, M., Shibasaki, K., Wu, S., Inaba, T., Tsurumi, S., and Baskin, T.I.** (2010). Gravitropism of *Arabidopsis thaliana* Roots Requires the Polarization of PIN2 toward the Root Tip in Meristematic Cortical Cells. *Plant Cell* **22**: 1762–1776.
- Rahni, R. and Birnbaum, K.D.** (2019). Week-long imaging of cell divisions in the *Arabidopsis* root meristem. *Plant Methods* **15**: 30.
- Ranocha, P., Dima, O., Nagy, R., Felten, J., Corratgé-Faillie, C., Novák, O., Morreel, K., Lacombe, B., Martinez, Y., Pfrunder, S., Jin, X., Renou, J-P., Thibaud, J-B., Ljung, K., Fischer, U., Martinoia, E., Boerjan, W., and Goffner, D.** (2013). *Arabidopsis* WAT1 is a vacuolar auxin transport facilitator required for auxin homeostasis. *Nat. Commun.* **4**.
- Rashotte, A.M., Brady, S.R., Reed, R.C., Ante, S.J., and Muday, G.K.** (2000). Basipetal Auxin Transport Is Required for Gravitropism in Roots of *Arabidopsis*. *Plant Physiol.* **122**: 481–490.
- Rashotte, A.M., DeLong, A., and Muday, G.K.** (2005). Genetic and Chemical Reductions in Protein Phosphatase Activity Alter Auxin Transport, Gravity Response, and Lateral Root Growth. *Plant Cell* **17**: 2614–2614.
- Rashotte, A.M., Poupard, J., Waddell, C.S., and Muday, G.K.** (2003). Transport of the Two Natural Auxins, Indole-3-Butyric Acid and Indole-3-Acetic Acid, in *Arabidopsis*. *Plant Physiol.* **133**: 761–772.
- Reinhardt, D., Mandel, T., and Kuhlemeier, C.** (2000). Auxin Regulates the Initiation and Radial Position of Plant Lateral Organs. *Plant Cell* **12**: 507–518.
- Rigó, G., Ayaydin, F., Tietz, O., Zsigmond, L., Kovács, H., Páy, A., Salchert, K., Darula, Z., Medzihradzsky, K. F., Szabados, L., Palme, K., Koncz, C., and Cséplő, Á.** (2013). Inactivation of Plasma Membrane-Localized CDPK-RELATED KINASE5 Decelerates PIN2 Exocytosis and Root Gravitropic Response in *Arabidopsis*. *Plant Cell* **25**: 1592–1608.
- Rodriguez-Villalon, A., Gujas, B., Kang, Y.H., Breda, A.S., Cattaneo, P., Depuydt, S., and Hardtke, C.S.** (2014). Molecular genetic framework for protophloem formation. *Proc. Natl. Acad. Sci.* **111**: 11551–11556.
- Rodriguez-Villalon, A., Gujas, B., van Wijk, R., Munnik, T., and Hardtke, C.S.** (2015). Primary root protophloem differentiation requires balanced phosphatidylinositol-4,5-bisphosphate levels and systemically affects root branching. *Development* **142**: 1437–1446.
- Rowe, M.H., Dong, J., Weimer, A.K., and Bergmann, D.C.** (2019). A Plant-Specific Polarity Module Establishes Cell Fate Asymmetry in the *Arabidopsis* Stomatal Lineage. *bioRxiv*: 1–13.
- Rubery, P.H. and Sheldrake, A.R.** (1973). Effect of pH and Surface Charge on Cell Uptake of Auxin. *Nat. New Biol.* **244**: 285–288.
- Rubery, P.H. and Sheldrake, A.R.** (1974). Carrier-mediated auxin transport. *Planta* **118**: 101–121.
- Ruiz Rosquete, M., Barbez, E., and Kleine-Vehn, J.** (2012). Cellular Auxin Homeostasis: Gatekeeping Is Housekeeping. *Mol. Plant* **5**: 772–786.
- Růžička, K., Strader, L. C., Bailly, A., Yang, H., Blakeslee, J., Langowski, Ł., Nejedlá, E., Fujita, H., Itoh, H., Syōno, K., Hejátko, J., Gray, W. M., Martinoia, E., Geisler, M., Bartel, B., Murphy, A. S., and Friml, J.** (2010). *Arabidopsis* PIS1 encodes the ABCG37 transporter of auxinic compounds including the auxin precursor indole-3-butyric acid. *Proc. Natl. Acad. Sci.* **107**: 10749–10753.
- Sabatini, S., Beis, D., Wolkenfelt, H., Murfett, J., Guilfoyle, T., Malamy, J., Benfey, P., Leyser, O., Bechtold, N., Weisbeek, P., and Scheres, B.** (1999). An Auxin-Dependent Distal Organizer of Pattern and Polarity in the *Arabidopsis* Root. *Cell* **99**: 463–472.
- Sakakibara, H.** (2006). Cytokinins: Activity, biosynthesis, and translocation. *Annu. Rev. Plant Biol.* **57**: 431–449.
- Sambrook, J., Fritsch, E.F., and Maniatis, T.** (1989). Molecular cloning: A laboratory manual. In Cold Spring Harbor, New York, Cold Spring Harbor Laboratory Press.

- Santelia, D., Henrichs, S., Vincenzetti, V., Sauer, M., Bigler, L., Klein, M., Bailly, A., Lee, Y., Friml, J., Geisler, M., and Martinoia, E.** (2008). Flavonoids Redirect PIN-mediated Polar Auxin Fluxes during Root Gravitropic Responses. *J. Biol. Chem.* **283**: 31218–31226.
- Santuari, L., Scacchi, E., Rodriguez-Villalon, A., Salinas, P., Dohmann, E.M.N., Brunoud, G., Vernoux, T., Smith, R.S., and Hardtke, C.S.** (2011). Positional Information by Differential Endocytosis Splits Auxin Response to Drive Arabidopsis Root Meristem Growth. *Curr. Biol.* **21**: 1918–1923.
- Sato, E.M., Hijazi, H., Bennett, M.J., Vissenberg, K., and Swarup, R.** (2015). New insights into root gravitropic signalling. *J. Exp. Bot.* **66**: 2155–2165.
- Sauer, M., Robert, S., and Kleine-Vehn, J.** (2013). Auxin: simply complicated. *J. Exp. Bot.* **64**: 2565–2577.
- Sawchuk, M.G., Edgar, A., and Scarpella, E.** (2013). Patterning of Leaf Vein Networks by Convergent Auxin Transport Pathways. *PLoS Genet.* **9**: e1003294.
- Scacchi, E., Osmont, K.S., Beuchat, J., Salinas, P., Navarrete-Gómez, M., Trigueros, M., Ferrándiz, C., and Hardtke, C.S.** (2009). Dynamic, auxin-responsive plasma membrane-to-nucleus movement of Arabidopsis BRX. *Development* **136**: 2059–2067.
- Schulz, P., Garcia-Celma, J.J., and Fendler, K.** (2008). SSM-based electrophysiology. *Methods* **46**: 97–103.
- Shin, H., Shin, H.-S., Guo, Z., Blancaflor, E.B., Masson, P.H., and Chen, R.** (2005). Complex regulation of Arabidopsis AGR1/PIN2-mediated root gravitropic response and basipetal auxin transport by cantharidin-sensitive protein phosphatases. *Plant J.* **42**: 188–200.
- Simon, S., Skůpa, P., Viaene, T., Zwiewka, M., Tejos, R., Klíma, P., Čarná, M., Rolčík, J., De Rycke, R., Moreno, I., Dobrev, P. I., Orellana, A., Zažímalová, E., and Friml, J.** (2016). PIN6 auxin transporter at endoplasmic reticulum and plasma membrane mediates auxin homeostasis and organogenesis in Arabidopsis. *New Phytol.* **211**: 65–74.
- Skokan, R., Medvecká, E., Viaene, T., Vosolobě, S., Zwiewka, M., Müller, K., Skůpa, P., Karady, M., Zhang, Y., Janacek, D. P., Hammes, U. Z., Ljung, K., Nodzyński, T., Petrášek, J., and Friml, J.** (2019). PIN-driven auxin transport emerged early in streptophyte evolution. *Nat. Plants* **5**: 1114–1119.
- Song, Y.** (2014). Insight into the mode of action of 2,4-dichlorophenoxyacetic acid (2,4-D) as an herbicide. *J. Integr. Plant Biol.* **56**: 106–113.
- Steinmann, T., Geldner, N., Grebe, M., Mangold, S., Jackson, C.L., Paris, S., Gälweiler, L., Palme, K., and Jürgens, G.** (1999). Coordinated Polar Localization of Auxin Efflux Carrier PIN1 by GNOM ARF GEF. *Science* (80-. ). **286**: 316–318.
- Strader, L.C. and Bartel, B.** (2009). The Arabidopsis PLEIOTROPIC DRUG RESISTANCE8/ABCG36 ATP Binding Cassette Transporter Modulates Sensitivity to the Auxin Precursor Indole-3-Butyric Acid. *Plant Cell* **21**: 1992–2007.
- Strader, L.C. and Bartel, B.** (2011). Transport and Metabolism of the Endogenous Auxin Precursor Indole-3-Butyric Acid. *Mol. Plant* **4**: 477–486.
- Strader, L.C., Monroe-Augustus, M., Rogers, K.C., Lin, G.L., and Bartel, B.** (2008). Arabidopsis iba response5 Suppressors Separate Responses to Various Hormones. *Genetics* **180**: 2019–2031.
- Su, N., Zhu, A., Tao, X., Ding, Z. J., Chang, S., Ye, F., Zhang, Y., Zhao, C., Chen, Q., Wang, J., Zhou, C. Y., Guo, Y., Jiao, S., Zhang, S., Wen, H., Ma, L., Ye, S., Zheng, S. J., Yang, F., Wu, S., and Guo, J.** (2022). Structures and mechanisms of the Arabidopsis auxin transporter PIN3. *Nature* **609**: 616–621.
- Su, S.-H., Gibbs, N.M., Jancewicz, A.L., and Masson, P.H.** (2017). Molecular Mechanisms of Root Gravitropism. *Curr. Biol.* **27**: R964–R972.
- Sussman, M.R. and Goldsmith, M.H.M.** (1981). The action of specific inhibitors of auxin transport on uptake of auxin and binding of N-1-naphthylphthalamic acid to a membrane site in maize coleoptiles. *Planta* **152**: 13–18.

- Swarup, K., Benková, E., Swarup, R., Casimiro, I., Péret, B., Yang, Y., Parry, G., Nielsen, E., De Smet, I., Vanneste, S., Levesque, M. P., Carrier, D., James, N., Calvo, V., Ljung, K., Kramer, E., Roberts, R., Graham, N., Marillonnet, S., Patel, K., Jones, J. D. G., Taylor, C. G., Schachtman, D. P., May, S., Sandberg, G., Benfey, P., Friml, J., Kerr, I., Beeckman, T., Laplace, L., and Bennett, M. J.** (2008). The auxin influx carrier LAX3 promotes lateral root emergence. *Nat. Cell Biol.* **10**: 946–954.
- Swarup, R., Friml, J., A., M., Ljung, K., Sandberg, G., Palme, G., and Bennett, M.J.** (2001). Localisation of the auxin permease AUX1 in the Arabidopsis root apex reveals two novel functionally distinct hormone transport pathways. *Genes Dev.* **15**: 2648–2653.
- Tan, S., Zhang, X., Kong, W., Yang, X.-L., Molnár, G., Vondráková, Z., Filepová, R., Petrášek, J., Friml, J., and Xue, H.-W.** (2020). The lipid code-dependent phosphoswitch PDK1–D6PK activates PIN-mediated auxin efflux in Arabidopsis. *Nat. Plants* **6**: 556–569.
- Tanaka, H., Dhonukshe, P., Brewer, P.B., and Friml, J.** (2006). Spatiotemporal asymmetric auxin distribution: a means to coordinate plant development. *Cell. Mol. Life Sci.* **63**: 2738–2754.
- Teale, W. and Palme, K.** (2018). Naphthylphthalamic acid and the mechanism of polar auxin transport. *J. Exp. Bot.* **69**: 303–312.
- Teale, W.D., Pasternak, T., Dal Bosco, C., Dovzhenko, A., Kratzat, K., Bildl, W., Schwörer, M., Falk, T., Ruperti, B., V. Schaefer, J., Shahriari, M., Pilgermayer, L., Li, X., Lübben, F., Plückthun, A., Schulte, U., and Palme, K.** (2021). Flavonol-mediated stabilization of PIN efflux complexes regulates polar auxin transport. *EMBO J.* **40**: 1–14.
- Thomson, K.-S., Hertel, R., Müller, S., and Tand vares, J.E.** (1973b). 1-N-naphthylphthalamic acid and 2,3,5-triiodobenzoic acid. *Planta* **109**: 337–352.
- Titapiwatanakun, B., Blakeslee, J. J., Bandyopadhyay, A., Yang, H., Mravec, J., Sauer, M., Cheng, Y., Adamec, J., Nagashima, A., Geisler, M., Sakai, T., Friml, J., Peer, W. A., aMurphy, A. S.** (2009). ABCB19/PGP19 stabilises PIN1 in membrane microdomains in Arabidopsis. *Plant J.* **57**: 27–44.
- Ulmasov, T., Murfett, J., Hagen, G., and Guilfoyle, T.J.** (1997). Creation of a Highly Active Synthetic AuxRE. *Society* **9**: 1963–1971.
- Ung, K.L., Winkler, M., Schulz, L., Kolb, M., Janacek, D.P., Dedic, E., Stokes, D.L., Hammes, U.Z., and Pedersen, B.P.** (2022). Structures and mechanism of the plant PIN-FORMED auxin transporter. *Nature* **609**: 605–610.
- Vernoux, T., Brunoud, G., Farcot, E., Morin, V., Van den Daele, H., Legrand, J., Oliva, M., Das, P., Larrieu, A., Wells, D., Guédon, Y., Armitage, L., Picard, F., Guyomarc'h, S., Cellier, C., Parry, G., Koumproglou, R., Doonan, J. H., Estelle, M., Godin, C., Kepinski, S., Bennett, M., De Veylder, L., and Traas, J.** (2011). The auxin signalling network translates dynamic input into robust patterning at the shoot apex. *Mol. Syst. Biol.* **7**: 508.
- Viaene, T., Delwiche, C.F., Rensing, S.A., and Friml, J.** (2013). Origin and evolution of PIN auxin transporters in the green lineage. *Trends Plant Sci.* **18**: 5–10.
- Vieten, A., Sauer, M., Brewer, P.B., and Friml, J.** (2007). Molecular and cellular aspects of auxin-transport-mediated development. *Trends Plant Sci.* **12**: 160–168.
- Wang, J., Guo, X., Xiao, Q., Zhu, J., Cheung, A.Y., Yuan, L., Vierling, E., and Xu, S.** (2021). Auxin efflux controls orderly nucellar degeneration and expansion of the female gametophyte in Arabidopsis. *New Phytol.* **230**: 2261–2274.
- Weijers, D. and Wagner, D.** (2016). Transcriptional Responses to the Auxin Hormone. *Annu. Rev. Plant Biol.* **67**: 539–574.
- Weller, B.** (2017). Auxin transport regulation through dynamic efflux carrier phosphorylation. Dissertation Technische Universität München.
- Weller, B., Zourelidou, M., Frank, L., Barbosa, I.C.R., Fastner, A., Richter, S., Jürgens, G., Hammes, U.Z., and Schwechheimer, C.** (2017). Dynamic PIN-FORMED auxin efflux carrier phosphorylation at the plasma membrane controls auxin efflux-dependent growth. *Proc. Natl. Acad. Sci.* **114**.
- Went, F.W.** (1928). Wuchsstoff und Wachstum. *Recl. Des Trav. Bot.* **25**: 1–116.

- Willige, B.C., Ahlers, S., Zourelidou, M., Barbosa, I.C.R., Demarsy, E., Trevisan, M., Davis, P.A., Roelfsema, M.R.G., Hangarter, R., Fankhauser, C., and Schwechheimer, C.** (2013). D6PK AGCVIII Kinases Are Required for Auxin Transport and Phototropic Hypocotyl Bending in Arabidopsis. *Plant Cell* **25**: 1674–1688.
- Wiśniewska, J., Xu, J., Seifertová, D., Brewer, P.B., Růžička, K., Blilou, I., Rouquié, D., Benková, E., Scheres, B., and Friml, J.** (2006). Polar PIN Localization Directs Auxin Flow in Plants. *Science* (80-. ). **312**: 883–883.
- Woodward, A.W. and Bartel, B.** (2005). Auxin: Regulation, action, and interaction. *Ann. Bot.* **95**: 707–735.
- Xiao, Y. and Offringa, R.** (2020). PDK1 regulates auxin transport and Arabidopsis vascular development through AGC1 kinase PAX. *Nat. Plants* **6**: 544–555.
- Xu, M., Zhu, L., Shou, H., and Wu, P.** (2005). A PIN1 Family Gene, OsPIN1, involved in Auxin-dependent Adventitious Root Emergence and Tillering in Rice. *Plant Cell Physiol.* **46**: 1674–1681.
- Yang, H. and Murphy, A.S.** (2009). Functional expression and characterization of Arabidopsis ABCB, AUX 1 and PIN auxin transporters in *Schizosaccharomyces pombe*. *Plant J.* **59**: 179–191.
- Yang, Y., Hammes, U.Z., Taylor, C.G., Schachtman, D.P., and Nielsen, E.** (2006). High-Affinity Auxin Transport by the AUX1 Influx Carrier Protein. *Curr. Biol.* **16**: 1123–1127.
- Yang, Y., Xu, R., Ma, C., Vlot, A.C., Klessig, D.F., and Pichersky, E.** (2008). Inactive Methyl Indole-3-Acetic Acid Ester Can Be Hydrolyzed and Activated by Several Esterases Belonging to the At MES Esterase Family of Arabidopsis. *Plant Physiol.* **147**: 1034–1045.
- Yang, Z., Xia, J., Hong, J., Zhang, C., Wei, H., Ying, W., Sun, C., Sun, L., Mao, Y., Gao, Y., Tan, S., Friml, J., Li, D., Liu, X., and Sun, L.** (2022). Structural insights into auxin recognition and efflux by Arabidopsis PIN1. *Nature* **609**: 611–615.
- Zegzouti, H., Li, W., Lorenz, T. C., Xie, M., Payne, C. T., Smith, K., Glenny, S., Payne, G. S., and Christensen, S. K.** (2006). Structural and Functional Insights into the Regulation of Arabidopsis AGC VIIIa Kinases. *J. Biol. Chem.* **281**: 35520–35530.
- Zhang, J., Nodzyński, T., Pěncík, A., Rolčík, J., and Friml, J.** (2010). PIN phosphorylation is sufficient to mediate PIN polarity and direct auxin transport. *Proc. Natl. Acad. Sci.* **107**: 918–922.
- Zhang, J. and Peer, W.A.** (2017). Auxin homeostasis: The DAO of catabolism. *J. Exp. Bot.* **68**: 3145–3154.
- Zhang, Y., Hartinger, C., Wang, X., and Friml, J.** (2020a). Directional auxin fluxes in plants by intramolecular domain–domain coevolution of PIN auxin transporters. *New Phytol.* **227**: 1406–1416.
- Zhang, Y., He, P., Ma, X., Yang, Z., Pang, C., Yu, J., Wang, G., Friml, J., and Xiao, G.** (2019a). Auxin-mediated statolith production for root gravitropism. *New Phytol.* **224**: 761–774.
- Zhang, Y., Rodriguez, L., Li, L., Zhang, X., and Friml, J.** (2020b). Functional innovations of PIN auxin transporters mark crucial evolutionary transitions during rise of flowering plants. *Sci. Adv.* **6**: 1–15.
- Zhang, Y., Xiao, G., Wang, X., Zhang, X., and Friml, J.** (2019b). Evolution of fast root gravitropism in seed plants. *Nat. Commun.* **10**: 3480.
- Zhao, Y.** (2010). Auxin biosynthesis and its role in plant development. *Annu. Rev. Plant Biol.* **61**: 49–64.
- Zolman, B.K., Martinez, N., Millius, A., Adham, A.R., and Bartel, B.** (2008). Identification and Characterization of Arabidopsis Indole-3-Butyric Acid Response Mutants Defective in Novel Peroxisomal Enzymes. *Genetics* **180**: 237–251.
- Zourelidou, M., Absmanner, B., Weller, B., Barbosa, I. CR, Willige, B. C., Fastner, A., Streit, V., Port, S. A., Colcombet, J., de la Fuente van Bentem, S., Hirt, H., Kuster, B., Schulze, W. X., Hammes, U. Z., and Schwechheimer, C.** (2014). Auxin efflux by PIN-FORMED proteins is activated by two different protein kinases, D6 PROTEIN KINASE and PINOID. *Elife* **3**: 1–25.

- Zourelidou, M., Müller, I., Willige, B.C., Nill, C., Jikumaru, Y., Li, H., and Schwechheimer, C.** (2009). The polarly localized D6 PROTEIN KINASE is required for efficient auxin transport in *Arabidopsis thaliana*. *Development* **136**: 627–636.
- Zwiewka, M., Bilanovičová, V., Seifu, Y.W., and Nodzyński, T.** (2019). The Nuts and Bolts of PIN Auxin Efflux Carriers. *Front. Plant Sci.* **10**.

## 11. Acknowledgements

*Men wanted for hazardous journey.  
Low wages, bitter cold, long hours of complete darkness.  
Safe return doubtful. Honour and recognition in event of success.*

Mit dieser Anzeige in einer Londoner Tageszeitung soll einst Ernest Shackleton nach Freiwilligen für die „British Imperial Trans-Antarctic Expedition“, einer Antarktisexpedition in den Jahren 1914 – 1917, gesucht haben. Es könnte aber auch die Ausschreibung für eine Doktorarbeit sein.

Meine Expedition startete in Regensburg, führte mich nach Freising und geht nun erfolgreich zu Ende. Sehr oft habe ich gesagt „Die Doktorarbeit ist so gut wie fertig“ oder „Bald reiche ich ein!“ oder „Jetzt aber dann wirklich!“ Nun ist es tatsächlich so weit. Aber mindestens genauso oft haben mich viele Menschen mit vielen Taten unterstützt, mich mit lieben Worten aufgebaut, mir in den Hintern getreten, mir gesagt, dass das schon wird, mir fachlichen Input zu meiner Forschung gegeben, mit mir Nacht- und Wochenendschichten im Labor eingelegt, aufmunternde Zettel an Laptop und Bildschirm geklebt oder einfach nichts gesagt und mir einen Drink eingeschenkt. An dieser Stelle möchte ich Euch meinen Dank aussprechen, weil Ihr im Großen wie im Kleinen dazu beigetragen haben, dass ich heute sehr stolz auf mich bin.

Lieber Claus,

ich danke Dir dafür, dass Du mir die Möglichkeit gegeben hast, an der TUM zu promovieren. Danke, dass wir als Arbeitsgruppe an Deinen Lehrstuhl kommen konnten und dort willkommen geheißen wurden. Es war eine intensive, einmalige Zeit und ich konnte viel lernen. Ich bin oft an meine Grenzen gekommen – und konnte doch über sie hinauswachsen! Vielen Dank für die fachlichen Impulse und die Unterstützung auch auf den letzten Metern meiner Arbeit.

Lieber Uli,

Hiwi, Praktikantin, Masterandin, Doktorandin: Vom „alten“ Regensburger Lehrstuhl bis heute sind über zehn Jahre vergangen, die wir uns nun schon kennen. Den größten Teil davon war ich ein Teil der AG Hammes. Und ich war es immer gern. Ohne Dich wüsste ich nicht, wer „der Brenner“ ist, hätte unzählige Alben nicht gehört und hätte viele großartige Menschen nicht kennengelernt, von denen viele enge Freundinnen und Freunde geworden sind. Und vor allem würde ich ohne Dich heute keine Doktorarbeit in den Händen halten. Du hast daran geglaubt, dass ich das Zeug dazu hab, mich für dieses tolle Projekt begeistert und mich als Chef, Doktorvater, Wissenschaftler und Freund begleitet. Ich danke Dir von Herzen.



Lieber Jürgen,

vielen Dank für den wissenschaftlichen Input, aber vor allem Deine unglaublich motivierende Art als mein Mentor!

Liebe Dorina,

unzählige injizierte Oozyten, unzählige Stunden Therapie... äh Efflux Assays bei Radio BUH im Isolab: Ich bin sehr stolz darauf, was wir, angefangen als Masterandinnen, in den letzten Jahren zusammen geleistet haben und ohne Dich als PIN-Partnerin wäre meine Doktorarbeit nicht zu dem geworden, was sie ist. Wir sind zusammen gewachsen und zusammengewachsen und waren gemeinsam stark. Die Zeiten waren oft *bäh bäh*, denn *Oozyten kennen kein Weekend*. Doch gemeinsam waren wir stets *nicer dicer* und *im Grünen* Bereich. Piep, piep! <3

Hallo! Heee Sie! Liebe Julia, mein Fels,

danke, dass Du mich unterstützt hast, mir so oft geholfen hast und einfach da warst mit Deiner wunderbaren Art. Immer. Wie groß der Berg auch war, der vor uns lag... Wir haben ihn „Spaten für Spaten“ abgetragen. Ich wusste Dich stets an meiner (rechten) Seite und hatte durch Dich immer ein Gefühl von Sicherheit, dass ich das schon alles irgendwie hinkriege. Danke!

Liebe Angela,

Du hast uns mit offenen Armen im Labor in Freising empfangen und durch Deine liebevolle, positive und engagierte Art so viel zur Arbeitsatmosphäre in unserer AG beigetragen. Vielen Dank für Deine praktische Unterstützung, die zu sehr vielen Ergebnissen in dieser Arbeit beigetragen haben!

“I think I broke my computer....”

Dear Alex, thank you for helping me patiently countless times with my computer, my plants and at the CLSM and for being such a supportive colleague to me. You cheered me up so many times, calmed me down when I freaked out and gave me confidence with a simple “Yes, Martini... you can do it.” I am so happy to have found in you not only a colleague but also a friend – and thanks to you, I know how delicious Pasteis de Nata are.

Liebe Helene, liebe Katrin,

vielen Dank für die Pflege der Frösche und Dorinas und meine Unterstützung bei allem was mit den unzähligen Oozyten zu tun hat.

Dear José,

as promised: forever on my “Thank you slide” and in my acknowledgements – thank you so much for the “angle root script”, I don’t know how I would have evaluated all those roots without it.

Danke an alle (ehemaligen) Kolleginnen und Kollegen des Lehrstuhls für Systembiologie der Pflanzen (TUM) und des Lehrstuhls für Zellbiologie und Pflanzenbiochemie (Universität Regensburg), allen voran der AG Hammes. Danke an Thomas Dresselhaus, bei dem meine Reise begann und an Veronika Mrosek, Petra Wick und Daniela Elephand-Dill, die die Lehrstühle zusammenhalten und gehalten haben!

Lieber Tom,

danke für’s Korrekturlesen und Deine Anmerkungen!

Liebe Sabrina,

wir gehen nun schon so viele Jahre gemeinsam durch unser Leben. Und auch durch die Doktorarbeit hast Du mich begleitet. Ich danke Dir fürs Zuhören, Deine aufbauenden Worte, Deinen Glauben an mich und dass ich wusste, dass Du immer für mich da bist. I didn’t lose the puppy – I found it!

Liebe Anna und Anastasiia,

danke, dass Ihr mich bis zum Schluss angefeuert und unterstützt habt! мяу, мяу!

Meinen lieben Eltern und meinem großartigen Bruder:

Wer hätte gedacht, dass das Ding jemals fertig wird... aber jetzt ist es wirklich so weit! Vielen Dank für Eure Unterstützung in den letzten Jahren auf dem Weg zur und durch die Doktorarbeit. Ich bin von Herzen dankbar, eine so wundervolle Familie zu haben! Und jetzt: Lasst uns bei einem guten Glas Wein mal darüber reden, woran ich da eigentlich geforscht hab...

And last but not least:

"I wanna thank me. I wanna thank me for believing in me. I wanna thank me for doing all this hard work. I wanna thank me for having no days off. I wanna thank me for never quitting"  
(~ Snoop Dogg, 2019, I Wanna Thank Me)

Tornado out.

## 12. Appendix

### Article

# Structures and mechanism of the plant PIN-FORMED auxin transporter

<https://doi.org/10.1038/s41586-022-04883-y>

Received: 4 January 2022

Accepted: 19 May 2022

Published online: 29 June 2022

Open access

 Check for updates

Kien Lam Ung<sup>1,4</sup>, Mikael Winkler<sup>1,4</sup>, Lukas Schulz<sup>2</sup>, Martina Kolb<sup>2</sup>, Dorina P. Janacek<sup>2</sup>, Emil Dedic<sup>1</sup>, David L. Stokes<sup>3</sup>, Ulrich Z. Hammes<sup>2,5\*</sup> & Björn Panyella Pedersen<sup>1,5\*</sup>

Auxins are hormones that have central roles and control nearly all aspects of growth and development in plants<sup>1–3</sup>. The proteins in the PIN-FORMED (PIN) family (also known as the auxin efflux carrier family) are key participants in this process and control auxin export from the cytosol to the extracellular space<sup>4–9</sup>. Owing to a lack of structural and biochemical data, the molecular mechanism of PIN-mediated auxin transport is not understood. Here we present biophysical analysis together with three structures of *Arabidopsis thaliana* PINs: two outward-facing conformations with and without auxin, and one inward-facing conformation bound to the herbicide naphthylphthalamic acid. The structure forms a homodimer, with each monomer divided into a transport and scaffold domain with a clearly defined auxin binding site. Next to the binding site, a proline–proline crossover is a pivot point for structural changes associated with transport, which we show to be independent of proton and ion gradients and probably driven by the negative charge of the auxin. The structures and biochemical data reveal an elevator-type transport mechanism reminiscent of bile acid/sodium symporters, bicarbonate/sodium symporters and sodium/proton antiporters. Our results provide a comprehensive molecular model for auxin recognition and transport by PINs, link and expand on a well-known conceptual framework for transport, and explain a central mechanism of polar auxin transport, a core feature of plant physiology, growth and development.

Auxins are a group of hormones that regulate nearly all growth and developmental processes in plants. Indole-3-acetic acid (IAA;  $pK_a = 4.7$ ) is the most prominent auxin, and is synonymously referred to as ‘auxin’. IAA provides a growth signal that orchestrates most complex environmental responses in plants, including phototropism and geotropism<sup>1</sup>.

Many of the effects on plant growth depend on the distribution of auxin in the plant body, which is controlled by the process of polar auxin transport<sup>2,3</sup>. This process relies on export of auxin out of cells by PIN transporters<sup>4–9</sup>. The physiological importance of PINs is underlined by often severe *pin* mutant phenotypes, which can be mimicked by auxin efflux inhibitors such as the commercially available herbicide naphthylphthalamic acid<sup>10</sup> (NPA (also known as naptalam);  $pK_a = 4.6$ ).

The PIN protein family is exclusive to the plant kingdom and is classified as part of the large bile/arsenite/riboflavin transporter (BART) superfamily, which also includes transporters of bile acid, arsenite and riboflavin with members distributed across all kingdoms of life<sup>11,12</sup>. PIN proteins are predicted to have ten transmembrane helices comprising two five-transmembrane helix repeats separated by a cytosolic loop. Canonical PINs (PIN1–4 and PIN7 in *A. thaliana*) are characterized by a long (323–355 residue) loop and are mostly located in the plasma membrane, whereas non-canonical PINs (PIN5 and PIN8) and the intermediate PIN6 in *A. thaliana* possess a much shorter loop and can be found in organellar membranes such as endoplasmic reticulum membranes<sup>13–15</sup>

(Extended Data Figs. 1 and 2a). The long loops of canonical PINs have phosphorylation sites that regulate activity; the loops have been shown to be auto-inhibitory, requiring kinase activity to initiate transport<sup>16</sup>.

Here we present structural and biophysical characterization of a PIN protein. In particular, cryo-electron microscopy (cryo-EM) has been used to solve structures in an outward-facing state with and without bound IAA as well as in an inward-facing state with bound NPA at resolutions between 2.9 and 3.4 Å. Combined with transport data from mutant protein, these structures suggest a molecular mechanism and model for auxin transport that is broadly applicable to the ubiquitous PIN family.

We chose to study PIN8 from *A. thaliana* after screening various PIN homologues for expression and purification. PIN8 is a non-canonical PIN of 40 kDa in size, with a short cytosolic loop of 43 residues that lacks the phosphorylation motifs seen in the long auto-inhibitory loops of canonical PINs. When expressed in oocytes, PIN8 exhibited robust IAA transport activity similar to that of kinase-activated PIN1. This activity is independent of activating kinases and sensitive to the inhibitor NPA, demonstrating that PIN8 is a constitutively active auxin transporter (Fig. 1a and Extended Data Fig. 2b).

To characterize electrogenic transport of IAA by PINs, we overexpressed the protein in *Saccharomyces cerevisiae* and, following purification, reconstituted it into proteoliposomes. We measured transport using capacitive coupling using solid supported membrane (SSM) electrophysiology,

<sup>1</sup>Department of Molecular Biology and Genetics, Aarhus University, Aarhus, Denmark. <sup>2</sup>Plant Systems Biology, School of Life Sciences Weihenstephan, Technical University of Munich, Freising, Germany. <sup>3</sup>Skirball Institute of Biomolecular Medicine, Department of Cell Biology, New York University School of Medicine, New York, NY, USA. <sup>4</sup>These authors contributed equally: Kien Lam Ung, Mikael Winkler. <sup>5</sup>e-mail: ulrich.hammes@tum.de; bpp@mbg.au.dk

## Article

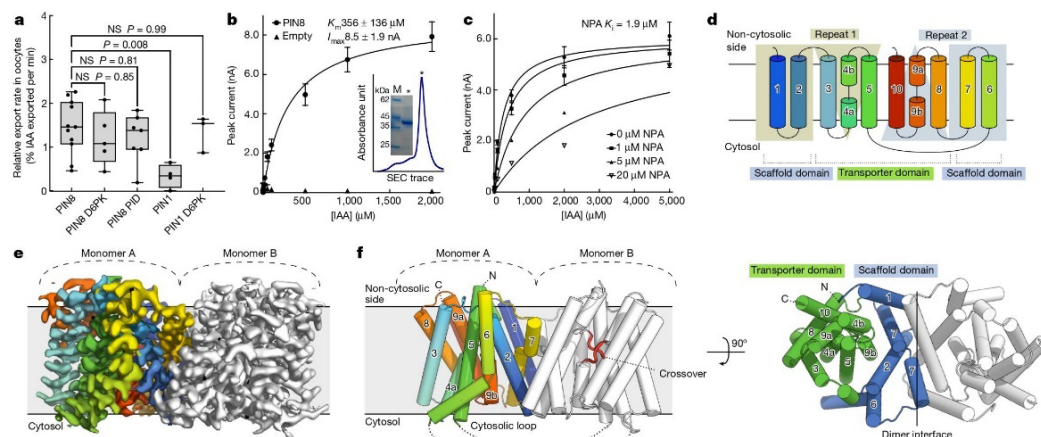


**Fig. 1 | Activity and overall structure of PIN8.** **a**, Relative IAA transport rates for PIN8 and PIN1 incubated with PIN-activating kinases D6PK and PID show that PIN8 is constitutively active in oocytes (internal oocyte IAA concentration = 1  $\mu\text{M}$ ). The centre line is the median, the box extends from the 25th to 75th percentile and whiskers extend to minimum and maximum values. Points represent biologically independent experiments (PIN8:  $n = 11$ , PIN8 D6PK:  $n = 5$ , PIN8 PID:  $n = 7$ , PIN1:  $n = 4$ , PIN1 D6PK:  $n = 3$ ). For differences between PIN8 and other groups, a one-way ANOVA followed by Dunnett's multiple comparisons test was performed. PIN8 versus PIN8 D6PK:  $P = 0.8508$ , PIN8 versus PIN8 PID:  $P = 0.8090$ , PIN8 versus PIN1:  $P = 0.0078$ , PIN8 versus PIN1 D6PK:  $P = 0.9968$ . **b**, Peak current response by SSM electrophysiology on PIN8 proteoliposomes. Transport is described by Michaelis–Menten kinetics ( $r^2 = 0.98$ ,  $K_m = 356 \pm 136 \mu\text{M}$ , maximum current ( $I_{max}$ ) =  $8.5 \pm 1.9 \text{ nA}$ ; data are

mean  $\pm$  s.e.m.; PIN8:  $n = 4$  different proteoliposome preparations, empty:  $n = 3$  liposome preparations). Inset, stained SDS–PAGE analysis and size-exclusion chromatography (SEC) trace for the PIN8 purification. **c**, Transport current in the presence of NPA shows inhibition ( $K_i = 1.9 \mu\text{M}$  (95% confidence interval: 0.9–3.8  $\mu\text{M}$ ;  $n = 3$  for 0 and 1  $\mu\text{M}$  NPA and  $n = 2$  for 5 and 20  $\mu\text{M}$  NPA); data are mean  $\pm$  s.e.m. ( $n > 2$ )). **d**, Topology of the PIN8 monomer shows an inverted repeat of five transmembrane helices and the relation between transporter and scaffold domains. **e**, Cryo-EM map of the PIN8 dimer with one monomer coloured according to panel **d**. **f**, Side view of PIN8 with M1–M10 labelled. The central crossover highlighted in red in monomer B. Right, top view from the non-cytosolic side displays the dimer interface and the two domains found in each monomer: the transporter domain (green) and the scaffold domain (blue).

and show that PIN8 has a relatively low apparent affinity for IAA, with a Michaelis constant ( $K_m$ ; Methods, 'SSM physiology assays') of  $356 \pm 136 \mu\text{M}$  ( $n = 4$ ) (Fig. 1b and Extended Data Fig. 2c). We measure the dissociation constant ( $K_d$ ) of IAA binding to be  $39.9 \mu\text{M}$  (Extended Data Fig. 2d). We observe a modest pH dependence with an optimum at 6.0–7.4 (Extended Data Fig. 2e). As in oocyte assays, transport can be inhibited by NPA, which inhibit with an inhibition constant ( $K_i$ ) of  $1.9 \mu\text{M}$ , suggesting an affinity one order of magnitude higher than that of IAA (Fig. 1c). We screened a number of additional PIN substrates (Extended Data Fig. 2f) and find that IAA analogues—for example, naphthaleneacetic acid (NAA) or the herbicide 2,4-dichlorophenoxyacetic acid (2,4-D), elicit a current response in PIN8, whereas uncharged auxins as well as some endogenous auxins does not. Comparison of these substrates suggests that shape complementary has a large role in recognition: for example, the larger size of indole-3-butyric acid (IBA) and the reduced ring system of 2-phenylacetic acid (PAA) both result in reduced currents.

We solved three distinct structures of PIN8 using single-particle cryo-EM after reconstitution of the purified protein into peptidisc: an apo form at 2.9  $\text{\AA}$  resolution, PIN8 with IAA bound at 3.2  $\text{\AA}$ , and PIN8 with NPA bound at 3.4  $\text{\AA}$  resolution (Extended Data Figs. 3–5 and Extended Data Table 1). In addition, a structure of the apo form that is indistinguishable from the apo peptidisc structure was produced from a detergent-solubilized preparation at 3.3  $\text{\AA}$  (Extended Data Table 1). The highest-resolution map of the apo form was used for initial model building, but all maps display excellent density for the entire protein except for 39 residues of the disordered cytosolic loop, which were not modelled (Fig. 1d, e). We could model multiple water molecules and lipids as well as IAA and NPA in the relevant structures.

The apo form of PIN8 displays a symmetric dimer of PIN8 (Fig. 1f) characterized by a twofold rotation axis perpendicular to the membrane

plane with a distinct concavity extending into the membrane along this axis from the non-cytosolic side. Within each monomer there are ten transmembrane helices (M1–M10), comprising an inverted repeat of five transmembrane helices<sup>17</sup> (Fig. 1d). In each repeat, the fourth helix is disrupted around a conserved proline residue in the middle of the membrane plane: Pro116 in M4 and Pro325 in M9. These disrupted helices make an X-shaped crossover that marks the auxin binding pocket (Fig. 1f).

The PIN8 monomer is divided into two domains that we name the scaffold domain and the transporter domain (Fig. 1d, f and Extended Data Fig. 6a). The scaffold domain comprises helices M1, M2, M6 and M7 and creates a large interface ( $1,512 \text{ \AA}^2$ ) to the other monomer in the dimeric complex. This interface is mediated mainly by M2 and M7, and is further stabilized by a lipid in a groove between M1 and the kinked M6 (Extended Data Fig. 6b). We also observe another lipid with an aliphatic tail sticking into a pocket of the transporter domain. We tested a dependence on lipids for activity and found that PIN8 functions similarly in mixed lipid and pure phosphatidylcholine liposomes (Extended Data Fig. 6c). The transporter domain consists of helices M3–M5 and M8–M10 and harbours the central X-shaped crossover (Fig. 1f). The overall fold of the monomer is similar to that of the bile acid/sodium symporters, but the membrane topology is inverted<sup>18</sup> (Extended Data Fig. 7). Next to the crossover, there is a well-defined water-filled binding pocket nestled between the scaffold domain and the transporter domain that is open to the non-cytosolic side of the protein via the concavity (Fig. 1f). By contrast, access to the cytosol is blocked, clearly defining the conformation of the apo-PIN8 dimer as an empty outward-open state.

The substrate-bound form of PIN8, IAA–PIN8, is almost identical to apo-PIN8 (root mean squared deviation of C $\alpha$  atoms (r.m.s.d.<sub>C $\alpha$</sub> ) = 0.6  $\text{\AA}$ )

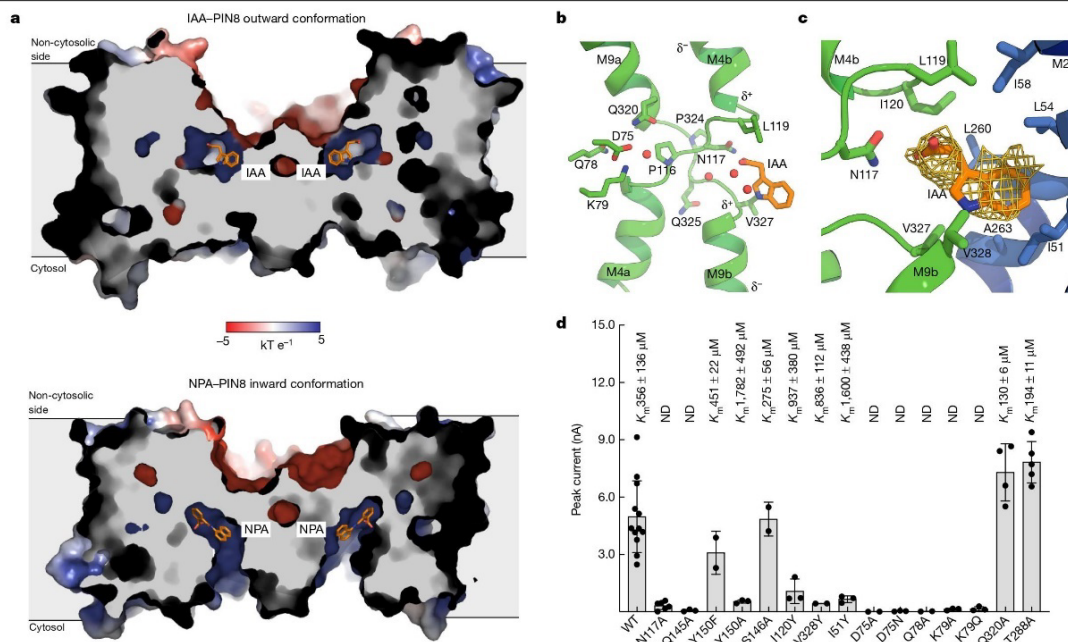


**Fig. 2 | Structures with IAA and NPA bound.** **a**, Cutaway view of electrostatic surface representation of IAA-PIN8 and NPA-PIN8 show the change in conformation. Whereas the concavity at the non-cytosolic side has negative potential, the binding pocket itself has a positive potential in both cases. **b**, View of the crossover and the position of IAA and the support site with central residues highlighted. **c**, Close-up view of IAA map density and the residues from the scaffold domain interacting with the indole ring. **d**, Peak current response evoked by 500  $\mu M$  IAA determined by SSM electrophysiology

(Fig. 2a). There is a clear density for IAA in the binding pocket, with three surrounding water molecules (Fig. 2b,c). Thus, the IAA-PIN8 structure represents a substrate-bound outward-open state, the expected release state for auxin.

IAA is bound with its carboxylate group oriented towards the crossover; although only two residues are within hydrogen-bonding distance (Asn117 and Gln145), IAA is stabilized by the positive dipole from M4b and M9b helices. The backbone carbonyl of Pro116 creates a polar pocket that is also lined by Tyr150 and Ser146. Here we observe three well-defined water molecules that may reflect partial disassociation of IAA from the binding pocket in the release state. Mutating either Asn117 and Gln145 to alanine abolishes transport, supporting their importance (Fig. 2d). Tyr150 mutants display mixed results: Y150F retains activity, affinity and sensitivity to NPA, whereas removal of the bulky side chain in Y150A results in very low activity and affinity (Extended Data Fig. 8a,b). By contrast, mutation of Ser146 had no effect on activity (Fig. 2d and Extended Data Fig. 8a).

In the transporter domain, the IAA carbon backbone contacts Leu119(M4b) and Ile120(M4b) towards the non-cytosolic side, whereas the indole ring contacts Val327(M9b) and Val328(M9b) towards the cytosolic side. These four hydrophobic residues are symmetrically located on the crossover immediately after the two key prolines as part of a duplicated and conserved crossover sequence motif (P(N/Q)X $\Phi$ ); where  $\Phi$  is a hydrophobic residue (Fig. 2b-d and Extended Data Figs. 1 and 8b). The hydrophobic residues of the crossover motif provide affinity for the auxin substrate. This is supported by the bulky I120Y and

V328Y mutants, which both reduce apparent affinity by interfering with substrate binding but still retain NPA sensitivity (Fig. 2d and Extended Data Fig. 8a,b). Together, the interactions between the transporter domain and IAA emphasize that PIN8 selects for IAA on the basis of shape complementarity, as also suggested by the SSM electrophysiology results. In the scaffold domain, the indole ring has additional non-specific hydrophobic interactions with Ile51 (M2) and Leu54 (M2) and the pseudo-symmetrically related Leu260 (M7) and Ala263 (M7). Bulky mutations in these hydrophobic residues (such as I51Y) lead to a considerably reduced transport current (Fig. 2d and Extended Data Fig. 8a,b). All the residues defining the binding pocket show high sequence conservation across different plant species and are fully conserved in all *A. thaliana* PIN proteins except PIN5 (Extended Data Figs. 1 and 8c).

The NPA-bound form of PIN8 adopts an inward-open conformation (Fig. 2a). The scaffold domains and dimeric interface is unchanged relative to the outward-open conformation (r.m.s.d.<sub>c $\alpha$</sub>  = 0.9 Å), but the two transporter domains are rotated by approximately 20° to expose the auxin binding site and Asn117 to the cytosolic side. This rotation results in a translation of the binding site by approximately 5 Å (Fig. 3a and Supplementary Video 1). NPA has more extensive interaction with the protein compared with IAA in the outward-open state (Fig. 3b,c and Extended Data Fig. 8c,d). Similar to IAA, the carboxylate group of NPA points towards the crossover, but has several stronger interactions that are not observed in the outward-open state. In addition to interactions seen for IAA, NPA interacts with main chain nitrogen atoms of Val327

and Val328 (M9b) towards the cytosolic side. These four hydrophobic residues are symmetrically located on the crossover immediately after the two key prolines as part of a duplicated and conserved crossover sequence motif (P(N/Q)X $\Phi$ ); where  $\Phi$  is a hydrophobic residue (Fig. 2b-d and Extended Data Figs. 1 and 8b). The hydrophobic residues of the crossover motif provide affinity for the auxin substrate. This is supported by the bulky I120Y and V328Y mutants, which both reduce apparent affinity by interfering with substrate binding but still retain NPA sensitivity (Fig. 2d and Extended Data Fig. 8a,b). Together, the interactions between the transporter domain and IAA emphasize that PIN8 selects for IAA on the basis of shape complementarity, as also suggested by the SSM electrophysiology results. In the scaffold domain, the indole ring has additional non-specific hydrophobic interactions with Ile51 (M2) and Leu54 (M2) and the pseudo-symmetrically related Leu260 (M7) and Ala263 (M7). Bulky mutations in these hydrophobic residues (such as I51Y) lead to a considerably reduced transport current (Fig. 2d and Extended Data Fig. 8a,b). All the residues defining the binding pocket show high sequence conservation across different plant species and are fully conserved in all *A. thaliana* PIN proteins except PIN5 (Extended Data Figs. 1 and 8c).

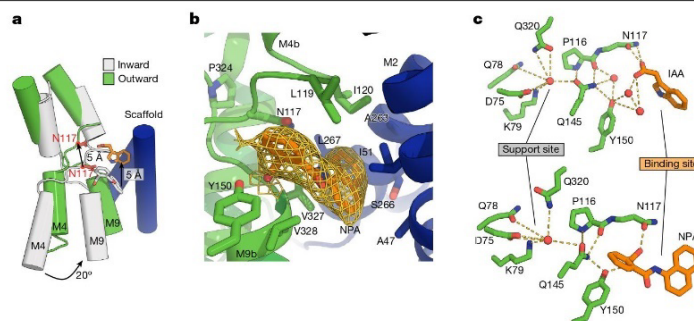


**Fig. 3 | Conformational change and the support site.** **a**, Inward and outward structures superposed on the scaffold domain (blue) reveal an elevator-type movement, with the substrate binding site moving 5 Å. **b**, Close-up view of the

NPA map density and the residues interacting with it. **c**, The hydrogen-bonding network linking the binding site to the support site through Gln145 in the outward state (top) and inward state (bottom).

and Val328, as well as with Gln145 and Tyr150 in a network that does not involve water. The benzene ring and naphthyl ring of NPA still interact with the two crossover motifs of the transporter domain, similar to IAA. Several new interactions are also observed with the scaffold domain, many of which are mediated by the naphthyl ring of NPA and are probably unique to the larger, more complex NPA molecule (Fig. 3b,c and Extended Data Fig. 8a–d). Inhibition by NPA can thus be explained by two components: (1) stronger binding due to engagement of additional residues from the scaffold domain, and (2) the larger size of NPA that prevents transition to the outward state.

Adjacent to the primary auxin binding site, an accessory ‘support site’ is apparent on the other side of the crossover between M3, M5 and M9. This support site is linked to the primary auxin binding site via an extensive hydrogen bond network bridged by the central Gln145 and the backbone carbonyl of Pro116. The higher-resolution apo-PIN8 map reveals two peaks in the site, which are modelled as water (Extended Data Fig. 8e). In the lower-resolution IAA–PIN8 and NPA–PIN8 map, the same site contains one single weak peak that is also modelled as water (Fig. 3c and Extended Data Fig. 8c–e). The presence of Na<sup>+</sup> at analogous sites in bile acid/sodium symporters led us to probe ion dependence by comparing PIN8 transport in sodium- and potassium-exclusive buffers. In both cases, PIN8 retains full activity, suggesting that specific counter-transport of ions does not take place (Extended Data Fig. 9a). In all structures, the water molecules in the support site engage in a hydrogen bond network with Asp75 (M3), Gln78 (M3), Lys79 (M3), Gln320 (M9a) and Gln145 (M5) (Fig. 3c). Mutational analysis indicates that all of these residues except Gln320 are absolutely essential for activity (Fig. 2d and Extended Data Fig. 8a). Notably, Asp75 and Lys79 are fully conserved and constitute a proton donor–acceptor pair with potential for proton transport; indeed, this idea is supported by isosteric mutations that remove the charge from either residue (D75N or K79Q) and abolish transport (Fig. 2d and Extended Data Fig. 8a,c,d). The distance from Asp75 to Lys79 is below 3 Å in all structures, consistent with an unprotonated state for Asp75. However, activity of PIN8 in proteoliposomes is not sensitive to proton-motive force decouplers and has minimal pH dependence, suggesting that a proton-motive force is not obligatory for transport (Extended Data Figs. 2e and 9b). Furthermore, export rates in oocytes are also indifferent to external pH (Extended Data Fig. 9c).

## Discussion

Plant growth and morphology are largely governed by polar auxin transport as mediated by canonical PINs. Comparison of all the PINs from *A. thaliana* with PIN8 studied here indicates that—with an exception of the unusual non-canonical PIN8—the auxin and support sites are

perfectly conserved. This conservation, which also extends to other plant species, indicates that our observations can be generalized<sup>19</sup> (Extended Data Figs. 1, 2a and 8c,d). The low apparent affinity for IAA measured in proteoliposome assays is 5–500-fold lower than the physiological concentrations of auxin in plant tissues<sup>20</sup> (0.1–10 μM). Although we cannot rule out experimental artifacts, this implies that distinct functions of *A. thaliana* PINs arise from differing localization, abundance and auto-inhibition properties rather than direct modulation of substrate affinity<sup>3</sup>. Some studies have suggested that ABCB transporters interact with PINs to generate selectivity in IAA transport<sup>21–23</sup>. Our work suggests that this interaction is not needed for activity *in vitro*, and is most probably not required in planta.

The PIN family is part of the BART superfamily, which includes the structurally characterized ASBT bile acid/sodium symporters from the BASS family<sup>18</sup>. Although PIN8 and ASBT adopt the same fold, ASBT assumes an inverted orientation and does not appear to dimerize (Extended Data Fig. 7). In addition, at least three other families of proteins adopt this same fold (DALI Z-score > 10), namely two Na<sup>+</sup>/H<sup>+</sup> antiporter families (CPA1 and CPA2) and the HCO<sub>3</sub><sup>-</sup>/Na<sup>+</sup> symporter family<sup>24–29</sup>. Similar to the bile acid/sodium symporters, these other protein families all share negligible sequence homology with PINs. The HCO<sub>3</sub><sup>-</sup>/Na<sup>+</sup> symporters adopt the same membrane orientation as PINs, whereas the Na<sup>+</sup>/H<sup>+</sup> antiporters share the inverted orientation with the bile acid/sodium symporters, perhaps explaining why the structural link between PINs and these divergent protein families has not been noted previously (Extended Data Fig. 7).

These other protein families are all secondary active transporters that use sodium or protons to drive transport, and all are proposed to function using an elevator mechanism in which the scaffold domain is fixed and the transporter domain pivots about the conserved proline crossover motif. Notably, the site occupied by the driving sodium and protons in these families is located at the same position as the support site in PINs (Extended Data Fig. 7), and it is clear from this work that PIN8 uses the same general proline crossover-based elevator mechanism (Fig. 3a and Supplementary Video 1).

Our data show that the negative charge of the IAA is sufficient for transport (Extended Data Figs. 2e and 9). However, the basic architecture of a support site is present that would allow for ion binding, as well as a conserved and functionally essential Asp75–Lys79 pair that could mediate proton translocation<sup>30</sup>. Most mutations of the support site completely abrogate activity, underlining the essential nature of this region, but neither oocyte nor SSM electrophysiology assays suggest dependence on counter-transport of either sodium or protons to drive auxin export. Our data thus support a uniport mechanism for PINs, although we cannot definitely rule out proton antiport *in vivo*.

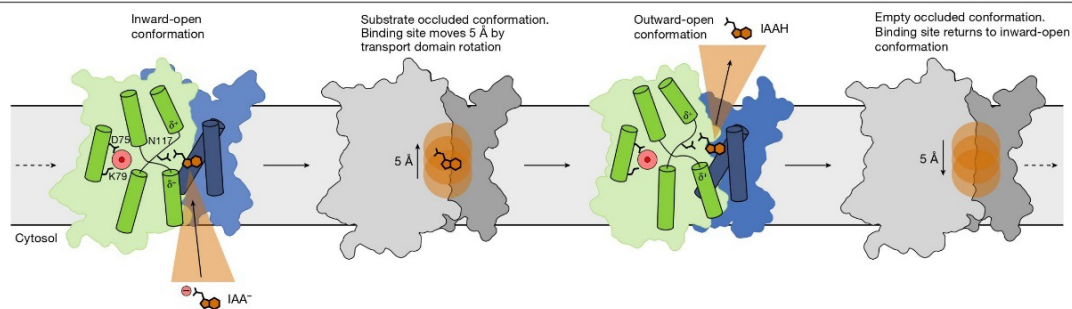


**Fig. 4 | Proposed mechanism of auxin export by PIN proteins.** In the inward-open conformation (left), IAA enters the binding site with a deprotonated carboxylate. The positive dipole of the M4b and M9b helices helps diffuse the charge. During rotation of the transporter domain, the binding site moves 5 Å towards the non-cytosolic side (second from left). At the

non-cytosolic side, IAA is released, probably assisted by a protonation event (second from right). The support site could also become protonated before reverting to the inward-facing conformation (right), but our data indicate that this is not obligatory for function.

On the basis of the data available, we propose the following model for auxin transport by PINs (Fig. 4): The inward-facing conformation allows an ionized auxin molecule to enter the binding site between transport and scaffold domains. The negatively charged carboxylate group is stabilized by the positive dipole of M4b and M9b, while being held in place by Asn117 and interacting with the support site through Gln145. The carbon backbone and indole ring are recognized by the four hydrophobic residues from the two crossover motifs of the scaffold domain. During transition to the outward-facing conformation, the proline crossover rotates 20° and the auxin binding site in the scaffold domain is translated away from the cytosol by 5 Å. Release of IAA in the outward-facing state is facilitated by a pH shift that protonates and neutralizes the carboxylate. After substrate release, the protein reverts back to the inward-open state.

It has been suggested that the oligomeric state of PINs might have a role in regulation, but the large dimer-interaction surface in PIN8 argues against a dynamic equilibrium<sup>31,32</sup>. Nevertheless, it is conceivable that the monomers operate independently and also that PINs could form hetero-oligomers<sup>33</sup>.

We have not directly addressed auto-inhibition by the cytosolic loop in canonical PINs, but the connection to other known protein families provides some hints: For HCO<sub>3</sub><sup>-</sup>/Na<sup>+</sup> symporters, it has been shown that a loop from a cytosolic regulatory partner locks the protein in an inward conformation by interacting with the binding site<sup>24,29</sup>. By analogy, it seems plausible that the auto-inhibitory loop in canonical PINs operates by a similar mechanism.

In conclusion, we have presented in vitro biochemical characterization of a PIN as well as structures representing two key conformational states in the presence and absence of auxin and the herbicide NPA. The structure with NPA demonstrates competitive inhibition in PIN proteins, and could provide the basis for structure-based development of novel herbicides. We describe the molecular mechanism of auxin transport by PINs that can function independently of monovalent ions or protons, thus expanding our understanding of the crossover elevator mechanism used by proteins from diverse protein superfamilies from all kingdoms of life. This work provides a comprehensive foundation for future studies aiming to elucidate PIN function in polar auxin transport, which is essential for plant growth and development.

### Online content

Any methods, additional references, Nature Research reporting summaries, source data, extended data, supplementary information, acknowledgements, peer review information; details of author contributions

and competing interests; and statements of data and code availability are available at <https://doi.org/10.1038/s41586-022-04883-y>.

- Weijers, D. & Wagner, D. Transcriptional responses to the auxin hormone. *Annu. Rev. Plant Biol.* **67**, 539–574 (2016).
- Goldsmith, M. H. M. The polar transport of auxin. *Annu. Rev. Plant Physiol.* **28**, 439–478 (1977).
- Hammes, U. Z., Murphy, A. S. & Schwechheimer, C. Auxin transporters—a biochemical view. *Cold Spring Harb. Perspect. Biol.* **14**, a039875 (2021).
- Gälweiler, L. et al. Regulation of polar auxin transport by AtPIN1 in *Arabidopsis* vascular tissue. *Science* **282**, 2226–2230 (1998).
- Chen, R. et al. The *Arabidopsis thaliana* AGR1/TROPIC 1 gene encodes a component of the polar-auxin-transport efflux carrier. *Proc. Natl. Acad. Sci. USA* **95**, 15112–15117 (1998).
- Luschnig, C., Gaxiola, R. A., Grisafi, P. & Fink, G. R. EIR1, a root-specific protein involved in auxin transport, is required for gravitropism in *Arabidopsis thaliana*. *Genes Dev.* **12**, 2175–2187 (1998).
- Petrásek, J. et al. PIN proteins perform a rate-limiting function in cellular auxin efflux. *Science* **312**, 914–918 (2006).
- Raven, J. A. Transport of indoleacetic acid in plant cells in relation to pH and electrical potential gradients, and its significance for polar IAA transport. *New Phytol.* **74**, 163–172 (1975).
- Rubery, P. H. & Shelldrake, A. R. Carrier-mediated auxin transport. *Planta* **118**, 101–121 (1974).
- Okada, K., Ueda, J., Komaki, M. K., Bell, C. J. & Shimura, Y. Requirement of the auxin polar transport system in early stages of *Arabidopsis* floral bud formation. *Plant Cell* **3**, 677–684 (1991).
- Chen, J. S. et al. Phylogenetic characterization of transport protein superfamilies: superiority of SuperfamilyTree programs over those based on multiple alignments. *J. Mol. Microbiol. Biotechnol.* **21**, 83–96 (2011).
- Mansour, N. M., Sawhney, M., Tamang, D. G., Vogl, C. & Saier Jr, M. H. The bile/arsenite/riboflavin transporter (BART) superfamily. *FEBS J.* **274**, 612–629 (2007).
- Ding, Z. et al. ER-localized auxin transporter PIN8 regulates auxin homeostasis and male gametophyte development in *Arabidopsis*. *Nat. Commun.* **3**, 941 (2012).
- Ditengou, F. A. et al. Characterization of auxin transporter PIN6 plasma membrane targeting reveals a function for PIN6 in plant bolting. *New Phytol.* **217**, 1610–1624 (2018).
- Mravec, J. et al. Subcellular homeostasis of phytohormone auxin is mediated by the ER-localized PIN5 transporter. *Nature* **459**, 1136–1140 (2009).
- Zourelidou, M. et al. Auxin efflux by PIN-FORMED proteins is activated by two different protein kinases, D6 PROTEIN KINASE and PINOID. *eLife* **3**, e02860 (2014).
- Duran, A. M. & Meiler, J. Inverted topologies in membrane proteins: a mini-review. *Comput. Struct. Biotechnol. J.* **8**, e201308004 (2013).
- Hu, N.-J., Iwata, S., Cameron, A. D. & Drew, D. Crystal structure of a bacterial homologue of the bile acid sodium symporter ASBT. *Nature* **478**, 408–411 (2011).
- Bennett, T. et al. Paralogous radiations of PIN proteins with multiple origins of noncanonical PIN structure. *Mol. Biol. Evol.* **31**, 2042–2060 (2014).
- Petersson, S. V. et al. An auxin gradient and maximum in the *Arabidopsis* root apex shown by high-resolution cell-specific analysis of IAA distribution and synthesis. *Plant Cell* **21**, 1659–1668 (2009).
- Bandyopadhyay, A. et al. Interactions of PIN and PGP auxin transport mechanisms. *Biochem. Soc. Trans.* **35**, 137–141 (2007).
- Deslauriers, S. D. & Spalding, E. P. Electrophysiological study of *Arabidopsis* ABCB4 and PIN2 auxin transporters: evidence of auxin activation and interaction enhancing auxin selectivity. *Plant Direct* **5**, e361 (2021).
- Noh, B., Murphy, A. S. & Spalding, E. P. Multidrug resistance-like genes of *Arabidopsis* required for auxin transport and auxin-mediated development. *Plant Cell* **13**, 2441–2454 (2001).

## Article

24. Fang, S. et al. Molecular mechanism underlying transport and allosteric inhibition of bicarbonate transporter SbtA. *Proc. Natl Acad. Sci. USA* **118**, e2101632118 (2021).
25. Hunte, C. et al. Structure of a Na<sup>+</sup>/H<sup>+</sup> antiporter and insights into mechanism of action and regulation by pH. *Nature* **435**, 1197–1202 (2005).
26. Lee, C. et al. A two-domain elevator mechanism for sodium/proton antiport. *Nature* **501**, 573–577 (2013).
27. Paulino, C., Wöhlert, D., Kapotova, E., Yıldız, Ö. & Kühlbrandt, W. Structure and transport mechanism of the sodium/proton antiporter MjNhaP1. *eLife* **3**, e03583 (2014).
28. Wöhlert, D., Kühlbrandt, W. & Yıldız, Ö. Structure and substrate ion binding in the sodium/proton antiporter PaNhaP. *eLife* **3**, e03579 (2014).
29. Liu, X.-Y. et al. Structures of cyanobacterial bicarbonate transporter SbtA and its complex with PII-like SbtB. *Cell Discov.* **7**, 63 (2021).
30. Buch-Pedersen, M. J., Pedersen, B. P., Veierskov, B., Nissen, P. & Palmgren, M. G. Protons and how they are transported by proton pumps. *Pflügers Arch.* **457**, 573–579 (2009).
31. Abbas, L. et al. Naphthylphthalamic acid associates with and inhibits PIN auxin transporters. *Proc. Natl Acad. Sci. USA* **118**, e2020857118 (2021).
32. Teale, W. D. et al. Flavonol-mediated stabilization of PIN efflux complexes regulates polar auxin transport. *EMBO J.* **40**, e104416 (2021).

33. Pařízková, B., Pernisová, M. & Novák, O. What has been seen cannot be unseen—detecting auxin in vivo. *Int. J. Mol. Sci.* **18**, E2736 (2017).

**Publisher's note** Springer Nature remains neutral with regard to jurisdictional claims in published maps and institutional affiliations.



**Open Access** This article is licensed under a Creative Commons Attribution 4.0 International License, which permits use, sharing, adaptation, distribution and reproduction in any medium or format, as long as you give appropriate credit to the original author(s) and the source, provide a link to the Creative Commons license, and indicate if changes were made. The images or other third party material in this article are included in the article's Creative Commons license, unless indicated otherwise in a credit line to the material. If material is not included in the article's Creative Commons license and your intended use is not permitted by statutory regulation or exceeds the permitted use, you will need to obtain permission directly from the copyright holder. To view a copy of this license, visit <http://creativecommons.org/licenses/by/4.0/>.

© The Author(s) 2022



## Methods

### Protein purification

*A. thaliana* protein sequences used in this study are publicly available at Uniprot (<https://www.uniprot.org/>) with the following accession codes. PIN1: Q9C6B8, PIN2: Q9LU77, PIN3: Q9S7Z8, PIN4: Q8RWZ6, PIN5: Q9FFD0, PIN6: Q9SQH6, PIN7: Q940Y5 and PIN8: Q9LFP6.

PIN genes were cloned into an *S. cerevisiae* overexpression plasmid based on p423\_GAL1 and tested for expression and purification properties. The *A. thaliana* PIN8 gene (Uniprot: Q9LFP6) was selected and put in frame with a tobacco etch virus (TEV) protease cleavage site and a deca-histidine affinity tag. This construct was used as the template for site-directed mutagenesis using the Quickchange commercial protocol (Agilent) for all point mutants.

Transformed *S. cerevisiae* strain DSY-5 were grown in 5 l shaking flasks or culture vessels, grown to high cell density and collected after 22 h induction with galactose<sup>34</sup>. Collected cells were washed three times in water and re-suspended in buffer A (0.1 M Tris pH 7.5, 0.6 M NaCl, 1 mM ethylenediamine tetraacetic acid (EDTA), 1.2 mM phenylmethylsulphonyl fluoride). Cells were lysed by bead beating and lysate was clarified by centrifugation at 5,000g for 20 min. Membrane fractions were pelleted by ultracentrifugation at 200,000g for 2 h and re-suspended in buffer B (0.05 M Tris pH 7.5, 0.5 M NaCl, 20% glycerol) before being frozen in liquid nitrogen.

For protein purification, 3–4 g of membrane was thawed and solubilized for 45 min in a total volume of 50 ml of buffer C (0.05 M Tris pH 7.5, 0.5 M NaCl, 10% glycerol) supplemented with 1% *n*-dodecyl- $\beta$ -D-maltoside (DDM) and 0.1% cholesterol hemisuccinate (CHS). Insoluble material was discarded by centrifugation at 17,000g for 30 min following by filtration using a 1.2  $\mu$ m filter. 20 mM imidazole pH 7.5 was added and the sample loaded on a 1 ml nickel-nitrilotriacetic (Ni-NTA) column. A two-step wash was performed with buffer D (buffer A with 20 mM imidazole, 0.1% DDM, 0.01% CHS) and buffer E (buffer A with 70 mM imidazole, 0.05% DDM, 0.005% CHS).

For SSM electrophysiology assays, the sample was eluted with buffer F (0.05 M Tris pH 7.5, 0.15 M NaCl, 10% glycerol, 0.05% DDM, 0.005% CHS, 500 mM imidazole). The eluate was incubated with TEV protease and dialysed against buffer F supplemented with 0.5 mM EDTA and 0.5 mM tris(2-carboxyethyl)phosphine (TCEP) overnight. The sample was then filtered and re-run on a Ni-NTA column to adsorb the His-tagged proteins consisting of TEV protease, cleaved tag and uncleaved tagged protein. The flow-through fraction, containing tag-free PIN8, was concentrated on a 100 kDa cut-off centricon (Vivaspin) and polished by SEC on a Biorad650 or Superdex200 10/300 column pre-equilibrated with buffer G optimized by a thermostability assay<sup>35</sup> (0.05 M Tris pH 7.5, 0.15 M NaCl, 10% glycerol, 0.05% DDM, 0.005% CHS, 0.5 mM EDTA).

For cryo-EM, peptidisc sample preparation followed general protocols<sup>36,37</sup>. In brief, after the two-step wash, proteins were re-lipidated using buffer I (0.05 M Tris pH 7.5, 0.15 M NaCl, 10% glycerol, 0.03% DDM, 0.003% CHS, 0.06 mg ml<sup>-1</sup> soybean extract polar lipids (Avanti)). Prior to starting the on-bead peptidisc reconstitution, the column was washed with buffer J (0.05 M Tris pH 7.5, 0.15 M NaCl, 10% glycerol, 0.008% DDM, 0.0008% CHS). Peptidisc reconstitution was initiated by washing the column with detergent-free buffer K (0.05 M Tris pH 7.5, 0.15 M NaCl, 10% glycerol) containing 1 mg ml<sup>-1</sup> peptidisc (Genscript). An additional washing step with buffer K was performed to eliminate residual free peptidisc prior to elution using buffer K supplemented with 500 mM imidazole. After this the sample was incubated with TEV protease and dialysed against buffer K supplemented with 0.5 mM EDTA and 0.5 mM TCEP.

For the cryo-EM detergent sample, immediately after the re-lipidation step with buffer I, the DDM detergent was exchanged to lauryl maltose neopentyl glycol (LMNG) using buffer L (0.05 M Tris pH 7.5, 0.15 M NaCl, 10% glycerol, 0.006% LMNG, 0.0006% CHS) prior to protein elution using buffer L supplemented with 500 mM imidazole. The sample

was then incubated with TEV protease and dialysed against buffer L supplemented with 0.5 mM EDTA and 0.5 mM TCEP. After dialysis, cryo-EM sample purification continued identically to the SURFE<sup>2</sup>R sample protocol described in 'SSM electrophysiology assays', with the exception that the SEC buffer was replaced with buffer K (peptidisc sample) or buffer L (LMNG sample) without glycerol and supplemented with 0.5 mM EDTA.

### SSM electrophysiology assays

For SSM electrophysiology, a SURFE<sup>2</sup>R N1 from Nanion Technologies was used. In brief, Soy Phospholipid Mixture (38% phosphatidylcholine, 30% phosphatidyl ethanolamine, 18% phosphatidyl inositol, 7% phosphatidic acid and 7% other soy lipids) and 1-palmitoyl-2-oleoyl-*sn*-glycero-3-phosphocholine (POPC) were purchased from Avanti. Liposomes were prepared in Ringer solution without Ca<sup>2+</sup> (115 mM NaCl, 2.5 mM KCl, 1 mM NaHCO<sub>3</sub>, 10 mM HEPES pH 7.4, 1 mM MgCl<sub>2</sub>) and homogenized using a Liposofast (Avestin Inc) with a 400 nm pore size. Triton X-100 was added to the liposomes to a final concentration of 1% (v/v). Protein was added to liposomes to a calculated liposome:protein ratio (LPR) of 10:1. The detergent was removed using 400 mg ml<sup>-1</sup> Bio Beads (BioRad) overnight at 4 °C in a rotary shaker. Proteoliposomes were frozen in liquid nitrogen and kept at -80 °C until use.

Sensor coating was performed as described<sup>38</sup>. Proteoliposomes were diluted 1:5 in Ringer solution without Ca<sup>2+</sup>, sonicated five times and then applied to the sensors by centrifugation (30 min, 3,000g, 4 °C). Non-activating buffer was Ringer solution without Ca<sup>2+</sup> as described unless specified otherwise and activating buffer contained the substrate of interest. To substitute Na<sup>+</sup>, K<sup>+</sup>-Ringer without CaCl<sub>2</sub> (117.5 mM KCl, 10 mM HEPES pH 7.4, 1 mM MgCl<sub>2</sub>) and to substitute K<sup>+</sup>, Na<sup>+</sup>-Ringer without CaCl<sub>2</sub> (117.5 mM NaCl, 10 mM HEPES pH 7.4, 1 mM MgCl<sub>2</sub>) were used. Uncouplers: carbonyl cyanide *m*-chlorophenyl hydrazone (CCCP) in ethanol was used at 5  $\mu$ M and 2,4-dinitrophenol (DNP) in ethanol was used at 100  $\mu$ M. All other chemicals were purchased from Roth or Sigma. Each experiment was performed on at least two individual sensors. On each sensor each measurement consists of three technical replicates where the mean is calculated.

In most instances, we used a single solution exchange experiment. In this case proteoliposomes, immobilized on the supported membrane are kept in non-activating buffer as specified. At the beginning of the experiment non-activating buffer was exchanged for fresh identical non-activating buffer and after 1 s activating buffer (same buffer containing substrate) was added. After a further 1 s, buffer was again exchanged to non-activating buffer. Current response was recorded throughout the entire 3 s. For competition or inhibition, the respective compound was present in non-activating and activating solution.

Currents in response to substrate in the activating solutions are responses to electrogenic events which occur (1) when a charged molecule is crossing the membrane; (2) when a substrate, which does not necessarily have to be charged, binds to the protein and this binding leads to a conformational change by which charges become displaced in the membrane; (3) currents are shielded or neutralized by the substrate; and (iv) any combination of these possibilities. The peak current in response to substrate application was used to describe the properties of the proteins.

To describe the current response to different substrate concentrations a Michaelis–Menten curve was fit. We use  $K_m$  throughout the manuscript, but since the peak current is a mixture of binding and transport signal (that is, pre-steady state and steady state currents), this parameter can also be more appropriately described as  $EC_{50}$ . A  $K_m$  derived from a biophysical assay will be specific to that experimental setup, and comparison to other types of assay or a physiological condition should be done cautiously. In the case of competitive studies, we explicitly use  $K_d$  or  $K_i$ , since in these instances the parameters were specifically determined. GraphPad Prism V9.3 was used for statistical analyses.

## Article

### Cryo-EM sample preparation

Peak fractions of freshly purified PIN8 were concentrated to 4–10 mg ml<sup>-1</sup>. C-flat Holey Carbon grids (CF-1.2/1.3, Cu-300 mesh) were glow-discharged for 45 s at 15 mA in a GloQube Plus (Quorum). A drop of 4 µl of sample was applied to the non-carbon side of the grids, and blotted with a Vitrobot Mark IV (ThermoFisher Scientific) operating at 4 °C and 100% humidity and using blot time of 4 s, before plunge-freezing into liquid ethane. The substrate-bound states were obtained by incubating the sample with 15 mM of IAA sodium salt or 2 mM of NPA for 2 h prior to grid freezing.

### Image collection and data processing

A Titan Krios G3i microscope (ThermoFisher Scientific) operating at 300 kV and equipped with a BioQuantum Imaging Filter (energy slit width of 20 eV) with a K3 detector (Gatan) was used to collect the movies. The datasets containing the peptidisc samples, were acquired using automated acquisition EPU v2.11.1.11 at nominal 130,000 magnification corresponding to a physical pixel size 0.647 Å. For all datasets, the movies were saved in super-resolution pixel size and binned 2× in EPU back to the nominal pixel size.

On-the-fly gain normalized exposures were imported into cryoSPARC (v3.2.0)<sup>39</sup> and processed in streaming mode for patch motion correction, patch contrast transfer function (CTF) estimation, particle picking and extraction. After several rounds of particle cleaning, an initial preliminary volume map was used to create templates for template picking. From a full dataset of apo-PIN8 with 7,900 movies, template picking provided a total of 2,082,448 particles. After two rounds of 2D classification, the best representative classes were selected manually. These particles served as an input for ab initio model reconstruction. After three rounds of particle sorting by heterogenous refinement using the ab initio 3D template, the remaining 327,193 particles were used for non-uniform refinement with C2 symmetry imposed and resulted in a global 2.9 Å resolution map. In parallel a C1 symmetry refinement job was performed but showed no differences between the two monomers.

To ensure the method of membrane protein stabilization did not influence oligomeric state and overall structure we solved apo PIN8 both in peptidisc (2.9 Å) and in the detergent LMNG (3.3 Å). The respective maps reveal no variation in conformation and we focus on the peptidisc-derived map given its higher resolution. There was also no evidence of monomers or higher oligomeric states in any of the grids screened.

The processing pipeline for the ligand-bound PIN8 was identical to the one from apo-PIN8. In brief, the entire IAA-PIN8 dataset comprised of 15,771 movies and template picking yielded a total of 2,639,895 particles. After several rounds of 2D classification and heterogenous refinement to obtain a final 200,061 particles, a non-uniform refinement with C2 symmetry imposition resulted in a global 3.2 Å resolution map. A full dataset of NPA-PIN8 comprised of 14,500 movies and template picking yielded a total of 3,345,146 particles. After several rounds of 2D classification and heterogenous refinement to obtain a final 77,608 particles, a non-uniform refinement with C2 symmetry imposition resulted in a global 3.4 Å resolution map. As for the apo form, a parallel C1 refinement was performed with no differences evident between the two monomers. Local resolution estimation was performed using cryoSPARC.

### Model building and refinement

A PIN8 model prediction was calculated using the RoseTTAFold server<sup>40</sup> and docked into the PIN8 map in Chimera<sup>41</sup>. Two molecules of PIN8 could be readily fitted into the map. The flexible cytoplasmic loop of PIN8 (residues 165 to 205) is not visible in the maps and was excluded from model building in Coot<sup>42</sup>. The final models include residues 1–164 and 206–367 (of 367 residues total). The initial PIN8 dimer model was analysed by molecular dynamics-based geometry fitting to the map

using MDFF<sup>43</sup> through Namdinator v2.0 (ref. <sup>44</sup>). Models could be further improved by iterative manual model building in Coot combined with real-space refinement using Phenix, initially with an Amber force-field molecular dynamic refinement<sup>45</sup>. The coordination of lipids and the ligand IAA was prepared using ligand builder eLBOW<sup>46</sup>. In all electron microscopy maps, although the lipid belt surrounding the PIN8 dimer is visible, the electron density only allowed for the tentative modelling of two phosphatidylcholine molecules for ligand-bound PIN8 and four molecules for apo-PIN8. Geometry was validated in MolProbity v4.2 including CaBLAM and Ramachandran-Z analysis<sup>47–49</sup> (Rama-Z). Figures were prepared using PyMOL Molecular Graphics System v1.5.0.4 (Schrödinger). Conservation of residues across species was analysed using ConSurf<sup>50</sup>. Sequence alignments were constructed with PROMALS3D<sup>51</sup>. Alignments were visualized using ALINE v1.0.025<sup>52</sup>. Structural similarity to other protein families were identified using DALI<sup>53</sup>. Phylogenetic analysis was made using NGPhylogeny.fr<sup>54</sup>. In brief, MAFFT was used for multiple sequence alignment (MSA), BMGE was used for MSA pruning and FastME was used for unrooted tree generation. Bootstrap values were calculated from 500 trials.

### Oocyte efflux assays

Oocyte efflux experiments were carried out as described<sup>55</sup>. In brief, oocytes were injected with 150 ng transporter cRNA without or with 75 ng kinase cRNA. <sup>3</sup>H-IAA (25 Ci mmol<sup>-1</sup>) was purchased from ARC or RC Tritec. Oocytes were injected with IAA to reach an internal IAA concentration of 1 µM, corresponding to 100%. Residual radioactivity was determined for each individual oocyte by liquid scintillation counting after the time points indicated and are expressed relative to the initial 100%. Each time point represents the mean and s.e.m. of ten oocytes. To calculate the relative transport rate in per cent per minute, linear regression was performed. Each data point in Fig. 1a and Extended Data Fig. 9c represents the transport rate of one biological replicate using oocytes collected from different *X. laevis* females. GraphPad Prism V 9.3 was used for statistical analyses.

### Reporting summary

Further information on research design is available in the Nature Research Reporting Summary linked to this paper.

### Data availability

Atomic models have been deposited in the Protein Data Bank (PDB) and cryo-EM maps have been deposited in the Electron Microscopy Data Bank (EMDB) under the following accession numbers. Apo outward state in peptidisc: PDB 7QP9 and EMDB EMD-14115, IAA-bound outward state in peptidisc: PDB 7QPA and EMDB EMD-14116, NPA-bound inward state in peptidisc: PDB 7QPC and EMDB EMD-14117, and apo outward state in detergent: EMDB EMD-14118. Source data are provided with this paper.

- Lyons, J. A., Shahsavar, A., Paulsen, P. A., Pedersen, B. P. & Nissen, P. Expression strategies for structural studies of eukaryotic membrane proteins. *Curr. Opin. Struct. Biol.* **38**, 137–144 (2016).
- Tomasiaik, T. M. et al. General qPCR and plate reader methods for rapid optimization of membrane protein purification and crystallization using thermostability assays. *Curr. Protoc. Protein Sci.* **77**, 29.111–29.114 (2014).
- Carlson, M. L. et al. The Peptidisc, a simple method for stabilizing membrane proteins in detergent-free solution. *eLife* **7**, e34085 (2018).
- Ung, K. L., Alsarraf, H., Kremer, L. & Blaise, M. MmpL3, the trehalose monomycolate transporter, is stable in solution in several detergents and can be reconstituted into peptidiscs. *Protein Express. Purif.* **191**, 106014 (2022).
- Bazzone, A. & Barthmes, M. Functional characterization of SLC transporters using solid supported membranes. *Methods Mol. Biol.* **2168**, 73–103 (2020).
- Punjani, A., Rubinstein, J. L., Fleet, D. J. & Brubaker, M. A. cryoSPARC: algorithms for rapid unsupervised cryo-EM structure determination. *Nat. Methods* **14**, 290–296 (2017).
- Baek, M. et al. Accurate prediction of protein structures and interactions using a three-track neural network. *Science* **373**, 871–876 (2021).
- Pettersen, E. F. et al. UCSF Chimera—a visualization system for exploratory research and analysis. *J. Comput. Chem.* **25**, 1605–1612 (2004).
- Emsley, P., Lohkamp, B., Scott, W. G. & Cowtan, K. Features and development of Coot. *Acta Crystallogr. D* **66**, 486–501 (2010).

43. Trabuco, L. G., Villa, E., Mitra, K., Frank, J. & Schulten, K. Flexible fitting of atomic structures into electron microscopy maps using molecular dynamics. *Structure* **16**, 673–683 (2008).
44. Kidmose, R. T. et al. Namdinator—automatic molecular dynamics flexible fitting of structural models into cryo-EM and crystallography experimental maps. *IUCr* **6**, 526–531 (2019).
45. Adams, P. D. et al. PHENIX: a comprehensive Python-based system for macromolecular structure solution. *Acta Crystallogr. D* **66**, 213–221 (2010).
46. Moriarty, N. W., Grosse-Kunstleve, R. W. & Adams, P. D. electronic Ligand Builder and Optimization Workbench (eLBOW): a tool for ligand coordinate and restraint generation. *Acta Crystallogr. D* **65**, 1074–1080 (2009).
47. Chen, V. B. et al. MolProbity: all-atom structure validation for macromolecular crystallography. *Acta Crystallogr. D* **66**, 12–21 (2010).
48. Prisant, M. G., Williams, C. J., Chen, V. B., Richardson, J. S. & Richardson, D. C. New tools in MolProbity validation: CaBLAM for CryoEM backbone, UnDowser to rethink 'waters,' and NGL Viewer to recapture online 3D graphics. *Protein Sci.* **29**, 315–329 (2020).
49. Sobolev, O. V. et al. A global Ramachandran score identifies protein structures with unlikely stereochemistry. *Structure* **28**, 1249–1258.e2 (2020).
50. Ashkenazy, H. et al. ConSurf 2016: an improved methodology to estimate and visualize evolutionary conservation in macromolecules. *Nucleic Acids Res.* **44**, W344–W350 (2016).
51. Pei, J., Kim, B.-H. & Grishin, N. V. PROMALS3D: a tool for multiple protein sequence and structure alignments. *Nucleic Acids Res.* **36**, 2295–2300 (2008).
52. Bond, C. S. & Schüttelkopf, A. W. ALINE: a WYSIWYG protein-sequence alignment editor for publication-quality alignments. *Acta Crystallogr. D* **65**, 510–512 (2009).
53. Holm, L. DALI and the persistence of protein shape. *Protein Sci.* **29**, 128–140 (2020).
54. Lemoine, F. et al. NGPhylogeny.fr: new generation phylogenetic services for non-specialists. *Nucleic Acids Res.* **47**, W260–W265 (2019).
55. Fastner, A., Absmanner, B. & Hammes, U. Z. Use of *Xenopus laevis* oocytes to study auxin transport. *Methods Mol. Biol.* **1497**, 259–270 (2017).

**Acknowledgements** We acknowledge the EMBION Cryo-EM Facility at iNANO, Aarhus University, for time under application ID 0137, where all data was collected with the assistance of A. Bøggild, J. Lykkegaard Karlsen and T. Boesen. We also thank eBIC (proposal BI27980) for data collection on the detergent PIN8 sample. This project has received funding from the European Research Council (ERC) under the European Union's Horizon 2020 research and innovation programme (grant agreement no. 101000936) to B.P.P. U.Z.H. is funded by the Deutsche Forschungsgemeinschaft (HA3468/6-1 and HA3468/6-3) and SFB924. D.L.S. is funded by the National Institutes of Health (R35 GM144109).

**Author contributions** Sample preparation: K.L.U. and M.W. Electron microscopy data collection and analysis: K.L.U., M.W., E.D., D.L.S. and B.P.P. Activity assays: D.P.J., L.S., M.K. and U.Z.H. Manuscript preparation: K.L.U., M.W., D.L.S., U.Z.H. and B.P.P.

**Competing interests** The authors declare no competing interests.

**Additional information**

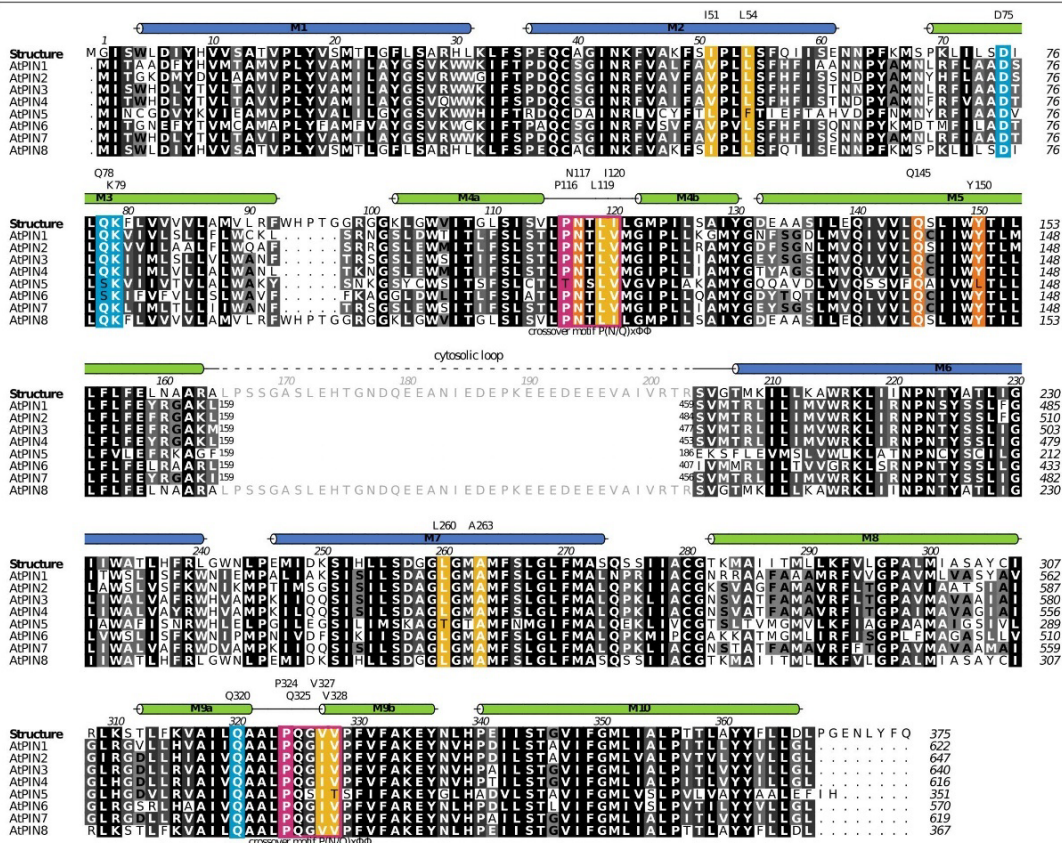
**Supplementary information** The online version contains supplementary material available at <https://doi.org/10.1038/s41586-022-04883-y>.

**Correspondence and requests for materials** should be addressed to Ulrich Z. Hammes or Bjørn Panyella Pedersen.

**Peer review information** Nature thanks Dolf Weijers and the other, anonymous, reviewer(s) for their contribution to the peer review of this work. Peer review reports are available.

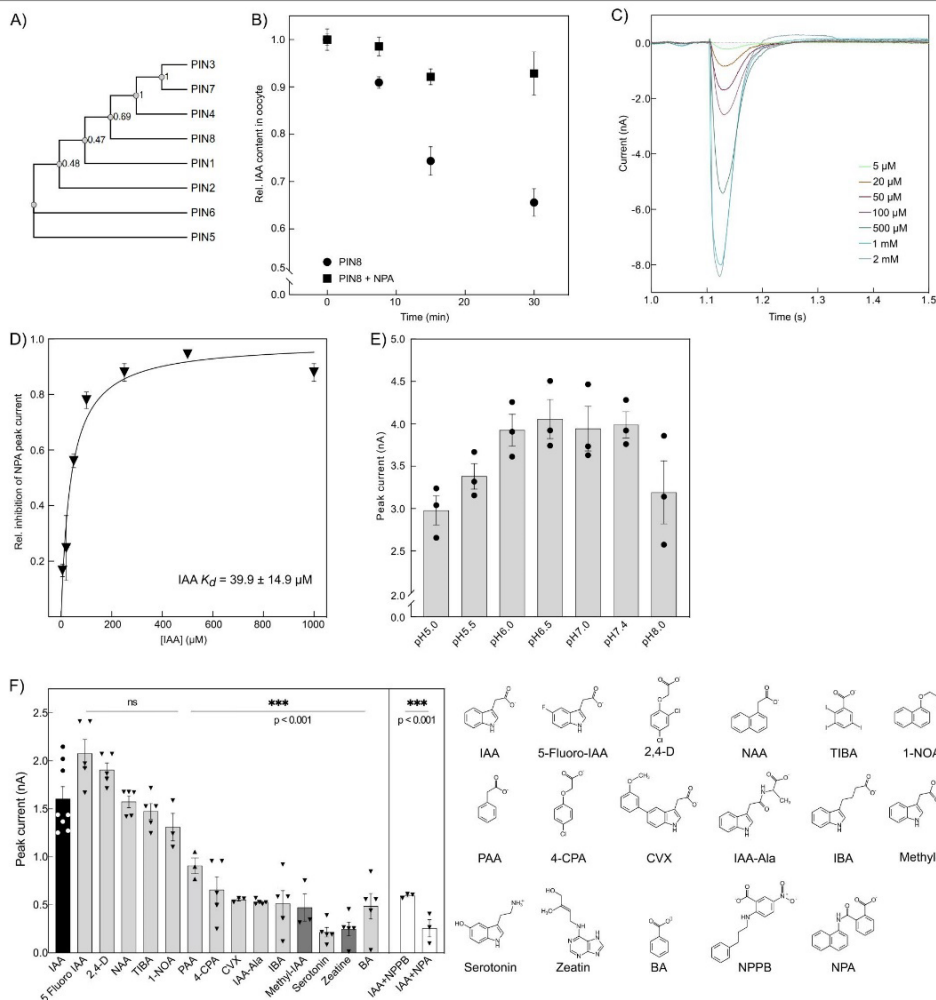
**Reprints and permissions information** is available at <http://www.nature.com/reprints>.

# Article



**Extended Data Fig. 1 | Multiple sequence alignment *A. thaliana* PINs.** Alignment between AtPIN1–8 with the following UniProt accession numbers. AtPIN1: Q9C6B8, AtPIN2: Q9LU77, AtPIN3: Q9S7Z8, AtPIN4: Q8RWZ6, AtPIN5: Q9FFD0, AtPIN6: Q9SQH6, AtPIN7: Q94OY5, AtPIN8: Q9LFP6. Conserved residues are highlighted with gray-scale, where black is perfectly conserved.

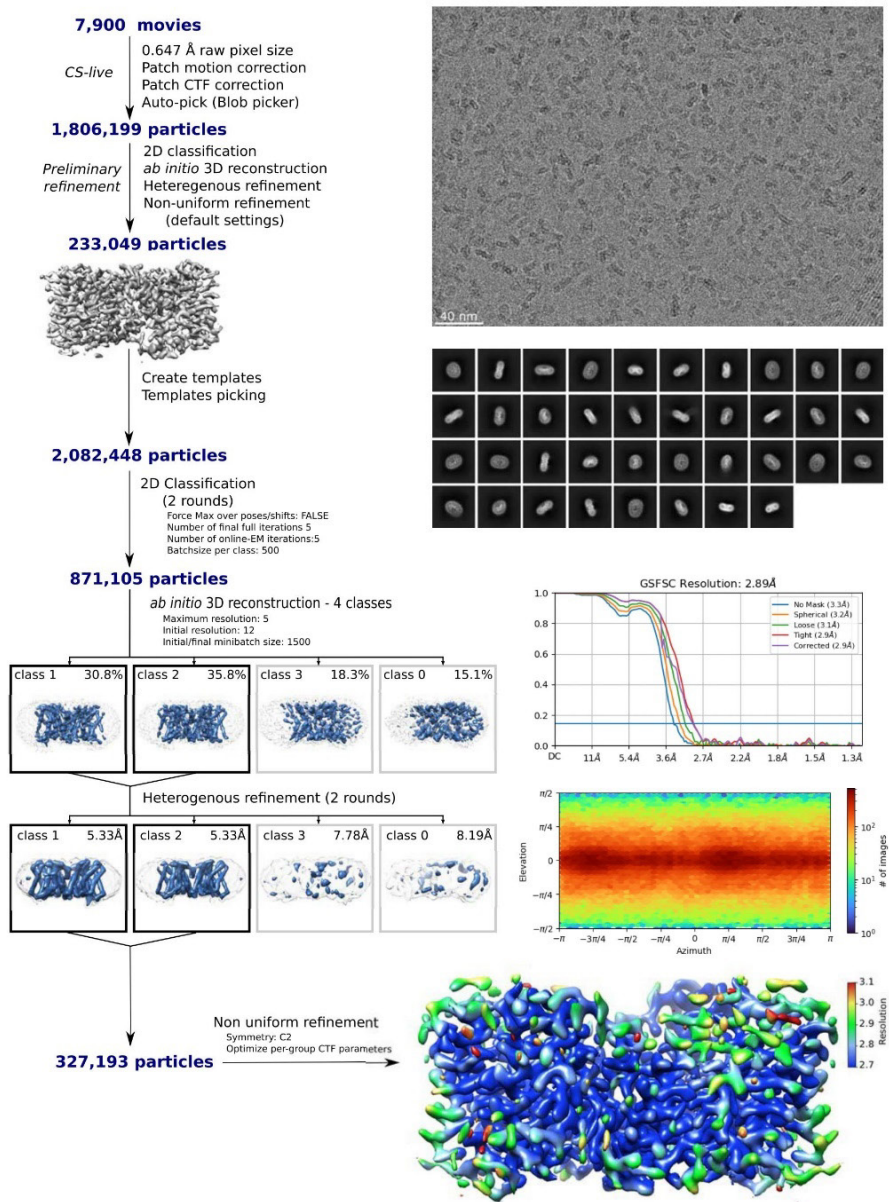
Colored tubes represent  $\alpha$ -helices found in the scaffold domain (blue) and transporter domain (green). Key residues are numbered above the  $\alpha$ -helix markings. Residues highlighted participate in IAA carboxylate recognition (orange) or IAA hydrophobic recognition (yellow), are part of the support site (blue) or form the central prolines of the crossover motif (pink).



**Extended Data Fig. 2 | Functional data on PINs. A)** Dendrogram of the relationship between *Arabidopsis thaliana* PIN1-8. Numbers denote bootstrap values of 500 trials. PIN8 is in a clade with the canonical PIN3, PIN4, and PIN7, unlike other non-canonical PINs (PIN5, PIN6). **B)** Figure time course of IAA export by PIN8 from oocytes. Relative IAA content of oocytes expressing PIN8 in the presence (■) or absence (●) of 10 μM NPA internally determined at the time indicated after substrate injection. Initial internal IAA concentration was 1 μM. n = 10 oocytes at each time point. Data points are mean ± SE. **C)** Raw current traces from SSM-electrophysiology for the PIN8 WT proteoliposomes. **D)** Relative inhibition of the peak binding current induced by 100 μM NPA in the presence of the indicated IAA concentration in non-activating as well as activating buffer. Half-maximal inhibition  $39.9 \pm 14.9 \mu M$  (mean ± SE, n = 3) corresponds to apparent  $K_d$ (IAA). **E)** Peak currents elicited by 500 μM IAA at the pH indicated (n = 3). Bars are mean ± SE. The points represent individual measurements. **F)** Substrate specificity of PIN8 measured at pH 7.4. Peak currents elicited by IAA (●) or a range of putative substrates tested at 100 μM (▼).

Synthetic auxins: 5-fluoro-IAA, 2,4-D, NAA, TIBA, 1-NOA, 4-CPA, CVX. Endogenous auxins: PAA, IAA-Ala, IBA, Methyl-IAA. Others: Serotonin, Zeatin (a cytokinin), BA (benzoic acid). Chemical structures at pH 7.4 are shown. Current response of substrates indicated with asterisks differed significantly from IAA, indicating that they are likely not substrates for the transporter, but we note that different chemical molecules have different electrostatic potentials and this can also have an influence on the observed current (5-Fluoro IAA p = 0.011; 2,4-D p = 0.272; NAA p = 0.999; TIBA p = 0.989; 1-NOA p = 0.539; PAA p = 0.0007, 4-CPA p < 0.0001; CVX p < 0.0001; IAA-Ala p < 0.0001; IBA p < 0.0001; Methyl-IAA p < 0.0001; Serotonin p < 0.0001; Zeatin p < 0.0001; BA p < 0.0001; IAA+NPPB p < 0.0001; IAA+NPA p < 0.0001). Substrates shown in dark grey are uncharged. Two inhibitors were tested in the presence of 100 μM IAA. Bars are mean ± SE; The data points represent individual measurements. (n = 8: IAA; n = 5: 5-Fluoro IAA, 2,4-D, NAA, TIBA, 4-CPA, IAA-Ala, IBA, Serotonin, Zeatin, BA; n = 3: 1-NOA, PAA, CVX, Methyl-IAA, IAA+NPPB, IAA+NPA).

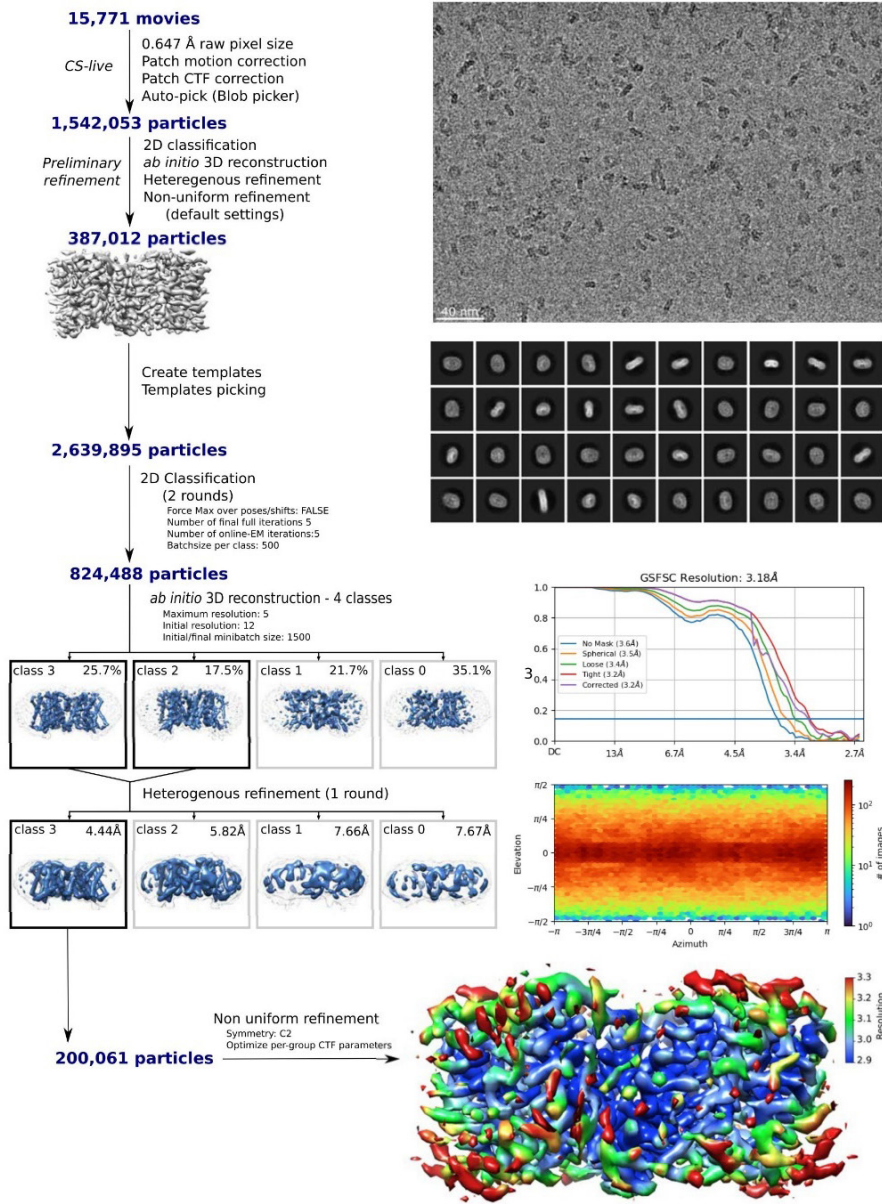
Cryo-EM Structure of apo-PIN8 in peptidisc



**Extended Data Fig. 3 | Image processing and reconstruction for apo-PIN8.** Workflow of image processing and 3D reconstruction in cryoSPARC, including a motion corrected micrograph from Titan Krios microscope using a K3 detector, 2D classes and sharpened density map from the final non-linear

refinement colored by local resolution. Corrected curve of the global Fourier shell correlation (FSC) indicates 2.89 Å based on the 0.143 gold-standard criterion. The cryo-EM experiment with this sample was repeated 7 times with data collection 1 time.

### Cryo-EM Structure of IAA-PIN8 in peptidisc

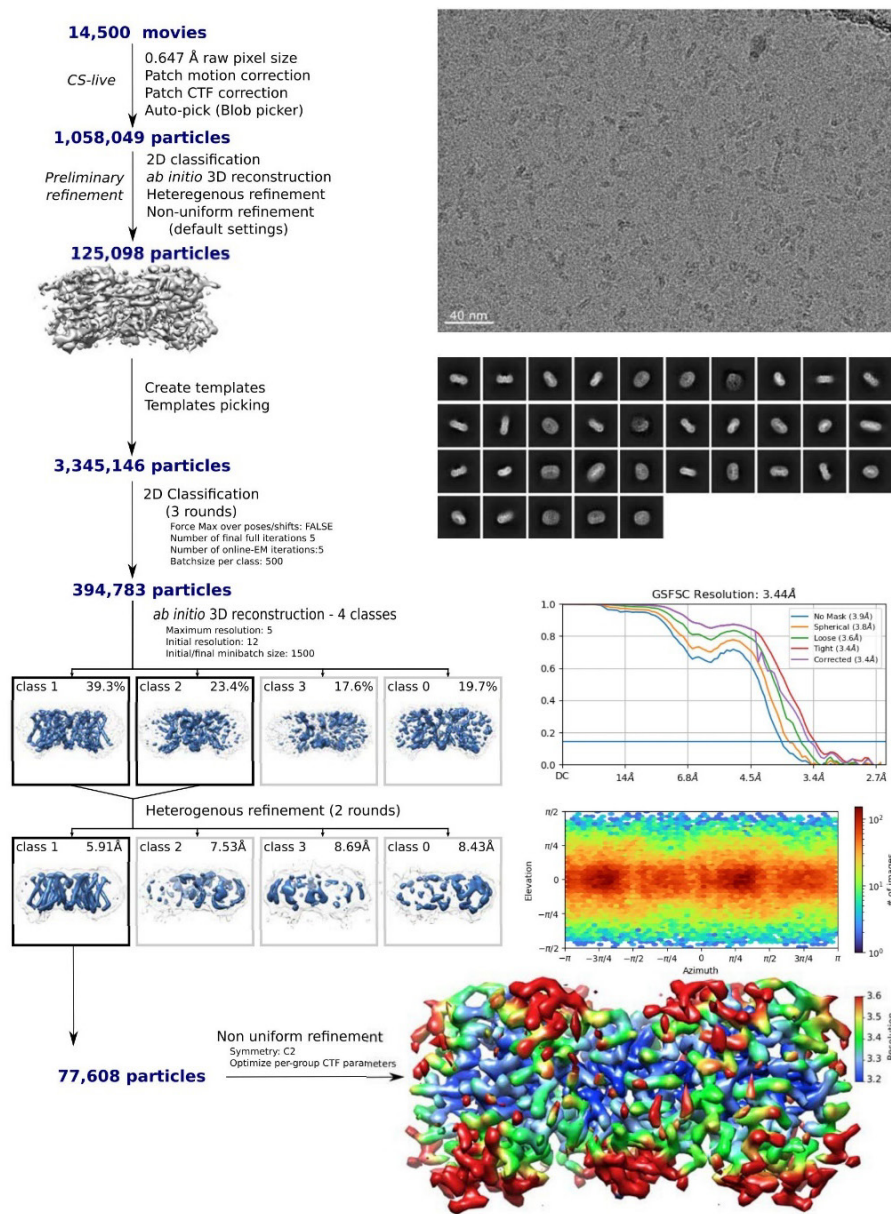


**Extended Data Fig. 4 | Image processing and reconstruction for IAA-PIN8.** Workflow of image processing and 3D reconstruction in cryoSPARC, including a motion corrected micrograph from Titan Krios microscope using a K3 detector, 2D classes and sharpened density map from the final non-linear

refinement colored by local resolution. Corrected curve of the global FSC indicates 3.18 Å based on the 0.143 gold-standard criterion. The cryo-EM experiment with this sample was repeated 6 times with data collection 1 time.

# Article

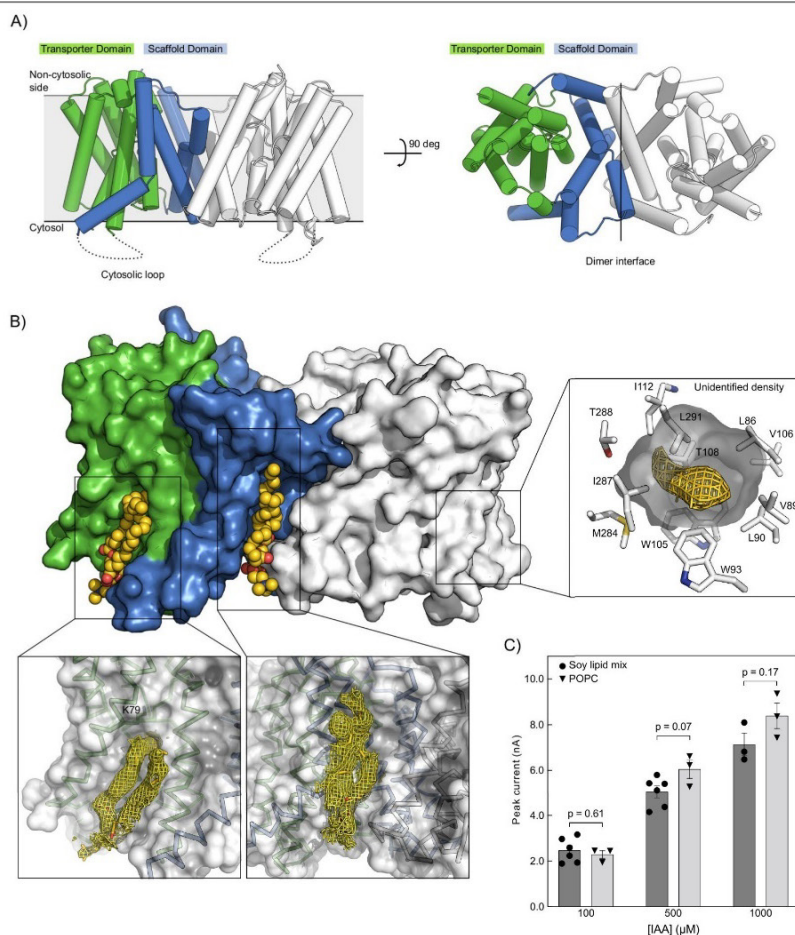
## Cryo-EM Structure of NPA-PIN8 in peptidisc



**Extended Data Fig. 5 | Image processing and reconstruction for NPA-PIN8.** Workflow of image processing and 3D reconstruction in cryoSPARC, including a motion corrected micrograph from Titan Krios microscope using a K3 detector, 2D classes and sharpened density map from the final non-linear

refinement colored by local resolution. Corrected curve of the global FSC indicates 3.44 Å based on the 0.143 gold-standard criterion. The cryo-EM experiment with this sample was repeated 2 times with data collection 1 time.

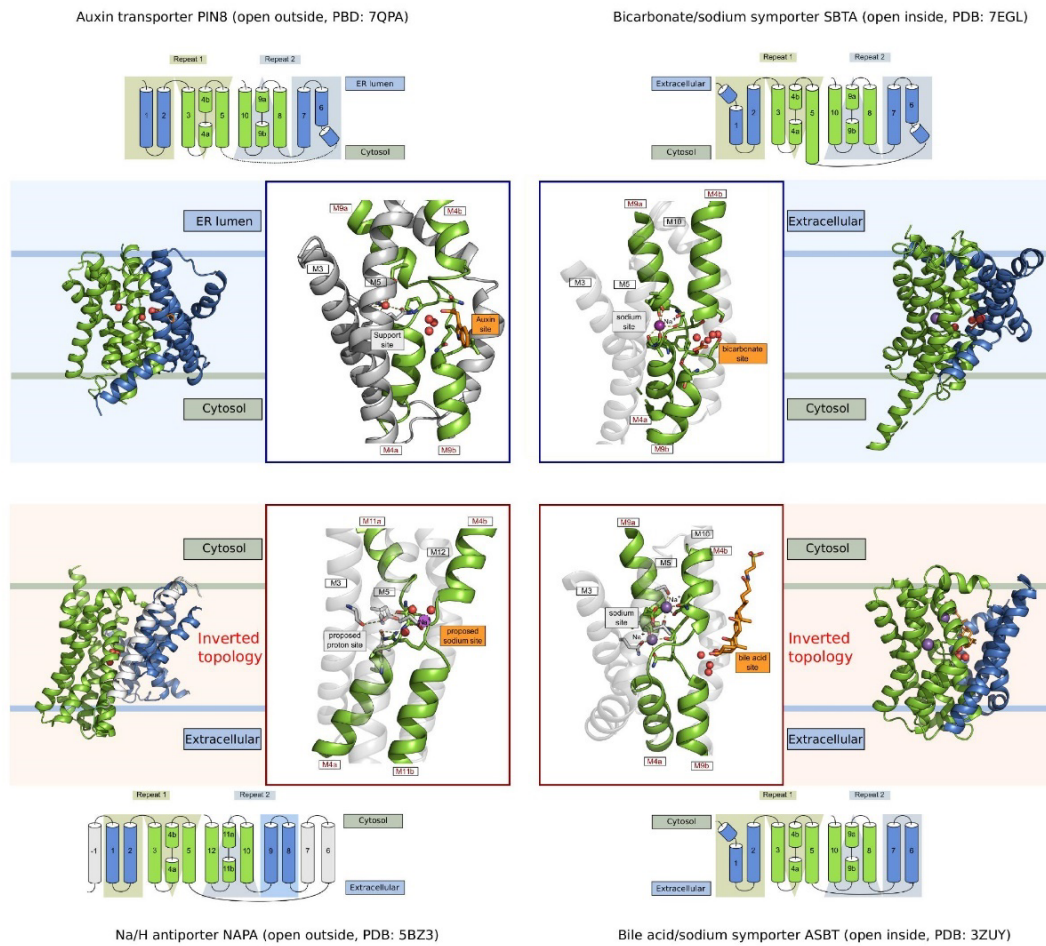




**Extended Data Fig. 6 | Domains and lipids in PINs.** **A)** Overview of the transporter (green) and scaffold (blue) domain in the monomer of PINs. **B)** Position of lipid modeled as phosphatidylcholine in PINs. One lipid is located in the groove between the two monomers, the other is located at the transporter domain with one aliphatic chain sticking into a cavity of the protein next to the support site. This links the support site to the lipid environment. An unidentified density was found in maps in a cavity towards the cytosolic side. Mutating T288A did not affect activity (Fig. 2d and Extended Data Fig. 9a).

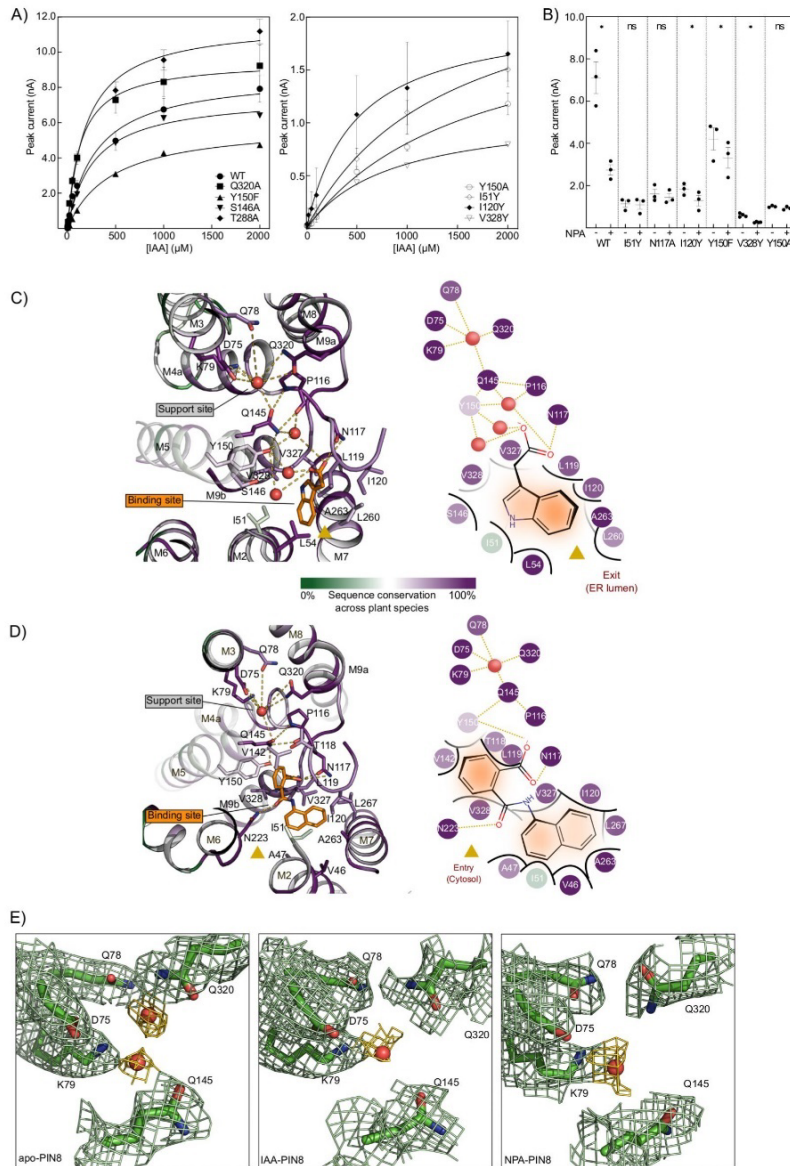
**C)** Peak currents elicited by the indicated IAA concentrations in liposomes consisting of soy lipid mix (●) or 1-palmitoyl-2-oleoyl-sn-glycero-3-phosphocholine (POPC) (▼). The current response did not differ between the liposomes at any concentration (two-sided unpaired t-test, 100 μM IAA p = 0.61, 500 μM IAA p = 0.07, 1000 μM p = 0.17). This supports that PINs is not dependent on specific lipids for activity. Bars are mean ± SE. Data points are independent experiments. (n = 6: soy lipid mix 100 μM and 500 μM; n = 3 all other conditions).

## Article



**Extended Data Fig. 7 | Topology of transporters with a crossover elevator mechanism.** Shown are the topologies of auxin transporters (PIN), bicarbonate/sodium symporters (SBTA), Na/H antiporters (NAPA) and bile

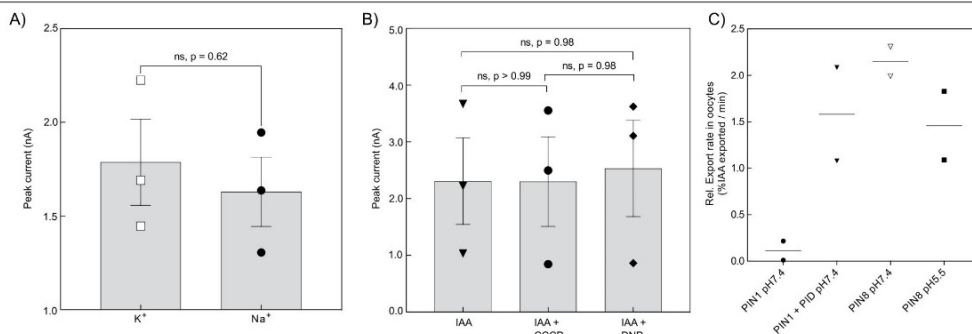
acid/sodium symporters (ASBT). NAPA and ASBT display an inverted topology compared to PINs and SBTA. All four families have a crossover with a substrate binding site to one side and a putative support site to the other side.



**Extended Data Fig. 8 | Details of mutants and support site. A)** Transport current using SSM-electrophysiology on PIN8 mutants in proteoliposomes. Transport can be described by Michaelis-Menten kinetics. Data points are mean or mean  $\pm$  SE ( $n > 2$ ) (WT  $n = 4$  different liposome preparations, for mutants  $n = 5$  (T288A),  $n = 4$  (Q320A),  $n = 3$  (I51Y, I120Y, Y150A),  $n = 2$  (Y150F, S146A, V328Y)). **B)** Sensitivity of WT and selected mutants to NPA inhibition. Peak current response to 2 mM IAA or 2 mM IAA and 20  $\mu$ M NPA presented in non-activating as well as activating buffer. Asterisks indicate significant differences between groups (two-sided paired t-test, WT  $p = 0.0131$ , I51Y  $p = 0.48$ , N117A  $p = 0.07$ , I120Y  $p = 0.03$ , Y150F  $p = 0.02$ , V328Y  $p = 0.01$ , Y150A  $p = 0.22$ ). Data points are mean  $\pm$  SE; data points are individual experiments

( $n = 4$  (V328Y),  $n = 3$  (all other mutants and WT)). **C)** View from the non-cytosolic side of the side chains interacting with IAA and forming the support site. Residues are colored by sequence conservation using ConSurf. 318 unique sequences from plants with sequence identity of 35–95% to AtPIN8 were identified, sorted by E-value and 150 selected at equal intervals for the alignment. **D)** View from the non-cytosolic side of the side chains interacting with NPA and forming the support site. Residues are colored by sequence conservation using ConSurf. **E)** Map density for the peaks found in the support site modeled as water. In the case of apo-PIN8 two peaks could be modeled as water with one having stronger density than the other.

## Article



**Extended Data Fig. 9 | Activity assays support PINS is independent of ions, pH and lipids. A)** Peak currents elicited by 100  $\mu$ M IAA in Na<sup>+</sup>-free K<sup>+</sup> buffer or K<sup>+</sup>-free Na<sup>+</sup> buffer. The current response was independent of the principal cation. Bars are mean  $\pm$  SE; n = 3. The points represent individual measurements. Means were compared by a two-tailed unpaired t-test (p = 0.62). **B)** Peak currents elicited by 100  $\mu$ M IAA, and with proton-motive force decouplers CCCP and DNP present. The current responses were similar in

all cases. Bars are mean  $\pm$  SE; n = 3. The points represent individual measurements. No difference (p = 0.97) between groups was found by one-way ANOVA multiple comparisons, followed by Tukey's Post Hoc test (IAA vs. IAA + CCCP p > 0.99, IAA vs. IAA + DNP p = 0.98, IAA + CCCP vs. IAA + DNP p = 0.98). **C)** Oocyte export assay using <sup>3</sup>H-IAA and PIN1 plus kinase PID as a control. PINS transport rate is unchanged at two different external pH values; n = 2. Data points are biologically independent experiments. The mean is indicated.

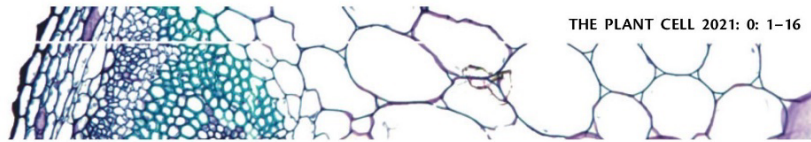
## Extended Data Table 1 | Statistics for cryo-EM data collection, model refinement and validation

### Cryo-EM data collection, refinement and validation statistics

	apo-PIN8 peptidisc	IAA-PIN8 peptidisc	NPA-PIN8 peptidisc	apo-PIN8 LM-NG
<b>Data Collection and processing</b>				
Magnification	130,000	130,000	130,000	130,000
Voltage (kV)	300	300	300	300
Electron exposure (e <sup>-</sup> /Å <sup>2</sup> )	59.100	60.122	59.379	60.000
Defocus range (µm)	0.5-2.5	0.4-2.6	0.5-2.5	0.5-2.5
Pixel size (Å)	0.647	0.647	0.647	0.653
Symmetry imposed	C2	C2	C2	C2
Collected micrographs (no.)	7,900	15,771	14,500	7,808
Initial particle images (no.)	2,082,448	2,639,895	3,345,146	973,540
Final particle images (no.)	327,193	200,061	77,608	74,743
Map resolution (Å)*	2.9	3.2	3.4	3.3
<b>Refinement</b>				
Initial model used (PDB code)	RosettaFold model	7QP9	7QP9	
Map sharpening B factor (Å <sup>2</sup> )	-126.9	-139.8	-128.3	
Model composition				
non-hydrogen atoms	5,421	5,276	5,292	
Protein residues	654	654	654	
Ligands	DLP: 4 **	DLP: 2 , IAC: 2	DLP: 2 , E7O: 2	
Waters	127	64	62	
R.m.s. deviations				
Bond lengths (Å)	0.003	0.003	0.002	
Bond angles (deg)	0.486	0.554	0.513	
Validation				
MolProbity score	1.57	1.50	1.40	
Clashscore	6.17	8.62	5.65	
Poor rotamers (%)	0	0	0	
Rama-Z score (Whole/Helix/Loop)	2.00 / 1.94 / -1.49	1.43 / 1.66 / -1.71	1.61 / 1.58 / -1.06	
CaBLAM score (Outliers/Disfavored/Cα)	0.78 / 3.45 / 0.00	0.78 / 5.17 / 0.31	0.78 / 4.86 / 0.16	
Ramachandran Plot				
Favored (%)	96.44	97.83	97.52	
Allowed (%)	3.56	2.17	2.48	
Disallowed (%)	0.00	0.00	0.00	
Deposited model (PDB id)	7QP9	7QPA	7QPC	
Deposited map (EMDB id)	EMD-14115	EMD-14116	EMD-14117	EMD-14118

\* Gold standard FSC with threshold of 0.143

\*\* DLP: 1,2-Dilinoleoyl-SN-Glycero-3-Phosphocholine



## Mapping and engineering of auxin-induced plasma membrane dissociation in BRX family proteins

Samuel W. H. Koh <sup>1</sup>, Petra Marhava <sup>1</sup>, Surbhi Rana <sup>1</sup>, Alina Graf <sup>2</sup>, Bernard Moret <sup>1</sup>,  
Alkistis E. L. Bassukas <sup>2</sup>, Melina Zourelidou <sup>2</sup>, Martina Kolb <sup>2</sup>, Ulrich Z. Hammes <sup>2</sup>,  
Claus Schwechheimer <sup>2</sup> and Christian S. Hardtke <sup>1,\*†</sup>

<sup>1</sup> Department of Plant Molecular Biology, University of Lausanne, Biophore Building, Lausanne 1015, Switzerland  
<sup>2</sup> Plant Systems Biology, Technical University of Munich, Freising 85354, Germany

\*Author for communication: christian.hardtke@unil.ch

†Senior author.

The author responsible for distribution of materials integral to the findings presented in this article in accordance with the policy described in the Instructions for Authors ([www.plantcell.org](http://www.plantcell.org)) is: Christian S. Hardtke ([christian.hardtke@unil.ch](mailto:christian.hardtke@unil.ch)).

C.S.H., C.S., and U.Z.H. designed the research. S.W.H.K. performed most of the experiments. P.M., S.R., and B.M. performed some of the experiments. A.G., A.E.L.B., and M.Z. performed kinase assays. M.K. performed oocyte assays. All authors analyzed data and commented on the manuscript. S.W.H.K., C.S., and C.S.H. wrote the manuscript.

### Abstract

Angiosperms have evolved the phloem for the long-distance transport of metabolites. The complex process of phloem development involves genes that only occur in vascular plant lineages. For example, in *Arabidopsis thaliana*, the *BREVIS RADIX (BRX)* gene is required for continuous root protophloem differentiation, together with *PROTEIN KINASE ASSOCIATED WITH BRX (PAX)*. BRX and its BRX-LIKE (BRXL) homologs are composed of four highly conserved domains including the signature tandem BRX domains that are separated by variable spacers. Nevertheless, BRX family proteins have functionally diverged. For instance, BRXL2 can only partially replace BRX in the root protophloem. This divergence is reflected in physiologically relevant differences in protein behavior, such as auxin-induced plasma membrane dissociation of BRX, which is not observed for BRXL2. Here we dissected the differential functions of BRX family proteins using a set of amino acid substitutions and domain swaps. Our data suggest that the plasma membrane-associated tandem BRX domains are both necessary and sufficient to convey the biological outputs of BRX function and therefore constitute an important regulatory entity. Moreover, PAX target phosphosites in the linker between the two BRX domains mediate the auxin-induced plasma membrane dissociation. Engineering these sites into BRXL2 renders this modified protein auxin-responsive and thereby increases its biological activity in the root protophloem context.

### Introduction

Angiosperms have evolved a vascular system that allows for the separation of the sites of water and nutrient acquisition from the sites of photosynthesis (Lucas et al., 2013). Shoot performance depends on water and inorganic nutrients delivered by the root system through the xylem, and in turn, root system growth depends on carbohydrates delivered by

the shoot through the phloem. More generally, the phloem connects source organs with sink organs and is, therefore, essential for sustained plant growth and development. Compared to other vascular tissues, the phloem is unique in its structure, function, and transport characteristics (Knoblauch et al., 2016). The phloem found in angiosperms consists of precisely aligned sieve elements, enucleated cells

Received October 15, 2020. Accepted March 3, 2021. Advance access publication March 5, 2021

© American Society of Plant Biologists 2021. All rights reserved. For permissions, please email: [journals.permissions@oup.com](mailto:journals.permissions@oup.com)

that form the phloem sap-conducting sieve tubes, and their neighboring, supporting companion cells. Genes that are involved in the formation of phloem are typically specific to land plants. For example, *BREVIS RADIX* (*BRX*) and its homologs constitute small gene families in angiosperms (Briggs et al., 2006; Beuchat et al., 2010), but *BRX* homologs can already be found in mosses or lycophytes (One Thousand Plant Transcriptomes, 2019).

*BRX* was originally identified as the causative loss-of-function locus for the short root phenotype in the *Arabidopsis thaliana* stock center accession Umkirch-1 (Mouchel et al., 2004). Research based on a null allele in the Col-0 reference accession confirmed requirement of *BRX* for primary root growth vigor (Rodrigues et al., 2009) and led to the realization that the causative cellular defect in *brx* mutants is their incapacity to form fully differentiated protophloem sieve element (PPSE) strands in the root meristem (Scacchi et al., 2010; Anne and Hardtke, 2017). Protophloem is early, meristematic phloem that is essential for root growth and maintenance (Furuta et al., 2014; Rodriguez-Villalon et al., 2014; Anne and Hardtke, 2017). Matching the location of the defect in *brx* mutants, the *BRX* protein is specifically expressed in developing protophloem, albeit at very low level (Bauby et al., 2007; Rodriguez-Villalon et al., 2014; Marhava et al., 2018).

The protophloem differentiation defects in *brx* mutants are not fully penetrant but rather occur in a nonrandom pattern, which has recently been explained by competition among neighboring sieve element precursors for auxin (Moret et al., 2020). Auxin flux through developing PPSE cell files controls the timing of their differentiation (Santuari et al., 2011; Marhava et al., 2018), and *BRX* has been implicated in regulating this polar auxin transport (Santuari et al., 2011; Marhava et al., 2018; 2020). *BRX* is a conditional plasma membrane-associated protein, which typically localizes to the rootward end of developing PPSEs. There it interacts and co-localizes with PROTEIN KINASE ASSOCIATED WITH *BRX* (*PAX*), a positive regulator of PIN-FORMED-1 (PIN)-mediated auxin efflux (Barbosa et al., 2018; Marhava et al., 2018). Because the plasma membrane association of *BRX* is negatively regulated by auxin and because *BRX* can interfere with PIN activation by *PAX* (Scacchi et al., 2009; Marhava et al., 2018), the three proteins are thought to constitute a molecular rheostat. In this model, inhibition of *PAX* by *BRX* suppresses PIN efflux activity, which in turn leads to increases in cytosolic auxin levels and thus the eventual dissociation of *BRX*, followed by *PAX* and PIN activation (Marhava et al., 2018). The ensuing dynamic equilibrium fine-tunes auxin flux through the developing protophloem.

The *A. thaliana* genome encodes five highly related *BRX* family proteins, which display four conserved domains that are separated by spacer regions: the N-terminus with a putative palmitoylation site (Rowe et al., 2019), an adjacent domain with a conserved “KDMA” motif, and two so-called “*BRX* domains” in tandem (Supplemental Figure S1A). Besides the *bona fide* *BRX* family genes, the *A. thaliana*

genome contains another partial *BRX* homolog (AT2G21030), which encodes a nearly identical but incomplete first *BRX* domain, the linker, and part of the second *BRX* domain, whereas the N-terminal parts of *BRX* are missing (Supplemental Figure S1B). Ectopic expression and promoter-swapping experiments suggested that only the closest *BRX* homolog, *BRX-LIKE1* (*BRXL1*), can fully substitute for *BRX*, whereas *BRXL2*–*BRXL4* at best confer partial rescue of *brx* mutants (Briggs et al., 2006; Beuchat et al., 2010). In contrast to *BRX*, the plasma membrane association of *BRXL2* is not auxin-responsive, and its capacity to inhibit *PAX* is reduced (Marhava et al., 2020). These differential features may be responsible for the incapacity of *BRXL2* to fully substitute for *BRX* function, as other protein–protein interaction properties and polar, rootward plasma membrane association are shared (Marhava et al., 2020). However, *BRX* and *BRXL2* are fully redundant in the context of stomata development, where *BRXL2* is the dominant family member (Bringmann and Bergmann, 2017; Rowe et al., 2019). Here, we embarked on a detailed comparative analysis of *BRX* family protein domains to further our understanding of this interesting class of land plant-specific proteins. Our data suggest that the auxin response of *BRX* is conferred by the linker region between the tandem *BRX* domains and by *PAX* kinase target phosphosites. Engineering these sites into *BRXL2* renders the protein auxin-responsive and increases its biological activity in the root protophloem.

## Results

### Expression level and auxin response determine redundancy among *BRX* family proteins

The defect in *A. thaliana* *brx* root meristems manifests itself in developing PPSE strands that are interrupted by PPSE precursors that do not properly differentiate, i.e. so-called gap cells. Gap cell frequency in one or both PPSE strands is one of the quantitative readouts of phenotypic severity in pertinent mutants (Breda et al., 2017). Typically, ~50%–60% of *brx* root meristems show gap cells in one PPSE strand, whereas ~20%–30% show gap cells in both strands (Supplemental Figure S2A). In available *brx brx1 brx2 brx3* quadruple mutants (Rowe et al., 2019), this defect tended to be enhanced relative to *brx* single mutants (Supplemental Figure S2A), and in extremis, PPSE differentiation was nearly absent (Supplemental Figure S2B). The enhanced severity of the quadruple mutant also manifested itself in eventually even further reduced root growth compared to the *brx* single mutant (Supplemental Figure S2C). In contrast, knockout of the partial *BRX* homolog AT2G21030, whose promoter is active in the mature root vasculature but not in developing protophloem (Supplemental Figure S2D), did not result in any detectable root development defects (Supplemental Figure S1B). These results suggest limited yet tangible redundancy between *BRX* and other *BRX* family genes in the root.

Previous work suggested that the closest *BRX* homolog, *BRXL1*, is mainly expressed in the mature vasculature (Scacchi et al., 2009; Cattaneo et al., 2019). However, some

weak expression and rootward polar localization in the protophloem was observed when a BRXL1–CITRINE fusion protein was expressed in the genomic *BRXL1* context (Figure 1A). In contrast, BRXL2–CITRINE fusion protein expressed in the genomic *BRXL2* context was observed throughout the root and also displayed rootward polarity (Marhava et al., 2020), which was accentuated in developing protophloem (Figure 1B). Interestingly, BRXL2–CITRINE expression was also observed in the stem cell niche and in the columella-root cap. Although the *BRX* promoter confers expression in these tissues as well (Scacchi et al., 2009) (Supplemental Figure S2E), BRX protein is barely detectable there (Marhava et al., 2018). The latter might reflect destabilization of BRX by auxin (Supplemental Figure S2F), which accumulates in and around the stem cell niche (Sabatini et al., 1999; Grieneisen et al., 2007).

When expressed in a *brx* background, increased *BRXL1* dosage through *BRXL1:gBRXL1-CITRINE* transgene expression conferred partial rescue of the *brx* mutant phenotype (Figure 1, C and D), and this rescue was quantitatively comparable to the partial rescue conferred by expression of the *BRXL2:gBRXL2-CITRINE* transgene in *brx* (Figure 1, E and F). However, *brx* rescue was nearly perfect when BRXL1–CITRINE was expressed under the control of the BRX promoter (Figure 1, G–I), but not when BRXL2–CITRINE was expressed in the same context (see below) (Marhava et al., 2020). Moreover, similar to BRX–CITRINE (Figure 1J), the plasma membrane association and stability of BRXL1–CITRINE were auxin-responsive (Figure 1, K and L), in stark contrast to BRXL2–CITRINE (Marhava et al., 2020) (Figure 1M). In summary, these observations support the notion that the auxin-responsiveness of BRX is critical for its regulatory function in protophloem development and that the closely related BRXL1, but not the divergent BRXL2, shares this functionally important property. Furthermore, the strong functional overlap between BRX and BRXL1 proteins is only set aside by divergent expression levels, with the BRX promoter conferring substantially higher expression than the *BRXL1* promoter.

#### Plasma membrane association is a robust feature of BRX function

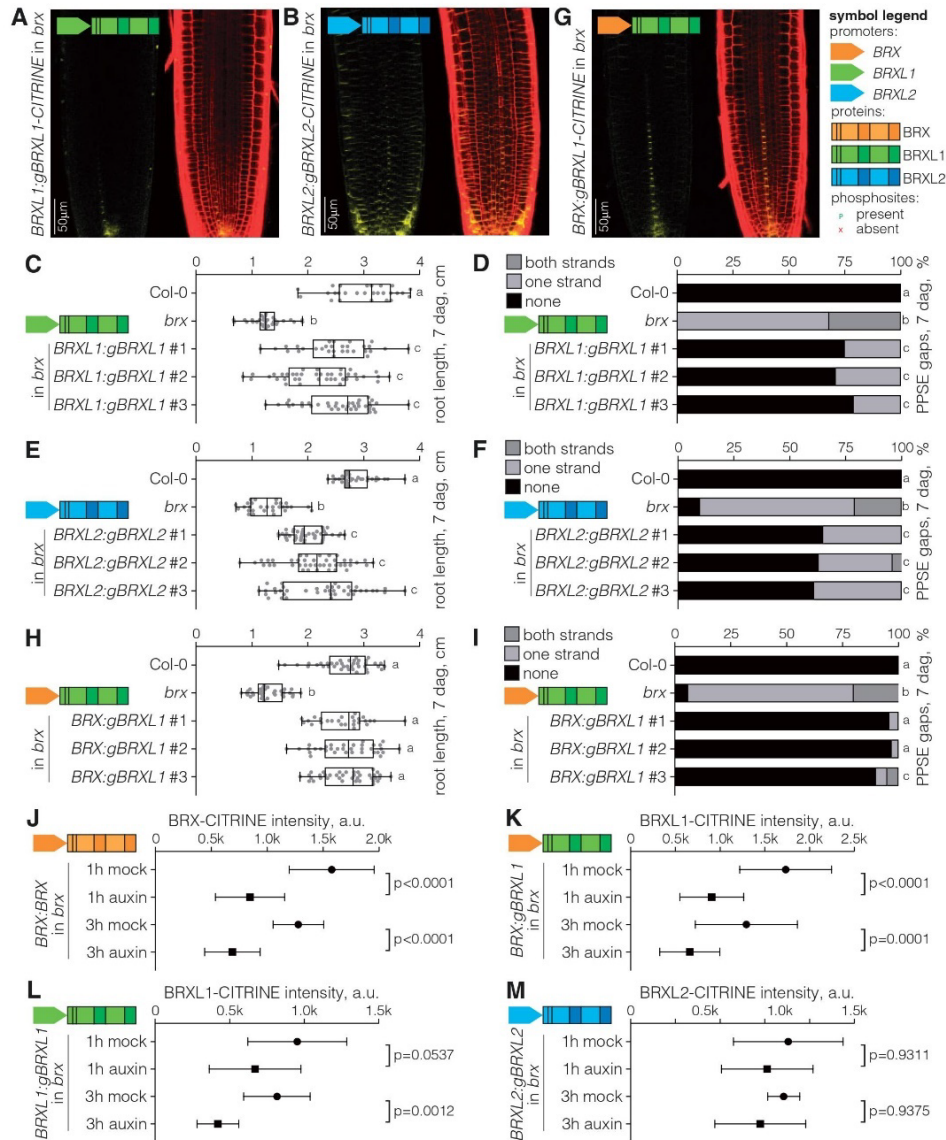
To better understand putative BRX functional domains, we explored sequence features that could be related to BRX localization, stability, or turnover (Supplemental Figure S3). First, we targeted the N-terminal amino acids, which confer robust plasma membrane association in the case of BRX (Scacchi et al., 2009) and contain a putative palmitoylation site (Rowe et al., 2019). Interestingly, BRX and BRXL1 differ at amino acid 2 (phenylalanine) from the other family members (leucine). Because BRX might be targeted by the ubiquitin–proteasome pathway (Scacchi et al., 2009), we replaced the destabilizing N-end rule phenylalanine residue by methionine ( $BRX^{F2M}$ ). However, this  $BRX^{F2M}$  version did not display any substantially different stability compared to wild-type BRX (Figure 2, A and B). Next, we added a

myristoylation signal to the N-terminus ( $BRX^{N-MYR}$ ) (Bologna et al., 2004) and compared it to a control protein with a similar sized added random sequence ( $BRX^{N-EXT}$ ). Again, no substantially different localization was observed (Figure 2, C and D), except that the plasma membrane association of  $BRX^{N-MYR}$  appeared somewhat “cleaner.” Interestingly, the myristoylation signal neither interfered with BRX polarity nor with its auxin response (Figure 2, E and F). This matches the idea that auxin-induced BRX dissociation from the plasma membrane could involve clathrin-mediated endocytosis (Scacchi et al., 2009; Santuari et al., 2011). Finally, we revisited the potential nuclear localization requirement of BRX (Scacchi et al., 2009) by either mutating its nuclear exclusion signal ( $BRX^{NES > mut}$ ), replacing it with a nuclear localization signal ( $BRX^{NES > NLS}$ ), or adding an artificial nuclear localization signal to the C-terminus ( $BRX^{C-NLS}$ ). Whereas the  $BRX^{NES > mut}$  protein appeared somewhat stabilized (Supplemental Figure S4A), the  $BRX^{NES > NLS}$  and  $BRX^{C-NLS}$  proteins appeared to be less abundant than wild-type BRX (Supplemental Figure S4, B and C). Yet remarkably, both  $BRX^{NES > NLS}$  and  $BRX^{C-NLS}$  were predominantly plasma membrane associated and were barely visible in the nucleus, suggesting that the presence of a nuclear localization signal could not override its plasma membrane association. Despite these slightly divergent behaviors of different BRX variant proteins, all of them fully rescued the root growth defect of *brx* (Supplemental Figure S4D), and no protophloem gaps were observed in these lines. In summary, none of our amino acid exchanges or additions had a major impact on the plasma membrane association of BRX or the capacity to rescue the signature defects of the *brx* mutant.

#### The tandem BRX domains comprise the essential features of BRX activity

To delimit functionally relevant domains of BRX, we expressed deletion constructs in the *brx* mutant background. To this end, the potentially palmitoylated BRX N-terminus (Rowe et al., 2019) (amino acids 1–9) was combined with different BRX subfragments that were designed to encompass the different conserved domains (Supplemental Figure S1A). These fragments were expressed as CITRINE fusions under the control of the BRX promoter. All five fragments tested showed plasma membrane association and expression in PPSEs (Figure 3, A–E). Yet, the fragments that contained no or only one BRX domain displayed more variable plasma membrane localization and at times expression outside of the PPSE strands (Figure 3, A–C). This also matched expression pattern of a nuclear localized NLS–VENUS fusion protein under the control of the full-length BRX promoter or its rather extended 2,314 bp 5′-UTR only (Figure 3, F and G). In contrast, the fragment that comprised both BRX domains ( $BRX^{104-344}$ ) invariably and precisely mimicked the plasma membrane localization and expression pattern of full-length BRX (Figure 3D). This highly PPSE-specific expression was also consistent with the striking, serendipitous observation that expression of the full-length





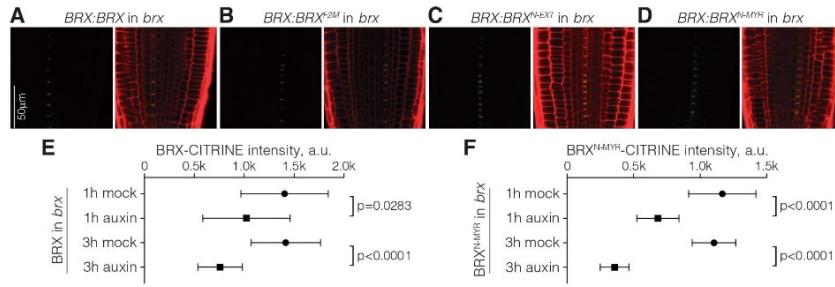


**Figure 2** Robust plasma membrane association of BRX N-terminal variants. A–D, Confocal microscopy images of variant BRX–CITRINE fusion proteins (see Supplemental Figure S3) expressed under the control of the BRX promoter in the *brx* mutant background (yellow fluorescence, left). (Right) Overlay with PI cell wall staining (red fluorescence). E and F, Quantification of the indicated CITRINE fusion protein signal intensity at the rootward plasma membrane of developing PPSEs, 1 or 3 h after mock or auxin treatment ( $n = 12\text{--}23$  roots, average of 12–15 cells per root). Plot circles and squares display the mean, error bars indicate standard deviation. Statistical significance was determined by ordinary one-way ANOVA.

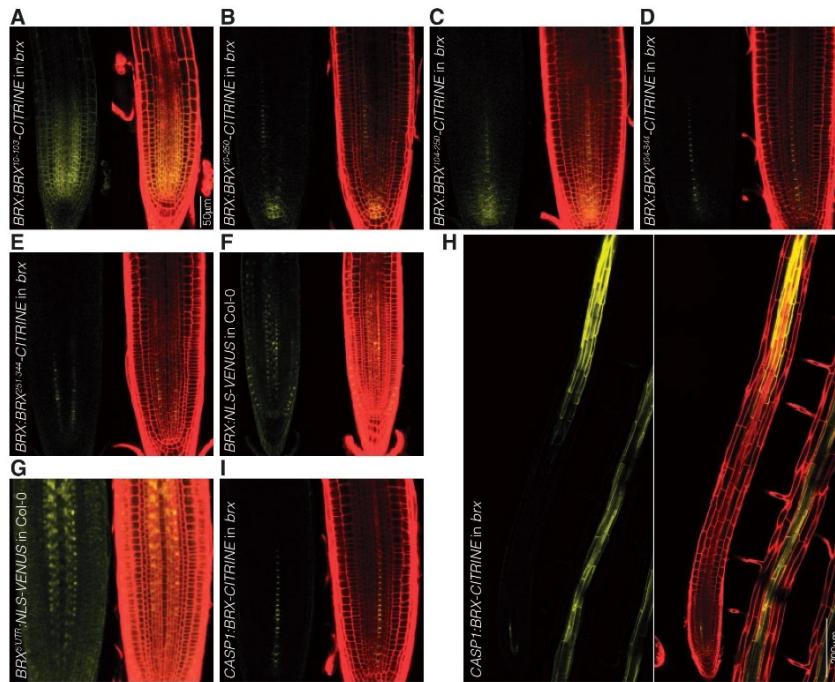


**Figure 3** The BRX transcript sequence confers expression in the root protophloem. A–E, Confocal microscopy images of BRX protein fragments fused with CITRINE tags (yellow fluorescence, left), expressed under the control of the BRX promoter in the *brx* mutant background. (Right) Overlay with PI cell wall staining (red fluorescence). Superscripts indicate the amino acid fragments. Note that all fragments were preceded by amino acids 1–9. F and G, Confocal microscopy images of NLS–VENUS fusion protein expressed in Col-0 under the control of the full-length BRX promoter (F) or the 5'-UTR only (G). H and I, Confocal microscopy images of full-length BRX–CITRINE fusion protein expressed in *brx* under the control of the CASP1 promoter, illustrating expression in the late endodermis (H) but also the protophloem (I).

BRX coding sequence under the control of ectopic promoters, such as the late endodermis-specific CASPARIAN STRIP MEMBRANE DOMAIN PROTEIN1 (CASP1) promoter

(Roppolo et al, 2011), fully rescued the *brx* root phenotype (Supplemental Figure S5, A and B) and conferred BRX–CITRINE expression in PPSEs, outside the CASP1 domain (Figure 3, H

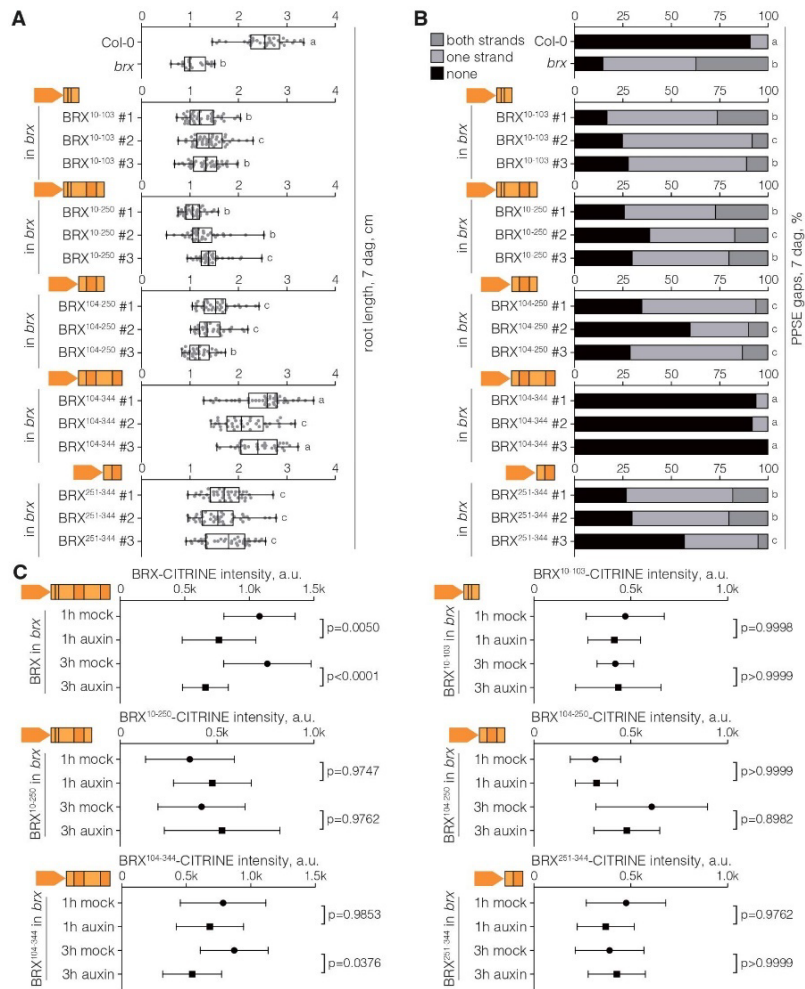


**Figure 4** The tandem BRX domains are necessary and sufficient for BRX function in the protophloem. **A**, Root length of Col-0, *brx*, and plants harboring the indicated transgenic BRX fragments (three representative independent lines,  $n = 20\text{--}45$  roots). Superscripts indicate the amino acid fragments. Note that all fragments were preceded by amino acids 1–9 and fused to C-terminal CITRINE tags. Box plots display second and third quartiles and the median, bars indicate maximum and minimum. Statistical significance was determined by ordinary one-way ANOVA. **B**, PPSE strand defects in roots of the indicated genotypes ( $n = 15\text{--}24$ ), corresponding to (A). Statistical significance was determined by Fisher's exact test. **C**, Quantification of the indicated CITRINE fusion protein signal intensity at the rootward plasma membrane of developing PPSEs, 1 or 3 h after mock or auxin treatment ( $n = 10\text{--}23$  roots, average of 12–15 cells per root). Plot circles and squares display the mean, error bars indicate standard deviation. Statistical significance was determined by ordinary one-way ANOVA. Statistically significant different groups are indicated by different lowercase letters.

and I). Collectively, these observations suggest that the coding region encompassing the BRX domains is a major determinant for the PPSE-specific BRX expression pattern.

At the level of biological function, the BRX<sup>104–344</sup> fragment was also the only one that nearly perfectly normalized both the root growth and protophloem differentiation defects of

*brx* mutants (Figure 4, A and B). Moreover, it was also the only fragment whose plasma membrane association displayed a statistically significant response to auxin treatment (Figure 4C). In summary, our experiments suggest that, together with the short, conserved N-terminus, the fragment comprising the tandem BRX domains is sufficient to convey

the biological outputs of BRX function that are captured by our assays.

#### The linker between the BRX domains functionally differentiates BRX family proteins

Next, we sought to map the differential plasma membrane association in response to auxin in BRX and BRXL2. To this end, we created a number of hybrids between the two proteins (Supplemental Figure S6). In each case, expression of these BRX–BRXL2 hybrids as CITRINE fusion proteins under the control of the BRX promoter in the *brx* background displayed the PPSE-specific pattern observed for wild-type BRX (Figure 5, A–D). However, the hybrid proteins differed in their capacity to normalize the protophloem and root growth defects of *brx* (Figure 5, E–L). Essentially, the capacity for complementation gradually increased as the portion of BRX extended from the N-terminus, and only the hybrid that combined the BRX N-terminal fragment including the first BRX domain with the second, C-terminal BRX domain of BRXL2 (BRX<sup>HYB250/254</sup>) was able to largely (although not perfectly) rescue the hallmark *brx* phenotypes (Figure 5, H and L). Matching these observations, the hybrids with a larger portion of BRXL2 did not display a significant auxin response (Figure 6, A–C), whereas the BRX<sup>HYB250/254</sup> hybrid was as auxin-responsive as wild-type BRX (Figure 6D). These results suggest that the sequence determinants for the auxin-responsive plasma membrane dissociation of BRX reside between amino acids 138 and 250, that is within, or close to, the first of the two BRX domains.

Sequence alignment pointed toward a potential role for the linker between the tandem BRX domains, because it is clearly different between BRX and BRXL1 on the one side and BRXL2–BRXL4 on the other (Supplemental Figure S1A; Figure 7A). Interestingly, the portion of the BRX linker that was present in BRX<sup>HYB250/254</sup>, encompassing amino acids 197–250, contained two R(D/E)S motifs that are also conserved in BRXL1 but absent from other BRX family proteins (Supplemental Figure S1A). These motifs, as well as another BRX/BRXL1-specific RES site before the first BRX domain (Figure 7A), could constitute potential target sites for AGC kinases such as D6 PROTEIN KINASE (D6PK) or PAX (Huang et al., 2010; Zourelidou et al., 2014). Indeed, in replicate in vitro kinase assays with recombinant GST–BRX fusion protein and phosphosite-mutant variants including S (serine) to A (alanine) substitutions of the pertinent serines 123, 217, and 228, the S228A mutation led to the strongest reduction in BRX phosphorylation by D6PK as well as by PAX compared to BRX wild-type protein phosphorylation (Figure 7, B and C). Finally, in phospho-proteomics replicates of BRX–CITRINE fusion protein that was immuno-purified from VISUAL assays (Kondo et al., 2016; Marhava et al., 2018), S228 was identified as a high confidence in vivo phosphosite (Figure 7A). In contrast, these data did not provide evidence for phosphorylation on S123, and S217 was not covered in these analyses. Although the intersection of our various assays points to a key role for the S228 phosphosite,

at this point, we cannot exclude the possibility that the other phosphosites do not at least contribute to the response. Nevertheless, together, these experiments suggest that the linker between the tandem BRX domains, which includes S228, has a crucial function in the differential activity of BRX and BRXL2 and that phosphosites targeted by PAX or D6PK might have a role in this differentiation.

#### Engineered phosphosites are sufficient to impart an auxin response to a BRX family protein

To assess the functional significance of these findings *in planta*, we investigated a BRX variant in which the three serines in the potential D6PK/PAX R(D/E)S target sites (S123, S217, and S228) were substituted by alanines (BRX<sup>3PKCO</sup>) (Supplemental Figure S7). Expression and localization of BRX<sup>3PKCO</sup>–CITRINE fusion protein appeared normal (Supplemental Figure S8A) and largely rescued the protophloem and root growth phenotypes of *brx* (Figure 8A). However, compared to the rescue obtained with wild-type BRX (Figure 8B), the rescue was never perfect. Even in the best-complemented lines, some level of PPSE defect persisted, and root growth rescue was highly variable (Figure 8, C and D). Most importantly, plasma membrane-associated BRX<sup>3PKCO</sup> no longer displayed a significant auxin response (Figure 8, E and F), but BRX<sup>3PKCO</sup> was still about as efficient as wild-type BRX in inhibiting D6PK-stimulated auxin efflux in *Xenopus laevis* oocyte assays (Supplemental Figure S8B). Together, these data suggest that PAX- and D6PK-targeted phosphosites contribute to the fine-tuning of BRX function and modulate its auxin-responsiveness.

To independently verify this finding, we investigated a BRX homolog from a descendant of the most ancient vascular plant lineage, the lycophyte *Selaginella moellendorffii*. As far as we could determine, the *S. moellendorffii* genome (Banks et al., 2011) contains a single BRX homolog (*SmBRX*). The encoded protein already possesses all the highly conserved domains found in *A. thaliana* BRX family proteins, but the linker between the two BRX domains is by comparison very short and does not contain any putative D6PK or PAX target phosphosites (Figure 9A). Expression of an *A. thaliana* codon-optimized version of *SmBRX* as a CITRINE fusion under the control of the BRX promoter in the *brx* background recapitulated the *A. thaliana* BRX PPSE-specific expression pattern and protein localization (Supplemental Figure S8C). However, similar to BRX<sup>3PKCO</sup>, *SmBRX* did not fully rescue the *brx* mutant phenotypes (Figure 9, B and C), corroborating the importance of the linker and phosphosites for BRX function. Finally, as would be predicted from our previous observations, *SmBRX* protein was also not significantly auxin-responsive (Figure 9, D and E).

Because the lack of auxin-responsive plasma membrane dissociation was pinpointed as one of the factors that differentiate BRXL2 from BRX (Marhava et al., 2020), we modified BRXL2 by adding three putative D6PK/PAX target phosphosites at the positions corresponding to S123, S217, and S228 in BRX (BRXL2<sup>3PADDD</sup>) (Supplemental Figure S7). This

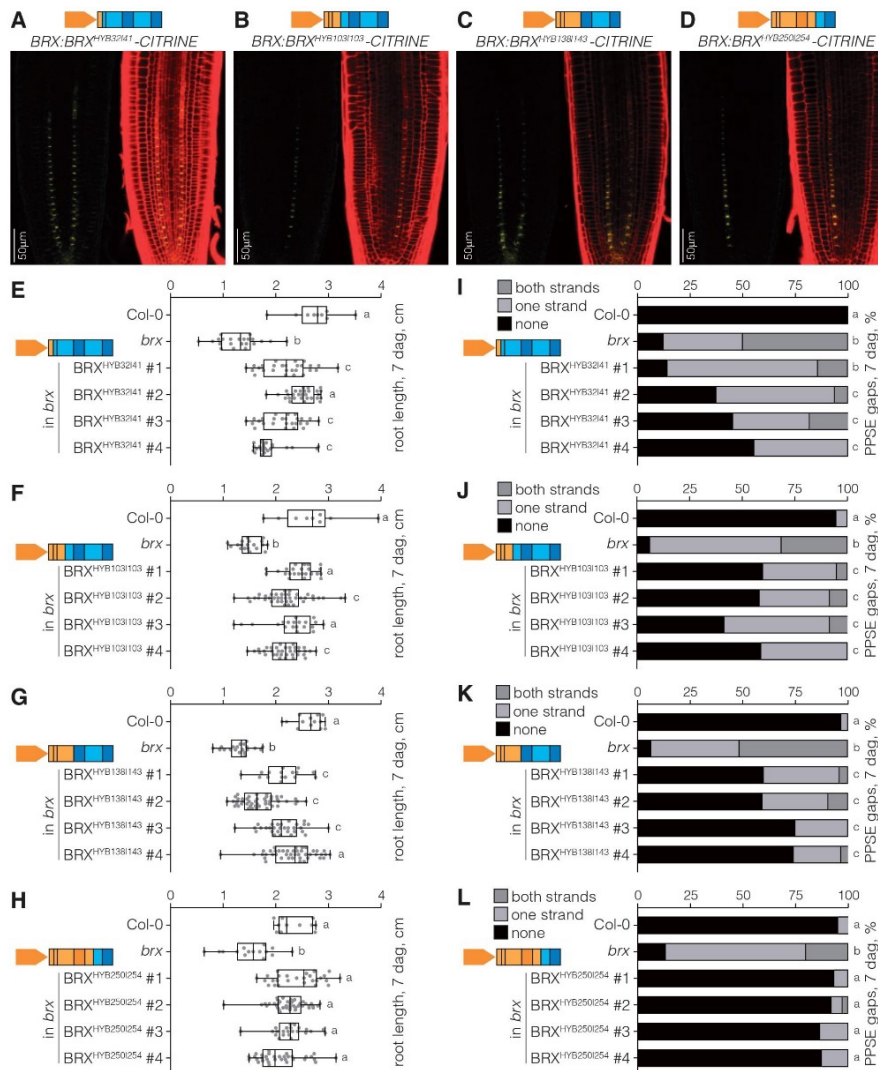


**Figure 5** Differential activity of BRX versus BRXL2 resides in the tandem BRX domains. A–D, Confocal microscopy images of BRX–BRXL2 hybrid fusion proteins, tagged with CITRINE and expressed under the control of the *BRX* promoter in the *brx* mutant background (yellow fluorescence, left). Right: overlay with PI cell wall staining (red fluorescence). Superscripts indicate the last amino acid in the BRX portion and the first amino acid in the BRXL2 portion. E–H, Root length of Col-0, *brx*, and the indicated transgenic lines corresponding to (A–D) (four representative independent lines,  $n = 10$ –48 roots). Box plots display second and third quartiles and the median, bars indicate maximum and minimum. Statistical significance was determined by ordinary one-way ANOVA. I–L, PPSE strand defects in the roots of the indicated genotypes, corresponding to (E–H) ( $n = 15$ –38 roots). Statistical significance was determined by Fisher's exact test. Statistically significant different groups are indicated by different lowercase letters.

BRXL2<sup>3PADD</sup>-CITRINE fusion protein displayed PPSE-specific expression and polar, rootward plasma membrane association when expressed under the control of the *BRX* promoter in the *brx* background (Supplemental Figure S8D).

Moreover, this fusion protein partially rescued the proto-phloem and root growth defects of *brx* (Figure 10, A and B), and this rescue appeared to be substantially better than the partial rescue observed with BRXL2 wild-type protein

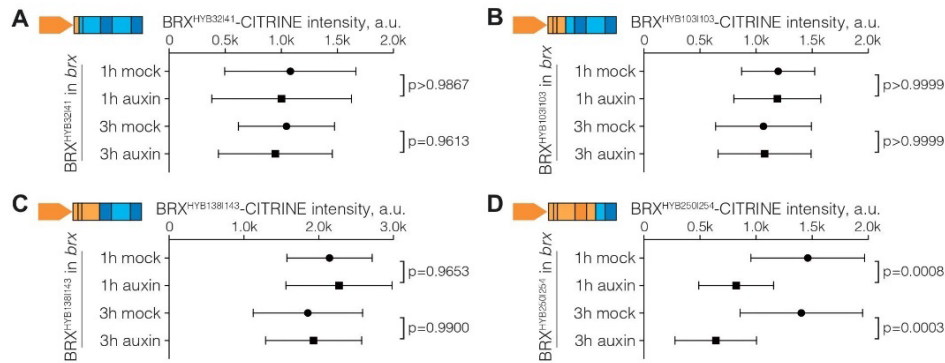


**Figure 6** Mapping of the BRX auxin response using BRX–BRXL2 hybrid fusion proteins. A–D, Quantification of the indicated BRX–BRXL2 hybrid CITRINE fusion protein signal intensity at the rootward plasma membrane of developing PPSEs, 1 or 3 h after mock or auxin treatment ( $n = 10$ –18 roots, average of 12–15 cells per root). Plot circles and squares display the mean, error bars indicate standard deviation. Statistical significance was determined by ordinary one-way ANOVA.

(Marhava et al., 2020). Indeed, in direct comparisons, *brx* rescue was consistently more efficient with BRXL2<sup>3PADDD</sup> than with BRXL2 wild-type protein (Figure 10, C and D). Finally, and most strikingly, unlike BRXL2 wild-type protein (Figure 10E), the plasma membrane association of BRXL2<sup>3PADDD</sup> was sensitive to auxin treatment (Figure 10, F and G), at about the same magnitude as BRX (Figure 8E). These observations suggest that the addition of the three putative D6PK/PAX phosphosites is sufficient to impart an auxin response on BRXL2 and thereby increase its biological activity in the context of protophloem development.

## Discussion

Recent work established that during protophloem development, BRX primarily acts as a switch element in conjunction with PAX to fine-tune auxin flux through developing PPSE strands (Marhava et al., 2018, 2020). In this study, we mapped functionally important regions of BRX and found that the plasma membrane-associated tandem BRX domains and their linker are sufficient to convey BRX action in the protophloem. This linker includes critical phosphosites that mediate the BRX auxin response and can impart this response on a modified BRXL2 protein. The modified, auxin-responsive BRXL2 displays increased functionality in PPSE development, where native, auxin-insensitive BRXL2 can only partially replace BRX (Briggs et al., 2006; Beuchat et al., 2010; Marhava et al., 2020). Our data thus suggest that among the *A. thaliana* BRX family proteins, BRX and its close homolog BRXL1 are uniquely suited to transmit both a PPSE-specific on-off signal through their regulated plasma membrane association and directional information through their asymmetric distribution. Only the latter part of this dual role seems to be required in the stomata context, where BRX can replace BRXL2 (Rowe et al., 2019). Our results also reiterate that auxin-responsive plasma

membrane dissociation is one of the features that quantitatively determine BRX activity in the protophloem context.

## Intragenic BRX sequences contribute to its root protophloem-specific expression

An unexpected finding in our study was that the plasma membrane-associated tandem BRX domains and their linker are not only sufficient to convey BRX protein function in the root protophloem, but apparently also confer its highly PPSE-specific expression. Such contribution of intragenic sequences to gene expression patterns has been reported repeatedly (Sieburth and Meyerowitz, 1997; Cattaneo et al., 2019) and reiterates the finding that reporters of promoter activity do not always capture the exact expression domain. Notably, in the case of BRX, the genuine expression pattern has been verified by anti-BRX immunostaining (Marhava et al., 2018). Thus, it appears that the BRX promoter and intragenic sequences have co-evolved to synergistically confer highly PPSE-specific expression in the root meristem. The finding that BRXL1 can only fully substitute for BRX when expressed under the control of the *BRX* promoter supports this idea. Future comparative studies between *BRX* family genes as well as codon-optimized *BRX* versions might be able to pinpoint the key regulatory sequences and determine their relative contributions. In summary, our results suggest that the tandem BRX domains constitute a module that is intimately associated with protophloem differentiation on several regulatory levels.

## BRX acts primarily at the plasma membrane

Interestingly, it has been demonstrated that mutation of cysteines 4 and 7 compromises the plasma membrane association of BRX and its function in stomata (Rowe et al., 2019). It was thus suggested that the BRX N-terminus could be reversibly palmitoylated, and that the auxin-induced plasma membrane dissociation of BRX might involve

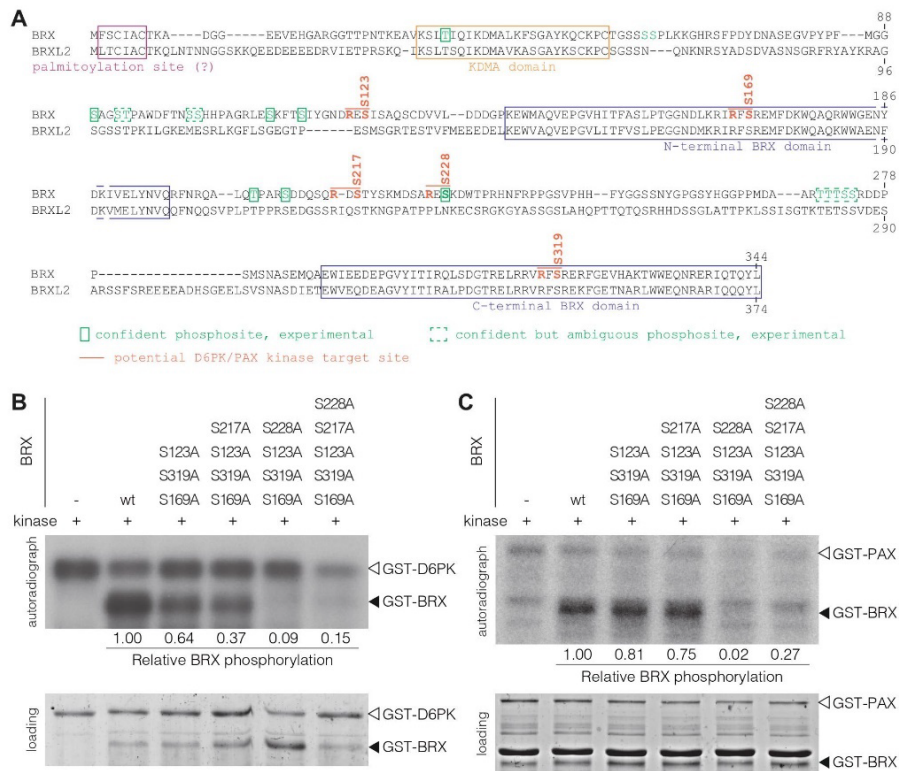


**Figure 7** D6PK/PAX phosphosites in BRX. **A**, Amino acid sequence alignment of BRX and BRXL2, highlighting key features and phosphosites identified by proteomics in BRX. The R(D/E)S D6PK/PAX target site motifs present in BRX and BRXL1, but not in BRXL2–BRXL4, are highlighted. **B** and **C**, Representative results of *in vitro* kinase assays with bacterially expressed GST fusions of BRX wild-type protein and point mutant variants with the indicated (multiplexed) serine to alanine substitutions as the substrate, and a GST fusion of D6PK (**B**) or PAX (**C**) as the kinase. Substitutions of S123, S169, S217, S228, and S319 are in hypothetical D6PK/PAX target sites where the phosphosite serine is preceded by a variable residue and an arginine. The relative phosphorylation strength (as determined by density measurements) is specified below the autoradiograph. Please note that identical amounts of BRX were loaded in the PAX and D6PK reactions but that, in the PAX reactions, BRX loading is covered by a GST-PAX degradation product.

de-palmitoylation. Yet, the addition of myristoylation signals neither affected the intracellular polarity (Rowe et al., 2019) nor auxin-response of BRX. Because myristoylation is an irreversible post-translational modification, BRX internalization could reflect proteolytic removal of the N-terminus. Alternatively, the turnover of plasma membrane-localized BRX might involve clathrin-mediated endocytosis (Scacchi et al., 2009; Santuari et al., 2011), for which the rootward plasma membrane domain of PPSEs is a hotspot (Dettmer et al., 2014; Marhava et al., 2020).

BRX is an auxin-responsive plasma membrane-localized regulator of protophloem development. Our domain analyses suggest that the plasma membrane-associated tandem BRX domains (amino acids 1–9 plus 139–344) are sufficient to convey the biological functions of BRX that are captured in our phenotypic assays. Substantial but still partial rescue

of *brx* by the tandem BRX domains has been reported before (Scacchi et al., 2009). However, in those experiments, the fragment was constitutively over-expressed under the control of the 35S cauliflower mosaic virus promoter, and the BRX N-terminal amino acids 1–9 added in this study were missing. Because the (ectopically) over-expressed fragment showed relatively little plasma membrane association and, instead, was mostly found in the nucleus, this was taken as evidence that BRX has a function in the nucleus. This notion was supported by the observation that BRX could interact with transcription factors (Scacchi et al., 2009; 2010), accumulated in the nucleus when transiently expressed in onion (*Allium cepa*) epidermal cells, and stimulated transcription in yeast (Mouchel et al., 2004). Our findings are not in conflict with these earlier observations, but they diminish the functional importance of the nuclear

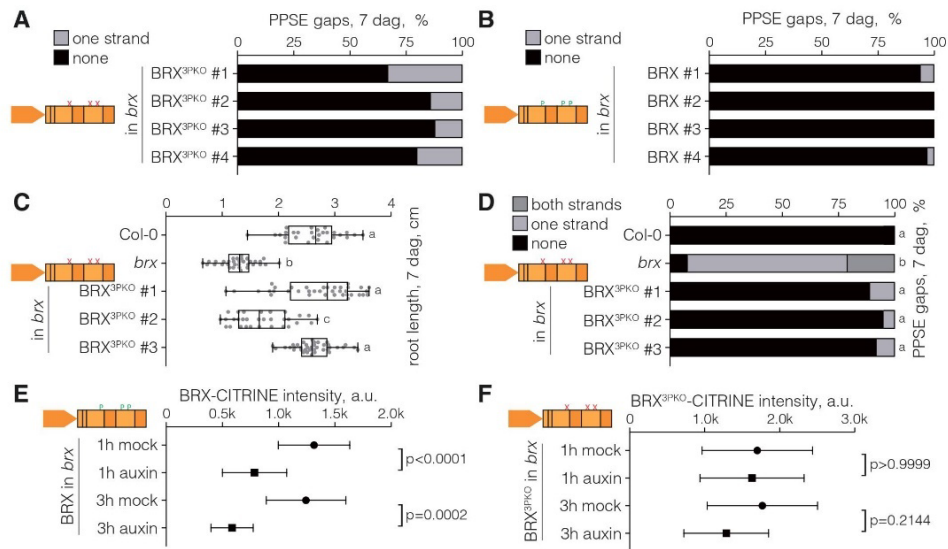


**Figure 8** Amino acid substitutions in putative PAX phosphosites diminish BRX activity. A and B, PPSE strand defects in the roots of the indicated genotypes (four representative independent lines,  $n = 13\text{--}20$  roots). BRX<sup>3PKO</sup> (B) carries three alanine substitutions for serines 123, 217, and 228. C, Root length of Col-0, *brx*, and three “best” BRX<sup>3PKO</sup> independent transgenic lines ( $n = 28\text{--}38$  roots). Box plots display second and third quartiles and the median, bars indicate maximum and minimum. Statistical significance was determined by ordinary one-way ANOVA. D, PPSE strand defects in the roots of the indicated genotypes, corresponding to the samples scored in (C) ( $n = 37\text{--}42$  roots). Statistical significance was determined by Fisher’s exact test. E and F, Quantification of the indicated CITRINE fusion protein signal intensity at the rootward plasma membrane of developing PPSEs, 1 or 3 h after mock or auxin treatment ( $n = 15\text{--}20$  roots, average of 12–15 cells per root). Plot circles and squares display the mean, error bars indicate standard deviation. Statistical significance was determined by ordinary one-way ANOVA. Statistically significant different groups are indicated by different lowercase letters.

localization of BRX with regard to its known phloem functions. We found that BRX variants expressed in the root protophloem in the native context always display substantial plasma membrane association and are barely visible in the nucleus, even when explicitly targeted to the nucleus. Such variants are also still able to rescue the *brx* root growth and protophloem phenotypes. Our findings, therefore, suggest that, for now, no biological role can be firmly associated with the nuclear localization of BRX and that its previously proposed central function as a transcriptional regulator (Mouchel et al., 2004; Scacchi et al., 2009) has to be revised. Our data also resonate with the role of BRX in stomata formation, which requires the plasma membrane association of BRX, but not its nuclear localization (Rowe et al., 2019).

#### Phosphosites in the linker contribute to the functional divergence of BRX family proteins

Besides the possible role of post-translational modifications, the plasma membrane association of BRX in the protophloem largely depends on PAX, presumably by a direct protein–protein interaction (Marhava et al., 2018, 2020). Interestingly, the plasma membrane association of PAX is not sensitive to auxin, but auxin stimulates its kinase activity (Marhava et al., 2018). The latter may be conferred by recently identified, functionally

redundant upstream regulators of D6PK and PAX, the 3-PHOSPHOINOSITIDE-DEPENDENT PROTEIN KINASES (PDK1) and PDK2 (Zegzouti et al., 2006; Tan et al., 2020; Xiao and Offringa, 2020). It is, therefore, tempting to speculate that BRX turnover and dissociation from the plasma membrane are modulated by PAX-mediated phosphorylation. PAX activation by auxin and, therefore, the stimulation of PIN-mediated auxin efflux would thus be amplified by simultaneous removal of the PAX inhibitor BRX. A direct test of this conceptually attractive model through experimental means is unfortunately currently out of reach. Yet, our striking observation that engineering of putative D6PK/PAX target phosphosites into BRXL2, which can also interact with PAX (Marhava et al., 2020), renders the modified protein auxin-responsive supports this model. The finding that this modification also augments the activity of BRXL2 in the context of root protophloem development, whereas, conversely, loss of the corresponding phosphosites diminishes the auxin response and activity of BRX, further corroborates the quantifiable contribution of the auxin-induced plasma membrane dissociation of BRX to integrated PPSE differentiation and the rheostat model (Marhava et al., 2018).

Finally, our results also suggest that the functional divergence within the BRX protein family resides mainly in the linker between the tandem BRX domains. The tandem



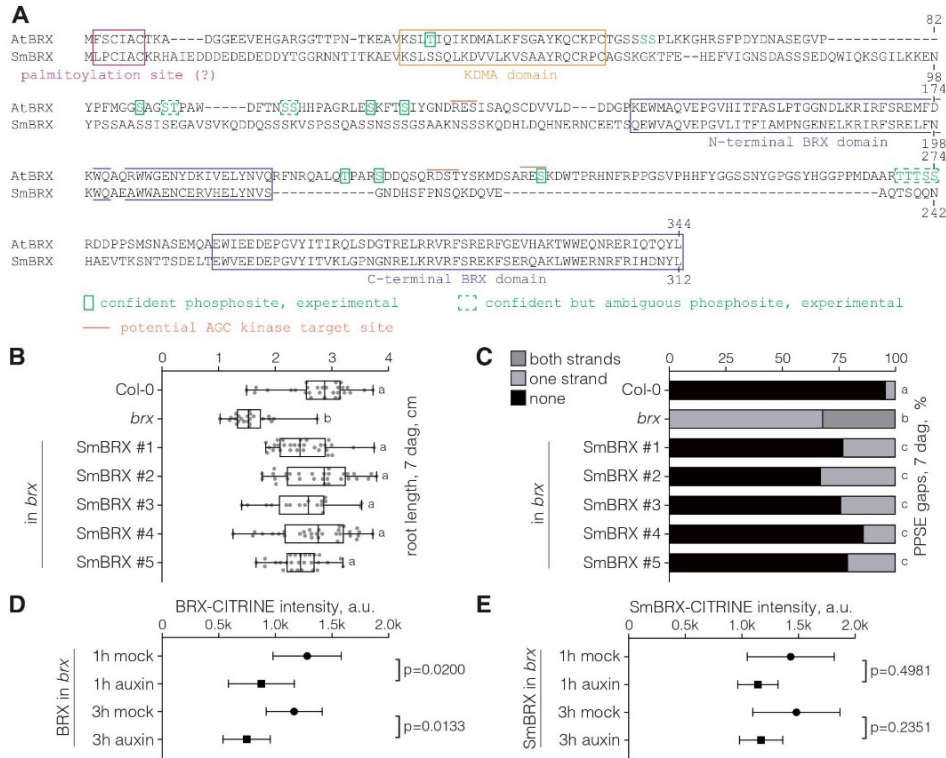


**Figure 9** Partial rescue of the *brx* phenotype by a *S. moellendorffii* BRX homolog. **A**, Amino acid sequence alignment of *A. thaliana* (AtBRX) and *S. moellendorffii* (SmBRX) BRX protein homologs, highlighting key features. **B**, Root length of Col-0, *brx*, and transgenic lines expressing *A. thaliana* codon-optimized SmBRX–CITRINE fusion protein (five representative independent lines,  $n = 17$ –31 roots). Box plots display second and third quartiles and the median, bars indicate maximum and minimum. Statistical significance was determined by ordinary one-way ANOVA. **C**, PPSE strand defects in the roots of the indicated genotypes, corresponding to (B) ( $n = 34$ –106 roots). Statistical significance was determined by Fisher's exact test. **D** and **E**, Quantification of the indicated CITRINE fusion protein signal intensity at the rootward plasma membrane of developing PPSEs, 1 or 3 h after mock or auxin treatment ( $n = 10$ –16 roots, average of 12–15 cells per root). Plot circles and squares display the mean, error bars indicate standard deviation. Statistical significance was determined by ordinary one-way ANOVA. Statistically significant different groups are indicated by different lowercase letters.

arrangement is the hallmark of BRX family proteins, and although single BRX domains are found in other proteins (Briggs et al., 2006; Furutani et al., 2020), their homology does not extend into the linker. Moreover, compared to the highly conserved BRX domains, the linker region is variable both in sequence and size. Because BRX family proteins are exchangeable in the context of stomata development (Rowe et al., 2019), but not in the context of root protophloem development (Briggs et al., 2006; Beuchat et al., 2010; Marhava et al., 2020), the linker region has apparently evolved to widen the developmental spectrum of BRX family protein functions. Indeed, the SmBRX protein is the smallest of the BRX homologs we could identify (One Thousand Plant Transcriptomes, 2019) because of its very short linker domain. It will be interesting to determine whether the evolution of the linker sequence correlates with the evolution of

PPSEs. Comprehensive testing of BRX homologs from various plant lineages for their functionality in *A. thaliana* could help to answer this question.

## Methods

### Plant material and growth conditions

The *A. thaliana* accession Columbia-0 (Col-0) was the wild-type background for all lines used or produced in this study. Transgenes were assayed in the Col-0 or *brx-2* mutant (Rodríguez et al., 2009) background. The *brx brx1 brx2 brx3* quadruple mutant has been described before (Briggs et al., 2006; Rowe et al., 2019). The two independent AT2G21030 mutant alleles were created in Col-0 via CRISPR/Cas9 gene editing as described (Fausser et al., 2014; Graeff et al., 2020), using guide RNA 5'-GCC GAG AGA UGU ACA

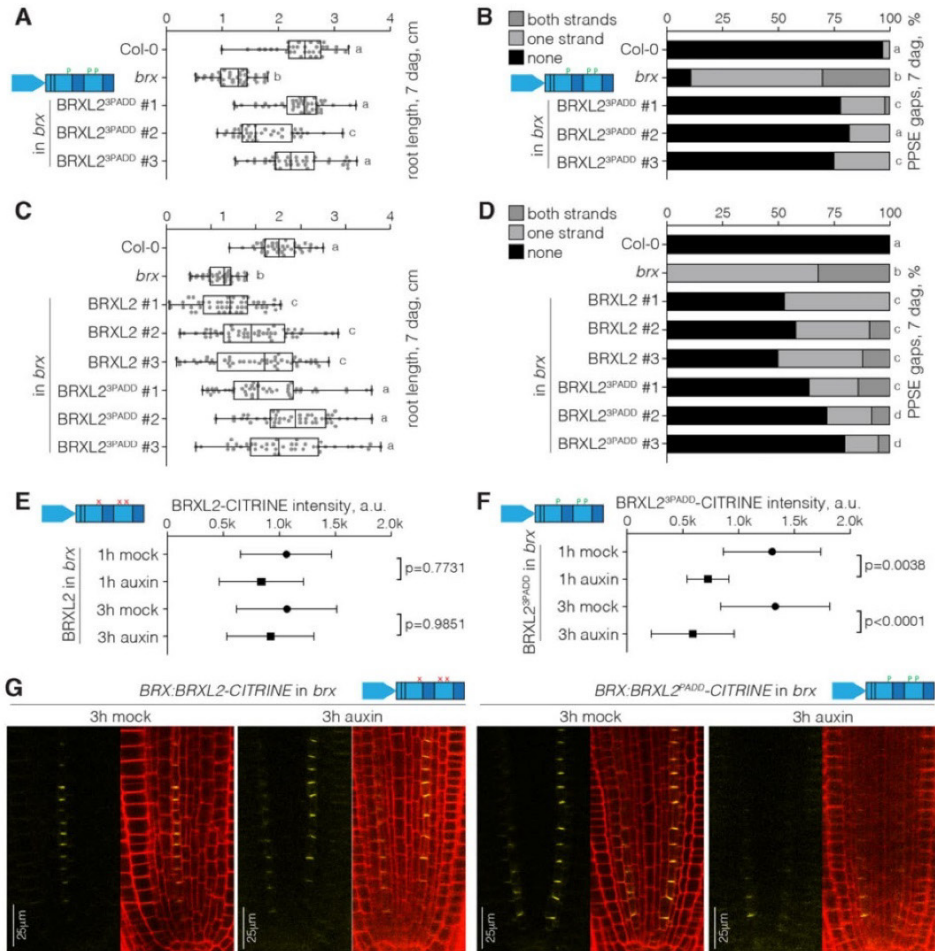


**Figure 10** Engineering of PAX phosphosites renders BRXL2 auxin-responsive. **A**, Root length of Col-0, *brx*, and transgenic lines expressing a modified BRXL2<sup>3PADD</sup>-CITRINE fusion protein (three representative independent lines,  $n = 33-44$  roots). BRXL2<sup>3PADD</sup> carries nine amino acid substitutions that introduce PAX target phosphosites (see Supplemental Figure S7). Box plots display second and third quartiles and the median, bars indicate maximum and minimum. Statistical significance was determined by ordinary one-way ANOVA. **B**, PPSE strand defects in the roots of the indicated genotypes, corresponding to (A) ( $n = 33-44$  roots). Statistical significance was determined by Fisher's exact test. **C**, Root length of Col-0, *brx*, and transgenic lines expressing either BRXL2-CITRINE or the modified BRXL2<sup>3PADD</sup>-CITRINE fusion protein (three "best" independent lines each, scored in parallel,  $n = 39-48$  roots). Box plots display second and third quartiles and the median, bars indicate maximum and minimum. Statistical significance was determined by ordinary one-way ANOVA. **D**, PPSE strand defects in the roots of the indicated genotypes, corresponding to (C) ( $n = 39-48$  roots). Statistical significance was determined by Fisher's exact test. **E** and **F**, Quantification of the indicated CITRINE fusion protein signal intensity at the rootward plasma membrane of developing PPSEs, 1 or 3 h after mock or auxin treatment ( $n = 15-30$  roots, average of 12-15 cells per root). Plot circles and squares display the mean, error bars indicate standard deviation. Statistical significance was determined by ordinary one-way ANOVA. **G**, Confocal microscopy images of BRXL2-CITRINE or BRXL2<sup>3PADD</sup>-CITRINE fusion protein expressed under the control of the *BRX* promoter in the *brx* mutant background (yellow fluorescence, left), illustrating auxin-induced plasma membrane dissociation of BRXL2<sup>3PADD</sup>-CITRINE. (Right) overlay with PI cell wall staining (red fluorescence). Statistically significant different groups are indicated by different lowercase letters.

AUA AG-3'. For phenotyping assays, seeds were surface sterilized and then stratified for 2 days in the dark at  $\sim 4^{\circ}\text{C}$  before germination and growth in continuous white light of  $\sim 140\ \mu\text{E}$  intensity at  $\sim 22^{\circ}\text{C}$  on vertically placed Petri dishes that contained  $0.5 \times$  Murashige and Skoog (MS) medium supplemented with 1% agar and 0.3% sucrose.

### Generation of transgenic lines

Transgenic constructs for plant transformation were created in suitable binary vectors and produced using standard molecular biology procedures and/or the Gateway<sup>TM</sup> cloning technology. The translational *BRX:BRX-CITRINE* and *BRX:BRXL2-CITRINE* fusions have been described before (Rodriguez-Villalon et al., 2014; Marhava et al., 2020). Similar constructs were created with *BRX* (AT1G31880) or *BRXL2* (AT3G14000) variants and *SmBRX* (SELMODRAFT\_229072), all of which was obtained by gene synthesis (GeneArt<sup>TM</sup>) (Supplemental File S1). *SmBRX* was *A. thaliana* codon-optimized. The *CASP1* promoter has been previously described (Roppolo et al., 2011). For the genomic *BRXL1* (AT2G35600) and *BRXL2* constructs, the *BRXL1* promoter (4,061 bp upstream of the start codon) and *BRXL2* promoter (2,616 bp upstream of the start codon) were amplified and cloned into pDONR P4P1R. Genomic fragments of the *BRXL1* and *BRXL2* transcript regions without the stop codons were amplified and cloned from genomic DNA template. Partial *BRX* fragments were amplified with suitable oligonucleotides (Supplemental Table S1) and cloned using standard procedures. *BRX-BRXL2* hybrids were obtained by gene synthesis (GeneArt<sup>TM</sup>) (Supplemental File S1). Genes were cloned into pDONR 221. These entry clones were combined together with *CITRINE* in pDONR P2RP3 into the destination vector pH7m34CW by the multisite Gateway recombination system. For the AT2G21030 promoter, the 551 bp upstream of the ATG codon were cloned in front of an NLS-3XVENUS reporter gene as described (Marhava et al., 2018). The binary constructs were introduced into *Agrobacterium tumefaciens* strain GV3101pMP90 and transformed using the floral dip method.

### Phenotyping

For root length measurements, plates were scanned and seedling root length was determined using Fiji software. For quantification of gap cells, root PPSEs were checked and counted by confocal microscopy (see below). Typically, 20–40 (length) and 15–20 (gap cells) roots were investigated for each genotype and/or treatment.

### Auxin treatments

Five- to six-day-old seedlings were transferred onto liquid MS medium with or without  $10\ \mu\text{M}$  1-naphthyl-acetic acid pre-dissolved in dimethyl sulfoxide (DMSO) and kept in continuous white light of  $\sim 140\ \mu\text{E}$  intensity at  $\sim 22^{\circ}\text{C}$ . Seedlings were removed for analysis at the indicated timepoints.

### Confocal imaging and image analysis

For confocal microscopy images, a Zeiss LSM 700 confocal scanning microscope was used with the following fluorescence excitation–emission settings to visualize reporter genes and staining signals: *CITRINE* excitation 514 nm, emission 529 nm; *VENUS* excitation 515 nm, emission 528 nm; propidium iodide (PI) excitation 536 nm, emission 617 nm. Pictures were taken with  $20\times$  or  $40\times$  water/oil immersion objectives. Samples within one experiment were imaged with identical settings. For image analyses, ImageJ and Zeiss Zen 2011 (black edition) image analysis software were used. For signal quantifications (raw intensity without background correction), regions of interest were analyzed at the plasma membrane of developing PPSEs (typically 10–16 PPSEs per time point and treatment) in the same area of the root meristem. The average signal intensity per transgenic line was calculated as the mean of means (typically 12–20 roots per time point and treatment).

### VISUAL assay and phosphoproteomics

The VISUAL assay was performed with *BRX:BRX-CITRINE* expressed in *brx* as described (Kondo et al., 2016; Marhava et al., 2018). Immuno-precipitated *BRX-CITRINE* samples were run on sodium dodecyl (lauryl) sulfate-polyacrylamide gel electrophoresis, and bands covering the *BRX-CITRINE* size range were cut out. Samples were prepared by semi-trypsin (two replicates) or semi-chymotrypsin (one replicate) digest for subsequent analysis by tandem mass spectrometry as described (Marhava et al., 2018).

### In vitro kinase phosphorylation assays

Kinase assays with bacterially expressed D6PK, PAX, and *BRX-GST* fusion proteins were performed as described (Marhava et al., 2018). *BRX* point mutants were created by site-directed mutagenesis using standard procedures (Zourelidou et al., 2014).

### Oocyte experiments

Auxin transport assays in *X. laevis* oocytes were performed as described (Marhava et al., 2018).

### Quantification and statistical analysis

Statistical analyses were performed in Graphpad Prism software version 8.4.3. ANOVA and T-test results are provided in Supplemental File S2.

### Sequence alignments

Sequence alignments were performed in SnapGene software version 5.1.3.

### Accession numbers

Sequence data from this article can be found in the GenBank/EMBL libraries under the following accession numbers: *BRX* (AT1G31880), *BRXL1* (AT2G35600), *BRXL2* (AT3G14000), AT2G21030, and *SmBRX* (SELMODRAFT\_229072).

## Acknowledgments

We would like to thank Prof. Thomas Berleth for helpful comments on the manuscript, and Ms. Amelia Amiguet-Vercher and Ms. Floriana Misceo for technical assistance.

## Funding

This work was funded by Swiss National Science Foundation grant 310030B\_185379 (awarded to C.S.H.), and by the Deutsche Forschungsgemeinschaft SCHW751/12-2 (awarded to C.S.) and HA3468/6-1 (awarded to U.Z.H.).

*Conflict of interest statement.* None declared.

## Supplemental data

The following materials are available in the online version of this article.

**Supplemental Figure S1.** Amino acid sequence alignment of *A. thaliana* BRX family proteins.

**Supplemental Figure S2.** Limited redundancy between BRX family genes in the root protophloem.

**Supplemental Figure S3.** Amino acid sequence alignment illustrating amino acid substitutions or additions to test putative functional features of BRX protein.

**Supplemental Figure S4.** Robust plasma membrane association of BRX variants.

**Supplemental Figure S5.** Ectopic expression of BRX-CITRINE fusion protein rescues the *brx* mutant.

**Supplemental Figure S6.** Schematic overview of the BRX-BRXL2 hybrid proteins tested in this study.

**Supplemental Figure S7.** Amino acid sequence alignment illustrating amino acid substitutions or additions to test the impact of putative D6PK/PAX target phosphosites on BRX and BRXL2 function in the root protophloem.

**Supplemental Figure S8.** Impact of amino acid substitutions in D6PK/PAX target phosphosites.

**Supplemental Table S1.** Primers used for genotyping and cloning.

**Supplemental File S1.** Sequences of BRX and BRXL2 hybrids and variants, and *A. thaliana*-codon-optimized *SmBRX*, obtained by site-directed mutagenesis or by gene synthesis.

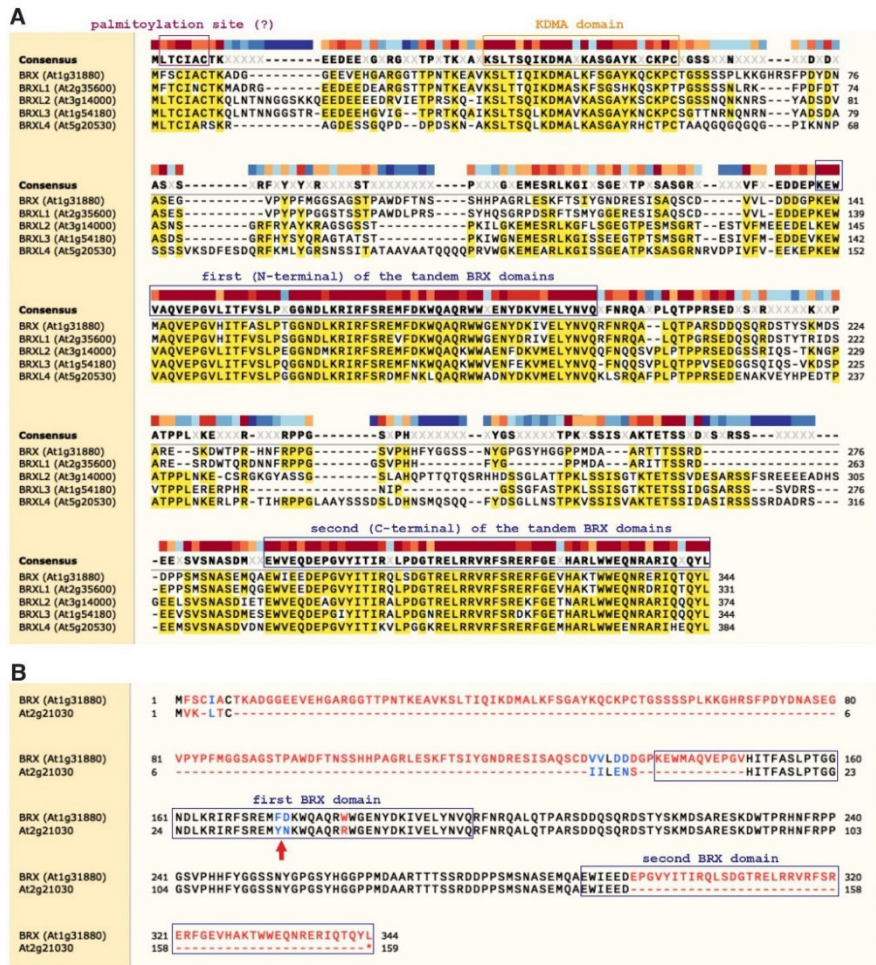
**Supplemental File S2.** ANOVA and T-test results.

## References

- Anne P, Hardtke CS (2017) Phloem function and development-biophysics meets genetics. *Curr Opin Plant Biol* **43**: 22–28
- Banks JA, Nishiyama T, Hasebe M, Bowman JL, Gribskov M, dePamphilis C, Albert VA, Aono N, Aoyama T, Ambrose BA et al. (2011) The Selaginella genome identifies genetic changes associated with the evolution of vascular plants. *Science* **332**: 960–963
- Barbosa ICR, Hammes UZ, Schwechheimer C (2018) Activation and polarity control of PIN-FORMED auxin transporters by phosphorylation. *Trends Plant Sci* **23**: 523–538
- Bauby H, Divol F, Truernit E, Grandjean O, Palauqui JC (2007) Protophloem differentiation in early *Arabidopsis thaliana* development. *Plant Cell Physiol* **48**: 97–109
- Beuchat J, Li S, Ragni I, Shindo C, Kohn MH, Hardtke CS (2010) A hyperactive quantitative trait locus allele of *Arabidopsis* BRX contributes to natural variation in root growth vigor. *Proc Natl Acad Sci USA* **107**: 8475–8480
- Bologna G, Yvon C, Duvaud S, Veuthey AL (2004) N-Terminal myristoylation predictions by ensembles of neural networks. *Proteomics* **4**: 1626–1632
- Breda AS, Hazak O, Hardtke CS (2017) Phosphosite charge rather than shootward localization determines OCTOPUS activity in root protophloem. *Proc Natl Acad Sci USA* **114**: 201703258
- Briggs GC, Mouchel CF, Hardtke CS (2006) Characterization of the plant-specific BREVIS RADIX gene family reveals limited genetic redundancy despite high sequence conservation. *Plant Physiol* **140**: 1306–1316
- Bringmann M, Bergmann DC (2017) Tissue-wide mechanical forces influence the polarity of stomatal stem cells in *Arabidopsis*. *Curr Biol* **27**: 877–883
- Cattaneo P, Graeff M, Marhava P, Hardtke CS (2019) Conditional effects of the epigenetic regulator JUMONJI 14 in *Arabidopsis* root growth. *Development* **146**: dev183905
- Dettmer J, Ursache R, Campilho A, Miyashima S, Belevich I, O'Regan S, Mullendore DL, Yadav SR, Lanz C, Beverina L, et al. (2014) CHOLINE TRANSPORTER-LIKE1 is required for sieve plate development to mediate long-distance cell-to-cell communication. *Nat Commun* **5**: 4276
- Fauser F, Schiml S, Puchta H (2014) Both CRISPR/Cas-based nucleases and nickases can be used efficiently for genome engineering in *Arabidopsis thaliana*. *Plant J* **79**: 348–359
- Furuta KM, Yadav SR, Lehesranta S, Belevich I, Miyashima S, Heo JO, Vaten A, Lindgren O, De Rybel B, Van Isterdael G et al. (2014) Plant development. *Arabidopsis* NAC45/86 direct sieve element morphogenesis culminating in enucleation. *Science* **345**: 933–937
- Furutani M, Hirano Y, Nishimura T, Nakamura M, Taniguchi M, Suzuki K, Oshida R, Kondo C, Sun S, Kato K et al. (2020) Polar recruitment of RLD by LAZY1-like protein during gravity signaling in root branch angle control. *Nat Commun* **11**: 76
- Graeff M, Rana S, Marhava P, Moret B, Hardtke CS (2020) Local and systemic effects of brassinosteroid perception in developing phloem. *Curr Biol* **30**: 1626–1638 e1623
- Grieneisen VA, Xu J, Maree AF, Hogeweg P, Scheres B (2007) Auxin transport is sufficient to generate a maximum and gradient guiding root growth. *Nature* **449**: 1008–1013
- Huang F, Zago MK, Abas L, van Marion A, Galván-Ampudia CS, Offringa R (2010) Phosphorylation of conserved PIN motifs directs *Arabidopsis* PIN1 polarity and auxin transport. *Plant Cell* **22**: 1129–1142
- Knoblauch M, Knoblauch J, Mullendore DL, Savage JA, Babst BA, Beecher SD, Dodgen AC, Jensen KH, Holbrook NM (2016) Testing the Munch hypothesis of long distance phloem transport in plants. *Elife* **5**: e15341
- Kondo Y, Nurani AM, Saito C, Ichihashi Y, Saito M, Yamazaki K, Mitsuda N, Ohme-Takagi M, Fukuda H (2016) Vascular cell induction culture system using *Arabidopsis* leaves (VISUAL) reveals the sequential differentiation of sieve element-like cells. *Plant Cell* **28**: 1250–1262
- Lucas WJ, Groover A, Lichtenberger R, Furuta K, Yadav SR, Helariutta Y, He XQ, Fukuda H, Kang J, Brady SM, et al. (2013) The plant vascular system: evolution, development and functions. *J Integr Plant Biol* **55**: 294–388
- Marhava P, Bassukas AEL, Zourelidou M, Kolb M, Moret B, Fastner A, Schulze WX, Cattaneo P, Hammes UZ, Schwechheimer C, et al. (2018) A molecular rheostat adjusts auxin flux to promote root protophloem differentiation. *Nature* **558**: 297–300
- Marhava P, Aliaga Fandino AC, Koh SWH, Jelinkova A, Kolb M, Janacek DP, Breda AS, Cattaneo P, Hammes UZ, Petrasek J, et al. (2020) Plasma membrane domain patterning and self-reinforcing polarity in *Arabidopsis*. *Dev Cell* **52**: 223–235 e225

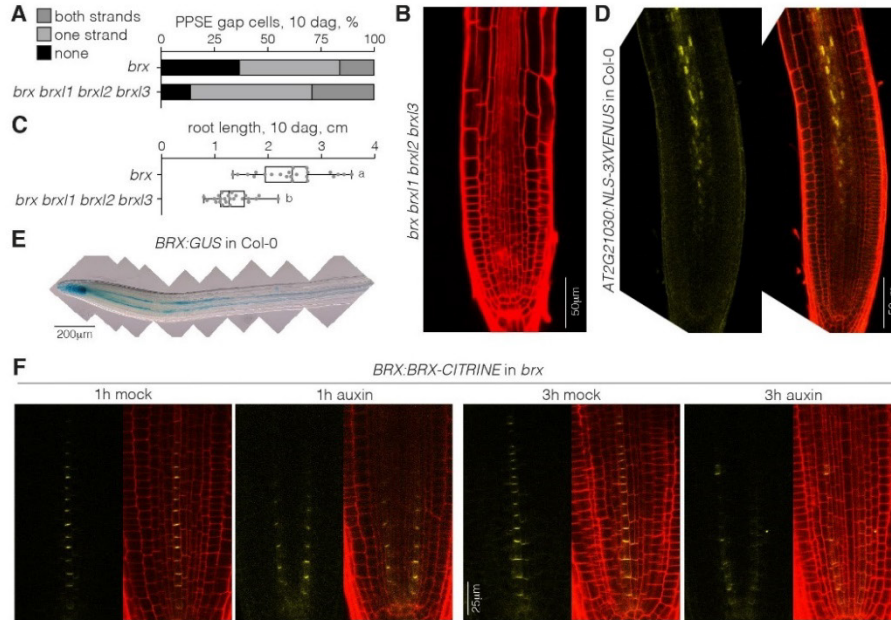
- Moret B, Marhava P, Aliaga Fandino AC, Hardtke CS, Ten Tusscher KHW** (2020) Local auxin competition explains fragmented differentiation patterns. *Nat Commun* **11**: 2965.
- Mouchel CF, Briggs GC, Hardtke CS** (2004) Natural genetic variation in *Arabidopsis* identifies BREVIS RADIX, a novel regulator of cell proliferation and elongation in the root. *Genes Dev* **18**: 700–714
- One Thousand Plant Transcriptomes Initiative** (2019) One thousand plant transcriptomes and the phylogenomics of green plants. *Nature* **574**: 679–685
- Rodrigues A, Santiago J, Rubio S, Saez A, Osmont KS, Gadea J, Hardtke CS, Rodriguez PL** (2009) The short-rooted phenotype of the brevis radix mutant partly reflects root abscisic acid hypersensitivity. *Plant Physiol* **149**: 1917–1928
- Rodriguez-Villalon A, Gujas B, Kang YH, Breda AS, Cattaneo P, Depuydt S, Hardtke CS** (2014) Molecular genetic framework for protofloeum formation. *Proc Natl Acad Sci USA* **111**: 11551–11556
- Roppolo D, De Rybel B, Denervaud Tendon V, Pfister A, Allassimone J, Vermeer JE, Yamazaki M, Stierhof YD, Beekman T, Geldner N** (2011) A novel protein family mediates Casparian strip formation in the endodermis. *Nature* **473**: 380–383
- Rowe MH, Dong J, Weimer AK, Bergmann DC** (2019) A plant-specific polarity module establishes cell fate asymmetry in the *Arabidopsis* stomatal lineage. *bioRxiv*. doi.org/10.1101/614636
- Sabatini S, Beis D, Wolkenfelt H, Murfett J, Guilfoyle T, Malamy J, Benfey P, Leyser O, Bechtold N, Weisbeek P, et al.** (1999) An auxin-dependent distal organizer of pattern and polarity in the *Arabidopsis* root. *Cell* **99**: 463–472
- Santuari L, Scacchi E, Rodriguez-Villalon A, Salinas P, Dohmann EM, Brunoud G, Vernoux T, Smith RS, Hardtke CS** (2011) Positional information by differential endocytosis splits auxin response to drive *Arabidopsis* root meristem growth. *Curr Biol* **21**: 1918–1923
- Scacchi E, Osmont KS, Beuchat J, Salinas P, Navarrete-Gomez M, Trigueros M, Ferrandiz C, Hardtke CS** (2009) Dynamic, auxin-responsive plasma membrane-to-nucleus movement of *Arabidopsis* BRX. *Development* **136**: 2059–2067
- Scacchi E, Salinas P, Gujas B, Santuari L, Krogan N, Ragni L, Berleth T, Hardtke CS** (2010) Spatio-temporal sequence of cross-regulatory events in root meristem growth. *Proc Natl Acad Sci USA* **107**: 22734–22739
- Sieburth LE, Meyerowitz EM** (1997) Molecular dissection of the AGAMOUS control region shows that cis elements for spatial regulation are located intragenically. *Plant Cell* **9**: 355–365
- Tan S, Zhang X, Kong W, Yang XL, Molnar G, Vondrakova Z, Filepova R, Petrasek J, Friml J, Xue HW** (2020) The lipid code-dependent phosphoswitch PDK1-D6PK activates PIN-mediated auxin efflux in *Arabidopsis*. *Nat Plants* **6**: 556–569
- Xiao Y, Offringa R** (2020) PDK1 regulates auxin transport and *Arabidopsis* vascular development through AGC1 kinase PAX. *Nat Plants* **6**: 544–555
- Zegzouti H, Li W, Lorenz TC, Xie M, Payne CT, Smith K, Glenny S, Payne GS, Christensen SK** (2006) Structural and functional insights into the regulation of *Arabidopsis* AGC VIIIa kinases. *J Biol Chem* **281**: 35520–35530
- Zourelidou M, Absmanner B, Weller B, Barbosa IC, Willige BC, Fastner A, Streit V, Port SA, Colcombet J, de la Fuente van Bentem S, et al.** (2014) Auxin efflux by PIN-FORMED proteins is activated by two different protein kinases, D6 PROTEIN KINASE and PINOID. *Elife* **3**: e02860

Supplemental Data. Koh et al. (2021). Mapping and engineering of auxin-induced plasma membrane dissociation in BRX family proteins. Plant Cell.



Supplemental Figure S1. Amino acid sequence alignment of *A. thaliana* BRX family proteins (Supports Figure 1). (A) Alignment of the five *bona fide* BRX family proteins, highlighting the conserved domains. (B) Alignment of BRX and the partial BRX homolog AT2G21030. The red arrowhead indicates the location of two independent CRISPR/Cas9-induced deletions. The first mutant allele carried a 4 bp deletion, leading to a frameshift after arginine 37 and the addition of 105 unrelated amino acids followed by a stop codon. The second mutant allele carried a 5 bp deletion, leading to a frameshift after tyrosine 36 and the addition of 8 unrelated amino acids followed by a stop codon. Neither of the two mutants displayed any apparent root growth or protophloem phenotype.

Supplemental Data. Koh et al. (2021). Mapping and engineering of auxin-induced plasma membrane dissociation in BRX family proteins. Plant Cell.



**Supplemental Figure S2.** Limited redundancy between *BRX* family genes in the root protophloem (Supports Figure 1). **(A)** PPSE strand defects in the roots of *brx* single and *brx brx1 brx12 brx13* quadruple mutants ( $n=23-24$  roots). dag, days after germination. **(B)** Confocal microscopy image (PI staining, red fluorescence) of a severely affected *brx brx1 brx12 brx13* quadruple mutant root meristem. **(C)** Root length of mutants, corresponding to **(A)** ( $n=23-24$  roots). Box plots display 2<sup>nd</sup> and 3<sup>rd</sup> quartiles and the median, bars indicate maximum and minimum. Statistical significance was determined by Student's t-test. **(D)** Confocal microscopy images of NLS-3XVENUS protein expressed under the control of the *AT2G21030* promoter in Col-0 (yellow fluorescence, left panel). Right panel: overlay with PI cell wall staining (red fluorescence). **(E)** Beta-glucuronidase (GUS) staining of a transgenic Col-0 root expressing GUS under the control of the *BRX* promoter. **(F)** Confocal microscopy images of BRX-CITRINE fusion protein expressed under the control of the *BRX* promoter in the *brx* mutant background (yellow fluorescence, left panels), illustrating auxin-induced plasma membrane dissociation of BRX-CITRINE. Right panels: overlay with PI cell wall staining (red fluorescence).

Supplemental Data. Koh et al. (2021). Mapping and engineering of auxin-induced plasma membrane dissociation in BRX family proteins. Plant Cell.

```

94
BRX -----MFSCLACTKADGGEEVEHARGGTTPTNKEAVKSLTIQIKDMALKFSGAYKQCKPCTGSSSSPLKKGHRSPDYDNASEGVPYPFMGGGAGSTP
BRX29k -----MMSCLACTKADGGEEVEHARGGTTPTNKEAVKSLTIQIKDMALKFSGAYKQCKPCTGSSSSPLKKGHRSPDYDNASEGVPYPFMGGGAGSTP
BRX143T MAAGAGAFSCLACTKADGGEEVEHARGGTTPTNKEAVKSLTIQIKDMALKFSGAYKQCKPCTGSSSSPLKKGHRSPDYDNASEGVPYPFMGGGAGSTP
BRX307S MGSVSLFSCCLACTKADGGEEVEHARGGTTPTNKEAVKSLTIQIKDMALKFSGAYKQCKPCTGSSSSPLKKGHRSPDYDNASEGVPYPFMGGGAGSTP
BRX259del -----MFSCLACTKADGGEEVEHARGGTTPTNKEAVKSLTIQAKDKGACKFSGAYKQCKPCTGSSSSPLKKGHRSPDYDNASEGVPYPFMGGGAGSTP
BRX259-362 -----MFSCLACTKADGGEEVEHARGGTTPTNKEAVKSLTIQKKRKKVGFSGAYKQCKPCTGSSSSPLKKGHRSPDYDNASEGVPYPFMGGGAGSTP
BRX318L -----MFSCLACTKADGGEEVEHARGGTTPTNKEAVKSLTIQIKDMALKFSGAYKQCKPCTGSSSSPLKKGHRSPDYDNASEGVPYPFMGGGAGSTP

194
BRX AWDFTNSSHHIPAGRLESKFTSIYGNDRSISAQSCDVLLDDGPKKEMAQVEPGVHIITFASLPTGGNDLKRIRFSREMPDKWQQRWGENYDKIVELYN
BRX29k AWDFTNSSHHIPAGRLESKFTSIYGNDRSISAQSCDVLLDDGPKKEMAQVEPGVHIITFASLPTGGNDLKRIRFSREMPDKWQQRWGENYDKIVELYN
BRX143T AWDFTNSSHHIPAGRLESKFTSIYGNDRSISAQSCDVLLDDGPKKEMAQVEPGVHIITFASLPTGGNDLKRIRFSREMPDKWQQRWGENYDKIVELYN
BRX307S AWDFTNSSHHIPAGRLESKFTSIYGNDRSISAQSCDVLLDDGPKKEMAQVEPGVHIITFASLPTGGNDLKRIRFSREMPDKWQQRWGENYDKIVELYN
BRX259del AWDFTNSSHHIPAGRLESKFTSIYGNDRSISAQSCDVLLDDGPKKEMAQVEPGVHIITFASLPTGGNDLKRIRFSREMPDKWQQRWGENYDKIVELYN
BRX259-362 AWDFTNSSHHIPAGRLESKFTSIYGNDRSISAQSCDVLLDDGPKKEMAQVEPGVHIITFASLPTGGNDLKRIRFSREMPDKWQQRWGENYDKIVELYN
BRX318L AWDFTNSSHHIPAGRLESKFTSIYGNDRSISAQSCDVLLDDGPKKEMAQVEPGVHIITFASLPTGGNDLKRIRFSREMPDKWQQRWGENYDKIVELYN

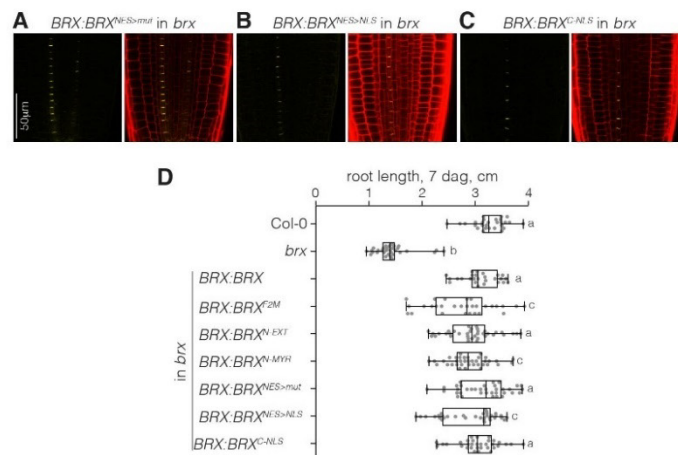
294
BRX VQRFNRQALQTPARSDQSQRDSTYSKMDSARESKDWTFRHINFRPPGSSVPHHIFYGSSNYGPGSYHGGPPMDAARTTSSRRDPPSMSNASEMQAEWIEE
BRX29k VQRFNRQALQTPARSDQSQRDSTYSKMDSARESKDWTFRHINFRPPGSSVPHHIFYGSSNYGPGSYHGGPPMDAARTTSSRRDPPSMSNASEMQAEWIEE
BRX143T VQRFNRQALQTPARSDQSQRDSTYSKMDSARESKDWTFRHINFRPPGSSVPHHIFYGSSNYGPGSYHGGPPMDAARTTSSRRDPPSMSNASEMQAEWIEE
BRX307S VQRFNRQALQTPARSDQSQRDSTYSKMDSARESKDWTFRHINFRPPGSSVPHHIFYGSSNYGPGSYHGGPPMDAARTTSSRRDPPSMSNASEMQAEWIEE
BRX259del VQRFNRQALQTPARSDQSQRDSTYSKMDSARESKDWTFRHINFRPPGSSVPHHIFYGSSNYGPGSYHGGPPMDAARTTSSRRDPPSMSNASEMQAEWIEE
BRX259-362 VQRFNRQALQTPARSDQSQRDSTYSKMDSARESKDWTFRHINFRPPGSSVPHHIFYGSSNYGPGSYHGGPPMDAARTTSSRRDPPSMSNASEMQAEWIEE
BRX318L VQRFNRQALQTPARSDQSQRDSTYSKMDSARESKDWTFRHINFRPPGSSVPHHIFYGSSNYGPGSYHGGPPMDAARTTSSRRDPPSMSNASEMQAEWIEE

344
BRX DEPGVYITIRQLSDGTRELRRVFRSRERFGEVHAKTWWEQNRERIQTYL-----
BRX29k DEPGVYITIRQLSDGTRELRRVFRSRERFGEVHAKTWWEQNRERIQTYL-----
BRX143T DEPGVYITIRQLSDGTRELRRVFRSRERFGEVHAKTWWEQNRERIQTYL-----
BRX307S DEPGVYITIRQLSDGTRELRRVFRSRERFGEVHAKTWWEQNRERIQTYL-----
BRX259del DEPGVYITIRQLSDGTRELRRVFRSRERFGEVHAKTWWEQNRERIQTYL-----
BRX259-362 DEPGVYITIRQLSDGTRELRRVFRSRERFGEVHAKTWWEQNRERIQTYL-----
BRX318L DEPGVYITIRQLSDGTRELRRVFRSRERFGEVHAKTWWEQNRERIQTYLKKKKRKG

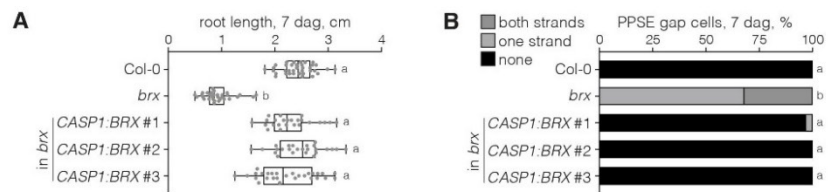
```

Supplemental Figure S3. Amino acid sequence alignment illustrating amino acid substitutions or additions (highlighted in red) to test putative functional features of BRX proteins. (Supports Figure 2).



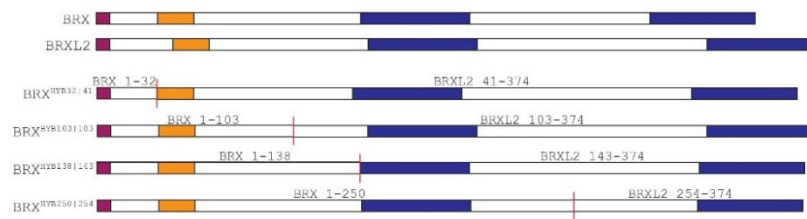


**Supplemental Figure S4.** Robust plasma membrane association of BRX variants. (Supports Figure 2). (A) to (C) Confocal microscopy images of variant BRX-CITRINE fusion proteins (see Supplemental Figure S3) expressed under the control of the *BRX* promoter in the *brx* mutant background (green fluorescence, left panels). Right panels: overlay with PI cell wall staining (red fluorescence). (D) Root length of Col-0, *brx*, and transgenic lines expressing modified BRX-CITRINE fusion proteins (see Supplemental Figure S3) (n=26-37 roots). Box plots display 2<sup>nd</sup> and 3<sup>rd</sup> quartiles and the median, bars indicate maximum and minimum. Statistical significance was determined by ordinary one-way ANOVA. Statistically significant different groups are indicated by different lowercase letters.



**Supplemental Figure S5.** Ectopic expression of BRX-CITRINE fusion protein rescues the *brx* mutant. (Supports Figure 3). **(A)** Root length of Col-0, *brx*, and transgenic lines expressing BRX-CITRINE fusion protein under the control of the *CASP1* promoter in *brx* (three representative independent lines, n=24-36 roots). Box plots display 2<sup>nd</sup> and 3<sup>rd</sup> quartiles and the median, bars indicate maximum and minimum. Statistical significance was determined by ordinary one-way ANOVA. **(B)** PPSE strand defects in roots of the indicated genotypes, corresponding to **(A)** (n=29-60 roots). Statistical significance was determined by Fisher's exact test. Statistically significant different groups are indicated by different lowercase letters.

Supplemental Data. Koh et al. (2021). Mapping and engineering of auxin-induced plasma membrane dissociation in BRX family proteins. *Plant Cell*.

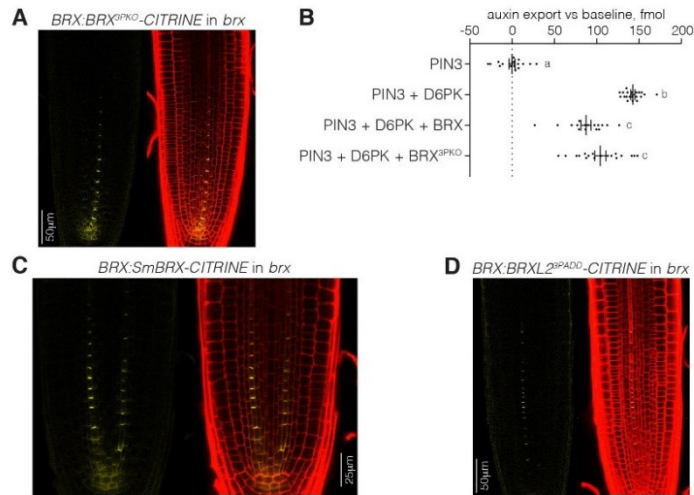


**Supplemental Figure S6.** Schematic overview of the BRX-BRXL2 hybrid proteins tested in this study. (Supports Figure 5). Colored bars represent the conserved N-terminal (purple), KDMA (orange) and BRX (blue) domains.

Supplemental Data. Koh et al. (2021). Mapping and engineering of auxin-induced plasma membrane dissociation in BRX family proteins. Plant Cell.



Supplemental Figure S7. Amino acid sequence alignment illustrating amino acid substitutions or additions (highlighted in red) to test the impact of putative D6PK/PAX target phosphosites on BRX and BRXL2 function in the root protophloem. (Supports Figure 8).



**Supplemental Figure S8.** Impact of amino acid substitutions in D6PK/PAX target phosphosites. (Supports Figure 9). **(A)** Confocal microscopy images of BRX<sup>3PKO</sup>-CITRINE fusion protein expressed under the control of the *BRX* promoter in the *brx* mutant background (yellow fluorescence, left panel). Right panel: overlay with PI cell wall staining (red fluorescence). **(B)** Auxin transport assays performed in *Xenopus laevis* oocytes, measuring retention of radio-labeled auxin in oocytes in the presence of the indicated heterologous plant proteins. Data points indicate fmol of auxin exported after 15 min. as compared to the baseline set by the average of the PIN1 sample (n=16-20). Statistically significant different groups (ordinary one-way ANOVA) are indicated by different lowercase letters. **(C)** Confocal microscopy images of SmBRX-CITRINE fusion protein expressed under the control of the *BRX* promoter in the *brx* mutant background (yellow fluorescence, left panel). Right panel: overlay with PI cell wall staining (red fluorescence). **(D)** Confocal microscopy images of BRXL2<sup>3PADD</sup>-CITRINE fusion protein expressed under the control of the *BRX* promoter in the *brx* mutant background (yellow fluorescence, left panel). Right panel: overlay with PI cell wall staining (red fluorescence).



# Naphthylphthalamic acid associates with and inhibits PIN auxin transporters

Lindy Abas<sup>a,1,2</sup>, Martina Kolb<sup>b,1</sup>, Johannes Stadlmann<sup>c</sup>, Dorina P. Janacek<sup>b</sup>, Kristina Lukic<sup>d</sup>, Claus Schwechheimer<sup>b</sup>, Leonid A. Sazanov<sup>d</sup>, Lukas Mach<sup>a</sup>, Jifi Friml<sup>d</sup>, and Ulrich Z. Hammes<sup>b,2</sup>

<sup>a</sup>Department of Applied Genetics and Cell Biology, University of Natural Resources and Life Sciences (BOKU), 1190 Vienna, Austria; <sup>b</sup>Plant Systems Biology, School of Life Sciences Weihenstephan, Technical University of Munich, 85354 Freising, Germany; <sup>c</sup>Department of Chemistry, University of Natural Resources and Life Sciences (BOKU), 1190 Vienna, Austria; and <sup>d</sup>Institute of Science and Technology Austria, 3400 Klosterneuburg, Austria

Edited by Julian I. Schroeder, University of California at San Diego, La Jolla, CA, and approved November 12, 2020 (received for review October 5, 2020)

***N*-1-naphthylphthalamic acid (NPA) is a key inhibitor of directional (polar) transport of the hormone auxin in plants. For decades, it has been a pivotal tool in elucidating the unique polar auxin transport-based processes underlying plant growth and development. Its exact mode of action has long been sought after and is still being debated, with prevailing mechanistic schemes describing only indirect connections between NPA and the main transporters responsible for directional transport, namely PIN auxin exporters. Here we present data supporting a model in which NPA associates with PINs in a more direct manner than hitherto postulated. We show that NPA inhibits PIN activity in a heterologous oocyte system and that expression of NPA-sensitive PINs in plant, yeast, and oocyte membranes leads to specific saturable NPA binding. We thus propose that PINs are a bona fide NPA target. This offers a straightforward molecular basis for NPA inhibition of PIN-dependent auxin transport and a logical parsimonious explanation for the known physiological effects of NPA on plant growth, as well as an alternative hypothesis to interpret past and future results. We also introduce PIN dimerization and describe an effect of NPA on this, suggesting that NPA binding could be exploited to gain insights into structural aspects of PINs related to their transport mechanism.**

auxin transport | NPA | PIN | auxin transport inhibitor | naphthylphthalamic acid

Many aspects of plant growth are controlled by the hormone auxin. A distinct feature of auxin is that its hormonal action requires it to be actively transported between cells and ultimately throughout the whole plant in a controlled directional or polarized manner, a process known as polar auxin transport (PAT). The ability of plants to perform PAT is ascribed to the auxin export activity of PIN transporters (1). Plasma membrane PINs can be restricted to a specific side of cells (2), and when this polarity is maintained in continuous plant cell files, the combined activity of identically localized PINs results in auxin flowing in that direction (3). This lays the vectorial foundations for PAT to create local auxin gradients and plant-wide PAT streams that are critical for auxin action and normal plant growth (4, 5).

Synthetic PAT inhibitors such as *N*-1-naphthylphthalamic acid (NPA) were initially developed as herbicides and then subsequently exploited by researchers to identify and characterize the unique PAT-based mechanisms that drive plant development (6). Having been used for over six decades, the question as to how NPA actually inhibits PAT has been keenly pursued. Several putative modes of action have been proposed, but the topic remains to date not fully or satisfactorily resolved (6).

Early studies established NPA binding with high affinity to membrane-integral components of plant membranes (7–10). With the later discovery of *pin1* mutants bearing their distinct bare inflorescences reminiscent of NPA-treated plants (11), followed by identification of the PIN gene family and gradual confirmation that PINs were NPA-sensitive auxin transporters that mediated PAT (1–5), it was apparent that the physiological and genetic evidence overwhelmingly linked NPA to inhibition of PIN activity

(6). However, direct molecular association of NPA with PINs has never been reported (6). Instead, a substantial body of data has accumulated suggesting that the NPA target is not PIN itself, but rather other proteins or complexes that either actively coparticipate in PAT or are indirectly involved in control of PAT components (6, 12). Members of the B-family of ABC transporters, such as ABCB1 and ABCB19, showed high-affinity NPA binding and NPA-sensitive auxin export (1, 12–15), thus leading to proposals that they may either physically interact with PINs, or functionally interact such that their nonpolar auxin export activity contributes to PAT and/or to regulation of PINs (12, 16). In these scenarios, PIN/PAT would be rendered vulnerable to the NPA sensitivity of ABCB. However, these schemes are not yet fully resolved, are not fully consistent with key genetic and physiological data (6), and are particularly obfuscated by ABCB1/19 functioning both interactively and independently from PINs (1, 12, 15–20), with ABCB-PIN interaction occurring in an as-yet-unclarified manner (15, 18).

A further twist in assigning ABCBs as the main NPA target is their regulation by their chaperone TWD1/FKBP42 (14, 16), with TWD1 itself also being an NPA-binding protein (14, 17). NPA interferes with this regulation and affects TWD1-ABCB interaction, but curiously NPA cannot bind stably to the ABCB-TWD1 complex (14, 17). As TWD1 has also been implicated in NPA-sensitive actin-based PIN trafficking (17), this has led to a model proposing that TWD1 could mediate the NPA

## Significance

The plant hormone auxin regulates many aspects of plant life and has the unique ability to flow throughout the plant in defined directions, as observed by Darwin over a century ago. The chemical NPA inhibits this directional flow, thereby severely affecting plant growth. In studying the specific effects of NPA, researchers have also uncovered general principles underlying plant development. Exactly how NPA inhibits directional auxin flow is unclear. NPA interacts with proteins that can transport auxin, such as ABCB transporters, and we show here that NPA also associates with and inhibits the major transporters that specialize in directional auxin flow—PINs. This explanation of NPA action will guide future research and may help reveal how PINs perform auxin transport.

Author contributions: L.A., M.K., C.S., L.M., J.F., and U.Z.H. designed research; L.A., M.K., J.S., and D.P.J. performed research; K.L., L.A.S., and J.F. contributed new reagents/analytic tools; L.A., M.K., J.S., and U.Z.H. analyzed data; and L.A. wrote the paper.

The authors declare no competing interest.

This article is a PNAS Direct Submission.

Published under the PNAS license.

<sup>1</sup>L.A. and M.K. contributed equally to this work.

<sup>2</sup>To whom correspondence may be addressed. Email: melinda.abas@boku.ac.at or ulrich.hammes@wzw.tum.de.

This article contains supporting information online at <https://www.pnas.org/lookup/suppl/doi:10.1073/pnas.2020857118/-/DCSupplemental>.

Published December 22, 2020.

sensitivities of both ABCB and PINs, thus presenting TWD1 as a modulator of PAT (17, 21). In an analogous scheme in some plant species, CYPB immunophilins such as tomato DGT, which are functionally similar to TWD1/FKBP42, are suggested to replace TWD1 in modulating auxin transporters and transducing NPA effects to PINs (12, 21).

Similar to TWD1, BIG/TIR3 has also been associated with NPA and PIN trafficking (22). Given the undisputed role of trafficking in controlling PIN polarity (5), these reported effects warrant attention, although they are inconsistent with other reports that NPA perturbs neither vesicular trafficking nor actin dynamics in conditions where auxin transport is inhibited (23, 24). Together with trafficking, phosphorylation is another key modulator of PIN polarity as well as activity (5), so it is not surprising to find hypotheses suggesting that NPA could interfere with critical phosphorylation events (6), particularly as PID, a kinase crucial for PIN trafficking and activation, has also been connected to ABCB function and TWD1/ABCB/NPA interactions (25). Others propose that NPA may mimic natural compounds in their capacity as endogenous regulators of PAT, with plant flavonoids being suspected candidates (6, 26). Since flavonoids can compete with or inhibit ATP-binding in mammalian kinases and ABC transporters (27, 28), and as flavonoids can bind to and inhibit PID (25), a phosphorylation-based NPA mode of action would overlap with this hypothesis and poses the question whether NPA acts similarly as an ATP mimic.

With these many potential NPA-affected pathways, there is a need to distinguish between low- and high-affinity NPA targets and possible secondary effects due to prolonged PAT inhibition. Current consensus is that low concentrations of NPA (<10  $\mu\text{M}$ ) cause direct inhibition of auxin transporters in PAT (21) and the consequent physiological effects seen in planta ( $\text{IC}_{50}$  0.1 to 10  $\mu\text{M}$ ) (7, 9, 19, 23, 29). This is associated with high-affinity binding to membranes ( $K_d$  0.01 to 0.1  $\mu\text{M}$ ) (7, 8) and the inhibition of PIN/ABCB activity in short-term auxin transport assays (1, 14, 18, 20, 23). In contrast, NPA is thought to affect trafficking (21, 30) and other non-PAT processes (31) when used at higher doses (50 to 200  $\mu\text{M}$  NPA), presumably via binding to its lower-affinity targets, although excessive NPA exposure may also have fast-acting toxic side effects (23). As the *in vitro* affinity of TWD1 for NPA is surprisingly low ( $K_d$  ~100  $\mu\text{M}$ ) (17), the TWD1-mediated NPA effects on PIN/PAT are thought to be of the low-affinity type and linked to trafficking perturbations (17, 21). However, as NPA is always externally applied to plants or cells, it is not clear how or where the drug distributes or accumulates, and thus there may be discrepancies between actual and reported/apparent effective concentrations, as might be the case for TWD1 (17). Finally, NPA also binds with low affinity to inhibit APM1, an aminopeptidase implicated in auxin-related plant growth, but as with trafficking effects, this low-affinity NPA interaction is not connected to direct regulation of PAT (31).

Thus, the available data proffer various indirect mechanisms that could lead to NPA inhibition of PIN-mediated PAT, but the proposed schemes have complicating aspects and struggle at times to satisfactorily explain the prime effects of NPA. Here we propose an alternative simpler scenario involving a more direct link between NPA and PINs that would resolve some of these currently outstanding issues. We present evidence from heterologous transport assays, classical *in situ* membrane binding, and oligomerization studies which collectively suggest that NPA can interact directly in a high-affinity manner with PINs, leading to conformational or structural effects and inhibition of auxin export activity.

## Results and Discussion

**NPA Inhibits PIN-Mediated Auxin Transport in Oocytes.** A notable advancement in auxin transport research was the recent establishment of a *Xenopus* oocyte assay to measure export activity of *Arabidopsis thaliana* PINs (32). As with previous assays, it monitors the

retention of radiolabeled  $^3\text{H}$ -indoleacetic acid (IAA). However, the ability to inject  $^3\text{H}$ -IAA as well as any inhibitory drugs directly into oocytes avoids the vagaries associated with external application and passive preloading of both in previous heterologous assays. More importantly, there is also a unique on/off activity switch for the expressed *At*PINs by virtue of the absence or presence of coexpressed mandatory activating kinases (32). We thus utilized this improved and tractable system to investigate NPA effects on PIN activity.

When coinjected with  $^3\text{H}$ -IAA into oocytes ( $\text{NPA}_{\text{in}}$ ), 10  $\mu\text{M}$  NPA (final internal concentration) abolished  $^3\text{H}$ -IAA export mediated by kinase-activated *At*PIN1 or *At*PIN3, whereas 1  $\mu\text{M}$   $\text{NPA}_{\text{in}}$  caused partial inhibition (Fig. 1A and C). We also saw  $\text{NPA}_{\text{in}}$  inhibition of *At*PIN6 export activity (SI Appendix, Fig. S1A), confirming that this noncanonical PIN is NPA-sensitive (33).  $\text{NPA}_{\text{in}}$  inhibition of PIN-dependent  $^3\text{H}$ -IAA export occurred with either PID or D6PK as the activating kinase (Fig. 1C); thus kinase identity was not crucial.

We checked that inhibition of PIN activity was not due to deleterious effects of NPA on general oocyte viability by measuring  $^3\text{H}$ -IAA or  $^{14}\text{C}$ -leucine import by *At*AUX1 and *At*CAT6, respectively. In contrast to PINs, the activity of these other plasma membrane transporters was not compromised by 10  $\mu\text{M}$   $\text{NPA}_{\text{in}}$  (SI Appendix, Fig. S1C and D), showing that NPA inhibits neither global transport nor  $^3\text{H}$ -IAA transport in general. We found no effect of  $\text{NPA}_{\text{in}}$  on  $^3\text{H}$ -IAA retention in control oocytes expressing inactive PIN without kinase, expressing kinase only, or neither (Fig. 1C and SI Appendix, Fig. S1A and E), confirming that NPA

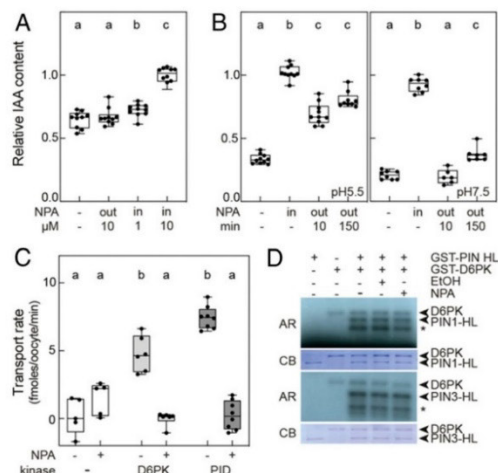


**Fig. 1.** NPA inhibits PIN-mediated  $^3\text{H}$ -IAA efflux in oocytes. (A) In oocytes, coinjected  $\text{NPA}_{\text{in}}$  fully (10  $\mu\text{M}$ ) or partially (1  $\mu\text{M}$ ) inhibits  $^3\text{H}$ -IAA efflux mediated by PIN1 (+YFP:D6PK), whereas external 10  $\mu\text{M}$   $\text{NPA}_{\text{out}}$  added immediately to the pH-7.5 medium has no effect (ANOVA;  $n = 12$ ; a-c,  $P < 0.001$ ; a-b,  $P = 0.029$ ). (B) In pH-5.5 medium (Left), external 10  $\mu\text{M}$   $\text{NPA}_{\text{out}}$  is effective at inhibiting  $^3\text{H}$ -IAA efflux mediated by PIN3 (+YFP:D6PK) after a 10-min preincubation whereas external  $\text{NPA}_{\text{out}}$  at pH 7.5 (Right) causes only partial inhibition after 2.5 h, compared to full inhibition by coinjected 10  $\mu\text{M}$   $\text{NPA}_{\text{in}}$  (ANOVA;  $n = 10$ ;  $P < 0.0001$  for all subsets). (C) Coinjected 10  $\mu\text{M}$   $\text{NPA}_{\text{in}}$  fully inhibits PIN3-mediated  $^3\text{H}$ -IAA efflux from oocytes independent of the choice of activating kinase, YFP:D6PK or PID (two-way ANOVA,  $n = 5$  to 8;  $P < 0.001$  for  $\pm$ kinase as well as  $\pm$ NPA subsets). (D) In [ $\gamma$ - $^{32}\text{P}$ ]-ATP *in vitro* kinase assays, 10  $\mu\text{M}$  NPA does not inhibit D6PK autophosphorylation or D6PK phosphorylation of PIN1 (Upper) or PIN3 (Lower) hydrophilic loops (HL); A single asterisk indicates PIN degradation products. AR, autoradiogram; CB, Coomassie Blue gel.

only affected outward movement of  $^3\text{H}$ -IAA when mediated by active PINs. As a further control, we ruled out NPA being a direct competitor of IAA transport by performing transport assays with  $^3\text{H}$ -NPA. We found that  $^3\text{H}$ -NPA was not transported by PIN1 or PIN3 (with YFP:D6PK) in oocytes (SI Appendix, Fig. S1B), complementing earlier in planta data that NPA is not polarly transported in maize (7). Collectively, these controls indicate that the effect of NPA on  $^3\text{H}$ -IAA retention in oocytes can be attributed to inhibition of PIN-mediated export activity.

Whereas previous auxin transport studies have used externally applied NPA by necessity, the oocyte system offers the opportunity to introduce NPA internally or externally, and as this has never been tested, we investigated this. In comparison to internally injected  $\text{NPA}_{\text{in}}$ , adding 10  $\mu\text{M}$  NPA to external medium ( $\text{NPA}_{\text{out}}$ ) of pH 7.5 at the start of the assay was ineffective in inhibiting PIN-mediated  $^3\text{H}$ -IAA export (Fig. 1A,  $\text{NPA}_{\text{out}}$ ). However, inhibition, was enhanced by either longer preincubation with 10  $\mu\text{M}$   $\text{NPA}_{\text{out}}$  at pH 7.5 or by changing to a plant-type medium pH of 5.5 (Fig. 1B). The more potent immediate effect of  $\text{NPA}_{\text{out}}$  at pH 5.5 and the delayed lesser effect at pH 7.5 suggest that NPA, a weak organic acid, diffuses into oocytes in the uncharged protonated state, with this species being more abundant at the lower pH of 5.5. This is consistent with previous suggestions of passive and pH-dependent uptake into maize coleoptiles (9). More importantly, we show that NPA has to enter cells and bind to an intracellular site to inhibit PIN-mediated  $^3\text{H}$ -IAA export.

PIN activity in oocytes is kinase-dependent. As the requirement is for active phosphorylation rather than kinase presence per se (32), it was necessary to check if kinase activity was being affected by NPA. PID phosphorylation activity has been reported as NPA-insensitive (25), and here, using in vitro assays, we found that NPA perturbed neither autophosphorylation nor phosphorylation of PIN1 or PIN3 hydrophilic loops by D6PK (Fig. 1D). Taken together, as NPA affects neither kinase nor general oocyte transport competence nor background leakage, we conclude that NPA may be targeting PINs themselves at an intracellular site to inhibit PIN-mediated auxin efflux in oocytes.

**NPA Binds to Plant Membranes Enriched in NPA-Sensitive PINs.** These results prompted us to see if NPA could indeed bind to PINs. Radioligand-binding assays were used to initially establish and characterize high-affinity  $^3\text{H}$ -NPA binding to plant microsomal membranes (7–10), followed by later reports linking microsomal  $^3\text{H}$ -NPA-binding profiles to the presence or absence (in mutant lines) of suspected target proteins such as ABCB1/19, TWD1, actin, PID, or BIG/TIR3 (13, 14, 17, 20, 34). Microsomes from *pin1* or *pin2* mutants have been used to argue for the lack of NPA binding by PINs (17, 20), although such interpretation may be unwarranted as single mutants are not devoid of other PIN members. As there are no reports using PIN-enriched samples, we tested this using transient overexpression of *AtPINs* in *Nicotiana benthamiana*. To remove nonexpressing cells, we isolated the lower epidermis of infiltrated leaves and used this pure population of transfected cells to prepare membranes highly enriched for the heterologously expressed *AtPINs* (SI Appendix, Fig. S2A). This enabled us to develop a microscale binding assay using minimal amounts of membranes, such that any endogenous NPA binding was at undetectable levels. We also minimized reaction volumes to  $<10\ \mu\text{L}$ , allowing us to monitor not just binding to membrane pellets but also the corresponding depletions from the supernatant (SN) (SI Appendix, Fig. S2D). The latter was a more reliable measure as bound  $^3\text{H}$ -NPA started to dissociate from membranes during washing of pellets. Such rapid dissociation has been reported (7, 8, 10) and agrees with reversible NPA inhibition of PAT in planta (7).

Using competition by excess unlabeled NPA to define specific/saturable binding (8), we found that  $^3\text{H}$ -NPA bound to membranes expressing *A. thaliana* PIN1, PIN2, PIN3, or PIN6 but not

to membranes from mock controls (Fig. 2A). Addition of excess IAA or another aromatic acid (benzoic acid [BA]) did not compete with  $^3\text{H}$ -NPA, showing that the observed binding was specific for NPA and reconfirming that IAA and NPA bind at different sites (7–9). Adding ATP did not hinder binding of  $^3\text{H}$ -NPA, revealing that NPA cannot mimic the known ability of flavonoids to compete for ATP-binding sites (27, 28). Furthermore, ATP did not enhance  $^3\text{H}$ -NPA binding in either controls or *AtPIN*-expressing membranes, arguing against active  $^3\text{H}$ -NPA transport into sealed vesicles by ATP-limited transporters (Fig. 2A). We could also exclude  $^3\text{H}$ -NPA transport by PINs, as the added excess IAA would have competed with such transport; this agrees with our oocyte results and confirms that we were detecting binding per se rather than vesicular uptake (8). Binding was reversible, as mentioned above, and saturable by about 100 nM  $^3\text{H}$ -NPA (SI Appendix, Fig. S2D), indicating high affinity.

The lack of binding in mock controls (Fig. 2A) indicated that overexpressed PINs were required for  $^3\text{H}$ -NPA binding. We also expressed *KjPIN*, a functional auxin transporter from the algae *Klebsormidium flaccidum*, but this did not lead to any specific binding of  $^3\text{H}$ -NPA (SI Appendix, Fig. S2A and B), which is consistent with *KjPIN*-mediated auxin export being NPA-insensitive in *Nicotiana* BY2 cells (35). As *KjPIN* was either exporting auxin by itself or integrating into NPA-insensitive auxin export complexes in the BY2 cells, when interpreted together with the NPA sensitivity of *AtPIN1/3/6*-mediated auxin export (1, 33) (Fig. 1A and C and SI Appendix, Fig. S1A), our results show that NPA sensitivity of PINs correlates with their NPA-binding capability, providing additional support for PINs being an NPA-binding component of auxin export.

#### **PIN-Expressing Plant Membranes Are Not Enriched for Other Potential NPA-Binding Proteins.**

The mock and *KjPIN* controls suggested that, in the absence of NPA-sensitive PINs, endogenous *N. benthamiana* proteins, membrane lipids or cell walls that were present in the membranes did not detectably contribute to  $^3\text{H}$ -NPA binding. We were able to exclude any involvement of PIN-cell-wall interactions (5) by using membranes released by enzymatic digestion; these cell-wall-free preparations also bound similar amounts of  $^3\text{H}$ -NPA (SI Appendix, Fig. S2C).

To test whether endogenous *N. benthamiana* proteins such as ABCBs or TWD1 were up-regulated in the PIN-overexpressing samples and thus potentially participating or contributing to  $^3\text{H}$ -NPA binding, we performed quantitative multiplexed mass spectrometry (QMS). Three control and three *AtPIN*-expressing samples were labeled with isobaric tags, allowing direct comparison of the relative abundances of endogenous *N. benthamiana* proteins between all six samples. About 3,600 *N. benthamiana* proteins could be quantified (Fig. 2B). Based on spectral counts, heterologous *AtPIN1*, *AtPIN2*, and *AtPIN3* were found to be much more abundant than the only endogenous PIN detected, *NbPIN7* (Fig. 2B and SI Appendix, Table S1). Direct quantitative comparison between *NbPIN7* and *AtPIN3* was possible using the relative abundances of shared peptides, revealing that *NbPIN7* was at least 20-fold less abundant than *AtPIN3*, although this difference is certainly underestimated as interference by technical noise greatly distorts comparison between peptides if they have vastly different relative abundance values, as is the case here (Materials and Methods). From immunoblot analysis (SI Appendix, Fig. S2A), we estimate that *AtPINs* were  $>200$ -fold more highly expressed in *N. benthamiana* samples when compared to native *AtPIN* expression in shoot (36) or to *AtPIN* expressed in *N. benthamiana* using native promoter expression (37), providing support that NPA binding could be attributed to an overabundance of *AtPINs*.

Global comparison of the relative abundances of 3,687 *N. benthamiana* proteins between controls and PIN samples in QMS revealed no up-regulation of any proteins comparable to the overabundant levels achieved by *AtPINs* (Fig. 2B and C). Major plasma



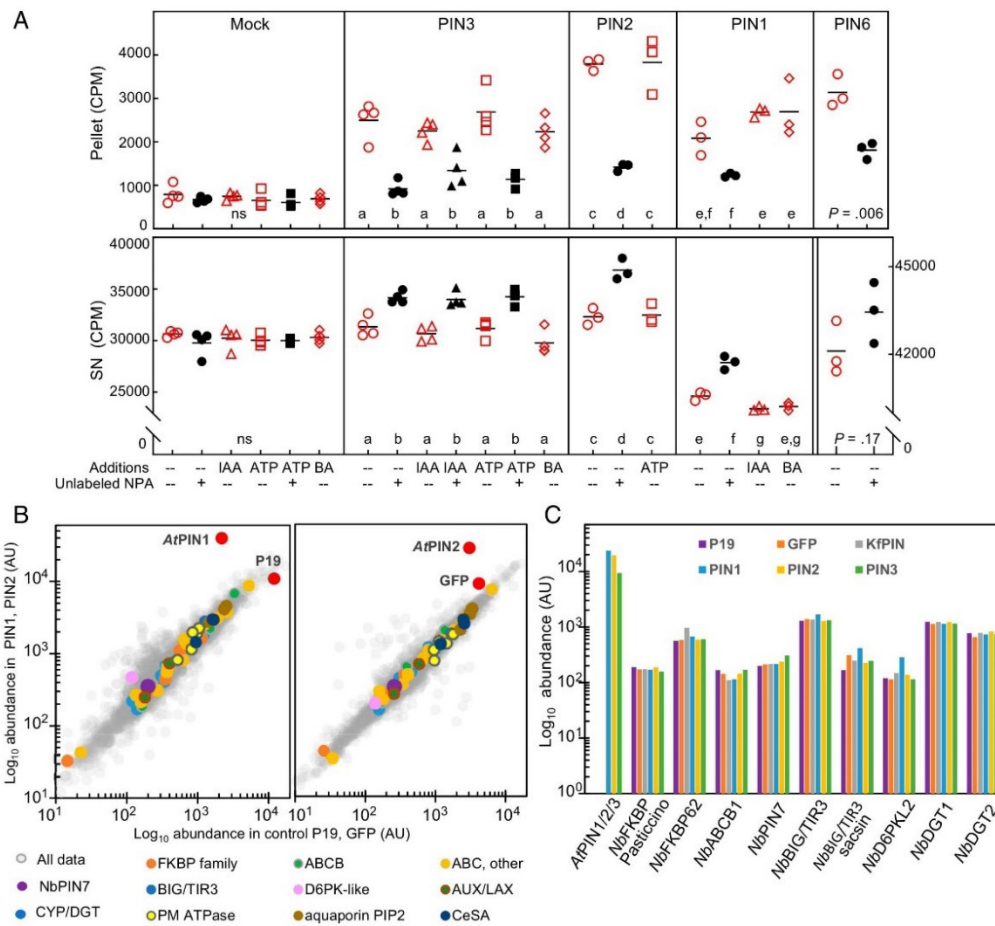


**Fig. 2.** NPA binds to leaf epidermal membranes overexpressing AtPINs. (A) <sup>3</sup>H-NPA binds in a specific/saturable manner to *N. benthamiana* epidermal peel membranes expressing AtPIN1/2/3/6 but not to membranes from mock controls, with accumulation (open red symbols) in pellet (Upper) and depletion from SN (Lower) competed by 20  $\mu$ M unlabeled NPA (filled black symbols). Addition of 20  $\mu$ M IAA or BA or 3 mM ATP did not compete for binding. Comparisons by t test (PIN6,  $n = 3$ ) or ANOVA ( $n = 3$  or 4). For pellet: a-b,  $P = 0.03$ ; c-d,  $P = 0.001$ ; e-f,  $P = 0.008$ . For SN: a-b,  $P = 0.004$ ; c-d,  $P = 0.003$ ; e-f, f-g,  $P = 0.001$ ; e-g,  $P = 0.04$ . (B) Relative abundance values of 3,687 endogenous *N. benthamiana* proteins from QMS analysis (gray cloud; log<sub>10</sub> scale; AU, arbitrary units) were compared between controls and PIN-expressing samples (Left, P19 vs. PIN1+P19; Right, GFP vs. PIN2+GFP). Highlighted *N. benthamiana* proteins are described in the text. Heterologous AtPIN1/PIN2, GFP, and P19 are shown as red dots; AtPIN1/PIN2 are plotted against the technical noise in their respective controls (Materials and Methods). GFP refers to GFP-KDEL (SI Appendix, Fig. S2F). (C) Relative abundance values of selected *N. benthamiana* proteins from QMS analysis compared across three nonbinding control (P19, GFP, KtPIN) and three overexpressing PIN (AtPIN1/2/3) samples (log<sub>10</sub> scale; AU, arbitrary units). Selected relative abundance values in B and C are in SI Appendix, Table S1.

membrane proteins such as ATPases, aquaporins, and cellulose synthases, as well the auxin transporters AUX/LAX and NbPIN7, were similar between all samples, also indicating equivalent amounts of plasma membranes (Fig. 2 B and C and SI Appendix, Table S1). BIG/TIR3, D6PK-like, and 20 ABC transporters were found, with 6 ABCB-family members including ABCB1 but not ABCB19. NbTWD1/FKBP42 was not detected, which may reflect low abundance in planta, as reported for AtTWD1 (14, 15). However, five other sequence-related FKBP proteins were detected with NbPasticcino and NbFKBP62 being most similar to

TWD1/FKBP42 (SI Appendix, Fig. S2H). Nine CYPs were present (SI Appendix, Fig. S2I), including two orthologs of tomato DGT, annotated here as NbDGT1 and NbDGT2. As NbDGT1/2 are more closely related to tomato DGT (95 to 96% identity) than *A. thaliana* orthologs (AtROC1/CYP1; 81% identity to tomato DGT), they may be potential PIN interactors (21). *N. benthamiana* has putative orthologs of AtAPM1 (SI Appendix, Fig. S2I), but none was detected in the QMS.

For all these endogenous proteins and identified potential NPA-binding or PIN-interacting proteins, we found no up-regulation

suggestive of a stoichiometric complex with overexpressed *At*PINs (Fig. 2 B and C and *SI Appendix*, Table S1). We cannot rule out that transient chaperone interactions were required to confer NPA-binding ability, or that complexes between overexpressed PINs and other unchanging abundant proteins may have occurred. However, as these along with *Nb*PIN7 and *Nb*ABC1 remained unchanged and showed no detectable binding in any controls (Fig. 2A and *SI Appendix*, Fig. S2 B–D), we conclude that, if present, any endogenous interactors did not contribute to the observed  $^3\text{H}$ -NPA binding and/or that PINs were the necessary NPA-binding component of any such complexes. The lack of detectable binding by *Nb*ABC1 or *Nb*PIN7 can be attributed to the minimal amounts of material used and low endogenous abundance compared to the highly overexpressed *At*PINs.

As a precise NPA-binding pocket in *At*TWD1 has been identified by NMR analysis (albeit using an unusually high concentration of 3.1 mM NPA due to methodological constraints) (17), we further checked if the other *N. benthamiana* FKBP found in QMS could be expected to bind NPA. Sequence alignment with *At*TWD1 revealed similarity in only one of the four clusters involved in binding (*SI Appendix*, Fig. S2 G and H), implying that these *N. benthamiana* FKBP are unlikely to bind NPA, particularly at the low concentrations ( $<0.1 \mu\text{M}$ ) of  $^3\text{H}$ -NPA used compared to the reported  $K_d$  of  $\sim 100 \mu\text{M}$  for *At*TWD1 (17). We also noted that K79 in the second cluster, identified as the most critical residue for NPA binding (17), is not conserved in *Nb*FKBP42, but is instead E79 (*SI Appendix*, Fig. S2G). We found that in other plant species, K79 frequently varies as E79/Q79/A79 within an otherwise conserved region of FKBP42 (*SI Appendix*, Fig. S2K). As mutating K79 to L79 abolished NPA binding in *At*TWD1 and conferred NPA insensitivity *in vivo* (17), it would thus be interesting to see if E79/Q79/A79 variants can bind NPA, particularly A79 which resembles the nonbinding L79 mutation.

Overall, our QMS and sequence analysis did not reveal any endogenous proteins that could potentially account for the observed NPA binding, leaving the enriched heterologous *At*PINs as the most plausible NPA-binding component in this experimental setup.

**NPA Binds to Heterologous PIN-Enriched Membranes and Is Independent of Phosphorylation.** To further confirm PINs as the NPA-binding component, we repeated the binding assays using *At*PINs expressed in nonplant hosts (*SI Appendix*, Fig. S3 C–E). Membranes from oocytes (PIN1) as well as yeast (PIN6:GFP) both bound  $^3\text{H}$ -NPA in a specific/saturable manner whereas nonexpressing controls did not, with excess BA in all samples not competing for binding (Fig. 3 A and B). This shows that plant-derived components are not required, agreeing with our QMS results that endogenous *N. benthamiana* proteins were not contributing to NPA binding. Furthermore, as PIN-expressing oocyte membranes bound NPA in this *in vitro* setting, this suggests that the *in vivo* transport inhibition observed was not due to NPA perturbing transient chaperone or trafficking events in oocytes, as these are not expected to occur in isolated membranes.

In oocyte membranes, NPA binding was independent of PIN1 hydrophilic loop phosphorylation as similar binding occurred with or without D6PK phosphorylation of PIN1 (Fig. 3A), which can be detected in PIN1 immunoblots by slower migration and a phosphorylation smear (32, 37) (Fig. 3C) and which was stable throughout the binding assay. D6PK itself did not participate in  $^3\text{H}$ -NPA binding, as it partitioned into the SN and was absent from the membrane fraction used for binding assays (Fig. 3D). The *N. benthamiana*  $^3\text{H}$ -NPA binding results also gave no indication of phosphorylation requirements in that we did not attempt to preserve phosphatase-sensitive phosphorylation during membrane extraction and thus PIN1 and PIN3 in the *N. benthamiana* membranes were no longer phosphorylated (no smear detected in immunoblots) whereas PIN2 had some residual smear (*SI Appendix*, Fig. S2A), yet all were able to bind NPA (Fig. 2A). We further checked the effect of NPA on *in vivo* steady-state phosphorylation of PIN in plant cells, where multiple kinases and phosphatases would contribute (37). Using *35S*:PIN1 to avoid complications from transcriptional responses, we found no reduction in the PIN1 phosphorylation smear, noting also that PIN stability was unaffected by NPA (Fig. 3E). Thus, NPA does not impinge on global PIN phosphorylation status *in vivo*, agreeing with our *in vitro* data (Fig. 1D), and neither phosphorylation nor

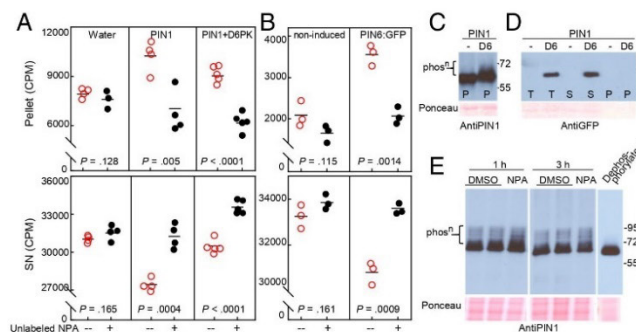


**Fig. 3.** NPA binds to oocyte and yeast membranes expressing PINs. (A)  $^3\text{H}$ -NPA binds in a specific/saturable manner to membranes from oocytes expressing PIN1 or PIN1+YFP:D6PK but not to membranes from control oocytes (injected with water instead of RNA), with an increase in pellet (red symbols, *Upper*) and depletion in SN (red symbols, *Lower*) compared to samples with  $30 \mu\text{M}$  unlabeled NPA (black symbols) (*t* test,  $n = 4$  to 5). All samples contained  $30 \mu\text{M}$  BA. (B)  $^3\text{H}$ -NPA binds in a specific/saturable manner to membranes from yeast expressing PIN6:GFP but not to noninduced control membranes with an increase in pellet (red symbols, *Upper*) and depletion in SN (red symbols, *Lower*) compared to samples with  $30 \mu\text{M}$  unlabeled NPA (black symbols) (*t* test,  $n = 3$ ). All samples contained  $15 \mu\text{M}$  BA. (C) Anti-PIN1 immunoblots using membranes from PIN1 + YFP:D6PK (D6) oocytes detect PIN1 traveling as a slower migrating species with a smear, indicative of YFP:D6PK-mediated phosphorylation, which is not seen when PIN1 is expressed alone. (D) YFP:D6PK (D6) partitioned into the soluble SN fraction (S) and was not detectable in the oocyte membrane pellet fraction (P) used for binding assays (T, total extract; antiGFP immunoblot). (E) In *35S*:PIN1 suspension culture cells,  $10 \mu\text{M}$  NPA treatment (1 to 3 h) did not reduce the endogenous PIN1 phosphorylation smear (antiPIN1 immunoblot). Dephosphorylated PIN1 is shown for comparison.

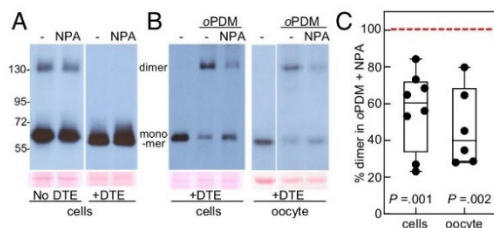


**Fig. 4.** NPA inhibits oPDM cross-linking of PIN1 into dimers. (A) Endogenous PIN1 dimers seen in nonreducing SDS/PAGE (No DTE) are unaffected by in vivo NPA treatment of suspension cells (10  $\mu$ M, 2 h; antiPIN1 immunoblot). (B) In membranes from suspension cells or oocytes, PIN1 is cross-linked into DTE-resistant dimers by oPDM in vitro, and this is inhibited by NPA (antiPIN1 immunoblot). (C) Monomers and cross-linked PIN1 dimers from oPDM treatments ( $\pm$  NPA) were quantified from immunoblots and dimer:monomer ratios were calculated. The ratio in oPDM+NPA was compared to oPDM+DMSO by a one-sample *t* test with the latter used as the test value of 100% as indicated by the dashed red line. NPA reduced the amount of oPDM-linked PIN1 dimers in both suspension cells ( $n = 8$ , 95% CI [26, 62]) and oocytes ( $n = 6$ , 95% CI [31, 75]).

kinase appear to be required or inhibitory for NPA association with PINs.

In summary, we found that  $^3$ H-NPA binding to *N. benthamiana*, oocytes, and yeast membranes correlates with the overexpression of *A*PINs, independent of host, phosphorylation status, or other plant proteins or cell-wall components, collectively supporting a direct association with PINs or a major role for PINs in enhancing NPA binding to PIN-enriched membranes.

**NPA Interferes with a PIN Dimer Interface.** As we saw NPA binding as well as NPA inhibition of PIN activity in oocytes, we sought a mechanism that might explain or connect these two observations. We found that PINs form disulfide-dependent dimers that are visible in nonreducing sodium dodecyl sulfate/polyacrylamide gel electrophoresis (SDS/PAGE) and which are not affected by NPA (Fig. 4A). However, we then treated plant or oocyte membranes with *ortho*-phenylenedimaleimide (oPDM), a bifunctional reagent that can covalently cross-link two vicinal free cysteines (Cys). This led to oPDM-linked PIN dimers now resistant to reducing agents such as dithioerythritol (DTE) (Fig. 4B), and we found that less cross-linking occurred when NPA was present (Fig. 4B and C). This effect was seen with both PIN1 and PIN2 from cultured plant cells as well as with PIN1 from oocytes (Fig. 4B and C and *SI Appendix*, Fig. S4A), indicating a property inherent of PINs and independent of the host membrane. The cross-linking of other proteins in the same sample was not affected by NPA (*SI Appendix*, Fig. S4C and D), and we further confirmed that NPA did not affect the chemical reactivity of oPDM or Cys (*SI Appendix*, Fig. S4B). We also checked other compounds and found that neither auxins (IAA or 1-naphthylacetic acid [NAA]) nor the alternative PAT inhibitor 2,3,5-triiodobenzoic acid (TIBA) could inhibit cross-linking of PINs by oPDM (*SI Appendix*, Fig. S4D and E).

These data support an inhibitory effect on cross-linking of PINs that was unique for NPA and suggestive of an interaction between NPA and PIN. Possible explanations are that NPA binds near a Cys to sterically hinder the reaction with oPDM, or elsewhere to cause a conformational change, or that NPA can prise PIN monomers apart beyond the 9-Å maximum cross-linking span of oPDM (38). This observation is reminiscent of NPA disrupting TWD1-ABCB1 interaction (14), although NPA is proposed to bind to soluble domains in TWD1 or ABCB1 (14, 17, 20), whereas all Cys in PIN1/2 are predicted to be in putative transmembrane domains or in short membrane-proximal cytoplasmic loops. Thus, the

NPA effect on PINs appears to be different from that of TWD1/ABCB in involving transmembrane domains rather than soluble regions, agreeing with reports describing NPA-binding sites as membrane-integral (10). We note that the predicted cytoplasmic locations for Cys in PIN1/2 are consistent with our oocyte results of an intracellular NPA-binding site.

Since we used intact membranes for both  $^3$ H-NPA binding and oPDM cross-linking, we cannot rule out that NPA interaction involves the immediate lipid environment of PINs, particularly as PIN activity (Fig. 1) and oligomerization (Fig. 4) are affected and as lipids are known to be important regulators of both in transporters and membrane proteins in general (39, 40). However, as we used three different phyla (plants, animals, fungi) known to have very different membrane lipid composition (39), it seems that PINs themselves are the determining factor in shaping any potential NPA-lipid interaction. Additionally, although ABCBs may stabilize PINs in certain sterol domains in plants and yeast (15), the ability of PINs to function in foreign oocyte membranes is now accepted as evidence that neither ABCB chaperoning nor specialized plant lipid domains are essential for PIN activity (12).

Notwithstanding any lipid involvement, NPA was able to bind to as well as inhibit cross-linking of PINs in oocyte membranes. Thus, a possible explanation for the transport inhibition in oocytes could be an NPA-PIN interaction that leads to conformational or structural perturbations in PINs, providing a potential mechanism for PIN inactivation and inviting consideration of using NPA as a structural or functional activity probe for PINs.

## Conclusions

Our data provide an evidential basis to invoke a straightforward mechanistic explanation for NPA inhibition of PINs, in which NPA can bind to PINs independently of other potential NPA-binding proteins. Direct PIN inhibition offers a physiologically relevant model of NPA action and a parsimonious hypothesis to plan and interpret future work, as an alternative to, or combined with, current indirect models. It may also be prudent to reinterpret past work in light of our results to reconsider possible overlooked effects or contributions due to NPA binding by PINs.

The combination of existing models with the one presented here means that NPA could synergistically inhibit both PIN- and ABCB-based major auxin streams. Since it is unlikely to be due to chance that a synthetic compound binds diverse targets (ABCB, PIN, TWD1) in a common auxin export pathway, one way to explain this apparent coincidence is the concept that NPA mimics an endogenous counterpart which has evolved to do precisely so. Our results provide hints as to how NPA or an endogenous inhibitor may interact with PINs, namely an intracellular allosteric site distinct from IAA substrate-binding sites, possibly involving membrane-proximal conserved Cys residues and an interface between monomers. Any involvement of the PIN hydrophilic loop is restricted to the  $\sim$ 100 residues shared between canonical PIN1/2/3 and the shorter loop of PIN6. Furthermore, binding is independent of the many phosphorylation sites contained therein and does not require loop kinases. Further investigations into these and other aspects of NPA-PIN interactions are warranted with the collateral benefit of gaining much needed structural and mechanistic insights into PINs.

## Materials and Methods

**Oocyte Transport.** Oocytes were injected with  $^3$ H-IAA or  $^3$ H-NPA (American Radiolabeled Chemicals) (32). NPA was coinjected with  $^3$ H-IAA (1 or 10  $\mu$ M final internal concentration; NPA<sub>in</sub>) or added into the medium (10  $\mu$ M final external; NPA<sub>out</sub>) at 0, 10, or 150 min before injecting  $^3$ H-IAA. Results are presented as "relative IAA content" ( $^3$ H-IAA cpm in oocytes at 30 vs. 0 min) or as transport rates from linear regression of a cpm vs. time plot, translated to fmol based on the specific activity of  $^3$ H-IAA. External medium was Barth's solution (32) with 10 mM Hepes, pH 7.5 or 5.5. For AUX1/ $^3$ H-IAA (41) and CAT6/ $^{14}$ C-leucine (ARC) (42) assays, oocytes were injected with 10  $\mu$ M NPA<sub>in</sub> and results are presented as cpm in oocytes at the end of assays.

**Phosphorylation and Dimers.** In vitro [ $\gamma$ - $^{32}$ P]-ATP phosphorylation assays were performed with  $\pm 10$   $\mu$ M NPA (32). For global phosphorylation or endogenous dimer analysis, 35S:PIN1 suspension cells were treated with 10  $\mu$ M NPA or dimethylsulfoxide (DMSO) (1 to 4 h in 0.5x Murashige-Skoog medium [MSM]), and membranes were extracted (36, 37).

***N. benthamiana* Membranes.** AtPIN1/2/3/6 or KPIN (in pMDC7 or pK7WG2D) were agroinfiltrated together with P19 (43) into *N. benthamiana* leaves. Mock controls received empty vectors and/or P19. Leaves with pMDC7 were induced (24 h, 2  $\mu$ M  $\beta$ -estradiol/0.2x MSM). The lower epidermis was peeled off, and membranes were extracted by homogenization (36) or released by digestion (1 h, 4  $^{\circ}$ C, 0.07% cellulase/0.03% macerozyme in 50 mM Tris-HCl, pH 7.4/5 mM ethylenediaminetetraacetic acid [EDTA]/0.05% casein/2% glycerol [EB] with 1 mM phenylmethylsulfonyl fluoride [PMSF]/1  $\mu$ g/mL aprotinin/leupeptin/pepstatin/E64 [PI]). Membranes were collected (45,000  $\times$  g, 30 min, 4  $^{\circ}$ C), washed (20 mM Tris-HCl, pH 8/5 mM EDTA [TE]), and resuspended in EB + PI.

**Yeast Membranes.** AtPIN6 in pDDGFP\_LEU2D was transformed into *Saccharomyces cerevisiae* BJ5460. Cultures started in LEU-dropout medium +2% lactate (from OD 0.05 to 0.6) were induced with 2% galactose (20 h, 30  $^{\circ}$ C) (SI Appendix, Fig. S3D). Yeast were spheroplasted using Zymolase 20T (Roth), disrupted in TE + PI, and twice spun through 5% glycerol/TE/1 mM PMSF onto a 0.1-mL 50% sucrose cushion (45,000  $\times$  g, 30 min, 4  $^{\circ}$ C). Membrane pellets were resuspended in 5% glycerol/TE/1 mM PMSF.

**Oocyte Membranes.** Oocytes were homogenized (100 mM Tris-HCl, pH 7.5/10 mM EDTA/5 mM EGTA/0.1% casein/10% glycerol/50 mM NaF/20 mM  $\beta$ -glycerol PO $_4$ /10 mM NaMoO $_4$ /Phosstop/PI), and a crude pellet was collected (45,000  $\times$  g, 30 min, 4  $^{\circ}$ C). Yolk proteins (vitellogenins) were removed from this pellet by successive washing with 100 mM MgCl $_2$ , 1 M NaCl, and TE (modified from ref. 44) (SI Appendix, Fig. S3A) and resuspended in EB + PI. Residual vitellogenin was similar in all samples (SI Appendix, Fig. S3B). Control water-injected and RNA-injected oocytes were prepared from the same batches.

**Radioligand Binding Assay.** We modified previous assays (7–10) into a microscale assay (<10  $\mu$ L). Each reaction contained membranes (1 to 3  $\mu$ L pellet volume) from 15 to 30 mg *N. benthamiana* peel, 12 OD units yeast or two oocytes, in all cases ~100 to 300x the amounts required to obtain a very strong signal in immunoblot analysis of PIN expression levels (SI Appendix, Figs. S2A and S3 C and E). For each series, equal aliquots of membranes were pelleted (21,000  $\times$  g, 30 min, 4  $^{\circ}$ C) and washed with 20 mM MgCl $_2$ , and all traces of supernatant removed. The pellet was carefully resuspended in an exact volume (3 to 6  $\mu$ L) of binding buffer (RB: 5% glycerol/0.1 mM MgSO $_4$ /5 mM KCl and 50 mM KH $_2$ PO $_4$ /NaH $_2$ PO $_4$ , pH 6.5 or 7.5) containing  $^3$ H-NPA (~0.05  $\mu$ Ci, 60 Ci/mmol) and 1- $\mu$ L additions (unlabeled NPA, BA, or IAA (20- to 30- $\mu$ M final concentrations) or ATP (3-mM final concentration, pH adjusted to 7.4 with two molar equivalents of Tris base) or solvent (DMSO or pH 7.4 Tris-HCl). When ATP was used, 5 mM MgCl $_2$  was included in the whole series. All yeast (15  $\mu$ M) and oocyte (30  $\mu$ M) samples contained BA. After 2 to 6 h, samples were spun (21,000  $\times$  g, 15 min, 4  $^{\circ}$ C), and a precise volume of SN was removed. Pellets were counted directly (as in refs. 7–9), or washed by quickly transferring to GF/F Whatman filters (as in ref. 10) using 10  $\mu$ L RB and rapidly washing with 3x 0.7 mL RB/0.1  $\mu$ M BA in a vacuum manifold. Radioactivity in pellets, filters, and SN was measured by liquid scintillation counting, and results are reported as cpm (61% counting efficiency). A typical reaction contained a 1.5- $\mu$ L membrane pellet resuspended in 6  $\mu$ L, from which 5 or 6  $\mu$ L SN was subsequently removed for washed or unwashed pellets, respectively (SI Appendix, Fig. S2D). Accurate pipetting was essential for this microscale assay; we used low-binding extrafine-tipped

pipette tips (10  $\mu$ L extralong Surphob Tips, Biozym) and an Eppendorf 10- $\mu$ L pipette with a metal-tip cone and volume lock.  $^3$ H-NPA was used within 2.5 y of purchase.

**Cross-linking.** Membranes from cells or oocytes were pretreated with 20 to 50  $\mu$ M NPA, TIBA, NAA, IAA, or DMSO (30 to 60 min; 0.2 M NaH $_2$ PO $_4$  pH 7.5/10% glycerol or RB), cross-linked (5 to 60 min, 0.2 to 0.5 mM oPDM [Sigma] or DMSO) and quenched (5 mM *N*-ethylmaleimide or 20 mM DTE followed by 60 mM *N*-ethylmaleimide). NPA did not affect the chemical reactivity or stability of oPDM or Cys, tested using Ellman's reagent/DTNB (Abs $_{412}$  nm) (SI Appendix, Fig. S4B).

**Immunoblotting.** Membrane fractions were prepared as above or as in ref. 36. Membranes from <0.1 mg *N. benthamiana* peel, 1/50th oocyte, or 0.1 OD units yeast were blotted (36, 37) and probed with antiPIN1 or antiPIN2 (36), antiPIN3 (45), antiKPIN (35), antiGFP (Roche) or rabbit antiPIN6 raised against residues 167 to 405 of AtPIN6. Molecular weight markers and Ponceau-stained blots are shown next to immunoblots. Bands were quantified from images captured using ImageLab/ChemIDocXRS (BioRad).

**QMS.** Equal amounts of *N. benthamiana* membranes from three controls (P19, GFP-KDEL, KPIN) and three AtPIN-expressing samples (PIN1, PIN2+GFP-KDEL, PIN3; all six samples contained P19) were sequentially solubilized with 2% dodecylmaltoide, 0.4% SDS, and 0.5% sodium deoxycholate (SI Appendix, Fig. S2 E and F), precipitated with CHCl $_3$ /MeOH, solubilized with a graded ethanol series, labeled using isobaric TMTsixplex as per the manufacturer's instructions (Thermo Fisher Scientific) and combined for QMS (46). We used the *N. benthamiana* NbDE proteome database (47). Sequences were analyzed in MEGA-X using multiple alignment by ClustalW or MUSCLE with manual curation. For heterologous proteins (AtPIN, GFP-KDEL), the apparent relative abundance values in the other nonexpressing samples are technical noise from the overtly overexpressing sample(s) due to precursor ion impurity and coisolation. We confirmed this using an alternate SP53 data-acquisition regime, where noise values for PIN1 were reduced from 5–11% (SI Appendix, Table S1) to 0–0.6% in SP53 and for PIN2 from 9–17% to 0.6–1.5%. Similarly, direct quantitative comparison using shared peptides between AtPIN and NbPIN7 was unreliable as the extreme differences in relative abundances caused technical noise in the nonexpressing samples. Fig. 2C uses relative abundance values normalized using global average relative abundance from 3,687 *N. benthamiana* proteins detected in each sample (SI Appendix, Table S1).

**Statistics.** Data were analyzed in Microsoft Excel 2016, IBM SPSS Statistics v24, or GraphPad Prism8. Unpaired *t* tests (two-tailed *P* values) were used, except for Fig. 3C (one-sample *t* test). One-way ANOVA was used unless otherwise stated and was not significant (ns) if *P* > 0.05. Post-hoc analysis was by Holm-Sidak, Dunn, or Tukey's tests; lowercase letters indicate homogeneous subsets. For  $^3$ H-NPA-binding data, bars show means.

**Data Availability.** All study data are included in the article and supporting information.

**ACKNOWLEDGMENTS.** This work was supported by Austrian Science Fund Grant FWF P21533-B20 (to L.A.); German Research Foundation Grant DFG HA3468/6-1 (to U.Z.H.); and European Research Council Grant 742985 (to J.F.). We thank Herta Steinkellner and Alexandra Castilho for *N. benthamiana* plants, Fabian Nagelreiter for statistical advice, Lanassa Bassukas for help with [ $\gamma$ - $^{32}$ P]-ATP assays, and Josef Penninger for providing access to mass spectrometry instruments at the Vienna BioCenter Core Facilities. We thank PNAS reviewers for the many comments and suggestions that helped to improve this manuscript.

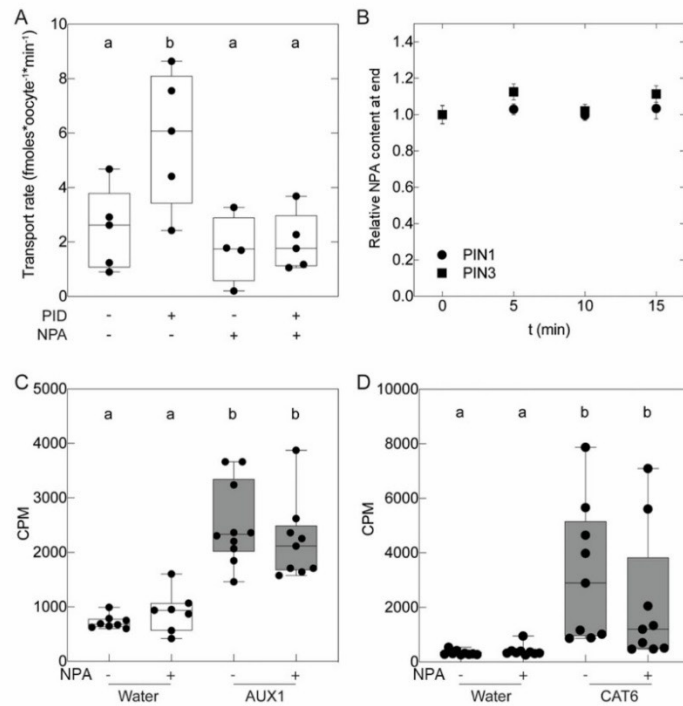
1. J. Petrášek *et al.*, PIN proteins perform a rate-limiting function in cellular auxin efflux. *Science* **312**, 914–918 (2006).
2. L. Gálweiler *et al.*, Regulation of polar auxin transport by AtPIN1 in Arabidopsis vascular tissue. *Science* **282**, 2226–2230 (1998).
3. J. Wiśniewska *et al.*, Polar PIN localization directs auxin flow in plants. *Science* **312**, 883 (2006).
4. E. Benková *et al.*, Local, efflux-dependent auxin gradients as a common module for plant organ formation. *Cell* **115**, 591–602 (2003).
5. M. Adamowski, J. Friml, PIN-dependent auxin transport: Action, regulation, and evolution. *Plant Cell* **27**, 20–32 (2015).
6. W. Teale, K. Palme, Naphthylphthalamic acid and the mechanism of polar auxin transport. *J. Exp. Bot.* **69**, 303–312 (2018).
7. K. S. Thomson, R. Hertel, S. Müller, J. E. Tavares, 1-N-naphthylphthalamic acid and 2,3,5-triiodobenzoic acid: In-vitro binding to particulate cell fractions and action on auxin transport in corn coleoptiles. *Planta* **109**, 337–352 (1973).

8. M. R. Sussman, G. Gardner, Solubilization of the receptor for N-1-naphthylphthalamic acid. *Plant Physiol.* **66**, 1074–1078 (1980).
9. M. R. Sussman, M. H. M. Goldsmith, The action of specific inhibitors of auxin transport on uptake of auxin and binding of N-1-naphthylphthalamic acid to a membrane site in maize coleoptiles. *Planta* **152**, 13–18 (1981).
10. P. Bernasconi, B. C. Patel, J. D. Reagan, M. V. Subramanian, The N-1-Naphthylphthalamic acid-binding protein is an integral membrane protein. *Plant Physiol.* **111**, 427–432 (1996).
11. K. Okada, J. Ueda, M. K. Komaki, C. J. Bell, Y. Shimura, Requirement of the auxin polar transport system in early stages of Arabidopsis floral bud formation. *Plant Cell* **3**, 677–684 (1991).
12. M. Geisler, B. Aryal, M. di Donato, P. Hao, A critical view on ABC transporters and their interacting partners in auxin transport. *Plant Cell Physiol.* **58**, 1601–1614 (2017).
13. B. Noh, A. S. Murphy, E. P. Spalding, Multidrug resistance-like genes of Arabidopsis required for auxin transport and auxin-mediated development. *Plant Cell* **13**, 2441–2454 (2001).

Abas *et al.*  
Naphthylphthalamic acid associates with and inhibits PIN auxin transporters

PNAS | 7 of 8  
<https://doi.org/10.1073/pnas.2020857118>

14. A. Bailly *et al.*, Modulation of P-glycoproteins by auxin transport inhibitors is mediated by interaction with immunophilins. *J. Biol. Chem.* **283**, 21817–21826 (2008).
15. B. Titapiwatanakun *et al.*, ABCB19/PGP19 stabilises PIN1 in membrane microdomains in *Arabidopsis*. *Plant J.* **57**, 27–44 (2009).
16. G. Wu, M. S. Otegui, E. P. Spalding, The ER-localized TWD1 immunophilin is necessary for localization of multidrug resistance-like proteins required for polar auxin transport in *Arabidopsis* roots. *Plant Cell* **22**, 3295–3304 (2010).
17. J. Zhu *et al.*, TWISTED DWARF1 mediates the action of auxin transport inhibitors on actin cytoskeleton dynamics. *Plant Cell* **28**, 930–948 (2016).
18. J. J. Blakeslee *et al.*, Interactions among PIN-FORMED and P-glycoprotein auxin transporters in *Arabidopsis*. *Plant Cell* **19**, 131–147 (2007).
19. J. Mravec *et al.*, Interaction of PIN and PGP transport mechanisms in auxin distribution-dependent development. *Development* **135**, 3345–3354 (2008).
20. J.-Y. Kim *et al.*, Identification of an ABCB/P-glycoprotein-specific inhibitor of auxin transport by chemical genomics. *J. Biol. Chem.* **285**, 23309–23317 (2010).
21. M. Geisler, A. Bailly, M. Ivanchenko, Master and servant: Regulation of auxin transporters by FKBP and cyclophilins. *Plant Sci.* **245**, 1–10 (2016).
22. T. Paciorek *et al.*, Auxin inhibits endocytosis and promotes its own efflux from cells. *Nature* **435**, 1251–1256 (2005).
23. J. Petrášek *et al.*, Do phytotropins inhibit auxin efflux by impairing vesicle traffic? *Plant Physiol.* **131**, 254–263 (2003).
24. P. Dhonukshe *et al.*, Auxin transport inhibitors impair vesicle motility and actin cytoskeleton dynamics in diverse eukaryotes. *Proc. Natl. Acad. Sci. U.S.A.* **105**, 4489–4494 (2008).
25. S. Henrichs *et al.*, Regulation of ABCB1/PGP1-catalysed auxin transport by linker phosphorylation. *EMBO J.* **31**, 2965–2980 (2012).
26. D. E. Brown *et al.*, Flavonoids act as negative regulators of auxin transport in vivo in *Arabidopsis*. *Plant Physiol.* **126**, 524–535 (2001).
27. G. Conseil *et al.*, Flavonoids: A class of modulators with bifunctional interactions at vicinal ATP- and steroid-binding sites on mouse P-glycoprotein. *Proc. Natl. Acad. Sci. U.S.A.* **95**, 9831–9836 (1998).
28. C. Gu *et al.*, Inhibition of inositol polyphosphate kinases by quercetin and related flavonoids: A structure-activity analysis. *J. Med. Chem.* **62**, 1443–1454 (2019).
29. H. Fujita, K. Syöno, PIS1, a negative regulator of the action of auxin transport inhibitors in *Arabidopsis thaliana*. *Plant J.* **12**, 583–595 (1997).
30. N. Geldner, J. Friml, Y.-D. Stierhof, G. Jürgens, K. Palme, Auxin transport inhibitors block PIN1 cycling and vesicle trafficking. *Nature* **413**, 425–428 (2001).
31. W. A. Peer *et al.*, Mutation of the membrane-associated M1 protease APM1 results in distinct embryonic and seedling developmental defects in *Arabidopsis*. *Plant Cell* **21**, 1693–1721 (2009).
32. M. Zourelidou *et al.*, Auxin efflux by PIN-FORMED proteins is activated by two different protein kinases, D6 PROTEIN KINASE and PINOID. *Elife* **3**, e02860 (2014).
33. S. Simon *et al.*, PIN6 auxin transporter at endoplasmic reticulum and plasma membrane mediates auxin homeostasis and organogenesis in *Arabidopsis*. *New Phytol.* **211**, 65–74 (2016).
34. M. Ruegger *et al.*, Reduced naphthylphthalamic acid binding in the *tir3* mutant of *Arabidopsis* is associated with a reduction in polar auxin transport and diverse morphological defects. *Plant Cell* **9**, 745–757 (1997).
35. R. Skokan *et al.*, PIN-driven auxin transport emerged early in streptophyte evolution. *Nat. Plants* **5**, 1114–1119 (2019).
36. L. Abas, C. Luchnig, Maximum yields of microsomal-type membranes from small amounts of plant material without requiring ultracentrifugation. *Anal. Biochem.* **401**, 217–227 (2010).
37. S. Tan *et al.*, Salicylic acid targets protein phosphatase 2A to attenuate growth in plants. *Curr. Biol.* **30**, 381–395.e8 (2020).
38. N. S. Green, E. Reisler, K. N. Houk, Quantitative evaluation of the lengths of homobifunctional protein cross-linking reagents used as molecular rulers. *Protein Sci.* **10**, 1293–1304 (2001).
39. M. Opekarová, W. Tanner, Specific lipid requirements of membrane proteins: A putative bottleneck in heterologous expression. *Biochim. Biophys. Acta* **1610**, 11–22 (2003).
40. K. Gupta *et al.*, The role of interfacial lipids in stabilizing membrane protein oligomers. *Nature* **541**, 421–424 (2017).
41. Y. Yang, U. Z. Hammes, C. G. Taylor, D. P. Schachtman, E. Nielsen, High-affinity auxin transport by the AUX1 influx carrier protein. *Curr. Biol.* **16**, 1123–1127 (2006).
42. U. Z. Hammes, E. Nielsen, L. A. Honaas, C. G. Taylor, D. P. Schachtman, ATCAT6, a sink-tissue-localized transporter for essential amino acids in *Arabidopsis*. *Plant J.* **48**, 414–426 (2006).
43. F. Garabagi, E. Gilbert, A. Loos, M. D. McLean, J. C. Hall, Utility of the P19 suppressor of gene-silencing protein for production of therapeutic antibodies in *Nicotiana* expression hosts. *Plant Biotechnol. J.* **10**, 1118–1128 (2012).
44. M. J. Bergeron *et al.*, Frog oocytes to unveil the structure and supramolecular organization of human transport proteins. *PLoS One* **6**, e21901 (2011).
45. M. M. Marqués-Bueno, J. Moreno-Romero, L. Abas, R. De Michele, M. C. Martínez, A dominant negative mutant of protein kinase CK2 exhibits altered auxin responses in *Arabidopsis*. *Plant J.* **67**, 169–180 (2011).
46. L. Zhang, J. E. Elias, “Relative protein quantification using tandem mass tag mass spectrometry” in *Proteomics. Methods in Molecular Biology*, L. Comai, J. Katz, P. Mallick, Eds. (Humana Press, New York, 2017), vol. 1550, pp. 185–198.
47. J. Kourelis *et al.*, A homology-guided, genome-based proteome for improved proteomics in the allopolyploid *Nicotiana benthamiana*. *BMC Genomics* **20**, 722 (2019).



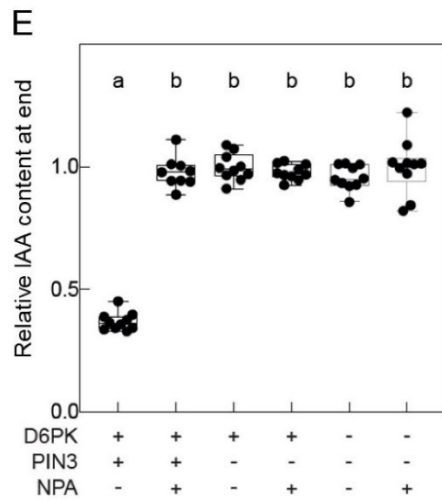
**SI Fig. S1. NPA inhibits PIN-mediated auxin efflux in oocytes but does not affect other plasma membrane transporters**

**(A)** PIN6 is activated by PID to mediate <sup>3</sup>H-IAA efflux in oocytes and this is inhibited by 10 μM NPA<sub>in</sub> (2-way ANOVA, *n*=5; *P* = .03 for ±kinase; a-b, *P* = .01).

**(B)** <sup>3</sup>H-NPA is not exported from oocytes expressing PIN1+YFP:D6PK or PIN3+YFP:D6PK (ANOVA, ns, *n*=10).

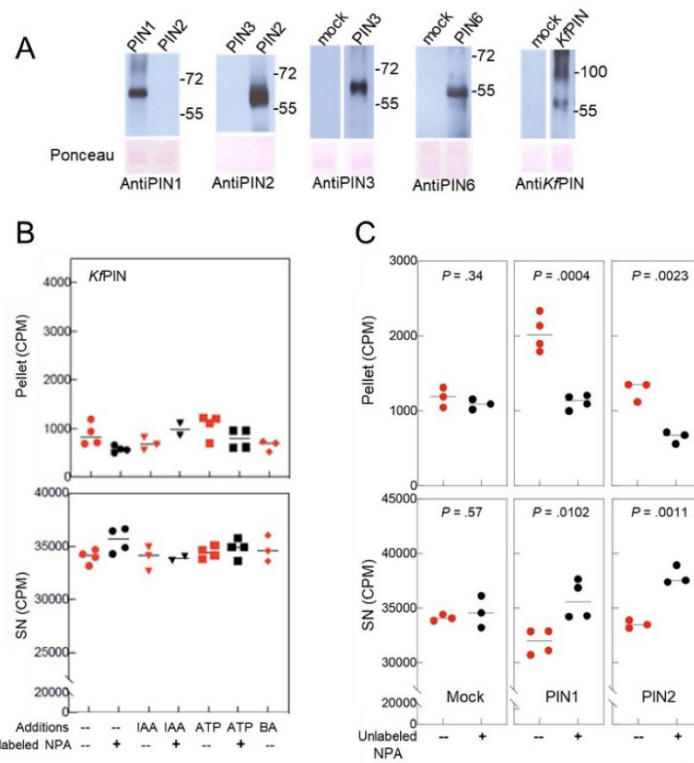
**(C)** AUX1-expressing oocytes import <sup>3</sup>H-IAA and this is not affected by 10 μM NPA<sub>in</sub>. Non-expressing oocyte controls (water-injected instead of cRNA) show no import activity or effect of NPA. Comparison by ANOVA (*n*=10; Kruskal-Wallis test (*P* < .0001) with Dunn's multiple comparison test (a-b, *P* < .032)).

**(D)** CAT6-expressing oocytes import <sup>14</sup>C-leucine and this is not affected by 10 μM NPA<sub>in</sub>. Non-expressing oocyte controls (water-injected instead of cRNA) show no import activity or effect of NPA. Comparison by ANOVA (*n*=10; Kruskal-Wallis test (*P* < .0001) with Dunn's multiple comparison test (a-b, *P* < .045)).



**SI Fig. S1. NPA inhibits PIN-mediated auxin efflux in oocytes but does not affect other plasma membrane transporters**

**(E)** Co-injected 10  $\mu\text{M}$   $\text{NPA}_{in}$  fully inhibits D6PK-activated PIN3-dependent  $^3\text{H}$ -IAA efflux in oocytes whereas retention of injected  $^3\text{H}$ -IAA is not affected by NPA in control oocytes expressing kinase only (D6PK) without PIN3 or in control oocytes expressing neither D6PK nor PIN (water-injected instead of cRNA). Comparison by ANOVA ( $n=10$ ; a-b,  $P < .0001$ ).



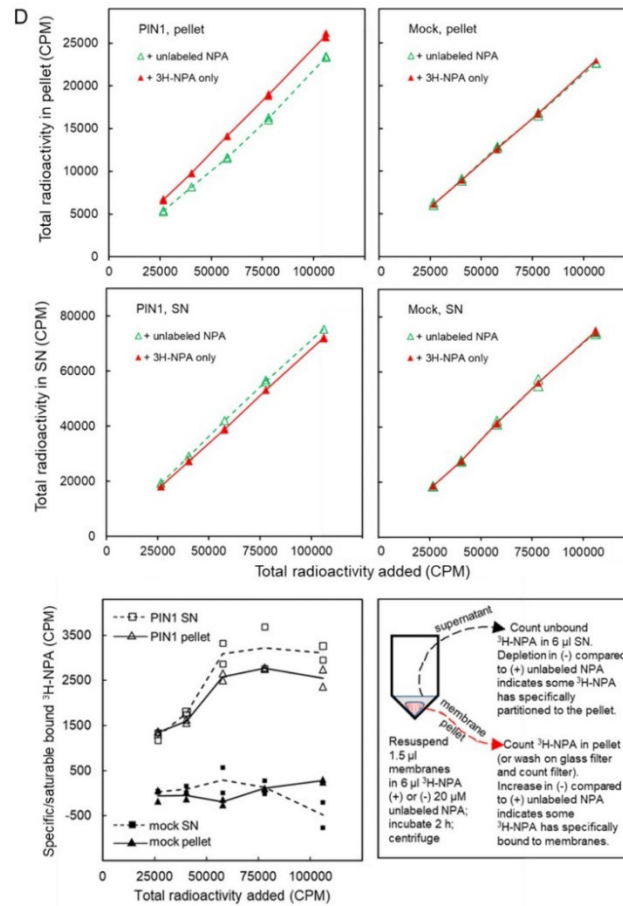
**SI Fig.S2. NPA binds to leaf epidermal membranes overexpressing AtPINs.**

**(A)** Immunoblot analysis of PIN expression in *N. benthamiana* peel membranes. Ponceau staining is weak as  $<1 \mu\text{g}$  total membrane protein was loaded due to abundant overexpression. In most cases, Ponceau is actually only staining casein present in the buffer, with *N. benthamiana* protein not detectable.

**(B)** *N. benthamiana* membranes with overexpressed *KfPIN* do not bind <sup>3</sup>H-NPA, with no change in pellet or SN in samples with excess unlabeled NPA (black symbols) compared to samples with only <sup>3</sup>H-NPA (red symbols). Additions of IAA, ATP or BA had no effect compared to no addition. Comparison by ANOVA ( $n=3$  or  $4$ , except *IAA+unlabeled NPA*  $n=2$ ) was ns for SN; for pellet ns between treatments except *+unlabeled NPA vs +ATP* ( $P = .016$ ).

**(C)** Cell wall-free *N. benthamiana* membranes obtained by enzymatic digestion and overexpressing *AtPIN1* or *AtPIN2* were able to bind <sup>3</sup>H-NPA in a specific/saturable manner, with increase in pellet and depletion in SN (red circles) compared to samples with  $20 \mu\text{M}$  unlabeled NPA (black circles). Mock membranes showed no specific/saturable binding (t-test,  $n=3$  or  $4$ ).

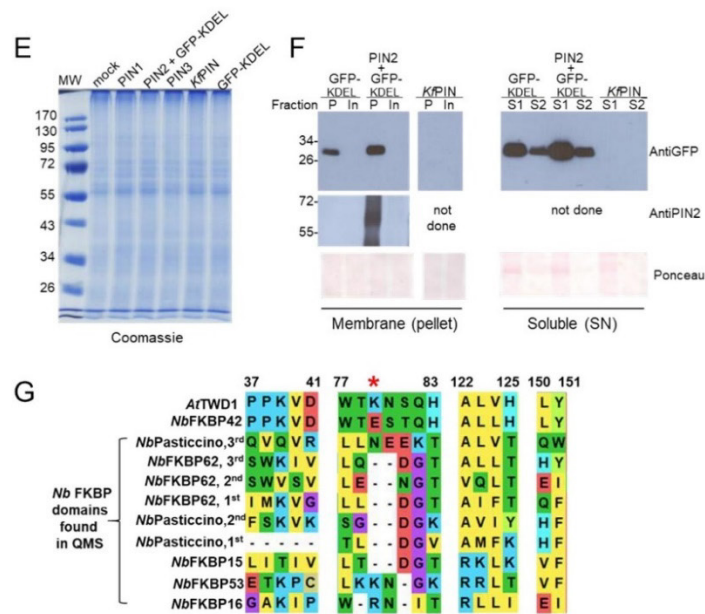




**SI Fig.S2. NPA binds to leaf epidermal membranes overexpressing AtPINs.**

**(D)** Binding of <sup>3</sup>H-NPA to PIN1-expressing *N. benthamiana* membranes is saturable. Total CPM in pellets (upper panels) or SN (centre panels) of PIN1-expressing or mock membranes increased with the amount of <sup>3</sup>H-NPA used in the binding reaction in the absence (+ <sup>3</sup>H-NPA only, filled red triangles) or presence (+ unlabeled NPA, open green triangles) of excess 20 µM unlabeled NPA. The difference between "+ unlabeled NPA" and "+ <sup>3</sup>H-NPA only" is the amount competed by excess unlabeled NPA and thus represents <sup>3</sup>H-NPA specifically bound to pellets and depleted from the SN (lower panels). Specifically-bound <sup>3</sup>H-NPA was seen in PIN1-expressing membranes, but not in mock membranes, both as an increase in pellet (open triangles) and depletion in SN (open squares) and was saturable at higher amounts of total <sup>3</sup>H-NPA added (lower left panel, note different y-axis scale). 60000 cpm theoretically corresponds to ≈90 nM NPA in the final reaction based on the apparent specific activity from supplier.

5



**SI Fig.S2. NPA binds to leaf epidermal membranes overexpressing AtPINs.**

**(E)** Coomassie stained gel of *N. benthamiana* membrane samples used for QMS.

**(F)** AntiPIN2 immunoblots shows complete solubilization of membranes for QMS (left panels). AntiGFP immunoblot shows that although GFP-KDEL partitioned mainly into the soluble SN (right panels), some was also in membrane pellet fraction (P) used for QMS. This may be due to retention in sealed endoplasmic reticulum (ER) vesicles or due to association with membrane-bound KDEL receptors. GFP-KDEL was expressed from a separate ORF (in plasmid pK7WG2D) as a soluble ER luminal protein with a signal peptide and C-terminal KDEL ER-retention marker, and was present in the vector only control and PIN2 (also in pK7WG2D). The K $\beta$ PIN sample (in pMDC7) was used as a negative control. Fractions are P, detergent-solubilized membrane pellet; In, detergent-insoluble membrane pellet; S1, S2, soluble SN. All fractions represent equal amounts of starting material (0.1 mg *N. benthamiana* peel).

**(G)** Sequence analysis of the four clusters of residues that form the NPA binding pocket/groove in AtTWD1/FKBP42 (amino acid residues 37-41, 77-83, 122-125 and 150-151) as identified by Zhu et al (17). All residues except P38 and N80 take part in binding. The *N. benthamiana* FKBP domains identified in QMS only retain limited similarity in the 3<sup>rd</sup> or 4<sup>th</sup> motifs, suggesting they would struggle to bind NPA. The most critical NPA-binding residue K79 (red asterisk \*) in the 2<sup>nd</sup> cluster is changed to E79 in NbFKBP42 and also *N. sylvestris*, *N. tomentosa* and *N. attenuata*, and would be expected to impact on NPA binding. Multiple FKBP domains in NbFKBP62 and NbPasticcino are explained in (H).

**SI Fig.S2. NPA binds to leaf epidermal membranes overexpressing AtPINs.**

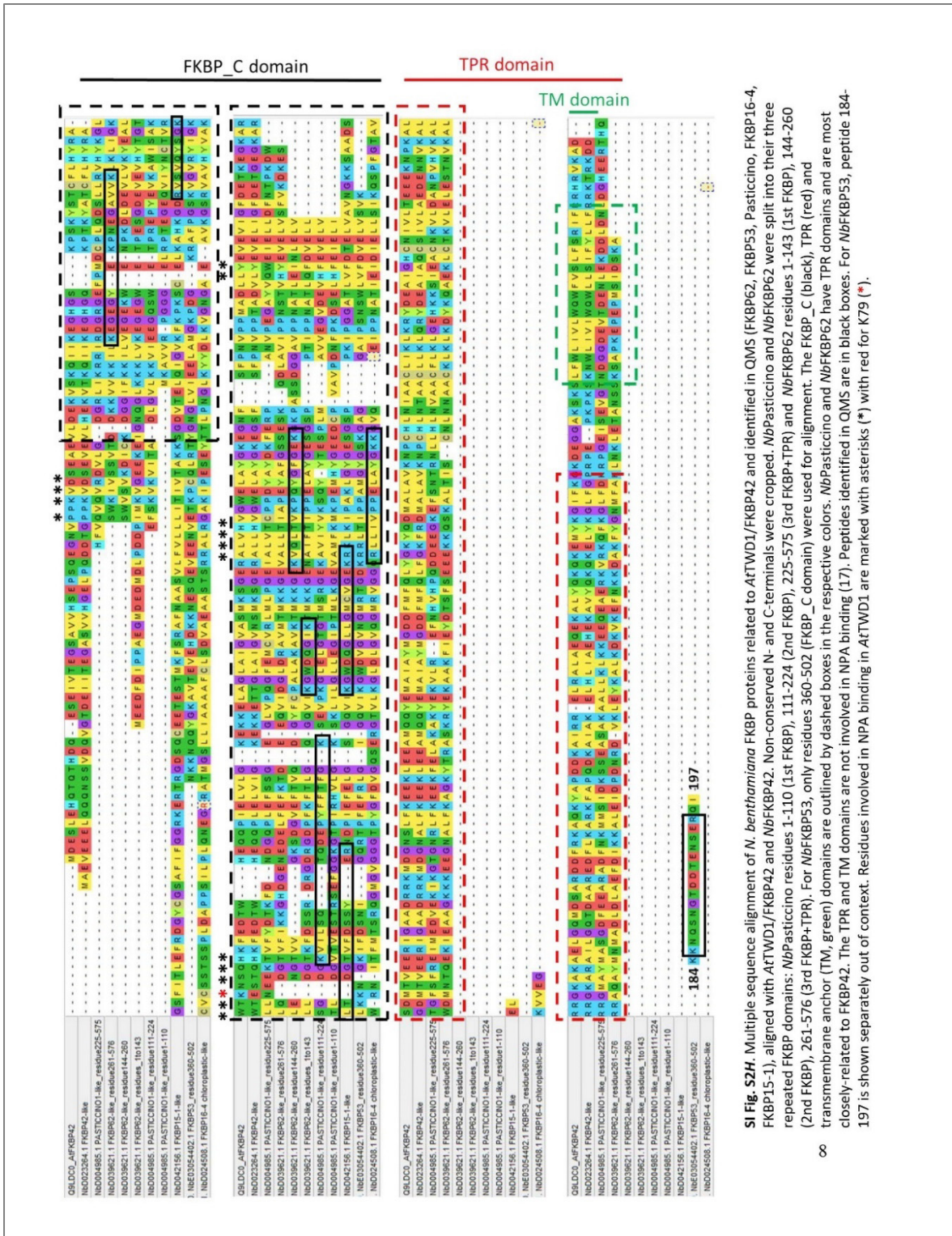
**(H)** Multiple sequence alignment of *N. benthamiana* FKBP proteins related to AtTWD1/FKBP42 and identified in QMS (FKBP62, FKBP53, Pasticcino, FKBP16-4, FKBP15-1), aligned with AtTWD1/FKBP42 and NbFKBP42. Non-conserved N- and C-terminals were cropped. NbPasticcino and NbFKBP62 were split into their 3 repeated FKBP domains: NbPasticcino residues 1-110 (1st FKBP), 111-224 (2nd FKBP), 225-575 (3rd FKBP+TPR) and NbFKBP62 residues 1-143 (1st FKBP), 144-260 (2nd FKBP), 261-576 (3rd FKBP+TPR). For NbFKBP53, only residues 360-502 (FKBP\_C domain) were used for alignment. The FKBP\_C (black), TPR (red) and transmembrane anchor (TM, green) domains are outlined by dashed boxes in the respective colors. NbPasticcino and NbFKBP62 have TPR domains and are most closely-related to FKBP42. The TPR and TM domains are not involved in NPA binding (17). Peptides identified in QMS are in black boxes. For NbFKBP53, peptide 184-197 is shown separately out of context. Residues involved in NPA binding in AtTWD1 are marked with asterisks (\*) with red for K79 (\*).

**(I)** Multiple sequence alignment of the closest *N. benthamiana* homologs of AtAPM1 found in the NbDE proteome. The putative NbAPM1 sequences have 71-75% identity and 82-86% similarity to AtAPM1. None was detected in our QMS analysis.

**(J)** Multiple sequence alignment of *N. benthamiana* CYP proteins identified in QMS (CYP/DGT, CYP19, CYP20, CYP21, CYP26, CYP38), aligned with AtROC1/CYP1 (AT4G38740), closely related *A. thaliana* rotamases and tomato DGT/CYP1. NbD002217 and NbD0014322 are the most closely-related to tomato DGT (95-96 % identical) and we annotate them as NbDGT1 and NbDGT2. Peptides identified in QMS are in black boxes. Identified shared/non-unique peptides are in dashed black boxes and were not used for quantitation. For *N. benthamiana* chloroplastic and mitochondrial sequences, only C-terminal CYP domains were used for alignment and non-conserved N-terminals were cropped. Peptides identified in these cropped regions are not shown, except NbCYP38 peptide 209-214 which is shown separately out of context.

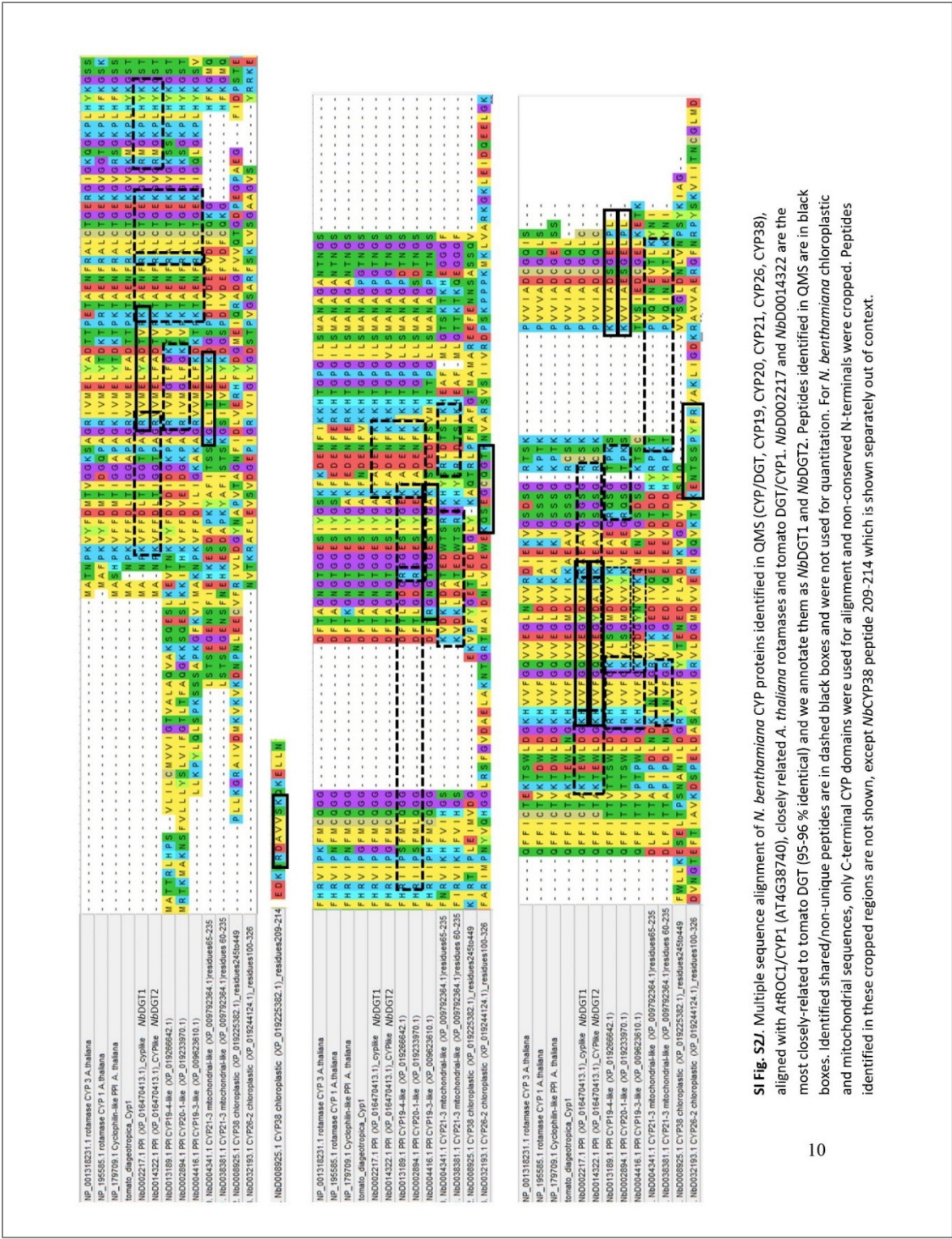
**(K)** Sequence alignment of the 2<sup>nd</sup> cluster of the AtTWD1 NPA binding motif (17) in FKBP42 proteins from selected di- and mono-cotyledons species. The six residues of the cluster are marked by asterisks (\*), K79 is marked by double red asterisks. N80 does not take part in NPA binding (17). K79 is not fully conserved in other species, and is replaced by E, Q or A, with E being the most abundant variant.

7



**SI Fig. S2H.** Multiple sequence alignment of *N. benthamiana* FKBP proteins related to AT1WD1/FKBP42 and identified in QMS (FKBP62, FKBP53, Pasticcino, FKBP16-4, FKBP15-1), aligned with AT1WD1/FKBP42 and *Nb*FKBP42. Non-conserved N- and C-terminals were cropped. *Nb*Pasticcino and *Nb*FKBP62 were split into their three repeated FKBP domains: *Nb*Pasticcino residues 1-110 (1st FKBP), 111-224 (2nd FKBP), 225-575 (3rd FKBP+TPR) and *Nb*FKBP62 residues 1-143 (1st FKBP), 144-260 (2nd FKBP), 261-576 (3rd FKBP+TPR). For *Nb*FKBP53, only residues 360-502 (FKBP\_C domain) were used for alignment. The FKBP\_C domain (black), TPR (red) and transmembrane anchor (TM), green domains are outlined by dashed boxes in the respective colors. *Nb*Pasticcino and *Nb*FKBP62 have TPR domains and are most closely-related to FKBP42. The TPR and TM domains are not involved in NPA binding (17). Peptides identified in QMS are in black boxes. For *Nb*FKBP53, peptide 184-197 is shown separately out of context. Residues involved in NPA binding in AT1WD1 are marked with asterisks (\*) with red for K79 (\*).

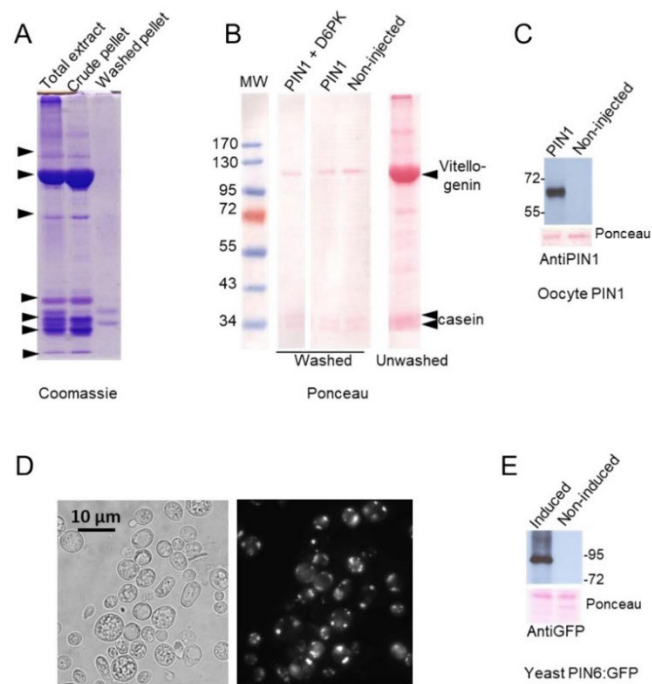




**SI Fig. S2J.** Multiple sequence alignment of *N. benthamiana* CYP proteins identified in QMS (CYP/DGT, CYP19, CYP20, CYP21, CYP26, CYP38), aligned with AtROC1/CYP1 (At4G38740), closely related *A. thaliana* rotamases and tomato DGT/CYP1. NBD002217 and NBD0014322 are the most closely-related to tomato DGT (95-96 % identical) and we annotate them as MBDGT1 and MBDGT2. Peptides identified in QMS are in black boxes. Identified shared/non-unique peptides are in dashed black boxes and were not used for quantitation. For *N. benthamiana* chloroplastic and mitochondrial sequences, only C-terminal CYP domains were used for alignment and non-conserved N-terminals were cropped. Peptides identified in these cropped regions are not shown, except NBD032193 peptide 209-214 which is shown separately out of context.

10





**SI Fig. S3. Expression of PIN1 in oocyte and PIN6:GFP in yeast**

**(A)** Coomassie-stained gel of oocyte samples. Oocyte yolk proteins (vitellogenins, *arrowheads*) were removed from the crude pellet by washing with 100 mM MgCl<sub>2</sub> and 1 M NaCl to give a washed membrane pellet depleted of vitellogenins. All lanes contain 1/50<sup>th</sup> of an oocyte, and in this amount, non-vitellogenin proteins are barely detectable in the washed pellet.

**(B)** Ponceau staining of blotted membrane samples. Washed membranes from PIN1, PIN1 + YFP:D6PK and non-injected oocytes used for <sup>3</sup>H-NPA binding assays contained similar amounts of residual oocyte vitellogenin. Casein is from the buffer. An equivalent amount of unwashed membrane sample with original vitellogenin content is shown as comparison.

**(C)** AntiPIN1 WB of washed membranes from PIN1 and control non-injected oocytes.

**(D)** Bright field (*left*) and epifluorescence (*right*) images of PIN6:GFP in yeast.

**(E)** AntiGFP WB of spheroplast membranes from induced and control non-induced PIN6:GFP yeast.





**SI Fig. S4. NPA inhibits oPDM crosslinking of PIN into dimers**

**(A)** PIN2 in membranes from suspension cells is crosslinked by oPDM *in vitro* into DTE-resistant dimers and this is inhibited by NPA (antiPIN2 WB).

**(B)** NPA did not affect the general chemical reactivity or stability of oPDM. The reactivity of maleimide groups in oPDM towards free thiols of Cys in the presence or absence of NPA was tested using the Ellman's reagent (DTNB) assay. Colorless DTNB is converted to yellow TNB (absorbance at 412 nm) by the free thiols of Cys. As oPDM consumes free thiols, this causes a reduction in Abs<sub>412</sub>. (from **a,b** to **c,d**). Equimolar NPA did not affect the reactivity of OPDM towards Cys (**c** vs. **d**), neither did it affect oPDM stability. NPA also did not affect the reaction between Cys thiols and DTNB (**a** vs. **b**).

**(C)** NPA inhibits oPDM crosslinking of PIN1 in oocyte membranes (WB, antiPIN1) but does not affect crosslinking of the oocyte lipovitellin component of vitellogenin in the same samples (Ponceau).

**(D)** NPA inhibits whereas TIBA, NAA and IAA do not inhibit oPDM crosslinking of PIN1 in oocyte membranes (WB, antiPIN1). Crosslinking of lipovitellin is unaffected in all treatments (Ponceau).

**(E)** Monomers and crosslinked PIN1 dimers from oPDM treatments ( $\pm$  TIBA, NPA, NAA or IAA) were quantified from WBs. Dimer:monomer ratios were calculated and the ratios in oPDM + TIBA/NPA/NAA/IAA expressed as % of the dimer:monomer ratio in oPDM+DMSO controls (100%). Comparison by ANOVA ( $n = 7$  (TIBA) ,11 (NPA) ,5 (NAA) ,8 (IAA); a-b,  $P < .001$ ).

**SI Table S1. Relative abundances of heterologous and selected endogenous *N. benthamiana* proteins from TMT6plex QMS of *N. benthamiana* peel membrane samples.**

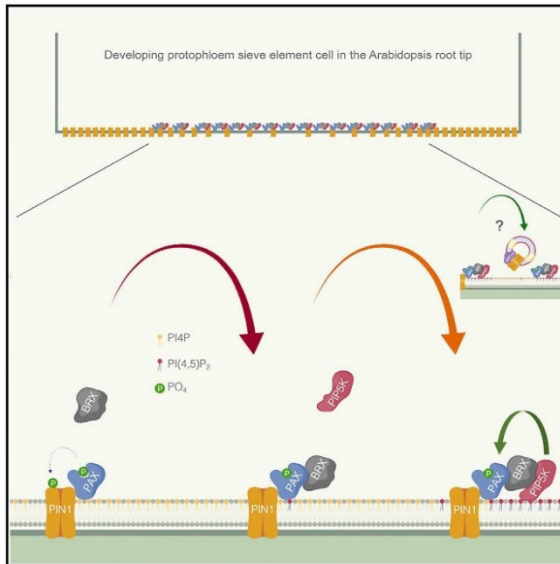
Relative abundance values were based on cumulative reporter ion intensities of all unique non-modified peptides identified for each protein. Raw relative abundance values were used for Fig. 2B. For Fig. 2C, values were normalized to the P19 control using average relative abundance from 3687 *N. benthamiana* proteins in each sample as shown in the table. This accounted for differences in overall protein loading, which was consistent across all proteins in each sample, as shown by the constant ratios between samples in Fig. 2B.



# Developmental Cell

## Plasma Membrane Domain Patterning and Self-Reinforcing Polarity in *Arabidopsis*

### Graphical Abstract



### Authors

Petra Marhava,  
Ana Cecilia Aliaga Fandino,  
Samuel W.H. Koh, ...,  
Ulrich Z. Hammes, Jan Petrášek,  
Christian S. Hardtke

### Correspondence

christian.hardtke@unil.ch

### In Brief

Cell polarity is an intriguing feature of animal and plant development, yet examples of molecular mechanisms that maintain context-specific polarity remain scarce. In their study, Marhava et al. present a self-reinforcing polarity module in plant development, which is necessary for proper differentiation of protophloem, an essential tissue of plant meristems.

### Highlights

- Unique PIN localization in root protophloem depends on the PIN regulators BRX and PAX
- Phosphatidylinositol-4,5-bisphosphate promotes the polarity of PAX and indirectly BRX
- Together, BRX and PAX recruit PIP5Ks to reinforce the polarity of all three proteins
- This self-reinforcing polarity module is required to maintain a local PIN minimum



Marhava et al., 2020, *Developmental Cell* 52, 223–235  
January 27, 2020 © 2019 Elsevier Inc.  
<https://doi.org/10.1016/j.devcel.2019.11.015>

CellPress

# Plasma Membrane Domain Patterning and Self-Reinforcing Polarity in *Arabidopsis*

Petra Marhava,<sup>1</sup> Ana Cecilia Aliaga Fandino,<sup>1</sup> Samuel W.H. Koh,<sup>1</sup> Adriana Jelínková,<sup>2</sup> Martina Kolb,<sup>3</sup> Dorina P. Janacek,<sup>3</sup> Alice S. Breda,<sup>1</sup> Pietro Cattaneo,<sup>1</sup> Ulrich Z. Hammes,<sup>3</sup> Jan Petrásek,<sup>2</sup> and Christian S. Hardtke<sup>1,4,\*</sup>

<sup>1</sup>Department of Plant Molecular Biology, University of Lausanne, Biophore Building, 1015 Lausanne, Switzerland

<sup>2</sup>Institute of Experimental Botany, Czech Acad Sci, Rozvojová 263, 165 02 Praha 6, Czech Republic

<sup>3</sup>Plant Systems Biology, Technical University of Munich, 85354 Freising, Germany

<sup>4</sup>Lead Contact

\*Correspondence: christian.hardtke@unil.ch

<https://doi.org/10.1016/j.devcel.2019.11.015>

## SUMMARY

Cell polarity is a key feature in the development of multicellular organisms. For instance, asymmetrically localized plasma-membrane-integral PIN-FORMED (PIN) proteins direct transcellular fluxes of the phytohormone auxin that govern plant development. Fine-tuned auxin flux is important for root protophloem sieve element differentiation and requires the interacting plasma-membrane-associated BREVIS RADIX (BRX) and PROTEIN KINASE ASSOCIATED WITH BRX (PAX) proteins. We observed “donut-like” polar PIN localization in developing sieve elements that depends on complementary, “muffin-like” polar localization of BRX and PAX. Plasma membrane association and polarity of PAX, and indirectly BRX, largely depends on phosphatidylinositol-4,5-bisphosphate. Consistently, mutants in phosphatidylinositol-4-phosphate 5-kinases (PIP5Ks) display protophloem differentiation defects similar to *brx* mutants. The same PIP5Ks are in complex with BRX and display “muffin-like” polar localization. Our data suggest that the BRX-PAX module recruits PIP5Ks to reinforce PAX polarity and thereby the polarity of all three proteins, which is required to maintain a local PIN minimum.

## INTRODUCTION

Cell polarity is a critical feature of animal and plant development alike (Thompson, 2013). For instance, planar polarity of animal epithelia is a central cue in organ formation (Goodrich and Strutt, 2011), and planar polarity also patterns the plant epidermis (Fischer et al., 2006). Polarly localized proteins frequently provide crucial information in symmetry breaking events, such as stomata formation in *Arabidopsis thaliana* (Dong et al., 2009; Houbaert et al., 2018; Pillitteri et al., 2011) or anteroposterior body axis establishment in *Caenorhabditis elegans* embryos (Nance et al., 2003; Scholze et al., 2018). Interestingly, correct polar segregation of PAR proteins in *C. elegans* one-cell embryos requires cortical patches of the plasma membrane

phospholipid phosphatidylinositol-4,5-bisphosphate (PI(4,5)P<sub>2</sub>), which is itself polarly distributed (Scholze et al., 2018). PI(4,5)P<sub>2</sub> is a phosphatidylinositol derivate found in all eukaryotes and is mainly produced from phosphatidylinositol-4-phosphate (PI4P) by PI4P 5-kinase (PIP5K) enzymes (Boss and Im, 2012; Heilmann, 2016; Meijer and Munnik, 2003; Mueller-Roeber and Pical, 2002) (Figure S1A). Localized PI(4,5)P<sub>2</sub> is important for various processes in *A. thaliana* (Heilmann, 2016; Heilmann and Heilmann, 2015), for example, pollen tube growth (Ischebeck et al., 2008; Sousa et al., 2008; Zhao et al., 2010).

The effects of localized PI(4,5)P<sub>2</sub> reflect at least partly the positive impact of PI(4,5)P<sub>2</sub> on clathrin-mediated endocytosis (Haucke, 2005; He et al., 2017; Heilmann, 2016; Ischebeck et al., 2013; König et al., 2008; Posor et al., 2015). For example, in plants, PI(4,5)P<sub>2</sub> modulates endocytosis of the plasma-membrane-integral PIN-FORMED (PIN) proteins (Ischebeck et al., 2013; Mei et al., 2012; Tejos et al., 2014). PIN proteins are efflux carriers for the phytohormone auxin, a key determinant in various developmental processes (Benjamins and Scheres, 2008). Coordinated polar localization of PIN proteins across cell files imposes directionality on transcellular auxin transport and can create local auxin accumulations that are critical for organ and tissue formation in meristems, the plant growth apices (Benková et al., 2003; Bililou et al., 2005; Friml et al., 2002, 2003; Grieneisen et al., 2007; Petersson et al., 2009). PINs are not only regulated by endocytosis (Geldner et al., 2001; Kleine-Vehn et al., 2011) but also by phosphorylation in their cytoplasmic, so-called hydrophilic loop. These phosphorylation events are catalyzed by plasma-membrane-associated AGC family kinases and generally activate PINs to transport auxin from the cytoplasm into the apoplast (Barbosa and Schwechheimer, 2014; Barbosa et al., 2014; Willige et al., 2013; Zourelidou et al., 2014), although they also influence PIN polarity (Friml et al., 2004; Galván-Ampudia and Offringa, 2007). Interestingly, AGC kinases, such as the prototypical D6 PROTEIN KINASE (D6PK), are themselves frequently polarly localized, together with PIN proteins, and their plasma membrane association depends on basic-hydrophobic patches that mediate interaction with plasma membrane phosphoinositides (Barbosa and Schwechheimer, 2014; Barbosa et al., 2016; Stanislas et al., 2015). PI4P is likely essential for basic AGC kinase plasma membrane association, whereas PI(4,5)P<sub>2</sub> is further required for polar localization (Barbosa et al., 2016; Platre et al., 2018). Both PIN and AGC kinase localization are disturbed in the root epidermis of double loss-of-function mutants for the *PIP5K1* and *PIP5K2*



genes, which together are essential for proper *A. thaliana* development (Barbosa et al., 2016; Ischebeck et al., 2013; Tejos et al., 2014).

We showed that the AGC kinase PROTEIN KINASE ASSOCIATED WITH BRX (PAX) is required for the development of the *A. thaliana* root protophloem, the early phloem that is essential for sustained root growth (Bonke et al., 2003; Depuydt et al., 2013; Rodríguez-Villalón et al., 2014). Phloem sieve tubes distribute nutrients and developmental signals from source to sink organs (Lucas et al., 2013) and are formed from interconnected, enucleated sieve elements (Furuta et al., 2014; Lucas et al., 2013; Rodríguez-Villalón et al., 2014). The peculiar sieve element differentiation process can be observed in the root meristem of *A. thaliana* seedlings, where it is laid out in a spatio-temporal gradient that encompasses ~20–25 cells from stem cell to mature sieve element. Mutants with disturbed root protophloem differentiation display discontinuous sieve tubes and consequently suboptimal sap delivery to the meristem as well as a number of secondary systemic effects collectively referred to as Disturbed Protophloem Syndrome (Anne and Hardtke, 2018). This phenotype is for instance observed in *pax* loss-of-function mutants (Marhava et al., 2018), and its severity can be quantified by the frequency at which developing sieve element precursors fail to differentiate. Such cells stand out because they neither degrade their nucleus nor build up a reinforced cell wall and thus appear as “gaps” that interrupt developing sieve element strand continuity (Anne and Hardtke, 2018).

PAX protein is polarly localized to the rootward end of nascent sieve elements, where it regulates the activity of rootward localized PIN1, the dominant PIN in the developing protophloem (Marhava et al., 2018). This regulation also requires BREVIS RADIX (BRX), a plant-specific plasma-membrane-associated protein that co-localizes with PAX. However, whereas PAX stimulates PIN-mediated cellular auxin export, BRX inhibits this activation. Because BRX plasma membrane association is negatively regulated by threshold auxin levels (Marhava et al., 2018; Scacchi et al., 2009), PAX and BRX are thought to constitute a “molecular rheostat” that fine-tunes auxin flux through the developing sieve element cell file (Marhava et al., 2018). Thus PAX and BRX together promote the gradual auxin increase observed in developing protophloem sieve elements that appears to be crucial for their earlier differentiation relative to neighboring cell files (Marhava et al., 2018; Santuari et al., 2011).

Interestingly, the Disturbed Protophloem Syndrome can also be triggered by overexpression of COTYLEDON VASCULAR PATTERN 2 (CVP2) (Rodríguez-Villalón et al., 2015), a 5-phosphatase that catalyzes the conversion of PI(4,5)P<sub>2</sub> into PI4P (Carland and Nelson, 2009) (Figure S1A). These findings suggest that the PI(4,5)P<sub>2</sub> to PI4P ratio matters for proper protophloem sieve element differentiation, a notion corroborated by partial rescue of the defective protophloem sieve element differentiation in *brx* mutants through *cvp2* second site mutation (Rodríguez-Villalón et al., 2015). Here, we show that BRX and PAX recruit PIP5Ks to partition the plasma membrane into distinct domains, thereby impinging on local PIN1 abundance. Our findings refine the molecular rheostat model and identify a polarity module that reinforces its own localization.

224 Developmental Cell 52, 223–235, January 27, 2020

## RESULTS

### Distinct Mutations in CVP2 Alleviate the *brx* Phenotype to Variable Degrees

We identified additional *cvp2* second site suppressor alleles obtained from random mutagenesis that reverted the *brx* phenotype to variable degrees (Figure S1B). Interestingly, the extent of rescue was not strictly correlated to the assumed allelic strength of the *cvp2* loss-of-function alleles (Figures S1C and S1D). To verify that the *brx* protophloem phenotype is nevertheless associated with elevated PI4P levels in the protophloem, we introduced a PI4P-specific fluorescent biosensor (Vermeer and Munnik, 2013; Vermeer et al., 2009) into the mutant. In comparison to Col-0 wildtype background, PI4P levels appeared to be higher in *brx* protophloem sieve elements (Figures S1E and S1F). Moreover, PI4P was more abundant at the plasma membrane, in line with previous observations (Platre et al., 2018; Simon et al., 2014, 2016) (Figure S1F). Similar experiments with a PI(4,5)P<sub>2</sub> biosensor were inconclusive because of the generally much lower abundance of PI(4,5)P<sub>2</sub> as compared to PI4P (Meijer and Munnik, 2003; Munnik and Nielsen, 2011; Simon et al., 2014). CVP2-CITRINE fusion protein detected by immunostaining with anti-GFP antibody displayed shootward plasma membrane association but also intracellular localization and some rootward plasma membrane association in developing protophloem cells (Gujas et al., 2017) (Figure S1G). Since *cvp2* mutation results in increased PI(4,5)P<sub>2</sub> levels (Carland and Nelson, 2004; Rodríguez-Villalón et al., 2015), our data support the idea that *cvp2* mutations alleviate the *brx* phenotype indirectly, through shifting the phosphoinositide balance in developing protophloem sieve elements.

### Polar PAX Localization Is Sensitive to PI(4,5)P<sub>2</sub> Levels

One component that could be sensitive to phosphoinositide balance is PAX, because similar to other AGC kinases it localizes to the plasma membrane through interaction of a basic-hydrophobic patch with phosphoinositides (Barbosa et al., 2016). This motif is essential for efficient plasma membrane association of AGC kinases but does not influence their kinase activity (Barbosa et al., 2016). We sought to confirm its relevance for PAX localization in the protophloem by expressing a PAX-CITRINE fusion protein variant in which six pertinent basic amino acids were replaced by alanines (PAX<sup>K/R>A</sup>) *in planta* (Barbosa et al., 2016). Indeed, this variant PAX protein did not display the strong, polar plasma membrane association typical of the wildtype protein (Figures 1A and 1B). Moreover, the PAX<sup>K/R>A</sup>-CITRINE variant could not complement the *pax* mutant phenotype (Figure 1C), corroborating that PAX plasma membrane association is essential for its function. BRX plasma membrane recruitment largely depends on PAX, while PAX-CITRINE plasma membrane association does not substantially depend on BRX, although PAX-CITRINE levels are more variable in *brx* mutants (Marhava et al., 2018). We generated an anti-PAX antibody for immunostaining to confirm that PAX abundance at the plasma membrane is more variable in *brx* as compared to wildtype but also found it to be overall reduced (Figures 1D and 1E). To determine whether this reduction might be related to shifted phosphoinositide balance in *brx*, we also monitored PAX abundance in different *brx cvp2* double

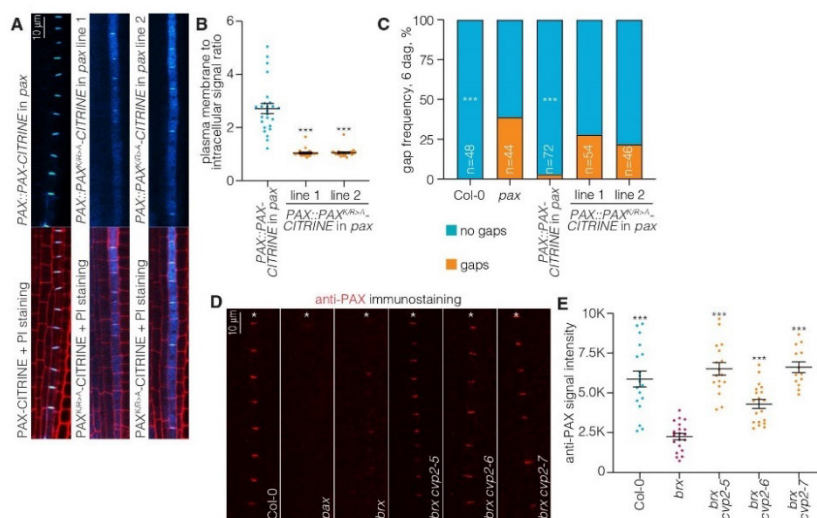


**Figure 1. PAX Plasma Membrane Association Is Determined by Phosphoinositides**

(A) Top, confocal microscopy of *A. thaliana* root meristems that express a PAX-CITRINE fusion protein under control of the PAX promoter (*PAX::PAX-CITRINE*) in a *pax* loss-of-function mutant, as compared to a *PAX<sup>KR5A</sup>-CITRINE* variant. Bottom, overlay of top with the cell outlines indicated by propidium iodide (PI) cell wall staining (red). In images throughout all figures, the root tip is toward the bottom.

(B) Quantification of plasma membrane versus cytoplasmic signal intensity (arbitrary units; 24–25 roots, 5–8 cells per root) of PAX-CITRINE or *PAX<sup>KR5A</sup>-CITRINE* fusion protein. Statistically significant difference (one-way ANOVA) compared to PAX-CITRINE is indicated.

(C) Quantification of gap cell frequency in protophloem strands of six-day-old root meristems of indicated genotypes. Col-0 is the wildtype background for all mutants analyzed in this study. Statistically significant difference (chi square test) compared to *pax* is indicated.

(D) Detection of endogenous PAX using anti-PAX antibody immunostaining in the protophloem strands (asterisks) of indicated genotypes.

(E) Quantification of anti-PAX signal intensity (arbitrary units; 13–20 roots, 5–8 cells per root). Statistically significant difference (one-way ANOVA) compared to *brx* is indicated.

Plots display individual values (dots), the mean (wide bars), and the standard error of the mean (whiskers). \* =  $p < 0.05$ ; \*\* =  $p < 0.001$ ; \*\*\* =  $p < 0.001$ ; See [Data S1](#) for statistical test details. See also [Figure S1](#).

mutants. Interestingly, compared to *brx*, PAX plasma membrane abundance was increased in *brx cvp2* double mutants, although the increase did not strictly correlate with the extent of phenotypic rescue ([Figures 1D, 1E, S1C, and S1D](#)). These results confirm that polar PAX plasma membrane association does not directly require BRX ([Marhava et al., 2018](#)) but is rather determined by PI(4,5)P<sub>2</sub> abundance ([Barbosa et al., 2016](#); [Platre et al., 2018](#)).

#### ***pip5k1 pip5k2* Double Mutants Display Severely Disturbed Protophloem Differentiation**

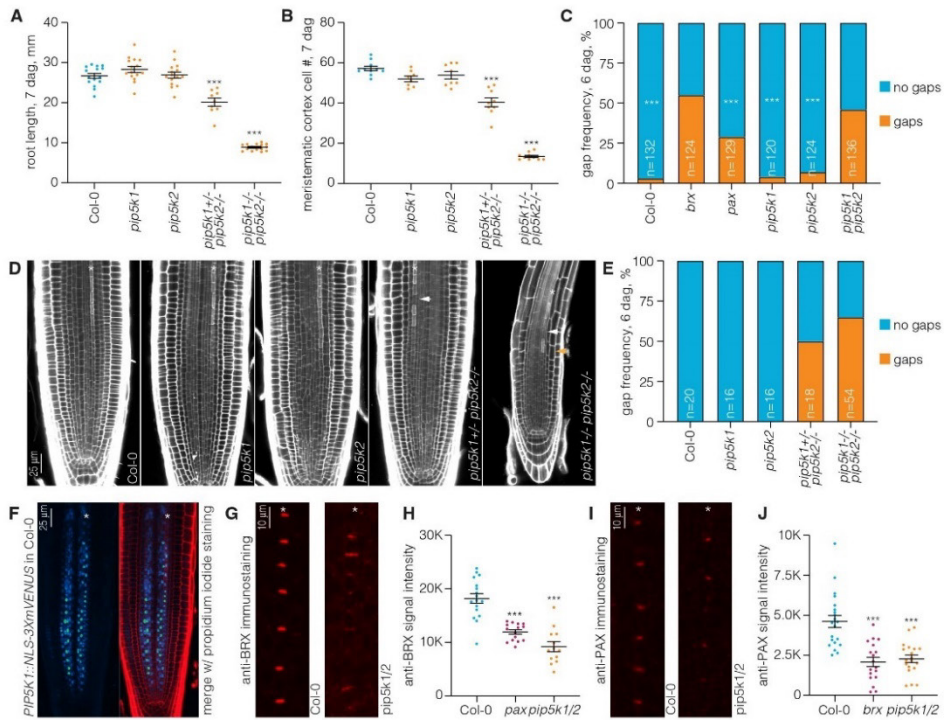
Involvement of PI(4,5)P<sub>2</sub> in protophloem development has also been suggested by the observation that *CVP2* overexpression in Col-0 wildtype mimics the *brx* phenotype ([Rodríguez-Villalon et al., 2015](#)). A genetically similar situation could be created through PIP5K knock out. Indeed, we found that *pip5k1 pip5k2* double mutants not only display a shorter root and a smaller root meristem ([Ischebeck et al., 2013](#); [Tejos et al., 2014](#); [Figures 2A and 2B](#)) but also severely disturbed protophloem development ([Figures 2C and 2D](#)). This phenotype was dosage-dependent, since *pip5k2* single mutants in combination with *pip5k1*

heterozygosity already showed an intermediate phenotype ([Figures 2D and 2E](#)).

Whereas broad expression throughout the root tip was reported for *PIP5K2*, *PIP5K1* expression was observed specifically in the vasculature ([Tejos et al., 2014](#)). Our analysis of the *PIP5K1* gene expression pattern by a reporter gene construct (*PIP5K1::NLS-3XmVENUS*) confirmed vascular *PIP5K1* expression but also indicated that it was restricted to the root phloem poles and procambial cells ([Figure 2F](#)). Thus, in line with the mutant phenotypes and transcriptomic data ([Table S1](#)), *PIP5K1* is dominant in the developing protophloem.

Since the severe sieve element differentiation defects of *pip5k1 pip5k2* double mutants mimicked the *brx* mutant root phenotype, we monitored both BRX and PAX abundance and localization by immunostaining. Consistent with PI(4,5)P<sub>2</sub> being a major determinant of PAX localization, and with PAX in turn being a major determinant of BRX localization, both BRX and PAX plasma membrane abundance were drastically reduced in *pip5k1 pip5k2* double mutants ([Figures 2G–2J](#)). In line with this observation, *pip5k* mutations did not further enhance the *brx* or *pax* phenotypes ([Figures S2A–S2C](#)). In summary, the *pip5k1*





*pip5k2* root phenotype was associated with severely reduced plasma membrane association of BRX and PAX and therefore could partly be interpreted in the context of the Disturbed Protophloem Syndrome.

#### PIP5K1 and PIP5K2 Interact and Co-localize with BRX and PAX in Developing Protophloem

We also obtained independent hints that PIP5Ks could play a role in protophloem development from proteomics data. In

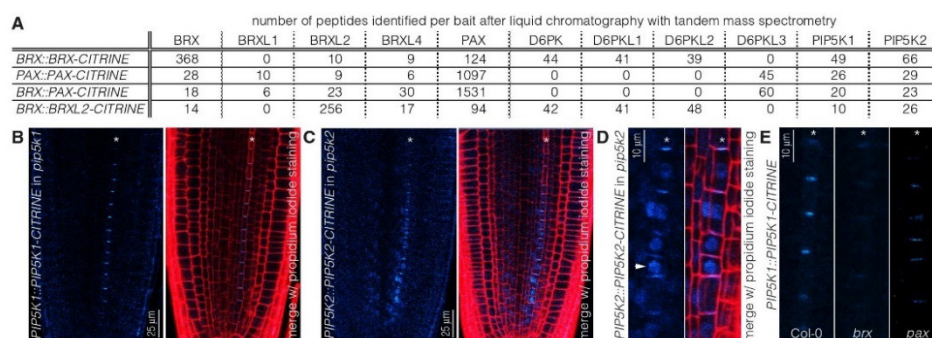


**Figure 3. Interaction and Co-localization of BRX and PAX with PIP5K1/2**

(A) Number of specific peptides isolated after immunoprecipitation of BRX, PAX, or BRXL2 CITRINE fusion proteins in the VISUAL transdifferentiation assay. (B and C) Confocal microscopy of root meristems expressing PIP5K1-CITRINE (B) and PIP5K2-CITRINE (C) fusion proteins expressed under control of their native promoters in the respective single mutant backgrounds (left panels) and overlaid with propidium iodide staining (right panels).

(D) Magnification of *PIP5K2::PIP5K2-CITRINE* expression closer the stem cell niche. Arrowhead points out PIP5K2 nuclear localization.

(E) Plasma membrane association of PIP5K1-CITRINE fusion protein detected by confocal live imaging in developing protophloem sieve elements of indicated genotypes.

Asterisks indicate protophloem sieve elements cell files.

immunoprecipitations of BRX-CITRINE fusion protein from transdifferentiating phloem sieve elements (Kondo et al., 2016; Marhava et al., 2018), combined PIP5K1 and PIP5K2 peptides were nearly as abundant as PAX peptides in replicate experiments (Figure 3A). Similar experiments with PAX-CITRINE fusion protein, expressed either under control of its native or the *BRX* promoter, not only confirmed its interaction with BRX but pulled down PIP5K1 and PIP5K2 as well (Figure 3A). Neither BRX, nor PAX or PIP5Ks were detected in similar immunoprecipitations with control fusion proteins, such as the plasma-membrane-associated MEMBRANE ASSOCIATED KINASE REGULATOR 5 (MAKR5) (Kang and Hardtke, 2016), the plasma-membrane-integral LOW TEMPERATURE INDUCED PROTEIN 6b (LTI6b) (Cutler et al., 2000), or cytoplasmic GFP. Consistently, confocal live imaging of PIP5K1-CITRINE and PIP5K2-CITRINE fusion proteins expressed under control of their native promoters confirmed the expression patterns (Tejos et al., 2014) and revealed strongly polar, rootward association of both proteins with the plasma membrane specifically in protophloem (Figures 3B and 3C). Closer to the stem cell niche, PIP5K2-CITRINE (unlike PIP5K1-CITRINE) was also often found in the nucleus (Gerth et al., 2017; Tejos et al., 2014) (Figure 3D). These findings suggested that both PIP5K1 and PIP5K2 could co-localize with BRX and PAX in developing sieve elements.

Although our proteomics data cannot be considered strictly quantitative, it was notable that the relative abundance of combined PIP5K peptides as compared to bait peptides was several fold higher in BRX-CITRINE pull-downs than in PAX-CITRINE pull-downs (Figure 3A), suggesting that BRX might be the primary interactor of PIP5Ks. Moreover, similar to BRX, PIP5K1-CITRINE polarity was strongly reduced and patchy in *pax* mutants and consistently barely detectable in *brx* mutants (Figure 3E). Together, these results suggest that BRX and PAX are in complex with PIP5Ks.

### PIN Proteins Display a Unique Localization in Developing Protophloem Sieve Elements

Detection of PIP5K1-CITRINE by immunostaining with anti-GFP antibody confirmed its rootward polarity in developing protophloem sieve elements (Figures 4A and 4B). Moreover, 3D reconstruction showed restriction of the signal to the inner area of the plasma membrane, in a round, “muffin-like” configuration (Figure 4C). We observed similar, “muffin-like” localization for both BRX and PAX-CITRINE by immunostaining with anti-BRX or anti-GFP antibody, respectively (Figure 4D), consistent with the mutual interactions between the three proteins suggested by the immunoprecipitations. This “muffin-like” localization was also evident in confocal live imaging (Figure S3A). Interestingly, the “muffin-like” localization was complementary to a partly overlapping “donut-like” localization of PIN1 around the edges of the rootward plasma membrane as detected by anti-PIN1 immunostaining (Figures 4E and 4F) or confocal live imaging (Figures S3B–S3D). Similar “donut-like” localization was observed for a PIN3-GFP fusion protein detected with anti-GFP antibody (Figure 4G), although it was in general barely visible because of its low abundance in the protophloem (Marhava et al., 2018). The peculiar “donut-like” PIN1 and PIN3 localization was specific for developing protophloem sieve elements and not observed in neighboring cell files, where PIN proteins were evenly distributed throughout the rootward plasma membrane (Figure 4H). Yet, PIN1 displayed a “muffin-like” configuration in a small portion of developing sieve elements. However, upon closer inspection we found that this localization typically occurred at the forming cell plate of dividing cells, as indicated by simultaneous immunostaining with an anti-KNOLLE antibody (Lauber et al., 1997) (Figure 4I). Interestingly, unlike PIN1, both BRX and PAX were absent from cell plates (Figures 4J and 4K). Finally, various plasma-membrane-integral control fusion proteins, such as eGFP-LTI6b (Cutler et al., 2000), YFP-AUX1 (Bennett et al., 1996), or protophloem-specific

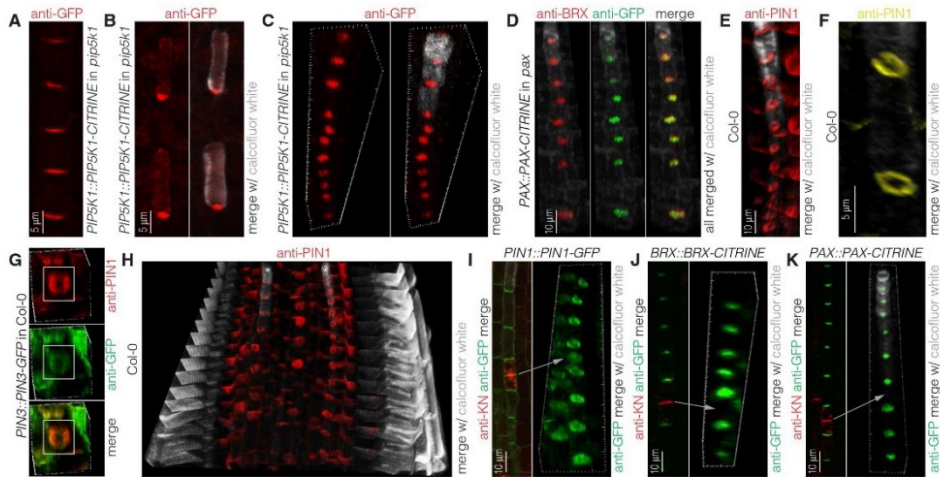


**Figure 4. PIP5K and PIN1 Localization in Developing Protophloem Sieve Elements**

(A and B) Immunolocalization of PIP5K1-CITRINE fusion protein by anti-GFP antibody in intact (A) and squashed (B) protophloem strands and counterstained with Calcofluor white (B, right panel). Note that developing sieve elements become detached in (B).

(C) Three-dimensional (3D) reconstruction of PIP5K1-CITRINE localization detected by immunostaining with anti-GFP antibody (left) and overlaid with Calcofluor white stain (right).

(D) 3D reconstruction of simultaneous detection of endogenous BRX using anti-BRX antibody (left panel, red) and PAX-CITRINE using anti-GFP antibody (middle panel, green), demonstrating co-localization (overlay, right panel) in the center of developing sieve elements ("muffin-like" localization).

(E) 3D reconstruction of PIN1 localization detected by anti-PIN1 antibody (red) in Col-0 protophloem sieve elements (overlaid with Calcofluor white staining).

(F) High-resolution close up 3D reconstruction of PIN1 detected by anti-PIN1 antibody (yellow) in Col-0 protophloem sieve elements (overlaid with Calcofluor white staining).

(G) 3D reconstruction of simultaneous PIN1 (detected by anti-PIN1 antibody, top panel, red) and PIN3-GFP (detected by anti-GFP antibody, middle panel, green) immunostaining and overlay (bottom panel). Developing protophloem sieve elements (boxed) viewed below from the root tip, note the localization around the plasma membrane edge ("donut-like" localization).

(H) 3D reconstruction of PIN1 localization detected by anti-PIN1 antibody (red) in a Col-0 root meristem, overlaid with Calcofluor white staining. Protophloem sieve element cell files are marked by asterisks.

(I–K) 2D images (left panels) and corresponding 3D reconstructions (right panels) of PIN1-GFP (I), BRX-CITRINE (J), and PAX-CITRINE (K) fusion proteins detected by anti-GFP antibody (green) and simultaneous co-staining with anti-KNOLLE antibody (left panels, red). The arrows indicate the corresponding positions of the newly forming cell plates marked by KNOLLE.

Axis scales in 3D panels (C) and (G–K) indicate 1- $\mu$ m steps, in each case  $\sim$ 150  $\mu$ m total protophloem strands were imaged. See also Figure S3.

BRASSINOSTEROID INSENSITIVE 1 (BRI1-CITRINE) (Kang et al., 2017), were detected throughout the rootward plasma membrane in anti-GFP immunostaining (Figures S3E–S3J), corroborating that the "donut-like" PIN localization was not a generic structural feature of developing sieve elements.

#### BRX, PAX, and PIP5Ks Determine PIN Localization in Developing Protophloem Sieve Elements

We confirmed the complementary, partially overlapping localizations of BRX and PAX on the one side and PIN1 on the other by simultaneous immunodetection of either BRX and PIN1-GFP (Figures 5A and 5B) or PAX-CITRINE and PIN1 (Figures 5C and 5D). Moreover, given the regulatory relation between BRX, PAX, and PIN1 in protophloem sieve element differentiation (Marhava et al., 2018), we sought to determine whether "donut-like" PIN1 localization depends on BRX or PAX. Immunostaining with anti-PIN1 antibody indicated that PIN1

abundance indeed increased in the muffin area both in *brx* and *pax* mutants (Figures 5E–5G and S3K). Moreover, a strong increase in the occurrence of aberrant PIN1 configuration was also observed in *pip5k1 pip5k2* double mutants (Figures 5F and 5G), consistent with the severely reduced BRX and PAX plasma membrane association in this background. Quantitatively, the absence of PAX had the strongest impact on PIN1 localization (Figure 5G). This was corroborated by the observation that in *brx cvp2* double mutants, in which PAX plasma membrane abundance was increased (Figures 1D and 1E), the proportion of "donut-like" PIN1 localization was substantially restored (Figures 5H and S4A).

Interestingly, PAX cannot be fully replaced by a fusion protein of the related D6PK that is expressed under control of the PAX promoter, despite rootward D6PK-CITRINE localization in *pax* protophloem sieve elements (Marhava et al., 2018; Figure S5A). Parallel anti-GFP and anti-PIN1 immunostaining indicated that

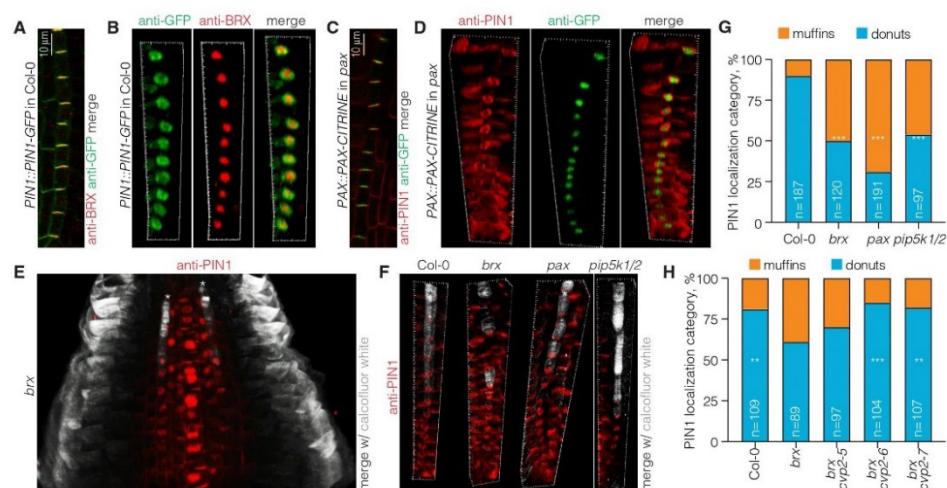


**Figure 5. PIN1 “Donut-like” Localization in Developing Protophloem Sieve Elements Depends on BRX, PAX, and PIP5Ks**

(A and B) 2D (A) and 3D reconstruction (B) of simultaneous immunolocalization of PIN1-GFP (detected by anti-GFP antibody, left panel, green) and BRX (detected by anti-BRX antibody, middle panel, red), revealing complementary-overlapping localization of BRX and PIN1 (overlay, right panel, and [A]). (C and D) 2D (C) and 3D reconstruction (D) of simultaneous immunolocalization of PIN1 (detected by anti-PIN1 antibody, left panel, red) and PAX-CITRINE (detected by anti-GFP antibody, middle panel, green), revealing complementary-overlapping localization of PAX and PIN1 (overlay, right panel, and [C]).

(E) 3D reconstruction of PIN1 localization detected by anti-PIN1 antibody (red) in a *brx* root meristem, overlaid with Calcofluor white staining. Protophloem sieve element cell files are marked by asterisks.

(F) 3D reconstruction of PIN1 localization detected by anti-PIN1 antibody (red) in root meristems of indicated genotypes, overlaid with Calcofluor white staining. Protophloem sieve element cell files are marked by asterisks.

(G) Quantification of PIN1 localization in protophloem strands of five-day-old root meristems of indicated genotypes, categorized into “donut-like” or “muffin-like” configuration as detailed in Figure S3K. Statistically significant difference (chi square test) compared to Col-0 is indicated.

(H) Quantification of PIN1 localization in protophloem strands of 5-day-old root meristems of indicated genotypes, categorized into “donut-like” or “muffin-like” configuration. Statistically significant difference (chi square test) compared to *brx* is indicated.

(E) Quantification of PIN1 localization in protophloem strands of 5-day-old root meristems of indicated genotypes, categorized into “donut-like” or “muffin-like” configuration. Statistically significant difference (chi square test) compared to *brx* is indicated. Axis scales in 3D panels (B), (D), (E), and (F) indicate 1- $\mu$ m steps, in each case  $\sim$ 150  $\mu$ m total protophloem strands were imaged. \* =  $p < 0.05$ ; \*\* =  $p < 0.001$ ; \*\*\* =  $p < 0.001$ ; See Data S1 for statistical test details. See also Figure S4.

consistently, “donut-like” PIN1 localization was not fully restored by D6PK-CITRINE (Figure S5B) although BRX plasma membrane association was essentially recovered (Figure S5C). Moreover, D6PK-CITRINE localization was broader than PAX localization and also showed a wider overlap with PIN1 (Figure S5A). Collectively, our observations suggest that the “donut-like” PIN1 localization observed in developing protophloem sieve elements specifically depends on the combined presence of BRX and PAX.

#### Unique PIN1 Localization Contributes to Properly Integrated Protophloem Differentiation

The finding that (partially) restored “donut-like” PIN1 localization coincided with partial rescues of *brx* or *pax* protophloem defects suggested that PIN1 localization contributes to sieve element differentiation, which we sought to corroborate independently. *BRX* and the related *BRX-LIKE* (*BRXL*) genes are highly conserved among the angiosperms, yet they cluster into distinct groups (Beuchat et al., 2010). In *A. thaliana*, the closest *BRX* homolog *BRXL1* is not expressed in the proto-

phloem (Scacchi et al., 2009). However, ectopic expression of *BRXL1* can rescue the *brx* mutant phenotype (Beuchat et al., 2010; Briggs et al., 2006). By contrast, at best partial rescue was observed with ectopic expression of the more distantly related *BRXL2-4* genes. To confirm this result, we expressed a CITRINE fusion of the representative *BRXL2* protein under control of the *BRX* promoter (*BRX::BRXL2-CITRINE*) in the *brx* mutant background. Again, only partial rescue was observed, both with respect to overall root growth and the frequency of protophloem gaps (Figures 6A and 6B), despite correct *BRXL2-CITRINE* expression and localization at the rootward end of developing protophloem sieve elements, in a “muffin-like” configuration, similar to *BRX* (Figures 6C and 6D). However, “donut-like” PIN1 localization was essentially restored by *BRXL2-CITRINE* (Figure 6E). In line with this observation, *BRXL2-CITRINE* immunoprecipitation from transdifferentiating phloem sieve elements pulled down PAX as well as PIP5K1 and PIP5K2 with roughly the same efficiency as *BRX-CITRINE* (Figure 3A). In summary, *BRXL2* displayed similar protein localization and interaction characteristics as *BRX*.

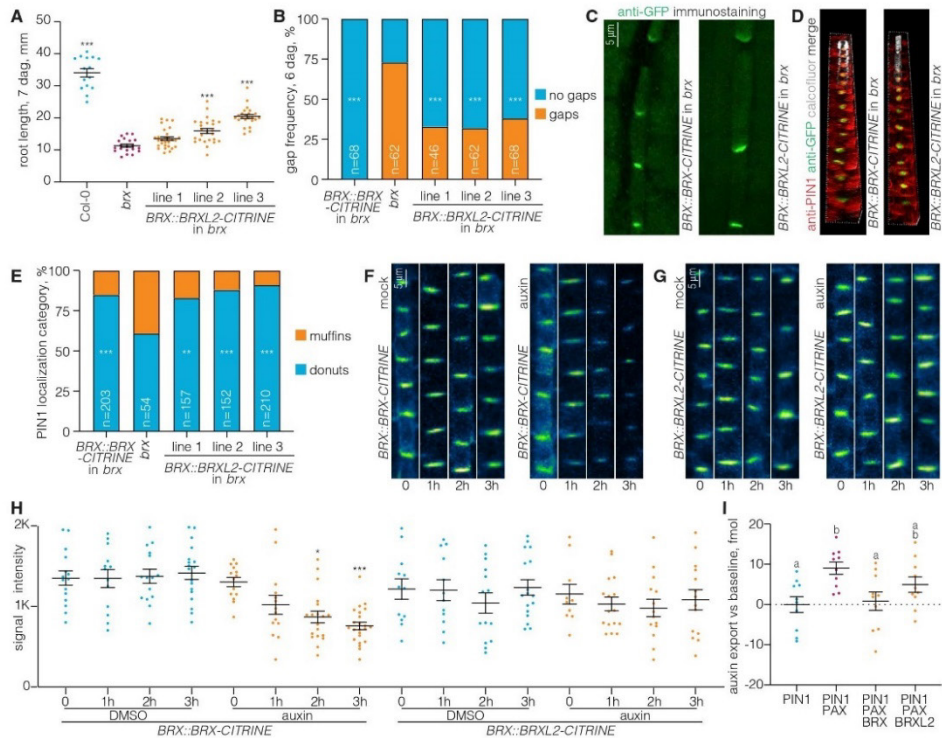


**Figure 6. Comparison of BRX and BRXL2 Characteristics**

(A) Quantification of primary root length of 7-day-old seedlings expressing BRXL2-CITRINE fusion protein under control of the *BRX* promoter (*BRX::BRXL2-CITRINE*) in *brx* mutant background as compared to controls (three independent representative lines). Statistically significant difference (one-way ANOVA) compared to *brx* is indicated.

(B) Quantification of gap cell frequency in protophloem strands of 6-day-old root meristems of indicated genotypes. Statistically significant difference (chi square test) compared to *brx* is indicated.

(C) Immunolocalization of BRX-CITRINE (left) and BRXL2-CITRINE (right) fusion protein detected by anti-GFP antibody in the protophloem of squashed roots, note that developing sieve elements become detached.

(D) 3D reconstruction overlay of simultaneously immunolocalized PIN1 (detected by anti-PIN1 antibody, red) and BRXL2-CITRINE fusion protein (detected by anti-GFP antibody, green), contrasted with Calcofluor white staining.

(E) Quantification of PIN1 localization in protophloem strands of 6-day-old root meristems of indicated genotypes, categorized into “donut-like” or “muffin-like” configuration. Statistically significant difference (chi square test) compared to *brx* is indicated.

(F and G) Response of BRX-CITRINE (F) and BRXL2-CITRINE (G) fusion proteins to treatment with 10  $\mu$ M auxin (NAA) at indicated time points compared to mock treatment (DMSO).

(H) Quantification of BRX-CITRINE and BRXL2-CITRINE signal intensities (arbitrary units; 10–23 roots, 5–8 cells per root). Statistically significant difference (one-way ANOVA) compared to mock-treated parallel sample is indicated.

(I) Auxin transport assays performed in *Xenopus laevis* oocytes, measuring retention of radio-labeled auxin in oocytes in the presence of indicated heterologous plant proteins ( $n = 10$  oocytes per time point). Data points indicate fmol of auxin exported after 1 h as compared to the baseline set by the average of the PIN1 sample. Statistically significant different groups (a and b) (one-way ANOVA) are indicated.

Axis scales in 3D panels (D) indicate 1- $\mu$ m steps, in each case  $\sim 150$   $\mu$ m total protophloem strands were imaged. Plots display individual values (dots), the mean (wide bars), and the standard error of the mean (whiskers). \* =  $p < 0.05$ ; \*\* =  $p < 0.001$ ; \*\*\* =  $p < 0.0001$ ; See [Data S1](#) for statistical test details. See also [Figure S5](#).

To determine why BRXL2 can only partially rescue the *brx* protophloem defects despite these similarities with BRX, we monitored additional BRX hallmarks that are integral for the “molecular rheostat” model ([Marhava et al., 2018](#)). Auxin treatment results in

gradual BRX dissociation from the plasma membrane and its degradation ([Marhava et al., 2018](#); [Scacchi et al., 2009](#)). Parallel experiments with plants expressing either BRX-CITRINE or BRXL2-CITRINE confirmed this behavior for BRX-CITRINE

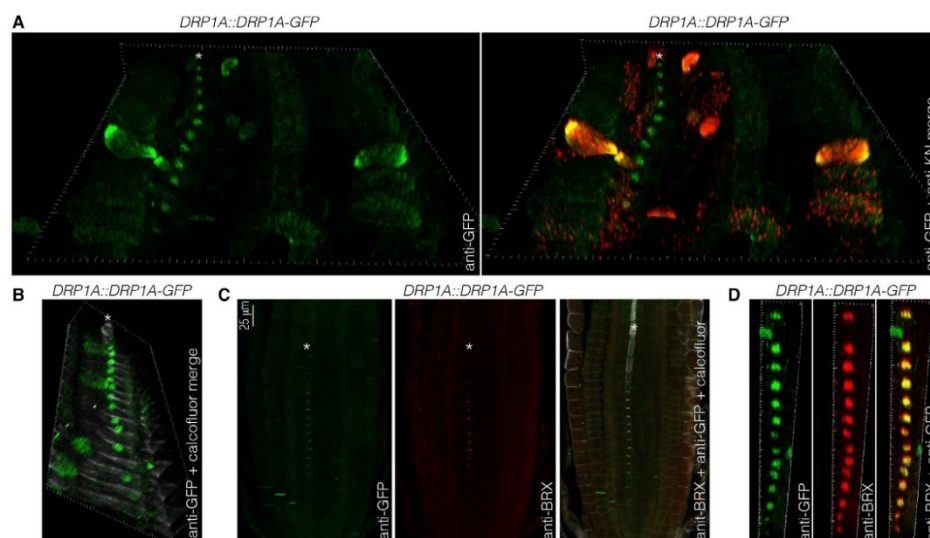


**Figure 7. The BRX-PAX-PIP5K1 Module Correlates with a Marker of Active Endocytosis**

(A) 3D reconstruction of simultaneous immunolocalization of DRP1A-GFP (detected by anti-GFP antibody, left panel, green) and KNOLLE (detected by anti-KNOLLE antibody, overlaid in right panel, red) in a Col-0 root meristem. Note that outside of the protophloem sieve element cell file, equally strong DRP1A signal is only found at the cell plate of dividing cells.

(B) 3D reconstruction of DRP1A-GFP detected by anti-GFP antibody immunostaining, counterstained with Calcofluor white.

(C) Simultaneous immunolocalization of DRP1A-GFP (detected by anti-GFP antibody immunostaining, left panel, green) and BRX (detected by anti-BRX antibody immunostaining, middle panel, red), counterstained with Calcofluor white (overlay, right panel).

(D) Same immunolocalization as in (C), 3D reconstruction.

Axis scales in 3D panels (A), (B), and (D) indicate 1- $\mu$ m steps, in each case  $\sim$ 150  $\mu$ m total protophloem strands were imaged. Protophloem sieve element cell files are marked by asterisks.

(Figure 6F); however, it was not observed for BRXL2-CITRINE, which remained associated with the plasma membrane and did not change in abundance (Figures 6G and 6H). Moreover, in *Xenopus laevis* oocytes, auxin efflux through PIN proteins is stimulated upon co-expression of D6PK or related AGC kinases such as PAX, although PAX is a comparatively weak activator (Marhava et al., 2018; Zourelidou et al., 2014). Additional co-expression of BRX inhibits auxin efflux stimulation by PAX (Marhava et al., 2018). By comparison, BRXL2 could not reduce auxin efflux to the same extent in this assay (Figure 6I). In summary, our data suggest that BRXL2 is not auxin-responsive and only a weak antagonist of PAX. This difference in functionality as compared to BRX might explain why BRXL2 could not fully rescue the *brx* mutant phenotype. The observation that this partial rescue coincided with restored “donut-like” PIN1 localization (Figure 6E) suggests that the latter is partly responsible for the correct progression of protophloem sieve element differentiation, but not sufficient.

#### The BRX-PAX-PIP5K Module Creates a Plasma Membrane Domain of Reduced PIN Abundance

The observation that BRXL2 could restore correct PIN1 localization suggested that PIP5K recruitment was sufficient to mediate

this aspect of BRX action. Because PI(4,5)P<sub>2</sub> enhances clathrin-mediated PIN endocytosis (Ischebeck et al., 2013; Mei et al., 2012; Tejos et al., 2014), this could also mean that the “donut-like” configuration is created by a local increase of PIN1 endocytosis in the “muffin-like” area of the plasma membrane. A specific component of clathrin-mediated endocytosis in plants is DYNAMIN-RELATED PROTEIN 1 A (DRP1A), which catalyzes fission of endocytic vesicles and is a marker of sites of active endocytosis (Fujimoto et al., 2010). DRP1A is typically found at the cell plate of dividing cells, where it is required for correct PIN localization (Mravec et al., 2011; Figure 7A). Interestingly however, it has been observed that DRP1A is rootward polar localized in developing protophloem sieve elements (Dettmer et al., 2014). By monitoring a DRP1A-GFP fusion protein by immunostaining, we could confirm this localization (Figures 7A and 7B) and again observed its association with the “muffin-like” subdomain, co-localizing with BRX (Figures 7C and 7D). Collectively, these observations are congruent with the notion that PIP5K recruitment to the rootward plasma membrane by the BRX-PAX-PIP5K module creates a local hotspot of clathrin-mediated PIN endocytosis that could be responsible for the complementary, “donut-like” PIN1 localization.

## DISCUSSION

### BRX, PAX, and PIP5Ks Constitute a Self-Reinforcing Polarity Module

Cell polarity is a fundamental characteristic of eukaryotic cells, from yeast to human, including plants (Goodrich and Strutt, 2011; Thompson, 2013; Zhang and Dong, 2018). Although an increasing number of polar proteins and polarity determinants have been described over recent years, it often remains unclear how they organize their own polarity. Self-reinforcing polarity mechanisms have been predicted, but examples remain scarce (Thompson, 2013). Our study proposes a scenario for self-reinforcing cellular polarity in plants. Although it remains unclear which mechanisms confer initial, PIP5K-independent PAX polarity, our data support a model in which PAX recruits BRX into a polar “bridgehead” that once established, allows both proteins to stabilize their localization through their interaction with PIP5Ks. That is, because PI(4,5)P<sub>2</sub> promotes PAX plasma membrane association (Barbosa et al., 2016; Platre et al., 2018), local PI(4,5)P<sub>2</sub> biosynthesis reinforces the polarity of all three components. Simultaneously, the local PI(4,5)P<sub>2</sub> accumulation creates a subdomain of high PIN1 endocytosis (Ischebeck et al., 2013; Posor et al., 2015; Tejos et al., 2014), which leads to enhanced removal of PIN1 from the center of the rootward plasma membrane and explains the local PIN1 minimum in developing sieve elements. Enhanced PIN1 removal could result in reduced auxin efflux, which could contribute to the reported buildup of auxin in developing sieve elements that appears to be crucial for the timing of their differentiation (Marhava et al., 2018; Santuari et al., 2011). Because BRX, PAX, and PIP5Ks are under feedback control of auxin at the transcriptional and/or post-translational level (Marhava et al., 2018; Scacchi et al., 2009; Tejos et al., 2014), the activity of the BRX-PAX-PIP5K polarity module would eventually reach a dynamic steady-state equilibrium that matches a particular auxin threshold.

### Polarity Reinforcement Might Be a Generic Activity of BRX Family Proteins

Although this model intuitively explains how BRX could reduce auxin efflux, the incapacity of BRXL2 and D6PK to fully complement *brx* or *pax* mutants, respectively, suggests that patterning of PIN1 plasma membrane localization and abundance is not sufficient to restore proper sieve element differentiation. However, these results emphasize that aberrant PIN1 localization is not merely an indicator of impaired protophloem development. In terms of biochemical interactions and localization, BRX and BRXL2 appear to be very similar. Yet, given the observed differences in their physiological behavior, BRXL2 only appears to possess a subset of BRX functionality and uncouples the effect of plasma membrane domain patterning from the effect on auxin efflux regulation through PAX (Marhava et al., 2018). Therefore, it appears that both the PIN1 minimum as well as PAX inhibition are necessary facets of BRX action in guiding protophloem sieve element differentiation.

The observation that BRX and BRXL2 differ in their activities is interesting in the light of reports that implicate polarly localized BRX family proteins in another developmental process, stomatal patterning (Bringmann and Bergmann, 2017; Rowe et al., 2019). In this context, their polarity depends on another polar plasma-

membrane-associated protein, BREAKING OF ASYMMETRY IN THE STOMATAL LINEAGE (BASL) (Dong et al., 2009). Since BASL localization also partly depends on BRX family proteins (Rowe et al., 2019), the situation somewhat resembles our observations for BRX and PAX in the protophloem. Interestingly, BRX and BRXL2 are fully interchangeable in the stomata context (Rowe et al., 2019), which could mean that polarity enforcement represents the generic activity of BRX family proteins.

### Proper Protophloem Sieve Element Differentiation Requires Tight Control of Auxin Efflux

Our results reiterate the proposed impact of BRX action on polar auxin transport (Marhava et al., 2018; Scacchi et al., 2009) and indicate that it possibly emerges from a multi-layered synergism. That is while BRX inhibits auxin efflux stimulation by PAX, together with PAX it simultaneously creates a local PIN1 minimum, possibly because recruitment of PIP5K promotes PIN1 endocytosis (Ischebeck et al., 2013; Mei et al., 2012; Tejos et al., 2014). Interestingly, this effect appears to be PIN-specific, since BRI1, which is also a cargo for clathrin-mediated endocytosis (Di Rubbo et al., 2013; Russinova et al., 2004), did not display such a local minimum. Whether reduced PIN1 abundance at this position necessarily equals reduced auxin efflux remains unclear however, although the impact could be substantial because of the small rootward membrane area of developing protophloem sieve elements. It also appears possible that PIN activation by AGC kinases and PIN endocytosis might be intricately linked in a regulatory cycle where the former is a prerequisite for the latter. Such a scenario could also reconcile the proposed separate impact of AGC kinases on PIN activity and polarity (Barbosa et al., 2018). However, the observation that D6PK cannot substitute for PAX in the developing protophloem, although it partially restores the PIN1 localization pattern and recruits BRX, suggests that it is not that straightforward. In this context it is noteworthy that within the AGC kinases, PAX is an outlier and considerably less active than D6PK (Marhava et al., 2018). However, auxin-induced PAX phosphorylation amplifies its activity to D6PK levels (Marhava et al., 2018), and this difference in dynamic range might explain the lack of interchangeability between PAX and D6PK in the developing sieve elements. The fact that BRX, PAX and PIP5Ks all respond to auxin at transcriptional and/or post-translational level also suggests that the self-reinforcing polarity module formed by these proteins controls its own activity in an auxin-dependent manner. How the input of auxin is exactly conveyed into BRX and PAX action at the plasma membrane is one of the most interesting follow up questions to our study.

## STAR★METHODS

Detailed methods are provided in the online version of this paper and include the following:

- KEY RESOURCES TABLE
- LEAD CONTACT AND MATERIALS AVAILABILITY
- EXPERIMENTAL MODEL AND SUBJECT DETAILS
  - Plant Material Growth Conditions
  - Growth Conditions
- METHOD DETAILS

- Constructs and Generation of Transgenic Lines
- Auxin Treatments
- Confocal Imaging and Image Processing
- VISUAL Assay and Proteomics
- Protein Immunolocalization
- Oocyte Experiments
- QUANTIFICATION AND STATISTICAL ANALYSIS
- DATA AND CODE AVAILABILITY

#### SUPPLEMENTAL INFORMATION

Supplemental Information can be found online at <https://doi.org/10.1016/j.devcel.2019.11.015>.

#### ACKNOWLEDGMENTS

This work was supported by SNSF grants 31003A\_166394 and 310030B\_185379 (awarded to C.S.H.) and MEYS CR CZ.02.1.01/0.0/0.0/16\_013/0001775 (awarded to J.P.). We would like to thank Prof. C. Schwechheimer for the PAX<sup>KR-A</sup> variant, Dr. U. Mayer and Prof. G. Juergens for the anti-KNOLLE antibody gift, Prof. A. Rodriguez-Villalon for CVP2::CVP2-GFP seeds, Prof. T. Munnik for PIP biosensors, and K. Holecková and A.-M. Amiguet-Vercher for technical support.

#### AUTHOR CONTRIBUTIONS

P.M. and C.S.H. conceived and designed this project. P.M., A.C.A.F., S.W.H.K., A.J., M.K., D.P.J., A.B., and P.C. performed the experiments, designed together with U.Z.H., J.P., and C.S.H. U.Z.H., J.P., and C.S.H. supervised the research. P.M. and C.S.H. drafted the manuscript. All authors analyzed the data and contributed to the writing of the final manuscript.

#### DECLARATION OF INTERESTS

The authors declare no competing interests.

Received: August 1, 2019

Revised: October 8, 2019

Accepted: November 21, 2019

Published: December 19, 2019

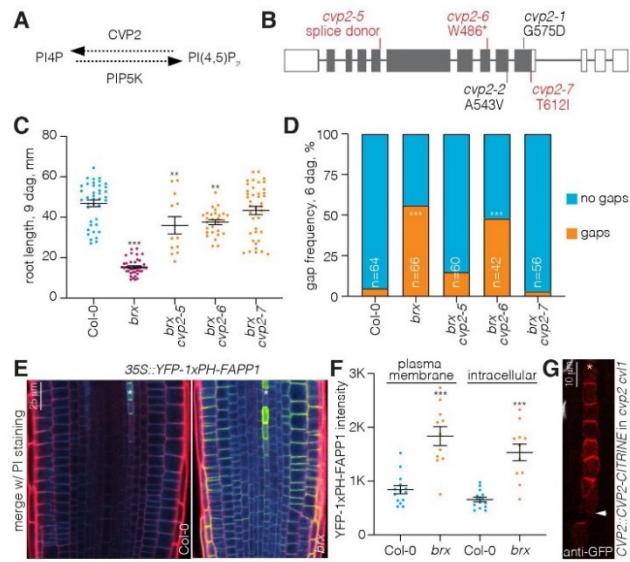
#### REFERENCES

- Anne, P., and Hardtke, C.S. (2018). Phloem function and development—biophysics meets genetics. *Curr. Opin. Plant Biol.* **43**, 22–28.
- Barbosa, I.C., and Schwechheimer, C. (2014). Dynamic control of auxin transport-dependent growth by AGCVIII protein kinases. *Curr. Opin. Plant Biol.* **22**, 108–115.
- Barbosa, I.C., Shikata, H., Zourelidou, M., Heilmann, M., Heilmann, I., and Schwechheimer, C. (2016). Phospholipid composition and a polybasic motif determine D6 protein kinase polar association with the plasma membrane and tropic responses. *Development* **143**, 4687–4700.
- Barbosa, I.C., Zourelidou, M., Willige, B.C., Weller, B., and Schwechheimer, C. (2014). D6 PROTEIN kinase activates auxin transport-dependent growth and PIN-FORMED phosphorylation at the plasma membrane. *Dev. Cell* **29**, 674–685.
- Barbosa, I.C.R., Hammes, U.Z., and Schwechheimer, C. (2018). Activation and polarity control of PIN-FORMED auxin transporters by phosphorylation. *Trends Plant Sci.* **23**, 523–538.
- Benjamins, R., and Scheres, B. (2008). Auxin: the looping star in plant development. *Annu. Rev. Plant Biol.* **59**, 443–465.
- Benková, E., Michniewicz, M., Sauer, M., Teichmann, T., Seifertová, D., Jürgens, G., and Friml, J. (2003). Local, efflux-dependent auxin gradients as a common module for plant organ formation. *Cell* **115**, 591–602.
- Bennett, M.J., Marchant, A., Green, H.G., May, S.T., Ward, S.P., Millner, P.A., Walker, A.R., Schulz, B., and Feldmann, K.A. (1996). Arabidopsis AUX1 gene: a permease-like regulator of root gravitropism. *Science* **273**, 948–950.
- Beuchat, J., Li, S., Ragni, L., Shindo, C., Kohn, M.H., and Hardtke, C.S. (2010). A hyperactive quantitative trait locus allele of Arabidopsis BRX contributes to natural variation in root growth vigor. *Proc. Natl. Acad. Sci. USA* **107**, 8475–8480.
- Billou, I., Xu, J., Wildwater, M., Willemsen, V., Paponov, I., Friml, J., Heidstra, R., Aida, M., Palme, K., and Scheres, B. (2005). The PIN auxin efflux facilitator network controls growth and patterning in Arabidopsis roots. *Nature* **433**, 39–44.
- Bonke, M., Thitamadee, S., Mähönen, A.P., Hauser, M.T., and Helariutta, Y. (2003). APL regulates vascular tissue identity in Arabidopsis. *Nature* **426**, 181–186.
- Boss, W.F., and Im, Y.J. (2012). Phosphoinositide signaling. *Annu. Rev. Plant Biol.* **63**, 409–429.
- Briggs, G.C., Mouchel, C.F., and Hardtke, C.S. (2006). Characterization of the plant-specific BREVIS RADIX gene family reveals limited genetic redundancy despite high sequence conservation. *Plant Physiol.* **140**, 1306–1316.
- Bringmann, M., and Bergmann, D.C. (2017). Tissue-wide mechanical forces influence the polarity of stomatal stem cells in Arabidopsis. *Curr. Biol.* **27**, 877–883.
- Carland, F., and Nelson, T. (2009). CVP2- and CVL1-mediated phosphoinositide signaling as a regulator of the ARF GAP SFC/VAN3 in establishment of foliar vein patterns. *Plant J.* **59**, 895–907.
- Carland, F.M., and Nelson, T. (2004). Cotyledon vascular pattern2-mediated inositol (1,4,5) triphosphate signal transduction is essential for closed venation patterns of Arabidopsis foliar organs. *Plant Cell* **16**, 1263–1275.
- Cutler, S.R., Ehrhardt, D.W., Griffiths, J.S., and Somerville, C.R. (2000). Random GFP::cDNA fusions enable visualization of subcellular structures in cells of Arabidopsis at a high frequency. *Proc. Natl. Acad. Sci. USA* **97**, 3718–3723.
- Depuydt, S., Rodriguez-Villalon, A., Santuari, L., Wyser-Rmili, C., Ragni, L., and Hardtke, C.S. (2013). Suppression of Arabidopsis protophloem differentiation and root meristem growth by CLE45 requires the receptor-like kinase BAM3. *Proc. Natl. Acad. Sci. USA* **110**, 7074–7079.
- Detmer, J., Ursache, R., Campilho, A., Miyashima, S., Belevich, I., O'Regan, S., Mullendore, D.L., Yadav, S.R., Lanz, C., Beverina, L., et al. (2014). Choline transporter-LIKE1 is required for sieve plate development to mediate long-distance cell-to-cell communication. *Nat. Commun.* **5**, 4276.
- Di Rubbo, S., Irani, N.G., Kim, S.Y., Xu, Z.Y., Gadeyne, A., Dejonghe, W., Vanhoutte, I., Persiau, G., Eeckhout, D., Simon, S., et al. (2013). The clathrin adaptor complex AP-2 mediates endocytosis of brassinosteroid insensitive1 in Arabidopsis. *Plant Cell* **25**, 2986–2997.
- Dong, J., MacAlister, C.A., and Bergmann, D.C. (2009). BASL controls asymmetric cell division in Arabidopsis. *Cell* **137**, 1320–1330.
- Fischer, U., Ikeda, Y., Ljung, K., Serralbo, O., Singh, M., Heidstra, R., Palme, K., Scheres, B., and Grebe, M. (2006). Vectorial information for Arabidopsis planar polarity is mediated by combined AUX1, EIN2, and GNOM activity. *Curr. Biol.* **16**, 2143–2149.
- Friml, J., Benková, E., Billou, I., Wisniewska, J., Hamann, T., Ljung, K., Woody, S., Sandberg, G., Scheres, B., Jürgens, G., et al. (2002). AtPIN4 mediates sink-driven auxin gradients and root patterning in Arabidopsis. *Cell* **108**, 661–673.
- Friml, J., Vieten, A., Sauer, M., Weijers, D., Schwarz, H., Hamann, T., Offringa, R., and Jürgens, G. (2003). Efflux-dependent auxin gradients establish the apical-basal axis of Arabidopsis. *Nature* **426**, 147–153.
- Friml, J., Yang, X., Michniewicz, M., Weijers, D., Quint, A., Tietz, O., Benjamins, R., Ouwerkerk, P.B., Ljung, K., Sandberg, G., et al. (2004). A PINOID-dependent binary switch in apical-basal PIN polar targeting directs auxin efflux. *Science* **306**, 862–865.
- Fujimoto, M., Arimura, S., Ueda, T., Takanashi, H., Hayashi, Y., Nakano, A., and Tsutsumi, N. (2010). Arabidopsis dynamin-related proteins DRP2B and DRP1A participate together in clathrin-coated vesicle formation during endocytosis. *Proc. Natl. Acad. Sci. USA* **107**, 6094–6099.



- Furuta, K.M., Yadav, S.R., Lehesranta, S., Belevich, I., Miyashima, S., Heo, J.O., Vatin, A., Lindgren, O., De Rybel, B., Van Isterdael, G., et al. (2014). Plant development. *Arabidopsis* NAC45/86 direct sieve element morphogenesis culminating in enucleation. *Science* **345**, 933–937.
- Galván-Ampudia, C.S., and Offringa, R. (2007). Plant evolution: AGC kinases tell the auxin tale. *Trends Plant Sci.* **12**, 541–547.
- Geldner, N., Friml, J., Stierhof, Y.D., Jürgens, G., and Palme, K. (2001). Auxin transport inhibitors block PIN1 cycling and vesicle trafficking. *Nature* **413**, 425–428.
- Gerth, K., Lin, F., Daamen, F., Menzel, W., Heinrich, F., and Heilmann, M. (2017). *Arabidopsis* phosphatidylinositol 4-phosphate 5-kinase 2 contains a functional nuclear localization sequence and interacts with alpha-importins. *Plant J.* **92**, 862–878.
- Goodrich, L.V., and Strutt, D. (2011). Principles of planar polarity in animal development. *Development* **138**, 1877–1892.
- Griensen, V.A., Xu, J., Marée, A.F., Hogeweg, P., and Scheres, B. (2007). Auxin transport is sufficient to generate a maximum and gradient guiding root growth. *Nature* **449**, 1008–1013.
- Gujas, B., Cruz, T.M.D., Kastanaki, E., Vermeer, J.E.M., Munnik, T., and Rodríguez-Villalón, A. (2017). Perturbing phosphoinositide homeostasis oppositely affects vascular differentiation in *Arabidopsis thaliana* roots. *Development* **144**, 3578–3589.
- Haucke, V. (2005). Phosphoinositide regulation of clathrin-mediated endocytosis. *Biochem. Soc. Trans.* **33**, 1285–1289.
- He, K., Marsland, R., III, Upadhyayula, S., Song, E., Dang, S., Capraro, B.R., Wang, W., Skillern, W., Gaudin, R., Ma, M., et al. (2017). Dynamics of phosphoinositide conversion in clathrin-mediated endocytic traffic. *Nature* **552**, 410–414.
- Heilmann, I. (2016). Phosphoinositide signaling in plant development. *Development* **143**, 2044–2055.
- Heilmann, M., and Heilmann, I. (2015). Plant phosphoinositides-complex networks controlling growth and adaptation. *Biochim. Biophys. Acta* **1851**, 759–769.
- Houbaert, A., Zhang, C., Tiwari, M., Wang, K., de Marcos Serrano, A., Savatin, D.V., Urs, M.J., Zhiponova, M.K., Gudesblatt, G.E., Vanhoutte, I., et al. (2018). POLAR-guided signalling complex assembly and localization drive asymmetric cell division. *Nature* **563**, 574–578.
- Ischebeck, T., Stenzel, I., and Heilmann, I. (2008). Type B phosphatidylinositol-4-phosphate 5-kinases mediate *Arabidopsis* and *Nicotiana tabacum* pollen tube growth by regulating apical pectin secretion. *Plant Cell* **20**, 3312–3330.
- Ischebeck, T., Werner, S., Krishnamoorthy, P., Lerche, J., Mejón, M., Stenzel, I., Löffke, C., Wiessner, T., Im, Y.J., Perera, I.Y., et al. (2013). Phosphatidylinositol 4,5-bisphosphate influences PIN polarization by controlling clathrin-mediated membrane trafficking in *Arabidopsis*. *Plant Cell* **25**, 4894–4911.
- Kang, B.H., Busse, J.S., and Bednarek, S.Y. (2003). Members of the *Arabidopsis* dynamin-like gene family, ADL1, are essential for plant cytokinesis and polarized cell growth. *Plant Cell* **15**, 899–913.
- Kang, Y.H., Breda, A., and Hardtke, C.S. (2017). Brassinosteroid signaling directs formative cell divisions and protophloem differentiation in *Arabidopsis* root meristems. *Development* **144**, 272–280.
- Kang, Y.H., and Hardtke, C.S. (2016). *Arabidopsis* MAKR5 is a positive effector of BAM3-dependent CLE45 signaling. *EMBO Rep.* **17**, 1145–1154.
- Kleine-Vehn, J., Wabnik, K., Martinière, A., Langowski, I., Willig, K., Naramoto, S., Leitner, J., Tanaka, H., Jakobs, S., Robert, S., et al. (2011). Recycling, clustering, and endocytosis jointly maintain PIN auxin carrier polarity at the plasma membrane. *Mol. Syst. Biol.* **7**, 540.
- Kondo, Y., Nurani, A.M., Saito, C., Ichihashi, Y., Saito, M., Yamazaki, K., Mitsuda, N., Ohme-Takagi, M., and Fukuda, H. (2016). Vascular cell induction culture system using *Arabidopsis* Leaves (VISUAL) reveals the sequential differentiation of sieve element-like cells. *Plant Cell* **28**, 1250–1262.
- König, S., Ischebeck, T., Lerche, J., Stenzel, I., and Heilmann, I. (2008). Salt-stress-induced association of phosphatidylinositol 4,5-bisphosphate with clathrin-coated vesicles in plants. *Biochem. J.* **415**, 387–399.
- Lauber, M.H., Waizenegger, I., Steinmann, T., Schwarz, H., Mayer, U., Hwang, I., Lukowitz, W., and Jürgens, G. (1997). The *Arabidopsis* KNOLLE protein is a cytokinesis-specific syntaxin. *J. Cell Biol.* **139**, 1485–1493.
- Lucas, W.J., Groover, A., Lichtenberger, R., Furuta, K., Yadav, S.R., Helariutta, Y., He, X.Q., Fukuda, H., Kang, J., Brady, S.M., et al. (2013). The plant vascular system: evolution, development and functions. *J. Integr. Plant Biol.* **55**, 294–388.
- Marhava, P., Bassukas, A.E.L., Zourelidou, M., Kolb, M., Moret, B., Fastner, A., Schulze, W.X., Cattaneo, P., Hammes, U.Z., Schwechheimer, C., et al. (2018). A molecular rheostat adjusts auxin flux to promote root protophloem differentiation. *Nature* **558**, 297–300.
- Mei, Y., Jia, W.J., Chu, Y.J., and Xue, H.W. (2012). *Arabidopsis* phosphatidylinositol monophosphate 5-kinase 2 is involved in root gravitropism through regulation of polar auxin transport by affecting the cycling of PIN proteins. *Cell Res.* **22**, 581–597.
- Meijer, H.J., and Munnik, T. (2003). Phospholipid-based signaling in plants. *Annu. Rev. Plant Biol.* **54**, 265–306.
- Mravec, J., Petrášek, J., Li, N., Boeren, S., Karlova, R., Kitakura, S., Pařezová, M., Naramoto, S., Nodzyński, T., Dhonukshe, P., et al. (2011). Cell plate restricted association of DRP1A and PIN proteins is required for cell polarity establishment in *Arabidopsis*. *Curr. Biol.* **21**, 1055–1060.
- Mueller-Roeber, B., and Pical, C. (2002). Inositol phospholipid metabolism in *Arabidopsis*. Characterized and putative isoforms of inositol phospholipid kinase and phosphoinositide-specific phospholipase C. *Plant Physiol.* **130**, 22–46.
- Munnik, T., and Nielsen, E. (2011). Green light for polyphosphoinositide signals in plants. *Curr. Opin. Plant Biol.* **14**, 489–497.
- Nance, J., Munro, E.M., and Pries, J.R. (2003). *C. elegans* PAR-3 and PAR-6 are required for apicobasal asymmetries associated with cell adhesion and gastrulation. *Development* **130**, 5339–5350.
- Peterson, S.V., Johansson, A.I., Kowalczyk, M., Makoveychuk, A., Wang, J.Y., Moritz, T., Grebe, M., Benfey, P.N., Sandberg, G., and Ljung, K. (2009). An auxin gradient and maximum in the *Arabidopsis* root apex shown by high-resolution cell-specific analysis of IAA distribution and synthesis. *Plant Cell* **21**, 1659–1668.
- Pillitteri, L.J., Peterson, K.M., Horst, R.J., and Torii, K.U. (2011). Molecular profiling of stomatal meristemoids reveals new component of asymmetric cell division and commonalities among stem cell populations in *Arabidopsis*. *Plant Cell* **23**, 3260–3275.
- Platre, M.P., Noack, L.C., Doumane, M., Bayle, V., Simon, M.L.A., Maneta-Peyret, L., Fouillen, L., Stanislas, T., Armengot, L., Pejchar, P., et al. (2018). A combinatorial lipid code shapes the electrostatic landscape of plant endomembranes. *Dev. Cell* **45**, 465–480.e11.
- Posor, Y., Eichhorn-Grünig, M., and Haucke, V. (2015). Phosphoinositides in endocytosis. *Biochim. Biophys. Acta* **1851**, 794–804.
- Rodríguez, A., Santiago, J., Rubio, S., Saez, A., Osmont, K.S., Gadea, J., Hardtke, C.S., and Rodríguez, P.L. (2009). The short-rooted phenotype of the *brevis radix* mutant partly reflects root abscisic acid hypersensitivity. *Plant Physiol.* **149**, 1917–1928.
- Rodríguez-Villalón, A., Gujas, B., Kang, Y.H., Breda, A.S., Cattaneo, P., Depuydt, S., and Hardtke, C.S. (2014). Molecular genetic framework for protophloem formation. *Proc. Natl. Acad. Sci. USA* **111**, 11551–11556.
- Rodríguez-Villalón, A., Gujas, B., van Wijk, R., Munnik, T., and Hardtke, C.S. (2015). Primary root protophloem differentiation requires balanced phosphatidylinositol-4,5-bisphosphate levels and systemically affects root branching. *Development* **142**, 1437–1446.
- Rowe, M.H., Dong, J., Weimer, A.K., and Bergmann, D.C. (2019). A plant-specific polarity module establishes cell fate asymmetry in the *Arabidopsis* stomatal lineage. *bioRxiv*. <https://doi.org/10.1101/614636>.
- Russinova, E., Borst, J.W., Kwaaitaal, M., Caño-Delgado, A., Yin, Y., Chory, J., and de Vries, S.C. (2004). Heterodimerization and endocytosis of *Arabidopsis* brassinosteroid receptors BRI1 and AtSERK3 (BAK1). *Plant Cell* **16**, 3216–3229.

- Santuari, L., Scacchi, E., Rodríguez-Villalón, A., Salinas, P., Dohmann, E.M., Brunoud, G., Vernoux, T., Smith, R.S., and Hardtke, C.S. (2011). Positional information by differential endocytosis splits auxin response to drive Arabidopsis root meristem growth. *Curr. Biol.* 27, 1918–1923.
- Sauer, M., Balla, J., Luschig, C., Wisniewska, J., Reinöhl, V., Friml, J., and Benková, E. (2006). Canalization of auxin flow by Aux/IAA-ARF-dependent feedback regulation of PIN polarity. *Genes Dev.* 20, 2902–2911.
- Scacchi, E., Osmont, K.S., Beuchat, J., Salinas, P., Navarrete-Gómez, M., Trigueros, M., Ferrándiz, C., and Hardtke, C.S. (2009). Dynamic, auxin-responsive plasma membrane-to-nucleus movement of Arabidopsis BRX. *Development* 136, 2059–2067.
- Scholze, M.J., Barbleux, K.S., De Simone, A., Boumasmoud, M., Suess, C.C.N., Wang, R., and Gonczy, P. (2018). PI(4,5)P<sub>2</sub> forms dynamic cortical structures and directs actin distribution as well as polarity in *Caenorhabditis elegans* embryos. *Development* 145, dev164988.
- Simon, M.L., Platte, M.P., Assil, S., van Wijk, R., Chen, W.Y., Chory, J., Dreux, M., Munnik, T., and Jaillais, Y. (2014). A multi-colour/multi-affinity marker set to visualize phosphoinositide dynamics in Arabidopsis. *Plant J.* 77, 322–337.
- Simon, M.L., Platte, M.P., Marqués-Bueno, M.M., Armengot, L., Stanislas, T., Bayle, V., Caillaud, M.C., and Jaillais, Y. (2016). A PtdIns(4)P-driven electrostatic field controls cell membrane identity and signalling in plants. *Nat. Plants* 2, 16089.
- Sousa, E., Kost, B., and Malhó, R. (2008). Arabidopsis phosphatidylinositol-4-monophosphate 5-kinase 4 regulates pollen tube growth and polarity by modulating membrane recycling. *Plant Cell* 20, 3050–3064.
- Stanislas, T., Hüser, A., Barbosa, I.C., Kiefer, C.S., Brackmann, K., Pietra, S., Gustavsson, A., Zourelidou, M., Schwechheimer, C., and Grebe, M. (2015). Arabidopsis D6PK is a lipid domain-dependent mediator of root epidermal planar polarity. *Nat. Plants* 1, 15162.
- Swarup, R., Kargul, J., Marchant, A., Zadik, D., Rahman, A., Mills, R., Yemm, A., May, S., Williams, L., Millner, P., et al. (2004). Structure-function analysis of the presumptive Arabidopsis auxin permease AUX1. *Plant Cell* 16, 3069–3083.
- Tejos, R., Sauer, M., Vanneste, S., Palacios-Gomez, M., Li, H., Heilmann, M., van Wijk, R., Vermeer, J.E., Heilmann, I., Munnik, T., et al. (2014). Bipolar plasma membrane distribution of phosphoinositides and their requirement for auxin-mediated cell polarity and patterning in Arabidopsis. *Plant Cell* 26, 2114–2128.
- Thompson, B.J. (2013). Cell polarity: models and mechanisms from yeast, worms and flies. *Development* 140, 13–21.
- Vermeer, J.E., and Munnik, T. (2013). Using genetically encoded fluorescent reporters to image lipid signalling in living plants. *Methods Mol. Biol.* 1009, 283–289.
- Vermeer, J.E., Thole, J.M., Goedhart, J., Nielsen, E., Munnik, T., and Gadella, T.W., Jr. (2009). Imaging phosphatidylinositol 4-phosphate dynamics in living plant cells. *Plant J.* 57, 356–372.
- Willige, B.C., Ahlers, S., Zourelidou, M., Barbosa, I.C., Demarsy, E., Trevisan, M., Davis, P.A., Roelfsema, M.R., Hangarter, R., Fankhauser, C., et al. (2013). D6PK AGC VIII kinases are required for auxin transport and phototropic hypocotyl bending in Arabidopsis. *Plant Cell* 25, 1674–1688.
- Zádníková, P., Petrásek, J., Marhavy, P., Raz, V., Vandenbussche, F., Ding, Z., Schwarzerová, K., Morita, M.T., Tasaka, M., Hejátko, J., et al. (2010). Role of PIN-mediated auxin efflux in apical hook development of Arabidopsis thaliana. *Development* 137, 607–617.
- Zhang, Y., and Dong, J. (2018). Cell polarity: compassing cell division and differentiation in plants. *Curr. Opin. Plant Biol.* 45, 127–135.
- Zhao, Y., Yan, A., Feijó, J.A., Furutani, M., Takenawa, T., Hwang, I., Fu, Y., and Yang, Z. (2010). Phosphoinositides regulate clathrin-dependent endocytosis at the tip of pollen tubes in Arabidopsis and tobacco. *Plant Cell* 22, 4031–4044.
- Zourelidou, M., Absmanner, B., Weller, B., Barbosa, I.C., Willige, B.C., Fastner, A., Streit, V., Port, S.A., Colcombet, J., de la Fuente van Bentem, S., et al. (2014). Auxin efflux by PIN-FORMED proteins is activated by two different protein kinases, D6 PROTEIN KINASE and PINOID. *eLife* 3, 02860.



**Supplemental Figure S1. Phosphoinositide balance in *brx* mutants, related to Figure 1.**

(A) Illustration of the enzymatic reaction catalyzed by phosphatidylinositol-4-phosphate 5-kinases (PIP5Ks), and the reverse reaction presumably catalyzed by the phosphoinositide 5-phosphatase COTYLEDON VASCULAR PATTERN 2 (CVP2). PI4P: phosphatidylinositol-4-phosphate; PI(4,5)P<sub>2</sub>: phosphatidylinositol-4,5-bisphosphate.

(B) New (red) and previously isolated (black) *cvp2* second site mutations obtained from a *brx* suppressor screen. The *cvp2-5* mutation abolishes a splice donor site and presumably results in a frameshift that adds eight amino acids after G128 and then introduces a premature stop codon.

(C) Quantification of primary root length of indicated genotypes. Statistically significant difference (one-way ANOVA) compared to Col-0 wildtype is indicated.

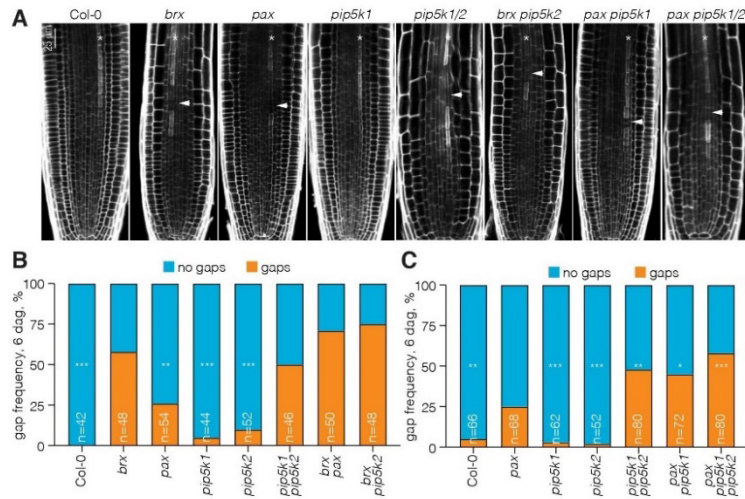
(D) Quantification of gap cell frequency in protophloem strands of six-day-old root meristems of indicated genotypes. Statistically significant difference (Chi square test) compared to Col-0 is indicated.

(E) Confocal microscopy of the PI4P fluorescent biosensor 35S::YFP-1xPH-FAPP1 (green) in Col-0 (left) and *brx* (right) root meristems, cellular outline stained with propidium iodide (PI) (red).

(F) Quantification of 35S::YFP-1xPH-FAPP1 signal intensities at the plasma membrane and intracellularly in developing protophloem sieve elements of Col-0 and *brx* (arbitrary units; 11-14 roots, 5-8 cells per root). Statistically significant difference (one-way ANOVA) compared to Col-0 is indicated.

(G) Localization of CVP2-CITRINE in developing protophloem sieve elements detected by immunolocalization using anti-GFP antibody. Note shootward plasma membrane association, intracellular localization as well as some rootward plasma membrane association in detached cells (arrowhead).

Asterisks indicate sieve element cell files. Plots display individual values (dots), the mean (wide bars) and the standard error of the mean (whiskers). \* =  $p < 0.05$ ; \*\* =  $p < 0.001$ ; \*\*\* =  $p < 0.0001$ ; See Data S1 for statistical test details.



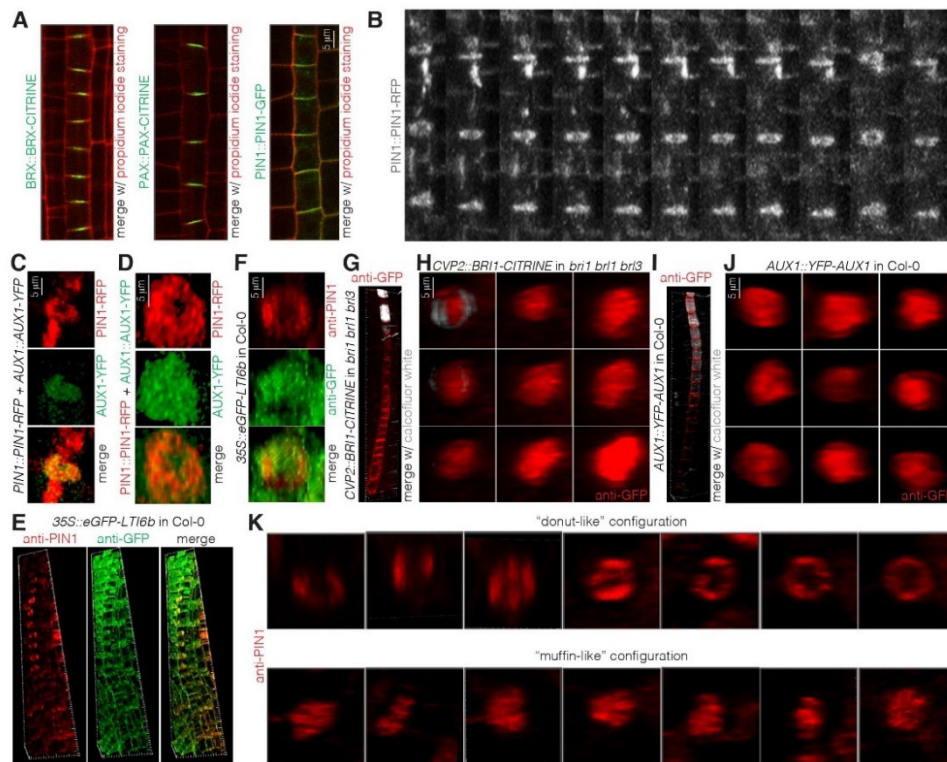
**Supplemental Figure S2. Analysis of *brx*, *pax* and *pip5k* multiple mutants, related to Figure 2.**

**(A)** Confocal microscopy of five-day-old root meristems stained with propidium iodide. Asterisks indicate developing protophloem sieve element strands. Arrowheads point out "gap cells" that fail to differentiate.

**(B)** Quantification of gap cell frequency in protophloem strands of six-day-old root meristems of indicated genotypes. Statistically significant difference (Chi square test) compared to *brx* is indicated.

**(C)** Quantification of gap cell frequency in protophloem strands of six-day-old root meristems of indicated genotypes. Statistically significant difference (Chi square test) compared to *pax* is indicated.

\* =  $p < 0.05$ ; \*\* =  $p < 0.001$ ; \*\*\* =  $p < 0.001$ ; See Data S1 for statistical test details.



**Supplemental Figure S3. PIN1 localization in developing protofloeem sieve elements, related to Figure 4.**

(A) Confocal live imaging of BRX-CITRINE, PAX-CITRINE and PIN1-GFP fusion proteins in developing protofloeem sieve elements viewed from the side. Note that BRX-CITRINE and PAX-CITRINE signals do not extend to the corners of the cells.

(B) Confocal live imaging time lapse of PIN1-RFP fusion protein in developing protofloeem sieve elements (maximum projections, 32 sections each), difference between frames is 1 min. Note that the "donut-like" localization remains stable.

(C) Sequential confocal live imaging of PIN1-RFP and AUX1-YFP fusion proteins in a developing protofloeem sieve element.

(D) 3D reconstruction of PIN1-RFP and AUX1-YFP fusion proteins imaged sequentially as in (C).  
 (E) 3D reconstruction of simultaneously immunolocalized PIN1 (detected by anti-PIN1 antibody, left panel, red) and eGFP-LTI6b fusion protein (detected by anti-GFP antibody, middle panel, green) in developing protofloeem sieve element strand (asterisks), and overlay (right panel).

(F) Close up of (E): 3D reconstruction of simultaneous detection of endogenous PIN1 (detected by anti-PIN1 antibody, top panel, red) and the integral plasma membrane marker eGFP-LTI6b (detected by anti-GFP antibody, middle panel, green) in developing protofloeem sieve elements viewed below from the root tip.

(G) 3D reconstruction of BR11-CITRINE fusion protein (detected by anti-GFP antibody, red) specifically expressed in developing protofloeem sieve element strands under control of the *COTYLEDON VASCULAR PATTERN 2 (CVP2)* promoter.

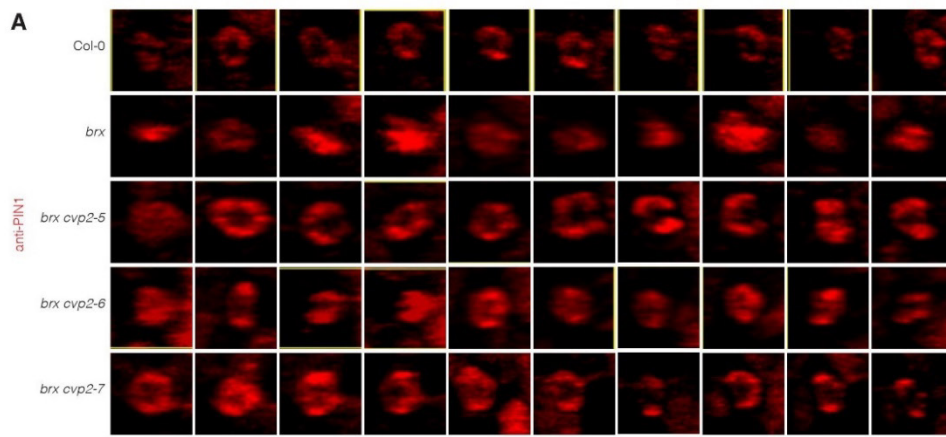
(H) Close ups of (G): 3D reconstructions of BR11-CITRINE fusion protein (detected by anti-GFP antibody, red) in representative individual developing protofloeem sieve elements viewed below from the root tip.

(I) 3D reconstruction of YFP-AUX1 fusion protein (detected by anti-GFP antibody, red) in developing protofloeem sieve element strands.

(J) Close ups of (I): 3D reconstructions of YFP-AUX1 fusion protein (detected by anti-GFP antibody, red) in representative individual developing protofloeem sieve elements viewed below from the root tip.

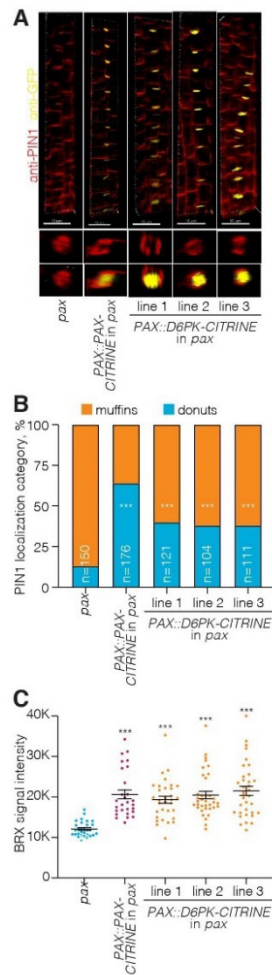
(K) Set of 3D reconstructions of PIN1 immunostainings (detected by anti-PIN1 antibody, red) in developing protofloeem sieve elements, viewed below from the root tip, illustrating the scope of "donut-like" and "muffin-like" localization categories.

Axis scales in 3D panels (E, G, I) indicate 1  $\mu\text{m}$  steps, in each case  $\sim 150 \mu\text{m}$  total protofloeem strands were imaged.



**Supplemental Figure S4. PIN1 localization in *brx cvp2* double mutants, related to Figure 5.**

**(A)** Set of 3D reconstructions of PIN1 immunostainings (detected by anti-PIN1 antibody, red) in developing protophloem sieve elements, viewed below from the root tip, illustrating representative cells from the indicated genotypes.



**Supplemental Figure S5. Analysis of D6PK expressed in *pax* mutants, related to Figure 6.**

**(A)** 3D reconstruction of simultaneously immunolocalized PIN1 (detected by anti-PIN1 antibody, red) and D6PK-CITRINE fusion protein (detected by anti-GFP antibody, yellow) expressed under control of the *PAX* promoter (*PAX::D6PK-CITRINE* independent representative lines) as compared to controls.

**(B)** Quantification of PIN1 localization in protophloem strands of six-day-old root meristems of indicated genotypes, categorized into "donut-like" or "muffin-like" configuration. Statistically significant difference (Chi square test) compared to *pax* is indicated.

**(C)** Quantification of anti-BRX signal intensity (arbitrary units; 28-36 roots, 5-8 cells per root). Statistically significant difference (one way ANOVA) compared to *pax* is indicated.

Axis scales in 3D panels (A) indicate 1  $\mu\text{m}$  steps, in each case  $\sim 150 \mu\text{m}$  total protophloem strands were imaged.

## A molecular rheostat adjusts auxin flux to promote root protophloem differentiation

P. Marhava<sup>1,5</sup>, A. E. L. Bassukas<sup>2,5</sup>, M. Zourelidou<sup>2</sup>, M. Kolb<sup>2,3</sup>, B. Moret<sup>1</sup>, A. Fastner<sup>3</sup>, W. X. Schulze<sup>4</sup>, P. Cattaneo<sup>1</sup>, U. Z. Hammes<sup>2,3</sup>, C. Schwechheimer<sup>2\*</sup> & C. S. Hardtke<sup>1\*</sup>

**Auxin influences plant development through several distinct concentration-dependent effects<sup>1</sup>. In the *Arabidopsis* root tip, polar auxin transport by PIN-FORMED (PIN) proteins creates a local auxin accumulation that is required for the maintenance of the stem-cell niche<sup>2–4</sup>. Proximally, stem-cell daughter cells divide repeatedly before they eventually differentiate. This developmental gradient is accompanied by a gradual decrease in auxin levels as cells divide, and subsequently by a gradual increase as the cells differentiate<sup>5,6</sup>. However, the timing of differentiation is not uniform across cell files. For instance, developing protophloem sieve elements (PPSEs) differentiate as neighbouring cells still divide. Here we show that PPSE differentiation involves local steepening of the post-meristematic auxin gradient. BREVIS RADIX (BRX) and PROTEIN KINASE ASSOCIATED WITH BRX (PAX) are interacting plasma-membrane-associated, polarly localized proteins that co-localize with PIN proteins at the rootward end of developing PPSEs. Both *brx* and *pax* mutants display impaired PPSE differentiation. Similar to other AGC-family kinases, PAX activates PIN-mediated auxin efflux, whereas BRX strongly dampens this stimulation. Efficient BRX plasma-membrane localization depends on PAX, but auxin negatively regulates BRX plasma-membrane association and promotes PAX activity. Thus, our data support a model in which BRX and PAX are elements of a molecular rheostat that modulates auxin flux through developing PPSEs, thereby timing PPSE differentiation.**

Auxin is a concentration-dependent permissive–restrictive signal in plant cell proliferation and differentiation–elongation that directly impinges on adaptive processes and growth rates<sup>1,2</sup>. Local auxin accumulations are important cues for organ organization. For example, high auxin concentration specifies the stem-cell niche in the *Arabidopsis* root tip<sup>2–4</sup>. Proximally, auxin concentration decreases gradually as stem-cell daughters repeatedly divide before they eventually differentiate. Notably, differentiation is accompanied by a renewed rise in auxin levels<sup>5,6</sup>. The underlying auxin distribution is generated by plasma-membrane-integral PINs, which are auxin efflux carriers with a coordinated asymmetric cellular localization that gives rise to directional polar auxin transport<sup>2–4</sup>. In root vasculature, PINs generally localize to the rootward end of cells, transporting auxin towards the root tip<sup>3</sup>. PINs are regulated by auxin, predominantly post-translationally<sup>7–9</sup>. Moreover, the AGC-family kinases D6 PROTEIN KINASE (D6PK) and PINOID (PID) activate auxin efflux through PIN phosphorylation<sup>10–12</sup>.

The proximo-distal auxin profile in root meristems intersects with differential auxin activity in the radial dimension. For example, developing PPSEs (Extended Data Fig. 1a, b) display higher auxin accumulation than surrounding cells<sup>6</sup> (Extended Data Fig. 2a–d) and differentiate, whereas neighbouring cells still remain meristematic<sup>6,13,14</sup> (Extended Data Fig. 2e). To explore whether PPSE differentiation depends on auxin activity, we manipulated the auxin response by expressing a constitutively active variant of an auxin-response factor, MONOPTEROS (MP<sup>Δ</sup>)<sup>15</sup>, under the control of PPSE-specific

*COTYLEDON VASCULAR PATTERN 2* (*CVP2*) promoter<sup>13,16</sup>. *CVP2::MP<sup>Δ</sup>* accelerated PPSE differentiation, indicating that auxin responses critically determine the differentiation process (Extended Data Fig. 2f, g).

How differential auxin activity is achieved in PPSEs remained unclear. BRX is plasma-membrane-associated, polarly localized and specifically expressed in developing PPSEs<sup>13,17</sup>. In *brx* mutants, PPSEs frequently fail to differentiate<sup>13</sup>. These cells lack the characteristic cell-wall changes and appear as gaps in the PPSE differentiation zone<sup>13,16,18</sup> (Extended Data Fig. 2h). A similar phenotype is observed in *octopus* (*ops*) mutants<sup>13,17</sup>, which are affected in a parallel genetic pathway required for PPSE differentiation<sup>19</sup>. Whereas OPS localizes to the shootward end of PPSEs, BRX co-localizes with PINs at the rootward end<sup>2,6,13,18</sup>. Auxin negatively regulates BRX protein abundance and plasma-membrane association, but induces *BRX* transcription<sup>18,20</sup>. Thus, BRX is a candidate for mediating auxin effects in PPSE differentiation. In *brx* PPSEs, auxin accumulation as compared to neighbouring cells was markedly lower and more variable than in the wild type (Extended Data Fig. 2i, j). Although *CVP2::MP<sup>Δ</sup>* expression in *brx* did not reduce the proportion of PPSE strands with gaps (Extended Data Fig. 2k), it significantly stimulated root growth (Extended Data Fig. 2l) and reduced gap size (Extended Data Fig. 2m). Such partial rescue was not observed with another PPSE-specific promoter that was inactive in gap cells (Extended Data Fig. 2k–n). Moreover, impaired PPSE differentiation was observed after pharmacological inhibition of auxin biosynthesis (Extended Data Fig. 2o, p), and *brx* protophloem defects were aggravated by genetic interference with auxin uptake (Extended Data Fig. 2q). These observations support the hypothesis that finely tuned auxin activity contributes to PPSE differentiation.

BRX protein is expressed only at low levels and in few cells, complicating cell-biological and biochemical investigations of BRX in its native context. However, a recently established trans-differentiation assay for sieve element formation<sup>21</sup> (Extended Data Fig. 3a, b) enabled us to perform proteomics analyses in a native cell type and identify specific BRX interactors by immunoprecipitation (Extended Data Fig. 3c, d). Among them, we retrieved D6PK and several D6PK-LIKE (D6PKL) kinases as well as PINs, but by far the most abundant was a D6PK/D6PKL-related kinase (AT2G44830)<sup>22</sup>, which we named PROTEIN KINASE ASSOCIATED WITH BRX (PAX).

To examine a potential role of AGC kinases in PPSE differentiation, we analysed *d6pk/d6pkl* as well as *pax* mutants. *D6PK/D6PKL* genes display substantial genetic redundancy and, consistent with normal PIN phosphorylation in their roots<sup>10,11,23</sup>, *d6pk0123* quadruple mutants had only a mild, possibly enhanced root-growth phenotype (Extended Data Fig. 4a). By contrast, *pax* loss-of-function mutants displayed reduced primary root growth (Fig. 1a), which was accompanied by PPSE differentiation defects (Fig. 1b–e). No phenotype was observed in a mutant of the closest PAX homologue, the uncharacterized PAX-LIKE (PAXL) kinase (AT5G40030)<sup>22</sup>, and *paxl* mutation only mildly enhanced the *pax* phenotype (Fig. 1b). A PAX–CITRINE fusion protein expressed

<sup>1</sup>Department of Plant Molecular Biology, University of Lausanne, Lausanne, Switzerland. <sup>2</sup>Plant Systems Biology, Technical University of Munich, Freising, Germany. <sup>3</sup>Department of Cell Biology and Plant Biochemistry, Regensburg University, Regensburg, Germany. <sup>4</sup>Department of Plant Systems Biology, University of Hohenheim, Stuttgart, Germany. <sup>5</sup>These authors contributed equally: P. Marhava, A. E. L. Bassukas. \*e-mail: claus.schwechheimer@wzw.tum.de; christian.hardtke@unil.ch



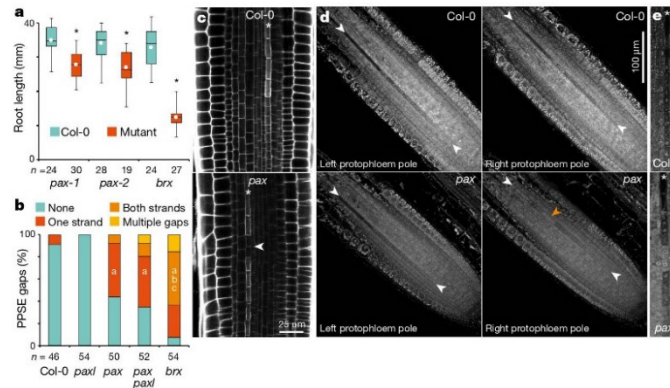


**Fig. 1 | Phenotypic characterization of *pax* mutants.** **a**, Root length of seven-day-old mutant and wild-type *A. thaliana* L. Heynh reference accession Columbia-0 (Col-0) seedlings. *pax-1* and *pax-2* are two independent PAX loss-of-function alleles. All data that are displayed subsequently were generated using *pax-1*. Box plots throughout show the second and third quartiles, maximum, minimum and mean (white dot). Statistically significant differences are indicated (two-sided Student's *t*-test; \* $P < 0.0008$ ). **b**, Quantification of protophloem strands with gap cells, 6-day-old seedlings. Statistically significant differences are indicated (Fisher's exact test, two-sided, all  $P$  values  $< 0.001$ ; a, significantly different

to Col-0; b, significantly different to *pax*; c, significantly different to *pax*). **c**, Confocal microscopy of propidium iodide (PI)-stained root meristems. Asterisks indicate PPSE strands and the arrowhead indicates a gap cell in the *pax* protophloem. **d**, Confocal microscopy of Col-0 and *pax* root meristems (ClearSee fixation with PI staining), showing both protophloem poles. Note PPSE cell files (white arrowheads) that start with meristematic cells and end with mature empty sieve elements. In one *pax* pole, PPSE differentiation is perturbed (gap cells, orange arrowhead). **e**, Expanded view, highlighting a gap cell in a *pax* PPSE cell file (arrowhead). *n*, number of independent biological replicates.

under its native promoter complemented the PPSE differentiation phenotype of *pax* mutants (Extended Data Fig. 4b) and revealed PAX expression in developing protophloem, as well as weaker expression in the xylem axis (Fig. 2a). PAX displayed rootward cellular polarity (Fig. 2b) and co-localized with BRX (Fig. 2c). Exclusive expression of PAX-CITRINE in developing PPSEs, under the BRX promoter, fully rescued the *pax* protophloem phenotype (Extended Data Fig. 4c, d). As previously observed in *brx*, the *pax* PPSE differentiation defects were accompanied by impaired phloem sap delivery into the meristem<sup>16</sup> (Extended Data Fig. 4e). In summary, *pax* mutants represent a (hypomorphic) phenocopy of *brx* mutants.

The *brx* phenotype was not enhanced in *brx pax* double mutants (Extended Data Fig. 4f), suggesting that *brx* is genetically epistatic to *pax*. In turn, the *pax* phenotype was not significantly enhanced by *d6pk/d6pkl* mutations (Extended Data Fig. 4g). However, similar to D6PK or PID, PAX (and PAXL) activated auxin efflux when co-expressed with PINs in *Xenopus laevis* oocytes<sup>12</sup> (Fig. 2d, Extended Data Fig. 4h). However, PAX was the weakest activator in this assay. Moreover, similar to D6PKL proteins, ADP-ribosylation factor-guanine-exchange factor (ARF-GEF) inhibition by brefeldin A (BFA) triggered rapid dissociation of PAX from the plasma membrane (Fig. 3a, Extended Data Fig. 4i). BRX is also BFA-sensitive<sup>18</sup>, yet in direct comparison, BFA-induced BRX plasma-membrane dissociation was slower than for PAX (Fig. 3a, Extended Data Fig. 4j, k). Consistently, BFA treatment also triggered PPSE differentiation defects in a dosage-dependent manner (Extended Data Fig. 4l, m). Moreover, BRX abundance, but not PIN abundance, was severely reduced in *pax* PPSEs (Fig. 3b–g). By contrast, PAX abundance or localization did not substantially depend on BRX (Extended Data Fig. 4n). In protoplasts, BRX localized evenly at the plasma membrane, whereas PAX accumulated in large patches<sup>24</sup> (Extended Data Fig. 4o). Their co-expression recruited BRX into PAX patches. However, a cytoplasmic PAX variant<sup>24</sup> did not disrupt the even plasma-membrane distribution of BRX. These results suggest that PAX is required for efficient BRX plasma-membrane recruitment.

Auxin activity is systemically reduced throughout *brx* root meristems<sup>16</sup>. We thus sought to monitor PIN activity in *brx* or *pax*. We focused our analysis on the dominant PIN in developing PPSEs, PIN1 (Extended

Data Fig. 5a). Corroborating the PIN1-green fluorescent protein (GFP) results, PIN1 abundance and localization in both the protophloem and the meristem were not affected in *pax* or *brx* mutants (Extended

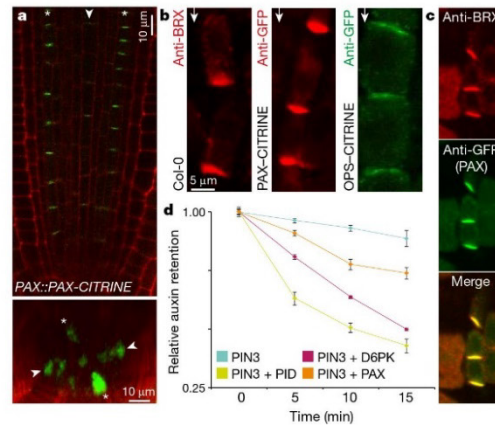


**Fig. 2 | Expression analysis of PAX protein.** **a**, Top, Confocal microscopy of the PAX-CITRINE fusion protein (green fluorescence) expressed under its native promoter in the meristem (longitudinal plane). Bottom, optical cross section. Asterisks indicate PPSE cell files and arrowheads indicate the xylem axis. **b**, Detection of endogenous BRX (red) using anti-BRX antibody staining, or PAX-CITRINE (red) or OPS-CITRINE (green) using anti-GFP antibody staining, in protophloem of fixed meristems (squashed after fixation). Arrows point rootward. **c**, Simultaneous detection of PAX-CITRINE (green) and BRX (red) by immunostaining, demonstrating co-localization. **d**, Auxin transport assays, average retention of radio-labelled auxin in *X. laevis* oocytes expressing the indicated heterologous plant proteins ( $n = 10$  per time point; error bars, s.e.m.).

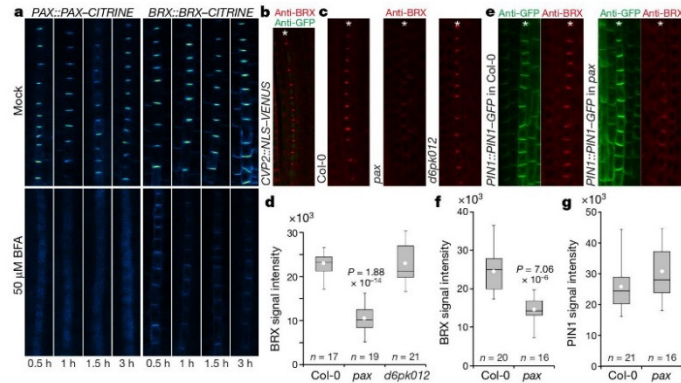


**Fig. 3 | PAX-dependence of efficient BRX plasma-membrane association.** **a**, Plasma-membrane dissociation of PAX-CITRINE and BRX-CITRINE in response to BFA treatment. **b**, Simultaneous detection of nuclear NLS-VENUS protein (green) expressed under the control of PPSE-specific *CYP2* promoter and BRX (red) by antibody staining. Asterisks in all microscopy images indicate the PPSE cell file. **c**, Detection of BRX (red) by antibody staining. **d**, BRX signal intensity quantification (anti-BRX antibody detection) in PPSEs (mean from approximately ten

cells per root, arbitrary units). **e**, Simultaneous immunolocalization of PIN1-GFP (anti-GFP, green) expressed under its native promoter and BRX (anti-BRX, red) by antibody staining in Col-0 and *pax*. **f**, **g**, BRX signal intensity quantification (**f**, anti-BRX antibody detection) and PIN1-GFP signal intensity (**g**, anti-GFP antibody detection) in PPSEs (means from approximately ten cells per root, arbitrary units). **d-g**, Statistically significant differences from Col-0 are indicated, two-sided Student's *t*-test.

Data Fig. 5b). To survey PIN1 activity, we performed immunostaining with antibodies against PIN1 phosphosites that are critical for PIN1 activation<sup>11,12</sup>. Phosphoserine S231 (J231) signal was significantly reduced in *pax* PPSEs, whereas phosphoserine S271 (J271) was not affected (Extended Data Fig. 5c-e). By contrast, both phosphoserines were barely detectable in *brx* meristems (Extended Data Fig. 5c, f). Reduced PIN1 phosphorylation was also observed in *ops* (Extended Data Fig. 5f), suggesting that meristem-wide reduced PIN1 activity is a secondary systemic consequence of severely disturbed PPSE differentiation, similar to other traits<sup>16</sup>. Yet, *brx* or *pax* protophloem defects

were aggravated in the presence of a *pin1* mutation (Extended Data Fig. 5g-i). In *brx pin1* double mutants, protophloem was frequently barely distinguishable, or even absent (approximately 20% of seedlings) (Extended Data Fig. 5i), underlining the importance of properly regulated auxin transport for PPSE differentiation.

The systemic ramifications of discontinuous protophloem on meristem development can be considered to be a post-catastrophic scenario that is triggered and enhanced by repeated PPSE differentiation failure, and is difficult to recover from once phloem sap (and thus auxin) delivery is impaired<sup>16</sup>. This complicates efforts to untangle cause and

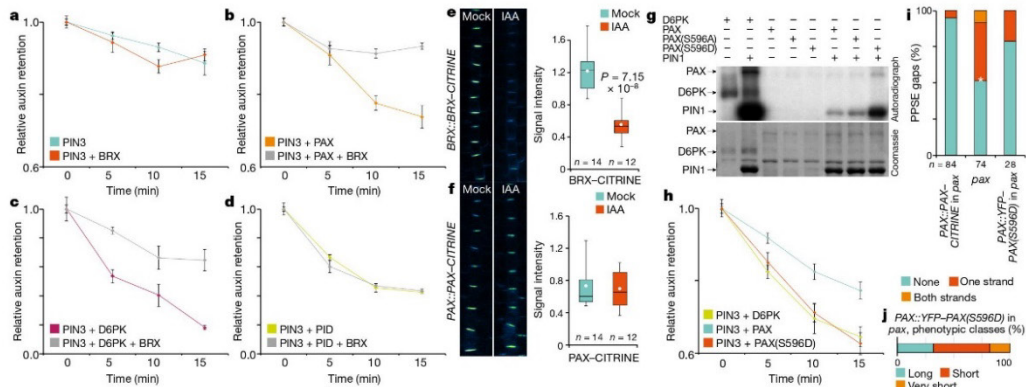


**Fig. 4 | Regulatory input of auxin on PAX and BRX activity.** **a-d**, Auxin transport assays in *X. laevis* oocytes expressing the indicated heterologous plant proteins ( $n = 10$  per time point; error bars, s.e.m.). **e-f**, Response of BRX (**e**) or PAX (**f**) fusion protein to 5  $\mu$ M auxin (IAA) treatment (3 h), with quantification (arbitrary units; means from approximately ten cells per root). The statistically significant difference is indicated, two-sided Student's *t*-test. **g**, Radioactive in vitro kinase assays with GST fusion proteins of D6PK, PAX or the PAX(S596A) and PAX(S596D) point mutants, with the PIN1 cytosolic loop as substrate (top), and

corresponding loading controls (bottom). **h**, Auxin transport assays in *X. laevis* oocytes expressing the indicated heterologous plant proteins ( $n = 10$  per time point; error bars: s.e.m.). **i**, Quantification of gap-cell frequency in PPSE strands. For *PAX::YFP-PAX(S596D)*, only long root seedlings (see **j**) were scored. *pax* alone was significantly different from *PAX::PAX-CITRINE* in *pax* (two-sided Fisher's exact test,  $*P < 0.0001$ ). *PAX::YFP-PAX(S596D)* was not significantly different from *PAX::PAX-CITRINE* in *pax* or from *pax* alone. **j**, Quantification of root phenotypic classes in a *PAX::YFP-PAX(S596D)* line ( $n = 50$ ).

effect in the cellular action of regulators from the multicellular context. For example, it remained unclear whether *pax* mutants display PPSE differentiation defects because of inefficient BRX plasma membrane recruitment, or whether *brx* mutants display PPSE differentiation defects because of a failure to control PAX activity. To investigate whether BRX interaction with AGC kinases affects auxin transport, we tested the effect of BRX co-expression on kinase-mediated PIN activation in oocytes. In these experiments, BRX substantially inhibited stimulation of auxin efflux by PAX or D6PK (Fig. 4a–c, Extended Data Fig. 5j, k). Because this inhibition was not observed in assays with the more distantly related PID (Fig. 4d), our findings suggest that BRX action affects a subset of related AGC kinases, and that its inhibitory effect is determined by kinase identity.

The observation that BRX inhibits auxin efflux appeared particularly interesting in light of its known auxin-induced plasma-membrane dissociation<sup>18</sup> (Fig. 4e, Extended Data Fig. 6a, b). By contrast, neither PAX abundance nor localization were affected by auxin (Fig. 4f). However, phosphoproteomics indicated auxin-induced phosphorylation of phosphoserine S596 in the PAX activation loop (Extended Data Fig. 6c), which correlated with simultaneously increased PIN1 phosphorylation (Extended Data Fig. 6d). In vitro, recombinant PAX phosphorylated PIN1 with comparably low efficiency, and S596 was dispensable for kinase activation (Fig. 4g, Extended Data Fig. 6e). A PAX(S596D) phosphomimic variant, however, was considerably more active than wild-type PAX and displayed increased phosphorylation activity towards PIN1 (Fig. 4g, Extended Data Fig. 6e). Matching this biochemical observation, PAX(S596D) also stimulated auxin efflux considerably more in oocytes, to a level approximately equal to D6PK (Fig. 4h, Extended Data Fig. 6f). However, unlike wild-type PAX, the PAX(S596D) variant at best partially rescued the *pax* mutant (Fig. 4i, Extended Data Fig. 6g). Moreover, PAX(S596D) frequently triggered a gain-of-function phenotype of even shorter, often barely developing roots (Fig. 4j). Consistent with the D6PK-like activity of PAX(S596D), D6PK expressed from the PAX promoter could not rescue the *pax* phenotype (Extended Data Fig. 6h, i). These findings suggest that fine-tuning of PAX activity is a feature of properly integrated PPSE development.

In a parsimonious interpretation of our results, PAX and BRX act together as a molecular rheostat to modulate auxin efflux dynamically (Extended Data Fig. 7). In this scenario, PAX recruits BRX to the plasma membrane, which inhibits PIN-mediated auxin efflux at lower auxin levels. Because of this inhibition, cellular auxin increases until BRX eventually becomes displaced from the plasma membrane. Concomitantly, PAX is activated and stimulates auxin efflux. Reinforced through auxin-induced BRX transcription<sup>6,18</sup> (Extended Data Fig. 6j, k), this interplay could reach a dynamic steady-state equilibrium, which would impair higher local auxin activity in the multicellular context to properly time PPSE differentiation.

### Online content

Any Methods, including any statements of data availability and Nature Research reporting summaries, along with any additional references and Source Data files, are available in the online version of the paper at <https://doi.org/10.1038/s41586-018-0186-z>.

Received: 14 September 2017; Accepted: 24 April 2018;  
Published online: 06 June 2018

1. Benjamins, R. & Scheres, B. Auxin: the looping star in plant development. *Annu. Rev. Plant Biol.* **59**, 443–465 (2008).
2. Billou, I. et al. The PIN auxin efflux facilitator network controls growth and patterning in *Arabidopsis* roots. *Nature* **433**, 39–44 (2005).
3. Grieneisen, V. A., Xu, J., Marée, A. F., Hogeweg, P. & Scheres, B. Auxin transport is sufficient to generate a maximum and gradient guiding root growth. *Nature* **449**, 1008–1013 (2007).
4. Sabatini, S. et al. An auxin-dependent distal organizer of pattern and polarity in the *Arabidopsis* root. *Cell* **99**, 463–472 (1999).

5. Brunoud, G. et al. A novel sensor to map auxin response and distribution at high spatio-temporal resolution. *Nature* **482**, 103–106 (2012).
6. Santuari, L. et al. Positional information by differential endocytosis splits auxin response to drive *Arabidopsis* root meristem growth. *Curr. Biol.* **21**, 1918–1923 (2011).
7. Sauer, M. et al. Canalization of auxin flow by Aux/IAA-ARF-dependent feedback regulation of PIN polarity. *Genes Dev.* **20**, 2902–2911 (2006).
8. Geldner, N., Friml, J., Stierhof, Y. D., Jürgens, G. & Palme, K. Auxin transport inhibitors block PIN1 cycling and vesicle trafficking. *Nature* **413**, 425–428 (2001).
9. Paciorek, T. et al. Auxin inhibits endocytosis and promotes its own efflux from cells. *Nature* **435**, 1251–1256 (2005).
10. Barbosa, I. C., Zourelidou, M., Willige, B. C., Weller, B. & Schwechheimer, C. D6 PROTEIN KINASE activates auxin transport-dependent growth and PIN-FORMED phosphorylation at the plasma membrane. *Dev. Cell* **29**, 674–685 (2014).
11. Weller, B. et al. Dynamic PIN-FORMED auxin efflux carrier phosphorylation at the plasma membrane controls auxin efflux-dependent growth. *Proc. Natl Acad. Sci. USA* **114**, E887–E896 (2017).
12. Zourelidou, M. et al. Auxin efflux by PIN-FORMED proteins is activated by two different protein kinases, D6 PROTEIN KINASE and PINOID. *eLife* **3**, e02860 (2014).
13. Rodriguez-Villalon, A. et al. Molecular genetic framework for protophloem formation. *Proc. Natl Acad. Sci. USA* **111**, 11551–11556 (2014).
14. Furuta, K. M. et al. *Arabidopsis* NAC45/86 direct sieve element morphogenesis culminating in enucleation. *Science* **345**, 933–937 (2014).
15. Ckurshumova, W., Smirnova, T., Marcos, D., Zayed, Y. & Berleth, T. Irrepressible *MONOPTEROS/ARF5* promotes *de novo* shoot formation. *New Phytol.* **204**, 556–566 (2014).
16. Rodriguez-Villalon, A., Gujas, B., van Wijk, R., Munnik, T. & Hardtke, C. S. Primary root protophloem differentiation requires balanced phosphatidylinositol-4,5-bisphosphate levels and systemically affects root branching. *Development* **142**, 1437–1446 (2015).
17. Truernit, E., Bauby, H., Belcram, K., Barthélémy, J. & Palauqui, J. C. OCTOPUS, a polarly localised membrane-associated protein, regulates phloem differentiation entry in *Arabidopsis thaliana*. *Development* **139**, 1306–1315 (2012).
18. Scacchi, E. et al. Dynamic, auxin-responsive plasma membrane-to-nucleus movement of *Arabidopsis* BRX. *Development* **136**, 2059–2067 (2009).
19. Breda, A. S., Hazak, O. & Hardtke, C. S. Phosphosite charge rather than shootward localization determines OCTOPUS activity in root protophloem. *Proc. Natl Acad. Sci. USA* **114**, E5721–E5730 (2017).
20. Mouchel, C. F., Osmond, K. S. & Hardtke, C. S. BRX mediates feedback between brassinosteroid levels and auxin signalling in root growth. *Nature* **443**, 458–461 (2006).
21. Kondo, Y. et al. Vascular cell induction culture system using *Arabidopsis* leaves (VISUAL) reveals the sequential differentiation of sieve element-like cells. *Plant Cell* **28**, 1250–1262 (2016).
22. Galván-Ampudia, C. S. & Offringa, R. Plant evolution: AGC kinases tell the auxin tale. *Trends Plant Sci.* **12**, 541–547 (2007).
23. Willige, B. C. et al. D6PK AGC/III kinases are required for auxin transport and phototropic hypocotyl bending in *Arabidopsis*. *Plant Cell* **25**, 1674–1688 (2013).
24. Barbosa, I. C. et al. Phospholipid composition and a polybasic motif determine D6 PROTEIN KINASE polar association with the plasma membrane and tropic responses. *Development* **143**, 4687–4700 (2016).

**Acknowledgements** We thank the University of Lausanne Protein Analysis Facility for mass spectrometry services, the Swiss National Science Foundation for Grant 31003A\_166394 (C.S.H.), the German-Israeli Foundation for I-236-203.17-2014 (C.S.) and the Deutsche Forschungsgemeinschaft for SCHW751/12-2 (C.S.), HA 3468/6-1 and SFB924 (U.Z.H.).

**Reviewer information** Nature thanks A. P. Mahonen, D. Weijers and the other anonymous reviewer(s) for their contribution to the peer review of this work.

**Author contributions** P.M., A.E.L.B., M.Z., M.K., B.M., A.F., W.X.S. and P.C. performed experiments and analysed data. P.M., A.E.L.B., M.Z., W.X.S., U.Z.H., C.S. and C.S.H. designed experiments. P.M., A.E.L.B., U.Z.H., C.S. and C.S.H. wrote the manuscript.

**Competing interests** The authors declare no competing interests.

### Additional information

**Extended data** is available for this paper at <https://doi.org/10.1038/s41586-018-0186-z>.

**Supplementary information** is available for this paper at <https://doi.org/10.1038/s41586-018-0186-z>.

**Reprints and permissions information** is available at <http://www.nature.com/reprints>.

**Correspondence and requests for materials** should be addressed to C.S. and C.S.H.

**Publisher's note:** Springer Nature remains neutral with regard to jurisdictional claims in published maps and institutional affiliations.

## METHODS

No statistical methods were used to predetermine sample size. The experiments were not randomized and investigators were not blinded to allocation during experiments and outcome assessment. Experiments were repeated two to four times. All attempts at replication were successful.

**Plant materials and growth conditions.** The wild-type *Arabidopsis* line used in this study was the *A. thaliana* L. Heynh reference accession Columbia-0 (Col-0), which was also the genetic background for the mutants and transgenic lines. For plant tissue culture, seeds were surface-sterilized, stratified for 2 days in the dark at 4 °C, and germinated in vertically placed Petri dishes on 0.9% agar and 0.5 × Murashige and Skoog (1/2 MS) medium (Duchefa) with 0.3% sucrose at 22 °C under continuous light. The mutant *pax-1* and *pax-2* alleles (T-DNA insertion lines SAIL\_688\_B04 and GABI\_274F04, respectively) were identified from available collections and obtained from the Nottingham *Arabidopsis* Stock Centre. The following transgenic and mutant lines have been described elsewhere: *BRX::BRX-CITRINE*<sup>13</sup>, *PIN1::PIN1-GFP*<sup>25</sup>, *PIN3::PIN3-GFP*<sup>26</sup>, *PIN7::PIN7-GFP*<sup>27</sup>, *CVP2::NLS-VENUS*<sup>16</sup>, *35S::DII-NLS-VENUS* and *35S::mDII-NLS-VENUS*<sup>5</sup>, *brx-2*<sup>13</sup>, *ops-2*<sup>17</sup>, *pin1-613*<sup>28</sup>, *aux1-729*, *d6pk*, *d6pk1*, *d6pk2*, *d6pk3*, as well as their *d6pk012* triple and *d6pk0123* quadruple mutants<sup>12</sup>. Primers used for genotyping are summarized in Extended Data Table 1.

**Constructs and generation of transgenic lines.** Transgenes for plant transformation were created in suitable binary vectors and produced using standard molecular biology procedures and/or the NEBuilder HiFi DNA Assembly Reaction Protocol. The *35S::mDII-VENUS* and *35S::DII-VENUS* lines in Col-0 and *brx-2* backgrounds have previously been described<sup>9</sup>. For the *CVP2::MP*<sup>3</sup> or *CLE45::MP*<sup>3</sup> constructs, a 2.6-kb genomic promoter fragment upstream of the initiation codon of the *CVP2* gene<sup>16</sup> or a 2.0-kb genomic promoter fragment upstream of the initiation codon of the *CLAVATA3/EMBRYO SURROUNDING REGION 45 (CLE45)* gene<sup>19</sup> was amplified, combined with amino acids 1–794 of the *MP* open reading frame<sup>15</sup> and introduced into the pCambia1305.1 binary vector. To generate the translational *PAX::PAX-CITRINE* fusion, the *PAX* promoter region (4.5-kb upstream of the ATG start codon) was amplified and cloned into pDONR P4P1R as well as a genomic fragment of the *PAX* transcript region without a STOP codon into pDONR 221. The entry clones together with CITRINE in pDONR P2R3 were cloned into the destination vector pH7m34GW by the multisite Gateway recombination system. To create *UBQ10::PAX-CITRINE*, the entry clones containing the *UBQ10* promoter in pDONR P4P1R, the *PAX* coding sequence without a STOP codon in pDONR 221, and the CITRINE coding sequence in pDONR P2R3 were combined into binary vector pH7m34GW. The binary constructs were introduced into *Agrobacterium tumefaciens* strain GV3101<sup>PM190</sup> and transformed into the pertinent *Arabidopsis* genotypes using the floral dip method. For recombinant expression of the glutathione-S-transferase N-terminally tagged fusion proteins *GST-PAX*, *GST-PAX(S596D)* and *GST-PAX(S596A)*, a Gateway-compatible attB-flanked PCR product of *PAX* coding sequence was amplified from cDNA and cloned into the Gateway-compatible donor vector pDONR 201 (Invitrogen). The mutagenesis leading to *PAX(S596D)* phosphomimetic or *PAX(S596A)* phospho-mutant variants in the activation loop of the *PAX* coding sequence was achieved using site-directed mutation PCR on a pDONR 201 entry clone carrying the *PAX* coding sequence insert. The resulting pDONR 201 entry clones served as substrate to recombine the *PAX* coding sequences into the pDEST15 (Life Technologies) destination vector that was ultimately used for recombinant protein expression. The expression vectors pDEST15 containing *GST-D6PK* and *GST-PIN1* cytosolic loop have previously been described<sup>12</sup>. Primers used for cloning are summarized in Extended Data Table 1.

**Microscopy.** To visualize reporter genes and staining signals, fluorescence for CITRINE (excitation 514 nm, emission 529 nm), VENUS (excitation 515 nm, emission 528 nm), propidium iodide (PI) (excitation 536 nm, emission 617 nm), Alexa Fluor 488 (excitation 498 nm, emission 520 nm) and Alexa Fluor 546 (excitation 556 nm, emission 573 nm) were detected in seedlings examined under Zeiss LSM 700 or 710 inverted confocal scanning microscopes. Pictures were taken with 20× or 40× water/oil immersion objectives. PI staining of seven-day-old seedlings was used for quantification of protoplasm cell size. For presentation, composite images had to be assembled in various instances. Sequential scanning was used for co-localization studies to avoid any interference between fluorescence channels. For image analyses, ImageJ (NIH; <https://rsb.info.nih.gov/ij/>), Zeiss Zen (black edition) and Imaris software were used. If necessary, images were processed using the 'sharpen' tool for clearer visualization of cellular organization. For signal quantifications, all samples were analysed in the same area of the root meristem, and the average signal intensity per transgenic line was calculated as the mean of means. Statistical significance was evaluated with Student's *t* test.

**Pharmacological and hormonal treatments.** For treatments, 5–7-day-old seedlings were either grown on, or transferred either onto solid or into liquid 1/2 MS

medium with or without the chemicals and incubated for the indicated time. Drugs and hormones used were as follows: BFA (dissolved in DMSO), IAA (dissolved in DMSO), 1-kynurenine (dissolved in DMSO), PI (1 mg ml<sup>-1</sup> in water, diluted 1:25).

**VISUAL assay and proteomics.** The VISUAL protocol<sup>21</sup> was performed as previously described<sup>19</sup> with subsequent BRX-CITRINE or YFP pull down. In brief, cotyledons of six-day-old transgenic *Arabidopsis* seedlings were cultured for 3 days in induction medium and subsequently ground in extraction buffer. Supernatants (4 mg of total protein extract in two technical replicates) were incubated with anti-GFP beads (GFP-Trap\_MA, Chromotek). Beads were magnetically separated and protein was eluted in 2× SDS sample buffer, loaded on an SDS-PAGE gel for electrophoresis, and subsequently analysed by liquid chromatography with tandem mass spectrometry.

**Protein immunolocalization.** Whole mount immunolocalization on five-day-old seedlings was performed as described previously<sup>7</sup>. The primary antibody dilutions were: 1:600 for anti-GFP mouse (Roche), 1:500 for anti-BRX rabbit (this study), 1:100 for anti-PIN1 S1-P rabbit<sup>11</sup>, 1:300 for anti-PIN1 S4-P rabbit<sup>11</sup> and 1:100 for anti-PIN1 goat (Santa Cruz Biotechnology). The secondary antibody dilutions were: 1:600 for Alexa Fluor 488 anti-mouse (Molecular Probes) and 1:600 for Alexa Fluor 546 anti-rabbit (Molecular Probes). The anti-BRX antibody was obtained by custom antibody production directed against the keyhole-limpet hemocyanin (KLH)-conjugated BRX peptide GGSSNYGPGSYHGGC with affinity purification (Agrisera).

**Oocyte experiments.** Auxin transport assays in *X. laevis* oocytes were carried out as described<sup>12,30</sup>. The oocytes were obtained from the animal facility of the Technical University of Munich, Department of Nutritional Physiology. The animals were kept in accordance with local guidelines and regulations. To monitor expression levels, post-assay immunoblots were performed with anti-PIN1 sheep and anti-PIN3 sheep primary antibodies (Nottingham *Arabidopsis* Stock Centre, used at 1:5,000 dilution), and anti-GFP rabbit (custom antibody)<sup>31</sup>, 1:2,000 dilution). The secondary antibodies were anti-sheep from donkey (1:5,000, Santa Cruz Biotechnology) and anti-rabbit from goat (1:10,000, Santa Cruz Biotechnology).

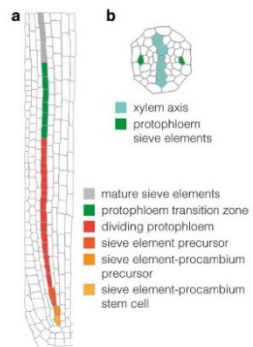
**Protoplast transformation.** Protoplasts were isolated from *Arabidopsis* suspension-cultured cells (Col-0) five to seven days after subculturing by incubation of 2 g of cell culture with 1% Cellulase R-10 (SERVA) and 0.25% Macerozyme R-10 (SERVA). Typically, protoplasts were transformed with 20 µg of plasmid DNA using polyethylene glycol-mediated transformation and analysed after 16 to 20 h of incubation as described<sup>24</sup>.

**In vitro kinase assay.** The in vitro kinase assay was performed using recombinant glutathione-S-transferase N-terminally tagged fusion proteins *GST-PIN1*<sup>12</sup> CL (cytosolic loop), *GST-D6PK*<sup>12</sup>, *GST-BRX*<sup>18</sup>, *GST-PAX*, *GST-PAX(S596D)* and *GST-PAX(S596A)*, expressed in the *Escherichia coli* strain BL21(DE3) and purified using Glutathione Sepharose 4B (GE Healthcare). The kinase reactions were performed by incubating the purified GST-fusion proteins for 60 min at 28 °C in the kinase reaction buffer (25 mM Tris HCl pH 7.5, 5 mM MgCl<sub>2</sub>, 0.2 mM EDTA, 1× cOmplete protease inhibitor cocktail (Roche)), supplemented with 10 µCi [<sup>32</sup>P] ATP (370 Mbq, specific activity 185 Tbq, Hartmann Analytics). The reactions were stopped by boiling the protein samples mixed with 5× concentrated Laemmli buffer for 10 min. Subsequently, the protein mixtures were separated by SDS-PAGE. After samples had been run, the SDS-PAGE gel was vacuum-dried and used for autoradiography. The same gel was later rehydrated and stained with Commae Brilliant Blue to serve as a loading control.

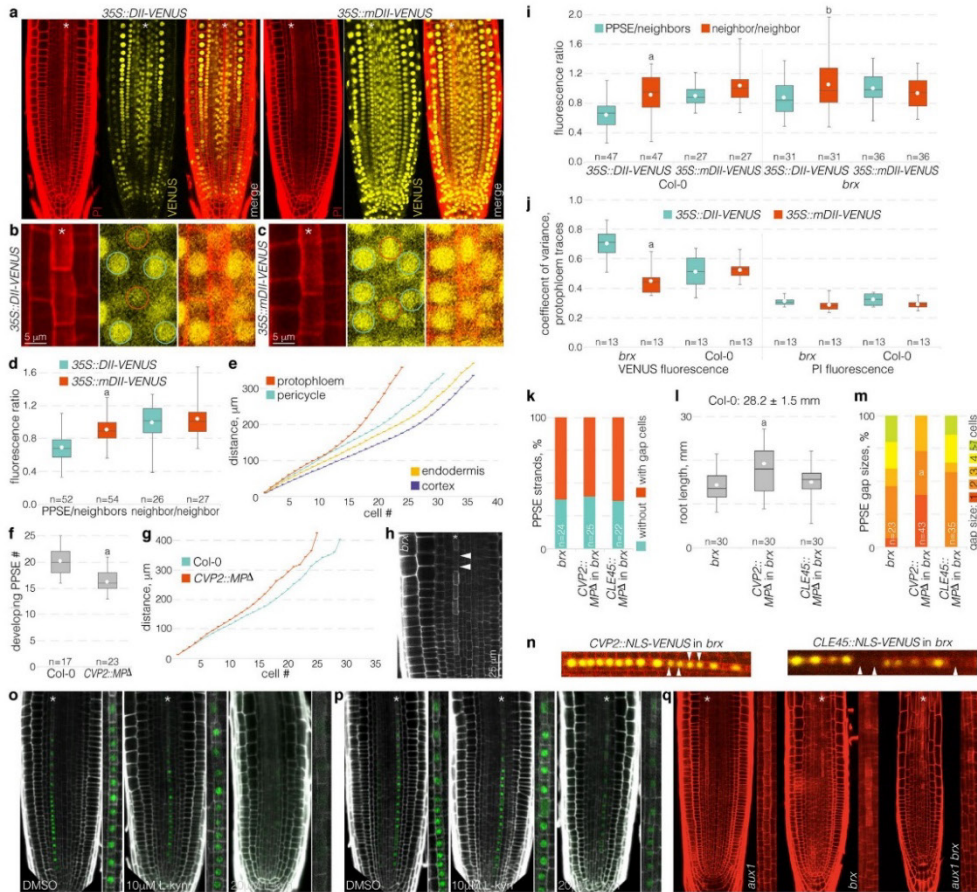
**Reporting summary.** Further information on experimental design is available in the Nature Research Reporting Summary linked to this paper.

**Data availability.** The datasets displayed in the current study are available from the corresponding authors upon reasonable request. For gel source images, see Supplementary Fig. 1.

25. Benková, E. et al. Local, efflux-dependent auxin gradients as a common module for plant organ formation. *Cell* **115**, 591–602 (2003).
26. Zádňíková, P. et al. Role of PIN-mediated auxin efflux in apical hook development of *Arabidopsis thaliana*. *Development* **137**, 607–617 (2010).
27. Friml, J. et al. Efflux-dependent auxin gradients establish the apical-basal axis of *Arabidopsis*. *Nature* **426**, 147–153 (2003).
28. Bennett, T. et al. The *Arabidopsis* MAX pathway controls shoot branching by regulating auxin transport. *Curr. Biol.* **16**, 553–563 (2006).
29. Marchant, A. et al. AUX1 promotes lateral root formation by facilitating indole-3-acetic acid distribution between sink and source tissues in the *Arabidopsis* seedling. *Plant Cell* **14**, 589–597 (2002).
30. Fastner, A., Absmanner, B. & Hammes, U. Z. Use of *Xenopus laevis* oocytes to study auxin transport. *Methods Mol. Biol.* **1497**, 259–270 (2017).
31. Absmanner, B., Stadler, R. & Hammes, U. Z. Phloem development in nematode-induced feeding sites: the implications of auxin and cytokinin. *Front. Plant Sci.* **4**, 241 (2013).



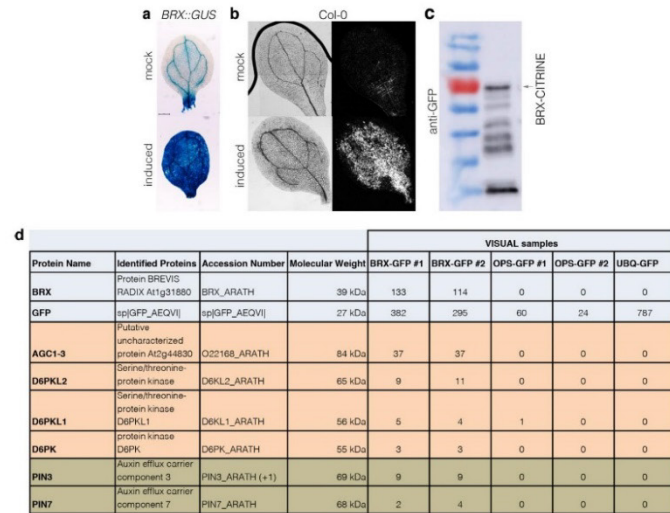
**Extended Data Fig. 1 | Overview of protophloem development.** a, Illustration of protophloem development from the stem cell to the mature sieve element in the *Arabidopsis* root meristem. b, Illustration of a cross section through the stele of an *Arabidopsis* root meristem, highlighting the arrangement of the two sieve element strands and the xylem axis.



Extended Data Fig. 2 | See next page for caption.

**Extended Data Fig. 2 | Auxin activity in developing PPSEs.** **a**, Confocal microscopy of the inverse auxin activity reporter DII-VENUS and its negative control mDII-VENUS (yellow fluorescence) in the root meristem (PI staining, red) of wild-type Col-0 plants. Asterisks indicate sieve element cell files. **b**, Confocal microscopy of constitutively expressed DII-VENUS in developing PPSEs and neighbouring cell files. Left, PI cell-wall staining (red); middle, DII-VENUS fluorescence (yellow; PPSE nuclei marked with red circles, nuclei in neighbouring cell files with blue circles); right, overlay. **c**, As in **b**, for mDII-VENUS. **d**, Relative intensity of the DII-VENUS reporter and its mDII-VENUS control in the nuclei of Col-0 PPSEs as compared to the nuclei of directly neighbouring cells. The statistically significant difference between DII-VENUS and mDII-VENUS in the PPSE/neighbours group is indicated (two-sided Student's *t*-test;  $a$ ,  $P = 5.86 \times 10^{-11}$ ). **e**, Cumulative average cell length in different root cell files, starting from the respective first stem-cell daughters (cell #1) ( $n = 11$  wild-type Col-0 roots). **f**, Number of developing PPSEs from the first stem-cell daughter up to the first transition zone PPSE (protophloem length) in seven-day-old Col-0 seedlings, and transgenic seedlings expressing a constitutively active derivative of the auxin response factor MONOPTEROS ( $MP^{\Delta}$ ) under control of the PPSE-specific *CVP2* promoter.  $a$ ,  $P = 3.16 \times 10^{-6}$ ; two-sided Student's *t*-test. **g**, Cumulative average cell length in the developing protophloem, starting from the first stem-cell daughter (cell #1) ( $n = 23$  each). Elongation occurs prematurely in *CVP2::MP^{\Delta}* plants. **h**, Confocal microscopy of a *brx* root meristem, focused on one of the sieve element strands (asterisk). Arrowheads point out gap cells, which fail to build up the characteristic PPSE cell wall owing to a failure to differentiate. **i**, Relative intensity of the DII-VENUS reporter and its mDII-VENUS control in the nuclei of Col-0 and *brx* PPSEs as

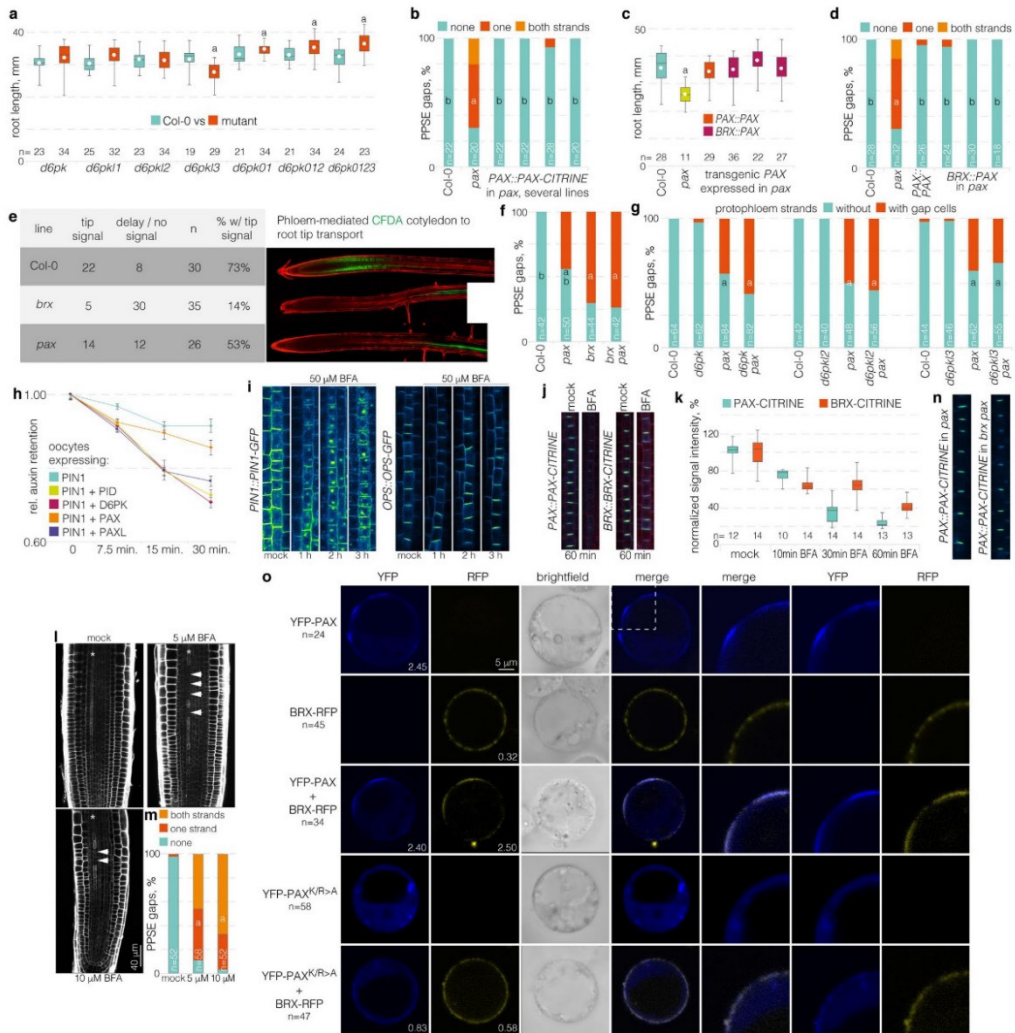
compared to nuclei of cells in directly neighbouring files. Statistically significant differences between PPSE/neighbours and neighbour/neighbour in the Col-0 and *brx* DII-VENUS groups are indicated (two-sided Student's *t*-test;  $a$ ,  $P = 2.49 \times 10^{-7}$ ;  $b$ ,  $P = 0.026$ ). **j**, Coefficient of variance for fluorescence traces of the DII-VENUS reporter and its mDII-VENUS control (left) and PI staining (right) along protophloem cell files. The statistically significant difference in VENUS fluorescence in the *brx* group is indicated (two-sided Student's *t*-test;  $a$ ,  $P = 2.30 \times 10^{-7}$ ). **k**, Quantification of PPSE strands with gaps in roots of indicated genotypes. **l**, Root length in seven-day-old seedlings for indicated genotypes. The statistically significant differences between *CVP2::MP^{\Delta}* in *brx* and *brx* alone ( $P = 0.0017$ ) and between *CVP2::MP^{\Delta}* in *brx* and *CLE45::MP^{\Delta}* in *brx* ( $P = 0.0052$ ) are indicated by the character  $\alpha$ . **m**, Distribution of gap size in protophloem strands of seven-day-old seedlings with gaps of indicated genotypes. The statistically significant differences between *CVP2::MP^{\Delta}* in *brx* and *brx* alone ( $P = 0.0008$ ) and between *CVP2::MP^{\Delta}* in *brx* and *CLE45::MP^{\Delta}* in *brx* ( $P = 0.0051$ ) are indicated by the character  $\alpha$  (two-sided  $\chi^2$  test). **n**, Expression of fluorescent NLS-VENUS reporter in PPSEs of *brx* mutants, driven by either *CVP2* or *CLE45* promoter. Arrowheads indicate gap cells. **o**, **p**, Expression of *CVP2::NLS-VENUS* reporter (green fluorescence) in PPSE cell files (asterisks) of six-day-old Col-0 root meristems (PI staining, white) grown in the presence of (**o**), or transferred for 48 h onto (**p**), increasing amounts of the auxin biosynthesis inhibitor L-kynurenine (L-kyn). On the higher concentration, PPSE cell files (magnified) were barely distinguishable. **q**, Confocal microscopy of seven-day-old root meristems (PI staining, red). Asterisks indicate sieve element cell files (magnified, barely distinguishable in *aux1 brx*).



**Extended Data Fig. 3 | Identification of BRX interactors.** **a**, Induction of *BRX* expression in cotyledons in the VISUAL transdifferentiation assay, as indicated by a *BRX::GUS* reporter gene. **b**, Visualization of successful tracheary element differentiation using polarized light

microscopy. **c**, Western analysis of BRX-CITRINE fusion protein after immunoprecipitation. **d**, List of the top BRX interactors, indicating the number of peptides isolated as compared to controls.

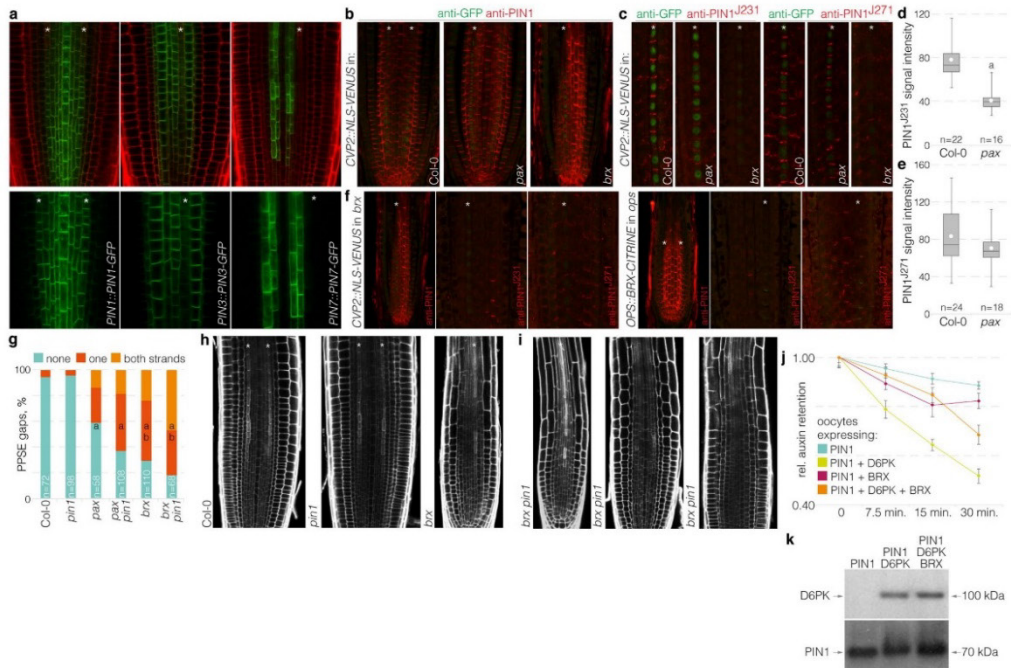




Extended Data Fig. 4 | See next page for caption

**Extended Data Fig. 4 | Phenotypic analysis of *pax*-related mutants and transgenic lines.** **a**, Root length in seven-day-old seedlings for indicated mutants and parallel Col-0 controls. Statistically significant differences between Col-0 and mutants are indicated (Student's *t*-test, two-sided; *a*,  $P < 0.02$ ). **b**, Quantification of gap-cell frequency in protophloem strands of six-day-old seedlings. Statistically significant differences are indicated (two-sided Fisher's exact test; *a*, *pax* versus Col-0; *b*, others versus *pax*; all  $P$  values  $< 0.001$ ). **c**, Root length in seven-day-old seedlings for Col-0, *pax* and transgenic lines in the *pax* mutant background that expressed *PAX* under the control of its native promoter or the *BRX* promoter. The statistically significant difference between *pax* and Col-0 is indicated (two-sided Student's *t*-test; *a*,  $P = 0.00016$ ). **d**, Quantification of gap-cell frequency in protophloem strands of six-day-old seedlings. Statistically significant differences are indicated (two-sided Fisher's exact test; *a*, *pax* versus Col-0; *b*, others versus *pax*; all  $P$  values  $< 0.001$ ). **e**, Phloem-mediated translocation of carboxyfluorescein diacetate succinimidyl ester (CFDA) dye (green fluorescence) into the phloem-unloading zone of the root tip 45 min after CFDA application to the cotyledons of four-day-old seedlings, and corresponding classification of CFDA signal at the end of the experiment. **f**, Quantification of gap-cell frequency in protophloem strands of six-day-old seedlings. Statistically significant differences are indicated (two-sided Fisher's exact test; *a*, others versus Col-0; *b*, Col-0 and *pax* versus *brx*; all  $P$  values  $< 0.01$ ). **g**, Quantification of gap-cell frequency in protophloem strands of six-day-old seedlings. Statistically significant

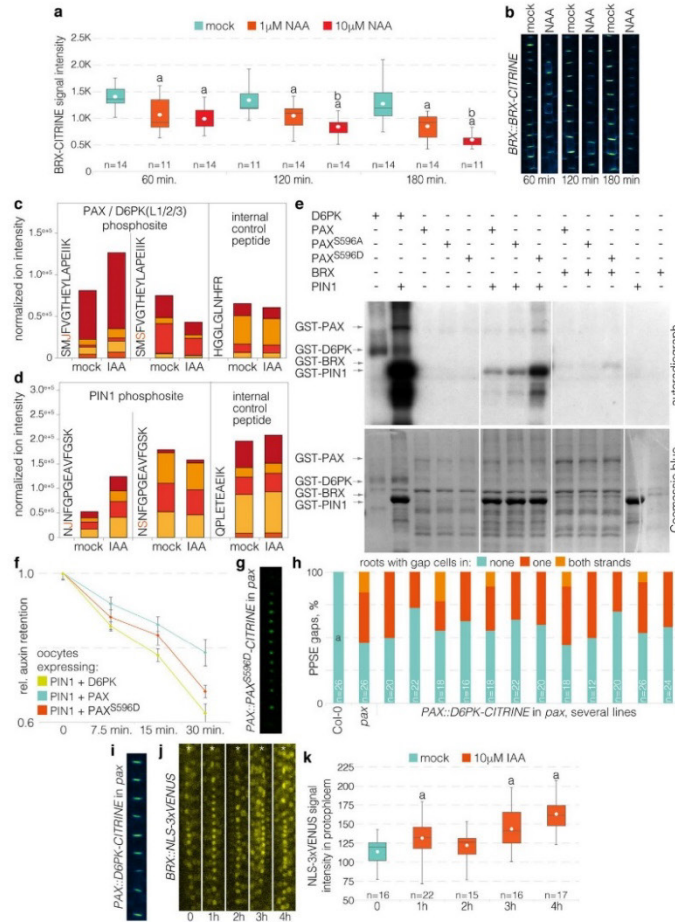
differences are indicated (two-sided Fisher's exact test; *a*, others versus Col-0, all  $P$  values  $< 0.001$ ). **h**, Auxin transport assays performed in *X. laevis* oocytes expressing the indicated heterologous plant proteins ( $n = 10$  oocytes per time point; error bars, s.e.m.). **i**, BFA control experiments. Accumulation of PIN1-GFP fusion protein in BFA compartments (left), and comparative BFA insensitivity of OPS-GFP fusion protein (right). **j**, Dissociation of PAX-CITRINE and BRX-CITRINE fusion proteins from the plasma membrane in response to 5  $\mu$ M BFA treatment. **k**, Quantification of PAX-CITRINE and BRX-CITRINE fluorescence signal at the plasma membrane in response to 5  $\mu$ M BFA treatment, normalized to allow direct comparison (means of approximately ten cells per root). **l**, Confocal microscopy of six-day-old PI-stained root meristems grown on mock or low BFA concentration as indicated. Asterisks indicate PPSE cell files and arrowheads indicate gap cells. **m**, Quantification of gap-cell frequency in PPSE strands of roots shown in (l). Statistically significant differences are indicated (two-sided Fisher's exact test; *a*, others versus mock,  $P < 0.0001$ ). **n**, Expression of PAX-CITRINE fusion protein under its native promoter, in *pax* single or *brx pax* double mutants. **o**, Transient expression of the indicated fusion proteins, alone or in combination, in *Arabidopsis* protoplasts. The PAX<sup>K/R>A</sup> variant carries point mutations in a polybasic stretch that is required for plasma membrane interaction<sup>24</sup>. The average number of patches per protoplast is indicated.



**Extended Data Fig. 5 | PIN activity in the root protophloem.**

**a**, Confocal microscopy of indicated reporter genes (green fluorescence) in the root meristem (PI staining, red) of Col-0 wild-type plants (top), and magnification without PI background (bottom). Asterisks indicate sieve element cell files. **b**, Immunolocalization of nuclear localized NLS-VENUS (green) expressed under control of PPSE-specific *CVP2* promoter, and PIN1 (red) by antibody staining. Asterisks indicate PPSE cell files. **c**, Simultaneous immunolocalization of *CVP2*-driven NLS-VENUS (green) with different anti-PIN1 antibodies that specifically detect phosphorylated PIN1 residues S231 (J231) or S271 (J271). **d**, Quantification of the J231 phosphosite signal intensity (means from approximately ten cells per root, arbitrary units). The statistically significant difference is indicated (two-sided Student's *t*-test;  $a$ ,  $P = 1.2 \times 10^{-9}$ ). **e**, Quantification of the J271 phosphosite signal intensity (means from approximately ten cells per root, arbitrary units). **f**, Immunolocalization of PIN1, and the J231 and J271 PIN1 phosphosites (red) in *brx* (left) or *ops* (right) by antibody staining, with an *OPS::BRX-CITRINE*

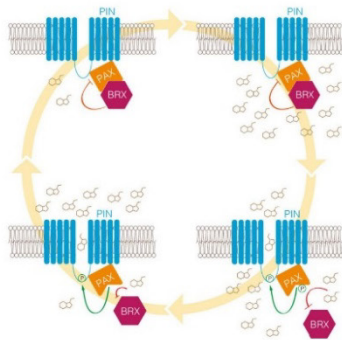
or *CVP2::NLS-VENUS* reporter in the background for the identification of PPSE cell files (asterisks). **g**, Quantification of gap-cell frequency in protophloem strands of six-day-old seedlings for the indicated genotypes. Statistically significant differences are indicated (two-sided Fisher's exact test; **a**, Col-0 and *pin1* versus others,  $P < 0.0001$ ; **b**, *brx* or *pax* single mutant versus *brx pin1* or *pax pin1* double mutants,  $P < 0.02$ ). **h**, Confocal microscopy of representative six-day-old Col-0, *pin1*, and *brx* root meristems (PI staining, white). Asterisks indicate PPSE cell files. **i**, Different phenotypic classes occurring in *brx pin1* double mutant root meristems (PI staining, white). PPSE cell files were frequently barely distinguishable or missing. **j**, Auxin transport assays performed in *X. laevis* oocytes expressing the indicated heterologous plant proteins ( $n = 10$  oocytes per time point; error bars, s.e.m.). **k**, Western blot analysis of the oocytes used in **j**, demonstrating that BRX expression does not interfere with D6PK or PIN1 expression or stability (detection of YFP-D6PK and PIN1 with anti-GFP and anti-PIN1 antibodies, respectively).



### Extended Data Fig. 6 | BRX auxin response and PAX specificity.

**a, b**, Response of BRX-CITRINE fusion protein to treatment with 1  $\mu$ M or 10  $\mu$ M auxin (NAA), time course experiment (**b**) with quantification (**a**, means from approximately ten cells per root, arbitrary units). Statistically significant differences are indicated (two-sided Student's *t*-test; a, mock versus others,  $P < 0.0094$ ; b, 1  $\mu$ M versus 10  $\mu$ M auxin,  $P < 0.0028$ ). **c**, Phosphoproteomics of auxin-treated seedlings, showing normalized abundance of a conserved phosphosite in PAX, D6PK, D6PKL1-3, and AGC1-6, with subfragments indicated in different colours. **d**, Same as **c**, for a PIN1 phosphosite. **e**, Radioactive *in vitro* kinase assays with GST fusion proteins of D6PK, PAX, or PAX(S596A) and PAX(S596D) point mutants, with BRX or the PIN1 cytosolic loop as substrate (top) and corresponding loading controls (bottom). **f**, Auxin transport assays performed in *X. laevis* oocytes expressing the indicated heterologous

plant proteins ( $n = 10$  oocytes per time point; error bars, s.e.m.). **g**, Polar localization of the YFP-PAX(S596D) variant in developing PPSEs of a *pax* mutant. **h**, Quantification of gap-cell frequency in protophloem strands of seven-day-old *pax* mutant seedlings that express a D6PK-CITRINE fusion protein under the control of the PAX promoter. The statistically significant difference is indicated (two-sided Fisher's exact test; a, Col-0 versus *pax* and transgenic lines,  $P < 0.0001$ ). **i**, Polar localization of D6PK-CITRINE fusion protein in developing PPSEs of a *pax* mutant. **j, k**, Auxin induction of BRX transcription in developing PPSE cell files (asterisks) visualized using an NLS-3 $\times$ VENUS reporter gene (**j**), with corresponding quantification of nuclear fluorescence signal (**k**). Statistically significant differences are indicated (one-sided Student's *t*-test; a, versus preceding time point,  $P < 0.0153$ ).



**Extended Data Fig. 7 | Molecular rheostat model for PAX-BRX action in the regulation of auxin efflux.** Proposed model for the cellular action of PAX and BRX as elements of a molecular rheostat. BRX interacts with PAX at the plasma membrane, where it inhibits PIN-mediated auxin efflux at lower auxin levels. Because of reduced PIN-mediated auxin efflux, cellular auxin levels increase so that, eventually, BRX becomes displaced from the plasma membrane. Concomitantly, PAX becomes activated and increasingly stimulates auxin efflux. Reinforced through auxin-induced *BRX* transcription and decreasing cellular auxin levels, BRX can return to the plasma membrane and again inhibit auxin efflux. This interplay would lead to a dynamic steady-state equilibrium that fine-tunes auxin levels along a cell file.



# Auxin methylation is required for differential growth in *Arabidopsis*

Mohamad Abbas<sup>a,b,1</sup>, Jorge Hernández-García<sup>a</sup>, Stephan Pollmann<sup>c</sup>, Sophia L. Samodelov<sup>d,e,2</sup>, Martina Kolb<sup>f</sup>, Jiří Friml<sup>b</sup>, Ulrich Z. Hammes<sup>f,3</sup>, Matias D. Zurbriggen<sup>d</sup>, Miguel A. Blázquez<sup>a,4</sup>, and David Alabadi<sup>a</sup>

<sup>a</sup>Instituto de Biología Molecular y Celular de Plantas, Consejo Superior de Investigaciones Científicas–Universidad Politécnica de Valencia, 46022 Valencia, Spain; <sup>b</sup>Institute of Science and Technology Austria, 3400 Klosterneuburg, Austria; <sup>c</sup>Centro de Biotecnología y Genómica de Plantas, Universidad Politécnica de Madrid–Instituto Nacional de Investigación y Tecnología Agraria y Alimentación, 28223 Pozuelo de Alarcón, Spain; <sup>d</sup>Institute of Synthetic Biology and Cluster of Excellence in Plant Sciences, University of Düsseldorf, 40225 Düsseldorf, Germany; <sup>e</sup>Spemann Graduate School of Biology and Medicine, University of Freiburg, 79085 Freiburg, Germany; and <sup>f</sup>Department of Cell Biology and Biochemistry, Regensburg University, 93053 Regensburg, Germany

Edited by Ottoline Leyser, University of Cambridge, Cambridge, United Kingdom, and approved May 21, 2018 (received for review April 16, 2018)

**Asymmetric auxin distribution is instrumental for the differential growth that causes organ bending on tropic stimuli and curvatures during plant development. Local differences in auxin concentrations are achieved mainly by polarized cellular distribution of PIN auxin transporters, but whether other mechanisms involving auxin homeostasis are also relevant for the formation of auxin gradients is not clear. Here we show that auxin methylation is required for asymmetric auxin distribution across the hypocotyl, particularly during its response to gravity. We found that loss-of-function mutants in *Arabidopsis* IAA CARBOXYL METHYLTRANSFERASE1 (*IAMT1*) prematurely unfold the apical hook, and that their hypocotyls are impaired in gravitropic reorientation. This defect is linked to an auxin-dependent increase in *PIN* gene expression, leading to an increased polar auxin transport and lack of asymmetric distribution of PIN3 in the *iamt1* mutant. Gravitropic reorientation in the *iamt1* mutant could be restored with either endodermis-specific expression of *IAMT1* or partial inhibition of polar auxin transport, which also results in normal *PIN* gene expression levels. We propose that IAA methylation is necessary in gravity-sensing cells to restrict polar auxin transport within the range of auxin levels that allow for differential responses.**

hormone regulation | auxin metabolism | homeostasis | gravitropism

The plant hormone auxin has long been known to act not only as a key morphogenetic component of differentiation pathways, but also as a coordinator of plant growth in response to environmental stimuli (1, 2). Particularly interesting is the involvement of auxin in the generation of curvatures, such as the apical hook of etiolated seedlings (3, 4), and in the reorientation of organ growth on lateral illumination or in response to gravity (5–7). An essential feature that explains the relevant role of auxin in these processes is the robust mechanism that directs the movement of this hormone through the plant, known as polar auxin transport (PAT) (8–10). Among other consequences, PAT allows the establishment of asymmetric distribution of auxin, which results in differential triggering of auxin responses in different parts of a given organ.

In the case of tropic responses, such as phototropism and gravitropism, it has been estimated that the concentration difference across the hypocotyl may range between 1.5-fold and 2-fold (11–13), similar to the difference in the root tip that triggers gravitropic reorientation (14). The fact that this small difference is sufficient to cause differential growth responses implies that the levels of auxin must be well maintained within a very specific range to ensure that this gradient is informative. Although regulation of the expression, tissue distribution, and cellular localization of the PIN-FORMED (PIN) auxin efflux carriers is presumably the most important mechanism for the maintenance of local auxin maxima (15, 16), it is likely that other mechanisms, such as the regulation of auxin homeostasis, also contribute to this effect (17–19).

Among the pathways that contribute to auxin homeostasis (2), conversion of indole-3-acetic acid (IAA) into methyl-IAA (Me-IAA) by an IAA CARBOXYL METHYLTRANSFERASE (*IAMT*) could be relevant, because ectopic overexpression of

*IAMT1* in *Arabidopsis* disrupts gravitropic responses (20). The specificity of *IAMT1* on IAA has been demonstrated for the orthologs in rice and *Arabidopsis* (21, 22). It has been reported that silencing of *IAMT1* in *Arabidopsis* using an RNAi strategy causes a dramatic phenotype that might be explained by simultaneous repression of additional members of the SABATH family (20), which includes methyltransferases for jasmonic acid and other substrates (Fig. 1A). Current models consider Me-IAA an inactive form of IAA, because the phenotype caused by *IAMT1* overexpression resembles that of auxin-deficient or auxin-resistant mutants (20), and also because exogenous application of Me-IAA produces the same effects as IAA application (23), which can be explained by hydrolysis of Me-IAA by auxin methyl esterases (24). Given that there is no indication of the physiological relevance of IAA methylation in the generation of differential auxin distribution, we identified and examined the behavior of single *iamt1* loss-of-function mutants under gravistimulation, and found that IAA methylation is required for asymmetric auxin distribution across the hypocotyl.

## Results and Discussion

We selected two T-DNA insertion lines (*iamt1-1* and *iamt1-2* in Col-0 and *Ler* backgrounds, respectively), the former of which would

### Significance

Auxin is a plant hormone required for the establishment of growth orientation. Redistribution of auxin across an organ allows reorientation, and this is achieved through changes in the polar localization of auxin efflux carriers. We have found that when auxin methylation is impaired, auxin is not correctly redistributed on gravistimulation, due to a general increase in basipetal auxin transport and deficient relocalization of auxin transporters. We conclude that auxin must be within a specific concentration range for its correct distribution, and this range is maintained by auxin methylation in the endodermis, the cell type that perceives gravity.

Author contributions: M.A., J.F., U.Z.H., M.D.Z., M.A.B., and D.A. designed research; M.A., J.H.-G., S.P., S.L.S., and M.K. performed research; M.A., J.H.-G., S.P., S.L.S., M.K., J.F., U.Z.H., M.D.Z., M.A.B., and D.A. analyzed data; and M.A.B. wrote the paper.

The authors declare no conflict of interest.

This article is a PNAS Direct Submission.

Published under the PNAS license.

<sup>1</sup>Present address: Plant and Crop Science, University of Nottingham, Loughborough LE12 5RD, United Kingdom.

<sup>2</sup>Present address: Department of Clinical Pharmacology and Toxicology, University Hospital Zurich, University of Zurich, 8091 Zurich, Switzerland.

<sup>3</sup>Present address: Plant Systems Biology, Technical University of Munich, 85354 Freising, Germany.

<sup>4</sup>To whom correspondence should be addressed. Email: mblazquez@ibmcp.upv.es.

This article contains supporting information online at [www.pnas.org/lookup/suppl/doi:10.1073/pnas.1806565115/-DCSupplemental](http://www.pnas.org/lookup/suppl/doi:10.1073/pnas.1806565115/-DCSupplemental).

Published online June 13, 2018.

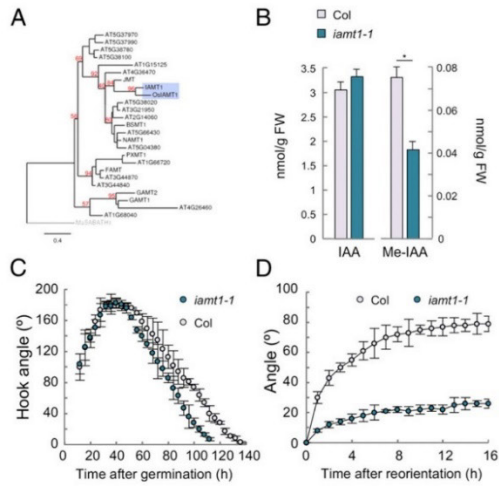


**Fig. 1.** IAMT1 is necessary for proper differential growth. (A) Phylogenetic tree of *Arabidopsis* methyltransferases. Numbers in red represent bootstrap values. (B) Levels of IAA and Me-IAA in 3-d-old etiolated seedlings of the *iamt1-1* mutant. Asterisk indicates that the difference is statistically significant (Student's *t* test, \**P* < 0.05). (C) Apical hook dynamics in the *iamt1-1* mutant. (D) Gravitropic reorientation of *iamt1* mutant hypocotyls.

putatively render a truncated version of IAMT1 lacking part of the active site (20) (*SI Appendix*, Fig. S1A). Hormone quantification in etiolated seedlings (Fig. 1B and *SI Appendix*, Fig. S2A) and light-grown seedlings (*SI Appendix*, Fig. S1B) showed at least a 50%

decrease in the levels of Me-IAA in *iamt1* mutants, confirming *in vivo* that IAMT1 encodes an IAA methyltransferase and suggesting that other methyltransferases can also act on IAA or, alternatively, that the truncated proteins encoded by the two *iamt1* alleles might retain some activity. It is also important to note that the decrease in Me-IAA was not accompanied by a significant increase in free IAA levels (Fig. 1B), indicating that Me-IAA represents a small proportion in the total IAA pool, in accordance with the observation that *iamt1-1* mutant plants do not display any obvious morphological defects that resemble IAA overaccumulation (*SI Appendix*, Fig. S1C).

To investigate if a reduction in IAA methyltransferase activity has an impact in the formation of auxin redistribution, we first examined the dynamics of apical hook development and the hypocotyl response to a gravitropic reorientation, two processes that involve auxin-dependent differential growth (4, 6, 25). The *iamt1* mutants did not display any severe defect in the formation or maintenance of the apical hook, showing only slightly faster opening of the hook (Fig. 1C and *SI Appendix*, Fig. S2B). In contrast, the ability of the mutant hypocotyls to reorient after gravistimulation was largely impaired (Fig. 1D and *SI Appendix*, Fig. S2C). Importantly, this different behavior of *iamt1* with respect to the two processes was correlated with the ability of the mutant to redistribute auxin across the hypocotyl in each situation. The asymmetry in the activity of the auxin signaling reporter DR5::GFP across the apical hook was similar in 3-d-old etiolated wild-type (WT) and *iamt1-1* mutant seedlings, despite the higher reporter signal in the mutant (*SI Appendix*, Fig. S3), suggesting no apparent defect in differential auxin distribution during hook formation in etiolated *iamt1-1* seedlings. Nonetheless, the seemingly high auxin signaling in the mutant apical hook might be the cause of its premature opening (Fig. 1C). On the other hand, gravistimulation of *iamt1-1* mutant hypocotyls did not provoke the typical accumulation of the DR5 reporter observed on the lower side of WT hypocotyls (6); instead, a similarly high signal was observed on both sides of the mutant hypocotyl before and after the stimulus (Fig. 2A and B). This

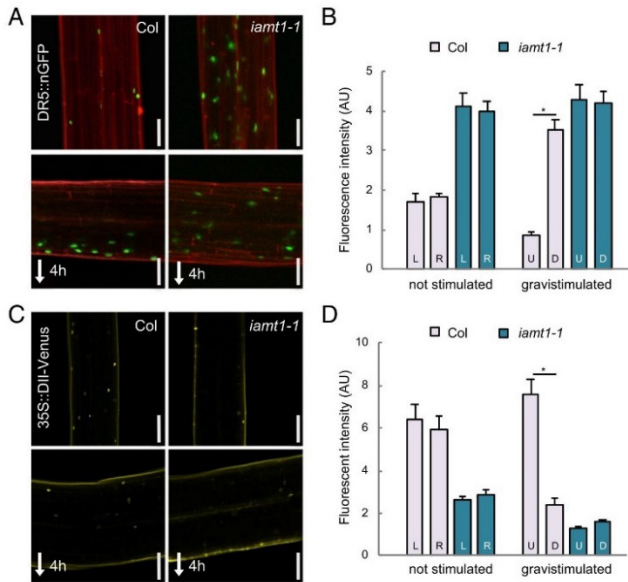


**Fig. 2.** IAMT1 modulates auxin levels in the hypocotyl. (A) DR5::nGFP signal in the hypocotyl of 3-d-old etiolated seedlings before and 4 h after gravistimulation. (B) Levels of DR5::nGFP in either side of the hypocotyl. (C) DII-Venus signal in the hypocotyl of 3-d-old etiolated seedlings before and 4 h after gravistimulation. (Scale bars: 100  $\mu$ m.) (D) Levels of DII-Venus signal in either side of the hypocotyl. D, down; L, left; R, right; U, up. Asterisks indicate that the difference is statistically significant (Student's *t* test, \**P* < 0.001).

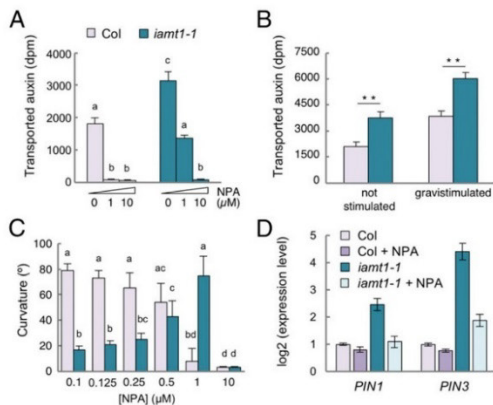


**Fig. 3.** IAMT1 restricts polar auxin transport in 3-d-old etiolated hypocotyls. (A) PAT in unstimulated etiolated hypocotyls. Seedling were treated for 6 h with NPA, followed by a 3-h incubation with [<sup>3</sup>H]-IAA. (B) Effect of 6 h of gravistimulation on PAT in etiolated hypocotyls. (C) Effect of NPA on hypocotyl curvature at 12 h after gravitropic reorientation. (D) Expression of *PIN1* and *PIN3* in seedlings gravistimulated for 4 h in 0.5 μM NPA or mock solution, determined by qRT-PCR. Values in A and B are the mean of three biological replicates. In C, values are the average of at least 15 seedlings. In all cases, the error bar represents SD. Asterisks indicate that the difference is statistically significant (Student's t test, \**P* < 0.05; \*\**P* < 0.01; \*\*\**P* < 0.001). Letters indicate significant differences between groups (*P* < 0.05, one-way ANOVA, Tukey's HSD post hoc test). In D, error bars represent SD from three technical replicates. Data from a representative experiment are shown. Two other biological replicates yielded similar results.

defect in the asymmetric auxin response is very likely caused by the inability of the *iamt1-1* mutant to differentially accumulate auxin, as indicated by the loss of signal of a more direct auxin reporter, DII-Venus, on both sides of the hypocotyl (Fig. 2 C and D).

The findings of no change in the amount of free IAA in whole seedlings in the *iamt1-1* mutant (Fig. 1B) and defects in local auxin distribution on gravistimulation (Fig. 2) suggest that alterations in PAT may contribute to the *iamt1* phenotype. In fact, auxin transport along the hypocotyl, measured using <sup>3</sup>H-IAA, was nearly twofold higher in the *iamt1-1* mutant compared with the WT (Fig. 3A). In both cases, transport was inhibited by incubation with 1-naphthylphthalamic acid (NPA), confirming that enhanced IAA movement was due to increased PAT.

To investigate the observed increase in the IAA transport in *iamt1-1* correlates with the agravitropic phenotype of the mutant, we measured PAT in WT and mutant seedlings with or without gravistimulation. Interestingly, PAT was enhanced in the wild-type and the *iamt1-1* mutant after reorientation (Fig. 3B). We next assayed the capacity of WT and mutant seedlings to reorient in the presence of NPA. As expected, the gravitropic reorientation of the hypocotyls of WT seedlings was gradually reduced with increasing doses of NPA (Fig. 3C). In contrast, low NPA doses promoted reorientation of *iamt1* seedlings and only a high concentration (10 μM) of NPA abolished it (Fig. 3C and *SI Appendix*, Fig. S5A). Remarkably, the same amount of NPA restored both the reorientation ability and auxin transport to WT levels in the mutant (Fig. 3A and C and *SI Appendix*, Fig. S5A). These results suggest a causal connection between the increased PAT in the *iamt1* mutant and its agravitropic phenotype.

The confirmation that a reduction of PAT alleviates the agravitropic phenotype of *iamt1* mutants suggests that PAT restriction by IAA methylation is an important element in asymmetric auxin redistribution. Given that auxin has been proposed to

indirectly regulate its own transport (26–28), we hypothesized that the primary effect of the auxin overaccumulation in *iamt1* mutants could in fact be an increase in the expression of *PIN* genes. To test this hypothesis, we measured the transcript levels of *PIN1*, *PIN2*, *PIN3*, and *PIN7* in 3-d-old etiolated seedlings and found at least twofold higher expression levels in *iamt1* mutants (Fig. 3D and *SI Appendix*, Figs. S4 and S5B). Moreover, transcriptional regulation of *PIN* genes by IAMT1 activity may be physiologically relevant for differential auxin distribution, since gravistimulation provoked not only an increase in PAT in WT seedlings (Fig. 3B), but also an increase in the expression of *PIN1* and *PIN3*, albeit with different kinetics (*SI Appendix*, Fig. S4A), and, to a lesser extent, of *PIN2* and *PIN7* (*SI Appendix*, Fig. S4B). The expression of *PIN* genes in the *iamt1-1* mutant followed the same transient induction on reorientation as in the wild-type, but with higher transcript levels (*SI Appendix*, Fig. S4 A and B). More importantly, the increased expression of *PIN* genes in the *iamt1-1* mutant was restored by incubation with NPA at a concentration that rescued gravitropic reorientation (Fig. 3D and *SI Appendix*, Fig. S4C), indicating that enhanced PAT and increased local accumulation of auxin in the *iamt1* hypocotyls are caused by a perturbation of the auxin-dependent feed-forward loop that promotes auxin transport.

The increase in *PIN3* gene expression in the *iamt1-1* mutant also resulted in higher levels of PIN3 protein, as indicated by the comparably stronger GFP signal in *PIN3::PIN3-GFP* lines throughout the mutant hypocotyls (Fig. 4). Gravistimulation of WT hypocotyls provokes the gradual asymmetrical redistribution of PIN3 to the inner side of endodermal cells in the upper half of hypocotyls (5, 6), being proposed as a major mechanism explaining how the gravity vector is translated into the directional auxin fluxes both in roots and shoots (29). However, we observed that the PIN3-GFP signal in the *iamt1-1* mutant remained in the outer side of endodermal cells even 6 h after gravistimulation (Fig. 4). This explains the mutant defects in both the gravity-mediated asymmetric auxin distribution and hypocotyl bending (Figs. 1D and 2 C and D and *SI Appendix*, Fig. S2C). Interestingly, we found that expression of *IAMT1* in the endodermis, but not in the epidermis, was able to rescue the agravitropic phenotype of *iamt1* mutants (Fig. 5 and *SI Appendix*, Fig. S6), indicating that IAA methylation acts locally in the endodermis to establish adequate rates of polar auxin transport. If Me-IAA is simply an inactive form of IAA, methylation could be a fine-tuning mechanism to correct local concentrations of auxin in the tissue that responds to gravity. On the other hand, the possibility that a reduction in auxin methylation can indirectly affect auxin conjugation, or that Me-IAA itself has a direct role as a modulator of auxin signaling or transport, cannot be ruled out. To evaluate this latter possibility, we resorted to orthogonal systems, which allowed the assessment of these processes in a context devoid of other endogenous components that may potentially affect the study. We first reconstructed the IAA perception complex in mammalian cells to observe the event of perception using a ratiometric sensor for auxin (30). Our results showed that Me-IAA neither mimicked the response to IAA in the activity of the auxin coreceptor complex nor interfered with the response triggered by IAA (*SI Appendix*, Fig. S7). Similarly, the presence of intracellular Me-IAA in auxin transport assays using *Xenopus* oocytes (31) reduced PIN1- and PIN3-mediated IAA efflux to the same extent as IAA itself (*SI Appendix*, Fig. S8), suggesting that Me-IAA can be transported by PINs and compete with IAA, and that it is rather unlikely that it acts as an allosteric inhibitor of these transporters.

In summary, we propose that IAA methylation is a biologically relevant mechanism in the endodermis for the maintenance of auxin homeostasis and the appropriate expression levels of *PIN* genes that allow asymmetric auxin distribution under certain circumstances, such as during gravitropic reorientation (Fig. 5B). Our results are in line with recent reports highlighting the importance of auxin conjugation in other developmental contexts, such as



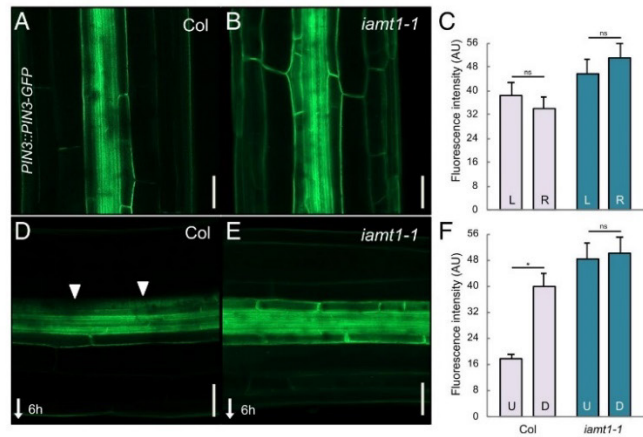


**Fig. 4.** The *iamt1-1* mutant shows defects in PIN3 lateralization after gravistimulation. (A and B) Localization of PIN3-GFP in 3-d-old etiolated WT (Col) and *iamt1-1* hypocotyls. (C) Quantitative analysis of PIN3-GFP fluorescence in the left and right sections on the hypocotyls. The graph represents the average intensity of fluorescence of the outer and inner endodermal plasma membranes. (D and E) Localization of PIN3-GFP at 6 h after gravistimulation. (Scale bars: 50  $\mu$ m.) (F) Quantitative analysis of PIN3-GFP in the upper and lower sections on the hypocotyls. Graphs represents the average intensity of fluorescence of endodermal plasma membranes facing away from the vasculature (left and right in vertical hypocotyls; upper and lower in horizontal hypocotyls). Arrows mark the lateralization of PIN3. Error bars represent SD. D, down; L, left; R, right; U, up. The asterisk indicates that the difference is statistically significant (Student's *t* test, \**P* < 0.001).

shade avoidance and root growth (17, 32). Moreover, the link between auxin transport and the control of an appropriate range of auxin concentrations shown here suggest that both mechanisms have necessarily coevolved to optimize plant adaptation.

**Materials and Methods**

**Plant Material and Growth Conditions.** *Arabidopsis thaliana* ecotype Col-0 was used as WT. The following published transgenic and mutant lines were used: *PIN3::PIN3-GFP* (4), *35S::DII-Venus* (33), and *DR5::nGFP* (34). *PIN3::PIN3-GFP*, *DII-Venus*, and *DR5::nGFP* were introgressed into the *iamt1-1* mutant background by crossing. The *iamt1-1* described in this work corresponds to the

T-DNA insertion line SALK\_072125 (35). This line was genotyped with *IAMT1*-specific oligonucleotides and with an oligonucleotide specific for the T-DNA left border (SI Appendix, Table S1). The presence of transgenes in progenies of crosses was determined by the corresponding antibiotic resistance when possible, and also by genotyping (SI Appendix, Table S1).

Seeds were sown on 1/2 M5 plates with 1% (wt/vol) sucrose and 8 g/L agar, pH 5.8. Seeds were stratified for 3 d at 4 °C, exposed to light for 6–8 h at 20 °C, and then cultivated in the dark. For experiments including chemicals, WT and *iamt1-1* seedlings were grown for 3 d in darkness and then transferred to medium containing 0.125, 0.25, 0.5, 1, and 10  $\mu$ M NPA (Sigma-Aldrich) for 2 h before rotating the plate 90° for 12 h.

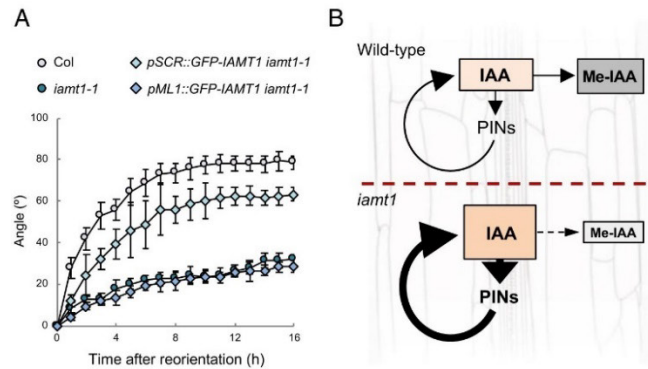


**Fig. 5.** Auxin methylation in the endodermis is sufficient to ensure gravitropic reorientation. (A) Endodermal expression of *IAMT1* is able to recover the *iamt1-1* gravitropic response. Gravitropic reorientation of *iamt1-1* mutant complemented with cell-specific expression of *IAMT1* in endodermis (*pSCR*) and epidermis (*pML1*). The experiments were carried out as described in *Materials and Methods*. Error bars represent SD. (B) Model for the role of auxin methylation on gravitropic reorientation. *IAMT1* is necessary to maintain relatively low levels of auxin in the responding tissue; in the absence of such mechanism, auxin levels locally increase and enhance the PAT-mediated feedforward loop that causes auxin hyperaccumulation. The relevance of this feedforward loop is highlighted by the rescue of the *iamt1* mutant phenotype by NPA.

**In Vivo Plant Imaging.** Apical hook development and gravitropic reorientation were monitored as described previously (36, 37). For analysis of the gravity response, 3-d-old etiolated seedlings grown in vertical plates were imaged at 1-h intervals for 16 h after rotating the plate 90°. Hypocotyl angles were measured by ImageJ. Three replicates of at least 10 seedlings with a synchronized germination start were processed.

**Confocal Imaging and Signal Quantification.** In some cases, hypocotyl cells were visualized by propidium iodide (PI) staining. In these cases, seedlings were rinsed first for 2 min with 10 µg/mL of PI and then for 5 min with water. Fresh stained seedlings were mounted on slides only with water. Images were obtained with a Zeiss 780 Axio Observer confocal microscope for *DR5::nGFP* and with a Zeiss LSM 800 confocal microscope for *DII-Venus* and *PIN3::PIN3-GFP*. For GFP and Venus detection, channel 1 was configured between 500 and 540 nm, and for PI detection, channel 2 was configured between 590 and 660 nm.

Fluorescence intensity was measured in the apical hook and in the bent region of the hypocotyl. The *DII-Venus* and *DR5::nGFP* fluorescence intensity was compared between the inner and outer sides of the apical hook and between the lower and upper sides of the hypocotyl in the responsive part as described previously (6). For quantification of the gravity-induced PIN3-GFP relocation, the PIN3-GFP fluorescence intensity was compared between the outer and inner sides of endodermal cells in both sides of hypocotyls as described previously (6). ImageJ software was used for all intensity measurements. Three replicates of at least 10 seedlings of similar size were processed. Values are presented as the mean of averages. The *t* test was used for statistic evaluation. Error bars in graphs represent SE.

**Real-Time Quantitative RT-PCR.** Total RNA from 3-d-old etiolated seedlings was extracted using the RNeasy Plant Mini Kit (Qiagen). cDNA synthesis and quantitative RT-PCR, as well as primer sequences for amplification of *PIN1*, *PIN2*, *PIN3*, *PIN7*, *IAMT1*, and *EF1α* genes, have been described previously (37, 38).

**Auxin Transport Assay.** For this assay, 3-d-old etiolated seedlings grown on vertical plates containing control medium were transplanted for 6 h to plates with mock or NPA at the indicated concentrations. The upper half of seedlings was placed on top of a small strip of Parafilm M, and a droplet containing 6.75 nM [<sup>3</sup>H]-IAA (specific activity, 25 Ci/mmol, 1 µCi/µL; Amersham) in 0.1% Tween-20 (Sigma-Aldrich) was applied to cotyledons for 3 h. For auxin transport during gravistimulation, [<sup>3</sup>H]-IAA was added after seedlings were either allowed to grow straight for another 6 h or plates were rotated 90° for the same time. The lowest 5 mm of the hypocotyl was collected, and radioactivity was measured as described previously (39).

**IAA and Me-IAA Quantification.** Whole seedlings were immediately frozen in liquid N<sub>2</sub>. Approximately 100 mg of tissue was pooled per sample, and at least three biological replicates were harvested for each independent experiment. Then 1 mL of methanol and 50 pmol of [<sup>2</sup>H<sub>2</sub>]-IAA or 100 pmol [<sup>2</sup>H<sub>2</sub>]-Me-IAA were added, the tissue was heated for 2 min at 60 °C, followed by further incubation without heating for at least 1 h. The sample was then taken to complete dryness.

For purification of IAA and Me-IAA, the sediments were dissolved in 2 mL of cold sodium phosphate buffer (50 mM, pH 7.0) containing 5% MeOH, followed by a 10-min ultrasonic treatment (B5510DTH; Branson Ultrasonics). Next, the pH was adjusted to 2.5 with 1 M hydrochloric acid, and the sample was purified by solid-phase extraction using 1 mL/30 mg Oasis HLB columns

(Waters) conditioned with 1 mL of methanol and 1 mL of water, and then equilibrated with 0.5 mL of sodium phosphate buffer (acidified with 1 M hydrochloric acid to pH 2.5). After sample application, the column was washed twice with 1 mL of 5% methanol and then eluted with 2 mL of 80% methanol. The elution fraction was taken to complete dryness using a vacuum concentrator (Vacufuge Plus; Eppendorf). After the addition of 20 µL of N,O-bis(trimethylsilyl) trifluoroacetamide containing 1% trimethylchlorosilane (99:1, vol/vol; Supelco) to each extract, the extracts were transferred into 400-µL GC-MS vials and incubated for 70 min at 60 °C.

To analyze IAA and Me-IAA contents in the same samples, 1 µL of each sample was injected splitless with a CombiPAL automated sample injector (CTC Analytics) into a Scion 455 gas chromatograph (Scion Instruments) equipped with a 30 m × 0.25 mm i.d. fused silica capillary column with a chemical bond 0.25-µm ZB35 stationary phase (Phenomenex). Helium at a flow rate of 1 mL/min served as the mobile phase. A pressure pulse of 25 psi over 1 min was used to force the transfer of compounds from the injector into the column. The injector temperature was 250 °C, and the column temperature was held at 50 °C for 1.20 min. Thereafter, the column temperature was increased by 30 °C/min to 120 °C. After reaching 120 °C, the temperature was further increased by 10 °C/min to 325 °C, at which point it was held for another 5 min. The column effluent was introduced into the ion source of a Scion TQ triple-quadrupole mass spectrometer. The mass spectrometer was used in EI-MRM mode. The transfer line temperature was set at 250 °C, and the ion source temperature was set at 200 °C. Ions were generated with -70 eV at a filament emission current of 80 µA. The dwell time was 100 ms, and the reactions *m/z* 247 to *m/z* 130 (endogenous IAA), *m/z* 249 to *m/z* 132 ([<sup>2</sup>H<sub>2</sub>]-IAA, internal standard), *m/z* 261 to *m/z* 202 (endogenous Me-IAA), and *m/z* 266 to *m/z* 207 ([<sup>2</sup>H<sub>2</sub>]-Me-IAA, internal standard) were recorded. Argon set at 1.5 mTorr was used as the collision gas. The amount of the endogenous compound was calculated from the signal ratio of the unlabeled over the stable isotope-containing mass fragment observed in the parallel measurements.

**Mammalian Cell Culture Orthogonal Platform for Determination of Me-IAA and IAA Signaling with an IAA Sensor.**

Human embryonic kidney 293-T cells (HEK-293T) were cultivated and transfected as described previously (30). For transfection of each well, 0.55 µg of a plasmid encoding rice TIR1 and 0.2 µg of a plasmid harboring a radiometric luminescent auxin sensor (with full-length *Arabidopsis* AUX/IAA17 as the sensor module) was mixed and diluted in 50 µL of OptiMEM (Life Technologies) and subsequently mixed with 2.5 µL of PEI solution (Polyscience, 1 M in H<sub>2</sub>O) in 50 µL of OptiMEM under vortexing. After 15 min at room temperature, this 100-µL mixture was added to the cells in a dropwise manner. To induce auxin-mediated protein degradation, appropriate IAA and Me-IAA dilution series were prepared in DMEM and added to the cells at 24 h posttransfection and incubated for 3.5 h, followed by firefly and *Renilla* luminescence analysis as described previously (30).

**ACKNOWLEDGMENTS.** We thank Cristina Ferrándiz and the members of the Hormone Signaling and Plasticity Laboratory at Instituto de Biología Molecular y Celular de Plantas for discussions and critical reading of the manuscript, and Malcolm Bennett for providing seeds of the reporter lines. Work in the authors' laboratories has been funded by grants from the Spanish Ministry of Economy and Competitiveness (BIO2013-43184-P, to D.A. and M.A.B., and BFU2014-55575-R, to S.P.), the German Research Foundation (EXC-1028-CEPLAS, EXC-294-BIOS and GSC 4-SGBM, to M.D.Z.), the European Union (H2020-MSCA-RISE-2014-644435, to M.A.B. and D.A.), and the European Research Council (Project ERC-2011-StG-20101109-PSDP, to J.F.).

1. Vanneste S, Friml J (2009) Auxin: A trigger for change in plant development. *Cell* 136: 1005–1016.
2. Woodward AW, Bartel B (2005) Auxin: Regulation, action, and interaction. *Ann Bot* 95:707–735.
3. Abbas M, Alabadi D, Blázquez MA (2013) Differential growth at the apical hook: All roads lead to auxin. *Front Plant Sci* 4:441.
4. Zádorníková P, et al. (2010) Role of PIN-mediated auxin efflux in apical hook development of *Arabidopsis thaliana*. *Development* 137:607–617.
5. Rakusová H, et al. (2016) Termination of shoot gravitropic responses by auxin feedback on PIN3 polarity. *Curr Biol* 26:3026–3032.
6. Rakusová H, et al. (2011) Polarization of PIN3-dependent auxin transport for hypocotyl gravitropic response in *Arabidopsis thaliana*. *Plant J* 67:817–826.
7. Spalding EP (2013) Diverting the downhill flow of auxin to steer growth during tropisms. *Am J Bot* 100:203–214.
8. Muday GK, DeLong A (2001) Polar auxin transport: Controlling where and how much. *Trends Plant Sci* 6:535–542.
9. Swarup R, Bennett M (2003) Auxin transport: The fountain of life in plants? *Dev Cell* 5: 824–826.
10. Adamowski M, Friml J (2015) PIN-dependent auxin transport: Action, regulation, and evolution. *Plant Cell* 27:20–32.
11. Esmo CA, et al. (2006) A gradient of auxin and auxin-dependent transcription precedes tropic growth responses. *Proc Natl Acad Sci USA* 103:236–241.
12. Fuchs I, Philippak K, Ljung K, Sandberg G, Hedrich R (2003) Blue light regulates an auxin-induced K<sup>+</sup>-channel gene in the maize coleoptile. *Proc Natl Acad Sci USA* 100: 11795–11800.
13. Hohm T, et al. (2014) Plasma membrane H<sup>+</sup>-ATPase regulation is required for auxin gradient formation preceding phototropic growth. *Mol Syst Biol* 10:751.
14. Band LR, et al. (2012) Root gravitropism is regulated by a transient lateral auxin gradient controlled by a tipping-point mechanism. *Proc Natl Acad Sci USA* 109: 4668–4673.
15. Kramer EM (2004) PIN and AUX/LAX proteins: Their role in auxin accumulation. *Trends Plant Sci* 9:578–582.
16. Grieneisen VA, Xu J, Marée AF, Hogeweg P, Scheres B (2007) Auxin transport is sufficient to generate a maximum and gradient guiding root growth. *Nature* 449: 1008–1013.

17. Mellor N, et al. (2016) Dynamic regulation of auxin oxidase and conjugating enzymes AtDAO1 and GH3 modulates auxin homeostasis. *Proc Natl Acad Sci USA* 113:11022–11027.
18. Porco S, et al. (2016) Dioxygenase-encoding AtDAO1 gene controls IAA oxidation and homeostasis in *Arabidopsis*. *Proc Natl Acad Sci USA* 113:11016–11021.
19. Zhang J, et al. (2016) DAO1 catalyzes temporal and tissue-specific oxidative inactivation of auxin in *Arabidopsis thaliana*. *Proc Natl Acad Sci USA* 113:11010–11015.
20. Qin G, et al. (2005) An indole-3-acetic acid carboxyl methyltransferase regulates *Arabidopsis* leaf development. *Plant Cell* 17:2693–2704.
21. Zhao N, et al. (2008) Structural, biochemical, and phylogenetic analyses suggest that indole-3-acetic acid methyltransferase is an evolutionarily ancient member of the SABATH family. *Plant Physiol* 146:455–467.
22. Zubieta C, et al. (2003) Structural basis for substrate recognition in the salicylic acid carboxyl methyltransferase family. *Plant Cell* 15:1704–1716.
23. Li L, et al. (2008) The possible action mechanisms of indole-3-acetic acid methyl ester in *Arabidopsis*. *Plant Cell Rep* 27:575–584.
24. Yang Y, et al. (2008) Inactive methyl indole-3-acetic acid ester can be hydrolyzed and activated by several esterases belonging to the AtMES esterase family of *Arabidopsis*. *Plant Physiol* 147:1034–1045.
25. Friml J, Wiśniewska J, Benková E, Mendgen K, Palme K (2002) Lateral relocation of auxin efflux regulator PIN3 mediates tropism in *Arabidopsis*. *Nature* 415:806–809.
26. Péret B, et al. (2013) Sequential induction of auxin efflux and influx carriers regulates lateral root emergence. *Mol Syst Biol* 9:699.
27. Sauer M, et al. (2006) Canalization of auxin flow by Aux/IAA-ARF-dependent feedback regulation of PIN polarity. *Genes Dev* 20:2902–2911.
28. Chen Q, et al. (2015) A coherent transcriptional feed-forward motif model for mediating auxin-sensitive PIN3 expression during lateral root development. *Nat Commun* 6:8821.
29. Rakusová H, Fendrych M, Friml J (2015) Intracellular trafficking and PIN-mediated cell polarity during tropic responses in plants. *Curr Opin Plant Biol* 23:116–123.
30. Wend S, et al. (2013) A quantitative ratiometric sensor for time-resolved analysis of auxin dynamics. *Sci Rep* 3:2052.
31. Zourelidou M, et al. (2014) Auxin efflux by PIN-FORMED proteins is activated by two different protein kinases, D6 PROTEIN KINASE and PINOID. *eLife* 3:02860.
32. Zheng Z, et al. (2016) Local auxin metabolism regulates environment-induced hypocotyl elongation. *Nat Plants* 2:16025.
33. Brunoud G, et al. (2012) A novel sensor to map auxin response and distribution at high spatio-temporal resolution. *Nature* 482:103–106.
34. Friml J, et al. (2003) Efflux-dependent auxin gradients establish the apical-basal axis of *Arabidopsis*. *Nature* 426:147–153.
35. Alonso JM, et al. (2003) Genome-wide insertional mutagenesis of *Arabidopsis thaliana*. *Science* 301:653–657.
36. Abbas M, et al. (2015) Oxygen sensing coordinates photomorphogenesis to facilitate seedling survival. *Curr Biol* 25:1483–1488.
37. Gallego-Bartolomé J, Kami C, Fankhauser C, Alabadi D, Blázquez MA (2011) A hormonal regulatory module that provides flexibility to tropic responses. *Plant Physiol* 156:1819–1825.
38. Frigerio M, et al. (2006) Transcriptional regulation of gibberellin metabolism genes by auxin signaling in *Arabidopsis*. *Plant Physiol* 142:553–563.
39. Willige BC, Isono E, Richter R, Zourelidou M, Schwechheimer C (2011) Gibberellin regulates PIN-FORMED abundance and is required for auxin transport-dependent growth and development in *Arabidopsis thaliana*. *Plant Cell* 23:2184–2195.

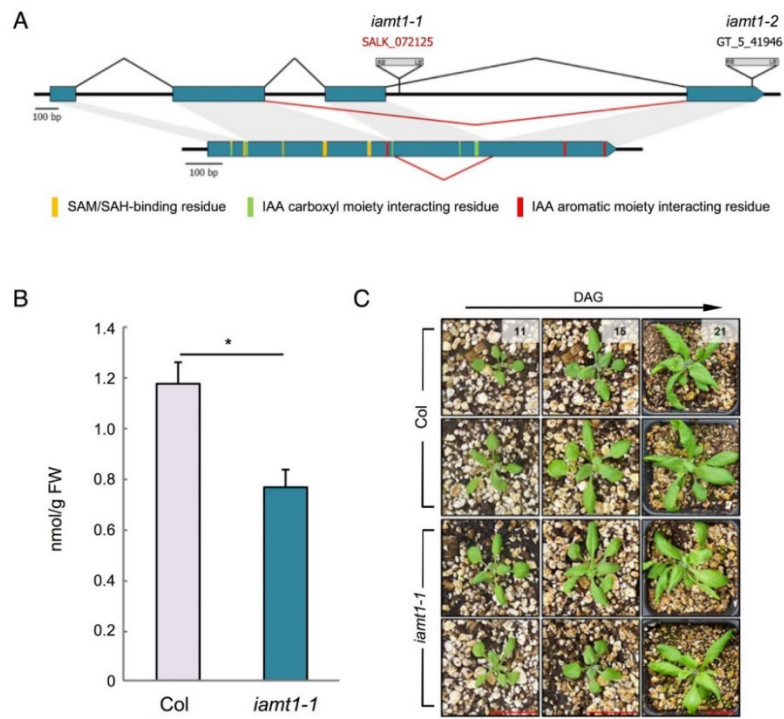


**Fig. S1.** Characterization of the *iamt1* mutant. (A) T-DNA insertion mutants. Blue boxes represent the exons, black lines represent the introns, and red lines indicate the splicing event in the *iamt1-1* allele. (B) Levels of Me-IAA in the *iamt1-1* mutant grown for 7 days in the light. Asterisk indicates that the difference is statistically significant (Student's t-test,  $n=4$ ,  $p<0.001$ ). (C) Overall phenotype of *iamt1-1* adult plants 11, 15, and 21 days after germination. Scale bars (red) = 2 cm.

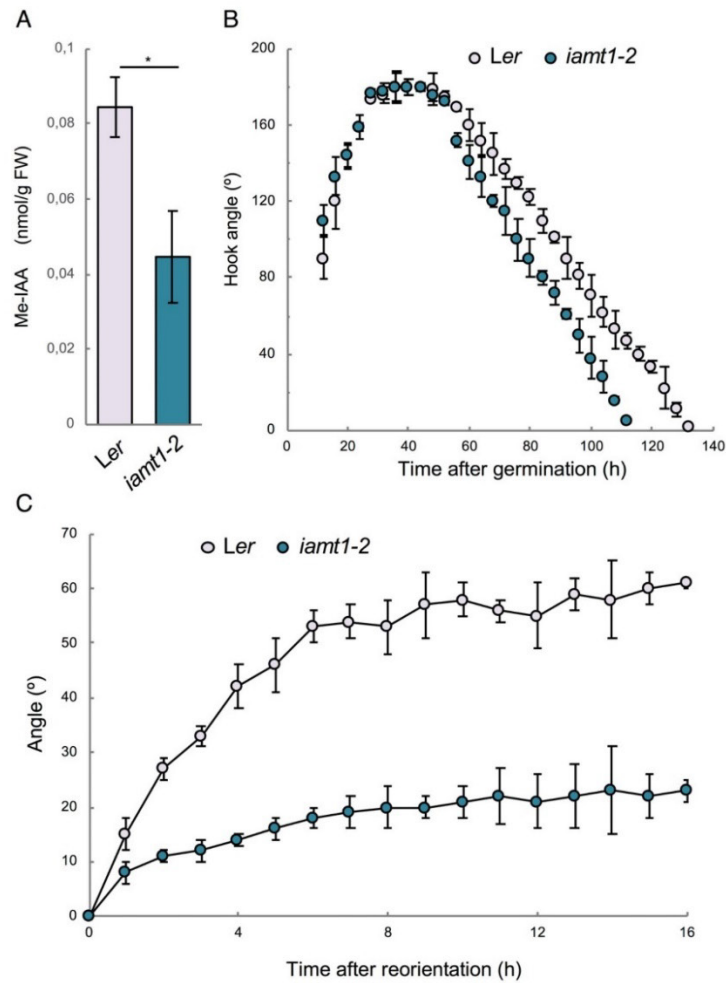


**Fig. S2.** The *iamt1-2* mutant displays a phenotype equivalent to that of *iamt1-1*. (A) Levels of IAA and Me-IAA in 3-day-old etiolated seedlings of the *iamt1-2* mutant. Asterisk indicates that the difference is statistically significant (Student's t-test, \* $p < 0.05$ ). (B) Hook opening dynamics in darkness. (C) Gravitropic reorientation. The experiments were carried out as described in Methods. Error bars represent SD.

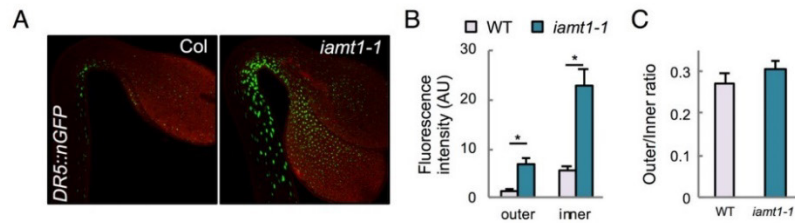


**Fig. S3.** IAMT1 modulates auxin levels in the apical hook. (A) DR5::nGFP expression in the apical hook of 3-day-old etiolated seedlings. (B) Levels of nGFP in either side of the apical hook of DR5::nGFP reporter lines. Graphs represents the average ratio of fluorescence of the outer and inner sides of the hook. (C) Ratio between outer and inner fluorescence measured in (B). Error bars represent SD. Asterisk indicates that the difference is statistically significant (Student's t-test, \*\* $p < 0.01$ ; \*\*\* $p < 0.001$ ).

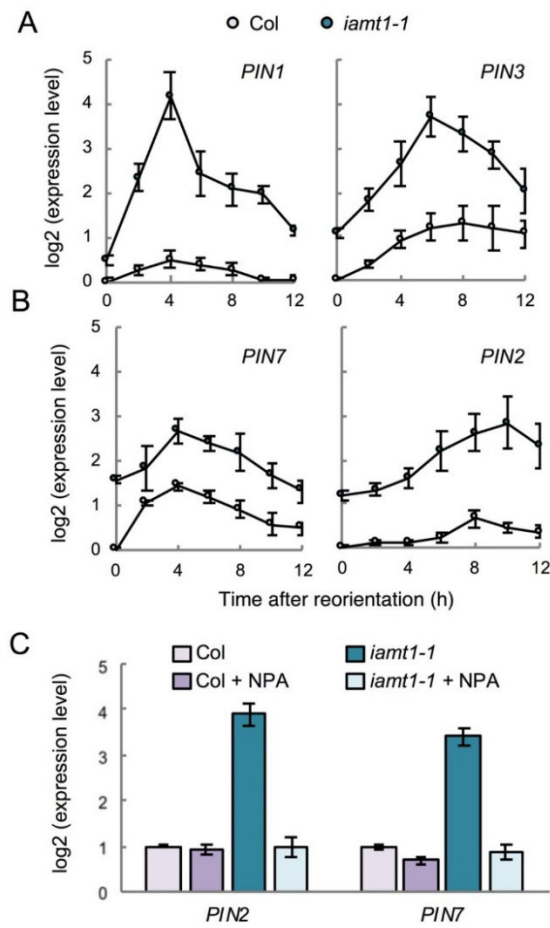


**Fig. S3.** Expression of PIN genes in the *iamt1-1* mutant. (A) and (B) Expression of *PIN1*, *PIN2*, *PIN3* and *PIN7* in gravistimulated hypocotyls, determined by RT-qPCR. (C) Expression of *PIN2* and *PIN7* in seedlings gravistimulated for 4 h in the presence of 0.5  $\mu$ M NPA or mock solution, determined by RT-qPCR. Error bars represent SD.

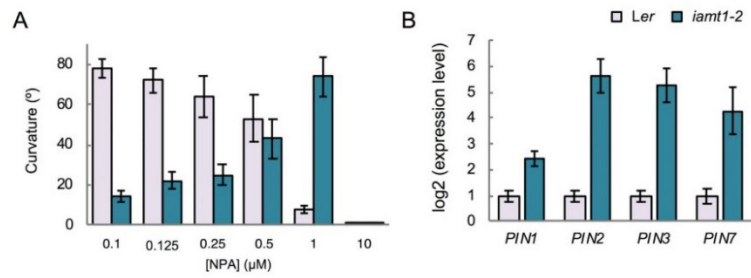


**Fig. S5.** The *iamt1-2* mutant is altered in polar auxin transport. (A) Effect of NPA on hypocotyl curvature 12 h after gravitropic reorientation. Error bars represent SD (n>10). (B) Expression of *PIN1*, *PIN2*, *PIN3*, and *PIN7* determined by RT-qPCR in wild-type and *iamt1-2* mutant 4 h after gravistimulation.



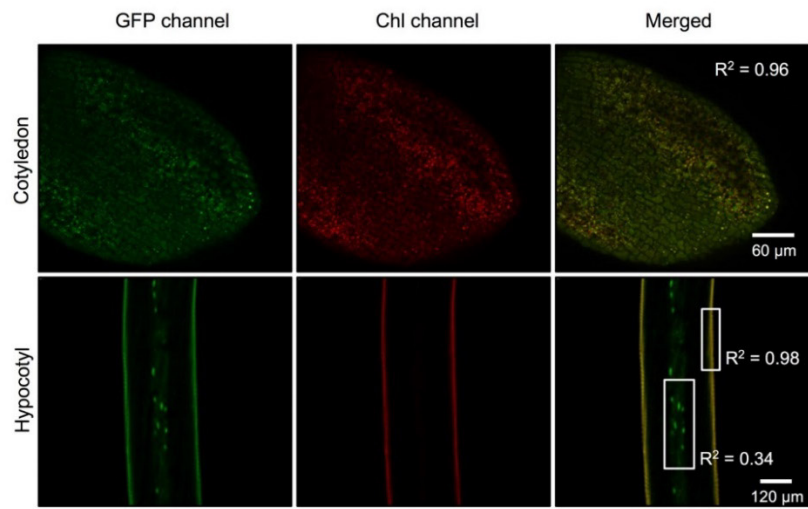


**Fig. S6.** In etiolated seedlings, *pSCR::nGFP::SCR* is only active in endodermal cells of the hypocotyl. The high  $R^2$  value (0.96) indicates that the signal detected in the cotyledons in the GFP channel corresponds to chlorophyll (Chl).

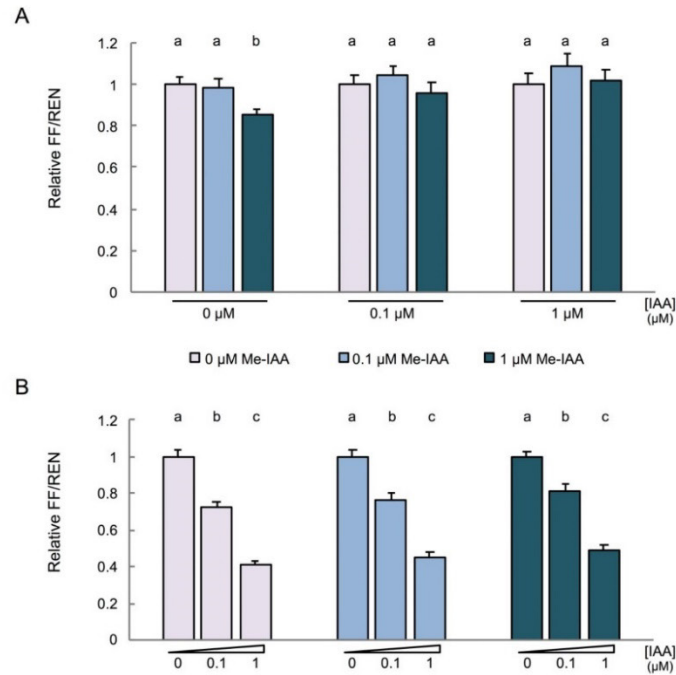


**Fig. S7.** Me-IAA does not mimic nor interfere with the activity of the auxin co-receptor complex. HEK-293T cells were co-transfected with a ratiometric luminescent IAA biosensor construct and rice TIR1. The sensor construct comprises two components: a sensor module (SM), fused to firefly luciferase (FF), and renilla luciferase (REN) for normalization. Both components are linked by a 2A peptide for stoichiometric co-expression of SM-FF and REN. The SM consisted of full length AtAUX/IAA17 and confers auxin-dependent degradation of FF. Auxin concentration-dependent degradation of the sensor could be monitored as a decrease in FF relative to REN luminescence (FF/REN). 24 h after transfection, the cell culture medium was supplemented with the indicated concentrations of IAA and/or Me-IAA for 3.5 hours before determination of luciferase activity. (A) Me-IAA does not mimic IAA. FF/REN ratios for increasing concentrations of IAA were normalized to the respective ratio obtained in the absence of Me-IAA (0 μM). (B) Me-IAA does not interfere with the ability of IAA to induce the degradation of the reporter. FF/REN ratios for increasing concentrations of Me-IAA were normalized to the respective ratio obtained in the absence of IAA (0 μM). Results are means ± SEM (n=5). Letters indicate significant differences between groups,  $p < 0.05$  (One way ANOVA, Tukey HSD Post Hoc test)

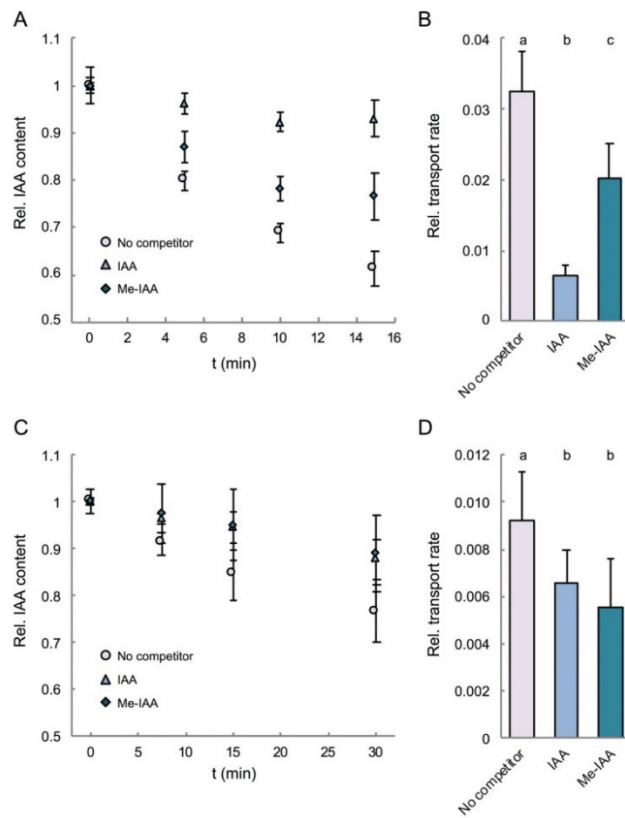


**Fig. S8.** Inhibition of [<sup>3</sup>H]-IAA efflux from *Xenopus laevis* oocytes by Me-IAA. (*A,B*) PIN3, (*C,D*) PIN1. (*A*) and (*C*) are data of a typical experiment, (*B*) and (*D*) are transport rates calculated from at least 3 biological replicates. Letters indicate significant differences between groups.  $p < 0.05$  (One way ANOVA, Student-Newman-Keuls Post Hoc test).